

Lorena Marrodán Bretón

Oxidation of organic compounds present in fuels under conditions of interest for combustion processes

Departamento

Ingeniería Química y Tecnologías del Medio
Ambiente

Director/es

MILLERA PERALTA, ÁNGELA
ALZUETA ANIA, MARIA UJUE

<http://zaguan.unizar.es/collection/Tesis>



Reconocimiento – NoComercial – SinObraDerivada (by-nc-nd): No se permite un uso comercial de la obra original ni la generación de obras derivadas.

© Universidad de Zaragoza
Servicio de Publicaciones

ISSN 2254-7606

Tesis Doctoral

OXIDATION OF ORGANIC COMPOUNDS PRESENT
IN FUELS UNDER CONDITIONS OF INTEREST
FOR COMBUSTION PROCESSES

Autor

Lorena Marrodán Bretón

Director/es

MILLERA PERALTA, ÁNGELA
ALZUETA ANIA, MARIA UJUE

UNIVERSIDAD DE ZARAGOZA

Ingeniería Química y Tecnologías del Medio Ambiente

2018



**Universidad
Zaragoza**

“Oxidation of organic compounds present in fuels under conditions of interest for combustion processes”

This dissertation is submitted to the Department of Chemical Engineering and Environmental Technologies at the University of Zaragoza (Spain) in fulfillment of the requirements for the degree of Doctor

Lorena Marrodán Bretón

Zaragoza, 2018



**Departamento de Ingeniería
Química y Tecnologías
del Medio Ambiente
Universidad Zaragoza**



**Instituto Universitario de Investigación
de Ingeniería de Aragón
Universidad Zaragoza**

GPT
Thermo-Chemical
Processes Group



Dña. María Ujué Alzueta Anía, Catedrática de Universidad, y **Dña. Ángela Millera Peralta**, Profesora Titular del Departamento de Ingeniería Química y Tecnologías del Medio Ambiente de la Universidad de Zaragoza,

INFORMAN

Que la presente memoria titulada:

“Oxidation of organic compounds present in fuels under conditions of interest for combustion processes”

ha sido realizada bajo su supervisión en el Grupo de Procesos Termoquímicos perteneciente al Instituto de Investigación en Ingeniería de Aragón (I3A) y en el Departamento de Ingeniería Química y Tecnologías del Medio Ambiente de la Universidad de Zaragoza, por **Dña. Lorena Marrodán Bretón**, y AUTORIZAN su presentación como compendio de publicaciones y con la mención internacional en el título de Doctor, cumpliendo con las condiciones requeridas para que su autora pueda optar al grado de Doctor en el Programa de Doctorado de Ingeniería Química y del Medio Ambiente de la Universidad de Zaragoza.

Y para que así conste, firmamos este certificado en Zaragoza a 17 de octubre de 2018.

Dña. María Ujué Alzueta Anía

Dña. Ángela Millera Peralta



Professor María Ujué Alzueta Anía and **Associate Professor Ángela Millera Peralta**, both belonging to the Department of Chemical and Environmental Engineering of the University of Zaragoza,

REPORT that:

The Doctoral Thesis entitled:

“Oxidation of organic compounds present in fuels under conditions of interest for combustion processes”

has been carried out under our supervision in the Thermo-Chemical Processes Group belonging to the Aragón Institute of Engineering Research (I3A) and in the Department of Chemical and Environmental Engineering of the University of Zaragoza, by **Ms. Lorena Marrodán Bretón**, and we AUTHORIZE and approve the presentation of this dissertation in the form of compendium of publications and with the international citation on the doctoral certificate, fulfilling the requirements for the degree of Doctor.

And for the record, we sign this document in Zaragoza on 17th October 2018.

Dña. María Ujué Alzueta Anía

Dña. Ángela Millera Peralta

El presente trabajo ha sido publicado, en gran parte, en los artículos que se mencionan a continuación y que se adjuntan al final de esta memoria.

The present work has been largely published in the articles mentioned below and attached at the end of this dissertation.

- A. **Marrodán, L.**; Millera, Á.; Bilbao, R.; Alzueta, M.U. (2014). High-pressure study of methyl formate oxidation and its interaction with NO. *Energy and Fuels* 28, 6107-6115.
- I. **Marrodán, L.**; Monge, F.; Millera, Á.; Bilbao, R.; Alzueta, M.U. (2016). Dimethoxymethane oxidation in a flow reactor. *Combustion Science and Technology* 188, 719-729.
- II. **Marrodán, L.**; Royo, E.; Millera, Á.; Bilbao, R.; Alzueta, M.U. (2015). High pressure oxidation of dimethoxymethane. *Energy and Fuels* 29, 3507-3517.
- III. **Marrodán, L.**; Arnal, Á.J.; Millera, Á.; Bilbao, R.; Alzueta, M.U. (2018). High-pressure ethanol oxidation and its interaction with NO. *Fuel* 223, 394-400.
- IV. **Marrodán, L.**; Berdusán, L.; Aranda, V.; Millera, Á.; Bilbao, R.; Alzueta, M.U. (2016). Influence of dimethyl ether addition on the oxidation of acetylene in the absence and presence of NO. *Fuel* 183, 1-8.
- V. **Marrodán, L.**; Arnal, Á.J.; Millera, Á.; Bilbao, R.; Alzueta, M.U. (2018). The inhibiting effect of NO addition on dimethyl ether high-pressure oxidation. *Combustion and Flame* 197, 1-10.
- VI. Song, Y.; **Marrodán, L.**; Vin, N.; Herbinet, O.; Assaf, E.; Fittschen, C.; Stagni, A.; Faravelli, T.; Alzueta, M.U.; Battin-Leclerc, F. (2018). The sensitizing effects of NO₂ and NO on methane low temperature oxidation in a jet stirred reactor. *Proceedings of the Combustion Institute*, DOI: 10.1016/j.proci.2018.06.115.
- VII. **Marrodán, L.**; Fuster, M.; Millera, Á.; Bilbao, R.; Alzueta, M.U. (2018). Ethanol as a fuel additive: high-pressure oxidation of its mixtures with acetylene. *Energy and Fuels* 32, 10078-10087.

Las publicaciones numeradas del I-VII forman parte del compendio de artículos, modalidad por la que se presenta esta Tesis Doctoral. La numeración de las mismas corresponde al orden en que se mencionan en la memoria. Al final de la misma, se pueden consultar las publicaciones completas.

The I-VII numbered publications are part of the compendium of publications, modality by which this Doctoral Thesis is presented. The numbering corresponds to the order in which they are mentioned in the memory, at the end of which, they can be consulted.

El artículo A, aunque no forma parte del compendio de publicaciones, ha sido incluido ya que se considera muy relevante en el contexto de esta investigación.

Article A has been included since it is considered very relevant in the context of this research, although it is not part of the compendium of publications.

Adicionalmente, en la parte final de la memoria, se muestran algunos resultados obtenidos durante esta tesis que todavía no han sido discutidos y publicados en revistas científicas.

Additionally, in the final part of this dissertation, some results obtained during this thesis, which have not yet been discussed and published in scientific journals, are shown.

Por otro lado, la doctoranda ha participado y presentado resultados parciales de la investigación en diferentes congresos nacionales e internacionales, relacionados con diferentes aspectos implicados en su trabajo.

On the other hand, the doctoral candidate has participated and presented partial results of this research in several national and international congresses, related to different aspects involved in her work.

- **Marrodán, L.**; Millera, Á.; Bilbao, R.; Alzueta, M.U. Methyl formate: an experimental and kinetic study of its oxidation at high-pressure. **III Jornada de Jóvenes Investigadores I3A**. Zaragoza (Spain), 29th May, 2014. *Oral presentation.*
- **Marrodán, L.**; Royo, E.; Millera, Á.; Bilbao, R.; Alzueta, M.U. A promising diesel fuel additive: dimethoxymethane. **ANQUE-ICCE-BIOTEC 2014**. Madrid (Spain), 1-4 July 2014. *Oral presentation.*
- **Marrodán, L.**; Millera, Á.; Bilbao, R.; Alzueta, M.U. Methyl formate oxidation at high-pressure. **23rd International Symposium on Gas Kinetics**. Szeged (Hungary), 20-25 July 2014. *Poster presentation.*
- **Marrodán, L.**; Royo, E.; Millera, Á.; Bilbao, R.; Alzueta, M.U. An updated kinetic mechanism for dimethoxymethane oxidation under high-pressure conditions. **35th**

International Symposium on Combustion. San Francisco (USA), 3-8 August 2014.
Poster presentation.

- **Marrodán, L.;** Royo, E.; Millera, Á.; Bilbao, R.; Alzueta, M.U. Oxidation of dimethoxymethane under high-pressure conditions. **13th Mediterranean Congress of Chemical Engineering.** Barcelona (Spain), 30-3 October 2014. *Poster presentation.*
- **Marrodán, L.;** Millera, Á.; Bilbao, R.; Alzueta, M.U. Compuestos oxigenados como aditivos para combustibles de automoción. **6^a Jornada de Jóvenes Investigadores de Aragón.** Zaragoza (Spain), 20th November 2014. *Oral presentation.*
- **Marrodán, L.;** Monge, F.; Millera, Á.; Bilbao, R.; Alzueta, M.U. Dimethoxymethane oxidation in a flow reactor. **Ninth Mediterranean Combustion Symposium.** Rhodes (Greece), 7-11 June 2015. *Oral presentation.*
- **Marrodán, L.;** Millera, Á.; Bilbao, R.; Alzueta, M.U. From rich to lean conditions, dimethoxymethane oxidation modeling at high pressures. **The 9th International Conference on Chemical Kinetics.** Ghent (Belgium), 28-2 July 2015. *Poster presentation.*
- **Marrodán, L.;** Arnal, J.; Millera, Á.; Bilbao, R.; Alzueta, M.U. Kinetic modeling improvements in the high-pressure oxidation of dimethyl ether. **24th International Symposium on Gas Kinetics.** York (United Kingdom), 17-21 July 2016. *Poster presentation.*
- **Marrodán, L.;** Millera, Á.; Bilbao, R.; Alzueta, M.U. Mecanismos cinético-químicos: cómo se forman y destruyen los contaminantes atmosféricos. **7^a Jornada de Jóvenes Investigadores (Química y Física) de Aragón.** Zaragoza (Spain), 24th November 2016. *Poster presentation.*
- **Marrodán, L.;** Fuster, M.; Millera, Á.; Bilbao, R.; Alzueta, M.U. Etanol como aditivo para combustibles: estudio de la oxidación a alta presión de sus mezclas con acetileno. **VI Jornada de Jóvenes Investigadores I3A.** Zaragoza (Spain), 2nd June 2017. *Poster presentation.*
- **Marrodán, L.;** Arnal, J.; Millera, Á.; Bilbao, R.; Alzueta, M.U. High-pressure ethanol oxidation and its interaction with NO. **13th International Conference Energy for a Clean Environment.** São Miguel, Azores (Portugal), 2-6 July 2017. *Oral presentation.*
- **Marrodán, L.;** Fuster, M.; Millera, Á.; Bilbao, R.; Alzueta, M.U. Ethanol as fuel additive: high-pressure oxidation of its mixtures with acetylene. **3rd General Meeting, COST Action 1404, Chemistry of Smart Energy Carriers and Technologies.** Prague (Czech Republic), 25-27 October 2017. *Oral presentation.*

- **Marrodán, L.**; Song, Y.; Herbinet, O.; Alzueta, M.U.; Battin-Leclerc, F. The effect of NO_x addition on the low-temperature oxidation of n-pentane in a jet stirred reactor. **“Gas-phase reaction kinetics of biofuels oxygenated molecules” Workshop**. Milan (Italy), 23-24 April 2018. *Oral presentation*.
- **Marrodán, L.**; Arnal, J.; Millera, Á.; Bilbao, R.; Alzueta, M.U. High-pressure oxidation of dimethyl ether: the effect of NO addition. **“Gas-phase reaction kinetics of biofuels oxygenated molecules” Workshop**. Milan (Italy), 23-24 April 2018. *Poster presentation*.
- **Song, Y.**; **Marrodán, L.**; Vin, N.; Herbinet, O.; Assaf, E.; Fittschen, C.; Stagni, A.; Alzueta, M.U.; Battin-Leclerc, F. The sensitizing effects of NO₂ and NO on methane low temperature oxidation in a jet stirred reactor. **“Gas-phase reaction kinetics of biofuels oxygenated molecules” Workshop**. Milan (Italy), 23-24 April 2018. *Poster presentation*.
- **Marrodán, L.**; Song, Y.; Vin, N.; Herbinet, O.; Assaf, E.; Fittschen, C.; Stagni, A.; Alzueta, M.U.; Battin-Leclerc, F. The sensitizing effects of NO₂ and NO on methane low temperature oxidation in a jet stirred reactor. **“Gas-phase reaction kinetics of biofuels oxygenated molecules” VII Jornada de Jóvenes Investigadores del I3A**. Zaragoza (Spain), 8th June 2018. *Poster presentation*.
- **Marrodán, L.**; Song, Y.; Herbinet, O.; Alzueta, M.U.; Battin-Leclerc, F. Jet-stirred low-temperature oxidation of n-pentane: the effect of NO_x addition. **25th International Symposium on Gas Kinetics & Related Phenomena**. Lille (France), 22-26 July 2018. *Poster presentation*.
- **Marrodán, L.**; Millera, Á.; Bilbao, R.; Alzueta, M.U. Evaluation of DME as a possible fuel additive through the study of the high-pressure oxidation of its mixtures with acetylene. **25th International Symposium on Gas Kinetics & Related Phenomena**. Lille (France), 22-26 July 2018. *Poster presentation*.
- **Marrodán, L.**; Millera, Á.; Bilbao, R.; Alzueta, M.U. Experimental and modeling study of the oxidation of prospective fuel additives and acetylene mixtures under high-pressure conditions. **37th International Symposium on Combustion**. Dublin (Ireland), 29-3 August 2018. *Poster presentation*.

*A MI FAMILIA,
a aquellos que, sin poder estar presentes,
lo están en nuestro recuerdo.*

Acknowledgements. Agradecimientos

La presente Tesis Doctoral ha sido realizada en el Grupo de Procesos Termoquímicos (GPT) perteneciente al Instituto de Investigación en Ingeniería de Aragón (I3A), dentro del programa de doctorado de Ingeniería Química y del Medio Ambiente (Departamento de Ingeniería Química y Tecnologías del Medio Ambiente), bajo la dirección y supervisión de las Dras. M^a Ujué Alzueta Anía y Ángela Millera Peralta.

La investigación ha sido financiada por el Gobierno de Aragón (Grupo GPT), el Fondo Social Europeo y MINECO (Proyectos CTQ2012-34423 y CTQ2015-65226). Así mismo, el Gobierno de Aragón concedió un contrato predoctoral a la doctoranda para la realización de la presente tesis. Parte de este trabajo de investigación se realizó en el *Laboratoire des Réactions et Génie des Procédés* (LRGP) de la Universidad de Lorraine en Nancy (Francia), bajo la supervisión de la Dra. Frédérique Battin-Leclerc, en el marco de una estancia corta de investigación, financiada por la Unión Europea a través del programa COST (Acción CM1404, SMARTCATs). *I would like to say thanks to Prof. Battin-Leclerc and all the group in Nancy for the help and assistance during my stay in the LRGP group. I always felt like at home.*

Quisiera aprovechar para expresar mi más profundo y sincero agradecimiento a mis directoras de tesis, las Dras. M^a Ujué Alzueta y Ángela Millera, por toda la dedicación y esfuerzo que han puesto para que esta tesis saliera adelante, por su paciencia y apoyo, por sus consejos y por todo lo que me han enseñado en estos años que hemos compartido. Quisiera agradecer igualmente al Dr. Rafael Bilbao, una pieza muy importante en este puzzle, por todos los debates científicos en los que nos hemos visto involucrados y por su enorme contribución a este trabajo.

A toda la familia del GPT, por esos cafés, meriendas científicas, excursiones... y, porque siempre que he necesitado de vuestra ayuda y consejos, he podido contar con vosotros. A María, por todos esos ratitos que hemos compartido estos años, incluso por su sabiduría, porque ya se sabe que "la investigación es el motor para alcanzar un desarrollo sostenible y, el fruto de la misma, es el progreso"; a Olga, mi mami zaragozana; a mi pelirroja favorita; a mis compañeros de despacho, laboratorio y nave, por vuestra santa paciencia para aguantarme. A todos, porque además de compañeros creo que me llevo grandes amigos.

A los IQs, esos Ingenieros Químicos con los que siempre he podido contar, en los buenos y en los no tan buenos momentos, qué sería de mí sin mis queridas Fichas, mi Evu siempre optimista, los Cuquis o los Lacheta. A mis Cerbunos del alma, siempre digo y diré que

el Cerbuna marcó un antes y un después en mi vida. A todas aquellas personas que han pasado por mi vida en estos últimos años, compañeros de batallas, de piso (mi querido otomaño Hakan), de entrenamientos, a mis tudelillanas favoritas y, por su puesto, a mi familia porque siempre están ahí.

A todos.....MIL GRACIAS!!

Abstract

The use of alternative fuels may be a possible solution to minimize the formation of pollutants from diesel engines, such as nitrogen oxides (NO_x) and soot, with diverse potential harmful effects on environment and/or human health. In this field, fuel reformulation by the addition of oxygenated compounds seems to be a promising solution. However, the behavior of these alternative fuels under combustion environments is less known compared to that of conventional ones. Therefore, experiments under well-controlled conditions accompanied by chemical kinetic studies, that help to interpret and understand the reaction schemes that occur during such processes, are desired to design and optimize future combustion devices.

In this context, the aim of the present work is to analyze the role, as fuel additives, of three oxygenated compounds proposed in literature as possible fuel additives, namely, ethanol, dimethyl ether (DME), and dimethoxymethane (DMM), with different functional groups and/or number of carbon atoms, under conditions of interest for combustion processes. To achieve this global goal, different studies have been carried out. First, the oxidation of intermediates of interest, methyl formate (MF) and methane (CH_4), generated during the oxidation of these oxygenated compounds, has been analyzed. Later, the high-pressure oxidation of the oxygenated compounds has been individually characterized and, in the case of DMM, its atmospheric pressure oxidation has also been studied. During these individual studies, a chemical kinetic mechanism has been developed to describe the oxidation of the corresponding compound under the different experimental conditions. Finally, the role as fuel additives of ethanol, DME and DMM has been analyzed by performing oxidation experiments of their mixtures with acetylene (C_2H_2) under high-pressure conditions, more representative of the real operating conditions. C_2H_2 has been selected as the main fuel because is considered a soot precursor and/or an intermediate compound found during the combustion of hydrocarbons.

The wide range of experimental conditions tested has allowed to compile and validate a detailed chemical kinetic mechanism able to describe the high-pressure oxidation of the mixtures of the oxygenates studied with acetylene, and analyze their role as fuel additives. Results indicate that the functional group has a strong influence on the oxidation behavior of the mixtures. While the addition of ethanol (an alcohol) has almost no effect on the oxidation of C_2H_2 , the addition of DME or DMM (ethers) shifts the conversion of C_2H_2 to lower temperatures, and the smaller the ether, the lower the temperatures. Thus, DME is the most effective in reducing the onset temperature of C_2H_2 conversion. Moreover, an increase in the

O/OH radical pool composition due to the oxygen present in these molecules, promotes the oxidation of C_2H_2 towards CO and CO_2 , removing carbon from the reaction pathways which lead to the formation of soot.

Resumen

El uso de combustibles alternativos puede ser una posible solución para minimizar la formación de contaminantes en los motores diésel, como, por ejemplo, los óxidos de nitrógeno (NO_x) y el hollín, que presentan una gran variedad de efectos perjudiciales para el medio ambiente y/o la salud humana. En este campo, la reformulación de combustibles, mediante la adición de compuestos oxigenados, parece ser una solución muy prometedora. Sin embargo, el comportamiento de estos combustibles alternativos en un entorno de combustión es menos conocido en comparación con los combustibles convencionales. Por lo tanto, para diseñar y optimizar los futuros equipos de combustión, se requieren experimentos bajo condiciones de laboratorio bien controladas, acompañados por estudios cinético-químicos, que ayuden a interpretar y a entender los mecanismos de reacción que ocurren durante dichos procesos.

En este contexto, el objetivo del presente trabajo es analizar el papel como aditivos de combustible de tres compuestos oxigenados propuestos en la bibliografía como posibles aditivos: etanol, dimetil éter (DME) y dimetoximetano (DMM), con diferentes grupos funcionales y/o número de átomos de carbono, en condiciones de interés para los procesos de combustión. Para lograr este objetivo global, se han llevado a cabo diferentes estudios. En primer lugar, se ha analizado la oxidación de intermedios de interés, formiato de metilo (MF) y metano (CH_4), generados durante la oxidación de estos compuestos oxigenados. Posteriormente, se ha caracterizado individualmente la oxidación a alta presión de los compuestos oxigenados y, en el caso del DMM, también se ha estudiado su oxidación a presión atmosférica. Durante los estudios individuales de los compuestos, se ha desarrollado un mecanismo cinético químico para describir la oxidación de los diferentes compuestos en las diversas condiciones experimentales estudiadas. Finalmente, se ha analizado el papel como aditivos de etanol, DME y DMM. Para ello, se han realizado experimentos de oxidación de sus mezclas con acetileno (C_2H_2) en condiciones de alta presión, más representativas de las condiciones reales de operación en motores. Se ha seleccionado el acetileno como combustible principal ya que se le considera un precursor de hollín y/o un intermedio durante la combustión de hidrocarburos.

El amplio intervalo de condiciones experimentales probadas ha permitido compilar y validar un mecanismo cinético químico detallado capaz de describir la oxidación a alta presión de las mezclas acetileno-compuesto oxigenado, y analizar el papel de los compuestos oxigenados como aditivos de combustible. Los resultados indican que el grupo funcional tiene

una gran influencia en la oxidación de las mezclas. Mientras que la adición de etanol (un alcohol) casi no tiene ningún efecto sobre la oxidación de C_2H_2 , la adición de DME o DMM (éteres) desplaza la conversión de C_2H_2 a menores temperaturas, y cuanto más pequeño es el éter, menor es dicha temperatura de conversión. Así, el DME es el compuesto más efectivo para reducir la temperatura de inicio de la conversión de C_2H_2 . Además, un aumento en la composición de la reserva de radicales O/OH, debido al oxígeno presente en estas moléculas, promueve la oxidación de C_2H_2 hacia CO y CO_2 , eliminando, de esta manera, carbono de las rutas de reacción que conducen a la formación de hollín.

Acronyms

CHEC	Combustion and Harmful Emission Control
CI	Compression ignition
cw-CRDS	Continuous wave cavity ring-down spectroscopy
DME	Dimethyl ether
DMM	Dimethoxymethane
DTU	Technical University of Denmark
EGR	Exhaust gas recirculation
FAME	Fatty acid methyl esters
FTIR	Fourier Transform Infrared
GPT	Thermo-Chemical Processes Group
HC	Hydrocarbons
HCCI	Homogeneous charge compression-ignition
JSR	Jet-stirred reactor
I3A	Aragón Institute of Engineering Research
IEA	International Energy Agency
JCR	Journal of Citation Reports
LPG	Liquified petroleum gas
LRGP	Laboratoire Réactions et Génie des Procédés
LTC	Low-temperature combustion
MF	Methyl formate
NTC	Negative temperature coefficient
PAH	Polycyclic aromatic hydrocarbons
POLIMI	Politecnico di Milano
POMDMEs	Polyoxymethylene dimethyl ethers
PM	Particulate matter
R	Radicals
ROP	Rate of production
SI	Spark ignition
STP	Standard Temperature and Pressure
TCD	Thermal conductivity detectors

Content

1. INTRODUCTION AND OBJECTIVES	1
1.1 INTRODUCTION.....	1
1.2 SCOPE AND OBJECTIVES.....	2
2. BACKGROUND	7
2.1 STATE OF THE ART	7
2.2 ETHANOL.....	12
2.3 DIMETHYL ETHER	14
2.4 DIMETHOXYMETHANE	18
2.5 INTERMEDIATES OF OXIDATION: METHYL FORMATE AND METHANE	19
3. EXPERIMENTAL METHODOLOGY	25
3.1 ATMOSPHERIC-PRESSURE FLOW REACTOR SET-UP	25
3.2 HIGH-PRESSURE FLOW REACTOR SET-UP.....	28
3.3 ATMOSPHERIC PRESSURE JET-STIRRED REACTOR (JSR) SET-UP	31
4. MODELING. REACTION MECHANISM	37
4.1 METHYL FORMATE REACTION SUBSET AT HIGH PRESSURE	39
4.2 DIMETHOXYMETHANE REACTION SUBSET AT ATMOSPHERIC AND HIGH PRESSURE	40
4.3 ETHANOL REACTION SUBSET AT HIGH PRESSURE	41
4.4 DIMETHYL ETHER REACTION SUBSET AT ATMOSPHERIC PRESSURE, IN ITS MIXTURES WITH C ₂ H ₂ AND AT HIGH PRESSURE.....	42
4.5 METHANE REACTION SUBSET AT ATMOSPHERIC PRESSURE IN A JET STIRRED REACTOR.....	45
5. RESULTS AND DISCUSSION	49
5.1 OXIDATION OF METHYL FORMATE AND METHANE	49
5.1.1 High-pressure oxidation of MF and its interaction with NO in a flow reactor.....	50
5.1.2 Low-temperature oxidation of CH ₄ in a jet-stirred reactor in the presence of NO _x	54
5.2 HIGH-PRESSURE OXIDATION OF DIMETHYL ETHER AND ETHANOL AND THEIR INTERACTION WITH NO	60
5.2.1 Evaluation of the effect of gas residence time	62
5.2.2 High-pressure oxidation of DME and ethanol in the absence of NO	63
5.2.3 Influence of the presence of NO on the high-pressure oxidation of DME and ethanol	67
5.3 HIGH-PRESSURE OXIDATION OF DIMETHOXYMETHANE.....	70
5.3.1 Atmospheric-pressure oxidation of DMM in a flow reactor	70
5.3.2 High-pressure oxidation of DMM in a flow reactor	75

CONTENT

5.4	HIGH-PRESSURE OXIDATION OF ACETYLENE-OXYGENATED COMPOUND MIXTURES IN A FLOW REACTOR	79
5.4.1	High-pressure oxidation of acetylene-ethanol mixtures	79
5.4.2	High-pressure oxidation of acetylene-dimethyl ether mixtures.....	87
5.4.2.1	Atmospheric-pressure oxidation of acetylene-dimethyl ether mixtures in the absence and presence of NO	87
5.4.2.2	High-pressure oxidation of acetylene-dimethyl ether mixtures.....	96
5.4.3	High-pressure oxidation of acetylene-dimethoxymethane mixtures	101
5.4.4	Evaluation of the high-pressure oxidation of acetylene-oxygenated compound mixtures.....	107
6.	SUMMARY AND CONCLUSIONS.....	113
6.1	OXIDATION OF THE INTERMEDIATES: METHYL FORMATE AND METHANE	113
6.1.1	High-pressure oxidation of methyl formate and its interaction with NO in a flow reactor.....	113
6.1.2	Low-temperature oxidation of CH ₄ in a jet-stirred reactor in the presence of NO _x	114
6.2	HIGH-PRESSURE OXIDATION OF DIMETHYL ETHER AND ETHANOL AND THEIR INTERACTION WITH NO	115
6.3	ATMOSPHERIC AND HIGH-PRESSURE OXIDATION OF DIMETHOXYMETHANE IN A FLOW REACTOR	117
6.4	HIGH-PRESSURE OXIDATION OF ACETYLENE-OXYGENATED COMPOUND MIXTURES.....	118
6.4.1	High-pressure oxidation of acetylene-ethanol mixtures	118
6.4.2	Atmospheric-pressure oxidation of acetylene-dimethyl ether mixtures in the absence and presence of NO	119
6.4.3	High-pressure oxidation of acetylene-dimethyl ether mixtures.....	120
6.4.4	High-pressure oxidation of acetylene-dimethoxymethane mixtures	121
6.5	GENERAL CONCLUSION	121
6.	RESUMEN Y CONCLUSIONES	125
6.1	OXIDACIÓN DE LOS INTERMEDIOS: FORMIATO DE METILO Y METANO	125
6.1.1	Oxidación a alta presión de formiato de metilo y su interacción con NO en un reactor de flujo	125
6.1.2	Oxidación a baja temperatura de CH ₄ en un reactor perfectamente agitado en presencia de NO _x	126
6.2	OXIDACIÓN A ALTA PRESIÓN DE DIMETIL ÉTER Y ETANOL Y SU INTERACCIÓN CON NO.....	127
6.3	OXIDACIÓN A PRESIÓN ATMOSFÉRICA Y ALTA PRESIÓN DE DIMETOXIMETANO EN UN REACTOR DE FLUJO	129
6.4	OXIDACIÓN A ALTA PRESIÓN DE LAS MEZCLAS ACETILENO-COMPUESTO OXIGENADO	130
6.4.1	Oxidación a alta presión de mezclas acetileno-etanol.....	131

6.4.2	Oxidación a presión atmosférica de las mezclas acetileno-dimetil éter en ausencia y en presencia de NO.....	131
6.4.3	Oxidación a alta presión de las mezclas acetileno-dimetil éter	132
6.4.4	Oxidación a alta presión de las mezclas acetileno-dimetoximetano	133
6.5	CONCLUSIÓN GENERAL.....	134
	REFERENCES.....	135

Annexes

- Regulations required to submit a PhD Thesis by compendium of publications
- Article A
- Article I
- Article II
- Article III
- Article IV
- Article V
- Article VI
- Article VII
- Final mechanism

List of Figures

Figure 2.1.	Diagram showing the equivalence ratio (ϕ) and temperature ranges for soot and NO _x formation and the operating regions for CI, SI, HCCI and LTC engines (Dec, 2009).....	9
Figure 2.2.	Overview of different way to obtain biofuels from biomass (Hamelinck and Faaij, 2006). FT: Fischer Tropsch; SNG: Synthetic Natural Gas.....	10
Figure 2.3.	Diagram for dimethyl ether production (adapted from Azizi et al., 2014).	15
Figure 3.1.	Scheme of the experimental set-up used to carry out the oxidation experiments at atmospheric pressure in a flow reactor (adapted from Alexandrino, 2018).	26
Figure 3.2.	Scheme and dimensions (in mm) of the atmospheric-pressure flow reactor.	26
Figure 3.3.	Temperature profiles inside the reaction zone of the atmospheric-pressure flow reactor, for different nominal temperatures, as a function of distance. They have been measured with a K-type thermocouple for a total N ₂ flow rate of 1 L (STP)/min.....	27
Figure 3.4.	Scheme of the experimental set-up used to carry out the oxidation experiments at high pressure in a flow reactor (adapted from Alexandrino, 2018).	29
Figure 3.5.	Longitudinal temperature profiles inside the reaction zone of the high-pressure flow reactor, for different nominal temperatures and pressures, as a function of distance. They have been measured with a K-type thermocouple for a total N ₂ flow rate of 1 L (STP)/min. ...	30
Figure 3.6.	Scheme of the experimental set-up used to carry out the oxidation experiments at atmospheric pressure in a jet-stirred reactor.	32
Figure 3.7.	Schematic view of the JSR and CRDS coupling (from Bahrini et al., 2012).	32
Figure 4.1.	Development progress for a detailed gas-phase chemical kinetic mechanism for the description of the oxidation of the different C ₂ H ₂ -oxygenate mixtures studied in this work. Left, for the oxygenated compounds. Right, for the oxidation intermediates.	37
Figure 5.1.	Evaluation of the effect of NO presence on the high-pressure (20 bar) oxidation of MF, for the conditions denoted as set 1MF-3MF and 7MF-9MF, in Table 5.1.	52
Figure 5.2.	Comparison between experimental results and modeling calculations with the POLIMI mechanism and the final mechanism of the present work, for CH ₄ consumption, in the absence and presence of NO (500 ppm), for $\lambda = 1$	56
Figure 5.3.	Evaluation of the effect of the NO ₂ or NO presence on the jet-stirred oxidation of CH ₄ , for the conditions denoted as 1JSR-6JSR and 8JSR-10JSR, in Table 5.2.....	57
Figure 5.4.	Evolution with temperature for NO ₂ , NO and HCN concentrations during the jet-stirred oxidation of CH ₄ in the presence of NO _x , for the conditions denoted as 4JSR-6JSR and 8JSR-10JSR, in Table 5.2.....	58
Figure 5.5.	Evaluation of the effect of pressure and gas residence time on the high-pressure (20 or 40 bar) oxidation of DME, for the conditions denoted as sets (a) 1DME, 10DME and 4DME; (b) 2DME, 11DME and 5DME; (c) 3DME, 12DME and 6DME, in Table 5.3.....	63

Figure 5.6. Influence of the air excess ratio on the DME (left) and ethanol (right) concentration profiles, as a function of temperature, for the conditions denoted as 1DME-3DME, in Table 5.3 and 1EtOH, 4EtOH and 7EtOH, in Table 5.4. 64

Figure 5.7. Influence of the pressure change on the DME (left) and ethanol (right) concentration profiles, as a function of temperature, for the conditions denoted as 2DME, 5DME and 8DME, in Table 5.3, and 4EtOH-6EtOH, in Table 5.4. 65

Figure 5.8. Evaluation of the effect of NO presence on the high-pressure oxidation of DME (left) and ethanol (right), for the conditions denoted as sets 2DME, 5DME, 8DME, 14DME, 17DME and 20DME, in Table 5.3 and 4EtOH-6EtOH and 13EtOH-15EtOH, in Table 5.4. 68

Figure 5.9. Example of repeatability of the DMM oxidation experiments at atmospheric pressure (left). Influence of the air excess ratio on the DMM concentration profile, as a function of temperature, for the conditions denoted as sets 1DMM_{at}-5DMM_{at}, in Table 5.5 (right). 71

Figure 5.10. Influence of the air excess ratio on the concentration profile of the products from DMM oxidation, as a function of temperature, for the conditions denoted as sets 1DMM_{at}-5DMM_{at}, in Table 5.5. 73

Figure 5.11. Example of repeatability of the DMM oxidation experiments at high pressure for the conditions denoted as sets 4DMM_{HP} and 7DMM_{HP}, in Table 5.6. 76

Figure 5.12. Influence of pressure and air excess ratio on the DMM concentration profile, as a function of temperature, for the conditions denoted as sets 1DMM_{HP}-9DMM_{HP}, in Table 5.6. 77

Figure 5.13. Evolution of C₂H₂, C₂H₅OH, O₂, CO, CO₂, H₂ and CH₃CHO concentrations with temperature during the high-pressure (10 bar) oxidation of C₂H₂-C₂H₅OH mixtures, for the conditions denoted as set 2EtOHmix, in Table 5.7. 81

Figure 5.14. Influence of the amount of C₂H₅OH added to the mixture on the concentration profiles of C₂H₂ and C₂H₅OH during the C₂H₂-C₂H₅OH mixture oxidation as a function of temperature, for stoichiometric conditions ($\lambda = 1$) and 10 bar. The inlet conditions correspond to sets 1EtOHmix, 3EtOHmix, 9EtOHmix, 10EtOHmix and 12EtOHmix, in Table 5.7. 82

Figure 5.15. Influence of the air excess ratio (λ) on the concentration profiles of C₂H₂ and CO (upper part) and C₂H₅OH (lower part) during the C₂H₂-C₂H₅OH mixture oxidation as a function of temperature, for 10 bar and two different amounts of ethanol added to the mixture, 50 ppm (left side) and 200 ppm (right side). The inlet conditions correspond to sets 2EtOHmix-4EtOHmix and 11EtOHmix-14EtOHmix, in Table 5.7. 83

Figure 5.16. Influence of the pressure on the experimental and simulated concentration profile of C₂H₂ during the high-pressure oxidation of C₂H₂-C₂H₅OH mixtures as a function of temperature, for the conditions denoted as sets 3EtOHmix, 6EtOHmix-8EtOHmix, 12EtOHmix and 15EtOHmix, (left) and 3EtOHmix, 5EtOHmix and 7EtOHmix (right), in Table 5.7. Additional model calculations to evaluate the effect of pressure on the evolution of the C₂H₂ concentration. 84

Figure 5.17. Influence of the air excess ratio (λ) on the concentration profiles of C_2H_2 , DME and the sum of CO and CO_2 as a function of temperature, during the C_2H_2 -DME mixture oxidation for the conditions denoted as sets 2DMEmix_{at}, 6DMEmix_{at}, 11DMEmix_{at} and 15DMEmix_{at}, in Table 5.8..... 89

Figure 5.18. Influence of the DME inlet concentration on the C_2H_2 concentration profile as a function of temperature, for $\lambda = 0.7$ (upper part) and $\lambda = 20$ (lower part), for the conditions denoted as sets 5DMEmix_{at}, 6DMEmix_{at}, 9DMEmix_{at}, 14DMEmix_{at}, 15DMEmix_{at} and 18DMEmix_{at}, in Table 5.8. ⁽¹⁾ Alzueta et al. (2008)..... 93

Figure 5.19. Evaluation of the effect of NO presence on C_2H_2 and DME concentration profiles as a function of temperature, during the C_2H_2 -DME mixture oxidation at atmospheric pressure (a y b). Experimental results for NO concentration as a function of temperature in the presence and absence of DME (c). Conditions denoted as sets 3DMEmix_{at}, 4DMEmix_{at}, 7DMEmix_{at}, 8DMEmix_{at}, 12DMEmix_{at}, 13DMEmix_{at}, 16DMEmix_{at}, and 17DMEmix_{at}, in Table 5.8. ⁽¹⁾ Abián et al. (2010). 95

Figure 5.20. Influence of the air excess ratio (λ) on the concentration profiles of C_2H_2 , DME and CO+ CO_2 as a function of temperature, during the C_2H_2 -DME mixture oxidation, for 20 bar and two different amounts of DME added to the mixture, 100 ppm DME (left) and 400 ppm DME (right). The inlet conditions correspond to sets 1DMEmix_{HP}-6DMEmix_{HP}, in Table 5.9. 98

Figure 5.21. Influence of the pressure on the concentration profiles of C_2H_2 , DME and CO+ CO_2 as a function of temperature, during the C_2H_2 -DME mixture oxidation, for $\lambda = 1$ and 100 ppm of DME added to the mixture. The inlet conditions correspond to sets 3DMEmix_{HP}, 9DMEmix_{HP} and 15DMEmix_{HP}, in Table 5.9. 101

Figure 5.22. Influence of the air excess ratio (λ) on the concentration profiles of C_2H_2 , DMM and CO+ CO_2 as a function of temperature, during the C_2H_2 -DMM mixture oxidation, for 20 bar and two different amounts of DMM added to the mixture, 70 ppm DME (left) and 280 ppm DME (right). The inlet conditions correspond to sets 1DMMmix-6DMMmix, in Table 5.10. 103

Figure 5.23. Influence of the pressure on the concentration profiles of C_2H_2 , DMM and CO+ CO_2 as a function of temperature, during the C_2H_2 -DMM mixture oxidation, for $\lambda = 1$ and 70 ppm of DMM added to the mixture. The inlet conditions correspond to sets 3DMMmix, 9DMMmix and 15DMMmix, in Table 5.10. 106

Figure 5.24. Effect of the addition of the different additives studied on the high-pressure (40 bar) oxidation of C_2H_2 , for $\lambda = 0.7$ (left) and $\lambda = 20$ (right). 108

Figure 5.25. Evaluation through modeling calculations of the effect of pressure on the high-pressure C_2H_2 oxidation for $\lambda = 0.2$, in the absence and presence of DME..... 109

List of Tables

Table 2.1.	Main properties of diesel fuel and the oxygenated compounds under study: dimethyl ether (DME), ethanol and dimethoxymethane (DMM).....	11
Table 2.2.	Experimental works on ethanol conversion more recent than the works included in the review by Sarathy et al. (2014).	13
Table 2.3.	Experimental works on DME conversion not included in the review by Rodriguez et al. (2015).	16
Table 2.4.	Experimental works addressing the conversion of DMM.	19
Table 2.5.	Experimental works addressing the conversion of MF.	20
Table 2.6.	Experimental works addressing the conversion of CH ₄ and its interaction with NO _x	21
Table 4.1.	Reactions modified or included in DMM reaction subset. Kinetic parameters of the form $k = A \times T^n \times \exp(-E_a/RT)$. Units: A is in cm ³ mol ⁻¹ s ⁻¹ ; E _a is in cal/mol.	41
Table 4.2.	Reactions modified or added compared to Alzueta et al.'s DME oxidation work (Alzueta et al., 1999). Units: A is in cm ³ mol ⁻¹ s ⁻¹ ; E _a is in cal/mol.	43
Table 5.1.	Matrix of experimental conditions of the high-pressure study of MF oxidation ^a	51
Table 5.2.	Matrix of experimental conditions of the low-temperature oxidation of CH ₄ in a jet-stirred reactor ^a	55
Table 5.3.	Matrix of experimental conditions of the high-pressure study of DME oxidation ^a	60
Table 5.4.	Matrix of experimental conditions of the high-pressure study of ethanol oxidation ^a	61
Table 5.5.	Matrix of experimental conditions of the atmospheric-pressure study of DMM oxidation ^a	71
Table 5.6.	Matrix of experimental conditions of the high-pressure study of DMM oxidation ^a	75
Table 5.7.	Matrix of experimental conditions of the high-pressure study of C ₂ H ₂ -C ₂ H ₅ OH mixtures oxidation ^a	80
Table 5.8.	Matrix of experimental conditions of the atmospheric-pressure study of C ₂ H ₂ -DME mixtures oxidation ^a	88
Table 5.9.	Matrix of experimental conditions of the high-pressure study of C ₂ H ₂ -DME mixtures oxidation ^a	97
Table 5.10.	Matrix of experimental conditions of the high-pressure study of C ₂ H ₂ -DMM mixtures oxidation ^a	102

Chapter 1:

Introduction and objectives

“Chapter 1 briefly introduces the context of this PhD Thesis: the problems caused by the emission of atmospheric pollutants in transport sector and the search of possible solutions, such as fuel reformulation by the addition of oxygenated compounds. In addition, the main objectives of the present work are indicated”.

1. INTRODUCTION AND OBJECTIVES

1.1 INTRODUCTION

The interest in the protection of the environment is increasing nowadays. Global warming, climate change or atmospheric pollution are real concerns for the population. At the same time, in the last years, the world is facing a major energetic issue due to the growing demand for energy. The energy supply mainly depends on the combustion of fossil fuels, especially for transportation. One of the main disadvantages of the conventional ways to produce energy by combustion is related to the emission of different pollutants, with a variety of potential harmful effects on environment and/or human health. Important pollutants include: nitrogen oxides (NO, NO₂ and N₂O), sulfur oxides (SO₂ and SO₃), carbon monoxide (CO), carbon dioxide (CO₂), and particulate matter (such as soot).

Solutions to address such problems include, for example, the use of renewable energy sources or innovations in the transport sector (such as the electric vehicle). However, in the medium term, the dominant strategy is to increase the efficiency of the systems for energy production based on combustion, as well as to reduce the CO₂ net production and other harmful pollutants by using non-conventional fuels.

Modern internal combustion engines, such as Homogeneous Charge Compression Ignition (HCCI) engines, are more efficient and fuel-flexible compared to conventional engines. Low-temperature combustion devices have been designed to reduce the combustion temperature and prevent the formation of nitrogen oxides (NO_x), while assuring a good performance. Many modern combustion systems also include systems for the recirculation of the flue gases to favor mixing and reduce the temperature and, therefore, the formation of NO_x. Furthermore, to increase the efficiency, the current tendency in engines is to increase the injection pressure.

On the other hand, the use of alternative fuels can be another possible solution to minimize the formation of some pollutants. If biomass is used as feedstock to produce these alternative fuels, then, the net CO₂ released to the atmosphere is zero. Therefore, fuel reformulation by a total replacement of the conventional fuel (e.g. biodiesel) or by the addition of some additives, mainly oxygenated organic compounds, seems to be a promising solution to reduce the formation of some pollutants. However, the behavior of these alternative fuels under a combustion environment is less known compared to conventional

1. INTRODUCTION AND OBJECTIVES

fuels. Therefore, experiments and reliable chemical kinetic mechanisms are desired to design and optimize future combustion devices.

In this regard, our research group, the Thermo-Chemical Processes Group (GPT), has been working during the last years in the experimental and modeling kinetic study of the oxidation of different oxygenated compounds proposed as additives in automotive fuels. Most of the works have been carried out in flow reactors under atmospheric pressure conditions (Alzueta et al., 1999; Alzueta and Hernández, 2002; Alexandrino et al., 2014; Alexandrino et al., 2016; Alzueta et al., 2017). Also, Alexandrino et al. (2015) have reported a study of 2,5-dimethylfuran oxidation at high pressure, in a flow reactor.

In this context, the aim of this work is to contribute to the knowledge of the oxidation process of some oxygenated compounds proposed in literature as alternative fuels, thus following with the research line initiated in our group. Specifically, in this work, ethanol, dimethyl ether (DME) and dimethoxymethane (DMM) have been selected for their study. The first two are isomers, i.e. compounds with the same molecular formula (C_2H_6O) but different functional group, which may imply different properties and oxidation behavior. Both DME and DMM are included in the category of polyoxymethylene dimethyl ethers, POMDMEs, with the general formula of $CH_3O(CH_2O)_nCH_3$, with $n=0$ and 1 , respectively, which means a different number of carbon atoms. Previous literature studies indicate that methyl formate (MF) is an important intermediate in the oxidation of higher order oxygenated hydrocarbons and, due to the high CH_3 radical concentration expected from the conversion of these oxygenates, the formation of CH_4 is also expected. Therefore, the oxidation of methyl formate and methane has also been considered in the present work.

1.2 SCOPE AND OBJECTIVES

This work has been developed in the framework of the “*Combustion and reduction of pollutant emissions (NO_x , SO_x and soot)*” and “*Development of detailed kinetic modeling of combustion processes*” research lines of the Thermo-Chemical Processes Group (GPT) of the Aragón Institute of Engineering Research (I3A) of the University of Zaragoza.

The global goal of this thesis is to analyze the role as fuel additives of three different oxygenated compounds proposed in literature as alternative fuels, i.e. ethanol, dimethyl ether (DME) and dimethoxymethane (DMM), under conditions of interest for combustion processes.

In order to achieve this global goal, a number of specific objectives have been raised:

- To carry out a study of the oxidation of intermediates of interest generated during the oxidation of these oxygenated compounds. Hence, experiments of the oxidation of CH₄ and MF at atmospheric and high pressure, respectively, have been carried out. The impact of the NO or NO/NO₂ addition on the oxidation of MF and CH₄, respectively, has been also evaluated.
- To analyze the oxidation under high-pressure conditions of the isomers DME and ethanol, and afterwards, to compare the results obtained for both compounds. Therefore, experiments of the oxidation of these compounds have been performed in a high-pressure flow reactor. In addition to pressure, the temperature and stoichiometry have also been varied. Moreover, the impact of NO addition has also been evaluated and, during the oxidation of DME, the influence of gas residence time inside the reactor has also been considered.
- To characterize the oxidation of DMM under high-pressure conditions and compare with the other POMDME proposed, i.e. DME. But first, the atmospheric oxidation of DMM has been studied. Thus, experiments of the oxidation of DMM at atmospheric and high pressure have been carried out in different flow reactors.
- To analyze the role as fuel additives of DME, ethanol and DMM. To achieve this objective, oxidation experiments of their mixtures with acetylene have been carried out under high-pressure conditions, more representative of the real operating conditions. Acetylene has been selected as main fuel because it is considered as an important soot precursor (Frenklach, 2002) and it is an important intermediate in the combustion of hydrocarbons.
- To develop a chemical kinetic mechanism, based on individual literature mechanisms, updated and improved, to describe the oxidation of the different oxygenated compounds under the different experimental conditions tested. Several rate of production (ROP) analyses have been performed to investigate the most important pathways for the consumption of the reactants and the formation of the products. Moreover, the conducted sensitivity analyses have allowed the determination of the most relevant reactions in the mechanism; which are the indirect effects of kinetic parameter changes in modeling predictions.

Chapter 2:

Background

“Chapter 2 includes a review of the most important aspects related to this thesis, such as the properties and characteristics of the different oxygenated compounds analyzed, as well as previous studies on the conversion of such compounds found in literature”.

2. BACKGROUND

As stated in the introductory chapter (Chapter 1), fuel reformulation by the addition of oxygenated compounds could be a prospective solution for the minimization of atmospheric pollutants from transportation.

Therefore, in this chapter, the properties and characteristics of the oxygenated additives selected in this work for their study, and a literature review of different experimental and modeling previous works on the conversion of such compounds, are presented.

2.1 STATE OF THE ART

Air pollution is an important public health problem, and many of its root causes can be found in the sector of energy. According to the International Energy Agency (IEA), poor air quality is responsible for around 6.5 million deaths each year, becoming the world's fourth-largest threat to human health behind high blood pressure and smoking (IEA, 2016). The transport sector is an important contributor, given its high reliance on the combustion of petroleum-derived fuels. For example, road transport is by far the largest source of the sector's NO_x and primary particulate matter (PM_{2.5}) emissions (58% and 73% of the total of emissions of transport sector, respectively), while navigation accounts for the largest share of sulfur dioxide (SO₂) emissions (IEA, 2017).

Although in the last years the number of electric vehicles has increased considerably, internal combustion engines (commonly known as Diesel or Otto engines) are still the most common and demanded in the market. In addition to the passenger cars, the automotive industry also includes the transport sector: vans, trucks, buses; apart from agricultural, earthmoving or mining work machinery. This machinery require high engine power, and such a performance requirement is very difficult to supply with any system that does not relies on hydrocarbons.

In diesel engines, also known as compression-ignition (CI) engines, first the air is compressed by the movement of the piston and then the fuel is injected to the cylinder. Due to the high pressure and temperature of the gases at the moment of the injection, the mixture ignites without any external help, flame or spark. The cetane number is used to characterize diesel fuels and it is related to the ignition delay time in the way that, the higher cetane number, the faster the fuel ignites. If the fuel ignites faster, it will have more time to complete

2. BACKGROUND

the oxidation, and consequently, the emission of unburned hydrocarbons will decrease, and the process efficiency will improve. For example, conventional diesel fuels usually have a cetane number of 40-55 (Yanfeng et al., 2007).

On the other hand, the octane number is used for fuels of spark-ignited (SI) engines. In this type of engines, fuel and air are first premixed and later compressed by the movement of the piston. Afterwards, a spark ignites the mixture, so a flame is formed and progresses inside the cylinder. Unlike to CI engines, autoignition is not desired in the case of SI engines. The octane number shows the fuel resistance to autoignition. In SI engines, fuels with high octane numbers are preferred. A common fuel for SI engines, E85 gasoline, consists of a 15% of ethanol mixed with gasoline, and its octane number is around 102-105.

Despite their high efficiency, low-operating costs, high durability and reliability, diesel engines present the main drawback of the relatively high emissions of nitrogen oxides (NO_x) and particulate matter (PM, such as soot). The fuel and the air first react in a fuel-rich mixture, which may lead to the formation of soot, then this mixture burns out in a high-temperature diffusion flame leading to the formation of NO_x. In general, diesel engines work under fuel-lean conditions, so the CO and hydrocarbon (HC) emissions are less important than in gasoline engines. However, due to the oxygen excess and the high temperatures reached because of the high compression ratio, the formation of NO_x is favored.

While most vehicles use either SI or CI engines, there are some emerging technologies to improve engines, e.g. homogeneous charge compression ignition (HCCI) engines. HCCI is characterized by the fact that the fuel and the air are premixed before combustion and then the mixture enters the cylinder (similar to SI engines), but the oxidation only starts with the autoignition of the mixture as a result of the temperature increase in the compression stroke. The fuel-rich zone found in CI engines is avoided in HCCI engines because the mixture is homogeneously premixed, so the formation of soot and PM is limited. Moreover, if the temperature is lowered (low-temperature combustion, LTC), for example, by a high dilution of the mixture if exhaust gas recirculation (EGR) is used, the thermal formation of NO_x could be also inhibited, while maintaining the thermal efficiency of the engines close to that of conventional CI engines (Yao et al., 2009a).

Figure 2.1 shows the typical equivalence ratios (ϕ , defined as the stoichiometric oxygen divided by the real oxygen fed to the system) and temperature ranges for the formation of soot and NO_x. The operating regions for the different combustion approaches for engines, described above, i.e. conventional diesel (compression-ignition, CI), spark ignition (SI),

homogeneous charge compression ignition (HCCI) and low-temperature combustion (LTC) are also shown.

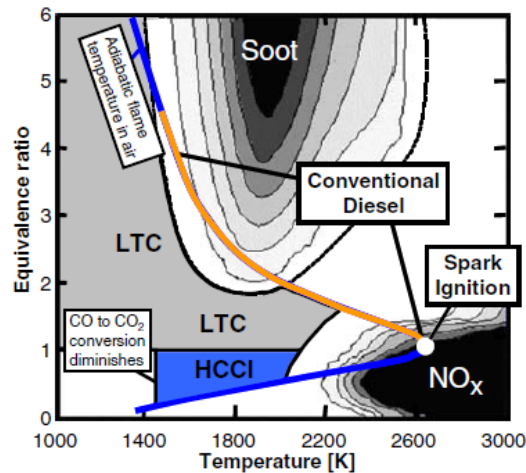


Figure 2.1. Diagram showing the equivalence ratio (ϕ) and temperature ranges for soot and NO_x formation and the operating regions for CI, SI, HCCI and LTC engines (Dec, 2009).

Combustion is a complex process during which chemical kinetics, mass transfer and fluid dynamics play an important role. For example, one of the major challenges in the design and operation of HCCI engines is controlling the moment of autoignition, which is governed by chemical kinetics. Therefore, reliable detailed chemical kinetic models are required for the design of such engines and modern combustion devices.

With advances in the development of engine combustion systems, such as HCCI or related strategies that can be adapted to a large variety of fuels, fuel reformulation of the conventional fuels by the use of alternative ones (such as biofuels) or by the use of additives seems to be possible (Yao et al., 2009a). A shift from hydrocarbon fossil fuels to biofuels is an interesting way to reduce CO_2 emissions, still using internal combustion engines.

Figure 2.2 reports an overview of the main routes to produce different biofuels: extraction of vegetable oils, fermentation of sugars to alcohol, gasification followed by chemical synthesis, and direct liquefaction. In this way, many different fuels can be produced such as hydrogen, methanol, dimethyl ether, ethanol or biodiesel, all of them with very different properties.

2. BACKGROUND

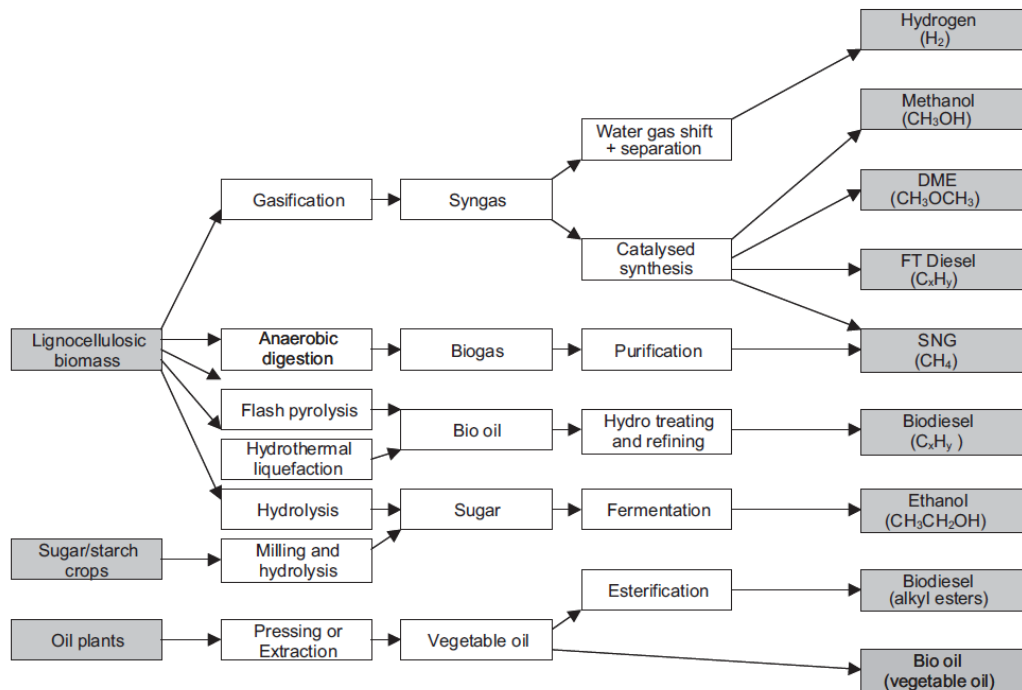


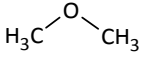
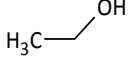
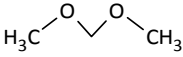
Figure 2.2. Overview of different way to obtain biofuels from biomass (Hamelinck and Faaij, 2006). FT: Fischer Tropsch; SNG: Synthetic Natural Gas.

It is also generally recognized today that one more significant benefit of adding biofuels to the fuel blend is the reduction in the emissions of particulate matter (PM) from diesel engines (Agarwal, 2007). Some of these biofuels, such as esters and DME, due to their chemical structure and composition, have an inherent tendency to reduce soot formation. As the oxygen content in the fuel molecule increases and/or the number of C-C bond decreases, the tendency to form soot precursors decreases (Arcoumanis et al., 2008). This is because the oxygen bonded to carbon atoms tends to form CO or CO₂ instead of participating in soot formation reactions (Szybist et al., 2007). Nowadays, ethanol, obtained from carbohydrates fermentation, and biodiesel, from transesterification of plant oils, are the most common biofuels in transportation. Whereas the combustion properties of ethanol are compatible with SI engines, the fatty acid methyl esters (FAMES), which mainly compose biodiesel, are suitable for CI (Leitner et al., 2017).

Oxygenates, organic compounds that contain one or more oxygen atoms in their molecular structure, have been considered as fuel additives since the early 1970's as a solution to environmental problems, to optimize energy consumption or to increase the antiknock power of gasoline, for example. As mentioned before, the oxygen content in the fuel molecule contributes to reduce soot emissions. But, besides the oxygen content, a good mixing of the additive with the fuel is also required for a correct engine performance.

Among all the possible oxygenated compounds that have been proposed in literature as possible fuel additives, in the present thesis: ethanol, dimethyl ether (DME), and dimethoxymethane (DMM), have been selected for the study of their oxidation under conditions relevant for engine applications. Ethanol and DME are isomers, that is, both have the same molecular formula (C_2H_6O) but a different chemical structure with a different functional group, which may imply different properties and, consequently, a different behavior during their oxidation. On the other hand, DME and DMM are polyoxymethylene dimethyl ethers, POMDMEs, with the general formula of $CH_3O(CH_2O)_nCH_3$, with $n=0$ and 1 respectively, which means different number of carbons while maintaining the functional group. Properties such as viscosity or boiling temperature are strongly influenced by the exact combination of the elements within the molecule. Whereas the functional group has a significant impact on the vapor pressure and viscosity, the carbon number determines the boiling temperature. Finally, the molecular structure influences the ignition and combustion kinetics and, hence, key engine parameters such as knocking or cold-start behavior (Khalife et al., 2017). Table 2.1 compares the main properties of these oxygenated compounds and conventional diesel fuel.

Table 2.1. Main properties of diesel fuel and the oxygenated compounds under study: dimethyl ether (DME), ethanol and dimethoxymethane (DMM).

Parameter	Diesel	DME	Ethanol	DMM
Chemical formula	C_x-H_y $C_{10}-C_{25}$	C_2H_6O	C_2H_6O	$C_3H_8O_2$
Chemical structure	-			
		CH_3OCH_3	CH_3CH_2OH	$CH_3OCH_2OCH_3$
Functional group	-	Ether	Alcohol	Ether
Carbon content (wt%)	86 ^a	52.2 ^b	52.20 ^a	46.20 ^a
Hydrogen content (wt%)	14 ^a	13 ^b	13 ^a	11.70 ^a
Oxygen content (wt%)	0 ^a	34.8 ^b	34.8 ^a	42.10 ^a
Cetane number	40-55 ^c	55-60 ^d	8 ^a	30 ^a
Auto-ignition (K)	588 ^b	508 ^b	639 ^e	510 ^f
Boiling point (K) at 1 atm	453-633 ^b	-248 ^b	351 ^a	316 ^a
Density (kg/m ³) at 293 K	830 ^a	667 ^b	794 ^a	0.865 ^f
Viscosity (mm ² /s) at 293 K	3.763 ^a	< 0.1 ^b	1.06 ^a	0.34 ^a
Lower heating value (MJ/kg)	42.5 ^b	27.6 ^d	27 ^a	22.4 ^f

^aWang et al. (2009), ^bArcoumanis et al. (2008), ^cYanfeng et al. (2007), ^dCrookes and Bob-Manuel (2007), ^eHansen et al. (2005), ^fZhu et al. (2011).

2. BACKGROUND

In the following sections, the properties, the methods commonly used for their production, and a review of previous literature studies on the compounds object of study, in the present thesis, will be briefly discussed.

2.2 ETHANOL

Ethanol (C₂H₅OH) had a long career as a transportation fuel in the early 20th century, until it was replaced by gasoline and diesel due to the growing supply of cheap petroleum from new oil field discoveries. Indeed, Henry Ford designed the Model T with the expectation that ethanol, obtained from renewable biomaterials, would be a major automobile fuel (Agarwal, 2007).

Nowadays, ethanol is one of the most common and abundant biofuels, especially in Brazil, Canada, USA and India (Balat, 2011; Awad et al., 2018). Ethanol can be produced through fermentation of sugars from renewable sources; typically, plants such as wheat, sugar beet, corn, straw and wood (Balat, 2011). It can also be produced at industrial scale by the catalyzed hydration of ethene (reaction R2.1).



Nevertheless, studies showed that not all methods of production of ethanol or other biofuels are environmentally acceptable. For example, Fargione et al. (2008) indicated that the devastation of rainforest or savannas to produce food crop-based biofuels in countries such as Brazil, Asia and USA, releases 17 to 420 times more CO₂ than the annual greenhouse gas reductions that would be achieved by replacing fossil fuels with these biofuels.

Several works in literature have analyzed the properties of diesel-ethanol blends, such as viscosity and lubricity, and the performance and emissions of the engine fueled with this type of blends. Ethanol has a good solubility in conventional diesel fuel and a high oxygen content. However, it presents a low cetane number (as low as merely eight) and, moreover, the addition of ethanol to diesel lowers fuel viscosity and lubricity (Hansen et al., 2005; Wang et al., 2009). Emission tests confirmed the ethanol effect of reducing particulate matter (Chen et al., 2007; Zhu et al., 2010; Zhang et al., 2011). However, the effect on CO, HC and NO_x emissions is less clear. Some authors (Kass et al., 2001) observed that the addition of ethanol produced no noticeable effect on NO_x emission, but small increases in CO and HC emissions. This is due to the reduction in the temperature inside the motor caused by the lowest calorific

value and the highest heat of vaporization of the fuel mixture. On the other hand, Huang et al. (2009a) found that CO and NO_x emissions were different depending on the engine speeds, loads and blends analyzed (10-30% by volume of ethanol). For example, CO emissions were reduced when the engine ran at and above its half load and were increased at low load; HC emissions from the engine fueled by the blends were higher than those obtained from the engine fueled by diesel fuel, except for the top loads and high speeds; and NO_x emissions were completely different in each case studied. Moreover, a widespread use of ethanol fuel may lead to an increased emission of aldehydes such as acetaldehyde (Yao et al., 2009b), which can cause serious health risks.

Ethanol combustion has been widely studied and modeled in shock-tube, flame, and flow reactor experiments over a wide range of temperature and pressure conditions. Sarathy et al. (2014) summarized the fundamental experimental studies of ethanol combustion in a review of the combustion chemistry of alcohols. Table 2.2 includes some of the most relevant and recent (from 2014) studies on ethanol combustion.

Table 2.2. Experimental works on ethanol conversion more recent than the works included in the review by Sarathy et al. (2014).

Reference	Type of experiment	Experimental conditions
Aghsaee et al. (2015)	Shock tube	T=1047-2518 K; P=1.06 and 2.07 bar; $\phi = \infty$ and 1 in Ne
	Spherical bomb	T=318-473 K; P=1, 2 and 5 bar; $\phi =0.7-1.5$
Kiecherer et al. (2015)	Shock tube	T=1300-1510 K; P=1.1 bar; $\phi = \infty$
Barraza-Botet et al. (2016)	Rapid compression machine	T=880-1150 K; P=3-10 bar; $\phi =1$ in Ar/N ₂
Li et al. (2017)	Constant volume bomb	T= 200°C; P=80-500 psi; $\phi =0.4-2$ in air
Mitu and Brandes (2017)	Closed vessel	T=298-373 K; P=10.1-101 kPa; $\phi =0.52$ and 3.57 in air
Hashemi et al. (2018)	Plug-flow reactor	T=600-900 K; P=50 bar; $\phi =0.1, 1, 43$ and ∞ in N ₂
Katoch et al. (2018)	Flame	T=350-620 K; P=1 atm; $\phi =0.7-1.3$ in air

Despite the huge number of works addressing ethanol combustion, detailed data for ethanol oxidation at high pressure, in plug flow reactor, are scarce. Therefore, in the present work, the oxidation of ethanol under high-pressure conditions in a flow reactor has been investigated. Additionally, the influence of the addition of NO to the reactant mixture has been

2. BACKGROUND

evaluated. Recently, a study of ethanol pyrolysis and oxidation in a flow reactor at high pressure (50 bar) has been performed by Hashemi et al. (2018).

Additionally, several detailed chemical kinetic mechanisms can be found in the literature for ethanol and/or multicomponent fuel mixtures including ethanol (Saxena and Williams, 2007; Leplat et al., 2011; Lee et al., 2012; Metcalfe et al., 2013; Burke et al., 2014, 2015a; Olm et al., 2016). These mechanisms are primarily based on revisions to the mechanism from Marinov (1999).

Beyond these kinetics-related investigations, there is also a substantial number of investigations focusing on the influence of ethanol addition to hydrocarbon fuels (such as acetylene, ethylene, n-heptane, propene, iso-octane, or benzene, among others) to investigate its effect on combustion performance and pollutant emissions. Those studies have been carried out in different experimental devices, such as flames (Inal and Senkan, 2005, Kohse-Höinghaus et al., 2007; Bennet et al., 2009; Bierkandt et al., 2015), jet-stirred reactors (Dagaut and Togbé, 2012; Rezgui and Guemini, 2014) and plug-flow reactors (Abián et al., 2008). Results indicate that the ethanol addition enhances the formation of some oxygenated species, such as acetaldehyde, rather than the formation of benzene, ethylene, aromatics and polycyclic aromatic hydrocarbons (PAH), all of them important soot precursors. Moreover, the effectiveness of ethanol to reduce the formation of soot has been previously demonstrated by Esarte et al. (2011) while studying the pyrolysis of acetylene and ethanol mixtures at atmospheric pressure. The results showed that adding very small concentrations of ethanol leads to a diminution on the production of soot from the acetylene pyrolysis. Moreover, Viteri et al. (2019) performed a study of the formation of soot and PAH during the pyrolysis of ethanol and their low formation, and the effluent low toxicity obtained suggest a good performance of the use of ethanol as a fuel additive.

However, despite its relevance for its applicability to internal combustion engines and the current tendency, in designing combustion systems, to work at high pressure to increase efficiency, to our knowledge, no experimental or modeling studies have been carried out evaluating the impact of ethanol addition to hydrocarbons at pressures higher than 10 atm.

2.3 DIMETHYL ETHER

Dimethyl ether (CH_3OCH_3 , DME), is an isomer of ethanol but with different structure and thermodynamic and ignition properties. DME, the simplest ether, is a volatile substance

which forms a liquid phase when pressurized above 50 atm; therefore, it is commonly handled and stored as liquid. It has handling characteristics similar to those of liquified petroleum gas (LPG). It has a high oxygen content, high cetane number, low boiling point and no carbon-carbon bond. It can be large-scale produced from a wide range of feedstocks such as natural gas, crude oil, residual oil, coal and waste products (Arcoumanis et al., 2008; Kohse-Höinghaus et al., 2010; Azizi et al., 2014).

DME can be produced in two distinct ways: the first one, called the indirect route, uses the methanol obtained from syngas to promote its dehydration (reaction R2.2); the second one, which is more efficient, is known as the direct route in which DME is produced in a single stage using bi-functional catalysts. Both ways are schematically represented in Figure 2.3.

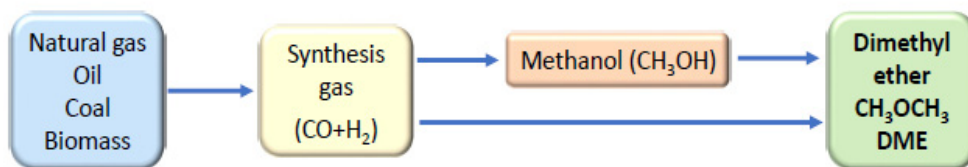


Figure 2.3. Diagram for dimethyl ether production (adapted from Azizi et al., 2014).

Besides its applications in diesel and in HCCI engines (Huang et al., 2009b), DME can also be used in gas turbines for power generation and for household purposes (Cocco et al., 2006). However, DME has some less favorable characteristics, not only because of its low calorific value, which decreases the performance of the motor; but because of its low viscosity, which leads to leakage problems and it could even cause lubricity problems. For this reason, the use of fuels, which contain certain amounts of DME, involves changes in the combustion system. A DME fuel storage tank must be twice the size of a conventional diesel fuel tank due to the lower energy density of DME compared to diesel fuel (Semelsberger et al., 2006).

DME is considered as a potential ultraclean replacement fuel, for being used in blend with diesel fuel in CI engines, with a potential reduction of soot formation (Arcoumanis et al., 2008). The use of DME has been experimentally studied in diesel engines (Ying et al., 2008; Junjun et al., 2009), showing its advantage in terms of emissions and engine efficiency. Particulate matter (PM) emissions were found to be reduced, as well as NO_x and SO_x emissions, while there was a slight increase in CO and HC emissions. DME conversion has also been subject of numerous studies carried out in different types of laboratory reactors and conditions. As an example, the review performed by Rodriguez et al. (2015) in their study of

2. BACKGROUND

the low-temperature oxidation of DME, includes 34 different DME oxidation experimental studies up to 2015, performed in jet-stirred and flow reactors, shock tubes, rapid compression machines, burners and spherical bombs. More recent experimental works on DME oxidation, that were not included in the work of Rodriguez et al. (2015), are presented in Table 2.3.

Table 2.3. Experimental works on DME conversion not included in the review by Rodriguez et al. (2015).

Reference	Type of experiment	Experimental conditions
Schönborn et al. (2014)	Plug-flow reactor	T=739-902 K; P=0.2-0.4 MPa; ϕ =0.225-0.675 in N ₂
Pan et al. (2014)	Shock tube	T=900-1700 K; P=1.2-10 atm; ϕ =0.5-2 in H ₂ /Ar
Pan et al. (2015)	Shock tube	T=1000-1600 K; P=1.2-20 atm; ϕ =0.5-2 in Ar
Moshammer et al. (2015)	Jet-stirred reactor	T=450-1000 K; P=933 mbar; ϕ =0.35; t_r =4 s
Wu et al. (2016)	Flame	T=966-1149 K; P=1 atm; ϕ =0.7
Zhao et al. (2016)	Plug-flow reactor	T=400-750 K; P=1 atm; O ₂ =3.65-3.87%; O ₃ =0-0.146%; t_r =0.45-0.24 s
Hajilou et al. (2017)	Flame	P=7.3 kPa; ϕ =0.4-1.4
Al-Noman et al. (2018)	Flame	P=1 atm; x_F =0.044, 0.055, 0.235

Several studies (e.g. Dagaut et al., 1998; Curran et al., 2000; Zhao et al., 2008; Rodriguez et al., 2015; Zhao et al., 2016) have reported a complicated behavior of DME during its oxidation at intermediate temperatures, the negative temperature coefficient (NTC) zone, where DME reactivity decreases with an increase in temperature. However, despite the fact that engine efficiency is increased by working under high-pressure conditions, DME oxidation has rarely been investigated at high pressure and intermediate temperatures.

On the other hand, numerous previous studies have analyzed the interaction between NO and different fuels, such as hydrocarbons or alcohols, showing that, depending on the combustion conditions, the impact of NO can be completely different. For example, at high temperatures and fuel-rich conditions, NO may be reduced to N₂ and HCN by reacting with hydrocarbon radicals in reburn-type reactions (e.g. Glarborg et al., 1998); whereas at low to intermediate temperatures, the presence of NO may promote the oxidation of the fuel (e.g. Bendtsen et al., 2000), but also the oxidation of NO to NO₂ may be promoted by the fuel in a mutually sensitized oxidation process (e.g. Dagaut and Nicolle, 2005). However, the presence of NO can also have inhibiting effects on fuel conversion at low temperatures, as reported by Moréac et al. (2006) in a n-heptane jet-stirred oxidation work at 10 atm.

Despite the large number of studies concerning the interaction of fuel components with NO or the DME oxidation, to our knowledge, only a previous work of our group focuses in the direct interaction of DME and NO in an atmospheric-pressure flow reactor (Alzueta et al., 1999). Therefore, the present work aims to analyze the DME oxidation at high pressure and the influence of the presence of NO on the process, which, to our knowledge, has not been considered earlier.

Over the years, several mechanisms have been developed to predict DME conversion under a wide range of experimental conditions and devices. Most of these models can be traced back to the one by Curran et al. (1998), which was developed to reproduce the oxidation of DME in a jet-stirred reactor (JSR) ($P=1$ and 10 atm, $T=800-1300$ K, $\phi =0.2-2.5$) and in a shock tube ($P=13$ and 40 bar, $T=650-1300$ K, $\phi =1$). This model was able to predict the ignition delay times and concentration profiles of the products in DME oxidation. Some years later, Curran et al. (2000) performed further experiments in a variable-pressure flow reactor ($P=12-18$ atm, $T=550-850$ K, $\phi =0.7-4.2$) and improved the model performance over a broad temperature range. More recently, different models that include updated rate coefficients for elementary reactions and thermodynamic data have been proposed (Zhao et al., 2008; Wang et al., 2015; Burke et al., 2015b; Rodriguez et al., 2015).

Since the attractiveness of DME lies in the possibility of being used as an additive in fuel mixtures, there are several research works on the oxidation of mixtures of different hydrocarbons and DME. Burke et al. (2015b) reported a promoting effect of DME on methane oxidation. The ignition promoting effect of DME is of importance for controlling ignition timing in internal combustion engines. The autoignition of propane/DME mixtures has also been recently studied in a rapid compression machine (Dames et al., 2016). Other studies have analyzed the effect of DME addition on the formation of aromatic species, which are known to be key intermediates in soot formation. These studies usually take as the base fuel: ethane, ethylene or acetylene, since they are small linear hydrocarbons considered as soot precursors, in the most accepted mechanism for describing soot formation (Frenklach, 2002). For example, Song et al. (2003) observed a decrease in aromatic species relative to pure ethane oxidation with the addition of DME. Moreover, the effect of the molecular structure has also been previously studied due to the isomeric character of ethanol and DME. For example, Esarte et al. (2010) studied the effect of ethanol and DME on the formation of soot when mixed with acetylene at atmospheric pressure. The results obtained showed that the presence of either ethanol or DME in the reactant mixture leads to a diminution in the formation of soot, and less

soot is produced in the case of the DME addition. In the present work, the oxidation of acetylene-DME mixtures is also addressed under atmospheric and high-pressure conditions.

2.4 DIMETHOXYMETHANE

Dimethoxymethane ($\text{CH}_3\text{OCH}_2\text{OCH}_3$, DMM) or methylal, is a diether considered to be a potential diesel fuel additive. In comparison to DME, the simplest ether, DMM has a higher quantity of oxygen, lower vapor pressure and better solubility with diesel fuel.

Nowadays, the most commonly used process for DMM production at the industrial scale is the “two-step selective synthesis”, characterized by a first oxidative reaction of methanol to formaldehyde followed by a second reaction of condensation. Synthesizing DMM in a single step directly from methanol is desirable but implies the use of highly selective catalysts for the oxidation of methanol to DMM. Developing these selective catalysts has become a widespread research subject in the recent years (Liu and Iglesia, 2003; Zhang et al., 2006; Thavornprasert et al., 2014). Also, DMM can be synthesized from the so-called bio-methanol obtained via biomass-derived syngas conversion.

DMM has shown to be a good fuel additive. In fact, diesel-DMM blends generally increase engine performance and decrease exhaust emissions. Several previous studies have analyzed the effect of adding DMM to base diesel fuel on emissions of CI engines. Huang et al. (2006) investigated the combustion characteristics and the emissions of a CI engine fueled with different blends of diesel and DMM. They found that a remarkable reduction in the exhaust CO and smoke (PM) can be achieved when operating with diesel-DMM blends, and a simultaneous reduction in both NO_x and smoke can be obtained when operating with large amounts of DMM. Zhu et al. (2009) also analyzed the effects of DMM addition on emissions and performance of a diesel engine. Their results showed that smoke and CO emissions decrease, NO_x remains almost unchanged, while HC increase. Some years later, Zhu et al. (2013) reported that the use of diesel-DMM blends could improve thermal efficiency and reduce smoke emissions with a slight increase in NO_x emissions. Moreover, engine performance and emissions can be optimized by adjusting the fuel injection timing.

Unlike DME and ethanol, the oxidation of DMM has not been deeply studied. The first experimental studies on DMM oxidation are dated in 1974 and reported by Molera et al. (1974). Later, the same authors tried to elucidate some features of DMM oxidation mechanism (Molera et al., 1977). Table 2.4 shows recent experimental studies on the oxidation and

pyrolysis of DMM. These works also include kinetic efforts to elucidate the facts observed experimentally. Recently, Kopp et al. (2018) have studied the kinetics and thermochemistry of dimethoxymethane using high-level ab initio and statistical mechanics methods.

Table 2.4. Experimental works addressing the conversion of DMM.

Reference	Type of experiment	Experimental conditions
Daly et al. (2001)	Jet-stirred reactor	T=800-1200 K; P=5.07 bar; ϕ =0.44, 0.89 and 1.78 in N ₂
Sinha and Thomson (2004)	Flame	P=1 atm; 8% DMM in air
Dias et al. (2010)	Flame	P=50 mbar; ϕ =0.24 and 1.72 in Ar
Zhang et al. (2014)	Shock tube	T=1103-1454 K; P=2, 4 and 10 atm; ϕ =0.5, 1 and 2 in Ar
Sun et al. (2018)	Jet-stirred reactor	^a LP: T=460-820 K; P=750 Torr; ϕ =0.5 in Ar ^b HP: T=500-1200 K; P=10 atm; ϕ =0.2, 0.5 and 1.5 in Ar
Vermeire et al. (2018)	Jet-stirred reactor	T=500-1100 K; P=1.07 bar; ϕ =0.25, 1, 2 and ∞ in He

^aLP: low-pressure experiments; ^bHP: high-pressure experiments.

As it can be seen in Table 2.4, previous studies on DMM oxidation are scarce and have been performed mainly in flames, jet-stirred reactors and shock tubes. Therefore, in the present work, DMM oxidation studies in flow reactors at atmospheric and high-pressure conditions have been carried out to fill the gap due to the lack of literature experiments under these conditions.

As already seen for DME and ethanol, the oxidation of mixtures of hydrocarbons and DMM has also been previously tested in the literature, mainly, in flames. For example, the effect of DMM addition on species concentration profiles has been tested in flames with ethylene (Renard et al., 2002), propane (Sinha and Thomson, 2004) or n-heptane (Chen et al., 2012). In the present work, the influence of DMM addition on the acetylene high-pressure oxidation will be addressed.

2.5 INTERMEDIATES OF OXIDATION: METHYL FORMATE AND METHANE

Some of the previous mentioned works indicate that methyl formate (CH₃OCHO, MF) is an important intermediate during the oxidation of higher order oxygenated hydrocarbons. For example, Sinha and Thomson (2004) measured significant quantities of MF in their study of

2. BACKGROUND

DMM combustion in diffusion flames; and Herrmann et al. (2014), in their experimental and numerical low-temperature oxidation study of ethanol and dimethyl ether, also identified MF as an oxygenated intermediate during DME oxidation. Furthermore, MF is the simplest methyl ester, belonging to a class of compounds that constitute biodiesel, which is a promising renewable fuel produced from a variety of vegetable oils, primarily constituted by methyl and ethyl esters. For these reasons, the study of the MF oxidation is addressed in the present work.

The combustion properties of MF have been investigated experimentally in relatively few studies compared to other oxygenated compounds such as DME or ethanol. Table 2.5 contains the most recent experimental works on the oxidation and pyrolysis of MF carried out in different experimental devices. MF combustion properties have also been analyzed from a modeling point of view. The first model including the combustion of MF was proposed by Fisher et al. (2000). Some years later, Westbrook et al. (2009) carried out a further development in the modeling of ester oxidation and proposed a new chemical kinetic mechanism for four different esters, which was constructed by relating reactivity in molecules of similar molecular structure to the esters investigated. Dooley et al. (2010) developed a mechanism for MF conversion with several rate constants estimated by investigating the hydrogen bond and reactivity of similar compounds. This reaction subset has been used in later MF oxidation studies, e.g. Alzueta et al. (2013) and Diévar et al. (2013).

Table 2.5. Experimental works addressing the conversion of MF.

Reference	Type of experiment	Experimental conditions
Akih-Kumgeh and Bergthorson (2010)	Shock tube	T=1053-1561 K; P=2, 4 and 10 atm; $\phi = 0.5, 1$ and 2 in Ar/ N ₂
	Plug-flow reactor	T=900 and 975 K; P=3 atm; $\phi = 0.5, 1, 1.5$ and ∞ in N ₂
Dooley et al. (2010)	Shock tube	T=1275-1935 K; P=2.7, 5.4 and 9.2 atm; $\phi = 1, 2$ and 0.5 in Ar
	Cylindrical bomb	P= 1 atm; $\phi = 0.8-1.6$ in air
Dooley et al. (2011)	Flame	P=22-30 Torr; $\phi = 1-1.8$ in Ar
Alzueta et al. (2013)	Plug-flow reactor	T=300-1100 K; P=1 atm; $\phi = \infty, 1.4, 1$ and 0.03 in N ₂
Ren et al. (2013a)	Shock tube	T=1266-1707 K; P=1.1-2.5 atm; MF=1 and 0.2% in Ar
Ren et al. (2013b)	Shock tube	T=1202-1607 K; P=1.36-1.72 atm; MF=0.1-3% in Ar
Wang et al. (2014)	Flame	T=298 and 333 K; P=1 atm; $\phi = 0.7-1.5$ in air
Christensen et al. (2015)	Flame	T=298-348 K; P=1 atm; $\phi = 0.7-1.6$ in air
Lee et al. (2018)	Flame	T=333 K; P=0.1-1 atm; $\phi = 0.9-1.5$ in air

However, high-pressure conditions (above 10 atm) have not been considered previously in works on the oxidation of methyl formate. Therefore, the present work aims to extend the experimental database on MF oxidation, in a flow reactor, to higher pressures, since these results will be helpful for future engine developments. Moreover, because of the fact that NO can be found in the combustion chamber of an engine, the interaction between MF and NO is also addressed in the present work.

On the other hand, methane (CH₄) has been object of numerous previous studies because it is the main component of natural gas. The consumption of natural gas is expected to increase from 113 trillion cubic feet in 2010 to 185 trillion cubic feet in 2040, becoming the world's fastest-growing fossil fuel and partially replace coal and liquid fuels in power generation for electricity and industrial processes (US EIA, 2013). However, the limited fossil fuel resources and their harmful effects on climate have increased the interest for environmentally friendly fuels. Biomass seems to be a promising fuel source due to its sustainability, secure supply and low threat to the environment. By the anaerobic digestion of biomass, it is possible to obtain a "biogas", which mainly consists of CH₄ and CO₂ with trace amounts of nitrogen and sulfur compounds, and with a high potential as renewable gas-phase fuel. Therefore, several literature studies have analyzed the conversion of methane and its interaction with NO_x (Table 2.6).

Table 2.6. Experimental works addressing the conversion of CH₄ and its interaction with NO_x.

Reference	Type of experiment	Experimental conditions
Dagaut et al. (1991)	Jet-stirred reactor	T=900-1300 K; P=1-10 atm; ϕ =0.1-1 in N ₂
Bromly et al. (1996)	Plug-flow reactor	T=723-923 K; P=1 atm; 0-14% O ₂ ; NO=0-200 ppm in N ₂
Alzueta et al. (1997)	Plug-flow reactor	T=900-1450 K; P=1 atm; 2300-6100 ppm O ₂ ; NO=100-1200 ppm in N ₂ ; t_r =80-270 ms
Hidaka et al. (1999)	Shock tube	T=1350-2400 K; P=1.6-4.4 atm; 0-4% O ₂ in Ar
Petersen et al. (1999)	Shock tube	T=1040-1500 K; P=40-260 atm; ϕ =0.4, 3 and 6 in Ar, N ₂ or He
Bendtsen et al. (2000)	Plug-flow reactor	T=750-1250 K; P=1 atm; 3.69-2.67% O ₂ ; NO _x =0, 200 ppm in N ₂
Huang et al. (2004)	Shock tube	T=1000-1350 K; P=16-40 atm; ϕ =0.7-1.3 in N ₂
Dagaut and Nicolle (2005)	Jet-stirred reactor	T=800-1150 K; P=1-10 atm; ϕ =0.1-1; NO=0, 200 ppm in N ₂
Rasmussen et al. (2008a)	Plug-flow reactor	T=600-900 K; P=20, 50 and 100 bar; $\phi \approx$ 100, 1 and 0.04 in N ₂ ; NO _x =200 ppm

2. BACKGROUND

Table 2.6. (Continued).

Chan et al. (2011)	Plug-flow reactor	T=823-948 K; P=1 atm; 2.5% methane-in-air mixture; NO _x =0-100 ppm T=873-1023 K; P=1 atm; 0.05% methane-in-air mixture; NO _x =0-100 ppm
Goswami et al. (2013)	Flame	P=1-5 atm; ϕ =0.8-1.4 in air
Dmitriev et al. (2015)	Flame	P=1, 3 and 5 atm; ϕ =0.8-1.2 in Ar
Zhang et al. (2015)	Plug-flow reactor	T=873-1223 K; P=0.2 MPa; X _{O₂} /X _{CH₄} =0.5-9, 0.03-0.6% NO ₂ in Ar
El Merhubi et al. (2016)	Shock tube	T=1400-2000 K; P=10, 20 and 40 bar; ϕ =0.5, 1 and 2 in Ar
Hashemi et al. (2016)	Plug-flow reactor	T=700-900 K; P=100 bar; ϕ =0.06-19.7 in N ₂
	Rapid compression machine	T=800-1250 K; P=15-80 bar; ϕ =0.5 and 1 in Ar or Ar/N ₂

Furthermore, methane has been widely found as intermediate during the oxidation of many hydrocarbons, such as ethylene (Dagaut et al., 1990) or ethane (Dagaut and Cathonnet, 1990). In the case of oxygenated compounds, high CH₃ radical concentration in the reaction environment is expected, from the conversion of these oxygenates, and, hence, the formation of CH₄ is also awaited. Therefore, the oxidation of methane has also been considered in the present work. The effect of the addition of NO and NO₂ on the oxidation of CH₄ has been mainly analyzed in flow reactors. In particular, in the case of jet-stirred reactor (JSR), the effect of NO₂ presence on the oxidation of CH₄, to our best knowledge, has not previously analyzed. Therefore, in the present work, to perform such a study, the configuration of a JSR coupled with different diagnostic techniques has been selected, since this type of reactor is well adapted for kinetic studies, and this configuration will allow a wide speciation.

Chapter 3:

Experimental methodology

“Chapter 3 describes the three experimental set-ups used to perform the different oxidation experiments; two of them include plug-flow reactors, and the third one, a jet-stirred reactor”.

3. EXPERIMENTAL METHODOLOGY

The oxidation experiments have been performed in three different experimental set-ups, with two different types of reactors. On the one hand, two plug-flow reactors (at atmospheric and high pressure) located in the facilities of the Thermo-Chemical Process Group (GPT group), in the framework of the Aragón Institute of Engineering Research (ISA) of the University of Zaragoza. And, on the other hand, a perfectly stirred reactor (commonly known as Jet-Stirred Reactor, JSR) available at the *Laboratoire Réactions et Génie des Procédés* (LRGP), in the city of Nancy (France), in which a research stay was performed during the development of the present thesis.

A brief description with the more relevant features of the different experimental set-ups is included in this chapter, while a more complete description of them and of the experimental methodology followed can be consulted in previous works, such as Esarte (2011), Abián (2013) and Rodríguez (2016).

On the other hand, the conditions of the different experiments performed are detailed in tables in Chapter 5 while analyzing the main results obtained in the corresponding study.

3.1 ATMOSPHERIC-PRESSURE FLOW REACTOR SET-UP

The oxidation experiments of DMM, and C₂H₂-DME mixtures in the presence and absence of NO, have been carried out in the gas-phase experimental set-up shown in Figure 3.1, which has been successfully used in a number of previous works by our research group, addressing homogeneous gas-phase reactions (e.g. Alzueta et al., 2001; Alzueta et al., 2008; Alexandrino, 2018).

In the case of this set-up, the reaction takes place in a quartz flow reactor (Figure 3.2), which has been built according to the design proposed by the CHEC Group (Combustion and Harmful Emission Control) of the Technical University of Denmark (DTU) (Kristensen et al., 1996). The reactor presents a reaction zone of 8.7 mm inside diameter and 200 mm in length. It is placed in a three-zone electrically heated furnace, ensuring a uniform temperature profile throughout the reaction zone within ± 5 K. An example of the longitudinal temperature profiles along the reaction zone for different nominal temperatures is shown in Figure 3.3.

The different gases are led to the reactor, through mass flow controllers (Bronkhorst High-Tech), in four separate streams: a main flow containing water vapor and nitrogen, and

3. EXPERIMENTAL METHODOLOGY

three injector tubes for the different reactants (DMM, C₂H₂, DME, O₂ and NO). Nitrogen is used to balance up to obtain a total flow rate of 1 L (STP)/min. Reactants are highly diluted in N₂, minimizing thermal effects. Reactants and nitrogen are fed from gas cylinders, while water vapor is injected by saturating a N₂ stream through a water bubbler at the adequate temperature to get the desired H₂O concentration in the reaction zone. The function of water is to minimize the impact of radical recombination in the reactor walls, the quenching effect. Moreover, water is a representative species of the mixture generated under combustion conditions.

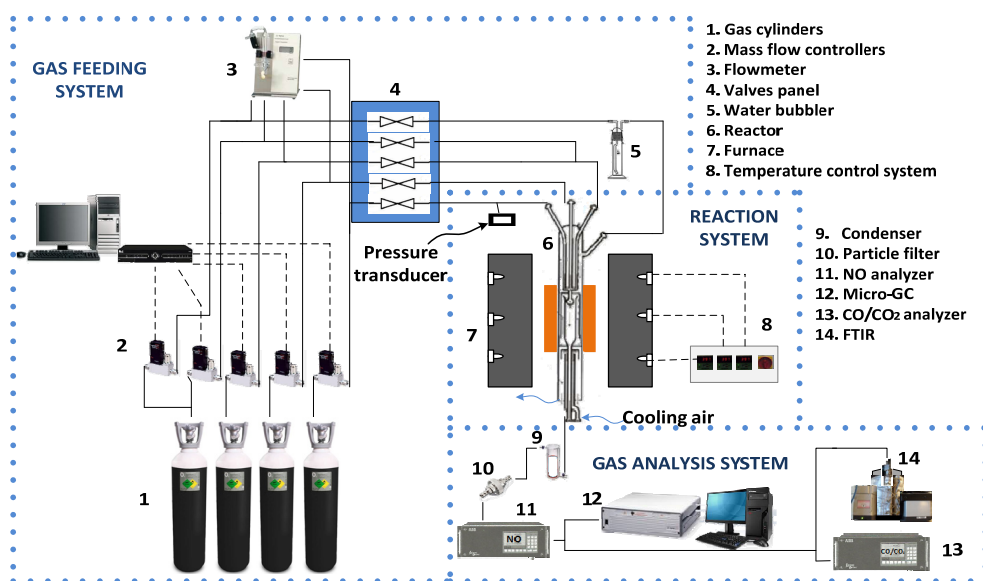


Figure 3.1. Scheme of the experimental set-up used to carry out the oxidation experiments at atmospheric pressure in a flow reactor (adapted from Alexandrino, 2018).

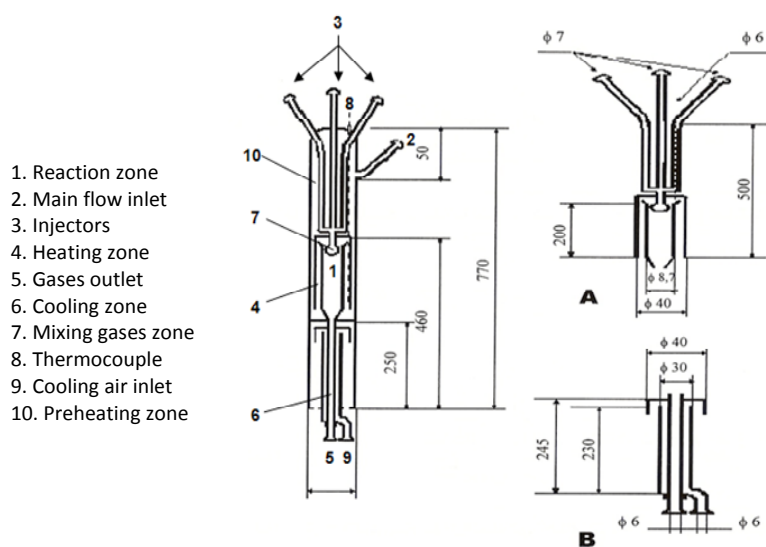


Figure 3.2. Scheme and dimensions (in mm) of the atmospheric-pressure flow reactor.

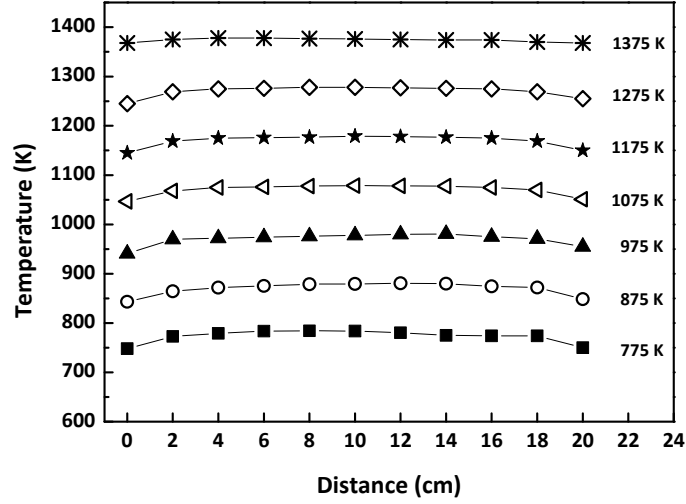


Figure 3.3. Temperature profiles inside the reaction zone of the atmospheric-pressure flow reactor, for different nominal temperatures, as a function of distance. They have been measured with a K-type thermocouple for a total N_2 flow rate of 1 L (STP)/min.

Under these conditions, the gas residence time (t_r) in the reaction zone depends on the temperature in this zone as follows:

$$t_r [s] = \frac{195}{T[K]} \quad (\text{Eq. 3.1})$$

The oxygen inlet concentration is determined by the air excess ratio (λ), which is defined as the real oxygen fed to the reactor ($O_{2, \text{fed}}$) divided by the stoichiometric oxygen ($O_{2, \text{st}}$), given the complete oxidation reaction of the fuel:



Thus, the amount of oxygen to be fed to the reactor is calculated by equation 3.2 depending on the air excess ratio analyzed,

$$\lambda = \frac{O_{2, \text{fed}}}{O_{2, \text{st}}} = \frac{O_{2, \text{fed}}}{x * [\text{fuel}]_{\text{inlet}}} \quad (\text{Eq. 3.2})$$

being $[\text{fuel}]_{\text{inlet}}$ the inlet fuel concentration. Therefore:

$\lambda > 1 \rightarrow$ fuel-lean or oxidizing conditions

$\lambda = 1 \rightarrow$ stoichiometric conditions

$\lambda < 1 \rightarrow$ fuel-rich or reducing conditions

3. EXPERIMENTAL METHODOLOGY

In the case of the mixtures with acetylene (C_2H_2), the value of lambda has been calculated considering the oxygen required for the stoichiometric conversion of both C_2H_2 and the oxygenated compound.

At the outlet of the reaction zone, the gas product is quenched by means of an external cooling air flow and, before analysis, it passes through a condenser and a particle filter to ensure gas cleaning. The outlet gas composition is analyzed by an Agilent 3000A micro-gas chromatograph (micro-GC) equipped with thermal conductivity detectors (TCD), an ATI Mattson Fourier Transform Infrared (FTIR) spectrometer, and ABB continuous infrared (IR) analyzers for CO, CO_2 and NO. The uncertainty of the measurements is estimated as $\pm 5\%$, except for the FTIR spectrometer, which is estimated as $\pm 10\%$.

3.2 HIGH-PRESSURE FLOW REACTOR SET-UP

The high-pressure oxidation experiments of methyl formate (MF), dimethyl ether (DME), ethanol, dimethoxymethane (DMM), and their mixtures with C_2H_2 (C_2H_2 -DME, C_2H_2 -ethanol and C_2H_2 -DMM) have been carried out in a laboratory-scale high-pressure flow reactor designed to approximate plug flow (Rasmussen et al., 2008b) which has been successfully used in a previous work by our research group, addressing homogeneous high-pressure gas-phase reactions (e.g. Alexandrino et al., 2015; Paper A). A scheme of the experimental set-up is shown in Figure 3.4.

In this set-up, the reaction takes place in a tubular quartz tube (inner diameter of 6 mm and length of 1500 mm). The reactor is enclosed in an AISI 316L stainless steel tube which acts as a pressure shell. Nitrogen is delivered to the shell side of the reactor by a pressure control system, to obtain a pressure similar to that inside the reactor avoiding in this way the stress in the reactor. The pressure inside the reactor is monitored by a differential pressure transducer (EL-PRESS Bronkhorst High-Tech), located at the reactor entrance and controlled by a pneumatic pressure valve (RCV-RC200) situated after the reactor. The maximum manometric pressure allowed in the system is 80 bar. The reactor-pressure shell system is placed inside a three-zone electrically heated furnace with individual temperature control, which allows a maximum temperature over the whole pressure range up to 1100 K.

Type K thermocouples, positioned in the void between the quartz reactor and the steel shell, were used to measure the longitudinal temperature profiles, obtaining an isothermal

reaction zone (± 10 K) of 56 cm. An example of the longitudinal temperature profiles along the reaction zone for different nominal temperatures and pressures is shown in Figure 3.5.

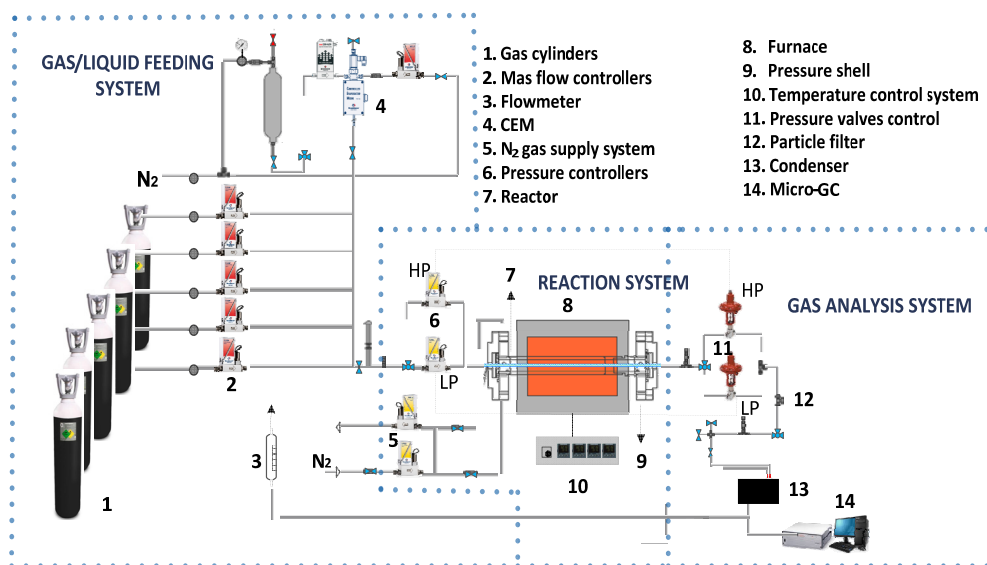


Figure 3.4. Scheme of the experimental set-up used to carry out the oxidation experiments at high pressure in a flow reactor (adapted from Alexandrino, 2018).

In the pure ethanol and methyl formate high-pressure oxidation experiments, due to the high concentrations considered, the corresponding fuel is fed into the reactor using a Controlled Evaporator Mixer (CEM) and N_2 as carrier gas. A mini CORI-FLOW meter/controller and an EL-FLOW meter/controller are used to measure the liquid and nitrogen flow, respectively. After fuel evaporation and to prevent condensation of reactants, all gas flow lines are heated and thermally insulated. The gases (DME, DMM, C_2H_5OH , C_2H_2 , O_2 , N_2 , and NO , when applicable) are fed into the reaction system from gas cylinders through mass flow controllers (Bronkhorst High-Tech). N_2 is used to balance up to obtain a total flow rate of 1 L (STP)/min.

The gas residence time (t_r) in the reaction zone is function of both temperature and manometric pressure in this zone and, for the previously described conditions, it is given by equation 3.3.

$$t_r [s] = \frac{261 * P [bar]}{T [K]} \quad (\text{Eq. 3.3})$$

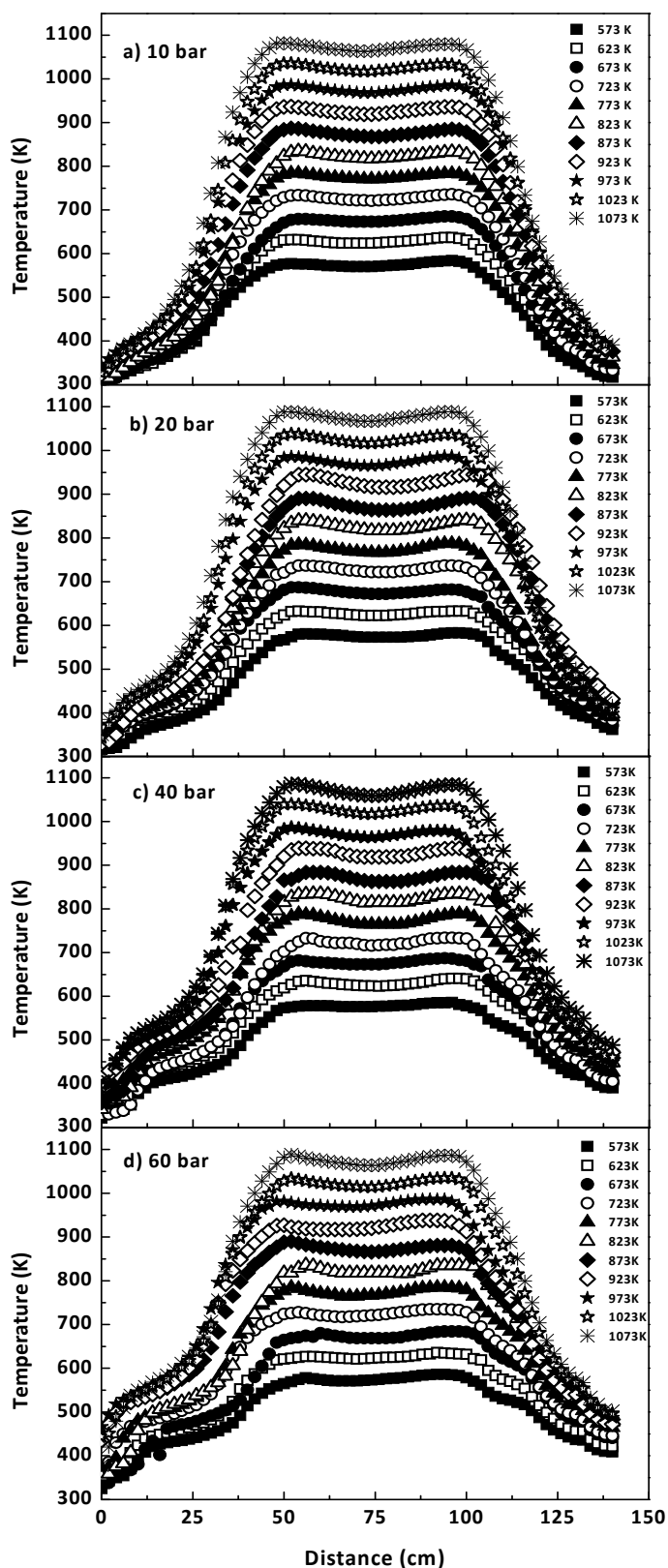


Figure 3.5. Longitudinal temperature profiles inside the reaction zone of the high-pressure flow reactor, for different nominal temperatures and pressures, as a function of distance. They have been measured with a K-type thermocouple for a total N_2 flow rate of 1 L (STP)/min.

Downstream the reactor, the pressure of the system is reduced to atmospheric level before product analysis, which is performed using a micro gas chromatograph (Agilent 3000A) equipped with thermal conductivity detectors (TCD), an ATI Mattson Fourier transform infrared (FTIR) spectrometer and an ABB NO analyzer. The uncertainty of the measurements is estimated as $\pm 5\%$, except for the FTIR spectrometer, which is estimated as $\pm 10\%$.

3.3 ATMOSPHERIC PRESSURE JET-STIRRED REACTOR (JSR) SET-UP

The oxidation experiments of pure methane (CH_4) and CH_4 doped with NO and NO_2 have been carried out in the experimental set-up shown in Figure 3.6 and available at the LRGP group in Nancy. This experimental set-up has been used with success in a number of previous works (e.g. Bahrini et al., 2012; Rodriguez et al., 2015; Rodriguez et al., 2017).

The jet-stirred reactor (JSR) used in this study is spherical with a volume of around 85 cm^3 . It is preceded by an annular preheater in which the reacting mixture is progressively heated up to the reaction temperature. The reactants enter the reactor through four injectors with nozzles, which creates a high turbulence and homogenous mixing. Both preheater and reactor are made of fused silica. The residence time inside the preheater is only 1% with respect to the one in the reactor, which is fixed at 1.5 s ($\pm 0.1 \text{ s}$) in all the experiments performed. The heating is provided through Thermocoax resistances rolled around the preheater and the reactor. The reaction temperature is measured by a type K thermocouple located in a glass finger (the intra-annular part of the preheater) at the center of the spherical reactor. Mass flow controllers (Bronkhorst High-Tech) are used to control the flow rates of the reactants (CH_4 , O_2 and NO or NO_2 , when applicable) and the inert gas (Ar). The role of the inert gas is to dilute the reacting mixture in order to minimize thermal effects as in the set-up described in Section 3.1. The pressure inside the reactor (1.07 bar) is controlled using a needle valve ($\pm 0.002 \text{ bar}$) located downstream of the reactor.

In the present study, the oxygen inlet concentration is determined by the equivalence ratio (ϕ) which is the inverse of the air excess ratio (λ) (equation 3.4).

$$\phi = \frac{1}{\lambda} \quad (\text{Eq. 3.4})$$

The gas stream is analyzed online downstream of the reactor with different diagnostic techniques: two gas chromatographs (Perichrom PR1250 and PR2500), a NO_x analyzer (Thermo Scientific Model 42i), a FTIR (Thermo Scientific Antaris) spectrometer and a continuous wave

3. EXPERIMENTAL METHODOLOGY

cavity ring-down spectroscopy (cw-CRDS) cell. The uncertainty for the different diagnostic instruments is estimated to be $\pm 5\%$, except for the FTIR and CRDS measurements that is $\pm 10\text{--}15\%$.

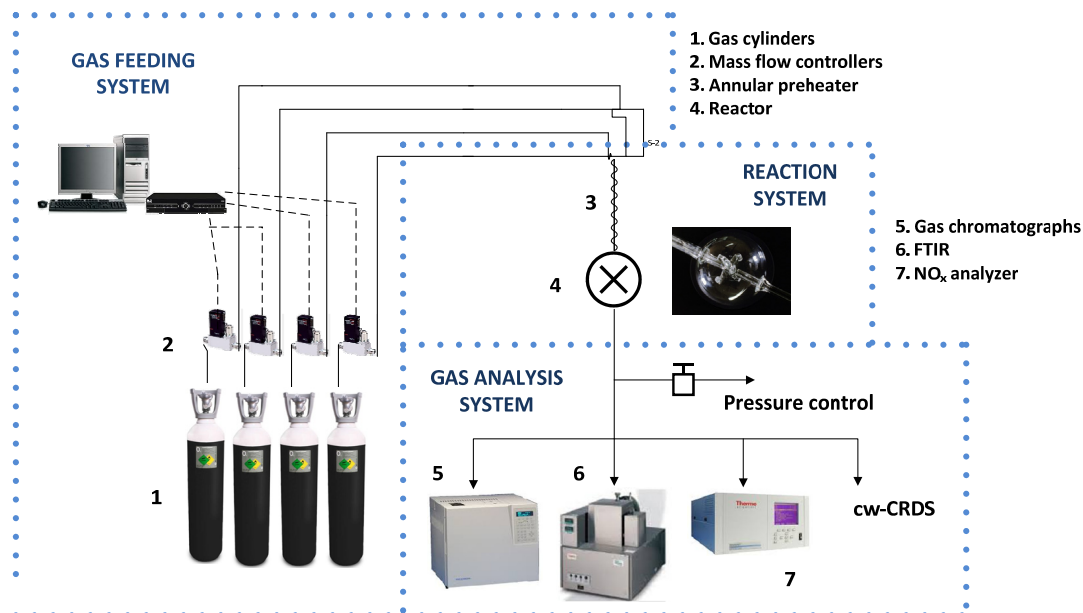


Figure 3.6. Scheme of the experimental set-up used to carry out the oxidation experiments at atmospheric pressure in a jet-stirred reactor.

A schematic view of the coupling between JSR and CRDS cell is shown in Figure 3.7. While only the main features are described here, a complete description can be found in Bahrini et al. (2012).

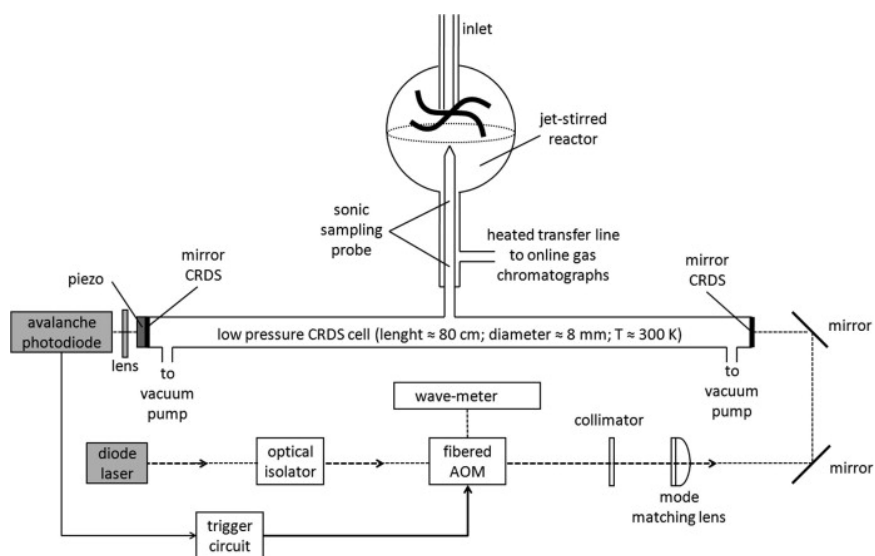


Figure 3.7. Schematic view of the JSR and CRDS coupling (from Bahrini et al., 2012).

The cw-CRDS cell is composed of a quartz tube with an outer diameter of 8 mm and a length of 80 cm. The total volume of the cell including the sampling probe is estimated to be 40 cm³. The cell is maintained at ambient temperature and the pressure in the CRDS cavity is kept at approximately 0.013 bar (10 Torr). The low pressure is obtained using a rotary vane pump. The reactor and the cell are connected by means of a sampling probe with a diameter of 6 mm and 10 cm in length.

CRDS analyses were carried out in the near infrared at wavelengths from 6638-6643 cm⁻¹. The near-infrared beam is provided by a diode laser, the wavelength can be varied in the 6640±13 cm⁻¹ range through changing the current applied to the diode laser. The diode laser emission passes through an optical isolator and an acousto-optical modulator (AOM). Two folding micrometric mirrors allow the alignment of the beam. After many round trips, the optical signal transmitted through the cavity is converted into current by an avalanche photodiode. A home designed amplifier-threshold circuit converts the current signal to an exploitable voltage signal. The ring-down signal is sampled every 800 ns and the data are transferred to PC in real time. The ring-down time is obtained by fitting the exponential decay by a Levenberg-Marquardt exponential fit in LabView. The concentration of a species, present during the hydrocarbon oxidation process in the jet-stirred reactor (JSR), can be obtained by measuring the ring-down time of the empty cavity, τ_0 , i.e., the ring down time before heating the reactor, and the ring-down time after turning on the heater, τ :

$$[A] \left[\frac{\text{mol}}{\text{cm}^3} \right] = \frac{R_L}{c \left[\frac{\text{cm}}{\text{s}} \right] * \sigma \left[\frac{\text{cm}^2}{\text{molecule}} \right]} \left(\frac{1}{\tau} - \frac{1}{\tau_0} \right) \left[\frac{1}{\text{s}} \right] * \left(\frac{1}{N_A \left[\frac{\text{molecule}}{\text{mol}} \right]} \right) \quad (\text{Eq. 3.5})$$

where σ is the absorption cross section; R_L is the ratio between the cavity length L , i.e. the distance between the two cavity mirrors, and the length L_A over which the absorber is present ($R_L=0.92$); and c is the speed of light. Knowing the absorption cross section (σ), the concentration $[A]$ of the target molecule can be calculated. An example of calculations for CH₄ quantification can be found in Bahrini et al. (2012).

Chapter 4:

Modeling. Reaction mechanism

“Chapter 4 explains how the detailed chemical kinetic mechanism has been compiled during the development of the present thesis. This mechanism has been used to perform modeling calculations to describe the oxidation of the oxygenated compounds and their mixtures with acetylene, under the different experimental conditions tested”.

4. MODELING. REACTION MECHANISM

Detailed chemical kinetic models are required to predict ignition, extinction, heat release, fuel consumption and pollutant formation during combustion processes. To develop a mechanism systematically, it is necessary to adopt or develop reaction subsets of the simpler molecules and then, step by step, add species and reactions relevant for more complex molecules.

Therefore, a detailed gas-phase chemical kinetic mechanism has been constructed progressively throughout the development of this thesis to numerically describe the oxidation, in laboratory reactors, of the different oxygenated compounds analyzed and their mixtures with acetylene. The construction progress will be described below and is schematically represented in Figure 4.1.

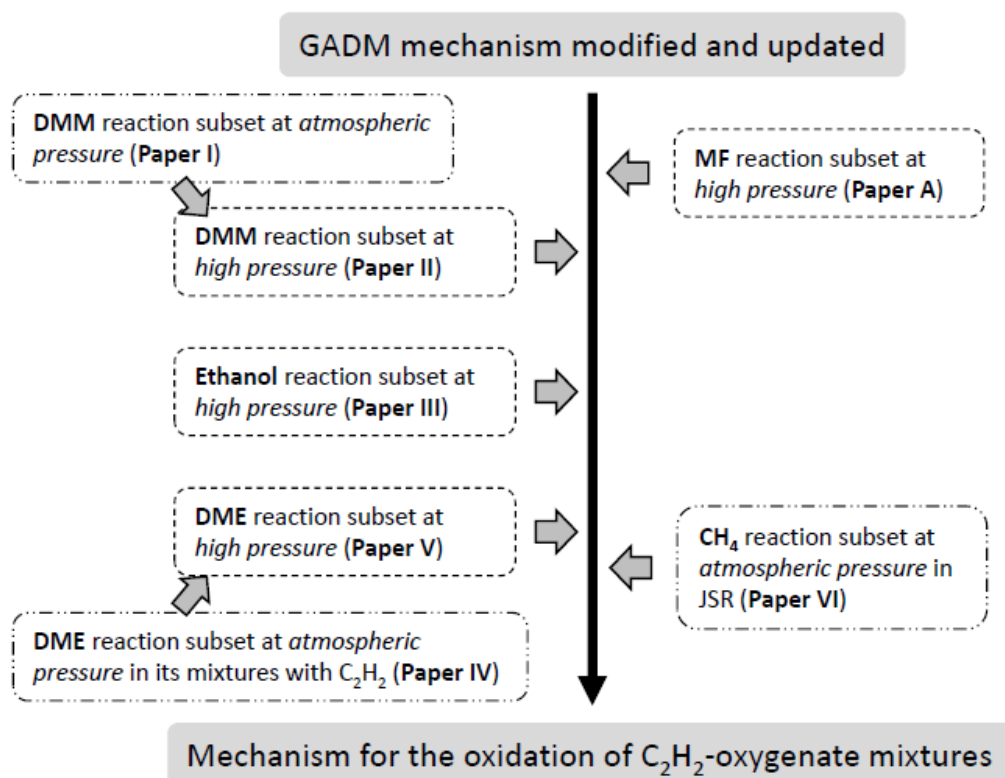


Figure 4.1. Development progress for a detailed gas-phase chemical kinetic mechanism for the description of the oxidation of the different C_2H_2 -oxygenate mixtures studied in this work. Left, for the oxygenated compounds. Right, for the oxidation intermediates.

The basis of the present gas-phase mechanism consists of a reaction mechanism to describe C_1 - C_2 and NO interactions, initially proposed by Glarborg et al. (1998), which has been progressively updated and modified (e.g. Glarborg et al., 1999; Alzueta et al., 2008). From now

on, this mechanism will be referred as GADM mechanism. To the GADM mechanism, the reaction subset for the conversion of the corresponding oxygenated compound studied (ethanol, DME or DMM), and other important intermediate species, has been added.

Traditionally, in our research group, the reaction subset for the species of interest has been first tested and validated under atmospheric-pressure conditions and, subsequently, under high-pressure conditions, which are of interest for combustion devices such as diesel engines. This is the case, for example, of methanol, which will be part of the mechanism used in this thesis because it is a possible intermediate of oxidation. Its oxidation was first studied at atmospheric pressure (Alzueta et al., 2001) and, some years later, at high pressure (Aranda et al., 2013), in both cases, in flow reactors. In this context, and as stated in the Chapter 1 of this thesis (Introduction and objectives), during the last years, the GPT group has studied the oxidation of different oxygenated compounds and proposed several kinetic mechanisms validated at atmospheric pressure, specifically for: ethanol (Alzueta and Hernández, 2002), DME (Alzueta et al., 1999) and MF (Alzueta et al., 2013), which will be part, as well, of the mechanism compiled in the present thesis, and improved or modified, if necessary.

To account the high-pressure conditions, which are the conditions of really interest for this work, some of the reaction subsets from the GADM mechanism have been revised and modified considering more recent works, as detailed below:

- H₂/O₂ and CO/CO₂ subsets, according to Rasmussen et al. (2008b).
- CH₄ subset, according to Rasmussen et al. (2008c).
- Methanol (CH₃OH) subset, according to Aranda et al. (2013).
- C₂H₂ subset, according to Giménez-López et al. (2016).
- Acetaldehyde (CH₃CHO) subset, according to Rasmussen et al. (2008c).
- H/N/O subset, according to Rasmussen et al. (2008a, 2008b).

The following sections describe, in more detail, what specifically refers to the reaction subsets of the different compounds of interest, i.e., the oxidation intermediates and the oxygenated compounds. Special emphasis will be put in the modifications and updates made to the different reaction subsets to obtain the final mechanism. The impact of the different modifications made is widely discussed in the corresponding publication of the compendium, as well as, in Chapter 5 (Results and discussion).

Model calculations have been performed using SENKIN, the plug flow reactor code that runs in conjunction with the Chemkin-II library (Lutz et al., 1988; Kee et al., 1991) and with

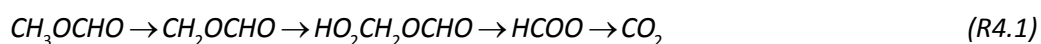
the Chemkin-Pro software package (ANSYS Chemkin-Pro, 2016). When Chemkin-Pro has been used, simulations have been conducted with the plug-flow reactor module and the fixed gas temperature assumption and taking into account the temperature profiles experimentally determined. The thermodynamic data have been taken from the same sources as the original mechanisms.

Several rate of production (ROP) and sensitivity analyses have been performed to identify the main reaction pathways occurring during reactant consumption and product formation at the different experimental conditions analyzed.

4.1 METHYL FORMATE REACTION SUBSET AT HIGH PRESSURE

A study of the oxidation of MF, as an important intermediate during the oxidation of higher oxygenates, has been carried out under high-pressure conditions from both experimental and modeling points of view (Paper A). This work takes as starting point a previous work from our research group on MF conversion at atmospheric pressure (Alzueta et al., 2013). With respect to the modeling part, the MF reaction subset proposed by Alzueta et al. (2013), which was mainly taken from the work of Dooley et al. (2010) with minor modifications, has been included in the mechanism developed in the present thesis.

Under high-pressure conditions, the results appeared to be sensitive to the $\text{HO}_2\text{CH}_2\text{OCHO}$ species, obtained from MF conversion, which are involved in the formation of the CO_2 , as oxidation product, through the reaction sequence represented in reaction R4.1.



Therefore, reactions involving HCOO and HCOOH (R4.2 and R4.3) have been added to the mechanism to improve modeling predictions. The values of the kinetic parameters for reaction R4.2 theoretically determined by Galano et al. (2002) have been adopted, and the experimental determination by Larson et al. (1988) for reaction R4.3 has been used.



The influence of NO addition has also been analyzed during the high-pressure oxidation of MF. When pressure is increased from atmospheric level to 20 bar, NO is almost

completely converted to NO_2 , being reaction R4.4 the main reaction involved in this conversion. The values of the kinetic parameters determined experimentally by Park et al. (1998), and later selected by Rasmussen et al. (2008b), have been adopted in the present work.



4.2 DIMETHOXYMETHANE REACTION SUBSET AT ATMOSPHERIC AND HIGH PRESSURE

As previously indicated, the reaction subsets are first validated at atmospheric pressure before being tested at higher pressures. Therefore, the reaction subset for DMM conversion has been validated with the experimental data obtained from the study of DMM oxidation at atmospheric pressure, in an isothermal quartz flow reactor (Paper I). To carry out the theoretical study, the subset proposed by Dias et al. (2010) has been included in the GADM mechanism without any modifications. In general, the chemical kinetic mechanism is able to represent the experimental trends observed. Therefore, due to the good agreement between experimental and modeling data achieved at atmospheric pressure, no further modifications to the DMM reaction subset have been done.

However, when this DMM reaction subset has been employed to simulate the oxidation of DMM under high-pressure conditions, the results obtained are not fully satisfactory. Thus, to improve the agreement between experimental results and modeling calculations, the kinetic parameters of some of the reactions involved in DMM conversion, under these conditions of high pressure, have been modified. Other reactions that were not included in the initial reaction subset of Dias et al. (2010), that can play an important role in DMM oxidation under high pressure and high oxygen concentration, have been included. A list of the reactions that have been modified or included can be found in Table 4.1. Details on these modifications can be found in Paper II.

Table 4.1. Reactions modified or included in DMM reaction subset. Kinetic parameters of the form $k = A \times T^n \times \exp(-E_a/RT)$. Units: A is in $\text{cm}^3 \text{mol}^{-1} \text{s}^{-1}$; E_a is in cal/mol.

Reaction	A	n	E_a	Reference
$\text{CH}_3\text{OCH}_2\text{OCH}_3 + \text{OH} \rightleftharpoons \text{CH}_3\text{OCH}_2\text{OCH}_2 + \text{H}_2\text{O}$	6.32×10^6	2.00	-652	Arif et al. (1997)
$\text{CH}_3\text{OCH}_2\text{OCH}_3 + \text{OH} \rightleftharpoons \text{CH}_3\text{OCH}_2\text{OCH}_2 + \text{H}_2\text{O}$	6.32×10^6	2.00	-652	Arif et al. (1997)
$\text{CH}_3\text{OCH}_2\text{OCH}_3 + \text{HO}_2 \rightleftharpoons \text{CH}_3\text{OCH}_2\text{OCH}_2 + \text{H}_2\text{O}_2$	1.00×10^{13}	0.00	17686	Curran et al. (1998)
$\text{CH}_3\text{OCH}_2\text{OCH}_3 + \text{HO}_2 \rightleftharpoons \text{CH}_3\text{OCHOCH}_3 + \text{H}_2\text{O}_2$	2.00×10^{13}	0.00	15296	Daly et al. (2001)
$\text{CH}_3\text{OCH}_2\text{OCH}_2 + \text{O}_2 \rightleftharpoons \text{CH}_2\text{O} + \text{CH}_3\text{OCHO} + \text{OH}$	2.50×10^{11}	0.00	-1700	Alzueta et al. (1999)
$\text{CH}_3\text{OCHOCH}_3 + \text{O}_2 \rightleftharpoons \text{CH}_2\text{O} + \text{CH}_3\text{OCHO} + \text{OH}$	2.50×10^{11}	0.00	-1700	Alzueta et al. (1999)
$\text{CH}_3\text{OCH}_2\text{OCH}_2 + \text{HO}_2 \rightleftharpoons \text{CH}_2\text{O} + \text{CH}_3\text{OCH}_2\text{O} + \text{OH}$	3.00×10^{11}	0.00	0	Daly et al. (2001)
$\text{CH}_3\text{OCHOCH}_3 + \text{HO}_2 \rightleftharpoons \text{CH}_3\text{OCHO} + \text{CH}_3\text{O} + \text{OH}$	1.00×10^{12}	0.00	0	Daly et al. (2001)
$\text{CH}_3\text{OCH}_2\text{OCH}_2 + \text{O}_2 \rightleftharpoons \text{CH}_3\text{OCH}_2\text{O}_2 + \text{CH}_2\text{O}$	6.40×10^{12}	0.00	91	Present work
$\text{CH}_3\text{OCH}_2\text{OCH}_2 + \text{HO}_2 \rightleftharpoons \text{CH}_3\text{OCH}_2\text{O}_2 + \text{CH}_2\text{OH}$	1.00×10^{12}	0.00	0	Present work

4.3 ETHANOL REACTION SUBSET AT HIGH PRESSURE

In the case of ethanol, as also happened for MF, there is an earlier work carried out by our research group on the ethanol oxidation at atmospheric pressure, from both experimental and theoretical points of view (Alzueta and Hernández, 2002). The mechanism used to describe ethanol conversion included the reaction subset proposed few years before by Marinov (1999), and the fitting to the experimental conditions was very good.

In the present work, the aforementioned ethanol reaction subset has been used, without any modification, to perform simulations of the experimental results obtained during the ethanol high-pressure oxidation, both in the absence and in the presence of NO, with a good performance.

In the case of the ethanol oxidation experiments in the presence of NO, due to the high-pressure conditions and the high concentration of oxygen, the NO fed to the reaction system is converted to NO_2 before entering the reactor. On the other hand, because of the interaction between CH_3 radicals and NO_2 , model calculations predicted an accumulation of nitromethane (CH_3NO_2), whose formation was not detected experimentally. Also, another

possible interaction between CH₃ and NO₂ could lead to the formation of CH₃ONO (reaction R4.5). Therefore, reaction R4.5 has been included in our mechanism with the kinetic parameters proposed by Canosa et al. (1979).



A more complete explanation of CH₃NO₂ and CH₃ONO formation, and the effect of this reaction on modeling results, can be found in Paper III.

4.4 DIMETHYL ETHER REACTION SUBSET AT ATMOSPHERIC PRESSURE, IN ITS MIXTURES WITH C₂H₂ AND AT HIGH PRESSURE

In an earlier work, Alzueta et al. (1999) validated a mechanism, which included a reaction subset for DME conversion, against experimental data on the atmospheric-pressure oxidation of DME in a flow reactor. This reaction subset was extracted mainly from Curran et al. (1998), but the kinetic parameters for selected reactions were updated.

In the present work, the Alzueta et al.'s DME subset has been included in the mechanism without any modifications. But before using it to simulate the high-pressure experimental data on DME oxidation, its performance has been evaluated against the results obtained during the oxidation of C₂H₂-DME mixtures at atmospheric pressure (Paper IV). Moreover, a reaction subset for glyoxal (OCHCHO) oxidation (Faßheber et al., 2015) has been added because this species is recognized as an important intermediate in hydrocarbons combustion and, at low temperatures, OCHCHO can be formed during the oxidation of C₂H₂ through the sequence represented in reaction R4.6.



In this way, modeling predictions obtained with this modified mechanism and the experimental data trends observed during the atmospheric-pressure oxidation of C₂H₂-DME mixtures are in good agreement.

However, when this modified mechanism has been used to simulate the high-pressure experimental results of DME oxidation, the mechanism was not able to properly describe the characteristic negative temperature coefficient (NTC) behavior of DME at low temperatures. Therefore, an improvement of the performance of the mechanism has been required. The

reaction subset for DME has been revised according to two kinetic mechanisms from literature, Zhao et al.'s (Zhao et al., 2008) and Burke et al.'s (Burke et al., 2015b) mechanisms, which have been validated against a wide range of experimental data. The modifications, that have been made in relation to the work of Alzueta et al. (1999), are listed in Table 4.2. For a matter of clarity, not all the pressure dependencies of the reactions involved in the low-temperature oxidation pathways for DME are shown. A more complete description can be checked in Paper V.

The performance of some of the most recent mechanisms for DME conversion (Zhao et al., 2008; Rodriguez et al., 2015; Wang et al., 2015; Dames et al., 2016) has been compared against the present high-pressure DME experimental data, and one interesting issue when comparing the various mechanisms is related to the presence and reactions of formic acid (HCOOH). Although some of them do not include HCOOH as an intermediate (such as the Rodriguez et al.'s mechanism), the present experimental results evidence the formation of HCOOH from DME (FTIR absorption spectra have been detected), and it has a significant role under the high-pressure conditions studied. Therefore, the more recent subset for the oxidation of HCOOH based on *ab initio* calculations proposed by Marshall and Glarborg (2015) has been included.

Table 4.2. Reactions modified or added compared to Alzueta et al.'s DME oxidation work (Alzueta et al., 1999). Units: A is in $\text{cm}^3 \text{mol}^{-1} \text{s}^{-1}$; E_a is in cal/mol.

Reaction		A	n	E_a	
$\text{CH}_3\text{OCH}_3 + (\text{M}) \rightleftharpoons \text{CH}_3 + \text{CH}_3\text{O} + (\text{M})$	HP ^a	4.37×10^{21}	-1.57	83842	(1)
	LP	1.13×10^{62}	-12.19	94882	
$\text{CH}_3\text{OCH}_3 + \text{OH} \rightleftharpoons \text{CH}_3\text{OCH}_2 + \text{H}_2\text{O}$		6.71×10^6	2.00	-629.88	(1)
$\text{CH}_3\text{OCH}_3 + \text{HO}_2 \rightleftharpoons \text{CH}_3\text{OCH}_2 + \text{H}_2\text{O}_2$		2.00×10^{13}	0.00	16500	(1)
$\text{CH}_3\text{OCH}_3 + \text{CH}_3 \rightleftharpoons \text{CH}_3\text{OCH}_2 + \text{CH}_4$		2.68×10^1	3.78	9631.1	(1)
$\text{CH}_3\text{OCH}_3 + \text{CH}_3\text{O}_2 \rightleftharpoons \text{CH}_3\text{OCH}_2 + \text{CH}_3\text{O}_2\text{H}$		1.27×10^{-3}	4.64	10556	(2)
$\text{CH}_3\text{OCH}_3 + \text{CH}_3\text{OCH}_2\text{O}_2 \rightleftharpoons \text{CH}_3\text{OCH}_2 + \text{CH}_3\text{OCH}_2\text{O}_2\text{H}$		5.00×10^{12}	0.00	17690	(2)
$\text{CH}_3\text{OCH}_3 + \text{OCHO} \rightleftharpoons \text{CH}_3\text{OCH}_2 + \text{HOCHO}$		1.00×10^{13}	0.00	17690	(2)
$\text{CH}_3\text{OCH}_2 \rightleftharpoons \text{CH}_3 + \text{CH}_2\text{O}$	(0.001 atm)	7.49×10^{23}	-4.52	25236	(2)
	(100 atm)	2.66×10^{29}	-4.94	31785	
$\text{CH}_3\text{OCH}_2 + \text{O}_2 \rightleftharpoons \text{CH}_3\text{OCH}_2\text{O}_2$	(0.001 atm)	1.12×10^{18}	-3.37	-4294	(2)
	(100 atm)	5.43×10^{17}	-1.73	2210	

4. MODELING. REACTION MECHANISM

Table 4.2. (Continued).

$CH_3OCH_2 + O_2 \rightleftharpoons CH_2OCH_2O_2H$	(0.001 atm)	5.08×10^{20}	-4.39	469	(2)
	(100 atm)	2.41×10^{27}	-4.50	16107	
$CH_3OCH_2O \rightleftharpoons CH_3O + CH_2O$		9.72×10^{15}	-1.10	20640	(1)
$CH_3OCH_2O_2 + CH_3OCH_2O_2 \rightleftharpoons O_2 + CH_3OCH_2O + CH_3OCH_2O$		1.60×10^{23}	-4.50	0	(1)
$CH_3OCH_2O_2 + CH_3OCH_2O_2 \rightleftharpoons O_2 + CH_3OCHO + CH_3OCH_2OH$		6.84×10^{22}	-4.50	0	(1)
$CH_3OCH_2O_2 \rightleftharpoons CH_2OCH_2O_2H$	(0.001 atm)	1.94×10^{29}	-6.99	22446	(2)
	(100 atm)	3.70×10^{14}	-1.13	20034	
$CH_3OCH_2O_2 \rightleftharpoons CH_2O + CH_2O + OH$	(0.001 atm)	2.06×10^{36}	-8.30	33415	(1)
	(0.01 atm)	2.07×10^{39}	-8.90	35842	
	(100 atm)	1.22×10^{30}	-5.20	39549	
$CH_2OCH_2O_2H \rightleftharpoons OH + CH_2O + CH_2O$	(0.001 atm)	1.66×10^{23}	-4.53	22243	(1)
	(0.01 atm)	5.30×10^{25}	-4.93	24158	
	(100 atm)	1.40×10^{22}	-2.72	24407	
$CH_2OCH_2O_2H + O_2 \rightarrow O_2CH_2OCH_2O_2H$	(0.001 atm)	9.42×10^{12}	-1.68	-4998	(2)
	(100 atm)	4.87×10^{12}	-0.32	428	
$CH_2OCH_2O_2H + O_2 \rightarrow HO_2CH_2OCHO + OH$	(0.001 atm)	5.90×10^{20}	-2.88	3234	(2)
	(100 atm)	3.96×10^{18}	-2.31	10500	
$O_2CH_2OCH_2O_2H \rightleftharpoons HO_2CH_2OCHO + OH$	(0.001 atm)	9.05×10^{23}	-4.88	18805	(2)
	(100 atm)	3.86×10^{07}	0.98	17467	
$HO_2CH_2OCHO \rightarrow OCH_2OCHO + OH$		3.00×10^{16}	0.00	43000	(1)
$CH_2O + OCHO \rightleftharpoons OCH_2OCHO$		1.25×10^{11}	0.00	11900	(2)
$HOCH_2OCO \rightleftharpoons HO_2CH_2O + CO$		2.18×10^{16}	-2.69	17200	(1)
$HOCH_2OCO \rightleftharpoons CH_2OH + CO_2$		5.31×10^{15}	-2.61	20810	(1)
$HOCH_2O \rightleftharpoons HCOOH + H$		1.00×10^{14}	0.00	14900	(1)
$CH_2O + OH \rightleftharpoons HOCH_2O$		4.50×10^{15}	-1.11	0	(1)

^aHP, LP: high- and low-pressure values; ⁽¹⁾ Zhao et al. (2008); ⁽²⁾ Burke et al. (2015b).

4.5 METHANE REACTION SUBSET AT ATMOSPHERIC PRESSURE IN A JET STIRRED REACTOR

During the research stay in the LRGP in Nancy (France), the oxidation of CH_4 and CH_4 doped with NO and NO_2 has been investigated in a jet-stirred reactor. This type of reactor is well suitable for kinetic studies: the gas phase inside the reactor is well stirred leading to homogenous concentrations and temperatures. JSR, coupled with different diagnostic techniques, such as gas-chromatography, time-of-flight mass spectrometry or CRDS spectroscopy, has been earlier used to study the low-temperature oxidation of organic compounds (Herbinet et al., 2011., Bahrini et al., 2012).

In this case, a detailed kinetic mechanism, derived from the POLIMI (*Politecnico di Milano*) kinetic framework (Ranzi et al., 2012), has been used to interpret the experimental data and has provided a good agreement between experimental and modeling results (Paper VI). Taking the POLIMI mechanism as a reference, some minor modifications to the mechanism compiled and validated during this thesis have been made to improve model performance. These modifications include the change in the kinetic parameters of reaction R4.7 and the thermodynamic data for the CH_3O_2 and CH_3NO_2 species.



Finally, the mechanism obtained during the construction process described above (Sections 4.1-4.5), which is the final mechanism developed in the present work, involves 138 species and contains 795 reactions. It can be found in the Annexes, at the end of this dissertation.

This final mechanism has been used to analyze the role of ethanol, DME and DMM as fuel additives under conditions of interest for real combustion processes. That is, to simulate the experimental results obtained during the high-pressure oxidation of their mixtures with acetylene.

Chapter 5:

Results and discussion

“Chapter 5 shows and analyzes the main results obtained during the study of the oxidation of the different compounds analyzed, intermediates and oxygenated compounds, and their mixtures with acetylene”.

5. RESULTS AND DISCUSSION

The main experimental and modeling results obtained in the different studies performed along this work, with a brief discussion of them, are presented below. These results have been structured according to the specific objectives addressed in Section 1.2 (Scope and objectives). First, the results of the oxidation of both intermediates MF and CH₄ at high and atmospheric pressure, respectively, are presented. Later, the high-pressure results obtained during the oxidation of the isomers ethanol and DME are compared. Next, the influence of the number of carbons in the molecule is analyzed by the comparison of the data got from the oxidation of DME and DMM, two POMDMEs with 2 and 3 C atoms, respectively. Finally, the results of the oxidation experiments of the C₂H₂-oxygenate mixtures are analyzed.

During the process of compiling of the different reaction subsets to obtain the final mechanism described in Chapter 4 (Modeling. Reaction mechanism), the kinetic parameters of several reactions have been modified, and also new reactions have been included in the final mechanism. Therefore, modeling calculations for the oxidation of the different compounds have been recalculated with the final mechanism and compared with modeling predictions obtained with the mechanism used during the corresponding oxidation study of each compound or acetylene-oxygenate mixture, which is described in detail in the related publication (Papers I-VII). Otherwise mentioned, modeling calculations obtained with the final mechanism are similar to those obtained with the mechanism used during the corresponding study. In the case of any change, a comparison of the results obtained with the different mechanisms will be shown in the corresponding section.

5.1 OXIDATION OF METHYL FORMATE AND METHANE

In this work, the oxidation of MF and CH₄, as interesting reaction intermediates, is addressed and the main results are presented below. The MF oxidation at atmospheric pressure and its interaction with NO was previously studied in a flow reactor by Alzueta et al. (2013). Therefore, in the present work, only the high-pressure MF oxidation in a flow reactor is discussed.

On the other hand, the CH₄ oxidation has been extensively studied, as has been reported in Section 2.5 of the Background, in the literature review of previous works, but to our best knowledge, this is the first study to investigate the oxidation of CH₄ doped with NO₂ in a jet-stirred reactor using various diagnostic techniques: GC, FTIR, cw-CRDS and NO_x analyzer,

to quantify different possible products, such as HCN, HONO and CH₃NO₂. These new experimental data and new species detection, along with a confirmation of the kinetics in these new conditions, could provide some novel insights into the mutual effect of NO_x on CH₄ oxidation. The work dealing with CH₄ has been carried out during the research stay in Nancy. It is considered of great value for the formation of the author of this thesis, because she could study a different configuration of reactor and complex diagnostic techniques, such as cw-CRDS.

5.1.1 High-pressure oxidation of MF and its interaction with NO in a flow reactor

MF has been found to be a byproduct and intermediate of the oxidation of several fuel additives, such as DME and DMM, and it has also been considered as a model molecule to try to understand the combustion of biodiesel. In this context, the present work aims to extend the experimental database of MF oxidation in flow reactor to pressures above atmospheric level, because these results would be helpful for future developments of engines. Because of the formation of NO_x in engines may happen, as discussed in Chapter 2 (Background), the interaction between MF and NO has also been analyzed.

Therefore, the oxidation of MF has been studied under flow-reactor conditions, at different pressures (1-60 bar), in the 573-1073 K temperature range, from reducing to very fuel-lean conditions ($\lambda = 0.7-20$). Additionally, at a constant pressure of 20 bar, the influence of the NO presence on MF oxidation has been considered for the different values of λ analyzed. The conditions of these experiments and the experimental set-up used are detailed in Table 5.1 and Section 3.2, respectively. Only some of the main results are discussed below. However, a more extensive discussion of the results obtained can be found in Paper A.

Figure 5.1 shows the evolution with temperature of the MF concentration profile for 20 bar and different values of λ , in the presence and absence of NO. The results for the rest of conditions and oxidation products quantified (CH₂O, CO₂, CO, CH₄, and H₂), that are not shown here, can be seen in Paper A. The discussion of the results will be made for all the conditions studied, including those that are not represented in Figure 5.1.

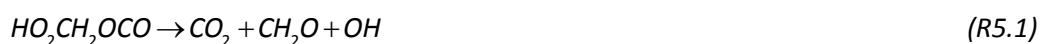
From now on, throughout all the thesis and the different publications, experimental results are denoted by symbols, while modeling calculations are denoted by lines.

Table 5.1. Matrix of experimental conditions of the high-pressure study of MF oxidation^a

MF oxidation at high pressure in a flow reactor					
T=573-1073 K; Flow rate: 1 L (STP)/min; $t_r [s] = \frac{261 * P [bar]}{T [K]}$					
Set	MF [ppm]	O ₂ [ppm]	NO [ppm]	λ	P [bar]
1MF	3000	4200	-	0.7	20
2MF	3000	6000	-	1	20
3MF	3000	120000	-	20	20
4MF	3000	6000	-	1	1
5MF	3000	6000	-	1	40
6MF	3000	6000	-	1	60
7MF	3000	4200	3000	0.7	20
8MF	3000	6000	3000	1	20
9MF	3000	120000	3000	20	20

^aThe balance is closed with N₂.

As mentioned before, modeling predictions have been recalculated with the final mechanism obtained in the present thesis. Figure 5.1 includes a comparison of modeling calculations obtained with this final mechanism and with the previously used mechanism to describe the high-pressure oxidation of MF (Paper A). In addition to all the modifications previously described (Chapter 4), the subset for MF oxidation has been revised according to a recent work by Rodriguez et al. (2015) on DME oxidation at low temperatures. In that study, MF appeared as an important primary product during DME conversion, therefore, a sub-mechanism for MF oxidation was included in their mechanism. By comparison of both mechanisms, Rodriguez et al.'s and ours, reactions R5.1 and R5.2 have been included in our final mechanism because they were not considered while the validation of MF reaction subset under high-pressure conditions (Paper A). It can be observed (Figure 5.1) that, in general, modeling predictions have improved after the modifications made to the mechanism, especially in the presence of NO.



In the absence of NO, the oxygen concentration in the reactant mixture has an almost imperceptible influence on the temperature for the onset of MF oxidation. According to the

5. RESULTS AND DISCUSSION

experimental results, the onset temperature for MF conversion is approximately 723 K, with MF almost totally converted at 873 K, independently of the stoichiometry. That is because MF oxidation is initiated by thermal decomposition, mainly by reaction R5.3. In the presence of highly reactive OH radicals, theoretical calculations indicate that MF also produces CH_2OCHO and CH_3OCO radicals by H-abstraction reactions R5.4 and R5.5, and it becomes really relevant under oxidizing conditions.

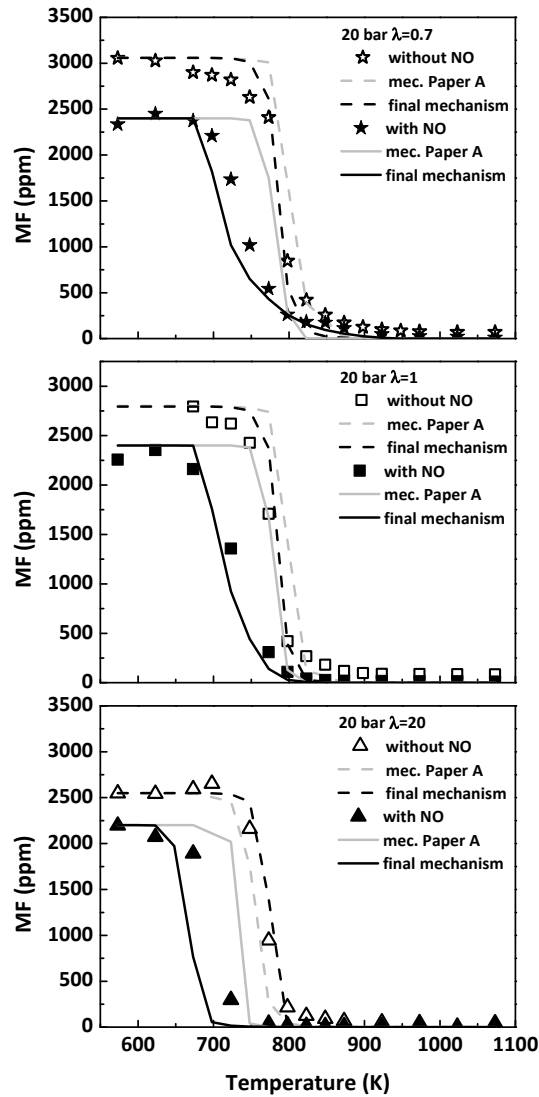


Figure 5.1. Evaluation of the effect of NO presence on the high-pressure (20 bar) oxidation of MF, for the conditions denoted as set 1MF-3MF and 7MF-9MF, in Table 5.1.



The CH_2OCHO radicals generated may thermally decompose to give CH_2O and formyl radicals (HCO) (R5.6) or continue the reaction sequence represented by reactions R5.7-R5.9; while the CH_3OCO radical decomposes to give CO_2 as the final product and methyl radicals (CH_3) (R5.10).



A study of the influence of varying the pressure on MF oxidation has also been performed. The results (Figure 4 in Paper A) indicate that an increase in pressure shifts the onset for MF conversion to lower temperatures. Moreover, the reaction rate analysis performed suggests that reaction pathways occurring at high pressure are a bit more complex than those observed at atmospheric pressure.

An increase in the working pressure has also an impact on NO to NO_2 conversion. At 20 bar, and the lowest temperatures studied, the NO concentration at the outlet of the experimental system is very low. It is attributed to the fact that most NO is converted to NO_2 when pressure is raised above atmospheric level through reaction R5.11 and the equilibrium between NO and NO_2 , reaction R5.12, which is relevant under high-pressure conditions (Giménez-López et al., 2011).



The presence of NO in the reactant mixture mainly produces a decrease of other final products different from CO or CO_2 , because CH_4 , CH_2O and H_2 have not been detected in an appreciable amount. Moreover, in the presence of NO , MF presents an increased reactivity, and the onset for MF conversion is shifted to lower temperatures because of the increased relevance of reactions involving OH radicals and MF (R5.4 and R5.5). In the presence of NO , CH_3 radicals from reaction R5.10 react with NO_2 giving nitromethane (CH_3NO_2), which

5. RESULTS AND DISCUSSION

continues the reaction sequence R5.13. Afterwards, CH_2O also reacts with NO_2 to form HONO (R5.14), which rapidly decomposes into NO and OH radicals (R5.15). These radicals are responsible for the increased reactivity of MF in the presence of NO.



However, results indicate that no net reduction of NO_x is achieved in the MF-NO interaction at high pressure, NO is converted to NO_2 , which exhibits a high reactivity, participating in several reactions with the different oxidation intermediates, and NO is formed again.

5.1.2 Low-temperature oxidation of CH_4 in a jet-stirred reactor in the presence of NO_x

The influence of the presence of NO_x (NO and NO_2) during the oxidation of CH_4 in a jet-stirred reactor has been analyzed at a pressure of 1.07 bar, in the 650-1200 K temperature range, with a fixed residence time of 1.5 s, and from fuel-lean to fuel-rich conditions. For the detection and quantification of the gases, different diagnostics techniques have been used: GC, cw-CRDS, FTIR and a NO_x analyzer. The experimental conditions analyzed in this study are presented in Table 5.2, and the experimental set-up is detailed in Section 3.3. The main results are reported in Paper VI of the compendium of publications.

Although in Paper VI the variable ϕ has been used to define the fuel air ratio, because it is the variable typically adopted by the Nancy group, in this work, to uniformize the different studies performed, the variable λ , will be used instead. As defined in Section 3.3, equation 3.4, ϕ is the inverse of λ ; so, for example, if $\phi > 1$, fuel-rich or reducing conditions are considered.

Table 5.2. Matrix of experimental conditions of the low-temperature oxidation of CH₄ in a jet-stirred reactor^a

CH₄ oxidation at low temperatures in a JSR					
T=650-1200 K; P=1.07 bar; t_r [s] = 1.5 s					
Set	CH ₄ [mole fraction]	O ₂ [mole fraction]	NO [ppm]	NO ₂ [ppm]	λ
1JSR	0.01	0.04	-	-	2
2JSR	0.01	0.02	-	-	1
3JSR	0.01	0.01	-	-	0.5
4JSR	0.01	0.04	500	-	2
5JSR	0.01	0.02	500	-	1
6JSR	0.01	0.01	500	-	0.5
7JSR	0.01	0.02	100	-	1
8JSR	0.01	0.04	-	400	2
9JSR	0.01	0.02	-	400	1
10JSR	0.01	0.01	-	400	0.5
11JSR	0.01	0.02	-	100	1
12JSR	0.01	0.02	1000	-	1

^aAr is used as bath gas.

As mentioned in the beginning of this chapter, modeling calculations for the different compounds have been recalculated with the final mechanism. As an example, Figure 5.2 shows a comparison of the modeling results obtained with the POLIMI mechanism and the final mechanism of the present work, for the JSR CH₄ oxidation, in the absence and presence of NO (500 ppm), for stoichiometric conditions ($\lambda=1$). As can be seen, the final mechanism is able to reproduce the experimental trends for CH₄ consumption. Although it is not shown, the agreement between experimental results and model calculations for the other air excess ratios analyzed is a little bit worse. Therefore, the discussion of the results will be done with the POLIMI mechanism.

As an example of the results obtained, Figure 5.3 shows the evolution with temperature of the CH₄ concentration profile in the absence of NO_x (open symbols), in the presence of NO₂ (left, solid symbols), and in the presence of NO (right, solid symbols), during the low-temperature oxidation of CH₄ in a JSR. The concentration profiles of CO and CO₂, as an example of the different products obtained, are also shown in Figure 5.3. The results for the rest of conditions and other products different from CO/CO₂, that have been quantified (H₂O, CH₂O, C₂H₄ and C₂H₆), can be seen in Paper VI.

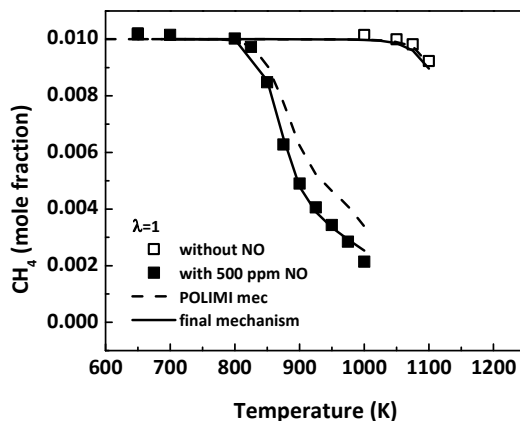


Figure 5.2. Comparison between experimental results and modeling calculations with the POLIMI mechanism and the final mechanism of the present work, for CH₄ consumption, in the absence and presence of NO (500 ppm), for $\lambda = 1$.

In the absence of NO_x, dynamic behaviors (oscillations) occur under oxidizing ($\lambda = 2$) and stoichiometric conditions when the temperature is above 1050 K and 1100 K, respectively. In the presence of NO or NO₂ and under stoichiometric conditions, oscillations even occur at temperatures above 1000 K, and, moreover, in the presence of NO₂, they also occur under oxidizing conditions and temperatures above 1100 K. Therefore, no more experimental data are available above these mentioned temperatures. Oscillations have been previously observed in the oxidation of several hydrocarbons in well-stirred reactors (e.g. Baulch et al., 1988; De Joannon et al., 2004). It is an interesting topic of research for such systems, but beyond the specific goals of the present study. Anyway, the POLIMI mechanism is able to reproduce these dynamic behaviors as shown in Supplementary Material of Paper VI.

The results represented in Figure 5.3 indicate that the onset temperature for CH₄ oxidation in the absence of NO_x (above 1025 K) is shifted to lower temperatures (825 K) by the addition of NO or NO₂, independently of the air excess ratio (λ). This fact indicates that, under the present conditions, CH₄ oxidation is promoted by the addition of NO_x. The consumption of CH₄ exhibits a similar trend in the presence of either NO and NO₂, and this is also reflected in the concentration profiles of CO and CO₂.

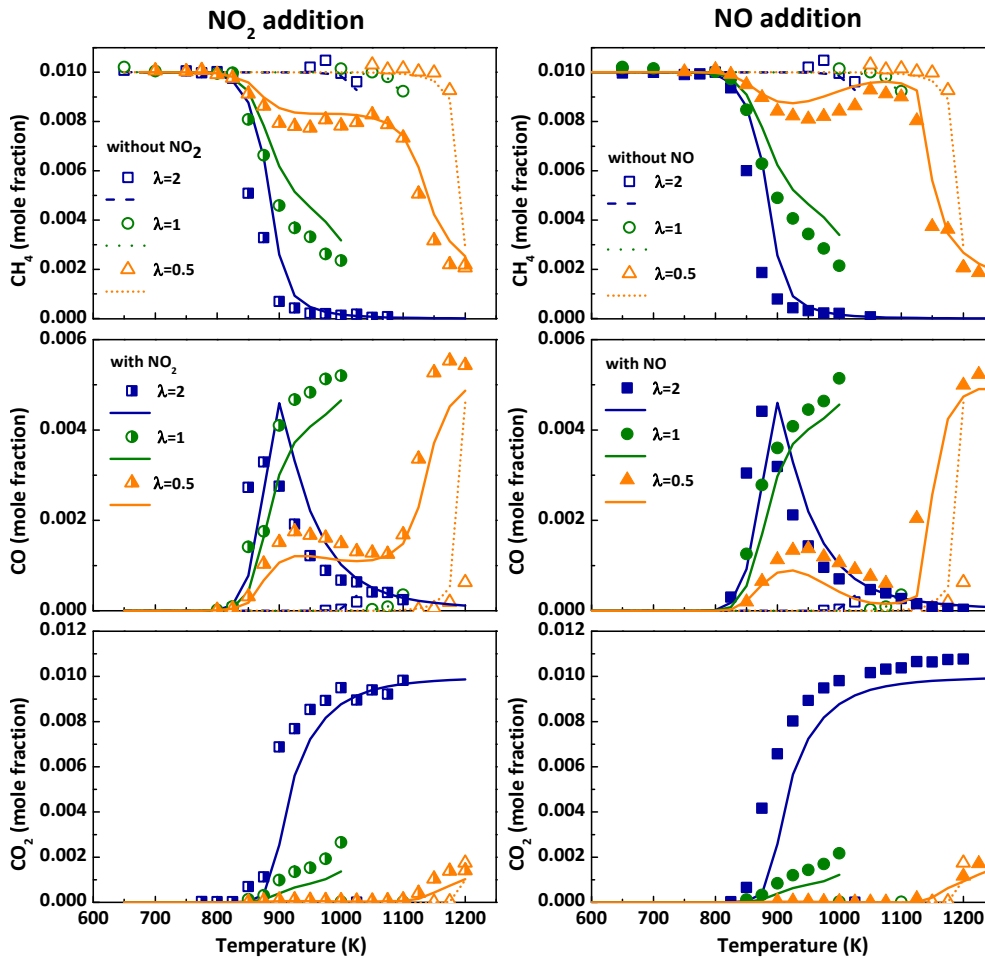


Figure 5.3. Evaluation of the effect of the NO_2 or NO presence on the jet-stirred oxidation of CH_4 , for the conditions denoted as 1JSR-6JSR and 8JSR-10JSR, in Table 5.2.

Figure 5.4 shows the evolution of NO_2 , NO and HCN concentration profiles as a function of temperature. In the presence of NO_2 (left), the conversion of NO_2 into NO is very similar, regardless the air excess ratio analyzed. At 800 K, the NO_2 concentration decreases while NO concentration increases until 900 K, when it attains a value of 300 ppm approximately, and then it remains constant. Only under reducing conditions ($\lambda = 0.5$) and temperatures above 1100 K, the NO concentration drops to 100 ppm, coinciding with the formation of HCN . On the other hand, in the presence of NO (right), the NO concentration remains almost constant, with the exception of the 800-900 K temperature range, when it decreases and NO_2 concentration increases. NO_2 concentration peaks at 850 K, which corresponds to the maximum NO consumption for all the air excess ratios analyzed. As in the case of NO_2 addition, under reducing conditions ($\lambda = 0.5$) and high temperatures (above 1100 K), the NO concentration decreases and HCN starts to be produced. The model captures well the experimental trends, with the biggest discrepancies between experimental and modeling

5. RESULTS AND DISCUSSION

calculations found in the NO concentration profile, in the 800-1000 K range, for the addition of NO₂.

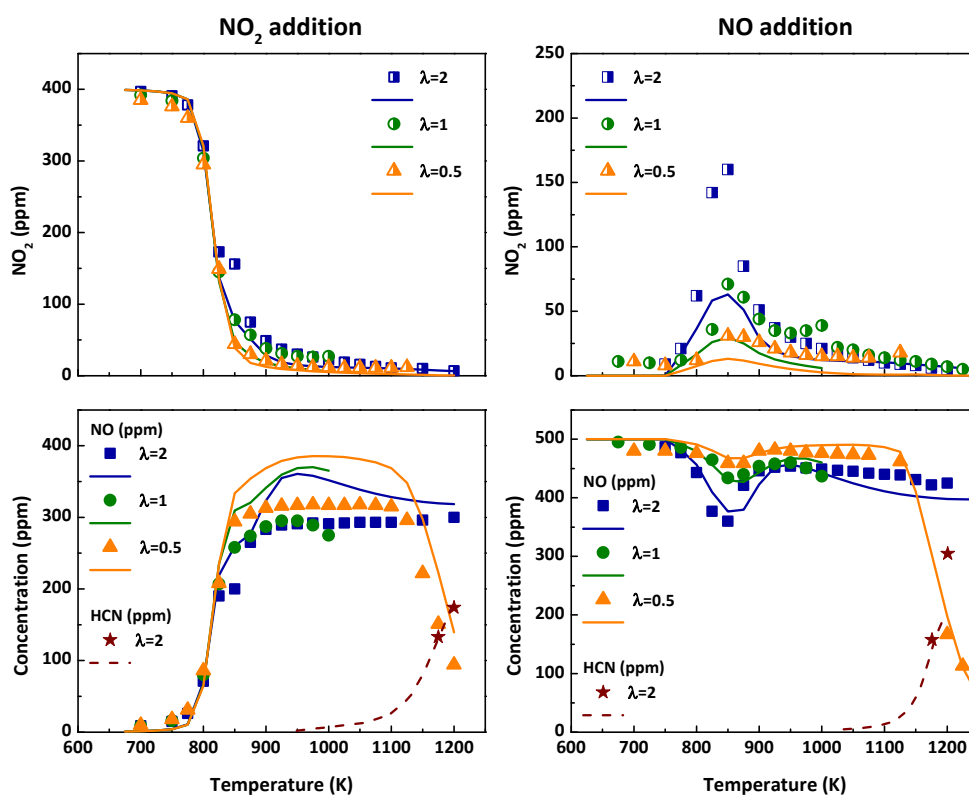
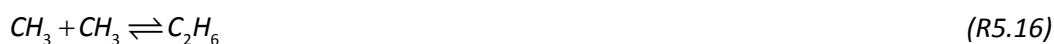


Figure 5.4. Evolution with temperature for NO₂, NO and HCN concentrations during the jet-stirred oxidation of CH₄ in the presence of NO_x, for the conditions denoted as 4JSR-6JSR and 8JSR-10JSR, in Table 5.2.

Regarding the possible detection and quantification of other nitrogen containing species, experimental results indicate that the maximum HONO concentration produced under the present conditions is below the estimated detection limit of 3 ppm. In the case of nitromethane (CH₃NO₂), no obvious FTIR absorption spectra have been observed. Therefore, the maximum CH₃NO₂ concentration produced is under 5 ppm, which is the FTIR estimated detection limit. The above-mentioned discrepancies between modeling and experimental results can be explained by the high modeling prediction of CH₃NO₂ formation in the 800-1000 K temperature range.

Reaction rate and sensitivity analyses have been performed to identify the main reaction routes and the most sensitive reactions for CH₄ consumption under the present conditions. Only the main results are discussed here, while a more complete description and a schematic diagram of the different reaction pathways occurring can be found in Paper VI (Figure 4).

In the absence of NO_x , the consumption of CH_4 proceeds through methyl radicals (CH_3), which react following four different routes represented by reactions R5.16-R5.19.



Both CH_3O and CH_3O_2 represent a source of CH_2O (R5.20 and R5.21), which reacts to produce formyl radicals (HCO) (R5.22), and finally CO (R5.23).



Under the present conditions, the similar behavior of NO and NO_2 promoting the oxidation of CH_4 is related to their exchange through reactions R5.24 and R5.25. The OH radicals produced during the NO - NO_2 exchanging cycle interact with CH_4 promoting its conversion ($\text{CH}_4 + \text{OH} \rightleftharpoons \text{CH}_3 + \text{H}_2\text{O}$), whereas the H and HO_2 radicals produced during the conversion of CH_4 (R5.20 and R5.23) promote the NO - NO_2 interconversion.



At high temperatures and reducing conditions, HCN is produced by means of well-known reburn type reactions of NO with hydrocarbon radicals (e.g. Bilbao et al., 1994; Glarborg et al., 1998; Miller et al., 2003).

5.2 HIGH-PRESSURE OXIDATION OF DIMETHYL ETHER AND ETHANOL AND THEIR INTERACTION WITH NO

DME and ethanol (C_2H_5OH , EtOH) are isomers, with the same molecular formula but a different functional group, ether and alcohol, respectively, what may imply different properties and different behavior during their oxidation. Therefore, in this section, the oxidation in a flow reactor of DME and ethanol at high pressure (20-60 bar), and for different air excess ratios (from reducing to oxidizing conditions), will be compared. The effect of the gas residence time and the presence of NO on the oxidation processes will be analyzed. The conditions of the oxidation experiments of DME and ethanol are detailed in Table 5.3 and Table 5.4, respectively; whereas the high-pressure experimental set-up used is described in Section 3.2. The main results are reported in Paper V, for DME, and Paper III, for ethanol, of the list of articles that are part of the compendium of publications.

Table 5.3. Matrix of experimental conditions of the high-pressure study of DME oxidation^a

DME oxidation at high pressure in a flow reactor						
T=450-1050 K						
Set	DME [ppm]	NO [ppm]	P [bar]	λ	t_r [s]	Flow rate [L (STP)/min]
1DME	700	-	20	0.7	5220/T	1
2DME	700	-	20	1	5220/T	1
3DME	700	-	20	35	5220/T	1
4DME	700	-	40	0.7	10440/T	1
5DME	700	-	40	1	10440/T	1
6DME	700	-	40	35	10440/T	1
7DME	700	-	60	0.7	15660/T	1
8DME	700	-	60	1	15660/T	1
9DME	700	-	60	35	15660/T	1
10DME	700	-	40	0.7	5220/T	2
11DME	700	-	40	1	5220/T	2
12DME	700	-	40	35	5220/T	2
13DME	700	500	20	0.7	5220/T	1
14DME	700	500	20	1	5220/T	1
15DME	700	500	20	35	5220/T	1
16DME	700	500	40	0.7	10440/T	1
17DME	700	500	40	1	10440/T	1
18DME	700	500	40	35	10440/T	1

Table 5.3. (continued)

19DME	700	500	60	0.7	15660/T	1
20DME	700	500	60	1	15660/T	1
21DME	700	500	60	35	15660/T	1

^aThe balance is closed with N₂.

Table 5.4. Matrix of experimental conditions of the high-pressure study of ethanol oxidation^a

Ethanol oxidation at high pressure in a flow reactor					
T=500-1100 K; Flow rate: 1 L (STP)/min; $t_r [s] = \frac{261 * P [\text{bar}]}{T [\text{K}]}$					
Set	Ethanol [ppm]	O ₂ [ppm]	NO [ppm]	λ	P [bar]
1EtOH	5000	10500	-	0.7	20
2EtOH	5000	10500	-	0.7	40
3EtOH	5000	10500	-	0.7	60
4EtOH	5000	15000	-	1	20
5EtOH	5000	15000	-	1	40
6EtOH	5000	15000	-	1	60
7EtOH	5000	60000	-	4	20
8EtOH	5000	60000	-	4	40
9EtOH	5000	60000	-	4	60
10EtOH	5000	10500	500	0.7	20
11EtOH	5000	10500	500	0.7	40
12EtOH	5000	10500	500	0.7	60
13EtOH	5000	15000	500	1	20
14EtOH	5000	15000	500	1	40
15EtOH	5000	15000	500	1	60
16EtOH	5000	60000	500	4	20
17EtOH	5000	60000	500	4	40
18EtOH	5000	60000	500	4	60

^aThe balance is closed with N₂.

5.2.1 Evaluation of the effect of gas residence time

Considering the experimental procedure followed in the high-pressure experimental set-up (Section 3.3), a change in the working pressure while maintaining constant the total gas flow rate, also implies a change in the residence time. That is, for a total flow rate of 1 L (STP)/min, the gas residence time in the reaction zone is given by equation 3.3 and depends on both temperature and pressure in this zone.

$$t_r[s] = \frac{261 * P[bar]}{T[K]} \quad (\text{Eq. 3.3})$$

Therefore, DME high-pressure oxidation experiments to distinguish between the effect of pressure or gas residence time have been carried out. To analyze the influence of the pressure, the total flow rate has been increased from 1 to 2 L (STP)/min, and the pressure from 20 to 40 bar. Thus, the gas residence time is $t_r[s]=5220/T[K]$ and only depends on the temperature. On the other hand, to analyze the influence of the gas residence time, the pressure has been kept constant at 40 bar, and the gas residence time has been changed from $t_r[s]=5220/T[K]$ to $t_r[s]=10440/T[K]$, by varying the flow rate from 2 to 1 L (STP)/min, respectively.

Figure 5.5 shows experimental results (symbols) and modeling calculations (lines) obtained in this way, for the different values of lambda analyzed. In general, there is a good agreement between experimental data and model predictions. For the same gas residence time and the different values of lambda analyzed, increasing the pressure from 20 to 40 bar does not seem to have a big effect on DME conversion. For the same pressure and $\lambda =0.7$ and $\lambda =1$, DME oxidation is favored by an increase in the gas residence time; whereas for $\lambda =35$ no big changes have been noticed. Under the conditions of the present study, the effect of gas residence time on DME high-pressure oxidation is clear and more noticeable than the effect of pressure.

In the case of the high-pressure oxidation of ethanol, an evaluation of the influence of pressure and gas residence time has also been carried out, but only from a modeling point of view. This evaluation can be found as Supplementary Material of the Paper III (Figure S1). Results indicate that both pressure and gas residence time had an appreciable impact on the ethanol oxidation process. Ethanol conversion is shifted to lower temperatures if any of these variables is increased.

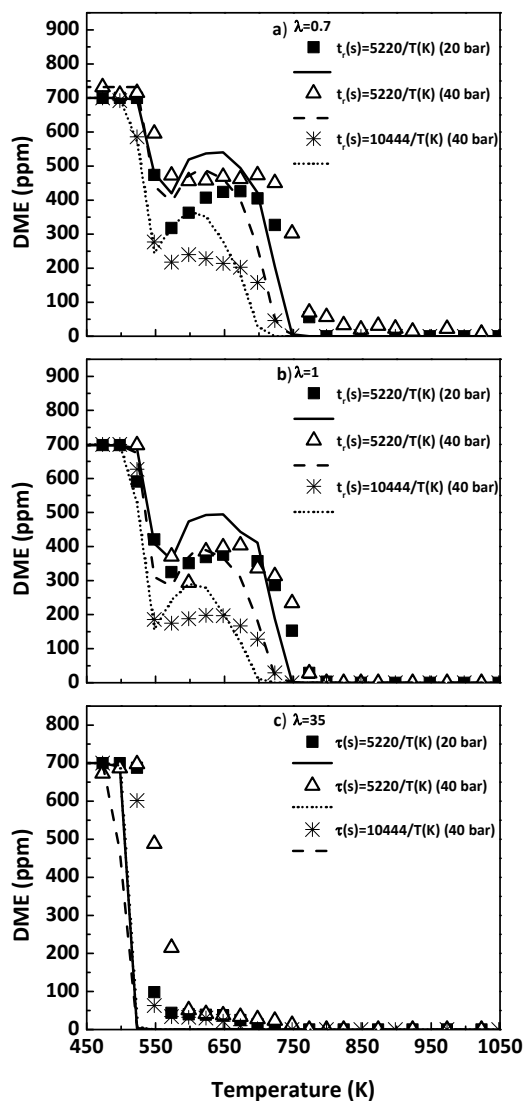


Figure 5.5. Evaluation of the effect of pressure and gas residence time on the high-pressure (20 or 40 bar) oxidation of DME, for the conditions denoted as sets (a) 1DME, 10DME and 4DME; (b) 2DME, 11DME and 5DME; (c) 3DME, 12DME and 6DME, in Table 5.3.

5.2.2 High-pressure oxidation of DME and ethanol in the absence of NO

Figure 5.6 shows a comparison of the influence of the air excess ratio on the DME and ethanol concentration profiles during their high-pressure (20 bar) oxidation. Different values of lambda have been analyzed, from reducing ($\lambda = 0.7$) to oxidizing ($\lambda = 35$ for DME and $\lambda = 4$ for ethanol) through stoichiometric ($\lambda = 1$) conditions. For oxidizing conditions, the difference in the value of λ studied is due to experimental limitations, because of the high ethanol concentration that has been tested. The results for the rest of conditions that are not shown in

5. RESULTS AND DISCUSSION

this section can be found in Paper V, for DME, and Paper III, for ethanol. In general, there is a good agreement between experimental and modeling calculations for both compounds.

Although DME and ethanol are isomers (C_2H_6O), their oxidation behavior is completely different as can be seen in Figure 5.6. During DME conversion, in the 550-700 K temperature range, there is a zone where DME concentration increases with temperature. It corresponds to the negative temperature coefficient (NTC) zone, where DME reactivity is constant or decreases with temperature. This is a distinctive feature of the low-temperature oxidation of hydrocarbons as discussed by Herbinet and Battin-Leclerc (2014). The NTC behavior is observed for all the conditions analyzed, although is less pronounced under very oxidizing conditions ($\lambda = 35$), because the high oxygen availability causes DME to be completely consumed at lower temperatures.

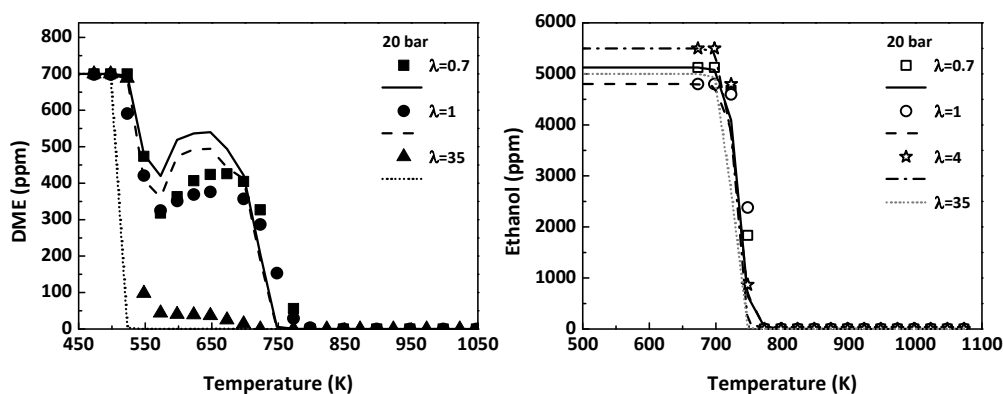


Figure 5.6. Influence of the air excess ratio on the DME (left) and ethanol (right) concentration profiles, as a function of temperature, for the conditions denoted as 1DME-3DME, in Table 5.3 and 1EtOH, 4EtOH and 7EtOH, in Table 5.4.

In the case of ethanol oxidation, the oxygen availability in the reactant mixture does not modify significantly the temperature for the onset of ethanol conversion at a constant pressure (20 bar). In a previous ethanol oxidation study at atmospheric-pressure in a flow reactor (Alzueta and Hernández, 2002), the ethanol oxidation happened at lower temperatures for very oxidizing conditions ($\lambda = 35$), and only small differences were found between $\lambda = 0.7$ and $\lambda = 1$. Therefore, given the little influence found for $\lambda = 1$ and 4, as seen in Figure 5.6 (right), in order to further evaluate the influence of the air excess ratio on ethanol oxidation, model calculations for $\lambda = 35$ have been carried out (Figure 5.6). The theoretical results obtained are almost the same than those for $\lambda = 4$. So, it can be deduced that for the high-pressure conditions studied in this work, there is almost no influence of the oxygen availability on the onset temperature for ethanol oxidation.

On the other hand, Figure 5.7 shows a comparison of the influence of the change in the working pressure, for stoichiometric conditions ($\lambda = 1$), on the DME and ethanol concentration profiles during their high-pressure oxidation. For DME, an increase in the pressure does not have a significant impact on the onset temperature for its conversion. However, as the pressure is increased, the DME consumption occurs at lower temperatures, and the reactivity of DME is favored in the NTC zone; that is, for the same temperature, a higher DME conversion is achieved by increasing the pressure from 20 to 40 bar. In the case of ethanol, its oxidation starts at lower temperatures as the pressure is increased, approximately 100 K when moving from 20 to 60 bar.

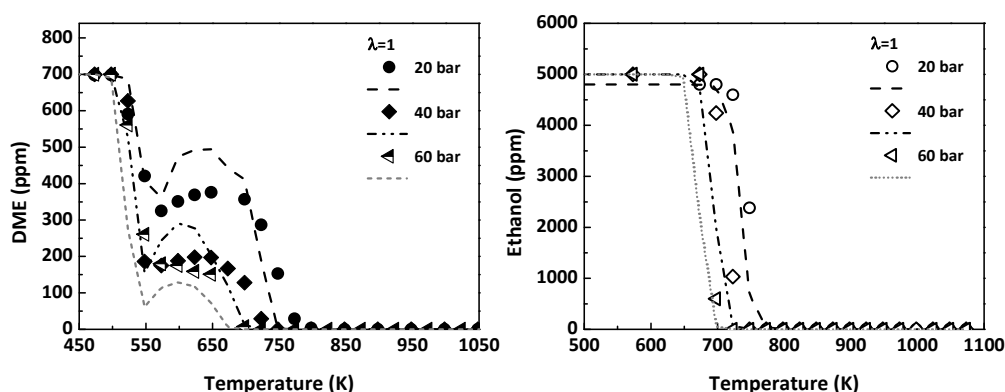


Figure 5.7. Influence of the pressure change on the DME (left) and ethanol (right) concentration profiles, as a function of temperature, for the conditions denoted as 2DME, 5DME and 8DME, in Table 5.3, and 4EtOH-6EtOH, in Table 5.4.

The main products obtained during the oxidation of each oxygenate are also different. In the case of DME, CO, CO₂, CH₄, HCOOH and H₂ have been detected; whereas during ethanol oxidation, besides CO, CO₂, CH₄, and H₂, species such as C₂H₄, CH₃OH and acetaldehyde (CH₃CHO) have been quantified.

The differences found during the high-pressure oxidation of DME and ethanol, such as the NTC zone or the different products detected, can be explained by the analysis of the main reaction pathways occurring during their consumption. Only the main reaction routes are described here, while more complete descriptions and schematic diagrams can be found in Paper V (for DME) and Paper III (for ethanol).

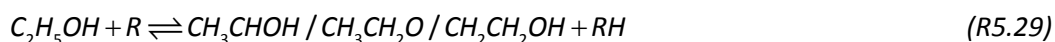
Ethanol consumption is initiated by its thermal dehydration to ethylene (R5.26), as this later has been detected by gas chromatography, and also by its thermal decomposition (R5.27). For example, for 20 bar and $\lambda = 0.7$, at 725 K, 86% of the ethanol consumption is produced through reaction R5.27. This fact could explain the almost negligible effect of the

5. RESULTS AND DISCUSSION

oxygen availability on the temperature for the onset of ethanol consumption. Alternatively, DME consumption is initiated by the abstraction of an H-atom from DME by oxygen molecules to form the CH_3OCH_2 radical (R5.28).



Once the consumption of DME and ethanol has been initiated, it continues, for both compounds, through hydrogen abstraction reactions by radicals (R: O, H, OH, CH_3 or HO_2). In the case of ethanol, the H-abstraction may occur on three different sites, leading to the formation of three different $\text{C}_2\text{H}_5\text{O}$ isomers (R5.29), although CH_3CHOH is the radical dominant under the present conditions; whereas for DME, it can only occur on one side leading to the formation of CH_3OCH_2 radical (R5.30), as in the case of the abstraction by molecular oxygen (R5.28).



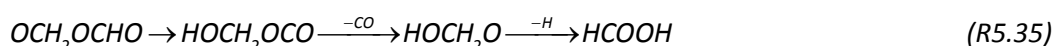
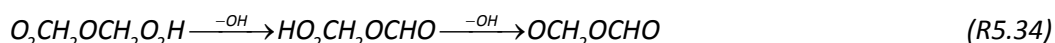
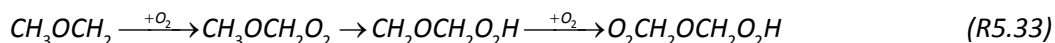
Under the present high-pressure conditions, HO_2 radicals may have a big relevance as in the case of ethanol. The hydroxymethyl radical (CH_2OH) formed through reaction R5.27 reacts with molecular oxygen to produce formaldehyde and HO_2 radicals (R5.31) which participate in reaction R5.29 producing CH_3CHOH radical.



Radicals from ethanol and DME (CH_3CHOH and CH_3OCH_2 , respectively) continue reacting, but in a completely different way. In the case of ethanol, CH_3CHOH radical reacts with molecular oxygen (R5.32) forming acetaldehyde (CH_3CHO), which has been detected by gas chromatography. Acetaldehyde interacts with the radical pool producing acetyl radical (CH_3CO), which thermally decomposes to CO and CH_3 radicals.



On the other hand, CH_3OCH_2 radicals produced from the consumption of DME, are involved in a more complex mechanism that includes two O_2 additions and several isomerizations and decompositions. The main reactions implicated in this mechanism are represented schematically by reaction sequences R5.33-R5.35, although a full description and a reaction pathways diagram can be found in Paper V.



During this complex reaction mechanism (R5.33-R5.35), OH radicals are released, which are responsible for the high reactivity of DME at low temperatures (R5.30). As temperature increases, β -scission of the $\text{CH}_2\text{OCH}_2\text{O}_2\text{H}$ radical forming 2 molecules of formaldehyde and only one reactive OH radical (R5.36) becomes more relevant and, therefore, the DME reactivity decreases (less formation of OH radicals) and the NTC zone appears. For example, at 20 bar and $\lambda = 1$, reaction R5.36 at 525 K represents a 6% of the $\text{CH}_2\text{OCH}_2\text{O}_2\text{H}$ radical total consumption; whereas at 600 K, it represents a 53% and at 700 K, a 94%.



Another β -scission reaction with increasing relevance with temperature is the decomposition of CH_3OCH_2 radical (R5.37). This decomposition is almost negligible at 600 K, it represents a 20% of radical consumption at 700 K and a 53% at 750 K, under the same conditions above specified (20 bar and $\lambda = 1$).



5.2.3 Influence of the presence of NO on the high-pressure oxidation of DME and ethanol

The influence of NO presence (500 ppm, approximately) on the high-pressure oxidation of DME and ethanol has been analyzed for reducing ($\lambda = 0.7$), stoichiometric ($\lambda = 1$) and oxidizing ($\lambda = 35$ for DME and $\lambda = 4$ for ethanol) conditions. Only the results obtained for

5. RESULTS AND DISCUSSION

$\lambda = 1$ are shown in Figure 5.8. The results for the rest of conditions can be found in Paper V, for DME, and Paper III, for ethanol.

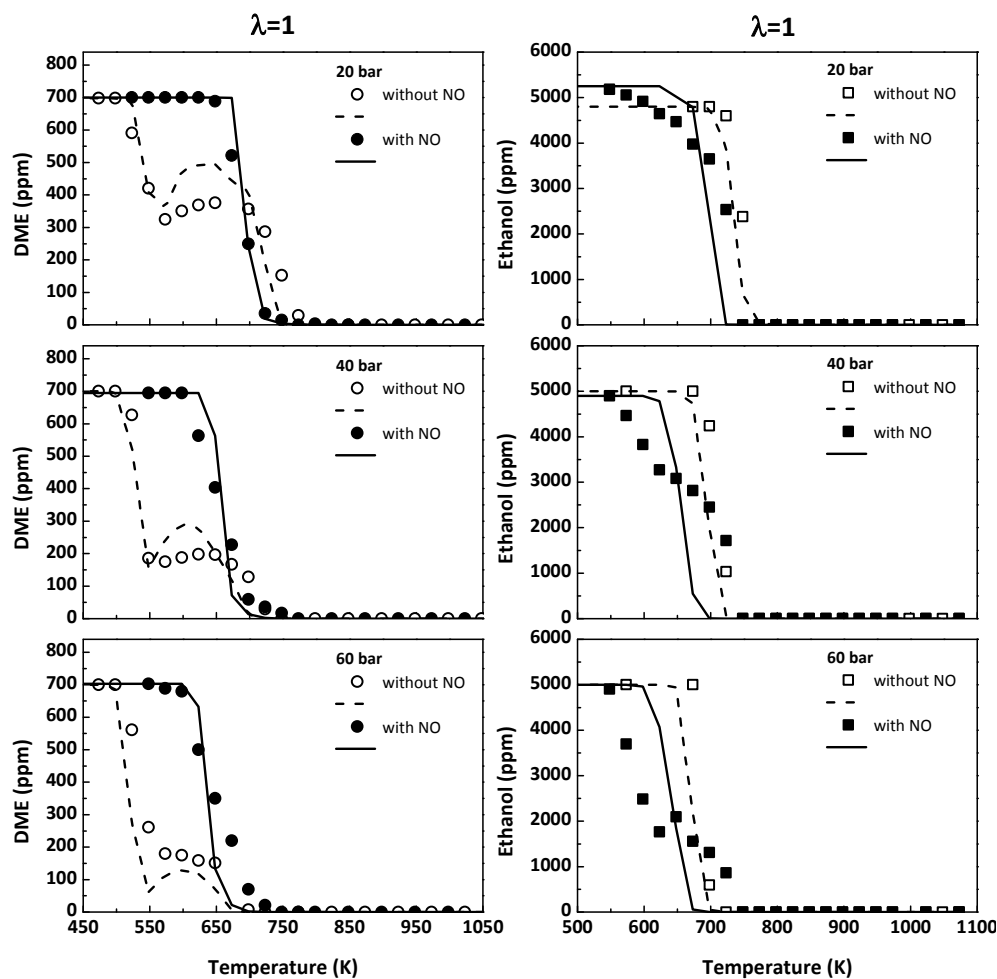


Figure 5.8. Evaluation of the effect of NO presence on the high-pressure oxidation of DME (left) and ethanol (right), for the conditions denoted as sets 2DME, 5DME, 8DME, 14DME, 17DME and 20DME, in Table 5.3 and 4EtOH-6EtOH and 13EtOH-15EtOH, in Table 5.4.

The presence of NO in the reactant mixture has a completely different effect on the high-pressure oxidation of each isomer. While the presence of NO clearly inhibits DME oxidation at low temperatures, in the 550-700 K range, where the NTC zone was previously observed in the absence of NO; the presence of NO promotes ethanol oxidation shifting the onset for ethanol consumption to lower temperatures, and the higher the pressure, the lower the temperature at which ethanol conversion occurs.

Under the present experimental conditions, and as reported while studying the high-pressure oxidation of MF (Section 5.1.1), it has been observed that NO added to the reactant

mixture can be converted to NO_2 before entering the reactor, because of the high-pressure conditions and the presence of O_2 , through reaction R5.11.



Both in the presence or absence of NO, the main consumption route for DME is through H-abstraction reactions forming CH_3OCH_2 radical (R5.30), which can continue the mechanism above described reacting with molecular oxygen to produce $\text{CH}_3\text{OCH}_2\text{O}_2$ radicals (see reaction sequence R5.33). However, a new reaction route involving NO and NO_2 is in competition with the O_2 addition: CH_3OCH_2 radical can react with NO_2 leading to the formation of a new radical $\text{CH}_3\text{OCH}_2\text{O}$ and NO (R5.38). This new radical can also be produced by reaction of $\text{CH}_3\text{OCH}_2\text{O}_2$ and NO (R5.39) and, finally, it decomposes to form methoxy radicals (CH_3O) and formaldehyde (CH_2O) (R5.40).



In conclusion, the presence of NO has an inhibiting effect on DME high-pressure oxidation at low temperatures, because of the competition between $\text{CH}_3\text{OCH}_2 + \text{O}_2$ and $\text{CH}_3\text{OCH}_2 + \text{NO}_2$ reactions and the participation of NO in reaction R5.39, preventing $\text{CH}_3\text{OCH}_2\text{O}_2$ radicals to continue reacting through the complex mechanism (R5.33-R5.35) during which highly reactive OH radicals are generated.

On the other hand, the promoting effect of NO presence on ethanol high-pressure oxidation can be explained by the increased relevance of the interactions of CH_3 radicals and NO_2 (from the conversion of NO to NO_2) through reactions R5.41 and R5.42, and the increased concentration of OH radicals from the interaction of NO_2 and water (R5.43) and the decomposition of HONO (R5.15).





5.3 HIGH-PRESSURE OXIDATION OF DIMETHOXYMETHANE

Poly(oxymethylene) dimethyl ether (POMDMEs) are polyethers with the general molecular formula $CH_3O(CH_2O)_nCH_3$, which are considered as attractive diesel additives or substitutes (Burger et al., 2010). Both, DME (with $n=0$) and DMM (with $n=1$), are POMDMEs, they have the same functional group but different number of carbons.

Therefore, in this section, the high-pressure oxidation of DMM in a flow reactor is shown, together with a comparison with DME oxidation. In the case of DME, the results shown in the previous section (Section 5.2) will be used, and the results for the rest of conditions can be found in Paper V. On the other hand, in the case of DMM, before addressing the main results obtained during its high-pressure oxidation (Paper II), a study of DMM oxidation under atmospheric-pressure conditions has been carried out (Paper I), as traditionally has been done by our research group.

5.3.1 Atmospheric-pressure oxidation of DMM in a flow reactor

Different DMM oxidation experiments have been carried in an atmospheric pressure gas-phase installation (complete description in Section 3.1), in the 573-1373 K temperature range, for different air/fuel ratios, from pyrolysis to fuel-lean conditions ($\lambda = 0, 0.4, 0.7, 1$ and 35). Table 5.5 summarizes the conditions of the different experiments that have been performed. In this section, a discussion of the main results obtained is addressed. A more complete discussion can be found in Paper I of the compendium of publications.

An example of the repeatability of the experiments of DMM oxidation at atmospheric pressure, under reducing ($\lambda = 0.7$) and very oxidizing conditions ($\lambda = 35$) is represented in the left side of Figure 5.9. As it can be seen, the experimental data show a good repeatability.

Table 5.5. Matrix of experimental conditions of the atmospheric-pressure study of DMM oxidation^a

DMM oxidation at atmospheric pressure in a flow reactor				
$T=573\text{-}1373\text{ K}; P=1\text{ atm}; \text{Flow rate: } 1\text{ L (STP)/min}; t, [s] = \frac{195}{T[K]}$				
Set	DMM [ppm]	O ₂ [ppm]	H ₂ O [ppm]	λ
1DMM _{at}	700	0	7000	0
2DMM _{at}	700	1120	7000	0.4
3DMM _{at}	700	1960	7000	0.7
4DMM _{at}	700	2800	7000	1
5DMM _{at}	700	98000	7000	35

^aThe balance is closed with N₂.

On the right side of the Figure 5.9, the experimental data and modeling results of DMM consumption are shown as a function of temperature and for the different values of λ analyzed. Modeling predictions have been recalculated with the final mechanism obtained in the present thesis (as explained in Chapter 4). A comparison of modeling calculations obtained with this final mechanism and with the mechanism used during the atmospheric-pressure oxidation study of DMM (Paper I) is also shown in Figure 5.9. As it can be seen, theoretical concentrations predicted by the final mechanism are slightly shifted to lower temperatures. Nonetheless, both mechanisms are able to satisfactorily reproduce the major trends experimentally observed.

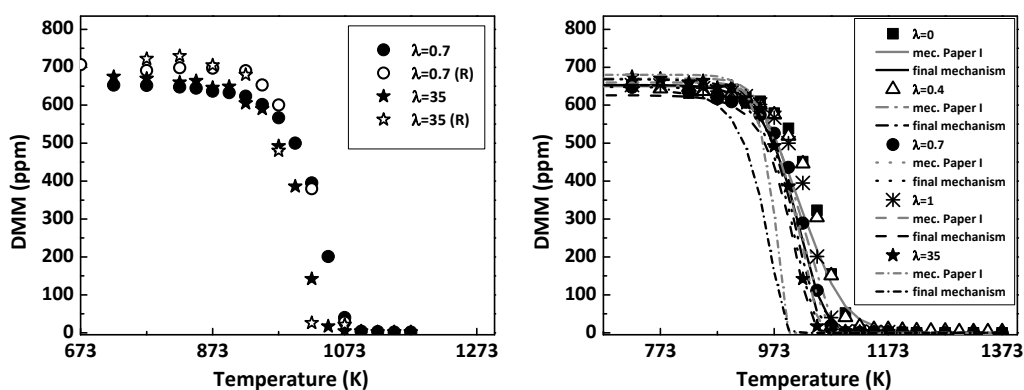


Figure 5.9. Example of repeatability of the DMM oxidation experiments at atmospheric pressure (left). Influence of the air excess ratio on the DMM concentration profile, as a function of temperature, for the conditions denoted as sets 1DMM_{at}-5DMM_{at}, in Table 5.5 (right).

DMM consumption occurs in the 973-1123 K temperature range. The temperature for the onset of DMM conversion is almost independent of the value of λ analyzed. Thus, it can be said that oxygen concentration in the reactant mixture slightly influences the conversion of DMM. Moreover, DMM is completely consumed for all the conditions studied at temperatures above 1123 K, independently of the oxygen availability.

Figure 5.10 shows the influence of the air excess ratio on the concentration profiles of the different products quantified during the oxidation of DMM at atmospheric pressure. For a better clarity of the results, only modeling calculations obtained with the mechanism used during the atmospheric oxidation study of DMM are shown, with the exception of methanol (CH_3OH). For CH_3OH , the concentrations predicted by the final mechanism are also included because of the clear improvement in modeling predictions achieved. In the case of the other compounds, modeling calculations obtained with both mechanisms are almost the same. In general, the mechanism is able to reproduce the main trends experimentally observed, with the main exception of MF.

The main products that have been quantified during the atmospheric oxidation of DMM are: CO , CO_2 , H_2 , CH_3OH , MF, CH_4 and different C_2 species: C_2H_6 , C_2H_4 and C_2H_2 . The presence of oxygen does have certain effects on some of the reaction products, which are described here. The onset for the formation of CO occurs approximately at the same temperature as the DMM starts to be consumed. When the temperature increases, the CO concentration increases as well, reaching a maximum value. As the air excess ratio increases, the temperature for this maximum CO concentration is slightly shifted towards lower temperatures, and also the width of the CO peak is narrower. The oxygen availability also influences the oxidation of CO to CO_2 . While under pyrolysis ($\lambda = 0$) and very reducing conditions ($\lambda = 0.4$), CO_2 is hardly formed; under reducing conditions ($\lambda = 0.7$), an appreciable amount of CO_2 is produced, which coexists with a not negligible amount of CO ; and for stoichiometric ($\lambda = 1$) and oxidizing conditions ($\lambda = 35$), CO is completely oxidized to CO_2 . Regarding H_2 production, the general trend is the opposite to the CO_2 case. The biggest concentration of H_2 is reached for pyrolysis conditions and the lowest one for oxidizing conditions. The H_2 concentration profile presents a maximum as a function of temperature; beyond it begins to drop to zero (stoichiometric and oxidizing conditions) or to an almost constant value (reducing and very reducing conditions). The only case where H_2 continues growing is in the absence of oxygen. In the case of CH_3OH , MF, CH_4 , C_2H_6 , C_2H_4 and C_2H_2 , all of these compounds reach a maximum concentration, which is shifted to lower temperatures when the reactant mixture becomes fuel-leaner.

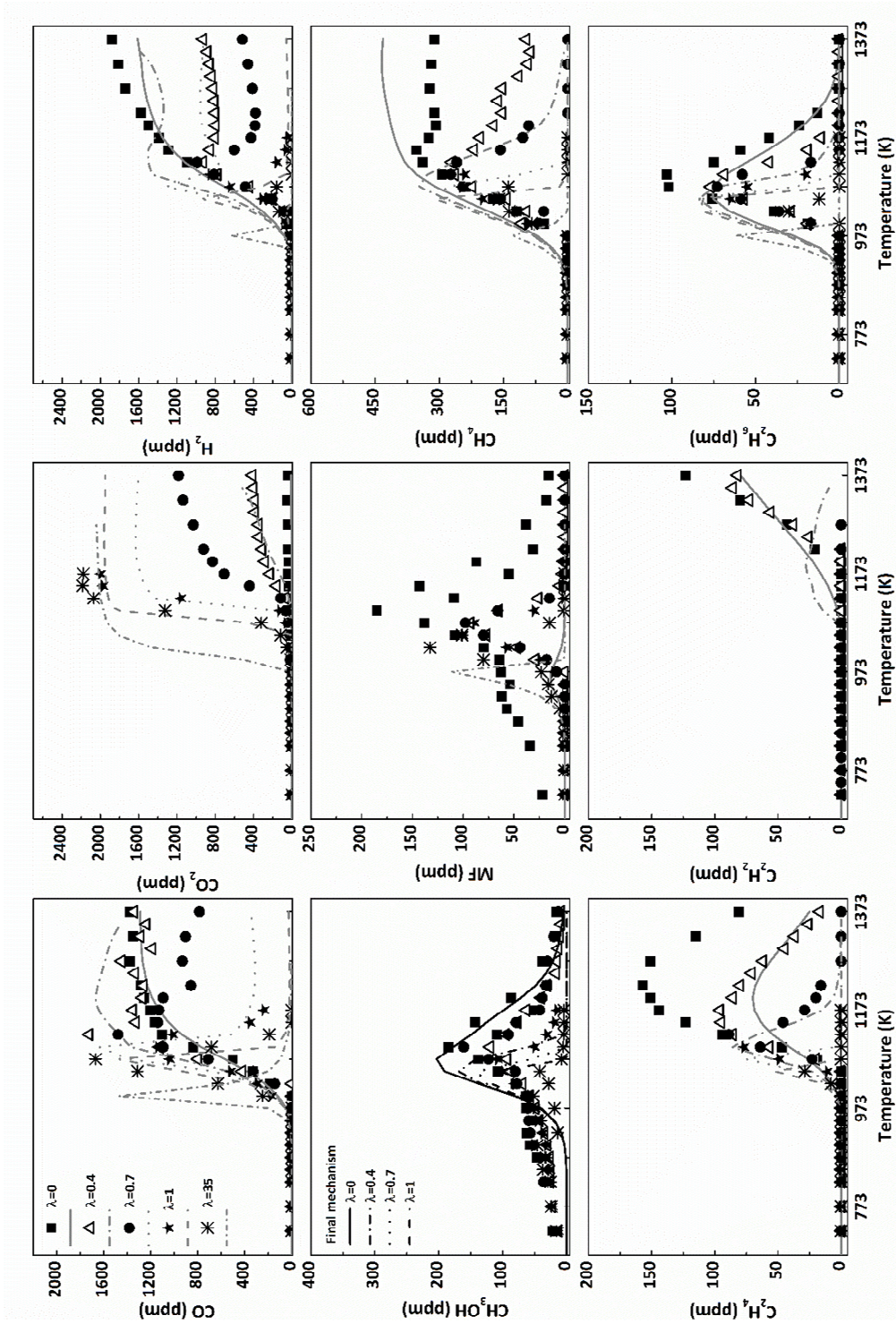


Figure 5.10. Influence of the air excess ratio on the concentration profile of the products from DMIM oxidation, as a function of temperature, for the conditions denoted as sets 1DMM_{air}-5DMM_{air}, in Table 5.5.

5. RESULTS AND DISCUSSION

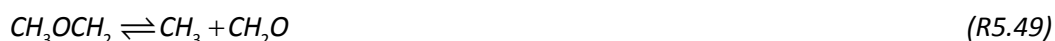
The formation of the different products, quantified during the DMM atmospheric oxidation, can be explained by the analysis of the main reaction routes occurring under the present conditions. DMM conversion is initiated by decomposition reactions (R5.44 and R5.45), even though its main consumption channel is by H-abstraction reactions by radicals (O, H, OH, CH₃) to obtain the primary radical (CH₃OCH₂OCH₂) or the secondary radical (CH₃OCHOCH₃).



Both DMM radicals, CH₃OCH₂OCH₂ and CH₃OCHOCH₃, may decompose through reactions R5.46 and R5.47.



The CH₃OCH₂O and the CH₃OCH₂ radicals generated in reactions R5.44 and R5.46 respectively, totally decompose to form MF (R5.48) and CH₃+CH₂O (R5.49).



Methyl formate obtained in reaction R5.48 is mainly consumed by reaction R5.50 producing CH₃OH, which produces hydroxymethyl radicals (CH₂OH) by H-abstraction reactions by O, OH or HO₂ radicals. Hydroxymethyl radicals mainly react with molecular oxygen to give CH₂O which continues the reaction sequence R5.51 until CO and CO₂ as final products. The formation of CH₄ is also possible from CH₂O (R5.52).



These reaction routes can explain the pattern for the maximum concentration, for MF, CH₃OH and CH₄, observed in Figure 5.10, for pyrolysis conditions, which increase in this order: first MF is obtained, later CH₃OH is formed from MF and, finally, CH₄ can be produced from CH₂O (obtained from CH₃OH).

On the other hand, self-reaction of methyl radicals (CH₃), obtained in many of the above described reactions, leads to the formation of ethane (C₂H₆), which reacts to produce ethylene (C₂H₄), and this last one produces acetylene (C₂H₂) as final product. For this reason, the order, in which the maximum concentration of these species appear is: C₂H₆, C₂H₄ and C₂H₂, from the lowest to the highest temperature (Figure 5.10).

5.3.2 High-pressure oxidation of DMM in a flow reactor

Once the atmospheric-pressure oxidation of DMM has been studied, and a chemical kinetic mechanism able to reproduce the experimental trends has been validated, the next step is to study its oxidation under high-pressure conditions. As has been mentioned, also the oxidation of DME and DMM in a flow reactor at high-pressure (20-60 bar), and for different air excess ratios, will be compared.

Table 5.6 lists the conditions of the different DMM experiments performed at high-pressure. In the case of DME, the experimental conditions are detailed in Table 5.3 (Section 5.2), and the results shown in the previous section (Section 5.2) will be used for the comparison.

Table 5.6. Matrix of experimental conditions of the high-pressure study of DMM oxidation^a

DMM oxidation at high pressure in a flow reactor				
T=373-1073 K; Flow rate: 1 L (STP)/min; t_r [s] = $\frac{261 * P[\text{bar}]}{T[\text{K}]}$				
Set	DMM [ppm]	O₂ [ppm]	λ	P (bar)
1DMM _{HP}	700	1960	0.7	20
2DMM _{HP}	700	1960	0.7	40
3DMM _{HP}	700	1960	0.7	60
4DMM _{HP}	700	2800	1	20
5DMM _{HP}	700	2800	1	40
6DMM _{HP}	700	2800	1	60
7DMM _{HP}	700	56000	20	20

5. RESULTS AND DISCUSSION

Table 5.6. (continued)

8DMM _{HP}	700	56000	20	40
9DMM _{HP}	700	56000	20	60

^aThe balance is closed with N₂.

An example of the repeatability of the experiments of DMM oxidation at high pressure (20 bar), under stoichiometric conditions ($\lambda = 1$) and oxidizing conditions ($\lambda = 20$), is represented in Figure 5.11. As it can be seen, the experimental data show a good repeatability.

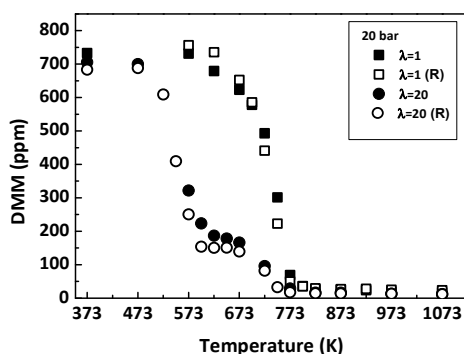


Figure 5.11. Example of repeatability of the DMM oxidation experiments at high pressure for the conditions denoted as sets 4DMM_{HP} and 7DMM_{HP}, in Table 5.6.

Figure 5.12 shows the DMM concentration results obtained during its high-pressure oxidation for the different pressures (20-60 bar) and air excess ratios ($\lambda = 0.7, 1$ and 20) analyzed. The concentration results for the main products quantified (CO, CO₂, CH₂O, CH₃OCHO and CH₄) can be found in Paper II. Experimental results (symbols) are compared against modeling calculations (lines) obtained with the mechanism used during the high-pressure oxidation study of DMM after the modifications described in Section 4.2 (mec. Paper II). In general, there is a good agreement between experimental results and modeling calculations with the suggested mechanism.

Furthermore, as previously reported, in the case of DMM high-pressure oxidation, modeling predictions have also been recalculated with the final mechanism obtained in the present thesis (as explained in Chapter 4). A comparison of modeling calculations obtained with this final mechanism and with the mechanism used during the high-pressure oxidation of DMM (Paper II) is also shown in Figure 5.12.

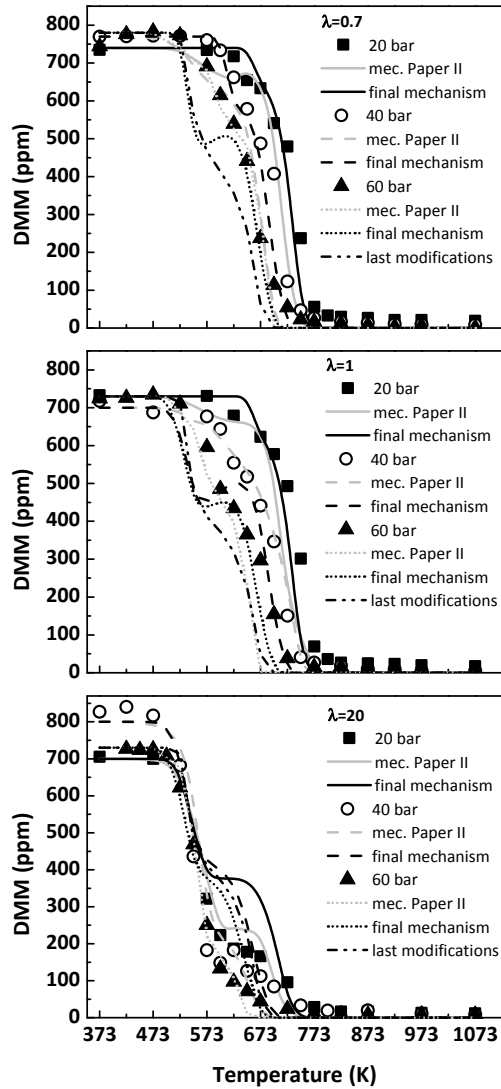


Figure 5.12. Influence of pressure and air excess ratio on the DMM concentration profile, as a function of temperature, for the conditions denoted as sets 1DMM_{HP}-9DMM_{HP}, in Table 5.6.

For reducing conditions ($\lambda = 0.7$), 20 and 40 bar, and for stoichiometric conditions ($\lambda = 1$), 20 bar, theoretical calculations with the final mechanism are in a slightly better agreement with experimental results. However, for $\lambda = 0.7$ and 60 bar, and $\lambda = 1$, 40 and 60 bar, at low temperatures, the final mechanism predicts an increased reactivity of DMM and a curve appears in modeling results, which appears to be an artifact of the model. It is mainly due to the modifications made to the DME reaction subset (Section 4.4). During the high-pressure oxidation study of DMM, for oxidizing conditions, a plateau in the DMM concentration profile has been observed. This zone seems to be associated with the peroxy intermediate, $\text{CH}_3\text{OCH}_2\text{O}_2$, whose formation and consumption reactions appear to be important for the description of DMM conversion under high-pressure and high-oxygen concentration conditions. Therefore, reactions involving this peroxy intermediate have been included in

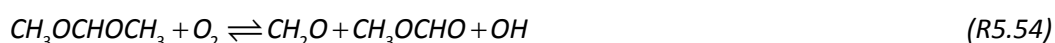
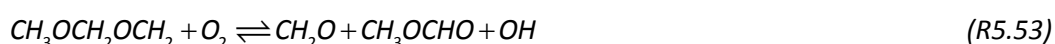
5. RESULTS AND DISCUSSION

DMM reaction subset (Table 4.1). On the other hand, this peroxy species seems to be also an important intermediate during the high-pressure conversion of DME, and some of the modifications that have been made to DME reaction subset (Table 4.2) include reactions involving $\text{CH}_3\text{OCH}_2\text{O}_2$. In conclusion, when recalculating modeling predictions with the final mechanism, during DMM high-pressure consumption an increased reactivity of DMM is predicted at low temperatures.

Attempts to improve modeling calculations have been made according to recent experimental and modeling studies on DMM pyrolysis and oxidation. Kopp et al. (2018) have studied the kinetics and the thermochemistry of DMM using *ab initio* and statistical mechanics methods. Furthermore, Vermeire et al. (2018) have performed an experimental and modeling study on the pyrolysis and oxidation of DMM in a jet-stirred reactor. An example of modeling predictions obtained after these modifications is shown in Figure 5.12, for 60 bar and the different values of lambda (last modifications). The DMM reactivity is still overpredicted and, in general, no big improvements are achieved. Although it is not shown, modeling predictions for DMM during its oxidation at atmospheric pressure have been also recalculated with this last modified mechanism, and modeling predictions are considerable worst. Therefore, those modifications have been rejected.

Slight differences are noticed in DMM concentration results when working under stoichiometric or somewhat fuel-rich conditions, although the DMM conversion is a bit different for oxidizing conditions. Moreover, working at 20, 40 and 60 bar does not have a big effect on neither the oxidation of DMM nor on the formation of the main products.

As in the case of DMM oxidation at atmospheric pressure, under high-pressure conditions, the main consumption of DMM is through H-abstraction reactions to form $\text{CH}_3\text{OCH}_2\text{OCH}_2$ and $\text{CH}_3\text{OCHOCH}_3$ radicals, specially by OH radicals. Under the present conditions, methyl formate plays an important role during DMM conversion. Both DMM radicals, $\text{CH}_3\text{OCH}_2\text{OCH}_2$ and $\text{CH}_3\text{OCHOCH}_3$, react with molecular oxygen to give MF and CH_2O as main products (R5.53 and R5.54). MF continues its conversion through the reactions detailed in Section 5.1.1 (R5.3-R5.10); whereas CH_2O continues the reaction sequence represented in reaction R5.51 until CO and CO_2 as final products.





Under oxidizing conditions, a new reaction path, involving the peroxy intermediate $CH_3OCH_2O_2$, becomes relevant. This peroxy species is also an intermediate during the oxidation of DME, and follows, in the case of DMM, almost the same reaction mechanism previously described in Section 5.2.2 during the high-pressure oxidation of DME in the absence of NO.

Once DMM high-pressure oxidation has been characterized, the results obtained can be compared with those obtained during the high-pressure oxidation of the other ether analyzed, DME (see Figure 5.6 and Figure 5.7). As it can be seen, the concentration profile obtained for each compound is completely different. While for DME the NTC zone has been observed for all the conditions analyzed (although is less pronounced for $\lambda = 35$), during the oxidation of DMM, only under very oxidizing conditions, a “plateau” where the DMM concentration remains almost constant has been observed in the 598-673 K temperature range. Furthermore, DME seems to be more reactive than DMM at low temperatures, although finally they are completely consumed at almost the same temperatures.

5.4 HIGH-PRESSURE OXIDATION OF ACETYLENE-OXYGENATED COMPOUND MIXTURES IN A FLOW REACTOR

Finally, once the oxidation of the different oxygenated compounds selected in this thesis for their study has been individually characterized, first at atmospheric and after at high pressure, in this section, the role as fuel additives of the oxygenates will be analyzed. It will be done by performing oxidation experiments of their mixtures with acetylene under high-pressure conditions, more representative of the real operating conditions. In this work, acetylene (C_2H_2) has been selected as the main fuel since it is considered as an important soot precursor, and also an intermediate species in the combustion of higher hydrocarbons (Frenklach, 2002; Giménez-López et al., 2016).

5.4.1 High-pressure oxidation of acetylene-ethanol mixtures

An experimental and modeling study of the oxidation of acetylene-ethanol (C_2H_2 - C_2H_5OH) mixtures under high-pressure conditions (10-40 bar) has been carried out, in the 575-1075 K temperature range, in a plug-flow reactor. The influence on the oxidation process of the oxygen inlet concentration (determined by the air excess ratio, λ) and the amount of

5. RESULTS AND DISCUSSION

ethanol (0-200 ppm) present in the reactant mixture has also been evaluated. The conditions of these experiments are detailed in Table 5.7, and the experimental set-up used is described in Section 3.2.

Table 5.7. Matrix of experimental conditions of the high-pressure study of C₂H₂-C₂H₅OH mixtures oxidation^a

C₂H₂-C₂H₅OH mixtures oxidation at high pressure in a flow reactor					
T=575-1075 K; Flow rate: 1 L (STP)/min; $t_r [s] = \frac{261 * P [\text{bar}]}{T [\text{K}]}$					
Set	C₂H₂ [ppm]	C₂H₅OH [ppm]	O₂ [ppm]	P (bar)	λ
1EtOHmix	500	-	1250	10	1
2EtOHmix	500	50	980	10	0.7
3EtOHmix	500	50	1400	10	1
4EtOHmix	500	50	28000	10	20
5EtOHmix	500	50	1400	20	1
6EtOHmix	500	50	980	40	0.7
7EtOHmix	500	50	1400	40	1
8EtOHmix	500	50	28000	40	20
9EtOHmix	500	100	1550	10	1
10EtOHmix	500	150	1700	10	1
11EtOHmix	500	200	1295	10	0.7
12EtOHmix	500	200	1850	10	1
13EtOHmix	500	200	37000	10	20
14EtOHmix	500	200	1295	40	0.7
15EtOHmix	500	200	1850	40	1
16EtOHmix	500	200	37000	40	20

^aThe balance is closed with N₂.

Figure 5.13 shows an example of the results of the consumption of the reactants (C₂H₂, C₂H₅OH and O₂) with temperature and of the formation of the different products quantified (CO, CO₂, H₂ and CH₃CHO). As it can be seen, in general, there is good agreement between experimental and modeling results obtained with the final mechanism compiled as described in Chapter 4.

Results obtained, during the high-pressure oxidation of C₂H₂-C₂H₅OH mixtures, of the influence of the amount of C₂H₅OH added to the mixture, the air excess ratio, and the pressure, on the different concentration profiles are shown for C₂H₂, C₂H₅OH and, in some

cases, also for CO as one of the major oxidation products. Additional information can be found in Paper VII.

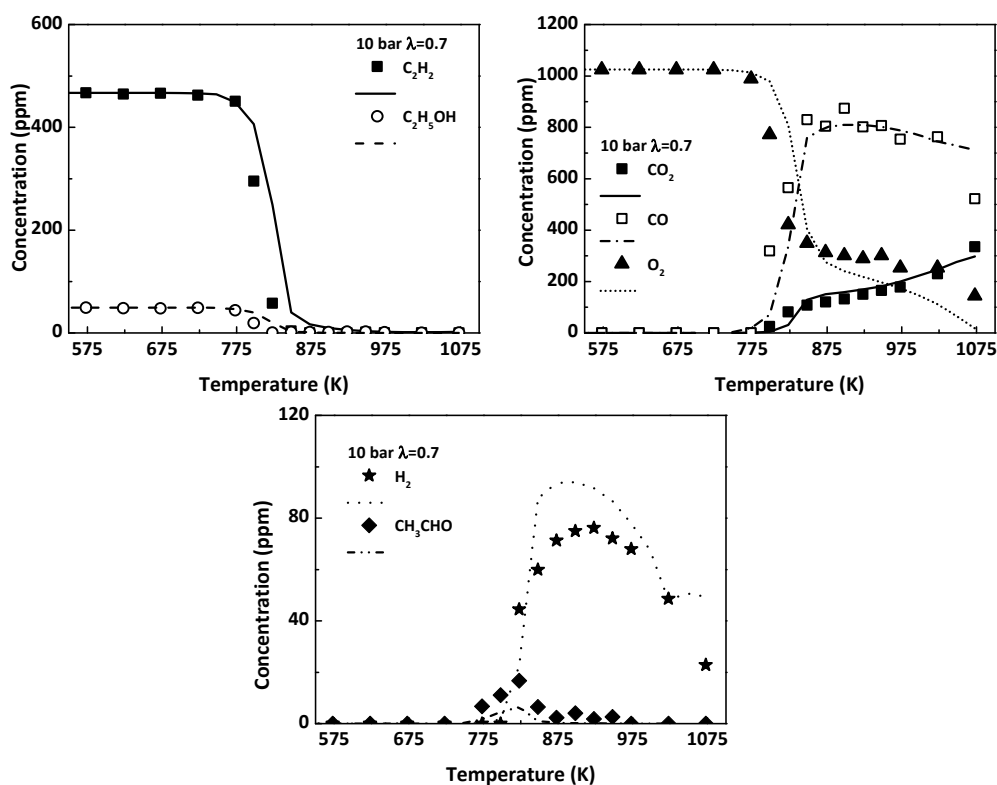


Figure 5.13. Evolution of C_2H_2 , C_2H_5OH , O_2 , CO , CO_2 , H_2 and CH_3CHO concentrations with temperature during the high-pressure (10 bar) oxidation of C_2H_2 - C_2H_5OH mixtures, for the conditions denoted as set 2EtOHmix, in Table 5.7.

Figure 5.14 shows the evolution with temperature of C_2H_2 and C_2H_5OH concentrations for stoichiometric conditions ($\lambda = 1$), 10 bar, and different inlet ethanol concentrations. Apparently, under the present high-pressure conditions, neither the presence nor the amount of ethanol significantly modify the onset temperature for acetylene oxidation or the acetylene conversion profile, in contrast to what was observed by Abián et al. (2008), in their atmospheric-pressure oxidation work of C_2H_2 - C_2H_5OH mixtures ($t_r[s]=195/T[K]$, 500 ppm of C_2H_2 , and 0-200 ppm of C_2H_5OH). In that study, as the amount of ethanol was increased, the acetylene conversion occurred at higher temperatures. Under the present high-pressure conditions (10 bar), the oxidation of C_2H_2 starts at 775-800 K approximately, independently of the amount of ethanol present in the reactant mixture. In the case of ethanol, it also starts to be consumed at the same temperature as C_2H_2 independently of the amount added to the mixture, whereas under atmospheric-pressure conditions (Abián et al., 2008), ethanol was

5. RESULTS AND DISCUSSION

more reactive, being completely consumed at lower temperatures than acetylene, and once ethanol was consumed, the C_2H_2 concentration sharply decayed.

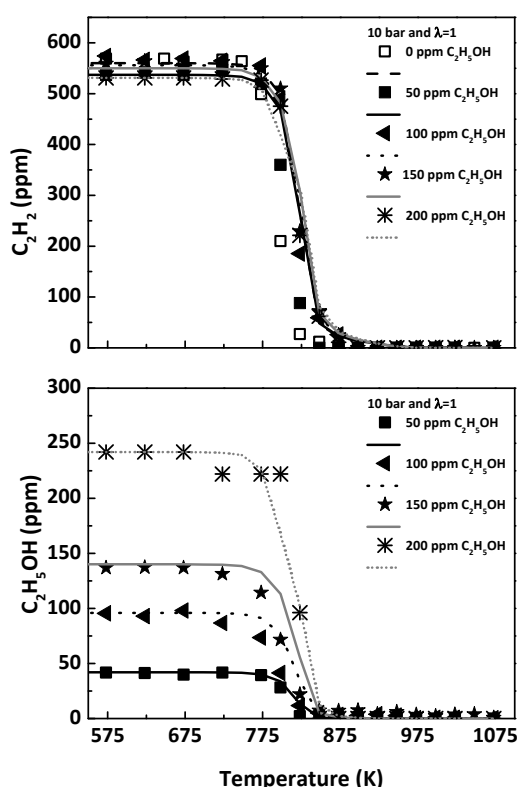


Figure 5.14. Influence of the amount of C_2H_5OH added to the mixture on the concentration profiles of C_2H_2 and C_2H_5OH during the C_2H_2 - C_2H_5OH mixture oxidation as a function of temperature, for stoichiometric conditions ($\lambda = 1$) and 10 bar. The inlet conditions correspond to sets 1EtOHmix, 3EtOHmix, 9EtOHmix, 10EtOHmix and 12EtOHmix, in Table 5.7.

To evaluate the influence of the oxygen availability in the reactant mixture on the oxidation of the mixtures, different air excess ratios (λ) have been used for two different ethanol concentrations in the mixture, 50 or 200 ppm, while keeping the value of the pressure at 10 bar and the C_2H_2 concentration constant (500 ppm, approximately). The experimental results obtained for acetylene and ethanol consumption and CO formation, as one of the major oxidation products, are compared to modeling calculations and represented in Figure 5.15.

The inlet oxygen concentration does not significantly modify acetylene conversion for either the lowest concentration of ethanol in the mixture (50 ppm, left side of Figure 5.15) or for the highest ethanol concentration in the mixture (200 ppm, right side of Figure 5.15). The temperature for the onset of C_2H_2 oxidation and, therefore, the onset of CO formation are almost independent of the value of λ analyzed.

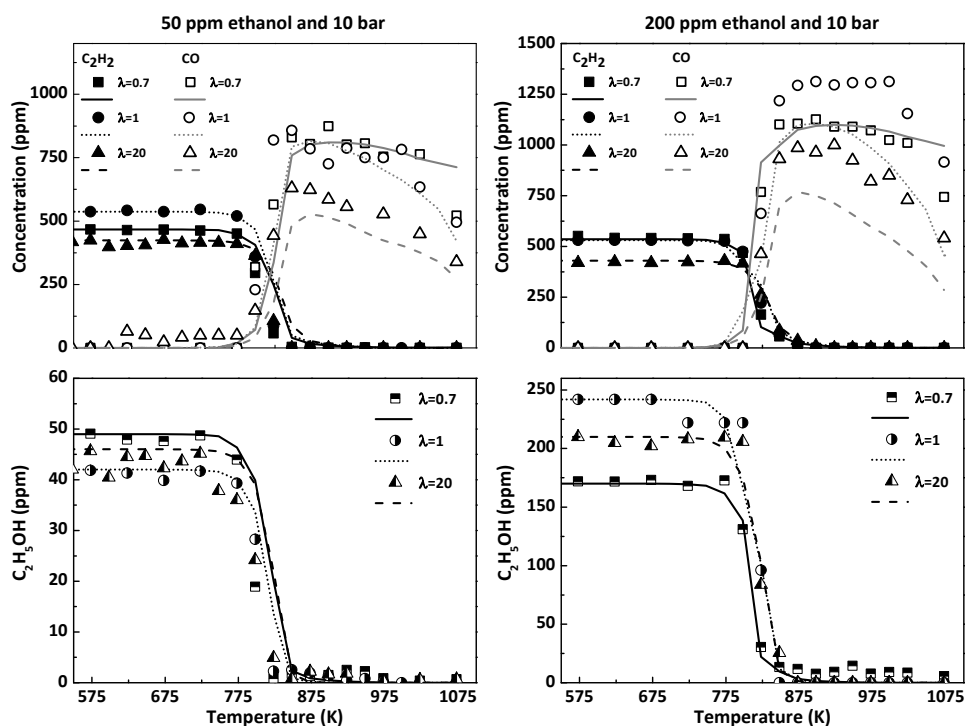


Figure 5.15. Influence of the air excess ratio (λ) on the concentration profiles of C_2H_2 and CO (upper part) and C_2H_5OH (lower part) during the C_2H_2 - C_2H_5OH mixture oxidation as a function of temperature, for 10 bar and two different amounts of ethanol added to the mixture, 50 ppm (left side) and 200 ppm (right side). The inlet conditions correspond to sets 2EtOHmix-4EtOHmix and 11EtOHmix-14EtOHmix, in Table 5.7.

In the case of C_2H_5OH , as previously reported during its high-pressure oxidation study (Section 5.2.2 and Paper III), for a given pressure, the inlet oxygen concentration does not clearly modify the C_2H_5OH oxidation, and C_2H_5OH is completely consumed for all of the stoichiometries analyzed at the highest temperatures considered. As mentioned, one possible explanation, to the almost negligible effect of the oxygen availability on the onset temperature for ethanol consumption, could be that ethanol oxidation is initiated by its thermal dehydration to ethylene (R5.26) and by its thermal decomposition (R5.27).



The study of the oxidation of C_2H_2 - C_2H_5OH mixtures, but at atmospheric pressure, above mentioned (Abián et al., 2008), also indicated that the onset temperature of C_2H_2 and C_2H_5OH conversion was almost the same (around 900 K) for all the values of λ analyzed, but

5. RESULTS AND DISCUSSION

the temperature range for the full consumption of C_2H_2 and C_2H_5OH was different depending on the value of λ , unlike what is observed at higher pressures.

The influence of a change in the working pressure (from 10 to 40 bar) on the oxidation of C_2H_2 - C_2H_5OH mixtures has also been evaluated. Figure 5.16 (left) shows the results obtained for C_2H_2 conversion under selected representative conditions. As it can be seen, an increase in the working pressure appears to shift the onset of C_2H_2 oxidation to lower temperatures, 50-75 K. A similar shift is observed in the onset temperature for C_2H_5OH conversion and CO formation (Paper VII). Therefore, the conversion of C_2H_2 at 40 bar starts at 725 K, which is approximately the same temperature as that obtained under similar experimental conditions by Giménez-López et al. (2016) in a high-pressure oxidation study of C_2H_2 (total flow rate of 3 L (STP)/min and residence times of 10-15 s in the isothermal reaction zone). The impact of the inlet oxygen concentration, at higher pressures, on the C_2H_2 - C_2H_5OH mixture oxidation is again almost negligible. Therefore, the effect of pressure is more noticeable than the concentration of oxygen. Moreover, since model provides good performance, theoretical calculations at different pressures have been performed to compare modeling predictions for C_2H_2 consumption under stoichiometric conditions, and approximately 50 ppm of ethanol. The results obtained from this theoretical evaluation are shown in the right side of Figure 5.16.

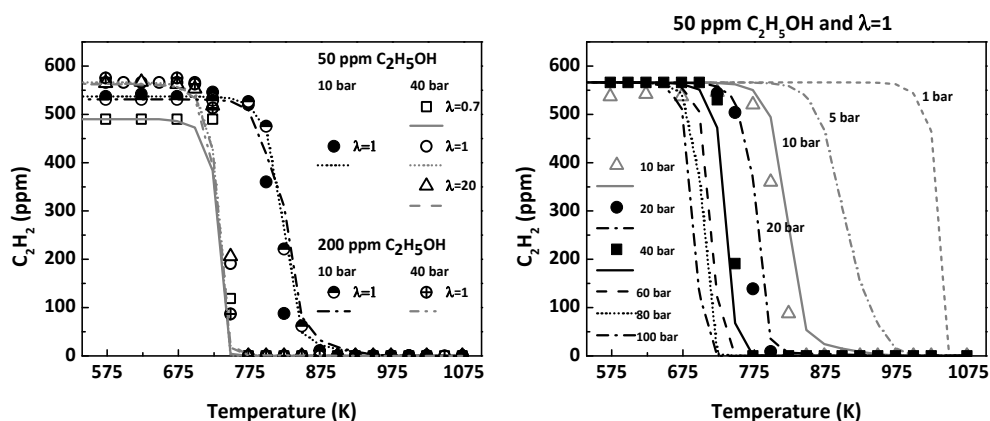


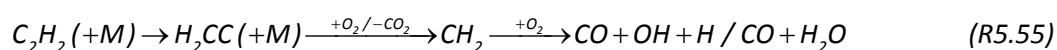
Figure 5.16. Influence of the pressure on the experimental and simulated concentration profile of C_2H_2 during the high-pressure oxidation of C_2H_2 - C_2H_5OH mixtures as a function of temperature, for the conditions denoted as sets 3EtOHmix, 6EtOHmix-8EtOHmix, 12EtOHmix and 15EtOHmix, (left) and 3EtOHmix, 5EtOHmix and 7EtOHmix (right), in Table 5.7. Additional model calculations to evaluate the effect of pressure on the evolution of the C_2H_2 concentration.

As it can be seen, the most significant changes occur in the 1-10 bar pressure range. As described in the Section 3.2, the gas residence time can be represented by

$t_r[s]=261 \cdot P[\text{bar}]/T[\text{K}]$ (equation 3.3). Therefore, when the pressure is increased from 1 to 10 bar, the residence time is also increased by a factor of 10, in addition to the increase in the species concentration by increasing the pressure system. As a consequence, the onset temperature for C_2H_2 conversion changes steeply.

In conclusion, a change in the working pressure from 10 to 40 bar has significant effects on the conversion of C_2H_2 and C_2H_5OH (not shown), but the effects are less pronounced when pressure is further increased.

With the final mechanism, a reaction rate analysis has been performed to identify the main routes for C_2H_2 and C_2H_5OH consumption and product formation during the oxidation of C_2H_2 - C_2H_5OH mixtures. In the case of acetylene, its conversion is initiated through the sequence described in reaction R5.55 and reactions with O_2 , such as reaction R5.56, to form HCO, which may react with molecular oxygen (R5.57).



Upon initiation, C_2H_2 undergoes addition reactions generating intermediate adducts, such as CHCHOH (R5.58), which is the main acetylene consumption route independent of the value of the air excess ratio analyzed.



The C_2H_2 combination with H radicals to form vinyl radicals (C_2H_3 , R5.59) is only important under stoichiometric ($\lambda = 1$) and fuel-rich conditions ($\lambda = 0.7$), whereas reactions of C_2H_2 and O radicals (R5.60 and R5.61) are of less importance compared to above mentioned reactions.

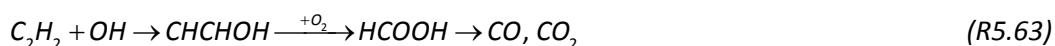


5. RESULTS AND DISCUSSION

Although the CHCHOH adduct could decompose thermally or react with O/H radicals, under the present conditions, it mainly reacts with O₂ to form formic acid (R5.62), and finally CO and CO₂ are produced.



In conclusion, under the present conditions, acetylene is mainly consumed following the sequence:



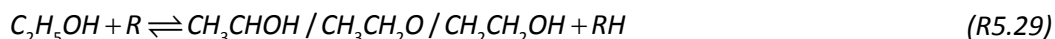
The C₂H₂ reaction routes are almost the same than those described by Giménez-López et al. (2016) in their high-pressure acetylene oxidation work. Only under reducing conditions differences have been found. In that work, C₂H₂ was mostly consumed by recombination with H radicals to form vinyl radicals; whereas, under the present conditions, C₂H₂ is mainly consumed by the reaction with OH radicals for all the values of λ analyzed. Thus, under the present conditions, the addition of ethanol to the reactant mixture does not modify the acetylene oxidation regime. It only modifies the composition of the radical pool, increasing the relevance of C₂H₂ reactions with OH radicals. Therefore, the effectiveness of ethanol in reducing soot formation from acetylene, that has been proved in different works (e.g. Esarte et al., 2011), is probably produced by the oxygen present in ethanol. Oxygen present in ethanol contributes to an increase of the O/OH radical pool, favoring C₂H₂ oxidation towards CO and CO₂ and, hence, removing carbon from the reaction paths that lead to soot formation.

On the other hand, as previously stated, ethanol conversion is initiated by its thermal dehydration to ethylene and water (R5.26). The water produced may react with O₂ (R5.64) or H radicals (R5.65) generated from the oxidation of C₂H₂ (for example, in reaction R5.56, C₂H₂ + O₂ \rightleftharpoons HCO + H + CO) and, therefore, HO₂ and OH radicals are formed.



After initiation, C₂H₅OH is mainly consumed by H-abstraction reactions by OH radicals, leading to the formation of three different ethanol radicals (R5.29). These radicals obtained

continue reacting through the same routes as those described during the high-pressure oxidation of ethanol (Section 5.2.2).



Therefore, it seems that, during the joint oxidation of ethanol and acetylene, there is no direct interaction between both compounds; each of them follows their corresponding reaction routes, and their oxidation is only modified by an increase in the O/OH radical pool composition produced during the conversion of the other reactant.

5.4.2 High-pressure oxidation of acetylene-dimethyl ether mixtures

Before addressing the high-pressure oxidation of C₂H₂-DME mixtures, and because no previous works on the oxidation of these mixtures at atmospheric pressure have been performed in our research group, an experimental and modeling study of the C₂H₂-DME mixture atmospheric-pressure oxidation has been performed in the present thesis.

5.4.2.1 Atmospheric-pressure oxidation of acetylene-dimethyl ether mixtures in the absence and presence of NO

The present study aims to achieve a better knowledge of the atmospheric-pressure oxidation of C₂H₂-DME mixtures, as well as of their interaction with NO. The influence of temperature, air excess ratio and DME concentration in these mixtures has been analyzed. Experiments have been performed both in the absence and presence of NO, thus allowing to determine both the impact of the NO presence on the oxidation regime of the mixtures and the capability of these mixtures to reduce NO. The experimental results have been interpreted in terms of the detailed kinetic mechanism compiled along the present thesis. Table 5.8 lists the conditions of the different experiments, both those performed in the present thesis and earlier experiments from our group, all carried out in the same experimental set-up, which is described in Section 3.1.

5. RESULTS AND DISCUSSION

Table 5.8. Matrix of experimental conditions of the atmospheric-pressure study of C₂H₂-DME mixtures oxidation^a

C₂H₂-DME mixtures oxidation at atmospheric pressure in a flow reactor							
T=575-1475 K; P=1 atm; Flow rate: 1 L (STP)/min; $t_r [s] = \frac{195}{T[K]}$							
Set	C₂H₂ [ppm]	DME [ppm]	O₂ [ppm]	NO [ppm]	H₂O [ppm]	λ	Source
1DMEmix _{at}	500	50	280	-	5000	0.2	pw
2DMEmix _{at}	500	200	370	-	5000	0.2	pw
3DMEmix _{at}	500	200	370	500	5000	0.2	pw
4DMEmix _{at}	500	-	250	500	7000	0.2	(*)
5DMEmix _{at}	500	50	980	-	5000	0.7	pw
6DMEmix _{at}	500	200	1295	-	5000	0.7	pw
7DMEmix _{at}	500	200	1295	500	5000	0.7	pw
8DMEmix _{at}	500	-	875	500	7000	0.7	(*)
9DMEmix _{at}	500	-	875	-	7000	0.7	(#)
10DMEmix _{at}	500	50	1400	-	5000	1	pw
11DMEmix _{at}	500	200	1850	-	5000	1	pw
12DMEmix _{at}	500	200	1850	500	5000	1	pw
13DMEmix _{at}	500	-	1250	500	7000	1	(*)
14DMEmix _{at}	500	50	28000	-	5000	20	pw
15DMEmix _{at}	500	200	37000	-	5000	20	pw
16DMEmix _{at}	500	200	37000	500	5000	20	pw
17DMEmix _{at}	500	-	25000	500	5000	20	pw
18DMEmix _{at}	500	-	25000	-	7000	20	(#)

^aThe balance is closed with N₂; pw: present work; (*) Abián et al. (2010); (#) Alzueta et al. (2008).

Figure 5.17 shows the influence of the temperature and air excess ratio (λ) on the concentration of DME, C₂H₂, and the sum of CO and CO₂. In general, the model provides good agreement between experimental results and modeling calculations, reproducing well the main experimental trends observed. However, certain discrepancies have been observed, especially for acetylene.

As it can be observed in Figure 5.17, the onset temperature for C₂H₂ and DME conversion depends on the oxygen availability. This temperature increases as the value of λ decreases, being quite similar for fuel-rich ($\lambda = 0.7$) and very fuel-rich conditions ($\lambda = 0.2$) for acetylene, and also for stoichiometric conditions for DME. The results differ from those

reported by Alzueta et al. (2008) in a study of the atmospheric oxidation of C_2H_2 , where the onset temperature for its conversion was approximately the same, independently of the value of λ . Something similar can be said about DME. In the DME atmospheric-pressure oxidation work by Alzueta et al. (1999), the oxygen availability had a slightly influence on the onset temperature of DME oxidation. Thus, the present results indicate an effective interaction of the compounds and/or their derivatives in the mixtures.

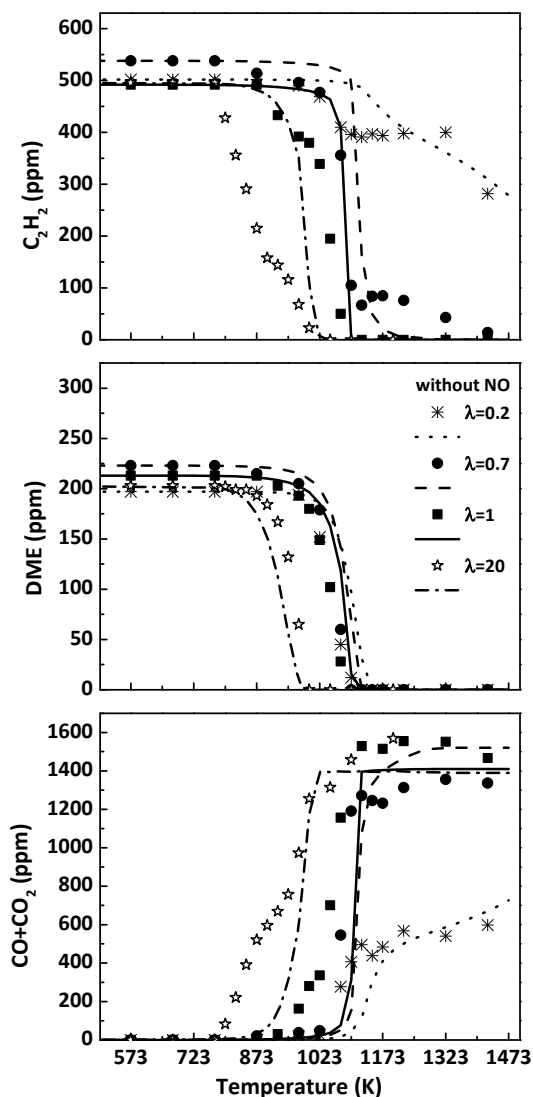
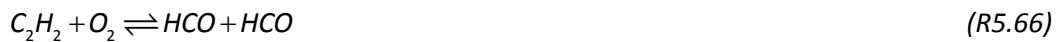


Figure 5.17. Influence of the air excess ratio (λ) on the concentration profiles of C_2H_2 , DME and the sum of CO and CO_2 as a function of temperature, during the C_2H_2 -DME mixture oxidation for the conditions denoted as sets 2DME $_{mix_{at}}$, 6DME $_{mix_{at}}$, 11DME $_{mix_{at}}$ and 15DME $_{mix_{at}}$ in Table 5.8.

At the highest temperatures considered, DME is completely consumed for all the λ values studied, even under reducing conditions. Alzueta et al. (1999) stated that DME

5. RESULTS AND DISCUSSION

oxidation does not take place or proceeds very slowly at temperatures lower than 1000 K, and this is the behavior observed for the different air excess ratios analyzed, except for $\lambda = 20$, where DME conversion starts at lower temperatures, approximately 100 K less. On the other hand, acetylene is not always completely consumed. For $\lambda = 0.2$ and the highest temperatures reached, about 250 ppm of C_2H_2 still remain unconverted, which is also predicted by the model. Moreover, at the fuel leanest conditions studied ($\lambda = 20$), the full conversion of acetylene occurs approximately at 75 K below, compared to stoichiometric conditions. It is also reflected in the $CO+CO_2$ experimental concentration profile, which start to be formed as C_2H_2 starts to be consumed, as follows. After the initiation of acetylene conversion, mainly by its reaction with O_2 forming formyl radicals (HCO) (R5.56 and R5.66), the main C_2H_2 consumption occurs through the interaction with O radicals (R5.60) generating the HCCO species. Afterwards, both HCO and HCCO give CO and subsequently CO_2 (R5.67-R5.69).



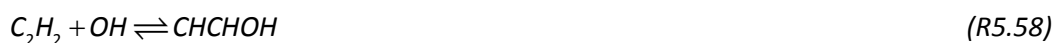
Furthermore, reaction rate analyses, for the oxidation of different C_2H_2 -DME mixtures, have been performed to identify the reactions that contribute to the C_2H_2 and DME consumption. The results indicate that the main routes for C_2H_2 consumption are similar to those reported by Alzueta et al. (2008) for the individual conversion of C_2H_2 at atmospheric pressure. In the case of the DME reaction pathways, which are very similar to those described by Alzueta et al. (1999), even though the presence of certain radicals (e.g. OH radicals) may increase the relevance of some of specific routes as described below.

The initiation reactions for C_2H_2 conversion include its interaction with O_2 (R5.66) and the H, O and OH radicals. The addition of H to C_2H_2 to form vinyl radicals (R5.59, $C_2H_2 + H (+M) \rightleftharpoons C_2H_3 (+M)$) appears to be an important C_2H_2 consumption reaction, especially for $\lambda = 0.2, 0.7$ and 1. This reaction is in competition with others involving interactions of C_2H_2

with O radicals (R5.60 and R5.61) and also with OH radicals, but with a minor relevance (R5.70-R5.72).



Under fuel-lean conditions ($\lambda = 20$), the C_2H_2 interaction with OH to form the adduct CHCHOH (R5.58) gains relevance. For example, at 873 K, the net rate of production of CHCHOH through reaction R5.58 increases from 1.00×10^{-15} mol/cm³ s, for $\lambda = 0.2$, to 1.00×10^{-11} mol/cm³ s, for $\lambda = 20$. The CHCHOH generated reacts with molecular oxygen to form glyoxal (OCHCHO, R5.73), which seems to be an important intermediate in combustion of hydrocarbons as it can be formed from C_2H_2 oxidation (Faßheber et al., 2015). Glyoxal reacts with OH radicals to form OCHCO (R5.74), which finally decomposes to formyl radicals and CO (R5.75).



On the other hand, the conversion of DME is mainly initiated by its molecular decomposition (R5.76), even though other important consumption reactions include H-abstraction reactions of DME by the radical pool (R5.30) to produce CH_3OCH_2 radicals, which decompose to obtain formaldehyde (R5.37), that follows the well-known reaction sequence R5.51 until CO and CO₂ are obtained as final products. These routes are the same as those described by Alzueta et al. (1999) for DME atmospheric-pressure oxidation in a flow reactor,

5. RESULTS AND DISCUSSION

and comparatively simpler than those previously described during the high-pressure oxidation of DME (Section 5.2.2).



The influence of the DME amount present in the mixture on the C₂H₂ consumption has been evaluated. Figure 5.18 shows a comparison of the results obtained for the experiments performed under fuel-rich ($\lambda = 0.7$) and fuel-lean ($\lambda = 20$), conditions for two different DME inlet amounts (50 or 200 ppm). Results of the C₂H₂ oxidation without DME have been taken from a previous work of our group (Alzueta et al., 2008). The presence of DME in the mixture has a different impact whether the ambient is fuel-rich or fuel-lean. Whereas for $\lambda = 0.7$, increasing the amount of DME seems to have an inhibiting effect on acetylene consumption, for $\lambda = 20$, the presence of DME shifts the C₂H₂ concentration profiles towards lower temperatures.

Reaction rate analyses have been performed to elucidate this fact. As mentioned before, the main C₂H₂ conversion occurs through its reaction with O₂ (R5.66) and O and OH radicals (reactions R5.60 and R5.61 and R5.70-R5.72), but for fuel-rich conditions, reaction R5.59 ($C_2H_2 + H (+M) \rightleftharpoons C_2H_3 (+M)$), that involves H-addition to form vinyl radicals, becomes a really important C₂H₂ consumption reaction. When DME is present in the mixture, some of these H radicals are then involved in DME consumption (R5.30, $CH_3OCH_3 + H \rightleftharpoons CH_3OCH_2 + H_2$). For example, at 1023 K, when DME is not present, H-radical consumption by reaction R5.59 is approximately 34%; when 50 ppm of DME are present, this value decreases to 29% (a 33% of H-radical consumption is by reaction R5.30); and, when the amount of DME is increased to 200 ppm, only a 13% of H radicals is consumed by reaction R5.59 and a 68%, by reaction R5.30. As a result, less H radicals participate in C₂H₂ consumption, and its conversion is shifted to higher temperatures when DME is present in the mixture.

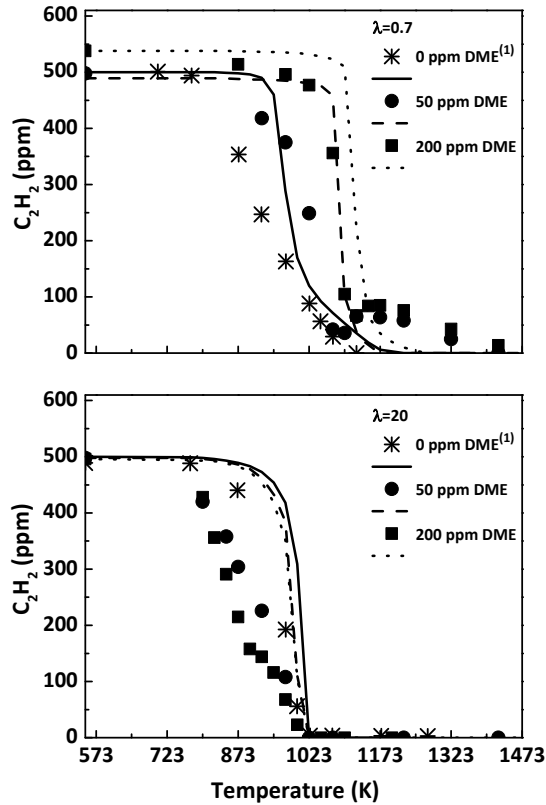


Figure 5.18. Influence of the DME inlet concentration on the C_2H_2 concentration profile as a function of temperature, for $\lambda = 0.7$ (upper part) and $\lambda = 20$ (lower part), for the conditions denoted as sets 5DME_{mix_{at}}, 6DME_{mix_{at}}, 9DME_{mix_{at}}, 14DME_{mix_{at}}, 15DME_{mix_{at}} and 18DME_{mix_{at}}, in Table 5.8. ⁽¹⁾ Alzueta et al. (2008).

On the other hand, when the oxygen availability is increased, the conversion of C_2H_2 is shifted to lower temperatures (i.e. $\lambda = 20$, lower part in Figure 5.18). The presence of DME in the reactant mixture promotes C_2H_2 conversion; although there is not a big difference of adding 50 or 200 ppm of DME to the reactant mixture, and it can only be observed experimentally. This can be explained because the formation of O and OH radicals is enlarged due to the increase in the available oxygen, because of the presence of DME in the mixture and the fuel-leaner conditions. As a result, both DME (see Figure 5.17) and C_2H_2 conversion (see Figure 5.17 and Figure 5.18) are shifted to lower temperatures than for fuel-rich conditions.

Although some authors indicate that NO_x emissions when DME is used as fuel are higher or of a similar level than when diesel fuel is used in a compression ignition engine at the same operating conditions (Cipolat, 2007), others indicate that when operating under optimized conditions (such as changing the injection system), NO_x emissions from DME are lower than those obtained using diesel fuel (Park and Yoon, 2015). Therefore, oxidation

5. RESULTS AND DISCUSSION

experiments of C₂H₂-DME mixtures in the presence of NO, for different air excess ratios, have been carried out (Table 5.8).

NO may interact with C₂H₂, DME and their derived species, achieving some degree of reduction depending on the operating conditions. Under fuel-rich conditions, NO could be reduced by reburn reactions by reacting with hydrocarbon radicals produced during the oxidation of DME and C₂H₂ (Bilbao et al., 1994; Alzueta et al., 1997; Miller et al., 2003). Under fuel-lean conditions, NO may favor the oxidation of the C₂H₂-DME mixture in a mutually sensitized oxidation process, similar to what has been observed for other compounds such as methane (Section 5.1.2).

To deeply analyze the influence of the presence of NO on the oxidation of C₂H₂-DME mixtures, Figure 5.19a and Figure 5.19b compare the results obtained in the absence of NO (open symbols, previously represented in Figure 5.17) and in the presence of NO (solid symbols) for the different values of λ analyzed. As an example of the model performance, only calculations for $\lambda = 0.2$ and $\lambda = 20$ are shown. The presence of NO has its major effect under fuel-lean conditions, causing a shift of more than 200 K in the temperature for the onset of DME oxidation, similar to what was observed by Alzueta et al. (1999) in their study of DME oxidation in the presence of NO at atmospheric pressure. In the case of the C₂H₂, the presence of NO does not affect significantly the C₂H₂ concentration profile.

Reaction rate analyses performed indicate that, for oxidizing conditions ($\lambda = 20$) and in the presence of NO, the main consumption of DME is by interaction with OH radicals to produce CH₃OCH₂ radicals (R5.30). The CH₃OCH₂ radicals generated react with molecular oxygen forming peroxy species ($CH_3OCH_2 \xrightarrow{+O_2} CH_3OCH_2O_2 \rightarrow CH_2OCH_2O_2H$), which continue reacting until formaldehyde is obtained (R5.36), in a similar way as previously described when analyzing the reaction routes for DME high-pressure conversion at high temperatures (Section 5.2.2).



As a consequence, for $\lambda = 20$ and in the presence of NO, the shape of the DME concentration profile reminds the shape of the NTC zone observed during the high-pressure oxidation of DME. This shape is also reflected in the NO concentration profile at low temperatures (Figure 5.19c).

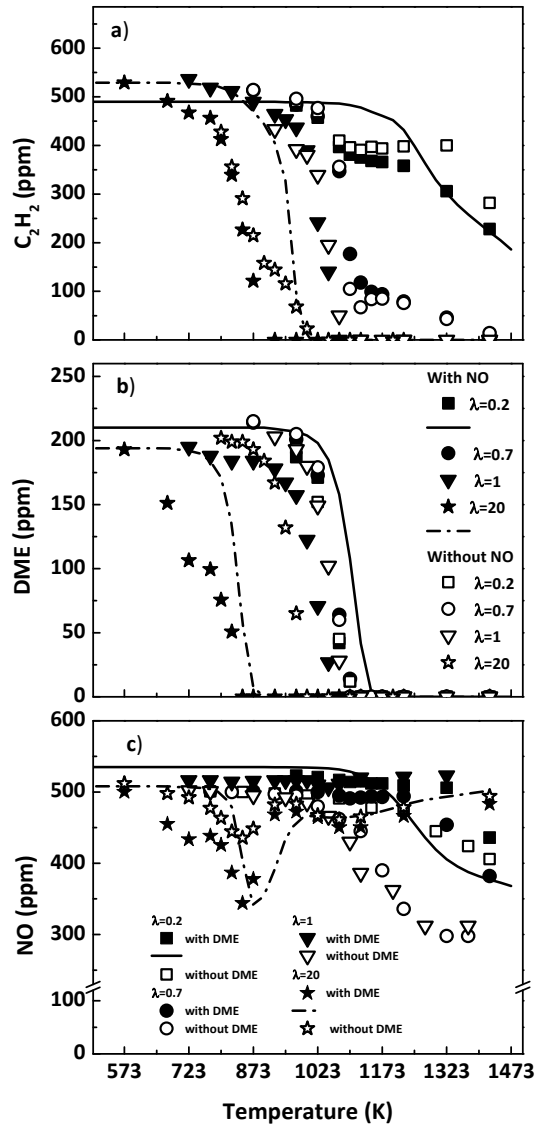


Figure 5.19. Evaluation of the effect of NO presence on C_2H_2 and DME concentration profiles as a function of temperature, during the C_2H_2 -DME mixture oxidation at atmospheric pressure (a y b). Experimental results for NO concentration as a function of temperature in the presence and absence of DME (c). Conditions denoted as sets 3DMEmix_{at}, 4DMEmix_{at}, 7DMEmix_{at}, 8DMEmix_{at}, 12DMEmix_{at}, 13DMEmix_{at}, 16DMEmix_{at}, and 17DMEmix_{at}, in Table 5.8.

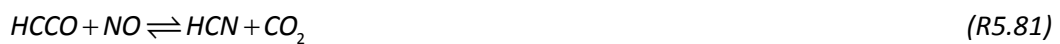
(¹) Abián et al. (2010).

Under fuel-lean conditions, NO interacts with CH_3 radicals (from the decomposition of DME, R5.76, $CH_3OCH_3 \rightleftharpoons CH_3O + CH_3$), and also with HO_2 (from the HCO reaction with O_2 , R5.77) and, as a consequence, in general, highly reactive OH radicals are generated (R5.78 and R5.79).





Moreover, C_2H_2 is an important source of HCCO radicals (R5.60), which can be involved in the NO concentration diminution. For fuel-rich conditions, HCCO radicals interact with NO (R5.80 and R5.81) explaining the NO concentration experimental decrease of 40% for $\lambda = 0.7$ and 1, and 15% for $\lambda = 0.2$, at 1300 K, in the absence of DME and at high temperatures. However, by increasing the oxygen concentration ($\lambda = 20$), the HCCO+NO reactions become less important and the HCCO+O₂ reactions (R5.82 and R5.83) predominate.



Thus, the competition between the consumption of HCCO by reaction with NO or O₂ determines the final concentration of NO.

5.4.2.2 High-pressure oxidation of acetylene-dimethyl ether mixtures

Oxidation experiments of several acetylene-dimethyl ether (C_2H_2 -DME) mixtures, under high-pressure conditions (20-60 bar), have been carried out in the 450-1050 K temperature range, in a flow reactor. Besides the influence of pressure and temperature on the oxidation process, the influence of the oxygen inlet concentration (determined by the air excess ratio, λ) and the amount of DME (100 or 400 ppm, approximately) present in the reactant mixture has also been evaluated. The experimental data have been compared with modeling predictions obtained with the final mechanism compiled in this work, as has been done throughout this thesis. Table 5.9 lists the conditions of the experiments, and the set-up used during this study is described in Section 3.2.

Table 5.9. Matrix of experimental conditions of the high-pressure study of C₂H₂-DME mixtures oxidation^a

C₂H₂-DME mixtures oxidation at high pressure in a flow reactor					
T=450-1050 K; Flow rate: 1 L (STP)/min; $t_r [s] = \frac{261 * P [bar]}{T [K]}$					
Set	C ₂ H ₂ [ppm]	DME [ppm]	O ₂ [ppm]	P [bar]	λ
1DMEmix _{HP}	1000	100	1960	20	0.7
2DMEmix _{HP}	1000	400	2590	20	0.7
3DMEmix _{HP}	1000	100	2800	20	1
4DMEmix _{HP}	1000	400	3700	20	1
5DMEmix _{HP}	1000	100	56000	20	20
6DMEmix _{HP}	1000	400	74000	20	20
7DMEmix _{HP}	1000	100	1960	40	0.7
8DMEmix _{HP}	1000	400	2590	40	0.7
9DMEmix _{HP}	1000	100	2800	40	1
10DMEmix _{HP}	1000	400	3700	40	1
11DMEmix _{HP}	1000	100	56000	40	20
12DMEmix _{HP}	1000	400	74000	40	20
13DMEmix _{HP}	1000	100	1960	60	0.7
14DMEmix _{HP}	1000	400	2590	60	0.7
15DMEmix _{HP}	1000	100	2800	60	1
16DMEmix _{HP}	1000	400	3700	60	1
17DMEmix _{HP}	1000	100	56000	60	20
18DMEmix _{HP}	1000	400	74000	60	20

^aThe balance is closed with N₂.

To evaluate the influence of the oxygen availability in the reactant mixture on the high-pressure oxidation of C₂H₂-DME mixtures, different values of the air excess ratio (λ) have been used for two different DME concentrations in the mixture, 100 or 400 ppm, while keeping the pressure and the C₂H₂ concentration (1000 ppm, approximately) constant. Figure 5.20 shows a comparison of the experimental results and modeling calculations obtained at a constant pressure of 20 bar, for the concentrations of C₂H₂ and DME and the sum of CO and CO₂, as the main products quantified. In the case of DME, for an easier comparison of the results with different DME inlet concentrations, DME concentration has been normalized with respect to its inlet concentration. For the other two values of the pressure analyzed, 40 and 60

5. RESULTS AND DISCUSSION

bar, although the results are not shown, the tendencies are the same. In general, there is a good agreement between experimental data and modeling calculations.

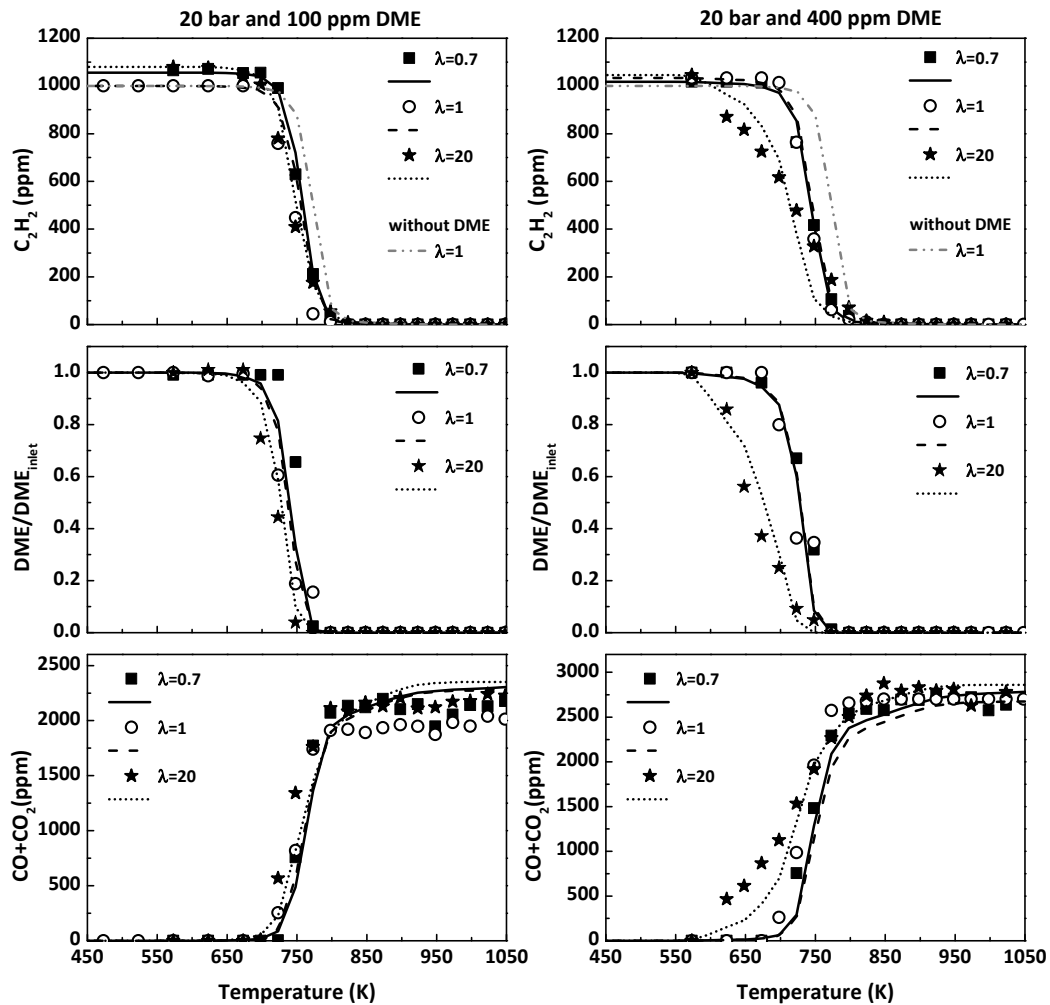


Figure 5.20. Influence of the air excess ratio (λ) on the concentration profiles of C_2H_2 , DME and $CO+CO_2$ as a function of temperature, during the C_2H_2 -DME mixture oxidation, for 20 bar and two different amounts of DME added to the mixture, 100 ppm DME (left) and 400 ppm DME (right). The inlet conditions correspond to sets 1DME_{mixHP}-6DME_{mixHP}, in Table 5.9.

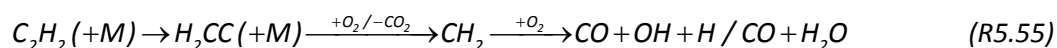
For a given pressure, the onset temperature for C_2H_2 and DME conversion is almost the same, independently of the oxygen available in the reactant mixture, except for the highest DME concentration analyzed (400 ppm) and oxidizing conditions ($\lambda = 20$). Under these conditions, both C_2H_2 and DME start to be consumed at lower temperatures, 100 K less, from 725 K to 625 K, and consequently, it is also reflected in the $CO+CO_2$ concentration.

On the other hand, the onset temperature for DME conversion during the high-pressure oxidation of C_2H_2 -DME mixtures is comparatively higher than the required for the DME oxidation itself. For example, at 20 bar, $\lambda = 1$ and in the absence of NO, DME starts to be

consumed at approximately 525 K (see Figure 5.6 left); whereas, under the same conditions but in its mixture with C₂H₂, DME consumption does not start until 700-725 K.

Because the model provides, in general, a good description of the oxidation process, model calculations, at 20 bar and stoichiometric conditions ($\lambda = 1$) for C₂H₂ oxidation without DME, have been carried out to analyze if the addition of DME has an effect on C₂H₂ conversion. As it can be seen (Figure 5.20), the presence of DME in the reactant mixture shifts the conversion of C₂H₂ to lower temperatures, and the higher the amount of DME, the lower the temperature.

Reaction rate analyses have been performed to identify the main consumption routes for C₂H₂ and DME and, therefore, to explain the observations previously discussed. The results indicate that, under the present conditions, both C₂H₂ and DME consumption routes in their mixtures are almost the same than those previously described while analyzing the high-pressure oxidation of C₂H₂-C₂H₅OH mixtures and DME, respectively. That is, C₂H₂ conversion is initiated by the R5.55 reaction sequence and DME conversion by reaction R5.28. After initiation, both compounds are mainly consumed by H-abstraction reactions with OH radicals, in the case of C₂H₂ to form the CHCHOH adduct (R5.58), and in the case of DME, to obtain CH₃OCH₂ radical (R5.30), even though other radicals, such as HO₂, can also participate in this reaction ($CH_3OCH_3 + HO_2 \rightleftharpoons CH_3OCH_2 + H_2O_2$). These HO₂ radicals can be generated directly from DME (R5.28), but also from the reaction with molecular oxygen of HCO radicals (R5.57) produced from C₂H₂ and CHCHOH (R5.56 and R5.62).



5. RESULTS AND DISCUSSION

The main source of OH radicals are reactions R5.84 and R5.85, included in the complex mechanism responsible for DME conversion under high-pressure conditions and low temperatures (R5.33-R5.35).



Therefore, as the amount of DME is increased in the reactant mixture, the amount of OH radicals generated is also increased and, as a consequence, the consumption of C₂H₂.

Furthermore, the influence of a change in the working pressure (20, 40 and 60 bar) on the oxidation of C₂H₂-DME mixtures has also been evaluated. Figure 5.21 shows a comparison of experimental results and modeling calculations for the concentrations of C₂H₂ and DME, and the sum of CO and CO₂, during the high-pressure oxidation of C₂H₂-DME mixtures, for stoichiometric conditions and 100 ppm of DME in the mixture. As it can be seen, modeling calculations are in very good agreement with the experimental trends.

An increase in the working pressure shifts the onset temperature for C₂H₂ and DME conversion to lower temperatures, as happened during the high-pressure oxidation of C₂H₂-C₂H₅OH mixtures. It is worth to mention that when the pressure is increased from 20 to 40 bar or from 40 to 60 bar, the residence time is also increased by a factor of 2. As a consequence, the change in the onset temperature can be attributed to both the increase in pressure and the related increase in the gas residence time.

As in the case of the high-pressure oxidation of C₂H₂-C₂H₅OH mixtures, the addition of DME to the reactant mixture does not modify the acetylene oxidation regime. It only modifies the composition of the radical pool, increasing the relevance of C₂H₂ reactions with OH radicals, favoring the C₂H₂ oxidation towards CO and CO₂ and, as a consequence, removing carbon from the reaction paths which leads to soot formation.

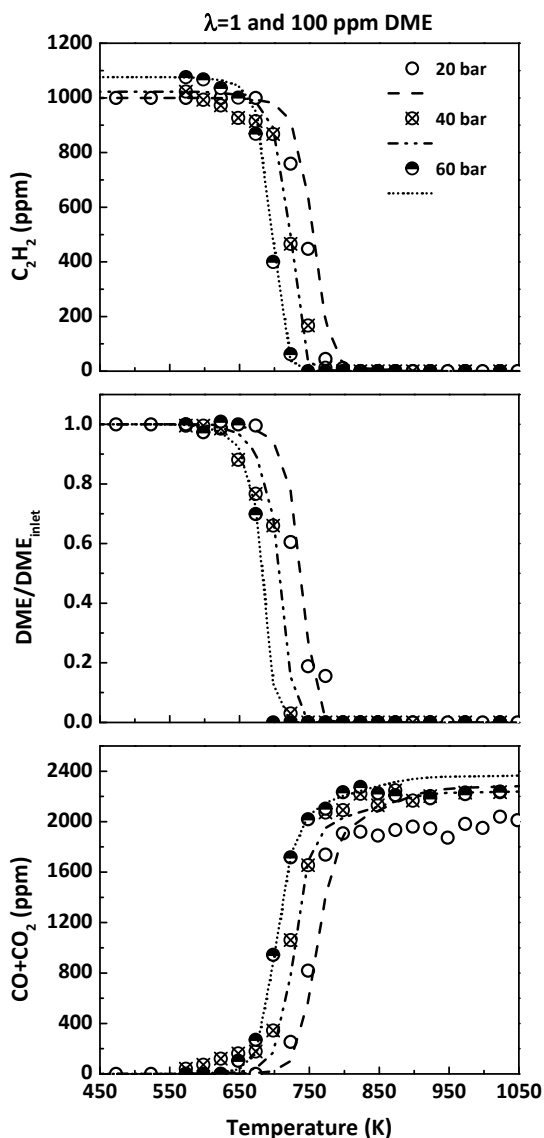


Figure 5.21. Influence of the pressure on the concentration profiles of C_2H_2 , DME and $CO+CO_2$ as a function of temperature, during the C_2H_2 -DME mixture oxidation, for $\lambda = 1$ and 100 ppm of DME added to the mixture. The inlet conditions correspond to sets 3DME_{mix,HP}, 9DME_{mix,HP} and 15DME_{mix,HP}, in Table 5.9.

5.4.3 High-pressure oxidation of acetylene-dimethoxymethane mixtures

To complete the investigation on the oxidation of C_2H_2 -oxygenate mixtures, the high-pressure oxidation of C_2H_2 -DMM mixtures has been studied in a flow reactor, in the 20-60 bar and 450-1050 K pressure and temperature ranges. The influence on the oxidation process of the oxygen inlet concentration (determined by the air excess ratio, λ) and the amount of DMM (70 or 280 ppm) present in the reactant mixture has also been evaluated. The conditions of these experiments are detailed in Table 5.10, whereas the experimental set-up used is

5. RESULTS AND DISCUSSION

described in Section 3.2. The oxidation of C₂H₂-DMM mixtures at atmospheric pressure, in a flow reactor, has been studied in a previous work of our research group (Martín, 2011); therefore, it is not addressed in the present work.

Table 5.10. Matrix of experimental conditions of the high-pressure study of C₂H₂-DMM mixtures oxidation^a

C₂H₂-DMM mixtures oxidation at high pressure in a flow reactor					
T=450-1050 K; Flow rate: 1 L (STP)/min; $t_r [s] = \frac{261 * P [bar]}{T [K]}$					
Set	C₂H₂ [ppm]	DMM [ppm]	O₂ [ppm]	P [bar]	λ
1DMMmix	700	70	1421	20	0.7
2DMMmix	700	280	2009	20	0.7
3DMMmix	700	70	2030	20	1
4DMMmix	700	280	2870	20	1
5DMMmix	700	70	40600	20	20
6DMMmix	700	280	57400	20	20
7DMMmix	700	70	1421	40	0.7
8DMMmix	700	280	2009	40	0.7
9DMMmix	700	70	2030	40	1
10DMMmix	700	280	2870	40	1
11DMMmix	700	70	40600	40	20
12DMMmix	700	280	57400	40	20
13DMMmix	700	70	1421	60	0.7
14DMMmix	700	280	2009	60	0.7
15DMMmix	700	70	2030	60	1
16DMMmix	700	280	2870	60	1
17DMMmix	700	70	40600	60	20
18DMMmix	700	280	57400	60	20

^aThe balance is closed with N₂.

Under high-pressure conditions, the influence of the oxygen availability on the oxidation of C₂H₂-DMM mixtures has been evaluated. Different values of the air excess ratio have been studied for two different DMM concentrations in the mixture, corresponding to 10 and 40% of the C₂H₂ concentration (700 ppm), that is, 70 and 280 ppm of DMM, respectively. Figure 5.22 shows a comparison of the experimental results and modeling calculations for the consumption of C₂H₂ and DME and the sum of CO and CO₂. As previously done in Section 5.4.2.2, while analyzing the results obtained during the high-pressure oxidation of C₂H₂-DME

mixtures, the concentration of DMM obtained has been normalized with respect to its inlet concentration. Only the results obtained for 20 bar are shown, although similar trends have been obtained in the case of the other pressures analyzed, 40 and 60 bar. In general, model predictions are in good agreement with experimental results.

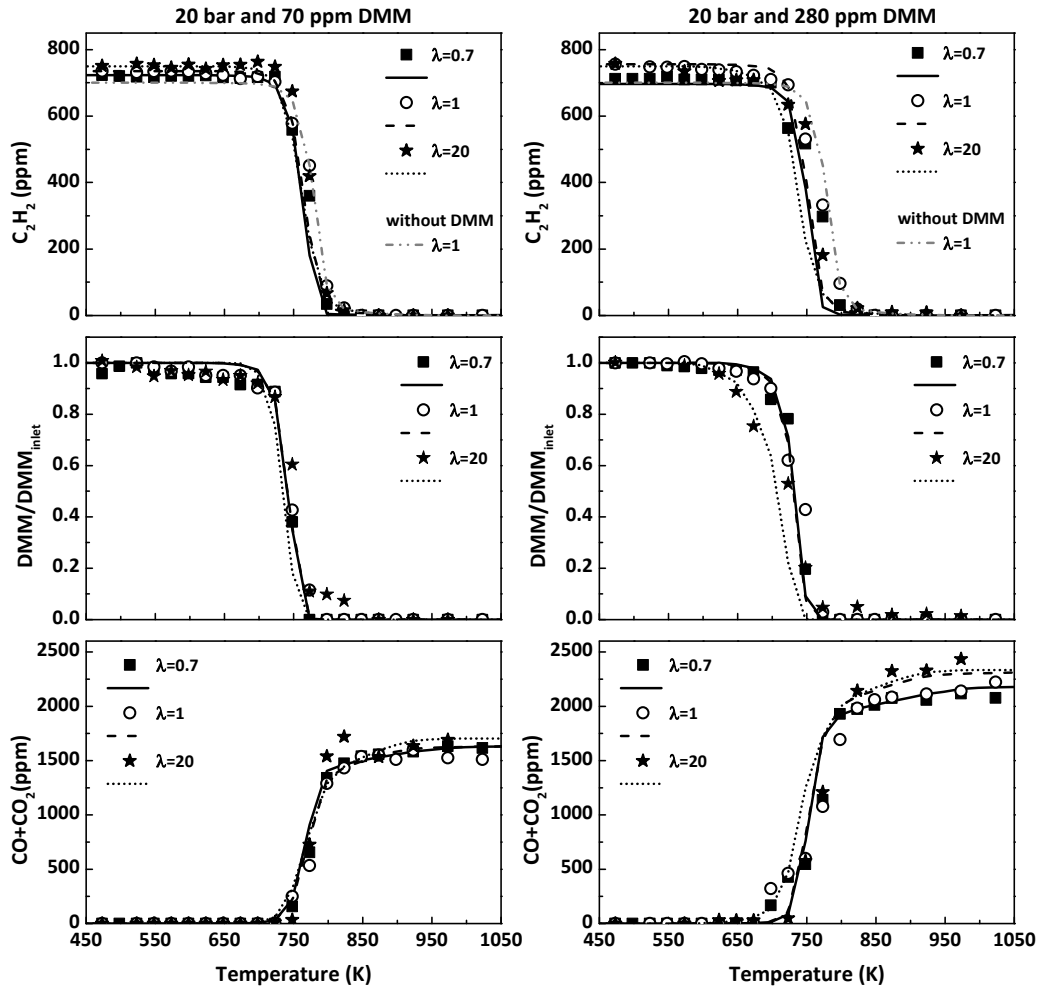


Figure 5.22. Influence of the air excess ratio (λ) on the concentration profiles of C_2H_2 , DMM and $CO+CO_2$ as a function of temperature, during the C_2H_2 -DMM mixture oxidation, for 20 bar and two different amounts of DMM added to the mixture, 70 ppm DME (left) and 280 ppm DME (right). The inlet conditions correspond to sets 1DMMmix-6DMMmix, in Table 5.10.

No significant differences have been found in the onset temperature for the conversion of C_2H_2 and DMM for the different values of lambda analyzed. For the lowest amount of DMM studied (Figure 5.22, left), independently of the oxygen availability, C_2H_2 starts to be consumed at temperatures around 750 K, whereas DMM conversion starts at lower temperatures, 725 K. However, for the higher amount of DMM (Figure 5.22, right), these onset temperatures for C_2H_2 and DMM consumption are slightly shifted to lower

temperatures, 25 K approximately, i.e. 725 K and 700 K, respectively. For oxidizing conditions, DMM starts to be consumed at even lower temperatures, 650 K. However, at atmospheric pressure (Martín, 2011), the availability of oxygen had an impact on the onset temperature for C₂H₂ and DMM conversions. These temperatures increased as the value of λ decreased, and C₂H₂ was not always completely consumed, for example, for $\lambda = 0.2$ and the highest temperatures reached. These results are similar to those obtained during the atmospheric-pressure oxidation of C₂H₂-DME mixtures (Section 5.4.2.1).

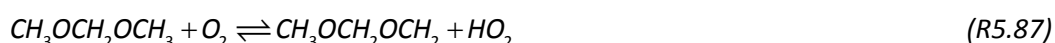
The experimental and modeling trends for C₂H₂ consumption, during the high-pressure oxidation of C₂H₂-DMM mixtures are quite similar to those obtained also during the high-pressure oxidation of C₂H₂-DME mixtures, for the lowest amount of DMM (Figure 5.22, left) and DME (Figure 5.20, left) in the reactant mixture.

On the other hand, the temperatures at which DMM starts to be consumed, during the high-pressure oxidation of its mixtures with C₂H₂, are considerably higher than those required for DMM conversion during its high-pressure oxidation itself under similar conditions (Figure 5.12), namely 650 K for $\lambda = 0.7$ and 1, and 600 K for $\lambda = 20$.

As previously done while analyzing the high-pressure oxidation of C₂H₂-DME mixtures (Section 5.4.2.2), model calculations, at 20 bar and $\lambda = 1$ without DMM, have been carried out to analyze if the addition of DMM has any effect on C₂H₂ conversion. As it can be seen in Figure 5.22, the presence of DMM in the reactant mixture shifts the C₂H₂ conversion to lower temperatures, 25 K approximately, with no big differences found between the lowest and the highest DMM concentrations.

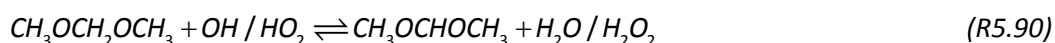
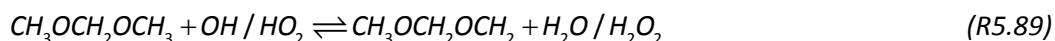
The results obtained in the reaction rate analyses performed indicate that there is no novelty in the main C₂H₂ consumption routes previously described during the high-pressure oxidation of C₂H₂-C₂H₅OH and C₂H₂-DME mixtures.

In the case of DMM, although no mentioned during the study of its high-pressure oxidation (Section 5.3.2), it may also decompose initially by reaction R5.86, generating more HCO radicals and afterwards HO₂ by reaction R5.77 ($HCO + O_2 \rightleftharpoons CO + HO_2$). Moreover, DMM reacts with molecular oxygen to obtain the primary radical (CH₃OCH₂OCH₂) and the secondary radical (CH₃OCHOCH₃) and more HO₂ radicals (R5.87 and R5.88).

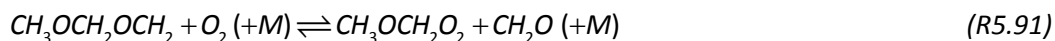




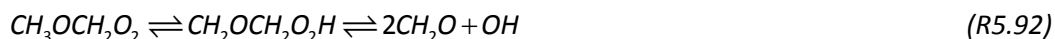
After initiation, the main consumption of DMM is through H-abstraction reactions. For $\lambda = 0.7$ and 1, reaction not only with OH radicals (as in the case of the high-pressure oxidation of DMM itself, Section 5.3.2), but also with HO₂ radicals can occur, to obtain both the primary and the secondary DMM radicals (R5.89 and R5.90) and H₂O₂, which afterwards decomposes to produce more OH radicals ($\text{H}_2\text{O}_2 (+M) \rightleftharpoons \text{OH} + \text{OH} (+M)$).



In comparison with the reaction routes described during the high-pressure oxidation of DMM itself, in the presence of C₂H₂, the secondary DMM radical (CH₃OCHOCH₃) also reacts with O₂ to produce MF and CH₂O as main products (R5.54, $\text{CH}_3\text{OCHOCH}_3 + \text{O}_2 \rightleftharpoons \text{CH}_2\text{O} + \text{CH}_3\text{OCHO} + \text{OH}$). However, in the case of the primary DMM radical (CH₃OCH₂OCH₂), it also reacts with molecular oxygen but instead of MF and CH₂O as products, the CH₃OCH₂O₂ radical is produced (R5.91).



This peroxy intermediate, CH₃OCH₂O₂, relevant under the high-pressure oxidation of DME and DMM (Section 5.2 and 5.3, respectively), instead of following the complex mechanism responsible for the low-temperature oxidation of DME (described in Section 5.2.2 by reactions R5.33-R5.35), it follows the routes described for higher temperatures (R5.92), where comparatively less OH radicals are generated.



Therefore, during the high-pressure oxidation of C₂H₂-DMM mixtures, for $\lambda = 0.7$ and 1, both reactants, C₂H₂ and DMM, compete for OH radicals and, as a consequence, the DMM conversion starts at higher temperatures than DMM oxidation itself. Moreover, the interaction of DMM with HO₂ radicals is comparatively stronger under the present conditions. Under oxidizing conditions and for the higher DMM concentration, the production of OH radicals is enhanced, and since those radicals are involved in DMM consumption by H-abstraction reactions, the result is that DMM starts to be consumed at lower temperatures than for the lower amount of DMM.

5. RESULTS AND DISCUSSION

The influence of a change in the working pressure on the oxidation of C_2H_2 -DMM mixtures has also been evaluated. As an example of the results obtained, Figure 5.23 shows a comparison of modeling predictions and experimental data for the concentrations of C_2H_2 and DMM, and the sum of CO and CO_2 , for stoichiometric conditions and 70 ppm of DMM in the reactant mixture. Although it is not shown, similar trends have been obtained for the other values of λ , pressures and amount of DMM analyzed.

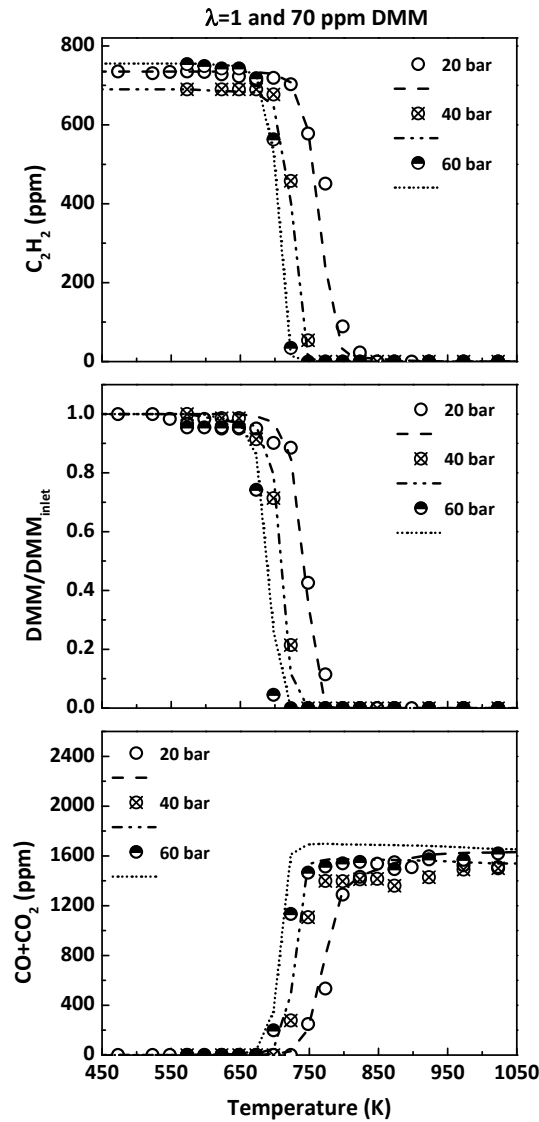


Figure 5.23. Influence of the pressure on the concentration profiles of C_2H_2 , DMM and $CO+CO_2$ as a function of temperature, during the C_2H_2 -DMM mixture oxidation, for $\lambda =1$ and 70 ppm of DMM added to the mixture. The inlet conditions correspond to sets 3DMMmix, 9DMMmix and 15DMMmix, in Table 5.10.

As it can be seen, the agreement between experimental and modeling results is very satisfactory and all the trends experimentally observed are well represented by the final kinetic model proposed in this work.

As previously reported when analyzing the high-pressure oxidation of the other C₂H₂-oxygenate mixtures, an increase in the working pressure shifts the onset temperature for the conversion of C₂H₂ and DMM, and consequently, the temperature for the formation of CO and CO₂, to lower temperatures.

The main reactions controlling the high-pressure oxidation of C₂H₂-DMM mixtures are the same independently of the working pressure. Therefore, the shift in the onset temperature of C₂H₂ and DMM conversion to lower temperatures, as pressure is increased, can be attributed to the increase in both the concentration of reactants and the gas residence time due to the increase in pressure, rather than to a change in the pathways that control the reaction rate.

5.4.4 Evaluation of the high-pressure oxidation of acetylene-oxygenated compound mixtures

After the high-pressure oxidation of the different C₂H₂-oxygenated compound mixtures has been individually analyzed, in this section, a comparison of the influence of the presence of each oxygenated compound on the high-pressure oxidation of C₂H₂ has been done, for $\lambda = 0.7$ and 20, for 40 bar and the highest amount of oxygenated compound studied.

The C₂H₂ inlet concentration is different for each mixture studied, therefore, for a clearer comparison, the C₂H₂ concentration has been normalized with respect to its inlet concentration. On the other hand, although the C₂H₂ inlet concentration is different for each mixture studied, the percentages selected of the oxygenated compound added to the mixture have been the same in all the cases, that is 10% and 40% of the C₂H₂ inlet concentration. For the comparison, only the highest percentage of additive has been selected, when the most relevant effects have been previously observed.

Figure 5.24 shows the comparison of results for two different values of lambda, reducing and oxidizing conditions ($\lambda = 0.7$ and 20), and 40 bar. It is the pressure selected because is the value experimentally analyzed for all the compounds under the same conditions. For the C₂H₂ high-pressure oxidation but in the absence of additives, modeling calculations have also been performed and are shown in Figure 5.24.

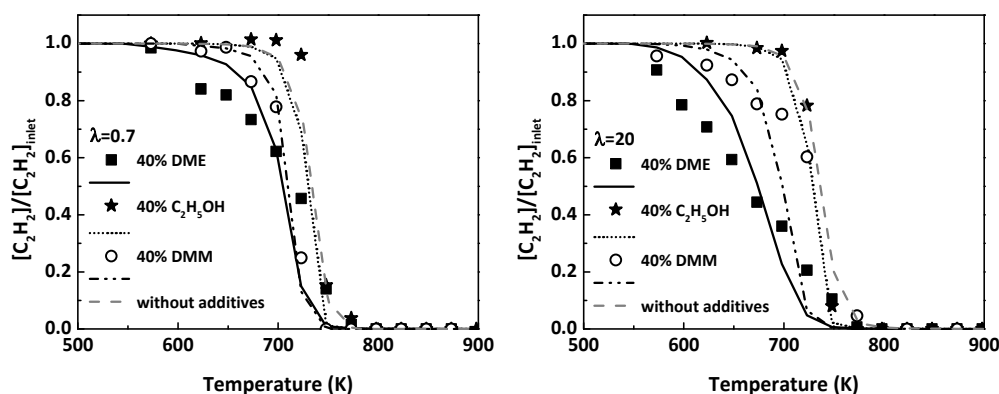


Figure 5.24. Effect of the addition of the different additives studied on the high-pressure (40 bar) oxidation of C_2H_2 , for $\lambda = 0.7$ (left) and $\lambda = 20$ (right).

It seems that the addition of ethanol has almost no effect on the oxidation of C_2H_2 , the predicted C_2H_2 concentration profile remains almost the same as without any additive, while the presence of an ether, DME or DMM, shifts the conversion of C_2H_2 to lower temperatures. This shifting in the onset temperature for C_2H_2 conversion is more significant for DME addition, the simplest ether considered, and it is more noticeable for oxidizing conditions. Moreover, the oxidation of C_2H_2 towards CO and CO_2 is favored by the addition of oxygenated compounds, instead of following reaction pathways which may lead to the formation of soot, due to an increase in the O/OH radical pool composition because of the oxygen present in such compounds.

The mechanism can be used as a prediction tool for conditions that can not be experimentally tested or that representative of real operating conditions. Therefore, theoretical calculations under very reducing ($\lambda = 0.2$) and high-pressure (20-100 bar) conditions have been performed for the C_2H_2 oxidation. This value of λ has been selected because the lowest value of lambda experimentally studied in the high-pressure flow reactor set-up is $\lambda = 0.7$. The reason is because particles of soot can be formed under very reducing conditions, deposited in the experimental set-up and cause severe damages. Moreover, during the atmospheric-pressure oxidation of C_2H_2 -DME mixtures (Section 5.4.2.1), for $\lambda = 0.2$, C_2H_2 was not completely consumed in all the temperature range analyzed. In this way, Figure 5.25 shows modeling predictions for the high-pressure oxidation of C_2H_2 in the absence of DME, at different pressures and very reducing conditions, $\lambda = 0.2$.

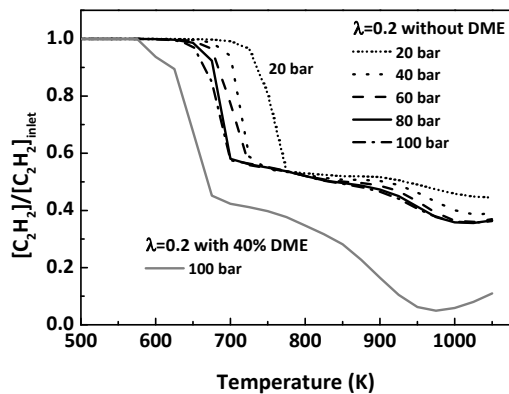


Figure 5.25. Evaluation through modeling calculations of the effect of pressure on the high-pressure C_2H_2 oxidation for $\lambda = 0.2$, in the absence and presence of DME.

As it can be seen, C_2H_2 is not completely consumed in all the temperature range analyzed. On the other hand, an increase in pressure from 20 to higher pressures, shifts the C_2H_2 conversion to lower temperatures, in the 700-800 K temperature range. However, this shift is less pronounced when pressure is increased from 40 to higher pressures. For the highest pressure analyzed, 100 bar, the effect of DME addition has also been evaluated since it has shown the biggest effect on C_2H_2 conversion. As it can be seen, DME presence effectively shifts the C_2H_2 conversion to lower temperatures and a higher C_2H_2 final consumption is achieved, so that, at temperatures around 1000 K, C_2H_2 is almost completely consumed.

Chapter 6:

Summary and conclusions

“Chapter 6 compiles and summarizes the main conclusions to be drawn from this thesis during the different oxidation studies of the oxygenated compounds, their mixtures with acetylene and intermediates, which have been performed along this work”.

6. SUMMARY AND CONCLUSIONS

In this thesis, the oxidation of three different oxygenated compounds, proposed as prospective fuel additives, namely dimethyl ether, ethanol and dimethoxymethane, has been investigated from both experimental and kinetic modeling points of view. The oxidation of intermediates of interest generated during the oxidation of these oxygenates has also been addressed. Finally, the role as fuel additives, of these oxygenated compounds, has been evaluated by studying the oxidation of their mixtures with acetylene, considered an important soot precursor and also an important intermediate in the combustion of higher hydrocarbons.

6.1 OXIDATION OF THE INTERMEDIATES: METHYL FORMATE AND METHANE

6.1.1 High-pressure oxidation of methyl formate and its interaction with NO in a flow reactor

MF has been found to be a byproduct and intermediate of the oxidation of several fuel additives, such as DME and DMM. Therefore, its oxidation has been studied in a quartz flow reactor, in the 573-1073 K temperature range, at different pressures (1-60 bar) and from reducing to oxidizing conditions ($\lambda = 0.7-20$). Furthermore, at a constant pressure of 20 bar, the effect of the NO presence on MF oxidation has also been evaluated for the different values of λ analyzed.

The experimental data obtained have been interpreted in terms of the final mechanism compiled in the present work as described in Chapter 4. Additionally, the MF subset has been revised and updated according to a recent work on DME oxidation at low temperatures (Rodriguez et al., 2015) and, after the modifications, modeling predictions have improved, especially in the results corresponding to the effect of the presence of NO, with respect to the mechanism previously used to describe the high-pressure oxidation of MF (Paper A). In general, there is a good agreement between experimental results and modeling calculations.

In the absence of NO, the oxygen availability in the reactant mixture has an almost imperceptible effect on the onset temperature for MF conversion. However, an increase in the working pressure shifts the onset for MF conversion to lower temperatures. Moreover, the reaction pathways occurring at high pressure are a bit more complex than those observed

under atmospheric conditions, because of the formation and evolution of CH_2OCHO and CH_3OCO radicals, which are not so relevant at atmospheric pressure.

An increase in the working pressure has also an impact on NO to NO_2 conversion. When pressure is raised above atmospheric level, most NO is converted to NO_2 , which exhibits a high reactivity, taking part in many reactions with the intermediates formed. As a consequence, in the presence of NO, MF presents an increased reactivity, and the onset for MF conversion is shifted to lower temperatures because of the increased relevance of reactions involving OH radicals and MF. However, results indicate that no net reduction of NO_x is achieved in the MF-NO interaction at high pressure. This is because NO_2 , from NO conversion, participates in several reactions and, finally, NO is formed again.

6.1.2 Low-temperature oxidation of CH_4 in a jet-stirred reactor in the presence of NO_x

Methane has been widely found as intermediate during the oxidation of many hydrocarbons and, in the case of the oxygenated compounds studied in this work, due to the high CH_3 radical concentration from the conversion of these oxygenates, the formation of CH_4 is, *a priori*, also expected.

The influence of the NO and NO_2 presence on the oxidation of CH_4 has been analyzed in a jet-stirred reactor from both experimental and modeling points of view, in the 650-1200 K temperature range, with a fixed residence time of 1.5 s, under oxidizing to reducing conditions. Different diagnostic techniques have been used for the detection and quantification of the gases: GC, cw-CRDS, FTIR and a NO_x analyzer. In general, there is a good agreement between experimental results and modeling calculations with the POLIMI mechanism.

The addition of NO_2 or NO causes comparable effects on CH_4 oxidation, shifting the onset temperature for CH_4 consumption to lower temperatures, from 1025 K to 825 K, regardless of the air excess ratio. The kinetic analysis made shows that the similar behavior of NO and NO_2 promoting CH_4 oxidation is related to their exchange via the reactions $\text{NO}_2 + \text{H} / \text{CH}_3 \rightleftharpoons \text{NO} + \text{OH} / \text{CH}_3\text{O}$ and $\text{NO} + \text{HO}_2 / \text{CH}_3\text{O}_2 \rightleftharpoons \text{NO}_2 + \text{OH} / \text{CH}_3\text{O}$, in a common oxidation-sensitizing mechanism. The OH radicals produced during the NO- NO_2 interconversion cycle interact with CH_4 promoting its conversion, whereas the H and HO_2 radicals produced during the oxidation of CH_4 promote the NO- NO_2 interconversion.

Regarding the detection and quantification of other important nitrogen containing species, at high temperatures and reducing conditions, the formation of HCN, by means of reburn type reactions of NO with hydrocarbon radicals, has been detected and quantified with a FTIR. On the other hand, modeling calculations predict the formation of CH_3NO_2 , in the 800-1000 K temperature range. However, no obvious FTIR absorption spectra for this species have been observed. Thus, the maximum CH_3NO_2 concentration produced is under 5 ppm, the estimated FTIR detection limit. In the case of HONO, the maximum concentration produced under the present conditions is below the estimated detection limit of 3 ppm (for the JSR and CRDS coupling).

The new experimental data and new species detection, along with the validation of a detailed kinetic model under these new conditions, have provided insight into understanding the mutual effect of CH_4 - NO_x interaction.

6.2 HIGH-PRESSURE OXIDATION OF DIMETHYL ETHER AND ETHANOL AND THEIR INTERACTION WITH NO

DME and ethanol are isomers; they present the same molecular formula but a different functional group, what may imply different properties and oxidation behaviors. Therefore, their high-pressure (20-60 bar) oxidation has been compared. The effect of the gas residence time and the effect of presence of NO on the oxidation process have been analyzed. Modeling predictions and experimental results are in good agreement for both compounds.

Experiments to distinguish between the effect of pressure or gas residence time have been carried out. Considering the experimental procedure followed in the high-pressure experimental set-up, a change in the working pressure, while maintaining constant the total gas flow rate, also implies a change in the gas residence time. Therefore, during the high-pressure oxidation of DME, pressure and total flow rate have been varied between 20 and 40 bar, and 1 and 2 L (STP)/min, respectively. Results (experimental and model) indicate that, under the conditions of this study, the effect of the gas residence time on DME high-pressure oxidation is clear and more noticeable than the effect of pressure. However, in the case of ethanol (only from a modeling point of view), results indicate that ethanol conversion is shifted to lower temperatures if either pressure or gas residence time are increased.

Although they are isomers, their high-pressure oxidation behavior is completely different. During DME conversion, the NTC zone, where DME reactivity is practically constant

6. SUMMARY AND CONCLUSIONS

or decreases with temperature, has been observed for all the conditions analyzed, although is less pronounced under very oxidizing conditions. In the case of ethanol oxidation, the oxygen availability in the mixture does not modify the temperature for the onset of ethanol conversion (at a constant pressure).

On the other hand, an increase in the working pressure implies different effects on the oxidation of each compound. For DME, an increase in the working pressure does not have a significant impact on the onset temperature for its conversion. However, ethanol oxidation starts at lower temperatures as the pressure is increased.

Furthermore, the presence of NO in the reactant mixture has a completely different effect on the high-pressure oxidation of each isomer. While the presence of NO clearly inhibits DME oxidation at low temperatures (550-700 K), the presence of NO promotes ethanol oxidation, shifting the onset for ethanol consumption to lower temperatures, and the higher the pressure, the lower the temperature.

Reaction rate analyses performed indicate that the main consumption of DME is through H-abstraction reactions forming the CH_3OCH_2 radical ($\text{CH}_3\text{OCH}_3 + R \rightleftharpoons \text{CH}_3\text{OCH}_2 + RH$). In the absence of NO, it reacts with O_2 to form $\text{CH}_3\text{OCH}_2\text{O}_2$ ($\text{CH}_3\text{OCH}_2 + \text{O}_2 \rightleftharpoons \text{CH}_3\text{OCH}_2\text{O}_2$) which continues reacting through a complex mechanism releasing OH radicals. However, the presence of NO has an inhibiting effect on DME high-pressure oxidation at low temperatures because of: (i) the competition between $\text{CH}_3\text{OCH}_2 + \text{O}_2$ and $\text{CH}_3\text{OCH}_2 + \text{NO}_2 \rightleftharpoons \text{CH}_3\text{OCH}_2\text{O} + \text{NO}$ reactions, and (ii) the participation of NO in the $\text{CH}_3\text{OCH}_2\text{O}_2 + \text{NO} \rightleftharpoons \text{CH}_3\text{OCH}_2\text{O} + \text{NO}_2$ reaction, preventing $\text{CH}_3\text{OCH}_2\text{O}_2$ radicals to continue reacting. Consequently, NO and NO_2 are interchanged in a cycle but never consumed.

The promoting effect of NO presence on the high-pressure ethanol oxidation can be explained by the increased relevance of the interactions of CH_3 and NO_2 (from the conversion of NO to NO_2 at high pressure and in presence of O_2) and the increased concentration of OH radicals from the interaction between NO_2 and water, and the decomposition of HONO ($\text{HONO} \rightleftharpoons \text{NO} + \text{OH}$).

6.3 ATMOSPHERIC AND HIGH-PRESSURE OXIDATION OF DIMETHOXYMETHANE IN A FLOW REACTOR

POMDMEs, $\text{CH}_3\text{O}(\text{CH}_2\text{O})_n\text{CH}_3$, such as DME or DMM, are polyethers considered as attractive diesel additives or substitutes. Therefore, the oxidation of DMM under high-pressure conditions has also been studied. But first, the atmospheric oxidation of DMM has been analyzed.

The oxidation of DMM has been studied in an atmospheric flow reactor, in the 573-1073 K temperature range and for different values of lambda ($\lambda = 0-35$), from pyrolysis to fuel-lean conditions. Theoretical concentrations, predicted by the final mechanism compiled in the present work, are slightly shifted to lower temperatures if compared with predictions obtained with the mechanism initially used in the atmospheric-oxidation study of DMM (Paper I). Nonetheless, both mechanisms are able to reproduce the major experimental trends.

On the other hand, the high-pressure oxidation of DMM has been investigated in a flow reactor in the 373-1073 K temperature range, for different air excess ratios ($\lambda = 0.7, 1$ and 20) and pressures (20-60 bar). The experimental results obtained have been interpreted in terms of the final mechanism compiled in the present work and the results obtained have been compared with those obtained with the mechanism used during the high-pressure oxidation study of DMM (Paper II). Although for some conditions ($\lambda = 0.7$ at 20 and 40 bar, and $\lambda = 1$ at 20 bar) the agreement with experimental results is better, for others, the final mechanism predicts an increased DMM reactivity. It is mainly due to the modifications made to DME reaction subset (Section 4.4) involving $\text{CH}_3\text{OCH}_2\text{O}_2$ reactions. Attempts to improve modeling calculations have been made according to recent DMM studies. However, no big improvements have been achieved, and, therefore, those modifications have not been finally included.

At atmospheric pressure, the temperature for the onset of DMM conversion is almost the same independently of the value of lambda analyzed. DMM consumption occurs in the 973-1123 K temperature range. At higher pressures, slight differences are also noticed when working under stoichiometric or somewhat fuel-rich conditions, although the DMM conversion is a bit different for oxidizing conditions. Under these conditions (high pressure and $\lambda = 20$) DMM consumption starts at lower temperatures and there is a temperature range (698-673 K) where DMM reactivity decreases and DMM concentration remains almost constant. On the other hand, an increase in the working pressure, does not have a big effect on neither the oxidation of DMM nor on the formation of the main products.

Independently of the environment (reducing, stoichiometric or oxidizing) and for atmospheric and high pressures, the main consumption of DMM occurs through H-abstraction reactions to obtain the primary radical ($\text{CH}_3\text{OCH}_2\text{OCH}_2$) or the secondary radical ($\text{CH}_3\text{OCHOCH}_3$). Furthermore, MF is an important intermediate formed during DMM oxidation. However, under oxidizing and high-pressure conditions, a new reaction pathway involving the peroxy intermediate, $\text{CH}_3\text{OCH}_2\text{O}_2$, which is also very important during the high-pressure oxidation of DME (Section 5.2.2), becomes relevant.

The concentration profile obtained during the high-pressure oxidation of each of the two ethers analyzed in this thesis, DME and DMM, is completely different. While for DME the NTC zone has been observed for all the conditions analyzed, although is less pronounced for $\lambda = 35$, for DMM only under very oxidizing conditions ($\lambda = 20$), a plateau where DMM concentration remains almost constant has been observed in the 598-673 K temperature range. Moreover, at low temperatures, DME seems to be more reactive than DMM with its conversion starting at lower temperatures.

6.4 HIGH-PRESSURE OXIDATION OF ACETYLENE-OXYGENATED COMPOUND MIXTURES

The role as fuel additives of the different oxygenated compounds has been analyzed by the characterization of the high-pressure oxidation of their mixtures with acetylene, which is considered an important soot precursor and also an intermediate during the oxidation of hydrocarbons.

6.4.1 High-pressure oxidation of acetylene-ethanol mixtures

The influence of the temperature (573-1073 K), pressure (10 or 40 bar), inlet oxygen concentration ($\lambda = 0.7, 1$ or 20), and ethanol concentration in the reactant mixture (50-200 ppm) has been evaluated during the high-pressure oxidation of C_2H_2 - $\text{C}_2\text{H}_5\text{OH}$ mixtures. The final detailed chemical kinetic mechanism compiled in the present thesis has been used for theoretical calculations. In general, the mechanism is able to reproduce the wide range of conditions experimentally tested.

Neither the oxygen concentration nor the amount of ethanol added to the reaction mixture have a significant influence on the onset temperature for the conversion of C_2H_2 . Only

an increase in the working pressure (when moving from 10 to 40 bar) shifts the onset for C₂H₂ conversion to lower temperatures.

The reaction routes for C₂H₂ consumption remain practically unaltered by the addition of ethanol in comparison to those obtained in the high-pressure oxidation study of C₂H₂ itself (Giménez-López et al., 2016). The interaction of C₂H₂ with OH radicals appears to be the main consumption route for the different values of lambda analyzed.

Apparently, under the present conditions, there is no interaction between acetylene and ethanol; their respective oxidation is only modified by an increase in the O/OH radical pool produced during the conversion of the other reactant. Therefore, the effectiveness of ethanol in reducing soot formation from C₂H₂ (Esarte et al., 2011), is probably due to the oxygen present in ethanol, which contributes to an increase in the O/OH radical pool composition, favoring C₂H₂ oxidation towards CO and CO₂ and, hence, removing carbon from the reaction paths which lead to soot formation.

6.4.2 Atmospheric-pressure oxidation of acetylene-dimethyl ether mixtures in the absence and presence of NO

A study of the oxidation of C₂H₂-DME mixtures at atmospheric pressure, analyzing the influence of temperature, air excess ratio (λ) and the presence of NO, has been performed under flow reactor conditions. The experimental results obtained have been compared against modeling calculations with the final mechanism compiled in the present thesis. In general, modeling predictions are in good agreement with the experimental trends obtained under the present conditions.

Unlike what is observed in their individual oxidations, the onset temperature for the C₂H₂ and DME conversion in the oxidation of their mixtures depends on the oxygen availability, being lower for the highest value of the air excess ratio considered ($\lambda = 20$).

The reaction pathways for C₂H₂ conversion, in the presence of DME, are basically the same as those in its absence. In this way, DME addition only modifies the radical pool composition, and it can act as an inhibitor or promoter, shifting the onset for C₂H₂ conversion to higher or lower temperatures, respectively, depending on the oxygen availability and the amount of DME present in the mixture. That is, for $\lambda = 0.7$, when DME is present in the mixture, less H radicals participate in C₂H₂ consumption through the H addition to form vinyl radicals ($C_2H_2 + H (+M) \rightleftharpoons C_2H_3 (+M)$), and as a consequence, C₂H₂ conversion is shifted to higher

temperatures; the higher the amount of DME in the mixture, the higher the temperature. However, for $\lambda = 20$, the trend is the opposite, and both DME and C_2H_2 conversions are shifted to lower temperatures due to the increase in O and OH radical formation.

Acetylene, DME and their intermediates may interact with NO, reaching different NO diminution levels depending on the conditions. The higher NO decrease levels are achieved in the absence of DME for temperatures above 1100 K and $\lambda = 0.7$ and $\lambda = 1$. This is due to the competition between reactions $HCCO+NO$ and $HCCO+O_2$. By increasing the oxygen availability, the $HCCO+O_2$ reactions predominate reaching a lower NO reduction. However, under fuel-lean conditions ($\lambda = 20$), the presence of DME increases NO diminution mainly due to CH_3 (from the decomposition of DME) and HO_2 (from HCO reaction with O_2) radicals, which can react with NO.

6.4.3 High-pressure oxidation of acetylene-dimethyl ether mixtures

The high-pressure oxidation of C_2H_2 -DME mixtures has been studied in the 450-1050 K temperature range in a flow reactor. The influence on the oxidation process of pressure (20-60 bar), oxygen inlet concentration (different values of the air excess ratio, λ), and the amount of DME (100 or 400 ppm) present in the reactant mixture, has also been evaluated. Experimental data have been compared with modeling predictions obtained with the final mechanism compiled in the present work, and, in general, there is a good agreement between experimental and modeling results.

Independently of the oxygen availability, for a constant pressure, the onset temperature for C_2H_2 and DME conversion is almost the same, except for oxidizing conditions, when both start to be consumed at lower temperatures, approximately 100 K less. In the case of DME, this temperature is comparatively higher than the required for DME oxidation itself, around 175-200 K more.

The presence of DME in the mixture shifts the conversion of C_2H_2 to lower temperatures due to the increased formation of OH radicals during DME consumption; the higher the DME amount, the lower the temperature. An increase in the working pressure also shifts the onset temperature for C_2H_2 and DME conversion to lower temperatures.

Under the present conditions, the main consumption routes for C_2H_2 and DME remain almost unchanged. Therefore, as in the case of the high-pressure oxidation of C_2H_2 - C_2H_5OH

mixtures, the addition of DME to the reactant mixture only modifies the composition of the radical pool, increasing the relevance of C_2H_2 reactions with OH radicals.

6.4.4 High-pressure oxidation of acetylene-dimethoxymethane mixtures

The influence of oxygen (λ) and DMM (70 or 280 ppm) inlet concentrations on the high-pressure (20-60 bar) oxidation of C_2H_2 -DMM mixtures has been studied in a flow reactor, in the 450-1050 K temperature range. Moreover, modeling calculations have also been performed with the final mechanism and compared against experimental results with a good agreement.

An increase in the amount of DMM in the reactant mixture or in the working pressure shifts the onset temperature for C_2H_2 and DMM conversion to lower temperatures.

For the different values of lambda analyzed, no significant differences have been found in the onset temperature for the conversion of C_2H_2 and DMM. Except for the highest amount of DMM tested and oxidizing conditions ($\lambda = 20$), when DMM starts to be consumed at lower temperatures mainly because of the enhanced production of OH radicals.

The main consumption routes for C_2H_2 are not modified by the addition of DMM. Its main consumption is by reaction with OH radicals. In the case of DMM, it is also consumed through the same reaction pathways as during its high-pressure oxidation itself, i.e. through H-abstraction reactions not only by OH radicals, but also with HO_2 radicals (from the conversion of C_2H_2). In the mixtures study, these routes are not modified by a change in the working pressure. Therefore, the shift in the onset temperature for C_2H_2 and DMM conversion to lower temperatures, as pressure is increased, is attributed to the increase in both the concentration of reactants and in the gas residence time, due to the increase in pressure, rather than to a change in the pathways that control the reaction rate.

6.5 GENERAL CONCLUSION

The individual knowledge of the oxidation of the three different oxygenated compounds, dimethyl ether, ethanol and dimethoxymethane, selected to be studied in this work because of their potential as prospective fuel additives, has allowed to compile and validate a detailed chemical kinetic mechanism able to describe the high-pressure oxidation of their mixtures with acetylene and analyze their role as fuel additives.

6. SUMMARY AND CONCLUSIONS

Results indicate that the functional group has a strong influence on the oxidation behavior of the mixtures. The addition of an alcohol, ethanol, has almost no effect on the oxidation of C_2H_2 ; whereas the addition of an ether, DME or DMM, shifts the conversion of C_2H_2 to lower temperatures, and the simpler the ether (lower carbon number) the lower the temperatures. Therefore, DME is the most effective in reducing the onset temperature for C_2H_2 conversion. The oxidation of C_2H_2 towards CO and CO_2 , and hence removing carbon from the reaction paths which lead to the formation of soot, is favored by an increase in the O/OH radical pool composition due to the oxygen present in the oxygenated compounds.

Chapter 6:

Resumen y conclusiones

“El Capítulo 6 recopila y resume las principales conclusiones que se pueden extraer de los diferentes estudios realizados, a lo largo de este trabajo, sobre la oxidación de los compuestos oxigenados, sus mezclas con acetileno y productos intermedios, que se han realizado a lo largo de este trabajo”.

6. RESUMEN Y CONCLUSIONES

En esta tesis, se ha investigado, tanto desde un punto de vista experimental como de modelado cinético, la oxidación de tres compuestos oxigenados diferentes, propuestos como posibles aditivos para combustible: dimetil éter, etanol y dimetoximetano. También se ha abordado el estudio de la oxidación de compuestos intermedios de interés generados durante la oxidación de dichos compuestos oxigenados. Finalmente, se ha evaluado el papel de estos compuestos oxigenados como aditivos para combustible, mediante el estudio de la oxidación de sus mezclas con acetileno, considerado como un importante precursor de hollín, además de un importante intermedio en la combustión de hidrocarburos.

6.1 OXIDACIÓN DE LOS INTERMEDIOS: FORMIATO DE METILO Y METANO

6.1.1 Oxidación a alta presión de formiato de metilo y su interacción con NO en un reactor de flujo

MF es un subproducto e intermedio en la oxidación de varios aditivos de combustible, como DME y DMM. Por lo tanto, se ha estudiado su oxidación en un reactor de flujo de cuarzo, en el intervalo de temperaturas de 573-1073 K, a distintas presiones (1-60 bar) y desde condiciones reductoras hasta condiciones oxidantes ($\lambda = 0.7-20$). Además, para una presión constante de 20 bar, se ha analizado el efecto de la presencia de NO en la oxidación de MF, para los distintos valores de λ analizados.

Los datos experimentales obtenidos han sido interpretados en términos del mecanismo final compilado en el presente trabajo, tal y como se ha descrito en el Capítulo 4. Además, se ha revisado y actualizado el subconjunto de reacciones de MF de acuerdo con un reciente trabajo sobre la oxidación de DME a bajas temperaturas (Rodríguez et al., 2015) y, tras las modificaciones realizadas, las predicciones del modelo han mejorado con respecto a las del mecanismo previamente utilizado para describir la oxidación a alta presión de MF (Artículo A), especialmente en el caso de los resultados correspondientes al efecto de la presencia de NO. En general, existe un buen acuerdo entre los resultados experimentales y los predichos por el modelo.

En ausencia de NO, la disponibilidad de oxígeno en la mezcla reaccionante tiene un efecto casi imperceptible en la temperatura de inicio para la conversión de MF. Sin embargo,

un aumento en la presión de trabajo desplaza la conversión de MF a menores temperaturas. Además, las vías de reacción que tienen lugar a alta presión son algo más complejas que las observadas a presión atmosférica, debido a la formación y evolución de los radicales CH_2OCHO y CH_3OCO , que no son tan relevantes a presión atmosférica.

Un aumento en la presión de trabajo también tiene un impacto en la conversión de NO a NO_2 . Cuando la presión se eleva por encima de la atmosférica, la mayor parte de NO se convierte en NO_2 , que presenta una alta reactividad y participa en varias reacciones con los diferentes intermedios formados. Como consecuencia, en presencia de NO, MF presenta una mayor reactividad, y el inicio de la conversión de MF se desplaza a temperaturas menores debido a la mayor relevancia de las reacciones que involucran a los radicales OH y a MF. Sin embargo, los resultados indican que no se logra una reducción neta de NO_x en la interacción MF-NO a alta presión. Ello se debe a que el NO_2 , procedente de la conversión de NO, participa en varias reacciones para finalmente volver a generar NO.

6.1.2 Oxidación a baja temperatura de CH_4 en un reactor perfectamente agitado en presencia de NO_x

El metano se ha encontrado frecuentemente como intermedio durante la oxidación de numerosos hidrocarburos y, en el caso de los compuestos oxigenados estudiados en este trabajo, se espera también, *a priori*, la formación de CH_4 debido a la alta concentración de radicales CH_3 procedentes de su conversión.

La influencia de la presencia de NO y NO_2 en la oxidación de CH_4 se ha analizado en un reactor de mezcla perfecta, desde un punto de vista tanto experimental como de modelado cinético, en el intervalo de temperaturas de 650 a 1200 K, con un tiempo de residencia fijo de 1.5 s, utilizando estequiometrías desde condiciones oxidantes a reductoras. Se han empleado diferentes técnicas de diagnóstico para la detección y cuantificación de los gases: GC, cw-CRDS, FTIR y un analizador de NO_x . En general, existe un buen acuerdo entre los resultados experimentales obtenidos y los predichos por el mecanismo POLIMI.

La adición de NO_2 o de NO tiene efectos similares sobre la oxidación de CH_4 , desplazando la temperatura de inicio para el consumo de CH_4 a menores temperaturas, de 1025 a 825 K, independientemente de la relación de exceso de aire. El análisis cinético realizado ha mostrado que el comportamiento similar de NO y de NO_2 , promoviendo la oxidación de CH_4 , está relacionado con su interconversión a través de las reacciones

$NO_2 + H / CH_3 \rightleftharpoons NO + OH / CH_3O$ y $NO + HO_2 / CH_3O_2 \rightleftharpoons NO_2 + OH / CH_3O$. Los radicales OH producidos durante dicha interconversión interaccionan con CH_4 promoviendo su conversión, mientras que los radicales H y HO_2 , producidos durante la oxidación de CH_4 , promueven la interconversión NO- NO_2 .

En lo que respecta a la detección y cuantificación de otras especies importantes que contienen nitrógeno, a altas temperaturas y en condiciones reductoras, se ha detectado la formación de HCN, a través de reacciones de tipo *reburning* de NO con radicales de hidrocarburos, y ha sido cuantificado con ayuda de un espectrómetro FTIR. Por otro lado, las simulaciones con el modelo predicen la formación de CH_3NO_2 , en el intervalo de temperatura 800-1000 K. Sin embargo, en el análisis con FTIR, no se han observado espectros de absorción obvios para esta especie. Por lo tanto, se deduce que la concentración máxima de CH_3NO_2 producida es inferior a 5 ppm, que es el límite estimado de detección en FTIR. En el caso de HONO, la máxima concentración producida en las condiciones de estudio está por debajo del límite de detección estimado de 3 ppm en CRDS.

Los nuevos datos experimentales y la detección de nuevas especies, junto con la validación del modelo cinético detallado en estas nuevas condiciones de trabajo, han proporcionado información necesaria para comprender la interacción CH_4+NO_x .

6.2 OXIDACIÓN A ALTA PRESIÓN DE DIMETIL ÉTER Y ETANOL Y SU INTERACCIÓN CON NO

DME y etanol son isómeros; tienen la misma fórmula molecular, pero su grupo funcional es diferente, lo que puede implicar diferentes propiedades y comportamiento durante su oxidación. Por lo tanto, se han comparado los resultados de su oxidación a alta presión (20-60 bar), analizando el efecto del tiempo de residencia del gas y de la presencia de NO en el proceso. Las predicciones del modelo y los resultados experimentales obtenidos concuerdan bien para ambos compuestos.

Se han llevado a cabo experimentos para distinguir entre el efecto de la presión o del tiempo de residencia del gas. Teniendo en cuenta el procedimiento experimental seguido en la instalación de alta presión, un cambio en la presión de trabajo, mientras se mantiene constante el caudal de gas total, también implica un cambio en el tiempo de residencia del gas. Por lo tanto, durante la oxidación a alta presión de DME, la presión y el caudal total se variaron de 20 a 40 bar, y de 1 a 2 L (STP)/min, respectivamente. Los resultados (experimentales y de

modelado) indican que, bajo las condiciones de este estudio, el efecto del tiempo de residencia del gas en la oxidación a alta presión de DME es más claro y notable que el efecto de la presión. Sin embargo, en el caso de etanol (sólo desde un punto de vista de modelado), los resultados indican que la conversión de etanol se desplaza a menores temperaturas si se aumenta la presión o el tiempo de residencia del gas.

Aunque son isómeros, su comportamiento durante la oxidación a alta presión es completamente diferente. Durante la conversión de DME, en todas las condiciones analizadas, aunque menos pronunciada en condiciones muy oxidantes, se ha observado la zona NTC (*negative temperature coefficient*) caracterizada por una reactividad de DME prácticamente constante o que disminuye con la temperatura. En el caso de la oxidación de etanol, la disponibilidad de oxígeno en la mezcla no modifica la temperatura para el inicio de la conversión de etanol (a una presión constante).

Por otro lado, un aumento en la presión de trabajo implica diferentes efectos en la oxidación de cada compuesto. Para DME, un aumento en la presión de trabajo no tiene un impacto significativo en la temperatura de inicio para su conversión. Sin embargo, la oxidación de etanol comienza a menores temperaturas a medida que se aumenta la presión.

La presencia de NO en la mezcla reaccionante tiene un efecto completamente diferente en la oxidación a alta presión de cada isómero. Si bien la presencia de NO inhibe claramente la oxidación de DME a bajas temperaturas (550-700 K), la presencia de NO promueve la oxidación de etanol, desplazando el inicio del consumo de etanol a menores temperaturas, tanto más cuanto mayor es la presión.

Los análisis de velocidad de reacción realizados indican que el principal consumo de DME se produce a través de reacciones de abstracción de H para formar el radical CH_3OCH_2 ($\text{CH}_3\text{OCH}_3 + \text{R} \rightleftharpoons \text{CH}_3\text{OCH}_2 + \text{RH}$). En ausencia de NO, este radical reacciona con O_2 para formar $\text{CH}_3\text{OCH}_2\text{O}_2$ ($\text{CH}_3\text{OCH}_2 + \text{O}_2 \rightleftharpoons \text{CH}_3\text{OCH}_2\text{O}_2$) que continúa reaccionando a través de un complejo mecanismo liberando radicales OH. Sin embargo, la presencia de NO tiene un efecto inhibitorio sobre la oxidación a alta presión de DME debido a: (i) la competencia entre las reacciones $\text{CH}_3\text{OCH}_2 + \text{O}_2$ y $\text{CH}_3\text{OCH}_2 + \text{NO}_2 \rightleftharpoons \text{CH}_3\text{OCH}_2\text{O} + \text{NO}$, y (ii) la participación de NO en la reacción $\text{CH}_3\text{OCH}_2\text{O}_2 + \text{NO} \rightleftharpoons \text{CH}_3\text{OCH}_2\text{O} + \text{NO}_2$, evitando que los radicales $\text{CH}_3\text{OCH}_2\text{O}_2$ continúen reaccionando. En consecuencia, NO y NO_2 se intercambian en un proceso cíclico, pero no se produce un consumo neto de los mismos.

El efecto promotor de la presencia de NO en la oxidación de etanol a alta presión puede explicarse por la mayor relevancia de las interacciones entre CH₃ y NO₂ (procedente de la conversión de NO a NO₂ a alta presión y en presencia de O₂) y el aumento de la concentración de radicales OH procedentes de la interacción entre NO₂ y agua, y de la descomposición de HONO ($HONO \rightleftharpoons NO + OH$).

6.3 OXIDACIÓN A PRESIÓN ATMOSFÉRICA Y ALTA PRESIÓN DE DIMETOXIMETANO EN UN REACTOR DE FLUJO

Los POMDMEs, CH₃O(CH₂O)_nCH₃, como DME o DMM, son poliéteres considerados atractivos aditivos o sustitutos del diésel. Por lo tanto, también se ha estudiado la oxidación de DMM en condiciones de alta presión, pero primero, se ha analizado su oxidación a presión atmosférica.

La oxidación de DMM se ha estudiado en un reactor de flujo a presión atmosférica, en el intervalo de temperaturas de 573-1073 K y para diferentes valores de lambda ($\lambda = 0-35$), desde condiciones de pirólisis hasta condiciones oxidantes. Las concentraciones predichas por el mecanismo final compilado en el presente trabajo se desplazan ligeramente a temperaturas más bajas si se comparan con las predicciones obtenidas con el mecanismo utilizado inicialmente en el estudio de oxidación a presión atmosférica de DMM (Artículo I). No obstante, ambos mecanismos son capaces de reproducir las principales tendencias experimentales.

Por otro lado, la oxidación a alta presión de DMM se ha investigado en un reactor de flujo en el intervalo de temperaturas de 373-1073 K, para diferentes relaciones de exceso de aire ($\lambda = 0.7, 1$ y 20) y presiones (20-60 bar). Los resultados experimentales obtenidos se han interpretado en términos del mecanismo final compilado en el presente trabajo, así como con el mecanismo utilizado durante el estudio de oxidación a alta presión de DMM (Artículo II). Aunque para algunas condiciones ($\lambda = 0.7, 20$ y 40 bar, y $\lambda = 1$ y 20 bar) el acuerdo de los resultados teóricos con los experimentales es mejor, para otras, el mecanismo final predice un aumento de la reactividad de DMM. Esto se debe principalmente a las modificaciones realizadas en el subconjunto de reacciones de DME (Sección 4.4), que involucra reacciones de la especie CH₃OCH₂O₂. Se han realizado diversos intentos para mejorar los cálculos de modelado considerando estudios recientes de la oxidación de DMM. Sin embargo, no se han

logrado mejoras significativas y, por lo tanto, esas modificaciones finalmente no se han incluido en el mecanismo final compilado.

A presión atmosférica, la temperatura de inicio de la conversión de DMM es casi la misma independientemente del valor de λ analizado. El consumo de DMM se produce en el intervalo de temperaturas de 973-1123 K. A mayores presiones, se notan ligeras diferencias cuando se trabaja en condiciones estequiométricas o ligeramente reductoras, pero la conversión de DMM es diferente en condiciones oxidantes. Bajo condiciones de alta presión y $\lambda = 20$, el consumo de DMM comienza a menores temperaturas, aunque la reactividad de DMM disminuye y la concentración de DMM permanece casi constante en el intervalo de temperaturas de 698-673 K. Por otro lado, un aumento en la presión de trabajo no tiene un gran efecto ni en la oxidación de DMM ni en la formación de los principales productos.

Independientemente de las condiciones (reductoras, estequiométricas u oxidantes) y tanto para presión atmosférica como para alta presión, el principal consumo de DMM se produce a través de reacciones de abstracción de H para obtener el radical primario ($\text{CH}_3\text{OCH}_2\text{OCH}_2$) o el radical secundario ($\text{CH}_3\text{OCHOCH}_3$). Además, MF es un intermedio importante en la oxidación de DMM. Sin embargo, bajo condiciones oxidantes y de alta presión, aparece una nueva vía de reacción que involucra al intermedio peróxido, $\text{CH}_3\text{OCH}_2\text{O}_2$, que también es muy importante durante la oxidación a alta presión de DME (Sección 5.2.2).

El perfil de concentraciones de DME y DMM (los dos éteres analizados en esta tesis) durante su oxidación a alta presión es completamente diferente. Mientras que para DME, la zona NTC se ha observado para todas las condiciones analizadas, aunque menos pronunciada para $\lambda = 35$, para DMM, sólo en condiciones muy oxidantes ($\lambda = 20$) se ha observado una meseta donde la concentración de DMM permanece casi constante en el intervalo de temperaturas de 598-673 K. Además, a bajas temperaturas, DME parece ser más reactivo que DMM y su conversión comienza a menores temperaturas.

6.4 OXIDACIÓN A ALTA PRESIÓN DE LAS MEZCLAS ACETILENO-COMPUESTO OXIGENADO

El papel como aditivos de combustible de los diferentes compuestos oxigenados se ha analizado mediante el estudio de la oxidación a alta presión de sus mezclas con acetileno, que se considera como un importante precursor de hollín y también un compuesto intermedio durante la oxidación de hidrocarburos.

6.4.1 Oxidación a alta presión de mezclas acetileno-etanol

La influencia de la temperatura (573-1073 K), la presión (10 o 40 bar), la concentración de oxígeno a la entrada ($\lambda = 0.7, 1$ o 20) y la concentración de etanol en la mezcla reaccionante (50-200 ppm) se han evaluado durante la oxidación a alta presión de las mezclas $C_2H_2-C_2H_5OH$. En general, el mecanismo cinético químico detallado final, compilado en la presente tesis, es capaz de reproducir los resultados obtenidos bajo las diferentes condiciones experimentales.

Ni la concentración de oxígeno ni la cantidad de etanol añadida a la mezcla reaccionante tienen una influencia significativa en la temperatura de inicio de la conversión de C_2H_2 . Sólo un aumento en la presión de trabajo (de 10 a 40 bar) desplaza el inicio de la conversión de C_2H_2 a menores temperaturas.

Las rutas de reacción durante el consumo de C_2H_2 permanecen prácticamente inalteradas por la adición de etanol, en comparación con las obtenidas en el estudio de oxidación a alta presión de C_2H_2 (Giménez-López y cols., 2016). La interacción de C_2H_2 con los radicales OH parece ser su principal ruta de consumo independientemente de la relación de exceso de aire.

Aparentemente, no existe interacción entre el acetileno y el etanol en las condiciones analizadas; su respectiva oxidación sólo se modifica por un aumento en los radicales O/OH producidos durante la conversión del otro reactivo. Por lo tanto, la efectividad del etanol en la reducción de la formación de hollín a partir de C_2H_2 (Esarte y cols., 2011) se debe probablemente al oxígeno presente en el etanol, que contribuye a un aumento en la concentración de los radicales O/OH, favoreciendo la oxidación de C_2H_2 hacia CO y CO_2 y, por tanto, eliminando carbono de las rutas de reacción que conducen a la formación de hollín.

6.4.2 Oxidación a presión atmosférica de las mezclas acetileno-dimetil éter en ausencia y en presencia de NO

Se ha realizado un estudio de la oxidación de mezclas de C_2H_2 -DME a presión atmosférica, analizando la influencia de la temperatura, la relación de exceso de aire (λ) y la presencia de NO, en un reactor de flujo. Los resultados experimentales obtenidos se han comparado con las simulaciones con el mecanismo final compilado en la presente tesis. En general, las predicciones de modelado están en buena concordancia con las tendencias experimentales obtenidas en las condiciones analizadas.

A diferencia de lo que se observa en el estudio de su oxidación individual, la temperatura de inicio para la conversión de C_2H_2 y DME en la oxidación de sus mezclas depende de la disponibilidad de oxígeno, siendo menor para el mayor valor de la relación de exceso de aire considerado ($\lambda = 20$).

Las vías de reacción para la conversión de C_2H_2 , en presencia de DME, son básicamente las mismas que en su ausencia. De esta manera, la adición de DME sólo modifica la composición de la reserva de radicales, y puede actuar como un inhibidor o promotor, desplazando el inicio de la conversión de C_2H_2 a temperaturas mayores o menores, respectivamente, dependiendo de la disponibilidad de oxígeno y de la cantidad de DME presente en la mezcla. Para $\lambda = 0.7$, cuando DME está presente en la mezcla participan menos radicales H en el consumo de C_2H_2 a través de reacciones de adición de H para formar radicales vinilo ($C_2H_2 + H (+M) \rightleftharpoons C_2H_3 (+M)$) y, como consecuencia, la conversión de C_2H_2 se desplaza a mayores temperaturas, tanto más cuanto mayor sea la cantidad de DME en la mezcla. Sin embargo, para $\lambda = 20$, la tendencia es la opuesta, y la conversión de DME y C_2H_2 se desplaza a temperaturas menores debido al aumento en la formación de los radicales O y OH.

El acetileno, el DME y sus derivados pueden interactuar con NO, alcanzando diferentes niveles de reducción de NO dependiendo de las condiciones de operación concretas. Los mayores niveles de reducción de NO se logran en ausencia de DME para temperaturas superiores a 1100 K y $\lambda = 0.7, 1$. Esto se debe a la competencia entre las reacciones de HCCO con NO y O_2 . Al aumentar la disponibilidad de oxígeno, predominan las reacciones $HCCO + O_2$, alcanzándose un nivel de reducción de NO menor. Sin embargo, en condiciones oxidantes ($\lambda = 20$), la presencia de DME aumenta la reducción de NO, principalmente debido a los radicales CH_3 (de la descomposición de DME) y HO_2 (de la reacción de HCO con O_2), que pueden reaccionar con NO.

6.4.3 Oxidación a alta presión de las mezclas acetileno-dimetil éter

Se ha estudiado la oxidación a alta presión de las mezclas C_2H_2 -DME en el intervalo de temperaturas de 450-1050 K en un reactor de flujo. También se ha evaluado la influencia de la presión (20-60 bar), la concentración de entrada de oxígeno (diferentes valores de la relación de exceso de aire, λ) y la cantidad de DME (100 o 400 ppm) presente en la mezcla reaccionante en el proceso de oxidación. Se han comparado los datos experimentales con las predicciones del modelo obtenidas con el mecanismo final compilado en el presente trabajo y, en general, existe una buena concordancia entre los resultados experimentales y de modelado.

Para una presión constante, la temperatura de inicio de la conversión de C_2H_2 y DME es casi la misma independientemente de la disponibilidad de oxígeno, excepto en condiciones oxidantes, cuando ambos compuestos comienzan a consumirse a temperaturas menores, aproximadamente 100 K menos. En el caso de DME, esta temperatura es comparativamente mayor que la requerida para la oxidación de DME, aproximadamente 175-200 K más.

La presencia de DME en la mezcla desplaza la conversión de C_2H_2 a menores temperaturas debido al aumento de la formación de radicales OH durante el consumo de DME; cuanto mayor es la cantidad de DME, menor es la temperatura. Un aumento en la presión de trabajo también desplaza la temperatura de inicio para la conversión de C_2H_2 y DME a menores temperaturas.

Las principales rutas de consumo para C_2H_2 y DME permanecen casi sin cambios con respecto a las que se observan en sus oxidaciones individuales. Por lo tanto, la adición de DME a la mezcla reaccionante sólo modifica la composición del conjunto de radicales, aumentando la relevancia de las reacciones de C_2H_2 con radicales OH, como ocurría en el caso de la oxidación a alta presión de las mezclas de C_2H_2 - C_2H_5OH .

6.4.4 Oxidación a alta presión de las mezclas acetileno-dimetoximetano

La influencia de la concentración de oxígeno (λ) y DMM (70 o 280 ppm) en la oxidación a alta presión (20-60 bar) de las mezclas de C_2H_2 -DMM se ha estudiado en un reactor de flujo, en el intervalo de temperaturas de 450-1050 K. Además, los cálculos de modelado realizados con el mecanismo final se han comparado con los resultados experimentales, obteniéndose un buen acuerdo.

Un aumento de la cantidad de DMM en la mezcla reaccionante, o de la presión de trabajo, desplaza la temperatura de inicio para la conversión de C_2H_2 y DMM a temperaturas menores.

Para los diferentes valores de lambda analizados, no se han encontrado diferencias significativas en la temperatura de inicio para la conversión de C_2H_2 y DMM; excepto para la mayor cantidad de DMM considerada y condiciones oxidantes ($\lambda = 20$), caso en el que DMM comienza a consumirse a temperaturas menores, principalmente debido a la mayor producción de radicales OH.

La adición de DMM no modifica las principales rutas de consumo de C_2H_2 . El principal consumo de C_2H_2 se produce a través de la reacción con radicales OH. En el caso de DMM, éste

también se consume a través de las mismas vías de reacción que durante su oxidación a alta presión, es decir, a través de reacciones de abstracción de H, no sólo con radicales OH sino también con radicales HO₂ (procedentes de la conversión de C₂H₂). En el estudio de las mezclas, estas rutas tampoco se modifican por un cambio en la presión de trabajo. Por lo tanto, el desplazamiento en la temperatura de inicio de la conversión de C₂H₂ y DMM, a temperaturas menores a medida que aumenta la presión, se atribuye al aumento tanto de la concentración de reactivos como del tiempo de residencia del gas, debido al aumento de la presión, en lugar de a un cambio en los caminos que controlan la velocidad de reacción.

6.5 CONCLUSIÓN GENERAL

El conocimiento de la oxidación individual de los tres compuestos oxigenados diferentes: dimetil éter, etanol y dimetoximetano, seleccionados para ser estudiados en este trabajo debido a su potencial como posibles aditivos de combustible, ha permitido compilar y validar un mecanismo químico cinético detallado capaz de describir la oxidación a alta presión de sus mezclas con acetileno y analizar su papel como aditivos al combustible.

Los resultados indican que el grupo funcional tiene una gran influencia en el comportamiento de las mezclas durante su oxidación. La adición de un alcohol, etanol, casi no tiene efecto en la oxidación de C₂H₂; mientras que la adición de un éter, DME o DMM, desplaza la conversión de C₂H₂ a menores temperaturas, tanto más cuanto más simple es el éter (menor número de carbonos). Por lo tanto, el DME es el más efectivo para reducir la temperatura de inicio para la conversión de C₂H₂. La oxidación de C₂H₂ hacia CO y CO₂ y, por lo tanto, la eliminación de carbono de las rutas de reacción que conducen a la formación de hollín se ven favorecidas por un aumento en la concentración de radicales O/OH debido al oxígeno presente en las moléculas de los compuestos oxigenados.

References

- Abián, M.; Esarte, C.; Millera, Á.; Bilbao, R.; Alzueta, M.U. (2008). Oxidation of acetylene-ethanol mixtures and their interaction with NO. *Energy and Fuels* 22, 3814-3823.
- Abián, M.; Silva, S.L.; Millera, Á.; Bilbao, R.; Alzueta, M.U. (2010). Effect of operating conditions on NO reduction by acetylene-ethanol mixtures. *Fuel Processing Technology* 91, 1204-1211.
- Abián, M. (2013). Pollutant reduction in combustion systems through flue gas recirculation (FGR). PhD Thesis, Universidad de Zaragoza, Spain.
- Agarwal, A.K. (2007). Biofuels (alcohols and biodiesel) applications as fuels for internal combustion engines. *Progress in Energy and Combustion Science* 33, 233-271.
- Aghsaee, M.; Nativel, D.; Bozkurt, M.; Fikri, M.; Chaumeix, N.; Schulz, C. (2015). Experimental study of the kinetics of ethanol pyrolysis and oxidation behind reflected shock waves and in laminar flames. *Proceedings of the Combustion Institute* 35, 393-400.
- Akih-Kumgeh, B.; Bergthorson, J.M. (2010). Shock tube study of methyl formate ignition. *Energy and Fuels* 24, 396-403.
- Alexandrino, K.; Millera, Á.; Bilbao, R.; Alzueta, M.U. (2014). Interaction between 2,5-dimethylfuran and nitric oxide: experimental and modeling study. *Energy and Fuels* 28, 4193-4198.
- Alexandrino, K.; Millera, Á.; Bilbao, R.; Alzueta, M.U. (2015). Novel aspects in the pyrolysis and oxidation of 2,5-dimethylfuran. *Proceedings of the Combustion Institute* 35, 1717-1725.
- Alexandrino, K.; Millera, Á.; Bilbao, R.; Alzueta, M.U. (2016). 2-methylfuran oxidation in the absence and presence of NO. *Flow Turbulence Combustion* 96, 343-362.
- Alexandrino, K. (2018). Study of the oxidation and pyrolysis of different oxygenated compounds proposed as alternative fuels. PhD Thesis, Universidad de Zaragoza, Spain.
- Al-Noman, S.M.; Choi, B.C.; Chung, S.H. (2018). Autoignited lifted flames of dimethyl ether in heated coflow air. *Combustion and Flame* 195, 75-83.

REFERENCES

- Alzueta, M.U.; Glarborg, P.; Dam-Johansen, K. (1997). Low temperature interactions between hydrocarbons and nitric oxide: an experimental study. *Combustion and Flame* 109, 25-36.
- Alzueta, M.U.; Muro, J.; Bilbao, R.; Glarborg, P. (1999). Oxidation of dimethyl ether and its interaction with nitrogen oxides. *Israel Journal of Chemistry* 39, 73-86.
- Alzueta, M.U.; Bilbao, R.; Finestra, M. (2001). Methanol oxidation and its interaction with nitric oxide. *Energy and Fuels* 15, 724-729.
- Alzueta, M.U.; Hernández, J.M. (2002). Ethanol oxidation and its interaction with nitric oxide. *Energy and Fuels* 16, 166-171.
- Alzueta, M.U.; Borruey, M.; Callejas, A.; Millera, Á.; Bilbao, R. (2008). An experimental and modeling study of the oxidation of acetylene in a flow reactor. *Combustion and Flame* 152, 377-386.
- Alzueta, M.U.; Aranda, V.; Monge, F.; Millera, Á.; Bilbao, R. (2013). Oxidation of methyl formate and its interaction with nitric oxide. *Combustion and Flame* 160, 853-860.
- Alzueta, M.U.; Salinas, P.; Millera, Á.; Bilbao, R.; Abián, M. (2017). A study of dimethyl carbonate conversion and its impact to minimize soot and NO emissions. *Proceedings of the Combustion Institute* 36, 3985-3993.
- ANSYS Chemkin-Pro 17.2 (2016). ANSYS Reaction Design: San Diego, USA.
- Aranda, V.; Christensen, J.M.; Alzueta, M.U.; Glarborg, P.; Gersen, S.; Gao, Y.; Marshall, P. (2013). Experimental and kinetic modeling study of methanol ignition and oxidation at high pressure. *International Journal of Chemical Kinetics* 45, 283-294.
- Arcoumanis, C.; Bae, C.; Crookes, R.; Kinoshita, E. (2008). The potential of di-methyl ether (DME) as an alternative fuel for compression-ignition engines: a review. *Fuel* 87, 1014-1030.
- Arif, M.; Dellinger, B.; Taylor, P.H. (1997). Rate coefficients of hydroxyl radical reaction with dimethyl ether and methyl tert-butyl ether over an extended temperature range. *Journal of Physical Chemistry A* 101, 2436-2441.

- Awad, O.I.; Mamat, R.; Ali, O.M.; Sidik, N.A.C.; Yusaf, T.; Kadirgama, K.; Kettner, M. (2018). Alcohol and ether as alternative fuels in spark ignition engine: a review. *Renewable and Sustainable Energy Reviews* 82, 2586-2605.
- Azizi, Z.; Rezaeimanesh, M.; Tohidian, T.; Rahimpour, M.R. (2014). Dimethyl ether: a review of technologies and production challenges. *Chemical Engineering and Processing* 82, 150-172.
- Bahrini, C.; Herbinet, O.; Glaude, P.A.; Schoemaeker, C.; Fittschen, C.; Battin-Leclerc, F. (2012). Detection of some stable species during the oxidation of methane by coupling a jet-stirred reactor (JSR) to cw-CRDS. *Chemical Physics Letters* 534, 1-7.
- Balat, M. (2011). Production of bioethanol from lignocellulosic materials via the biochemical pathway: a review. *Energy Conversion and Management* 52, 858-875.
- Barraza-Botet, C.L.; Wagnon, S.W.; Wooldridge, M.S. (2016). Combustion chemistry of ethanol: ignition and speciation studies in a rapid compression facility. *Journal of Physical Chemistry A* 120, 7408-7418.
- Baulch, D.; Griffiths, J.; Papin, A.J.; Sykes, A.F. (1988). Stationary-state and oscillatory combustion of hydrogen in a well-stirred flow reactor. *Combustion and Flame* 73, 163-185.
- Bendtsen, A.B.; Glarborg, P.; Dam-Johansen, K. (2000). Low temperature oxidation of methane: the influence of nitrogen oxides. *Combustion Science and Technology* 151, 31-71.
- Bennett, B.A.V.; McEnally, C.S.; Pfefferle, L.D.; Smooke, M.D.; Colket, M.B. (2009). Computational and experimental study of the effects of adding dimethyl ether and ethanol to nonpremixed ethylene/air flames. *Combustion and Flame* 156, 1289-1302.
- Bierkandt, T.; Kasper, T.; Akyildiz, E.; Lucassen, A.; Oßwald, P.; Köhler, M.; Hemberger, P. (2015). Flame structure of a low-pressure laminar premixed and lightly sooting acetylene flame and the effect of ethanol addition. *Proceedings of the Combustion Institute* 35, 803-811.
- Bilbao, R.; Millera, Á.; Alzueta, M.U. (1994). Influence of the temperature and oxygen concentration on NO_x reduction in the natural gas reburning process. *Industrial and Engineering Chemistry Research* 33, 2846-2852.

REFERENCES

- Bromly, J.H.; Barnes, F.J.; Muris, S.; You, X.; Haynes, B.S. (1996). Kinetic and thermodynamic sensitivity analysis of the NO-sensitized oxidation of methane. *Combustion Science and Technology* 115, 259-296.
- Burger, J.; Siegert, M.; Ströfer, E.; Hasse, H. (2010). Poly(oxyethylene) dimethyl ethers as components of tailored diesel fuel: properties, synthesis and purification concepts. *Fuel* 89, 3315-3319.
- Burke, S.M.; Metcalfe, W.; Herbinet, O.; Battin-Leclerc, F.; Haas, F.M.; Santner, J.; Dryer, F.L.; Curran, H.J. (2014). An experimental and modeling study of propene oxidation. Part 1: speciation measurements in jet-stirred and flow reactors. *Combustion and Flame* 161, 2765-2784.
- Burke, S.M.; Burke, U.; McDonagh, R.; Mathieu, O.; Osorio, I.; Keese, C.; Morones, A.; Petersen, E.L.; Wang, W.; DeVerter, T.A.; et al. (2015a). An experimental and modeling study of propene oxidation. Part 2: Ignition delay time and flame speed measurements. *Combustion and Flame* 162, 296-314.
- Burke, U.; Somers, K.P.; O'Toole, P.; Zinner, C.M.; Marquet, N.; Bourque, G.; Petersen, E.L.; Metcalfe, W.K.; Serinyel, Z.; Curran, H.J. (2015b). An ignition delay and kinetic modeling study of methane, dimethyl ether, and their mixtures at high pressures. *Combustion and Flame* 162, 315-330.
- Canosa, C.; Penzhorn, R.D.; Sonntag, C. (1979). Product quantum yields from the photolysis of NO₂ at 366 nm in presence of ethylene. The role of NO₃^{*}. *Berichte der Bunsengesellschaft für physikalische Chemie* 83, 217-225.
- Chan, Y.L.; Barnes, F.J.; Bromly, J.H.; Konnov, A.A.; Zhang, D.K. (2011). The differentiated effect of NO and NO₂ in promoting methane oxidation. *Proceedings of the Combustion Institute* 33, 441-447.
- Chen, H.; Shuai, S.J.; Wang, J.X. (2007). Study on combustion characteristics and PM emission of diesel engines using ester-ethanol-diesel blended fuels. *Proceedings of the Combustion Institute* 31, 2981-2989.
- Chen, G.; Yu, W.; Fu, J.; Mo, J.; Huang, Z.; Yang, J.; Wang, Z.; Jin, H.; Qi, F. (2012). Experimental and modeling study of the effects of adding oxygenated fuels to premixed n-heptane flames. *Combustion and Flame* 159, 2324-2335.

- Christensen, M.; Nilsson, E.J.K.; Konnov, A.A. (2015). The temperature dependence of the laminar burning velocities of methyl formate + air flames. *Fuel* 157, 162-170.
- Cipolat, D. (2007). Analysis of energy release and NO_x emissions of a CI engine fueled on diesel and DME. *Applied Thermal Engineering* 27, 2095-2103.
- Cocco, D.; Tola, V.; Cau, G. (2006). Performance evaluation of chemically recuperated gas turbine (CRGT) power plants fuelled by di-methyl-ether (DME). *Energy* 31, 1446-1458.
- Crookes, R.J.; Bob-Manuel, K.D.H. (2007). RME or DME: a preferred alternative fuel option for future diesel engine operation. *Energy Conversion and Management* 48, 2971-2977.
- Curran, H.J.; Pitz, W.J.; Westbrook, C.K.; Dagaut, P.; Boettner, J.C.; Cathonnet, M. (1998). A wide range modelling study of dimethyl ether oxidation. *International Journal of Chemical Kinetics* 30, 229-241.
- Curran, H.J.; Fischer, S.L.; Dryer, F.L. (2000). The reaction kinetics of dimethyl ether. II: Low-temperature oxidation in flow reactors. *International Journal of Chemical Kinetics* 32, 741-759.
- Dagaut, P.; Boettner, J.C.; Cathonnet, M. (1990). Ethylene pyrolysis and oxidation: a kinetic modeling study. *International Journal of Chemical Kinetics* 22, 641-664.
- Dagaut, P.; Cathonnet, M. (1990). Kinetics of ethane oxidation in a high pressure jet-stirred reactor: experimental results. *Journal de Chimie Physique* 87, 1173.
- Dagaut, P.; Boettner, J.C.; Cathonnet, M. (1991). Methane oxidation: experimental and kinetic modeling study. *Combustion Science and Technology* 77, 127-148.
- Dagaut, P.; Daly, C.; Simmie, J.M.; Cathonnet, M. (1998). The oxidation and ignition of dimethylether from low to high temperature (500-1600 K): experiments and kinetic modeling. *Symposium (International) on Combustion [Proceedings]* 27, 361-369.
- Dagaut, P.; Nicolle, A. (2005). Experimental study and detailed kinetic modeling of the effect of exhaust gas on fuel combustion: mutual sensitization of the oxidation of nitric oxide and methane over extended temperature and pressure range. *Combustion and Flame* 140, 161-171.

REFERENCES

- Dagaut, P.; Togbé, C. (2012). Oxidation kinetics of mixtures of iso-octane with ethanol or butanol in a jet-stirred reactor: experimental and modeling study. *Combustion Science and Technology* 184, 1025-1038.
- Daly, C.; Simmie, J.M.; Dagaut, P.; Cathonnet, M. (2001). Oxidation of dimethoxymethane in a jet-stirred reactor. *Combustion and Flame* 125, 1106-1117.
- Dames, E.E.; Rosen, A.S.; Weber, B.W.; Gao, C.W.; Sung, C.J.; Green, W.H. (2016). A detailed combined experimental and theoretical study on dimethyl ether/propane blended oxidation. *Combustion and Flame* 168, 310-330.
- Dec, J.E. (2009). Advanced compression-ignition engines-understanding the in-cylinder processes. *Proceedings of the Combustion Institute* 32, 2727-2742.
- De Joannon, M.; Sabia, P.; Tregrossi, A.; Cavaliere, A. (2004). Dynamic behavior of methane oxidation in premixed flow reactor. *Combustion Science and Technology* 176, 769-783.
- Dias, V.; Lories, X.; Vandooren, J. (2010). Lean and rich premixed dimethoxymethane/oxygen/argon flames: experimental and modeling. *Combustion Science and Technology* 182, 350-364.
- Diévar, P.; Won, S.H.; Gong, J.; Dooley, S.; Ju, Y. (2013). A comparative study of the chemical kinetic characteristics of small methyl esters in diffusion flame extinction. *Proceedings of the Combustion Institute* 34, 821-829.
- Dmitriev, A.M.; Knyazkov, D.A.; Bolshova, T.A.; Tereshchenko, A.G.; Paletsky, A.A.; Shmakov, A.G.; Korobeinichev, O.P. (2015). Structure of CH₄/O₂/Ar flames at elevated pressures studied by flame sampling molecular beam mass spectrometry and numerical simulation. *Combustion and Flame* 162, 3946-3959.
- Dooley, S.; Burke, M.P.; Chaos, M.; Stein, Y.; Dryer, F.L.; Zhukov, V.P.; Finch, O.; Simmie, J.M.; Curran, H.J. (2010). Methyl formate oxidation: speciation data, laminar burning velocities, ignition delay times, and a validated chemical kinetic model. *International Journal of Chemical Kinetics* 42, 527-549.
- Dooley, S.; Dryer, F.L.; Yang, B.; Wang, J.; Cool, T.A.; Kasper, T.; Hansen, N. (2011). An experimental and kinetic modeling study of methyl formate low-pressure flames. *Combustion and Flame* 158, 732-741.

- El Merhubi, H.; Kéromnès, A.; Catalano, G.; Lefort, B.; Le Moyne, L. (2016). A high pressure experimental and numerical study of methane ignition. *Fuel* 177, 164-172.
- Esarte, C.; Millera, Á.; Bilbao, R.; Alzueta, M.U. (2010). Effect of ethanol, dimethylether, and oxygen, when mixed with acetylene on the formation of soot and gas products. *Industrial and Engineering Chemistry Research* 49, 6772-6779.
- Esarte, C. (2011). Pyrolysis of acetylene with ethanol and other oxygenated compounds. Study of formation of soot and gaseous pollutants. PhD Thesis, Universidad de Zaragoza, Spain.
- Esarte, C.; Callejas, A.; Millera, Á.; Bilbao, R.; Alzueta, M.U. (2011). Influence of the concentration of ethanol and the interaction of compounds in the pyrolysis of acetylene and ethanol mixtures. *Fuel* 90, 844-849.
- Faßheber, N.; Friedrichs, G.; Marshall, P.; Glarborg, P. (2015). Glyoxal oxidation mechanism: implications for the reaction $\text{HCO} + \text{O}_2$ and $\text{OCHCHO} + \text{HO}_2$. *Journal of Physical Chemistry A* 119, 7305-7315.
- Fargione, J.; Hill, J.; Tilman, D.; Polasky, S.; Hawthorne, P. (2008). Land clearing and the biofuel carbon debt. *Science* 319, 1235-1238.
- Fisher, E.M.; Pitz, W.J.; Curran, H.J.; Westbrook, C.K. (2000). Detailed chemical kinetic mechanisms for combustion of oxygenated fuels. *Proceedings of the Combustion Institute* 28, 1579-1586.
- Frenklach, M. (2002). Reaction mechanism of soot formation in flames. *Physical Chemistry Chemical Physics* 4, 2028-2037.
- Galano, A.; Álvarez-Idaboy, J.R.; Ruiz-Santoyo, M.E.; Vivier-Bunge, A. (2002). Rate coefficient and mechanism of the gas phase OH hydrogen abstraction reaction from formic acid: a quantum mechanical approach. *Journal of Physical Chemistry A* 41, 9520-9528.
- Giménez-López, J.; Alzueta, M.U.; Rasmussen, C.T.; Marshall, P.; Glarborg, P. (2011). High pressure oxidation of $\text{C}_2\text{H}_4/\text{NO}$ mixtures. *Proceedings of the Combustion Institute* 33, 449-457.

REFERENCES

- Giménez-López, J.; Rasmussen, C.T.; Hashemi, H.; Alzueta, M.U.; Gao, Y.; Marshall, P.; Goldsmith, F.; Glarborg, P. (2016). Experimental and kinetic modeling study of C₂H₂ oxidation at high pressure. *International Journal of Chemical Kinetics* 48, 724-738.
- Glarborg, P.; Alzueta, M.U.; Dam-Johansen, K.; Miller, J.A. (1998). Kinetic modeling of hydrocarbon/nitric oxide interactions in a flow reactor. *Combustion and Flame* 115, 1-27.
- Glarborg, P.; Østberg, M.; Alzueta, M.U.; Dam-Johansen, K.; Miller, J.A. (1999). The recombination of hydrogen atoms with nitric oxide at high temperatures. *Proceedings of the Combustion Institute* 27, 219-227.
- Goswami, M.; Derks, S.C.R.; Coumans, K.; Slikker, W.J.; de Andrade Oliveira, M.H.; Bastiaans, R.J.M.; Luijten, C.C.M.; Goey, L.P.H.; Konnov, A.A. (2013). The effect of elevated pressures on the laminar burning velocity of methane + air mixtures. *Combustion and Flame* 160, 1627-1635.
- Hajilou, M.; Ombrello, T.; Won, S.H.; Blemont, E. (2017). Experimental and numerical characterization of freely propagating ozone-activated dimethyl ether cool flames. *Combustion and Flame* 176, 326-333.
- Hamelinck, C.N.; Faaij, A.P.C. (2006). Outlook for advanced biofuels. *Energy Policy* 34, 3268-3283.
- Hansen, A.C.; Zhang, Q.; Lyne, P.W.L. (2005). Ethanol-diesel fuel blends-a review. *Bioresource Technology* 96, 277-285.
- Hashemi, H.; Christensen, J.M.; Gersen, S.; Levinsky, H.; Klippenstein, S.J.; Glarborg, P. (2016). High-pressure oxidation of methane. *Combustion and Flame* 172, 349-364.
- Hashemi, H.; Christensen, J.M.; Glarborg, P. (2018). High-pressure pyrolysis and oxidation of ethanol. *Fuel* 218, 247-257.
- Herbinet, O.; Battin-Leclerc, F.; Bax, S.; Le Gall, H.; Glaude, P.A.; Fournet, R.; Zhou, Z.; Deng, L.; Guo, H.; Xie, M.; Qi, F. (2011). Detailed product analysis during the low temperature oxidation of n-butane. *Physical Chemistry Chemical Physics* 13, 296-308.

- Herbignet, O.; Battin-Leclerc, F. (2014). Progress in understanding low-temperature organic compound oxidation using a jet-stirred reactor. *International Journal of Chemical Kinetics* 46, 619-639.
- Herrmann, F.; Jochim, B.; Oßwald, P.; Cai, L.; Pitsch, H.; Kohse-Höinghaus, K. (2014). Experimental and numerical low-temperature oxidation study of ethanol and dimethyl ether. *Combustion and Flame* 161, 384-397.
- Hidaka, Y.; Sato, K.; Henmi, Y.; Tanaka, H.; Inami, K. (1999). Shock-tube and modeling study of methane pyrolysis and oxidation. *Combustion and Flame* 118, 340-358.
- Huang, J.; Hill, P.G.; Bushe, W.K.; Munshi, S.R. (2004). Shock-tube study of methane ignition under engine-relevant conditions: experiments and modeling. *Combustion and Flame* 136, 25-42.
- Huang, Z.H.; Ren, Y.; Jiang, D.M.; Liu, L.X.; Zeng, K.; Liu, B.; Wang, X.B. (2006). Combustion and emission characteristics of a compression ignition engine fueled with Diesel-dimethoxy methane blends. *Energy Conversion and Management* 47, 1402-1415.
- Huang, J.; Wang, Y.; Li, S.; Roskilly, A.P.; Yu, H.; Li, H. (2009a). Experimental investigation on the performance and emissions of a diesel engine fueled with ethanol-diesel blends. *Applied Thermal Engineering* 29, 2484-2490.
- Huang, C.; Yao, M.; Lu, X.; Huang, Z. (2009b). Study of dimethyl ether homogeneous charge compression ignition combustion process using a multi-dimensional computational fluid dynamics model. *International Journal of Thermal Sciences* 48, 1814-1822.
- Inal, F.; Senkan, S.M. (2005). Effects of oxygenate concentration on species mole fractions in premixed n-heptane flames. *Fuel* 84, 495-503.
- International Energy Agency, IEA. (2016). *World energy outlook special report: energy and air pollution*.
- International Energy Agency, IEA. (2017). *The future of trucks: implications for energy and the environment*.
- Junjun, Z.; Xinqi, Q.; Zhen, W.; Bin, G.; Zhen, H. (2009). Experimental investigation of low-temperature combustion (LTC) in an engine fueled with dimethyl ether (DME). *Energy and Fuels* 23, 170-174.

REFERENCES

- Kass, M.; Thomas, J.; Storey, J.; Domingo, N.; Wade, J.; Kenreck, G. (2001). Emissions from a 5.9 liter diesel engine fuelled with ethanol diesel blends. *SAE Technical Paper* 2001-01-2018.
- Katoch, A.; Milán-Merino, A.; Kumar, S. (2018). Measurement of laminar burning velocity of ethanol-air mixtures at elevated temperatures. *Fuel* 231, 37-44.
- Kee, R.J.; Rupley, F.M.; Miller, J.A. (1991). CHEMKIN-II: a Fortran chemical kinetics package for the analysis of gas-phase chemical kinetics; Sandia National Laboratories: Albuquerque; Report SAND87-8215.
- Khalife, E.; Tabatabaei, M.; Demirbas, A.; Aghbashlo, M. (2017). Impacts of additives on performance and emission characteristics of diesel engines during steady state operation. *Progress in Energy and Combustion Science* 59, 32-78.
- Kiecherer, J.; Bänsch, C.; Bentz, T.; Olzmann, M. (2015). Pyrolysis of ethanol: a shock-tube/TOF-MS and modeling study. *Proceedings of the Combustion Institute* 35, 465-472.
- Kohse-Höinghaus, K.; Oßwald, P.; Struckmeier, U.; Kasper, T.; Hansen, N.; Taatjes, C.A.; Wang, J.; Cool, T.A.; Gon, S.; Westmoreland, P.R. (2007). The influence of ethanol addition on premixed fuel-rich propene-oxygen-argon flames. *Proceedings of the Combustion Institute* 31, 1119-1127.
- Kohse-Höinghaus, K.; Oßwald, P.; Cool, T.A.; Kasper, T.; Hansen, N.; Qi, F.; Westbrook, C.K.; Westmoreland, P.R. (2010). Biofuel combustion chemistry: from ethanol to biodiesel. *Angewandte Chemie International Edition* 49, 3572-3597.
- Kopp, W.A.; Kröger, L.C.; Döntgen, M.; Jacobs, S.; Burke, U.; Curran, H.J.; Heufer, K.A.; Leonhard, K. (2018). Detailed kinetic modeling of dimethoxymethane. Part I: Ab initio thermochemistry and kinetics predictions for key reactions. *Combustion and Flame* 189, 433-442.
- Kristensen, P.G.; Glarborg, P.; Dam-Johansen, K. (1996). Nitrogen chemistry during burnout in fuel-staged combustion. *Combustion and Flame* 107, 211-222.
- Larson, C.W.; Steward, P.H.; Golden, D.M. (1988). Pressure and temperature dependence of reactions proceeding via a bound complex. An approach for combustion and

- atmospheric chemistry modelers. Application to $HCO + CO \rightarrow [HOCO] \rightarrow H + CO_2$. *International Journal of Chemical Kinetics* 20, 27-40.
- Lee, B.C.; Vranckx, S.; Heufer, K.A.; Khomik, S.V.; Uygun, Y.; Olivier, H.; Fernandes, R.X. (2012). On the chemical kinetics of ethanol oxidation: shock tube, rapid compression machine and detailed modeling study. *Zeitschrift für Physikalische Chemie* 226, 1-27.
- Lee, D.J.; Burrell, R.R.; Egolfopoulos, F.N. (2018). Propagation of sub-atmospheric methyl formate flames. *Combustion and Flame* 189, 24-32.
- Leitner, W.; Klankermayer, J.; Pischinger, S.; Pitsch, H.; Kohse-Höinghaus, K. (2017). Advanced biofuels and beyond: chemistry solutions for propulsion and production. *Angewandte Chemie International Edition* 56, 5412-5452.
- Leplat, N.; Dagaut, P.; Togbé, C.; Vandooren, J. (2011). Numerical and experimental study of ethanol combustion and oxidation in laminar premixed flames and in jet-stirred reactor. *Combustion and Flame* 158, 705-725.
- Li, R.; Liu, Z.; Han, Y.; Tan, M.; Xu, Y.; Tian, J.; Chong, D.; Chai, J.; Liu, J.; Li, Z. (2017). Experimental and numerical investigation into the effect of fuel type and fuel/air molar concentration on autoignition temperature of n-heptane, methanol, ethanol, and butanol. *Energy and Fuels* 31, 2572-2584.
- Liu, H.; Iglesia, E. (2003). Selective one-step synthesis of dimethoxymethane via methanol of dimethyl ether oxidation on $H_{3+n}V_nMo_{12-n}PO_{40}$ Keggin Structures. *Journal of Physical Chemistry B* 107, 10840-10847.
- Lutz, A.E.; Kee, R.J.; Miller, J.A. (1988). SENKIN: a Fortran program for predicting homogenous gas phase chemical kinetics with sensitivity analysis; Sandia National Laboratories: Livermore; Report SAND87-8248.
- Marinov, N.M. (1999). A detailed chemical kinetic model for high temperature ethanol oxidation. *International Journal of Chemical Kinetics* 31, 183-220.
- Marshall, P.; Glarborg, P. (2015). Ab initio and kinetic modeling studies of formic acid oxidation. *Proceedings of the Combustion Institute* 35, 153-160.

REFERENCES

- Martín, L. (2011). Oxidación de mezclas de acetileno y dimetoximetano. M.Sc. Thesis (in Spanish). Universidad de Zaragoza, Spain.
- Metcalf, W.K.; Burke, S.M.; Ahmed, S.S.; Curran, H.J. (2013). A hierarchical and comparative kinetic modeling study of C₁-C₂ hydrocarbon and oxygenated fuels. *International Journal of Chemical Kinetics* 45, 638-375.
- Miller, J.A.; Klippenstein, S.J.; Glarborg, P. (2003). A kinetic issue in reburning: the fate of HCNO. *Combustion and Flame* 135, 357-362.
- Mitu, M.; Brandes, E. (2017). Influence of pressure, temperature and vessel volume on explosion characteristics of ethanol/air mixtures in closed spherical vessels. *Fuel* 203, 460-468.
- Molera, M.J.; García Domínguez, J.A.; Santiuste, J.M. (1974). Slow gas-phase oxidation of methylal. *Anales de Química* 70, 579-586.
- Molera, M.J.; García Domínguez, J.A.; Santiuste, J.M. (1977). Gas-phase oxidation of dimethoxy methane-¹⁴C. *Anales de Química* 73, 467-471.
- Moréac, G.; Dagaut, P.; Roesler, J.F.; Cathonnet, M. (2006). Nitric oxide interaction with hydrocarbon oxidation in a jet-stirred reactor at 10 atm. *Combustion and Flame* 145, 512-520.
- Moshhammer, K.; Jasper, A.W.; Popolan-Vaida, D.M.; Wang, Z.; Shankar, V.S.B.; Ruwe, L.; Taatjes, C.A.; Dagaut, P.; Hansen, N. (2015). Quantification of the keto-hydroperoxide (HOOCH₂OCHO) and other elusive intermediates during low-temperature oxidation of dimethyl ether. *Journal of Physical Chemistry A* 120, 7890-7901.
- Olm, C.; Varga, T.; Valkó, E.; Hartl, S.; Hasse, C.; Turányi, T. (2016). Development of an ethanol combustion mechanism based on a hierarchical optimization approach. *International Journal of Chemical Kinetics* 48, 423-441.
- Pan, L.; Hu, E.; Zhang, J.; Zhang, Z.; Huang, Z. (2014). Experimental and kinetic study on ignition delay times of DME/H₂/O₂/Ar mixtures. *Combustion and Flame* 161, 735-747.
- Pan, L.; Hu, E.; Tian, Z.; Yang, F.; Huang, Z. (2015). Experimental and kinetic study on ignition delay times of dimethyl ether at high temperatures. *Energy and Fuels* 29, 3495-3506.

- Park, J.; Giles, N.D.; Moore, J.; Lin, M.C. (1998). A comprehensive kinetic study of thermal reduction of NO₂ by H₂. *Journal of Physical Chemistry A* 102, 10099-10105.
- Park, S.H.; Yoon, S.H. (2015). Injection strategy for simultaneous reduction of NO_x and soot emissions using two-stage injection in DME fueled engine. *Applied Energy* 143, 262-270.
- Petersen, E.L.; Davidson, D.F.; Hanson, R.K. (1999). Kinetics modeling of shock-induced ignition in low-dilution CH₄/O₂ mixtures at high pressures and intermediate temperatures. *Combustion and Flame* 117, 272-290.
- Ranzi, E.; Frassoldati, A.; Grana, R.; Cuoci, A.; Faravelli, T.; Kelley, A.P.; Law, C.K. (2012). Hierarchical and comparative kinetic modeling of laminar flame speeds of hydrocarbon oxygenated fuels. *Progress in Energy and Combustion Science* 38, 468-501.
- Rasmussen, C.L.; Rasmussen, A.E.; Glarborg, P. (2008a). Sensitizing effects of NO_x on CH₄ oxidation at high pressure. *Combustion and Flame* 154, 529-545.
- Rasmussen, C.L.; Hansen, J.; Marshall, P.; Glarborg, P. (2008b). Experimental measurements and kinetic modeling of CO/H₂/O₂/NO_x conversion at high pressure. *International Journal of Chemical Kinetics* 40, 454-480.
- Rasmussen, C.L.; Jakobsen, J.G.; Glarborg, P. (2008c). Experimental measurements and kinetic modeling of CH₄/O₂ and CH₄/C₂H₆/O₂ conversion at high pressure. *International Journal of Chemical Kinetics* 40, 778-807.
- Ren, W.; Dames, E.; Hyland, D.; Davidson, D.F.; Hanson, R.K. (2013a). Shock tube study of methanol, methyl formate pyrolysis: CH₃OH and CO time-history measurements. *Combustion and Flame* 160, 2669-2679.
- Ren, W.; Lam, K.Y.; Pyun, S.H.; Farooq, A.; Davidson, D.F.; Hanson, R.K. (2013b). Shock tube/laser absorption studies of the decomposition of methyl formate. *Proceedings of the Combustion Institute* 34, 453-461.
- Renard, C.; Van Tiggelen, P.J.; Vandooren, J. (2002). Effect of dimethoxymethane addition on the experimental structure of a rich ethylene/oxygen/argon flame. *Proceedings of the Combustion Institute* 29, 1277-1284.

REFERENCES

- Rezgui, Y.; Guemini, M. (2014). Effect of ethanol on soot precursors emissions during benzene oxidation in a jet-stirred reactor. *Environmental Science and Pollution Research* 21, 6671-6686.
- Rodriguez, A.; Frottier, O.; Herbinet, O.; Fournet, R.; Bounaceur, R.; Fittschen, C.; Battin-Leclerc, F. (2015). Experimental and modeling investigation of the low-temperature oxidation of dimethyl ether. *Journal of Physical Chemistry A* 119, 7905-7923.
- Rodriguez, A. (2016). Étude de la combustion de composés organiques grâce au couplage d'un réacteur parfaitement agité avec des méthodes analytiques spectroscopiques et spectrométriques: application à la détection des hydroperoxydes. PhD Thesis (in French), Université de Lorraine, France.
- Rodriguez, A.; Herbinet, O.; Wang, Z.; Qi, F.; Fittschen, C.; Westmoreland, P.R.; Battin-Leclerc, F. (2017). Measuring hydroperoxide chain-branching agents during n-pentane low-temperature oxidation. *Proceedings of the Combustion Institute* 36, 333-342.
- Sarathy, S.M.; Oßwald, P.; Hansen, N.; Kohse-Höinghaus, K. (2014). Alcohol combustion chemistry. *Progress in Energy and Combustion Science* 44, 40-102.
- Saxena, P.; Williams, F.A. (2007). Numerical and experimental studies of ethanol flames. *Proceedings of the Combustion Institute* 31, 1149-1156.
- Schönborn, A.; Sayad, P.; Konnov, A.A.; Klingmann, J. (2014). Autoignition of dimethyl ether and air in an optical flow-reactor. *Energy and Fuels* 28, 4130-4138.
- Semelsberger, T.A.; Borup, R.L.; Greene, H.L. (2006). Dimethyl ether (DME) as an alternative fuel. *Journal of Power Sources* 156, 497-511.
- Sinha, A.; Thomson, M.J. (2004). The chemical structures of opposed flow diffusion flames of C₃ oxygenated hydrocarbons (isopropanol, dimethoxy methane, and dimethyl carbonate) and their mixtures. *Combustion and Flame* 136, 548-556.
- Song, K.H.; Nag, P.; Litzinger, T.A.; Haworth, D.C. (2003). Effects of oxygenated additives on aromatic species in fuel-rich, premixed ethane combustion: a modeling study. *Combustion and Flame* 135, 341-349.

- Sun, W.; Tao, T.; Lailliau, M.; Hansen, N.; Yang, B.; Dagaut, P. (2018). Exploration of the oxidation chemistry of dimethoxymethane: jet-stirred reactor experiments and kinetic modeling. *Combustion and Flame* 193, 491-501.
- Szybist, J.P.; Song, J.; Alam, M.; Boehman, A.L. (2007). Biodiesel combustion, emissions and emission control. *Fuel Processing Technology* 88, 679-691.
- Thavornprasert, K.; Capron, M.; Jalowiecki-Duhamel, L.; Gardoll, O.; Trentesaux, M.; Mamede, A.S.; Fang, G.; Faye, J.; Touati, N.; Vezin, H.; Dubois, J.L.; Couturier, J.L.; Dumeignil, F. (2014). Highly productive iron molybdate mixed oxides and their relevant catalytic properties for direct synthesis of 1,1-dimethoxymethane from methanol. *Applied Catalysis B: Environmental* 145, 126-135.
- U.S. Energy Information Administration, EIA. (2013). *International Energy Outlook*. Washington: EIA, 2013.
- Vermeire, F.H.; Carstensen, H.H.; Herbinet, O.; Battin-Leclerc, F.; Marin, G.B.; Van Geem, K.M. (2018). Experimental and modeling study of the pyrolysis and combustion of dimethoxymethane. *Combustion and Flame* 190, 270-283.
- Viteri, F.; López, A.; Millera, Á.; Bilbao, R.; Alzueta, M.U. (2019). Influence of temperature and gas residence time on the formation of polycyclic aromatic hydrocarbons (PAH) during the pyrolysis of ethanol. *Fuel* 236, 820-828.
- Wang, J.; Wu, F.; Xiao, J.; Shuai, S. (2009). Oxygenated blend design and its effects on reducing diesel particulate emissions. *Fuel* 88, 2037-2045.
- Wang, Y.L.; Lee, D.J.; Westbrook, C.K.; Egolfopoulos, F.N.; Tsotsis, T.T. (2014). Oxidation of small alkyl esters in flames. *Combustion and Flame* 161, 810-817.
- Wang, Z.; Zhang, X.; Xing, L.; Zhang, L.; Herrmann, F.; Moshhammer, K.; Qi, F.; Kohse-Höinghaus, K. (2015). Experimental and kinetic modeling study of the low- and intermediate-temperature oxidation of dimethyl ether. *Combustion and Flame* 162, 1113-1125.
- Westbrook, C.K.; Pitz, W.J.; Westmoreland, P.R.; Dryer, F.L.; Chaos, M.; Osswald, P.; Kohse-Höinghaus, K.; Cool, T.A.; Wang, J.; Yang, B.; Hansen, N.; Kasper, T. (2009). A detailed chemical kinetic reaction mechanism for oxidation of four small alkyl esters in laminar premixed flames. *Proceedings of the Combustion Institute* 32, 221-228.

REFERENCES

- Wu, Z.; Zhang, Q.; Bao, T.; Li, L.; Deng, J.; Hu, Z. (2016). Experimental and numerical study on ethanol and dimethyl ether lifted flames in a hot vitiated co-flow. *Fuel* 184, 620-628.
- Yanfeng, G.; Shenghua, L.; Hejun, G.; Tiegang, H.; Longbao, Z. (2007). A new diesel oxygenate additive and its effects on engine combustion and emissions. *Applied Thermal Engineering* 27, 202-207.
- Yao, M.; Zheng, Z.; Liu, H. (2009a). Progress and recent trends in homogeneous charge compression ignition (HCCI) engines. *Progress in Energy and Combustion Science* 35, 398-437.
- Yao, C.; Yang, X.; Raine, R.R.; Cheng, C.; Tian, Z.; Li, Y. (2009b). The effects of MTBE/ethanol additives on toxic species concentration in gasoline flame. *Energy and Fuels* 23, 3543-3548.
- Ying, W.; Genbao, L.; Wei, Z.; Longbao, Z. (2008). Study on the application of DME/diesel blends in a diesel engine. *Fuel Processing Technology* 89, 1272-1280.
- Zhang, Y.; Drake, I.J.; Briggs, D.N.; Bell, A.T. (2006). Synthesis of dimethyl carbonate and dimethoxy methane over Cu-ZSM-5. *Journal of Catalysis* 244, 219-229.
- Zhang, Z.H.; Tsang, K.S.; Cheung, C.S.; Chan, T.L.; Yao, C.D. (2011). Effect of fumigation methanol and ethanol on the gaseous and particulate emissions of a direct-injection diesel engine. *Atmospheric Environment* 45, 2001-2008.
- Zhang, C.; Li, P.; Li, Y.; He, J.; Li, X. (2014). Shock-tube study of dimethoxymethane ignition at high temperatures. *Energy and Fuels* 28, 4603-4610.
- Zhang, J.; Burklé-Vitzthum, V.; Marquaire, P.M. (2015). An investigation on the role of NO₂ in the oxidation of methane to formaldehyde. *Combustion Science and Technology* 187, 1139-1156.
- Zhao, Z.; Chaos, M.; Kazakov, A.; Dryer, F. (2008). Thermal decomposition reaction and a comprehensive kinetic model of dimethyl ether. *International Journal of Chemical Kinetics* 40, 1-18.
- Zhao, H.; Yang, X.; Ju, Y. (2016). Kinetic studies of ozone assisted low temperature oxidation of dimethyl ether in a flow reactor using molecular-beam mass spectrometry. *Combustion and Flame* 173, 187-194.

- Zhu, R.; Wang, X.; Miao, H.; Huang, Z.; Gao, J.; Jiang, D. (2009). Performance and emission characteristics of diesel engines fueled with diesel-dimethoxymethane (DMM) blends. *Energy and Fuels* 23, 286-293.
- Zhu, L.; Cheung, C.S.; Zhang, W.G.; Huang, Z. (2010). Emissions characteristics of a diesel engine operating on biodiesel and biodiesel blended with ethanol and methanol. *Science of the Total Environment* 408, 914-921.
- Zhu, R.; Wang, X.; Miao, H.; Yang, X.; Huang, Z. (2011). Effect of dimethoxy-methane and exhaust gas recirculation on combustion and emission characteristics of a direct injection diesel engine. *Fuel* 90, 1731-1737.
- Zhu, R.; Miao, H.; Wang, X.; Huang, Z. (2013). Effects of fuel constituents and injection timing on combustion and emission characteristics of a compression-ignition engine fueled with diesel-DMM blends. *Proceedings of the Combustion Institute* 34, 3013-3020.

Annexes:

**Regulations required to submit a PhD Thesis
by compendium of publications**

Annexes

Regulations required to submit a PhD Thesis by compendium of publications

According to the specific regulations for the presentation of the PhD Thesis by a compendium of publications (Articles 19, 20 and 21 of the Regulation, of the Agreement of 20/12/2013 of the Governing Council of the University of Zaragoza), the following sections are presented below:

- Subject category and impact factor of the journals reported in this dissertation.
 - PhD student's contributions.
 - Resignation to claim authority rights by contributing authors, not holding a PhD degree, included in any of the publications of the present dissertation.
-

Según la normativa específica para la presentación de Tesis Doctoral como compendio de publicaciones (Artículos 19, 20 y 21 del Reglamento, del Acuerdo de 20/12/2013 del Consejo de Gobierno de la Universidad de Zaragoza), se presentan a continuación los siguientes apartados:

- Áreas temáticas y factor de impacto de las revistas en donde se ha publicado el trabajo realizado.
- Aportaciones del doctorando.
- Renuncia de los coautores no doctores participantes en los trabajos incluidos en esta Tesis Doctoral presentada por la modalidad de compendio de publicaciones.

Subject category and impact factor of the articles reported in this dissertation

The characteristics of the journals in which the articles that make up this dissertation have been published are shown below. Impact factor from the Journal of Citation Reports (JCR) corresponding to the year of publication, and the thematic areas, are also indicated. The numbering follows the same order as the indicated at the beginning of this dissertation.

- I. **Marrodán, L.**; Monge, F.; Millera, Á.; Bilbao, R.; Alzueta, M.U. (2016). Dimethoxymethane oxidation in a flow reactor. *Combustion Science and Technology* 188, 719-729. Citations: 6

Journal: Combustion Science and Technology

Impact Factor 2016: 1.241

Thematic Areas 2016:

- Thermodynamics 35/58
- Energy & Fuels 63/92
- Engineering, Multidisciplinary 36/85
- Engineering, Chemical 82/135

- II. **Marrodán, L.**; Royo, E.; Millera, Á.; Bilbao, R.; Alzueta, M.U. (2015). High pressure oxidation of dimethoxymethane. *Energy and Fuels* 29, 3507-3517. Citations: 9

Journal: Energy and Fuels

Impact Factor 2015: 2.835

Thematic Areas 2015:

- Energy & Fuels 33/88
- Engineering, Chemical 25/135

- III. **Marrodán, L.**; Arnal, Á.J.; Millera, Á.; Bilbao, R.; Alzueta, M.U. (2018). High-pressure ethanol oxidation and its interaction with NO. *Fuel* 223, 394-400.

Journal: Fuel

Impact Factor 2017: 4.908

Thematic Areas 2017:

- Energy & Fuels 19/97
- Engineering, Chemical 13/137

- IV. **Marrodán, L.**; Berdusán, L.; Aranda, V.; Millera, Á.; Bilbao, R.; Alzueta, M.U. (2016). Influence of dimethyl ether addition on the oxidation of acetylene in the absence and presence of NO. *Fuel* 183, 1-8. Citations: 1

Journal: Fuel

Impact Factor 2016: 4.601

Thematic Areas 2016:

- Energy & Fuels 16/92
- Engineering, Chemical 13/135

- V. **Marrodán, L.**; Arnal, Á.J.; Millera, Á.; Bilbao, R.; Alzueta, M.U. (2018). The inhibiting effect of NO addition on dimethyl ether high-pressure oxidation. *Combustion and Flame* 197, 1-10.

Journal: Combustion and Flame

Impact Factor 2017: 4.494

Thematic Areas 2017:

- Thermodynamics 5/59
- Energy & Fuels 21/97
- Engineering, Multidisciplinary 4/86
- Engineering, Chemical 17/137
- Engineering, Mechanical 17/128

- VI. Song, Y.; **Marrodán, L.**; Vin, N.; Herbinet, O.; Assaf, E.; Fittschen, C.; Stagni, A.; Faravelli, T.; Alzueta, M.U.; Battin-Leclerc, F. (2018). The sensitizing effects of NO₂ and NO on methane low temperature oxidation in a jet stirred reactor. *Proceedings of the Combustion Institute*, DOI: 10.1016/j.proci.2018.06.115.

Journal: Proceedings of the Combustion Institute

Impact Factor 2017: 5.336

Thematic Areas 2017:

- Thermodynamics 3/59
- Energy & Fuels 16/97
- Engineering, Chemical 12/137
- Engineering, Mechanical 3/128

- VII. **Marrodán, L.**; Fuster, M.; Millera, Á.; Bilbao, R.; Alzueta, M.U. (2018). Ethanol as a fuel additive: high-pressure oxidation of its mixtures with acetylene. *Energy and Fuels* 32, 10078-10087.

Journal: Energy and Fuels

Impact Factor 2017: 3.024

Thematic Areas 2017:

- Energy & Fuels 40/97
- Engineering, Chemical 36/137

Áreas temáticas y factor de impacto de las revistas en donde se ha publicado el trabajo realizado

Las características de las revistas en las que se han publicado los artículos que componen esta tesis se muestran a continuación. También se indica el factor de impacto según el *Journal of Citation Reports* (JCR) correspondiente al año de publicación, y las áreas temáticas. La numeración sigue el mismo orden que el indicado al comienzo de esta memoria.

- I. **Marrodán, L.**; Monge, F.; Millera, Á.; Bilbao, R.; Alzueta, M.U. (2016). Dimethoxymethane oxidation in a flow reactor. *Combustion Science and Technology* 188, 719-729. Citations: 6

Revista: Combustion Science and Technology

Factor de impacto 2016: 1.241

Áreas temáticas 2016:

- Thermodynamics 35/58
- Energy & Fuels 63/92
- Engineering, Multidisciplinary 36/85
- Engineering, Chemical 82/135

- II. **Marrodán, L.**; Royo, E.; Millera, Á.; Bilbao, R.; Alzueta, M.U. (2015). High pressure oxidation of dimethoxymethane. *Energy and Fuels* 29, 3507-3517. Citations: 9

Revista: Energy and Fuels

Factor de impacto 2015: 2.835

Áreas temáticas 2015:

- Energy & Fuels 33/88
- Engineering, Chemical 25/135

- III. **Marrodán, L.**; Arnal, Á.J.; Millera, Á.; Bilbao, R.; Alzueta, M.U. (2018). High-pressure ethanol oxidation and its interaction with NO. *Fuel* 223, 394-400.

Revista: Fuel

Factor de impacto 2017: 4.908

Áreas temáticas 2017:

- Energy & Fuels 19/97
- Engineering, Chemical 13/137

- IV. **Marrodán, L.**; Berdusán, L.; Aranda, V.; Millera, Á.; Bilbao, R.; Alzueta, M.U. (2016). Influence of dimethyl ether addition on the oxidation of acetylene in the absence and presence of NO. *Fuel* 183, 1-8. Citations: 1

Revista: Fuel

Factor de impacto 2016: 4.601

Áreas temáticas 2016:

- Energy & Fuels 16/92
- Engineering, Chemical 13/135

- V. **Marrodán, L.**; Arnal, Á.J.; Millera, Á.; Bilbao, R.; Alzueta, M.U. (2018). The inhibiting effect of NO addition on dimethyl ether high-pressure oxidation. *Combustion and Flame* 197, 1-10.

Revista: Combustion and Flame

Factor de impacto 2017: 4.494

Áreas temáticas 2017:

- Thermodynamics 5/59
- Energy & Fuels 21/97
- Engineering, Multidisciplinary 4/86
- Engineering, Chemical 17/137
- Engineering, Mechanical 17/128

- VI. Song, Y.; **Marrodán, L.**; Vin, N.; Herbinet, O.; Assaf, E.; Fittschen, C.; Stagni, A.; Faravelli, T.; Alzueta, M.U.; Battin-Leclerc, F. (2018). The sensitizing effects of NO₂ and NO on methane low temperature oxidation in a jet stirred reactor. *Proceedings of the Combustion Institute*, DOI: 10.1016/j.proci.2018.06.115.

Revista: Proceedings of the Combustion Institute

Factor de impacto 2017: 5.336

Áreas temáticas 2017:

- Thermodynamics 3/59
- Energy & Fuels 16/97
- Engineering, Chemical 12/137
- Engineering, Mechanical 3/128

- VII. **Marrodán, L.**; Fuster, M.; Millera, Á.; Bilbao, R.; Alzueta, M.U. (2018). Ethanol as a fuel additive: high-pressure oxidation of its mixtures with acetylene. *Energy and Fuels* 32, 10078-10087.

Revista: Energy and Fuels

Factor de impacto 2017: 3.024

Áreas temáticas 2017:

- Energy & Fuels 40/97
- Engineering, Chemical 36/137

PhD student contributions

The contribution of the author of this PhD Thesis, in the different publications included in this dissertation, has been the decision and realization of the different experiments in the laboratory and the analysis of the results, the update, modification and optimization of the chemical kinetic mechanisms used, and the performance of the modeling calculations. She has also had a very active participation in the writing of the different publications.

Aportaciones del doctorando

La contribución de la autora de esta Tesis Doctoral, en las diferentes publicaciones incluidas en esta memoria, ha sido la decisión y ejecución de los diferentes experimentos en el laboratorio y el análisis de los resultados obtenidos, la actualización, modificación y optimización de los mecanismos cinéticos químicos utilizados, y la realización de los cálculos de modelado. También ha tenido una participación muy activa en la redacción de los diferentes artículos.

Resignation to claim authority rights by contributing authors not holding a PhD degree included in any of the publications of the present dissertation

The non-doctor co-authors of the articles included in this PhD Thesis submitted in the form of compendium of publications have signed the corresponding resignation documents, which have been delivered at the time of the deposit of the present dissertation.

Renuncia de los coautores no doctores de los trabajos incluidos en la presente Tesis Doctoral presentada en la modalidad de compendio de publicaciones

Los coautores no doctores de los trabajos incluidos en la presente Tesis Doctoral, presentada en la modalidad de compendio de publicaciones, han firmado los correspondientes documentos de renuncia, los cuales han sido entregados en el momento del depósito de la presente memoria.

Article A:

Marrodán, L.; Millera, Á.; Bilbao, R.; Alzueta, M.U. (2014). High-pressure study of methyl formate oxidation and its interaction with NO. *Energy and Fuels* 28, 6107-6115.

High-Pressure Study of Methyl Formate Oxidation and Its Interaction with NO

Lorena Marrodán, Ángela Millera, Rafael Bilbao, and María U. Alzueta*

Aragón Institute of Engineering Research (I3A), Department of Chemical and Environmental Engineering, University of Zaragoza, C/Mariano Esquillor, s/n, 50018 Zaragoza, Spain

Supporting Information

ABSTRACT: An experimental and modeling study of the influence of pressure on the oxidation of methyl formate (MF) has been performed in the 1–60 bar pressure range, in an isothermal tubular quartz flow reactor in the 573–1073 K temperature range. The influence of stoichiometry, temperature, pressure, and presence of NO on the conversion of MF and the formation of the main products (CH_2O , CO_2 , CO , CH_4 , and H_2) has been analyzed. A detailed kinetic mechanism has been used to interpret the experimental results. The results show that the oxidation regime of MF differs significantly from atmospheric to high-pressure conditions. The impact of the NO presence has been considered, and results indicate that no net reduction of NO_x is achieved, even though, at high pressure, the NO – NO_2 interconversion results in a slightly increased reactivity of MF.

INTRODUCTION

Nowadays, there is increasing urgency in finding ways to improve fuel economy of motor vehicles while controlling exhaust emissions to meet ever tighter emission regulations. Diesel engines exhibit a better fuel economy and lower emissions of unburned hydrocarbons and CO compared to gasoline-fueled engines. However, they suffer from high emissions of particulate matter and NO_x , which are hard to reduce simultaneously.

Methods to reduce both emissions include high-pressure injection, turbocharging, and the use of fuel additives; the latest is thought to be one attractive and effective solution.¹ Dimethyl ether (DME) and dimethoxymethane (DMM) are two examples of promising additives for diesel fuel and/or substitutes.^{2–6} Methyl formate (MF, CH_3OCHO) has been found to be a byproduct of the oxidation of several proposed fuel alternatives, such as these two, DME^{7–9} and DMM.^{10,11} MF is the simplest ester, and esters are the primary constituents of biodiesel.^{12,13} MF has also been considered as a model molecule used to understand biodiesel and other such real fuel molecule combustion.^{14,15}

Esters are volatile organic compounds and may be released into the atmosphere during their employment (e.g., manufacture of perfumes and food flavoring, industrial solvents, and fuel burning) or from natural sources (i.e., vegetation). MF has been reported to be active as well in the atmosphere, and while many studies have been reported in the literature on the conversion of MF in the atmosphere (e.g., ref 16), few studies addressing the conversion of MF at high temperatures, from both experimental and kinetic modeling points of view, have been reported^{12,14,15,17–22} and even less in terms of high pressure. Francisco²¹ suggested a mechanism for CH_3OCHO decomposition with two parallel reactions forming $\text{CH}_3\text{OH} + \text{CO}$ and $\text{CH}_2\text{O} + \text{CH}_2\text{O}$, and later, Dooley et al.¹² found that the rate constant value for MF decomposition proposed by Francisco²¹ was not consistent with their experimental results. Metcalfe et al.¹⁵ computed pressure-dependent rate constants

for MF decomposition with *ab initio* methods and confirmed that computations of Francisco might be in error. The MF decomposition seems to be dominated by a single channel producing methanol and carbon monoxide over all temperatures and pressures. The other two possible channels (producing two molecules of formaldehyde and $\text{CH}_4 + \text{CO}_2$) appear to be of minor relevance.

Among all of the previous studies reported, it is worthwhile to mention an earlier work of our research group¹⁷ on MF conversion at atmospheric pressure, which has been taken as the starting point of the present work. The earlier study was carried out in an experimental setup that operates at atmospheric pressure in the 300–1000 K temperature range and for different stoichiometries ($\lambda = 0, 0.7, 1, \text{ and } 3.5$). That work suggests $\text{CH}_3\text{OCHO} \rightarrow \text{CH}_3\text{OH} \rightarrow \text{CH}_2\text{OH}/\text{CH}_3\text{O} \rightarrow \text{CH}_2\text{O} \rightarrow \text{HCO} \rightarrow \text{CO} \rightarrow \text{CO}_2$ as the main reaction pathway, and the $\text{HCOOCH}_3 (+\text{M}) \rightleftharpoons \text{CH}_3\text{OH} + \text{CO} (+\text{M})$ reaction was found to play an important role in MF conversion. That work also analyzed the influence of the presence of NO on MF conversion at atmospheric pressure, and it was found that the addition of NO does not produce any variation of the MF conversion regime, except for oxidizing conditions when MF conversion is shifted to lower temperatures, because of the fact that a route producing CH_2OCHO radicals becomes more active compared to the above-mentioned reaction pathway. Nevertheless, the consumption of MF does not result in a net decrease of NO_x .

In this context, the present work aims to extend the experimental database of flow reactor data on MF oxidation to different pressures (above atmospheric pressure), because these results will be helpful for engine developments. Because of the fact that NO can be produced in the combustion chamber of the engine, the interaction between MF and NO is also

Received: June 12, 2014

Revised: July 29, 2014

Published: July 31, 2014

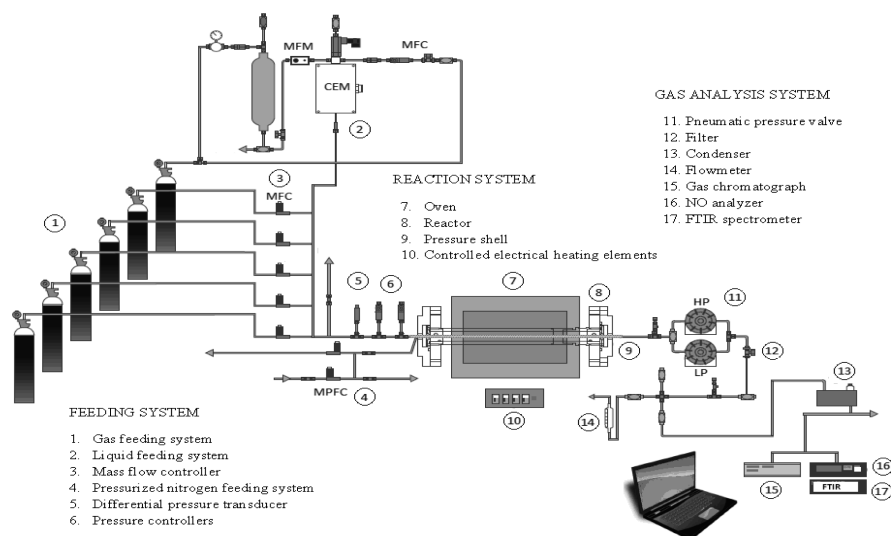


Figure 1. High-pressure gas-phase installation.

analyzed by adding a given amount of NO (at a constant pressure, 20 bar). The NO evolution at high pressure in the NO_x interaction with $\text{CO}/\text{H}_2/\text{O}_2$ has been previously studied by Rasmussen et al.²³ and in the $\text{C}_2\text{H}_4/\text{NO}_x$ interaction by Giménez-López et al.²⁴

Specifically, the oxidation of MF has been investigated under flow reactor conditions, in a new high-pressure setup, at different pressures (atmospheric, 20, 40, and 60 bar), in the 573–1073 K temperature interval, from reducing to very fuel-lean conditions, in both the absence and presence of NO. Additionally, the experimental data are interpreted in terms of a detailed kinetic modeling study based on the MF mechanism subset by Dooley et al.,¹² updated by Alzueta et al.¹⁷ and revised and completed in the present work.

EXPERIMENTAL SECTION

Oxidation experiments of MF (in both the presence and absence of NO) were carried out in an experimental installation (Figure 1), which consists of a feeding system (gas/liquid), a reaction system, and a gas analysis system.

This installation is provided with a controlled evaporation mixer (CEM), which evaporates liquids and mixes them with a carrier gas. MF liquid is supplied from a pressurized tank through a liquid mass flow controller (MFM) and evaporated in the CEM using N_2 as the carrier gas. A concentration of approximately 3000 ppm of MF is introduced in all experiments with an uncertainty of the measurements below 10%. Because of the fact that the feeding is a liquid, some punctual fluctuations may occur during the experiments.

All gases are supplied from gas cylinders through gas mass flow controllers (MFCs). The amount of O_2 used depends upon the air excess ratio (λ), defined as the inlet oxygen concentration divided by stoichiometric oxygen. A concentration of approximately 3000 ppm of NO has been used in the experiments conducted with NO. The NO concentration value of 3000 ppm was chosen to be of a similar order of magnitude as the MF feed (i.e., 6000 ppm of C), with a NO/C ratio of 1:2, which falls within the 1:12 to 1 NO/C range of previous studies of our research group.²⁵

Nitrogen is used to balance, resulting in a constant flow rate of 1000 mL [standard temperature and pressure (STP)]/min. All of the experimental mixtures are diluted in nitrogen. Therefore, little heat is released during the reaction, and isothermal conditions can be considered.

The reaction system consists of a quartz reactor (inner diameter of 6 mm and 1500 mm in length), enclosed in a stainless-steel tube that acts as a pressure shell. A pressure control system, consisting of two

thermal mass flow pressure controllers (MFPCs), automatically delivers N_2 to the shell side of the reactor to obtain a pressure similar to that inside the reactor, avoiding the reactor breaking. Pressure inside the reaction chamber is controlled within $\pm 1\%$. The steel tube is placed horizontally in a tubular oven, with three individually controlled electrical heating elements that ensure an isothermal reaction zone of approximately 56 cm with a uniform temperature profile (± 10 K). The reactor temperature is monitored by type K thermocouples positioned between the quartz reactor and the steel shell. An example of temperature profiles inside the reactor can be found in the Supporting Information.

The gas residence time, t_r , in the isothermal zone depends upon the reaction temperature and pressure, t_r (s) = $261.1P$ (bar)/ T (K). The experiments were carried out at different pressures (atmospheric, 20, 40, and 60 bar) and in the 573–1073 K temperature range. Table 1 lists the conditions of the experiments.

Table 1. Matrix of Experimental Conditions^a

experiment	MF (ppm)	O_2 (ppm)	NO (ppm)	λ	P (bar)
set 1	3056	4200	0	0.7	20
set 2	2794	6000	0	1	20
set 3	2547	120000	0	20	20
set 4	3166	6000	0	1	1
set 5	2489	6000	0	1	40
set 6	2238	6000	0	1	60
set 7	2375	4200	3020	0.7	20
set 8	2400	6000	2745	1	20
set 9	2209	120000	3000	20	20

^aThe experiments are conducted at a constant flow rate of 1000 mL (STP)/min, in the temperature interval of 573–1073 K. The balance is closed with N_2 . The residence time depends upon the reaction temperature and pressure: t_r (s) = $261.1P$ (bar)/ T (K).

All of the reactants (gases and the evaporated liquid) are premixed before entering the reactor and pressurized from gas cylinders. The reactor pressure is monitored upstream of the reactor by a differential pressure transducer and controlled by a pneumatic pressure valve positioned after the reactor, which can operate at pressures up to 80 bar. Downstream of the reactor, the pressure is reduced to atmospheric level. Previous to the gas analysis, gases pass through a filter and a condenser to ensure gas cleaning and water-free content, which could affect the analysis equipment.

Products are analyzed by a gas chromatograph equipped with thermal conductivity detectors (TCDs) able to detect MF, CO, CO_2 ,

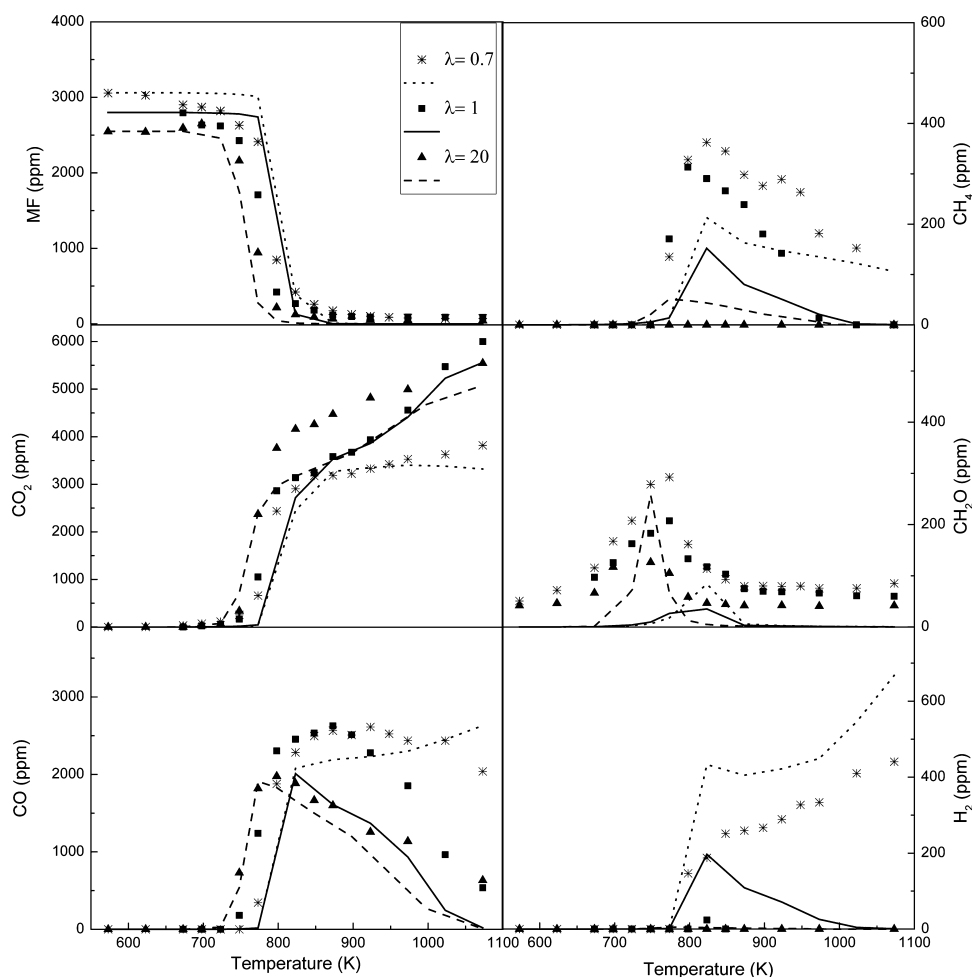


Figure 2. Influence of stoichiometry on the MF, CO₂, CO, CH₄, CH₂O, and H₂ concentration profiles as a function of the temperature in the absence of NO, with sets 1–3 (20 bar) in Table 1.

H₂, CH₃OH, CH₂O, and hydrocarbons (CH₄, C₂H₂, C₂H₄, and C₂H₆), a continuous infrared (IR) analyzer to measure the NO concentration, and a Fourier transform infrared (FTIR) spectrometer to check the formation of some nitrogen compounds, such as NO₂, HCN, or NH₃. The uncertainty of measurements is estimated as $\pm 5\%$, except for the FTIR spectrometer, which is estimated as $\pm 10\%$.

To evaluate the goodness of the experiments, the atomic carbon balance was checked in all experiments and resulted to close always better than 94%.

REACTION CHEMICAL KINETIC MECHANISM

The present experimental results have been analyzed in terms of a detailed chemical kinetic model for the oxidation of MF in the absence and presence of NO at different pressures. The full mechanism takes as the starting point an earlier work on MF conversion at atmospheric pressure,¹⁷ which includes the Dooley et al. MF reaction subset,¹⁸ even though it has been revised according to the present high-pressure conditions and the presence of NO, taking into account the considerations by Rasmussen et al.^{23,26,27} and Giménez-López et al.²⁴

The decomposition reaction of MF, with CH₃OH and CO as main products, constitutes the beginning of the MF oxidation. Methanol formed is rapidly consumed, giving mainly hydroxymethyl radicals and these, formaldehyde. Under oxidizing conditions, MF also produces CH₂OCHO and CH₃OCO radicals by hydrogen abstraction reactions. All of

these reactions will be discussed in depth later through the reaction path diagram for MF oxidation.

In particular, results appeared to be sensitive to the HO₂CH₂OCHO species, involved in the formation of CO₂ (HO₂CH₂OCHO → OCH₂OCHO → HCOO → CO₂). Therefore, to represent the experimental results by the model, reactions concerning HCOO and HCOOH had to be added to the mechanism. For the HCOOH + OH ⇌ HCOO + H₂O reaction, we have adopted the theoretically determined values of kinetic parameters by Galano et al.,²⁸ and for HCOO ⇌ H + CO₂, the determination by Larson et al.²⁹ was used.

Under the present combustion conditions and without NO, the main reaction products are formaldehyde, CO, CO₂, CH₄, and H₂. In the presence of NO in the reactant mixture, it has been observed that, when the pressure is increased from atmospheric to 20 bar, NO is converted almost completely to NO₂, as reported in previous works.^{24,26} The main reaction involved in this conversion is NO + NO + O₂ ⇌ NO₂ + NO₂, which gains relevance with the pressure. This reaction has already been studied;^{30–32} however, the pressure dependence of the kinetic parameters is not well-known presently, and the uncertainty related to it may be significant. For this reaction, we have adopted the value determined by Park et al.,³² which was also selected in the high-pressure work by Rasmussen et al.²⁶

Model calculations have been performed using SENKIN, the plug flow reactor code that runs in conjunction with the

CHEMKIN-II library,^{33,34} considering constant pressure and temperature in the reaction zone, which has been tested to be a fairly good assumption. The full mechanism listing and thermochemistry used can be found in the Supporting Information.

RESULTS AND DISCUSSION

In this work, a study of the oxidation of MF at different pressures (1, 20, 40, and 60 bar) and in the 573–1073 K temperature interval has been carried out. In addition to temperature and pressure, the influence of stoichiometry ($\lambda = 0.7, 1,$ and 20) and the presence of NO (approximately 3000 ppm) on the oxidation process have also been analyzed.

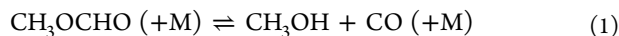
Oxidation of MF in the Absence of NO. Figure 2 shows the influence of the temperature and stoichiometry at a given pressure (20 bar) on the concentration of MF and the formation of the main products of the reaction: CH_2O , CO_2 , CO , CH_4 , and H_2 . The concentration values are shown as a function of the temperature for three different stoichiometries, $\lambda = 0.7, 1,$ and 20 . Figure 2 compares experimental (symbols) and simulation (lines) results. The model predicts the general trend of the different concentration profiles, but there are some discrepancies between experimental and simulation results. These discrepancies, especially in the profiles of CO_2 , may be attributed to the small fluctuations in the liquid flow fed using the CEM previously mentioned and/or the uncertainty in model calculations.

The temperature for the onset of the MF oxidation is approximately 723 K according to the experimental results, independent of the stoichiometry, with MF almost converted at 873 K in all of the cases. This onset temperature is lower than that needed in the case of MF oxidation at atmospheric pressure.¹⁷

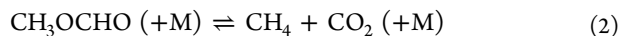
The oxygen concentration in the reactant mixture slightly influences the conversion of MF, similar to what has been observed in the oxidation behavior of other oxygenated compounds, such as DME.³⁵ However, the presence of oxygen does have certain effects on some of the reaction products. The conversion of MF is accompanied by the formation of both CO and CO_2 , which are the main products in all of the experiments performed. At higher temperatures, when CO has reached its maximum concentration and begins to drop, CO_2 increases its concentration up to an almost constant value, which is reached at lower temperatures for smaller values of λ .

Under oxidizing conditions, the formation of CO_2 is favored and, consequently, a lower amount of CO is produced, whereas other products, such as CH_4 or H_2 , are hardly formed.

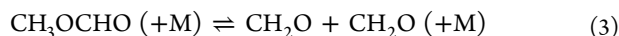
Figure 3 shows a reaction path diagram for MF oxidation obtained through a reaction rate analysis with the mechanism compiled in the present work. For the conditions of Figure 2, the MF oxidation is initiated by the following decomposition reaction, which is in agreement with other previous works:^{10,15}



with minor relevance of



and



Both products, CH_4 and CH_2O , are detected as final products in the reaction process.

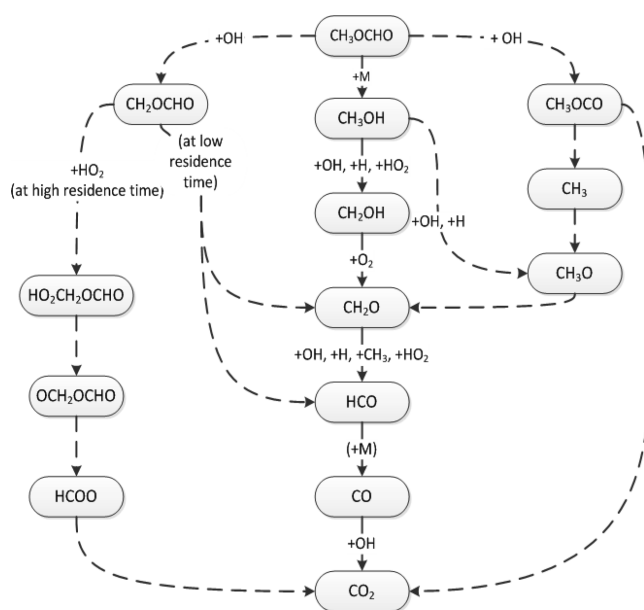
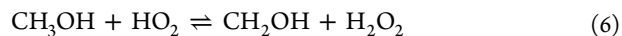
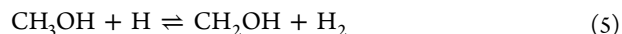
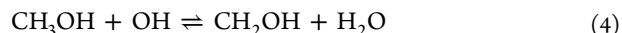
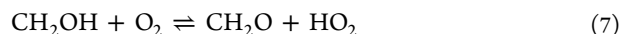


Figure 3. Reaction path diagram for MF oxidation in the absence of NO according to the current kinetic model. Solid lines represent the main reaction pathways for all of the conditions considered in the present work. The dashed lines refer to additional paths that occur under oxidizing conditions.

The methanol produced by reaction 1 is consumed by a number of reactions (reactions 4–6), giving mainly hydroxymethyl radicals

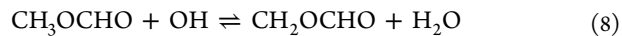


which react mainly with molecular oxygen to give formaldehyde



When formaldehyde has been produced, it continues the $\text{CH}_2\text{O} \rightarrow \text{HCO} \rightarrow \text{CO} \rightarrow \text{CO}_2$ reaction sequence.

Under oxidizing conditions, calculations indicate that MF also produces CH_2OCHO and CH_3OCO radicals by hydrogen abstraction reactions, as reported in previous studies,^{36,37} i.e.



For example, at 1 bar and stoichiometric conditions ($\lambda = 1$), reaction 1 [$\text{CH}_3\text{OCHO} (+\text{M}) \rightleftharpoons \text{CH}_3\text{OH} + \text{CO} (+\text{M})$] is the dominant reaction pathway, with a relative importance of 86%, whereas at 20 bar and oxidizing conditions ($\lambda = 20$), reaction 8 has a relative importance of approximately 62% and reaction 9 has a relative importance of approximately 20%.

At low residence times (i.e., around 0.3 s, at 1 bar), CH_2OCHO is found, in part, to decompose thermally to give formaldehyde and formyl radical through reaction 10, but at higher residence times (i.e., around 6–8 s, at 20 bar), it mostly follows the path represented by the reactions 11–13.

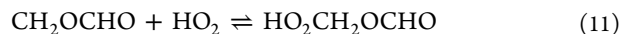


Table 2. Linear Sensitivity Coefficients for CO for Sets 1–9^a

reaction	set 1 (723 K)	set 2 (723 K)	set 3 (698 K)	set 4 (823 K)	set 5 (673 K)	set 6 (673 K)	set 7 (748 K)	set 8 (748 K)	set 9 (698 K)
CH ₃ OCHO (+M) = CH ₃ OH + CO (+M)	0.396	0.287	0.024	0.982	0.018	0.000	0.943	0.940	0.813
CH ₃ OCHO + OH = CH ₂ OCHO + H ₂ O	0.024	0.024	0.017		-0.023	0.008	0.423	0.450	1.983
CH ₃ OCHO + OH = CH ₃ OCO + H ₂ O	-0.030	-0.038	-0.015		0.067	0.142	-0.361	-0.392	-1.039
CH ₃ OCHO + HO ₂ = CH ₂ OCHO + H ₂ O ₂	0.309	0.411	0.566	0.001	0.720	0.564			
CH ₃ OCHO + HO ₂ = CH ₃ OCO + H ₂ O ₂	0.224	0.306	0.480	0.001	0.604	0.563			
CH ₃ OCHO + CH ₃ = CH ₂ OCHO + CH ₄	0.120	0.078	-0.015	0.001	0.032	-0.031			
CH ₃ OCHO + CH ₃ O ₂ = CH ₂ OCHO + CH ₃ OOH	0.267	0.335	0.707		1.116	0.911			
CH ₃ OCHO + CH ₃ O ₂ = CH ₃ OCO + CH ₃ OOH	0.202	0.256	0.582		0.895	0.732			
CH ₃ OCHO + CH ₃ O = CH ₃ OCO + CH ₃ OH	-0.050	-0.049	0.174		0.617	0.499	-0.005	-0.007	-0.020
CH ₃ + CO ₂ = CH ₃ OCO	-0.197	-0.197	0.000	-0.000	0.060	-0.003	-0.328	-0.332	-0.175
CH ₃ O + CO = CH ₃ OCO	0.197	0.197	-0.000	0.000	-0.060	0.003	0.328	0.331	0.175
CH ₂ O + HCO = CH ₂ OCHO	0.321	0.312	-0.003	0.000	-0.018	-0.001	1.034	1.048	0.114
CH ₃ OCO + CH ₃ OCHO = CH ₃ OCHO + CH ₂ OCHO	-0.143	-0.116	0.061		0.232	0.244	-1.220	-1.305	-2.490
CH ₃ + CH ₂ OCHO = CH ₃ CH ₂ OCHO	-0.269	-0.343	-0.048		-0.415	-0.570			
CH ₂ OCHO + HO ₂ = HO ₂ CH ₂ OCHO	0.006	0.025	0.016		0.391	0.627			
OOCH ₂ OCHO = HOOCH ₂ OCO	0.103	0.142	0.020		-0.082	-0.005	0.199	0.271	2.400
HO ₂ + HO ₂ = H ₂ O ₂ + O ₂	-0.160	-0.244	-0.423		-0.695	-1.113			
H ₂ O ₂ + M = OH + OH + M	0.374	0.498	0.921	0.000	1.059	1.911			
HCO + O ₂ = HO ₂ + CO				-0.000		-0.001	0.139	0.153	0.048
CH ₃ + CH ₃ (+M) = C ₂ H ₆ (+M)	-0.345	-0.370	-0.009		-0.189	-0.171			
CH ₄ + O ₂ = CH ₃ + HO ₂	-0.082	-0.109	-0.025		-0.127	-0.178			
CH ₃ + HO ₂ = CH ₃ O + OH	0.049	0.075	0.016		0.156	0.144			
CH ₃ O ₂ + HO ₂ = CH ₃ OOH + O ₂	0.006	0.014	0.097		0.225	0.282			
CH ₃ O ₂ + CH ₂ O = CH ₃ OOH + HCO	0.011	0.024	0.090		0.289	0.872			
CH ₃ O ₂ + CH ₃ = CH ₃ O + CH ₃ O	0.215	0.235	-0.365		-0.562	-0.646			
CH ₃ O ₂ + CH ₃ O ₂ = CH ₃ O + CH ₃ O + O ₂	0.001	0.001	-0.109		-0.035	-0.061			
CH ₃ O ₂ + CH ₃ O ₂ = CH ₃ OH + CH ₂ O + O ₂	0.000	-0.001	-0.063		-0.060	-0.119			
CH ₃ OOH = CH ₃ O + OH	0.008	0.011	0.087		0.174	0.249			
CH ₂ O + H (+M) = CH ₃ O (+M)	0.014	0.014	-0.029		-0.153	-0.243	0.001	0.001	0.006
CH ₂ O + HO ₂ = HCO + H ₂ O ₂	0.019	0.039	0.048		0.163	0.558			
NO + OH (+M) = HONO (+M)							0.017	0.018	0.187
NO ₂ + NO ₂ = NO + NO + O ₂							-0.073	-0.088	-0.414
CH ₂ O + NO ₂ = HONO + HCO							0.211	0.243	1.004
HCO + NO ₂ = NO + CO ₂ + H							-0.303	-0.274	-0.035
CH ₃ + NO ₂ = CH ₃ O + NO							0.884	0.914	0.596
CH ₃ OH + NO ₂ = HONO + CH ₂ OH							0.303	0.330	0.581
CH ₃ NO ₂ (+M) = CH ₃ + NO ₂ (+M)							-0.618	-0.642	-0.522

^aThe sensitivity coefficients are given as $A_i \delta Y_j / Y_j \delta A_i$, where A_i is the pre-exponential constant for reaction i and Y_j is the mass fraction of the j th species. Therefore, the sensitivity coefficients listed can be interpreted as the relative change in predicted concentration for the species j caused by increasing the rate constant for reaction i by a factor of 2.



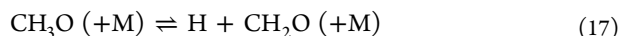
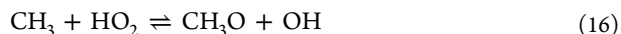
The hydrocarboxyl radical decomposes



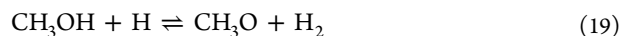
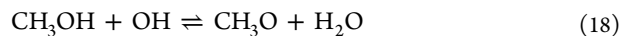
The CH₃OCO radical formed in reaction 9 decomposes thermally to give CO₂ as the final product and methyl radicals.



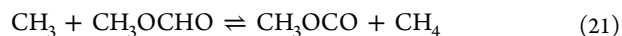
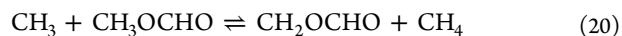
Under the high-pressure conditions of this work, the stable methyl radical can generate methane, which is found as a final reaction product, but can also form methoxy radicals through reaction 16, which further decomposes, giving formaldehyde (reaction 17) that can go through the already mentioned reaction sequence to give CO₂ as the final product.



Methanol also forms methoxy radicals by hydrogen abstraction reactions with OH and H radicals in oxidizing conditions.



For the highest value of λ studied ($\lambda = 20$), CH₄ produced is lower, as seen in Figure 2. This is attributed to the fact that reaction 16 is favored under oxidative conditions. In the case of stoichiometric or reducing conditions and for the high pressures of this work, other reactions of CH₃ (with MF) start to become more important and produce CH₄ as the product.



A first-order sensitivity analysis for CO has been performed for all of the sets in Table 1. The results obtained are shown in

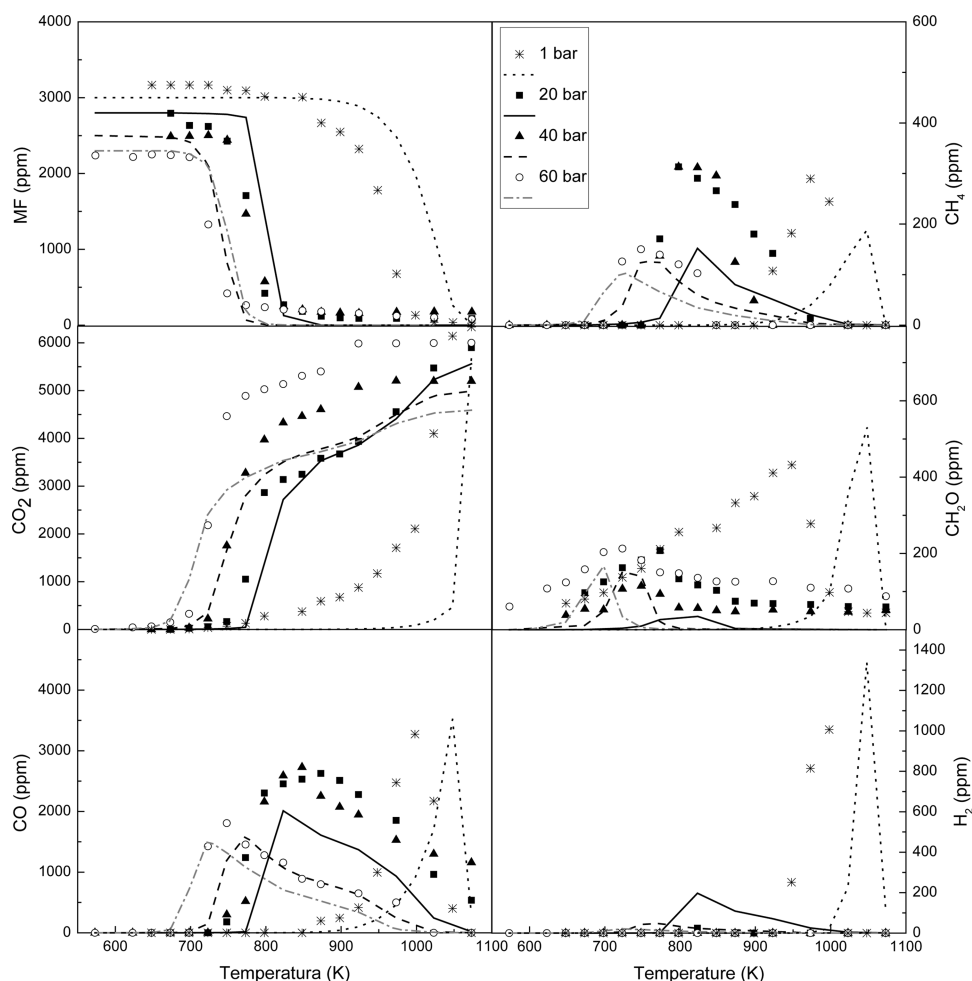


Figure 4. Influence of the pressure on the MF, CO₂, CO, CH₄, CH₂O, and H₂ concentration profiles as a function of the temperature in the absence of NO, with sets 2 and 4–6 ($\lambda = 1$) in Table 1.

Table 2. The data of Table 2 indicate that the conversion of MF is mostly sensitive to the unimolecular decomposition of MF to give methanol and carbon monoxide (reaction 1). Reactions giving CH₂OCHO and CH₃OCO radicals appear also to be sensitive, especially in the presence of NO and for the highest value of λ studied ($\lambda = 20$).

A study of the influence of varying pressure on MF oxidation has also been performed. Experiments at different pressures, from atmospheric to 60 bar and for stoichiometric conditions, have been carried out (Table 1). The results obtained are shown in Figure 4.

As seen, there is a huge difference between the results at atmospheric pressure and higher pressures. At 1 bar, the temperature for the onset of the conversion of MF is near 873 K and is clearly higher than the required for 20 bar (723 K). However, the effect of increasing pressure between 20 and 60 bar is seen to be less pronounced in comparison to the changes found from 1 to 20 bar. For example, as seen in Figure 4, the maximum concentration of CH₄ for atmospheric pressure is reached at approximately 973 K, the maximum concentration of CH₄ for 20 and 40 bar is reached at approximately 798 K, and finally, the maximum concentration of CH₄ for the highest value of pressure (60 bar) is reached at approximately 748 K. Increasing pressure above atmospheric conditions shifts the concentration profiles to almost approximately 200 K less.

Results indicate that, at the highest pressure studied (60 bar), the formation of CO₂ is favored and, therefore, a smaller amount of CO is produced. In the cases of 20 and 40 bar, the amounts of CO and CH₄ produced experimentally are almost similar and higher than those predicted by the model. Calculations match reasonably well with the experimental trends; the biggest discrepancy is found in the CO₂ concentration profile.

Under atmospheric pressure conditions, MF decomposes, giving CH₃OH via reaction 1 and with minor relevance via reactions 2 and 3.¹⁷ When the pressure is raised, the reaction pathways become slightly more complex. At 20 bar, the MF oxidation is also initiated by its decomposition into CH₃OH and CO (reaction 1), but as the pressure increases, all of the reactions become faster and reactions of MF with OH radicals (reactions 8 and 9) become more relevant (i.e., at 60 bar, 51 and 16% of relative importance for reactions 8 and 9, respectively), producing CH₂OCHO and CH₃OCO radicals. The CH₂OCHO radical reacts, in the presence of MF, to produce the CH₃OCO radical and also reacts with HO₂ by reaction 11 and following the reaction 12–14 sequence until CO₂ is generated. The CH₃OCO radical decomposes thermally producing CO₂ and methyl radicals (reaction 15).

All of these reaction sequences are responsible for the formation of CO₂, favored at high pressures, and it is found to

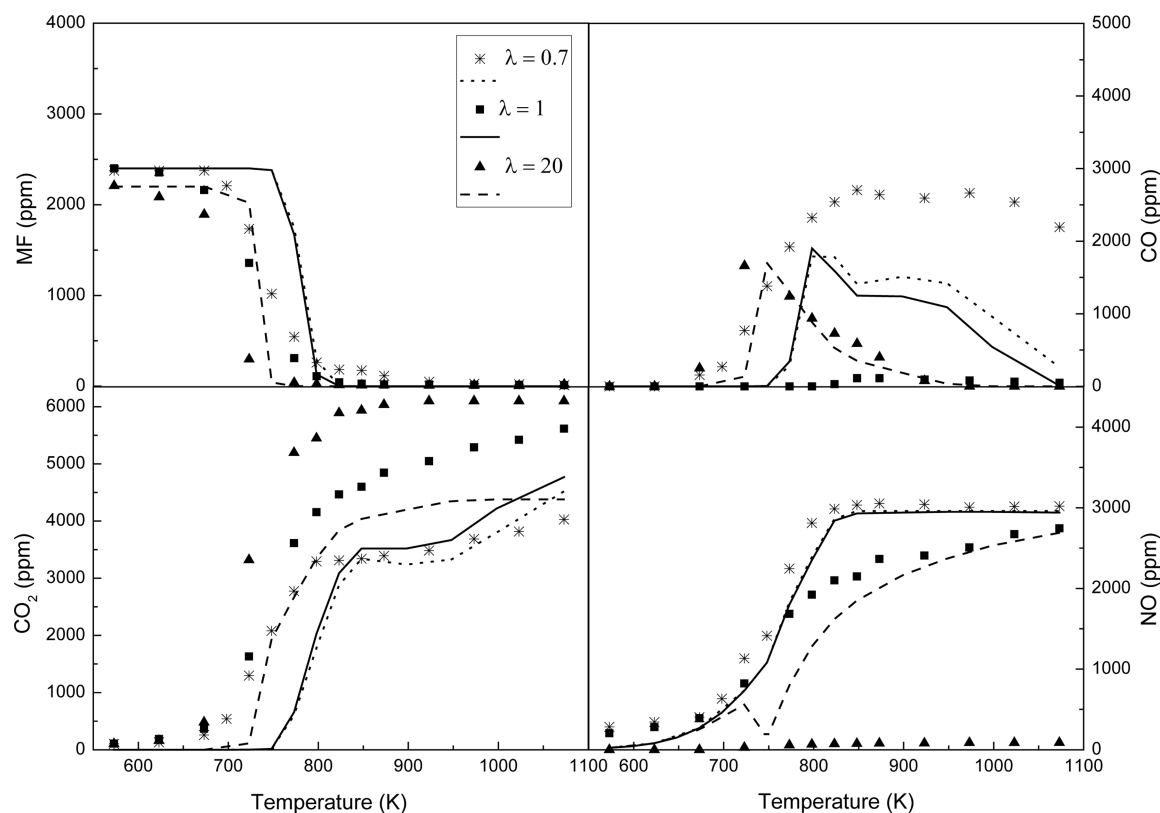
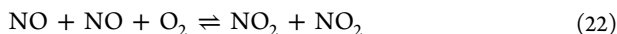


Figure 5. Influence of the presence of NO on the MF, CO₂, and CO concentration profiles as a function of the temperature for different values of λ and influence of the stoichiometry on the NO concentration profile as a function of the temperature, with sets 7–9 (20 bar) in Table 1.

occur at lower temperatures compared to the low-pressure conditions.

Oxidation of MF in the Presence of NO. The influence of the NO presence on MF oxidation has been considered for different stoichiometries at a given pressure of 20 bar. Figure 5 shows the results obtained of MF conversion and the formation of CO and CO₂. It is worthwhile to note that the presence of NO in the reactant mixture has its main effect on the decrease of other final products different from CO₂ or CO, because CH₄ or CH₂O is not formed in appreciable amounts. Besides, MF presents a slightly increased reactivity.

Figure 5 also shows the results of NO obtained under the conditions studied. For the high pressure considered (20 bar), principally for the lowest studied temperatures, the concentration of NO at the outlet of the reaction system is very low and attributed to the fact that the conversion of NO to NO₂ is clearly favored. This is attributed to the fact that most NO is converted to NO₂ when the pressure is raised above atmospheric pressure through



and through the important equilibrium between NO and NO₂



which is relevant under high-pressure conditions.²⁴ However, results indicate no net reduction of NO_x in the studied conditions.

Model calculations indicate that the reaction pathways change with the presence of NO and/or NO₂ formed. Figure 6 shows a reaction path diagram for MF oxidation in the presence of NO obtained in a manner similar to Figure 3, i.e., through a reaction rate analysis with the mechanism compiled

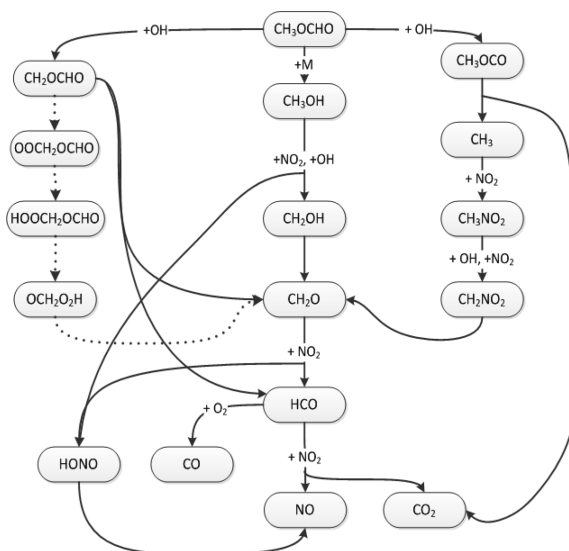
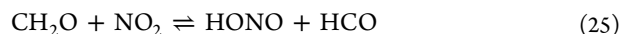


Figure 6. Reaction path diagram for MF oxidation in the presence of NO according to the current kinetic model. Solid lines represent the main reaction pathways for all of the conditions considered in the present work. The dashed lines refer to additional paths that occur under exclusively oxidizing conditions.

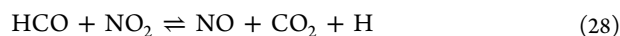
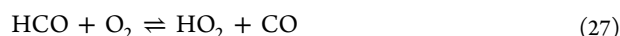
in the present work. Although the MF oxidation starts also by reaction 1, CH₂OCHO and CH₃OCO radicals are highly formed under the studied conditions. The CH₂OCHO radical, with MF, reacts giving the other radical, CH₃OCO, as the product. It decomposes thermally through reaction 15, and subsequently, CH₃ formed reacts with NO₂, giving nitromethane.



CH_3NO_2 continues the $\text{CH}_3\text{NO}_2 \rightarrow \text{CH}_2\text{NO}_2 \rightarrow \text{CH}_2\text{O}$ reaction sequence, and formaldehyde also reacts with NO_2 .



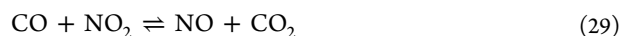
HCO produced can react with either molecular oxygen or NO_2



which contributes to the NO_2 –NO interconversion.

The last two reactions are in competition at stoichiometric and reducing conditions, but under oxidizing conditions, reaction with oxygen (reaction 27) becomes dominant.

For higher oxidizing conditions considered, i.e., $\lambda = 20$, the reaction pathways mentioned change slightly. With an excess of O_2 , the radical CH_2OCHO follows another reaction sequence through some intermediate oxygenated compounds, i.e., $\text{CH}_2\text{OCHO} \rightarrow \text{OOCH}_2\text{OCHO} \rightarrow \text{HOCH}_2\text{OCHO} \rightarrow \text{OCH}_2\text{O}_2\text{H} \rightarrow \text{CH}_2\text{O}$, to give formaldehyde as the product, which reacts with NO_2 as mentioned above (reaction 25). In the presence of NO_2 , CO can also react, producing CO_2 and NO



with no net NO_x reduction, as mentioned.

CONCLUSION

The oxidation of MF has been studied in a tubular quartz flow reactor in the 573–1073 K temperature interval, for different stoichiometries ($\lambda = 0.7, 1$, and 20) and also different pressures, from atmospheric conditions to 60 bar. The experimental data obtained have been interpreted in terms of a detailed chemical kinetic mechanism, taken from the literature and updated and revised in the present work.

The stoichiometry has been found to have certain effects on the main products of the oxidation of MF. Under oxidizing conditions, the formation of CO_2 is favored and, thus, a lower amount of CO is produced, whereas other products (CH_4 or H_2) are hardly formed. MF conversion is clearly shifted toward lower temperatures, around 200 K, when the pressure is increased from 1 to 20 bar and over.

The reaction pathways occurring at high pressure are a bit more complex than those observed at atmospheric conditions, because of the formation of CH_2OCHO and CH_3OCO radicals, which are not so relevant at atmospheric pressure.

The addition of NO to the reactant mixture has its main effect on the decrease of other final products different from CO_2 or CO. When the pressure is raised above atmospheric, most NO is converted to NO_2 , which exhibits a high reactivity, taking part in many reactions with the intermediates formed. However, results indicate that no net reduction of NO_x is achieved in the MF–NO interaction at high pressure.

ASSOCIATED CONTENT

Supporting Information

Information on temperature profiles inside the reactor, the full mechanism listing, and the thermochemistry used. This material is available free of charge via the Internet at <http://pubs.acs.org>.

AUTHOR INFORMATION

Corresponding Author

*Telephone: +34976761876. Fax: +34976761879. E-mail: uxue@unizar.es.

Notes

The authors declare no competing financial interest.

ACKNOWLEDGMENTS

The authors express their gratitude to the Aragón Government (GPT Group) and the Ministry of Economy and Competitiveness (MINECO) and the European Regional Development Fund (FEDER) (Project CTQ2012-34423) for financial support. The authors also acknowledge the “Servicio General de Apoyo a la Investigación-SAI” of the University of Zaragoza for its contribution to the development of the experimental setup.

REFERENCES

- (1) Yanfeng, G.; Shenghua, L.; Hejun, G.; Tiegang, H.; Longbao, Z. *Appl. Therm. Eng.* **2007**, *27*, 202–207.
- (2) Sorenson, S. C. *J. J. Eng. Gas Turbines Power* **2001**, *123*, 652–658.
- (3) Song, R.; Li, K.; Feng, Y.; Liu, S. *Energy Fuels* **2009**, *23*, 5460–5466.
- (4) Esarte, C.; Millera, A.; Bilbao, R.; Alzueta, M. U. *Ind. Eng. Chem. Res.* **2010**, *49*, 6772–6779.
- (5) Song, K. H.; Litzinger, T. A. *Combust. Sci. Technol.* **2006**, *178*, 2249–2280.
- (6) Sathiyagnanam, A. P.; Saravanan, C. G. *Fuel* **2008**, *87*, 2281–2285.
- (7) Gao, J.; Nakamura, Y. *Fuel* **2013**, *106*, 241–248.
- (8) Herrmann, F.; Jochim, B.; Oßwald, P.; Cai, L.; Pitsch, H.; Kohse-Höinghaus, K. *Combust. Flame* **2014**, *161*, 384–397.
- (9) Herrmann, F.; Oßwald, P.; Kohse-Höinghaus, K. *Proc. Combust. Inst.* **2014**, *34*, 771–778.
- (10) Daly, C. A.; Simmie, J. M.; Dagaut, P.; Cathonnet, M. *Combust. Flame* **2001**, *125*, 1106–1117.
- (11) Chen, G.; Yu, W.; Fu, J.; Mo, J.; Huang, Z.; Yang, J.; Wang, Z.; Jin, H.; Qi, F. *Combust. Flame* **2012**, *159*, 2324–2335.
- (12) Dooley, S.; Dryer, F. L.; Yang, B.; Wang, J.; Cool, T. A.; Kasper, T.; Hansen, N. *Combust. Flame* **2011**, *158*, 732–741.
- (13) Pitz, W. J.; Mueller, C. J. *Prog. Energy Combust. Sci.* **2011**, *37*, 330–350.
- (14) Ren, W.; Lam, K.-Y.; Pyun, S. H.; Farooq, A.; Davidson, D. F.; Hanson, R. K. *Proc. Combust. Inst.* **2014**, *34*, 453–461.
- (15) Metcalfe, W. K.; Simmie, J. M.; Curran, H. J. *J. Phys. Chem. A* **2010**, *114*, 5478–5484.
- (16) Wallington, T. J.; Hurley, M. D.; Maurer, T.; Barnes, I.; Becker, K. H.; Tyndall, G. S.; Orlando, J. J.; Pimentel, A. S.; Bilde, M. *J. Phys. Chem. A* **2001**, *105*, 5146–5154.
- (17) Alzueta, M. U.; Aranda, V.; Monge, F.; Millera, A.; Bilbao, R. *Combust. Flame* **2013**, *160*, 853–860.
- (18) Dooley, S.; Burke, M. P.; Chaos, M.; Stein, Y.; Dryer, F. L.; Zhukov, V. P.; Finch, O.; Simmie, J. M.; Curran, H. J. *Int. J. Chem. Kinet.* **2010**, *42*, 527–549.
- (19) Good, D. A.; Hanson, J.; Francisco, J. S.; Li, Z.; Jeong, G. R. *J. Phys. Chem. A* **1999**, *103*, 10893–10898.
- (20) Good, D. A.; Francisco, J. S. *J. Phys. Chem. A* **2000**, *104*, 1171–1185.
- (21) Francisco, J. S. *J. Am. Chem. Soc.* **2003**, *125*, 10475–10480.
- (22) Westbrook, C. K.; Pitz, W. J.; Westmoreland, P. R.; Dryer, F. L.; Chaos, M.; Osswald, P.; Kohse-Höinghaus, K.; Cool, T. A.; Wang, J.; Yang, B.; Hansen, N.; Kasper, T. *Proc. Combust. Inst.* **2009**, *32*, 221–228.
- (23) Rasmussen, C. L.; Jakobsen, J. G.; Glarborg, P. *Int. J. Chem. Kinet.* **2008**, *40*, 778–807.
- (24) Giménez-López, J.; Alzueta, M. U.; Rasmussen, C. L.; Marshall, P.; Glarborg, P. *Proc. Combust. Inst.* **2011**, *33*, 449–457.

- (25) Abián, M.; Silva, S. L.; Millera, A.; Bilbao, R.; Alzueta, M. U. *Fuel Process. Technol.* **2010**, *91*, 1204–1211.
- (26) Rasmussen, C. L.; Hansen, J.; Marshall, P.; Glarborg, P. *Int. J. Chem. Kinet.* **2008**, *40*, 454–480.
- (27) Rasmussen, C. L.; Rasmussen, A. E.; Glarborg, P. *Combust. Flame* **2008**, *154*, 529–545.
- (28) Galano, A.; Álvarez-Idaboy, J. R.; Ruiz-Santoyo, M. E.; Vivier-Bunge, A. *J. Phys. Chem. A* **2002**, *106*, 9520–9528.
- (29) Larson, C. W.; Steward, P. H.; Golden, D. M. *Int. J. Chem. Kinet.* **1998**, *20*, 27–40.
- (30) Olbregts, J. *Int. J. Chem. Kinet.* **1985**, *17*, 835–848.
- (31) Röhring, M.; Petersen, E. L.; Davidson, D. F.; Hanson, R. K. *Int. J. Chem. Kinet.* **1997**, *29*, 483–494.
- (32) Park, J.; Giles, N. D.; Moore, J.; Lin, M. C. *J. Phys. Chem. A* **1998**, *102*, 10099–10105.
- (33) Lutz, A. E.; Kee, R. J.; Miller, J. A. *SENKIN: A FORTRAN Program for Predicting Homogeneous Gas Phase Chemical Kinetics with Sensitivity Analysis*; Sandia National Laboratories: Livermore, CA, 1988; Report SAND87-8248.
- (34) Kee, R. J.; Rupley, F. M.; Miller, J. A. *CHEMKIN-II: A FORTRAN Chemical Kinetics Package for the Analysis of Gas-Phase Chemical Kinetics*; Sandia National Laboratories: Albuquerque, NM, 1991; Report SAND87-8215.
- (35) Alzueta, M. U.; Muro, J.; Bilbao, R.; Glarborg, P. *Isr. J. Chem.* **1999**, *39*, 73–86.
- (36) Tan, T.; Pavone, M.; Krisiloff, D. B.; Carter, E. A. *J. Phys. Chem. A* **2012**, *116*, 8431–8443.
- (37) Lam, K.-Y.; Davidson, D. F.; Hanson, R. K. *J. Phys. Chem. A* **2012**, *116*, 12229–12241.

Article I:

Marrodán, L.; Monge, F.; Millera, Á.; Bilbao, R.; Alzueta, M.U. (2016).
Dimethoxymethane oxidation in a flow reactor. *Combustion Science and
Technology* 188, 719-729.

Dimethoxymethane Oxidation in a Flow Reactor

Lorena Marrodán, Fabiola Monge, Ángela Millera, Rafael Bilbao, and María U. Alzueta

Aragón Institute of Engineering Research (I3A), Department of Chemical and Environmental Engineering, University of Zaragoza, Zaragoza, Spain

ABSTRACT

The simultaneous reduction of NO_x and soot emissions from diesel engines is a major research subject and a challenge in today's world. One prospective solution involves diesel fuel reformulation by addition of oxygenated compounds, such as dimethoxymethane (DMM). In this context, different DMM oxidation experiments have been carried out in an atmospheric pressure gas-phase installation, in the 573–1373 K temperature range, from pyrolysis to fuel-lean conditions. The results obtained have been interpreted by means of a detailed gas-phase chemical kinetic mechanism. Results indicate that the initial oxygen concentration slightly influences the consumption of DMM. However, certain effects can be observed in the profiles of the main products (CH_4 , CH_3OH , CH_3OCHO , CO , CO_2 , C_2H_2 , C_2H_4 , and C_2H_6). Acetylene, an important soot precursor, is only formed under pyrolysis and reducing conditions. In general, a good agreement between experimental and modeling data was observed.

ARTICLE HISTORY

Received 3 November 2014
Revised 22 June 2015
Accepted 19 November 2015

KEYWORDS

Dimethoxymethane (DMM);
Flow reactor; Kinetic model;
Oxidation

Introduction

In the past several years, diesel has been one of the most used fuels in transportation because of its higher fuel efficiency and lower exhaust emissions of hydrocarbons, CO , and CO_2 compared to gasoline. However, nitrogen oxides (NO_x) and particulate matter, mainly soot, are the most critical pollutants produced by diesel engines, and the reduction of both simultaneously becomes one of the main obstacles in its development because of the increasing environmental protection concern and the implementation of the emission restrictions. Some measures for their minimization have been proposed, such as increasing the injection pressure, recirculation of the exhaust gas, or fuel reformulation by adding oxygenated additives. The use of these additives increases the oxygen content, producing a cleaner burning of the fuel. Furthermore, the use of oxygenates modifies as well the fuel properties, such as density, viscosity, volatility, behavior at low temperatures, and cetane number (Ribeiro et al., 2007). The changes in the properties also lead to fuel combustion modifications, which may result in a simultaneous reduction of particulate matter and NO_x . For this reason, some compounds, such as methanol (Chao et al., 2001), ethanol (He et al., 2003), and dimethylether (Ying et al., 2008), have been extensively studied.

Dimethoxymethane (DMM; $\text{CH}_3\text{OCH}_2\text{OCH}_3$) is a diether of interest because it is a liquid, 100% miscible in diesel fuel, does not have C–C atomic bonds, and contains 42%

oxygen by weight. All of these characteristics, and the decrease of the cetane number compared to conventional diesel fuels, cause a delay of the ignition time, which allows more air to be drawn into the fuel jet and reduce the production of particulate matter (Song and Litzinger, 2006).

The first study on DMM oxidation found in the literature is reported by Molera et al. (1977). Their experimental data suggest that the DMM oxidation is initiated by hydrogen abstraction reactions forming $\text{CH}_3\text{OCH}_2\text{OCH}_2$ and $\text{CH}_3\text{OCHOCH}_3$ radicals. Daly et al. (2001) investigated the oxidation of DMM in a jet-stirred reactor at pressures of 5.07 bar, temperatures from 800 K to 1200 K, and equivalence ratios of 0.444, 0.889, and 1.778. The results obtained were interpreted by using a detailed chemical mechanism with a good agreement between experimental and calculated data. Some years later, Sinha and Thomson (2004) determined, at atmospheric pressure, the species concentrations and temperatures across opposed flow diffusion flames of three different C3 oxygenated hydrocarbons, among which DMM was considered. In addition, the results obtained were compared with those of propane-DMM blends, concluding that the presence of DMM reduces the formation of ethylene and acetylene, which are the main soot precursors. Dias et al. (2010) and Dias and Vandooren (2011) developed a reaction mechanism taking into account the formation and the consumption of oxygenated species involved in dimethoxymethane oxidation, which contained 480 reactions and 90 chemical species. Recently, Zhang et al. (2014) performed autoignition delay time measurements for dimethoxymethane/oxygen/argon mixtures at 2, 4, and 10 atm, temperatures of 1103–1454 K, and different dilution and equivalence ratios. Their results were compared with those calculated from the previously proposed mechanism by Dias et al. (2010) with good agreement.

In this context, the present work on the DMM oxidation under well controlled tubular flow reactor conditions at atmospheric pressure represents the starting point of a deep research of this compound, which will be extended with the study of its oxidation at higher pressures (20–60 bar), and both in the presence and absence of NO. Therefore, a large number of experimental results will be available. Further, the DMM sooting tendency will be studied in its mixtures with acetylene, which is considered to be one of the main soot precursors.

Experimental

The experiments of the dimethoxymethane oxidation have been carried out in an experimental installation successfully used by our research group and previously described in detail elsewhere (e.g., Alzueta et al., 1998); only a brief description is given here. The quartz flow reactor, built according to the design of Kristensen et al. (1996), has a reaction zone of 8.7 mm inside diameter and 200 mm in length. It is placed in a three-zone electrically heated oven ensuring a uniform temperature profile within ± 10 K throughout the reaction zone.

Gases are fed to the system through mass flow controllers, in four separate streams: one flow containing nitrogen and water vapor and three injector tubes containing dimethoxymethane, O_2 and N_2 , respectively. Water vapor, approximately 7000 ppm, is introduced in the reactor by saturating a N_2 stream through a water bubbler. N_2 is used to achieve a

Table 1. Matrix of experimental conditions.

Set	DMM (ppm)	O ₂ (ppm)	H ₂ O (ppm)	λ
1	653	0	6918	0
2	668	1113	6466	0.4
3	648	1946	6918	0.7
4	626	2782	6484	1
5	653	97,327	6918	35

Note. The experiments are conducted at a constant flow rate of 1000 mL(STP)/min, at atmospheric pressure, in the temperature interval of 573–1373 K. The residence time is dependent on the reaction temperature: t_r (s) = 195/T (K). The balance is closed with N₂.

total flow rate of 1000 mL(STP)/min, resulting in a gas residence time dependent on the reaction temperature of 195/T (K).

A concentration of approximately 700 ppm of DMM is introduced in all of the experiments. For a given value of the air excess ratio (λ), defined as the inlet oxygen concentration divided by the stoichiometric oxygen, the amount of O₂ is determined. This amount has been varied between 0–98,000 ppm. Each set of experiments has been carried out at atmospheric pressure covering the 573–1373 K temperature range. Table 1 summarizes the conditions of the experiments performed.

At the outlet of the reaction zone, the gas product is quenched by cooling air and before analysis it passes through a condenser and a filter to ensure gas cleaning. The outlet gas composition is analyzed by a micro-gas chromatograph equipped with TCD detectors, which detect and quantify DMM, CO, CO₂, CH₃OCHO, CH₃OH, CH₄, C₂H₂, C₂H₄, C₂H₆, and H₂. The uncertainty of the measurements is estimated as $\pm 5\%$. Carbon-balance was checked for the experiments and, in general, was found to be closed within $100 \pm 10\%$.

Modeling

The gas-phase chemical kinetic mechanism developed in the present work was initially built from the work of Glarborg et al. (1998), which describes the interactions among C1–C2 hydrocarbons and NO_x, extended and updated later by Glarborg et al. (2003) and Skjoth-Rasmussen et al. (2004). Additional reaction subsets for dimethyl ether (Alzueta et al., 1999), ethanol (Alzueta and Hernández, 2002), acetylene (Alzueta et al., 2008), and methyl formate (Marrodán et al., 2014) have been added. For the DMM oxidation, the subset proposed by Dias et al. (2010) was taken.

The resultant mechanism (which can be obtained directly from the authors), developed to describe the dimethoxymethane oxidation at atmospheric pressure under a wide range of operating conditions, has been validated with the present experimental data. Thermodynamic data for the involved species were taken from the same sources as the origin mechanisms. The modeling study was performed using SENKIN, the plug flow reactor code that runs in conjunction with the Chemkin-II library (Kee et al., 1991; Lutz et al., 1988), considering constant temperature and pressure in the reaction zone, which has been tested to be a fairly good assumption.

Results and discussion

In this work, a wide study of the oxidation of dimethoxymethane has been carried out, under flow reactor conditions at atmospheric pressure in the 573–1373 K temperature range and for different air/fuel ratios ($\lambda = 0, 0.4, 0.7, 1,$ and 35). From now on, $\lambda = 0.4$ is referred to as very reducing conditions and $\lambda = 0.7$ as reducing conditions. With the model validated with the present experimental results, reaction path and sensitivity analyses have been performed in order to identify the most important reactions involved in the conversion of DMM under the conditions of the present work.

Figures 1–3 show both the experimental and modeling results for the consumption of DMM, and the formation of the main products (CO , CO_2 , H_2 , CH_3OH , CH_3OCHO , CH_4 , C_2H_2 , C_2H_4 , and C_2H_6) as a function of temperature for the different air/fuel ratios. Symbols denote experimental results and lines denote modeling calculations. In general, the model is able to predict satisfactorily the main experimental trends under the present conditions.

Figure 1 shows the influence of the temperature and λ value on the concentration of DMM and the formation of the products CO , CO_2 , and H_2 . The DMM consumption occurs in the 973–1123 K temperature range. The temperature for the onset of the DMM conversion is almost independent of the stoichiometry studied, even though both experimental and theoretical results obtained under highly oxidizing conditions ($\lambda = 35$) are slightly shifted toward lower temperatures. Thus, it can be said that the oxygen

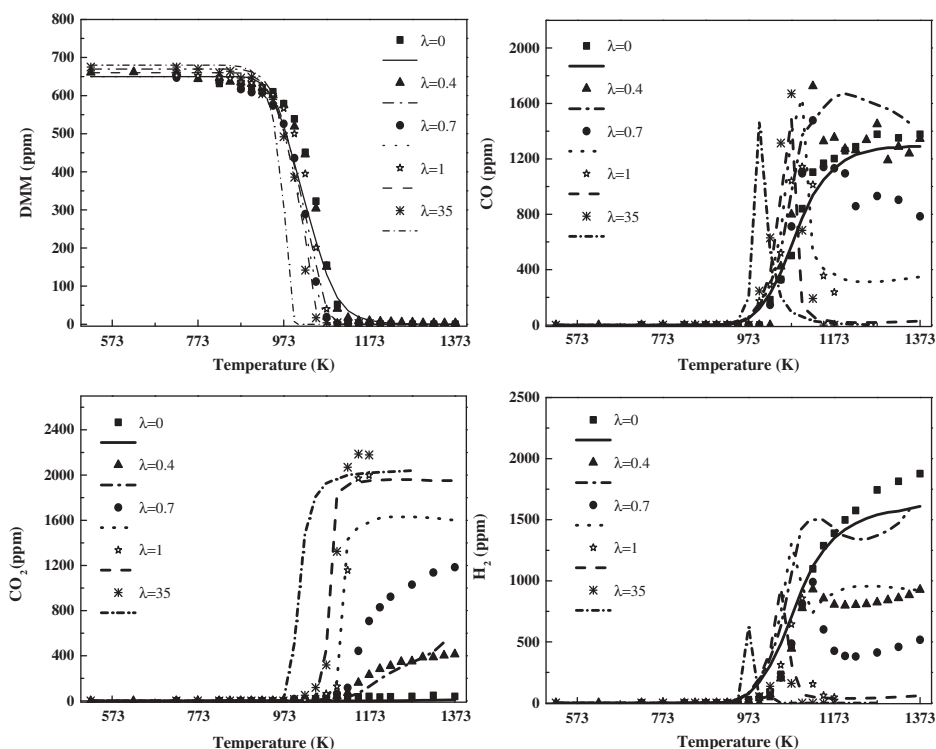


Figure 1. Influence of the air excess ratio (λ) on the DMM, CO , CO_2 , and H_2 concentration profiles as a function of the temperature.

concentration in the reactant mixture slightly influences the conversion of DMM, similar to what has been observed in the case of other oxygenated compounds, such as DME (Alzueta et al., 1999). Another important aspect to highlight is that DMM is consumed completely, independently of the oxygen availability, in all of the conditions studied at temperatures above 1150 K.

However, the presence of oxygen does have certain effects on some of the reaction products, which are described here. The onset for the formation of CO occurs approximately at the same temperature as the DMM starts to be consumed. When the temperature increases, the CO concentration increases as well, reaching a maximum value. As the air excess ratio increases, the temperature for this maximum CO concentration is slightly shifted towards lower temperature values, and also the width of the CO peak is narrower. The oxygen availability also influences the oxidation of CO to CO₂. While under pyrolysis and very reducing conditions, CO₂ is hardly formed; under reducing conditions, an appreciable amount of CO₂ is produced, which coexists with a non-negligible amount of CO; and for stoichiometric and oxidizing conditions, CO is completely oxidized to CO₂. In the case of the H₂ production, the general trend is the opposite of the CO₂ case. The biggest concentration of H₂ is reached for pyrolysis conditions and the lowest one for oxidizing conditions. The H₂ concentration profile presents a maximum as a function of temperature; beyond that it begins to drop to zero (stoichiometric and oxidizing conditions) or to an almost constant value (reducing and very reducing conditions). The only case where H₂ continues growing is in the absence of oxygen.

Figures 2 and 3 show the concentration profiles for CH₃OH and CH₃OCHO (MF), and CH₄, C₂H₆, C₂H₄, and C₂H₂, respectively, as a function of the temperature. All of these compounds reach a maximum concentration, which is shifted to lower temperatures when the reactant mixture becomes fuel-leaner. In general, there is a good agreement between experimental and calculated results, with the exception of MF and MeOH. As it will be discussed later, MF is an important intermediate in the DMM conversion and it produces methanol through reaction (r.1):

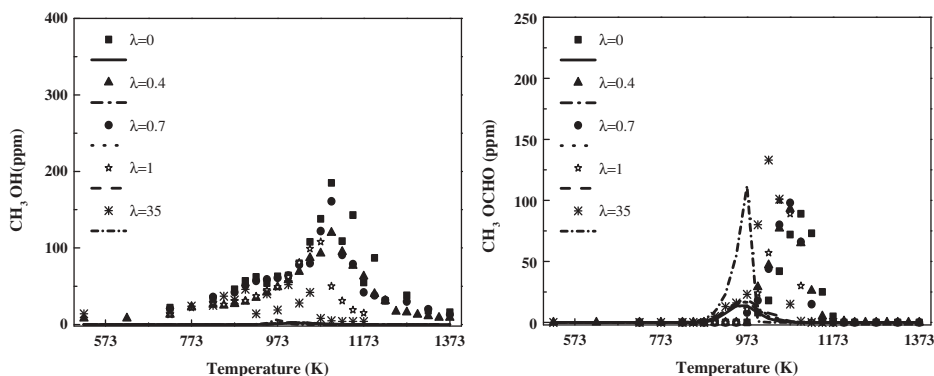


Figure 2. Influence of the air excess ratio (λ) on the CH₃OH and CH₃OCHO concentration profiles as a function of the temperature.

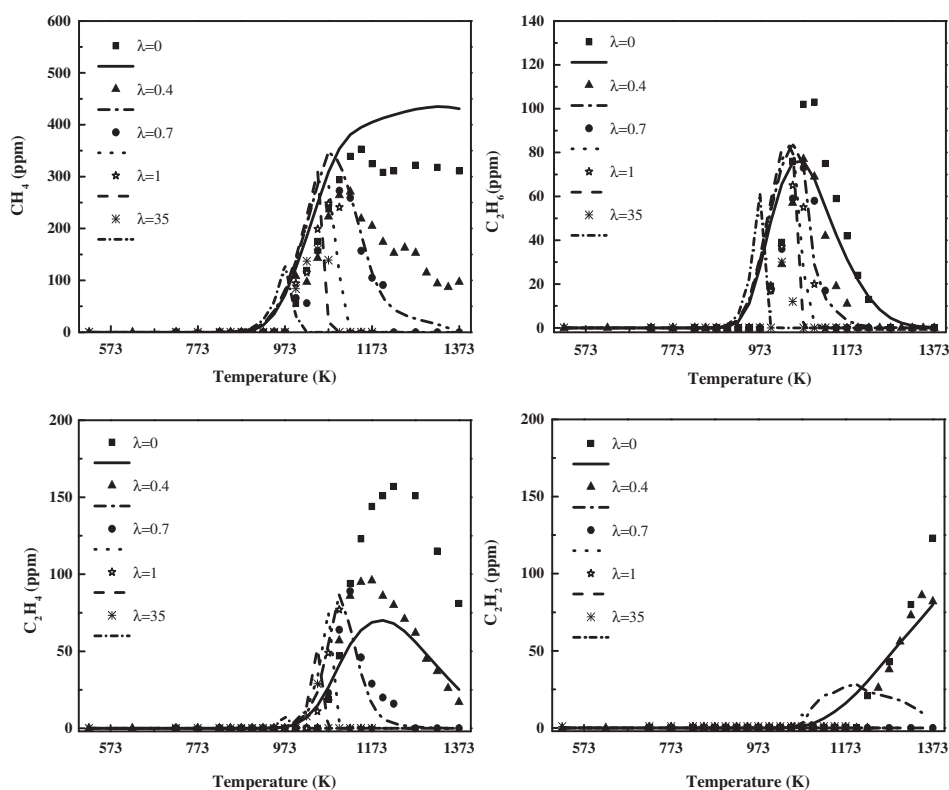


Figure 3. Influence of the air excess ratio (λ) on the CH_4 , C_2H_6 , C_2H_4 , and C_2H_2 concentration profiles as a function of the temperature.

There is a considerable uncertainty in the value of the activation energy for this reaction. In a previous work of our group on methyl formate oxidation at atmospheric pressure (Alzueta et al., 2013), the impact of varying the activation energy value was evaluated. Changes between 50.0 and 68.3 kcal/mol (values interval found in the literature) showed a great influence on the consumption of MF and formation of the main products. The value of 60.0 kcal/mol, following Dooley et al. (2010), was finally chosen. This value has been adopted in this work, although changes in this value have a considerable impact in the MF and MeOH predictions under the conditions of this work.

It is important to note that acetylene (C_2H_2) has only been detected under pyrolysis and very reducing conditions. For the latter ones, the model underpredicts the concentration of C_2H_2 .

In order to explain the experimental concentration profiles obtained and identify the main reaction routes, a reaction rate analysis with the mechanism compiled in the present work was performed. The reaction path diagram for DMM oxidation obtained is represented in Figure 4. As an example, for stoichiometric conditions and for different temperatures, the relative importance (%) of the two main DMM consumption steps is shown.

In most of the present conditions, the DMM conversion is initiated by the decomposition reactions (r.2) and (r.3), even though the main consumption channel of DMM is the

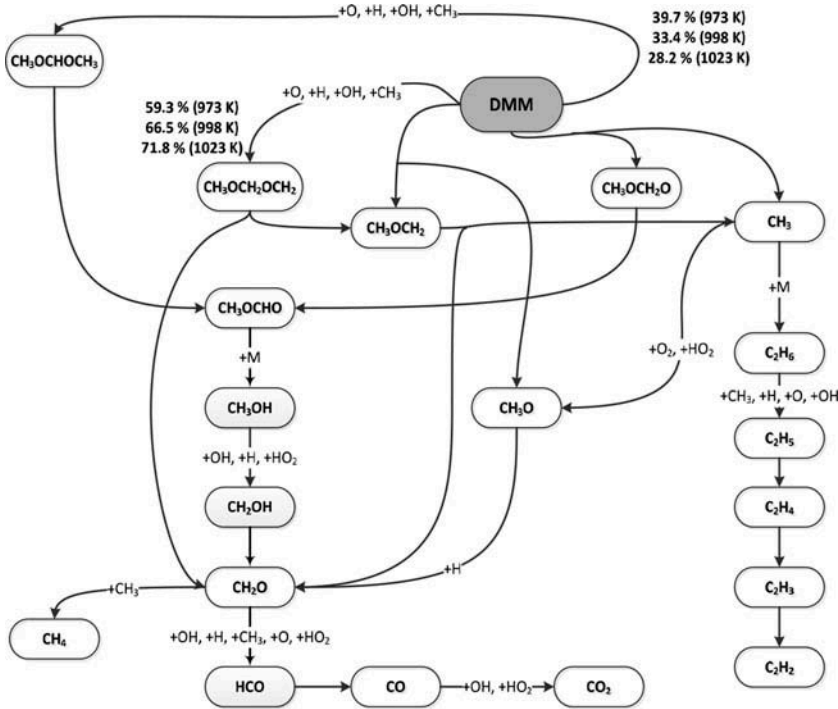
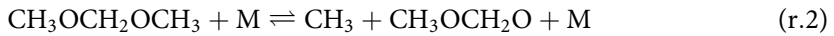
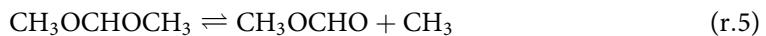
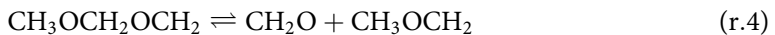


Figure 4. Reaction path diagram for DMM oxidation according to the current kinetic model.

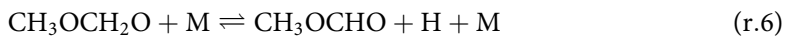
hydrogen abstraction by different radicals (H, OH, O, CH₃) to obtain the primary radical CH₃OCH₂OCH₂, or the secondary radical CH₃OCHOCH₃:



The DMM radicals generated (CH₃OCH₂OCH₂ and CH₃OCHOCH₃) decompose through reactions (r.4) and (r.5):



The CH₃OCH₂O and CH₃OCH₂ species, obtained in reaction (r.2) and reactions (r.3) and (r.4), decompose totally to CH₃OCHO (MF) [reaction (r.6)], and CH₃ and CH₂O [reaction (r.7)], respectively:



The methyl formate obtained by this route or from the CH₃OCHOCH₃ thermal degradation (r.5), follows the same reaction pathways described in detail in an earlier work of our research group (Marrodán et al., 2014) and only a brief discussion is given here.

Table 2. Elementary reactions and kinetic parameters for selected reactions.

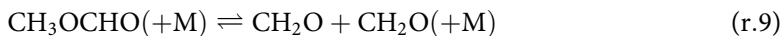
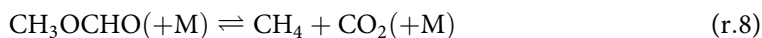
Reaction	<i>A</i>	<i>n</i>	<i>E_a</i>	Source
$\text{CH}_3\text{OCH}_2\text{OCH}_3 + \text{M} \rightleftharpoons \text{CH}_3 + \text{CH}_3\text{OCH}_2\text{O} + \text{M}$	2.62E+16	0.0	82,200	Dias et al. (2010)
$\text{CH}_3\text{OCH}_2\text{OCH}_3 + \text{M} \rightleftharpoons \text{CH}_3\text{O} + \text{CH}_3\text{OCH}_2 + \text{M}$	2.51E+15	0.0	76,800	Dias et al. (2010)
$\text{CH}_3\text{OCH}_2\text{OCH}_3 + \text{H} \rightleftharpoons \text{CH}_3\text{OCH}_2\text{OCH}_2 + \text{H}_2$	9.70E+13	0.0	6210	Dias et al. (2010)
$\text{CH}_3\text{OCH}_2\text{OCH}_3 + \text{H} \rightleftharpoons \text{CH}_3\text{OCH}_2\text{OCH}_3 + \text{H}_2$	3.70E+12	0.0	3240	Dias et al. (2010)
$\text{CH}_3\text{OCH}_2\text{OCH}_3 + \text{OH} \rightleftharpoons \text{CH}_3\text{OCH}_2\text{OCH}_2 + \text{H}_2\text{O}$	9.10E+12	0.0	986	Dias et al. (2010)
$\text{CH}_3\text{OCH}_2\text{OCH}_3 + \text{OH} \rightleftharpoons \text{CH}_3\text{OCHOCH}_3 + \text{H}_2\text{O}$	9.10E+12	0.0	986	Dias et al. (2010)
$\text{CH}_3\text{OCH}_2\text{OCH}_3 + \text{O} \rightleftharpoons \text{CH}_3\text{OCH}_2\text{OCH}_2 + \text{OH}$	5.00E+13	0.0	4570	Dias et al. (2010)
$\text{CH}_3\text{OCH}_2\text{OCH}_3 + \text{O} \rightleftharpoons \text{CH}_3\text{OCHOCH}_3 + \text{OH}$	6.00E+13	0.0	3970	Dias et al. (2010)
$\text{CH}_3\text{OCH}_2\text{OCH}_3 + \text{CH}_3 \rightleftharpoons \text{CH}_3\text{OCH}_2\text{OCH}_2 + \text{CH}_4$	2.26E-05	5.35	5810	Dias et al. (2010)
$\text{CH}_3\text{OCH}_2\text{OCH}_3 + \text{CH}_3 \rightleftharpoons \text{CH}_3\text{OCHOCH}_3 + \text{CH}_4$	5.00E+12	0.0	9750	Dias et al. (2010)
$\text{CH}_3\text{OCH}_2\text{OCH}_2 \rightleftharpoons \text{CH}_2\text{O} + \text{CH}_3\text{OCH}_2$	1.00E+13	0.0	32500	Dias et al. (2010)
$\text{CH}_3\text{OCH}_2\text{O} + \text{M} \rightleftharpoons \text{CH}_3\text{OCHO} + \text{H} + \text{M}$	7.00E+15	0.0	22,800	Dias et al. (2010)
$\text{CH}_3\text{OCH}_2 \rightleftharpoons \text{CH}_3 + \text{CH}_2\text{O}$	1.60E+13	0.0	25,500	Alzueta et al. (1999)
$\text{CH}_3\text{OCHOCH}_3 \rightleftharpoons \text{CH}_3\text{OCHO} + \text{CH}_3$	1.00E+13	0.0	32,500	Dias et al. (2010)
$\text{CH}_3\text{OCHO}(+\text{M}) \rightleftharpoons \text{CH}_3\text{OH} + \text{CO}(+\text{M})$	2.00E+13	0.0	60,000	Alzueta et al. (2013)
$\text{CH}_3\text{OCHO}(+\text{M}) \rightleftharpoons \text{CH}_4 + \text{CO}_2(+\text{M})$	1.50E+12	0.0	59,700	Alzueta et al. (2013)
$\text{CH}_3\text{OCHO}(+\text{M}) \rightleftharpoons \text{CH}_2\text{O} + \text{CH}_2\text{O}(+\text{M})$	1.00E+12	0.0	60,500	Alzueta et al. (2013)

Note. *A* in units of cm^3 , mol, s; *E_a* in cal/mol.

The MF oxidation is initiated by the following decomposition reaction:



with minor relevance of reactions (r.8) and (r.9):



The kinetic parameters used for these reactions are reported in Table 2.

The methanol produced (r.1) is consumed giving mainly hydroxymethyl radicals (CH_2OH), which react mainly with molecular oxygen to give formaldehyde. It continues the $\text{CH}_2\text{O} \rightarrow \text{HCO} \rightarrow \text{CO} \rightarrow \text{CO}_2$ reaction sequence. Methanol can also lead to the formation of CH_4 through formaldehyde as intermediate.

These reaction routes can explain the pattern observed in Figures 2 and 3, in which the temperature for the maximum concentration of these compounds follows, increasing in the following order: MF, CH_3OH , and CH_4 .

The recombination of methyl radicals obtained through different routes, leads to the formation of ethane, which gives ethylene, and this one reacts to form acetylene as the final product. For this reason, the order, from the lowest to the highest temperature, in which the maximum concentration of these species appear, is: C_2H_6 , C_2H_4 , and C_2H_2 .

A first-order sensitivity analysis for CO has been performed for all of the sets in Table 1. Figure 5 shows the results obtained. In the upper part of the figure, the sensitivity coefficients for reaction $\text{CH}_3\text{OCH}_2\text{OCH}_3 + \text{CH}_3 \rightleftharpoons \text{CH}_3\text{OCHOCH}_3 + \text{CH}_4$, which is clearly dominant, have been divided by two to clarify the representation and to better highlight the other reactions that are of comparatively minor importance. The results indicate that the conversion of DMM is mostly sensitive to the hydrogen abstraction by methyl radicals to obtain the secondary DMM radical ($\text{CH}_3\text{OCHOCH}_3$) and also to the already mentioned DMM degradation reactions [(r.2) and (r.3)]. In the case of methyl formate, its conversion is sensitive to its degradation to methanol and CO (r.1). There are no huge discrepancies between the different λ analyzed; only the

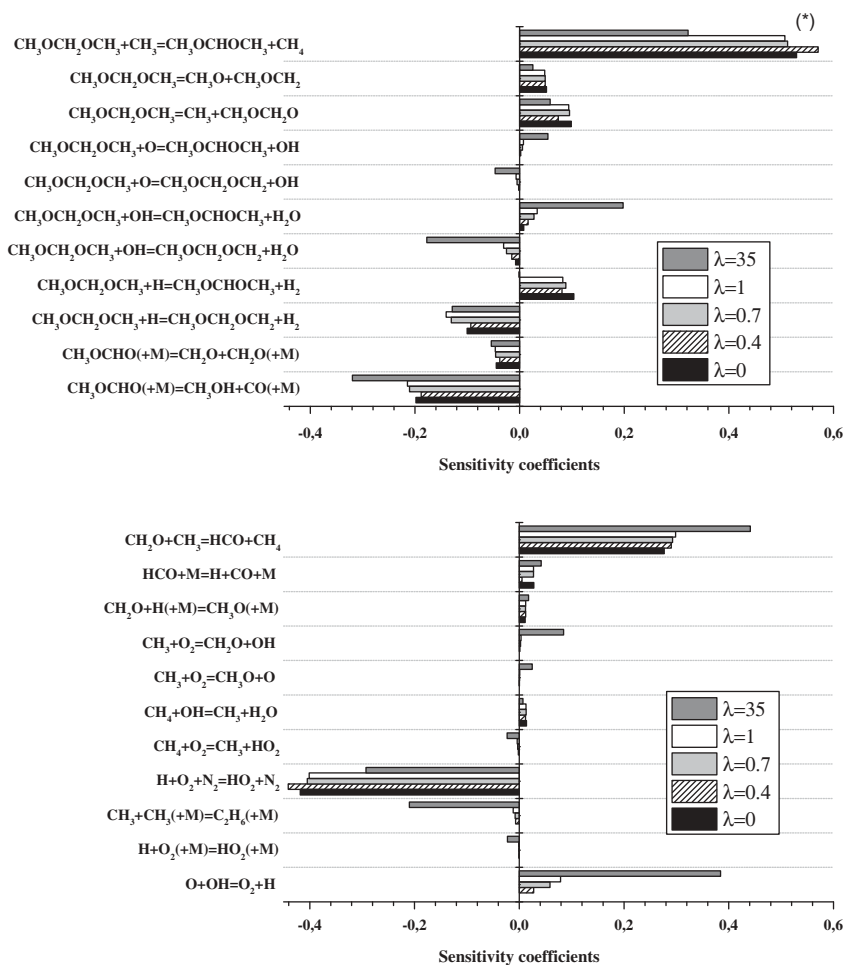


Figure 5. Sensitivity analysis for DMM for different air/fuel ratios. Upper part: sensitivity coefficients for DMM and MF reactions. Lower part: sensitivity coefficients for C0–C1 reactions. (*) The sensitivity coefficients have been divided by two.

reactions where OH radicals participate present a bigger sensitivity under oxidizing conditions.

Conclusions

The oxidation of DMM has been studied in a quartz flow reactor in the 573–1373 K temperature range, for different air/fuel ratios ($\lambda = 0, 0.4, 0.7, 1, \text{ and } 35$) at atmospheric pressure. The experimental data obtained have been interpreted in terms of a detailed chemical kinetic mechanism compiled from different works in the literature.

The oxygen concentration in the reactant mixture slightly influences the conversion of DMM; only for the oxidizing conditions, both experimental and theoretical results are shifted towards lower temperatures. However, in some reaction products, such as CO and CO_2 , certain effects can be observed. As the air excess ratio increases, the CO maximum

concentration is shifted to lower temperatures and the concentration peak becomes narrower. CO₂ formation is favored under stoichiometric and oxidizing conditions, where CO is completely oxidized to CO₂.

Methyl formate is an important intermediate formed during the DMM conversion. The analysis of its main reaction pathways indicates that they are similar to those obtained in previous works about MF oxidation (Alzueta et al., 2013; Marrodán et al., 2014). Modeling calculations have been found to be very sensitive to the activation energy value for MF conversion to methanol and CO ($\text{CH}_3\text{OCHO}(\text{+M}) \rightleftharpoons \text{CH}_3\text{OH} + \text{CO}(\text{+M})$).

Acetylene, considered as one of the main soot precursors, was only detected for pyrolysis and very reducing conditions.

Sensitivity and reaction rate analyses were performed to identify the main reactions involved in the DMM conversion. The results obtained indicate that the DMM conversion is initiated by degradation reactions, but hydrogen abstraction reactions also play an important role.

Funding

The authors express their gratitude to the Aragón Government and European Social Fund (GPT group), and to MINECO and FEDER (Project CTQ2012-34423) for financial support. Ms. L. Marrodán acknowledges the DGA (Diputación General de Aragón) for the predoctoral grant awarded.

References

- Alzueta, M.U., Aranda, V., Monge, F., Millera, A., and Bilbao, R. 2013. Oxidation of methyl formate and its interaction with nitric oxide. *Combust. Flame*, **160**, 853–860.
- Alzueta, M.U., Bilbao, R., Millera, A., Oliva, M., and Ibañez, J.C. 1998. Interactions between nitric oxide and urea under flow reactor conditions. *Energy Fuels*, **12**, 1001–1007.
- Alzueta, M.U., Borruey, M., Callejas, A., Millera, A., and Bilbao, R. 2008. An experimental and modeling study of the oxidation of acetylene in a flow reactor. *Combust. Flame*, **152**, 377–386.
- Alzueta, M.U., and Hernández, J.M. 2002. Ethanol oxidation and its interaction with nitrogen oxide. *Energy Fuels*, **16**, 166–171.
- Alzueta, M.U., Muro, J., Bilbao, R., and Glarborg, P. 1999. Oxidation of dimethyl ether and its interaction with nitrogen oxides. *Isr. J. Chem.*, **39**, 73–86.
- Chao, M., Lin, T., Chao, H., Chang, F., and Chen, C. 2001. Effects of methanol-containing additive on emission characteristics from a heavy-duty diesel engine. *Sci. Total Environ.*, **279**, 167–179.
- Daly, C.A., Simmie, J.M., Dagaut, P., and Cathonnet, M. 2001. Oxidation of dimethoxymethane in a jet-stirred reactor. *Combust. Flame*, **125**, 1106–1117.
- Dias, V., Lories, X., and Vandooren, J. 2010. Lean and rich premixed dimethoxymethane/oxygen/argon flames: Experimental and modeling. *Combust. Sci. Technol.*, **182**, 350–364.
- Dias, V., and Vandooren, J. 2011. Experimental and modeling studies of C₂H₄/O₂/Ar, C₂H₄/methylal/O₂/Ar and C₂H₄/O₂/Ar rich flames and the effect of oxygenated additives. *Combust. Flame*, **158**, 848–859.
- Dooley, S., Burke, M.P., Chaos, M., Stein, Y., Dryer, F.L., Zhukov, V.P., Finch, O., Simmie, J.M., and Curran, H.J. 2010. Methyl formate oxidation: Speciation data, laminar burning velocities, ignition delay times, and a validated chemical kinetic model. *Int. J. Chem. Kinet.*, **42**, 527–549.
- Glarborg, P., Alzueta, M.U., Dam-Johansen, K., and Miller, J.A. 1998. Kinetic modeling of hydrocarbon/nitric oxide interactions in a flow reactor. *Combust. Flame*, **115**, 1–27.

- Glarborg, P., Alzueta, M.U., Kjærgaard, K., and Dam-Johansen, K. 2003. Oxidation of formaldehyde and its interaction with nitric oxide in a flow reactor. *Combust. Flame*, **132**, 629–638.
- He, B., Shuai, S., Wang, J., and He, H. 2003. The effect of ethanol blended diesel fuels on emissions from a diesel engine. *Atmos. Environ.*, **37**, 4965–4971.
- Kee, R.J., Rupley, F.M., and Miller, J.A. 1991. CHEMKIN II: A FORTRAN chemical kinetics package for the analysis of gas-phase chemical kinetics. Report SAND87-8215. Sandia National Laboratories, Albuquerque, NM.
- Kristensen, P.G., Glarborg, P., and Dam-Johansen, K. 1996. Nitrogen chemistry during burnout in fuel-staged combustion. *Combust. Flame*, **107**, 211–222.
- Lutz, A.E., Kee, R.J., and Miller, J.A. 1988. SENKIN: A FORTRAN program for predicting homogeneous gas phase kinetics with sensitivity analysis. Report SAND87-8248. Sandia National Laboratories, Livermore, CA.
- Marrodán, L., Millera, A., Bilbao, R., and Alzueta, M.U. 2014. High-pressure study of methyl formate and its interaction with NO. *Energy Fuels*, **28**, 6107–6115.
- Molera, M.J., Domínguez, J.A., and Santiuste, J.M. 1977. Gas-phase oxidation of dimethoxy methane-¹⁴C. *An. Quím.*, **73**, 467–471.
- Ribeiro, N.M., Pinto, A.C., Quintella, C.M., da Rocha, G.O., Teixeira, L.S.G., Guarieiro, L.L.N., Rangel, M.C., Veloso, M.C.C., Rezende, M.J.C., da Cruz, R.S., Oliveira, A.M., Torres, E.A., and de Andrade, J.B. 2007. The role of additives for diesel and diesel blended (ethanol or biodiesel) fuels: A review. *Energy Fuels*, **21**, 2433–2445.
- Sinha, A., and Thomson, M.J. 2004. The chemical structures of opposed flow diffusion flames of C3 oxygenated hydrocarbons (isopropanol, dimethoxymethane, and dimethyl carbonate) and their mixtures. *Combust. Flame*, **136**, 548–556.
- Skjøth-Rasmussen, M.S., Glarborg, P., Østberg, M., Johannessen, J.T., Livbjerg, H., Jensen, A.D., and Christensen, T.S. 2004. Formation of polycyclic aromatic hydrocarbons and soot in fuel-rich oxidation of methane in a laminar flow reactor. *Combust. Flame*, **136**, 91–128.
- Song, K.H., and Litzinger, T.A. 2006. Effects of dimethoxymethane blending into diesel fuel on soot in an optically accessible DI diesel engine. *Combust. Sci. Technol.*, **178**, 2249–2280.
- Ying, W., Genbao, L., Wei, Z., and Longbao, Z. 2008. Study on the application of DME/diesel blends in a diesel engine. *Fuel Process. Technol.*, **89**, 1272–1280.
- Zhang, C., Li, P., Li, Y., He, J., and Li, X. 2014. Shock-tube study of dimethoxymethane ignition at high temperatures. *Energy Fuels*, **28**, 4603–4610.

Article II:

Marrodán, L.; Royo, E.; Millera, Á.; Bilbao, R.; Alzueta, M.U. (2015). High pressure oxidation of dimethoxymethane. *Energy and Fuels* 29, 3507-3517.

High Pressure Oxidation of Dimethoxymethane

Lorena Marrodán, Eduardo Royo, Ángela Millera, Rafael Bilbao, and María U. Alzueta*

Aragón Institute of Engineering Research (I3A), Department of Chemical and Environmental Engineering, University of Zaragoza, 50018 Zaragoza, Spain

Supporting Information

ABSTRACT: The oxidation of dimethoxymethane (DMM) has been studied under a wide range of temperatures (373–1073 K), pressures (20–60 bar) and air excess ratios ($\lambda = 0.7, 1$ and 20), from both experimental and modeling points of view. Experimental results have been interpreted and analyzed in terms of a detailed gas-phase chemical kinetic mechanism for describing the DMM oxidation. The results show that the DMM oxidation regime for 20, 40 and 60 bar is very similar for both reducing and stoichiometric conditions. For oxidizing conditions, a plateau in the DMM, CO and CO₂ concentration profiles as a function of the temperature can be observed. This zone seems to be associated with the peroxy intermediate, CH₃OCH₂O₂, whose formation and consumption reactions appear to be important for the description of DMM conversion under high pressure and high oxygen concentration conditions.

INTRODUCTION

Diesel engines are used for transportation because of their high fuel efficiency. However, they highly contribute to nitrogen oxides (NO_x) and particulate matter (PM) emissions, which are difficult to reduce simultaneously in conventional diesel engines (NO_x formation is favored under fuel-lean conditions, whereas PM is formed when there is a lack of oxygen). The addition of oxygenated compounds to diesel fuel can effectively reduce these emissions.^{1–4} For instance, the reduction of smoke has been reported to be strongly related to the oxygen content of blends⁵ without increasing the NO_x and engine thermal efficiency.

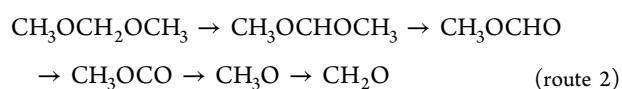
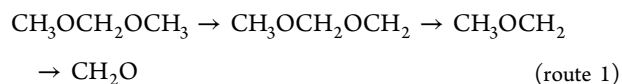
Dimethoxymethane (methylal or DMM, CH₃OCH₂OCH₃) is a diether considered to be a potential fuel additive. In comparison to the simplest ether, dimethyl ether (DME), which has been widely proposed and tested for using with diesel fuel as a means of reducing exhaust emissions,^{6,7} DMM has a higher quantity of oxygen, lower vapor pressure and better solubility with diesel fuel. Several studies have analyzed the effect of adding DMM to base diesel on emissions of compression ignition engines or direct injection engines (e.g., Ren et al.⁸) and, in general, diesel–DMM blends increase engine performance and decrease exhaust emissions.

Huang et al.⁹ studied the combustion and the emissions of a compression ignition engine fuelled with blends of diesel–DMM. They found that a remarkable reduction in the exhaust CO and smoke can be achieved when operating with diesel–DMM blends, and a simultaneous reduction in both NO_x and smoke can be obtained with large DMM additions. Sathiyagnanam and Saravanan¹⁰ also analyzed the effects of DMM addition to diesel, and obtained an appreciable reduction of emissions such as smoke density, particulate matter and a marginal increase in the performance when compared with the normal diesel run. Chen et al.¹¹ developed an experimental and modeling study of the effects of adding oxygenated fuels to premixed *n*-heptane flames and found that, as oxygenated fuels were added, mole fractions of most C₁–C₅ hydrocarbon

intermediates were significantly reduced together with an apparent decrease of benzene amount.

Although a great volume of experiments have been conducted to determine the effects of diesel–DMM blends in the CO and smoke emissions, few studies have been focused on the combustion characteristics of pure DMM fuel at high temperatures¹² and even less at high pressures.

Daly et al.¹³ investigated the oxidation of DMM in a jet-stirred reactor at a pressure of 5.07 bar, high temperatures of 800–1200 K and equivalence ratios of 0.444 ($\lambda = 2.25$), 0.889 ($\lambda = 1.13$) and 1.778 ($\lambda = 0.56$), and proposed a submechanism of 50 reactions relevant to describe the combustion of DMM, including a significant number of estimated rate constants. Recently, Dias et al.¹⁴ have studied lean and rich premixed DMM flames to build a submechanism taking into account the formation and the consumption of oxygenated species involved in DMM oxidation. They were able to build a new mechanism containing 480 elementary reactions and involving 90 chemical species, by using kinetic data from the literature about DMM, mainly drawn from Daly et al.,¹³ in order to simulate the DMM flames. Whatever the availability of oxygen in the flow, they established two main DMM conversion routes, with the first one being the fastest:



In this context, a study on DMM oxidation carried out under well controlled tubular flow reactor conditions at atmospheric pressure, from pyrolysis to high oxidizing conditions, from both

Received: March 3, 2015

Revised: April 22, 2015

Published: April 22, 2015

experimental and modeling points of view, was previously developed by our research group.¹⁵ The results obtained indicate that the initial oxygen concentration slightly influences the consumption of DMM. In general, a good agreement between experimental and modeling data was obtained and, accordingly, the final mechanism compiled in that work has been taken as the initial mechanism in the present work.

Therefore, the purpose of the present work is to carry out an experimental study of DMM conversion at high pressure covering a large range of temperature, pressure and different stoichiometries, together with the validation of a kinetic mechanism under high-pressure conditions, which would be of interest for diesel applications. Specifically, experiments have been performed under well-controlled flow reactor conditions, in the 373–1073 K temperature range and for different high pressures (20, 40 and 60 bar). Under these conditions, the oxygen concentration was varied from 1960 to 56 000 ppm, resulting in different air excess ratios (λ) ranging from 0.7 to 20. Additionally, a modeling study to describe the oxidation of DMM was performed using the gas-phase detailed chemical kinetic mechanism of our previous work,¹⁵ which has been updated in the present work to account for working at high pressures.

EXPERIMENTAL SECTION

The experimental installation used in the present work is described in detail elsewhere,¹⁶ and only a brief description is given here. It consists basically of a gas feeding system, a reaction system and a gas analysis system.

Gases are supplied from gas cylinders through mass flow controllers. A concentration of approximately 700 ppm of DMM is introduced in all the experiments. The amount of O₂ used has been varied between 1960 and 56 000 ppm, and is related to the air excess ratio (λ), defined as the inlet oxygen concentration divided by the stoichiometric oxygen. Therefore, values of λ lower than 1 refer to fuel rich conditions, and λ values larger than 1, refer to fuel lean conditions. Nitrogen is used to balance, resulting in a constant flow rate of 1000 (STP) mL/min.

The DMM oxidation takes place in a quartz flow reactor (inner diameter of 6 mm and 1500 mm in length) that is enclosed in a stainless steel tube that acts as a pressure shell. Nitrogen is delivered to the shell side of the reactor by a pressure control system, to obtain a pressure similar to that inside the reactor avoiding this way the stress in the reactor.

The reactor tube is placed horizontally in a three-zone electrically heated furnace, ensuring a uniform temperature profile within ± 10 K throughout the isothermal reaction zone (56 cm). The gas residence time, t_r , in the isothermal zone, is a function of the reaction temperature and pressure, t_r (s) = 261 · P (bar)/T (K).

Downstream the reactor, the pressure is reduced to atmospheric level. Before analysis, the product gases pass through a condenser and a filter to ensure gas cleaning. The outlet gas composition is measured using a gas micro chromatograph (Agilent 3000), which is able to detect and measure DMM and the main products of its oxidation: methyl formate (CH₃OCHO), formaldehyde (CH₂O), CO, CO₂ and CH₄. No other products were detected in a noticeable amount. The uncertainty of measurements is estimated as $\pm 5\%$. To evaluate the goodness of the experiments, the atomic carbon balance was checked in all the experiments and resulted to close always near 100%.

The experiments were carried out at different pressures (20, 40 and 60 bar) and in the 373–1073 K temperature range. Table 1 lists the conditions of the experiments.

MODELING

The experimental results have been analyzed in terms of a detailed gas-phase chemical kinetic mechanism for describing

Table 1. Matrix of Experimental Conditions^a

exp.	DMM (ppm)	O ₂ (ppm)	λ	P (bar)
set 1	720	1960	0.7	20
set 2	770	1960	0.7	40
set 3	770	1960	0.7	60
set 4	757	2800	1	20
set 5	720	2800	1	40
set 6	720	2800	1	60
set 7	688	56000	20	20
set 8	778	56000	20	40
set 9	706	56000	20	60

^aThe experiments are conducted at constant flow rate of 1000 mL (STP)/min, in the temperature interval of 373–1073 K. The balance is closed with N₂. The residence time depends on the reaction temperature and pressure: t_r (s) = 261 · P (bar)/T (K).

the oxidation of DMM. The model taken as starting point was the kinetic mechanism compiled in the previously appointed work about the DMM oxidation at atmospheric pressure by our research group.¹⁵ This one was built by adding different reaction subsets found in the literature to the model developed by Glarborg et al.¹⁷ updated and extended later.^{18,19} The additional reaction subsets included for the different expected or involved compounds of relevance for the present experiments were dimethyl ether (DME),²⁰ ethanol,²¹ acetylene²² and methyl formate (MF).²³ The last subset was revised by our group¹⁶ to account for high-pressure conditions in the methyl formate oxidation, which are similar to those of the present work. For DMM, the Dias et al. reaction subset¹⁴ developed for atmospheric pressure was also included. Thermodynamic data for the involved species are taken from the same sources as the cited mechanisms.

The model used in the previous work¹⁵ has been modified in the present work to account also for the high-pressure conditions studied in the DMM oxidation. The changes made to the mechanism are listed in Table 2 and will be described below. The final mechanism involves 726 reactions and 142 species.

Thermal decomposition of DMM is an important initiation step, and can occur through DMM breaking, reactions 1 and 2, or by losing a primary or a secondary hydrogen atom, reactions 3 and 4, respectively. The constants for these reactions were kept, without any modification, from the work of Dias et al.,¹⁴ originally proposed by Daly et al.¹³

For reaction 1, the value of $2.62 \times 10^{16} \exp(-41\,369/T) \text{ cm}^3 \text{ mol}^{-1} \text{ s}^{-1}$ for the rate constant was taken from the estimation made by Dagaut et al.²⁴ for DME, from a fit of the available NIST²⁵ data. For reaction 2, the value for the rate constant, $2.51 \times 10^{15} \exp(-38\,651/T) \text{ cm}^3 \text{ mol}^{-1} \text{ s}^{-1}$, estimated by Foucaut and Martin by analogy with diethyl ether²⁶ was taken, and for reaction 3, the kinetic parameters ($4.35 \times 10^{16} \exp(-50\,327/T) \text{ cm}^3 \text{ mol}^{-1} \text{ s}^{-1}$) were taken from the estimation for the similar reaction involving ethane.²⁷ Finally, for the loss of a secondary hydrogen atom from DMM, reaction 4, Dean²⁷ estimated the rate constant by analogy with the rate constant for the loss of a secondary atom of hydrogen from propane, with a value of $6.31 \times 10^{15} \exp(-47\,660/T) \text{ cm}^3 \text{ mol}^{-1} \text{ s}^{-1}$.

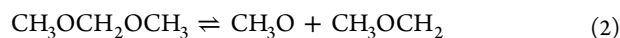
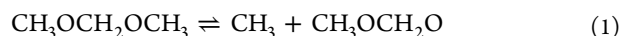


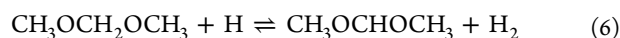
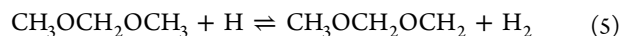
Table 2. Reactions Modified or Included in the Final Mechanism in Relation to the Mechanism Used in Reference 15 and Corresponding Kinetic Parameters^a

number	reaction	A	n	E _a	source
9	CH ₃ OCH ₂ OCH ₃ + OH ⇌ CH ₃ OCH ₂ OCH ₂ + H ₂ O	6.32 × 10 ⁶	2.00	-652	[refs 22, 32 and 34, see text]
10	CH ₃ OCH ₂ OCH ₃ + OH ⇌ CH ₃ OCHOCH ₃ + H ₂ O	6.32 × 10 ⁶	2.00	-652	[refs 22, 32 and 34, see text]
11	CH ₃ OCH ₂ OCH ₃ + HO ₂ ⇌ CH ₃ OCH ₂ OCH ₂ + H ₂ O ₂	1.00 × 10 ¹³	0.00	17686	35
12	CH ₃ OCH ₂ OCH ₃ + HO ₂ ⇌ CH ₃ OCHOCH ₃ + H ₂ O ₂	2.00 × 10 ¹²	0.00	15296	13
15	CH ₃ OCH ₂ OCH ₂ + O ₂ ⇌ CH ₂ O + CH ₃ OCHO + OH	2.50 × 10 ¹¹	0.00	-1700	22
16	CH ₃ OCHOCH ₃ + O ₂ ⇌ CH ₂ O + CH ₃ OCHO + OH	2.50 × 10 ¹¹	0.00	-1700	22
17	CH ₃ OCH ₂ OCH ₂ + HO ₂ ⇌ CH ₂ O + CH ₃ OCH ₂ O + OH	3.00 × 10 ¹¹	0.00	0	13
18	CH ₃ OCHOCH ₃ + HO ₂ ⇌ CH ₃ OCHO + CH ₃ O + OH	1.00 × 10 ¹²	0.00	0	13
19	CH ₃ OCH ₂ OCH ₂ + O ₂ ⇌ CH ₃ OCH ₂ O ₂ + CH ₂ O	6.40 × 10 ¹²	0.00	91	see text
20	CH ₃ OCH ₂ OCH ₂ + HO ₂ ⇌ CH ₃ OCH ₂ O ₂ + CH ₂ OH	1.00 × 10 ¹²	0.00	0	see text

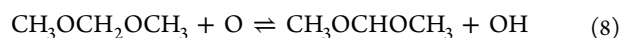
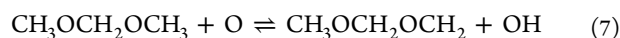
^aA is in cm³ mol⁻¹ s⁻¹; E_a is in cal/mol.



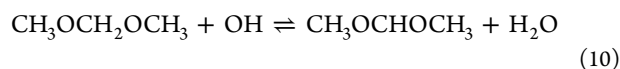
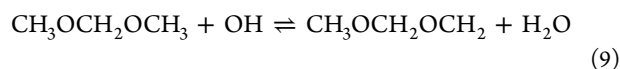
An important pathway for DMM consumption includes hydrogen abstraction reactions by the O/H radical pool. For the reactions with H (reactions 5 and 6), the rate expressions were taken from the DMM subset proposed by Dias et al.,¹⁴ which were, a priori, taken from Daly et al.¹³ The rate constant of reaction 5 was taken as that for the reaction between DME and a hydrogen atom,²⁸ that is $9.70 \times 10^{13} \exp(-3125/T) \text{ cm}^3 \text{ mol}^{-1} \text{ s}^{-1}$. For reaction 6, the $7.40 \times 10^{12} \exp(-1631/T) \text{ cm}^3 \text{ mol}^{-1} \text{ s}^{-1}$ rate constant was based on the abstraction of a secondary hydrogen atom from diethyl ether.²⁹ Although, Dias et al.¹⁴ included an A-factor for this reaction divided by 2 in their final mechanism, we adopted the value originally proposed by Daly et al.,¹³ which is $7.40 \times 10^{12} \text{ cm}^3 \text{ mol}^{-1} \text{ s}^{-1}$.



In the case of the reactions between DMM and O radicals (reactions 7 and 8), their rate constants were taken from the DMM subset proposed by Dias et al.¹⁴ without any modification, previously adopted from,³⁰ by analogy with CH₃OCH₂ for reaction 7, and by analogy with diethyl ether, for reaction 8.



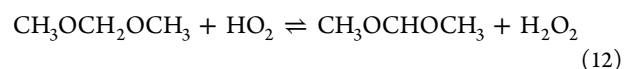
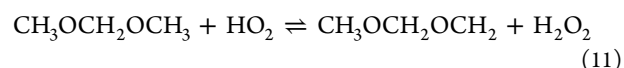
Reaction with hydroxyl radicals (OH) is an important step in the oxidation of organic compounds in combustion systems.³¹ Although it will be discussed later through the analysis of the different reaction pathways, the main consumption of DMM occurs through H abstraction reactions by OH to form CH₃OCH₂OCH₂ and CH₃OCHOCH₃ radicals (reactions 9 and 10). The kinetic parameters of these reactions have been modified from the previous work.¹⁵



In the Dias et al. DMM reaction subset,¹⁴ the rate constant of these reactions is estimated by analogy with the reaction CH₃OCH₃ + OH ⇌ CH₃OCH₂ + H₂O from DeMore and Bayes,³² with a proposed value of $9.10 \times 10^{12} \exp(-496/T)$

cm³ mol⁻¹ s⁻¹, determined experimentally in the 263–361 K temperature range. Arif et al.³¹ determined a rate constant of $6.32 \times 10^6 T^2 \exp(327/T) \text{ cm}^3 \text{ mol}^{-1} \text{ s}^{-1}$, in the 295–650 K temperature range, which is adopted in this study, also used in the work of Alzueta et al.,²⁰ and that is in agreement with the high-temperature (923–1423 K) determination of Cook et al.³³ With this value, the latest authors achieved a good fit for both the low and the high temperature measurements.

The prevalence of HO₂ radicals under high pressure, and preferably lean conditions, should make them to play an important role under the conditions of the present work. Reactions involving DMM and HO₂ radicals (reactions 11 and 12) were not included in the initial reaction subset of Dias et al.,¹⁴ and we have included them in the present work.



The rate constants for reactions 11 and 12 have not been measured to our knowledge and, therefore, there is some degree of uncertainty in their absolute values. For reaction 11, the rate parameters have been taken by analogy of the dimethyl ether and HO₂ reaction, following the same procedure described by Daly et al.,¹³ and likewise taking the value, $1.00 \times 10^{13} \exp(-8900/T) \text{ cm}^3 \text{ mol}^{-1} \text{ s}^{-1}$, from the work of Curran et al.³⁴ The rate constant for abstraction of a secondary hydrogen atom (reaction 12) was estimated by Daly et al.¹³ from the value for reaction 11, with the A factor divided by a factor of 6. These authors stated that DMM has six primary hydrogen atoms and only two secondary ones, so the probability of attack will therefore be lower for the attack on the CH₂ groups than on the CH₃ groups. Also, the proximity of two oxygen atoms to the central carbon atom of the molecule will make the hydrogen atoms attached to it more labile than those belonging to the methyl groups. As a result, the activation energy for reaction 12 should be lower than for reaction 11. Thus, a rate constant value of $2.00 \times 10^{12} \exp(-7698/T) \text{ cm}^3 \text{ mol}^{-1} \text{ s}^{-1}$ was proposed for reaction 12,¹³ which is adopted in the present mechanism.

The subset proposed by Dias et al.¹⁴ includes reactions involving DMM with molecular oxygen (reaction 13 and 14) and their corresponding rate constants, adopted here with no modification from the work of Daly et al.,¹³ were both estimated by analogy with the reaction of DME with oxygen. Therefore, the rate parameters for reaction 13 are the same as those considered by Dagaut et al.²⁴ (although for reaction 13,

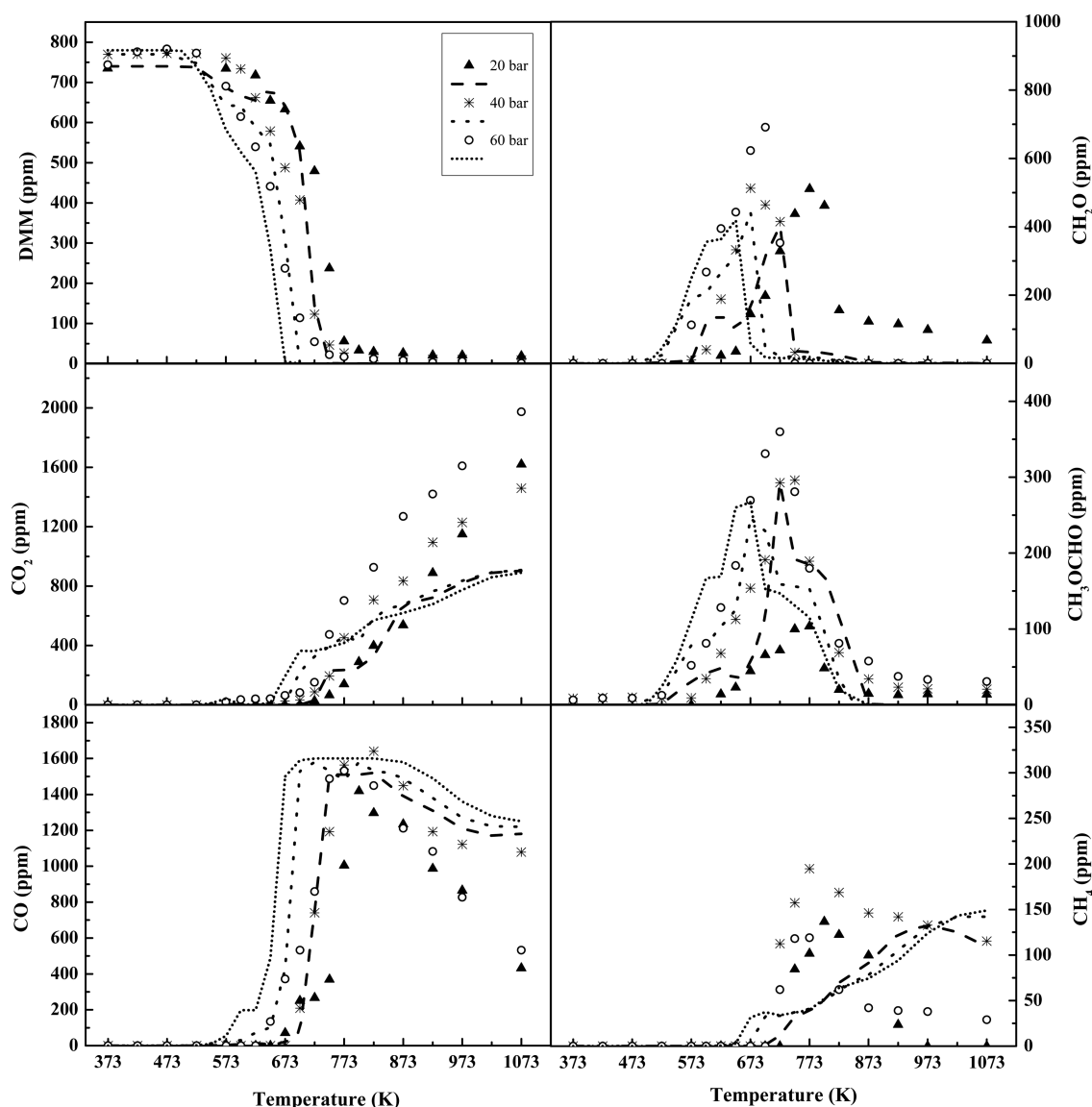
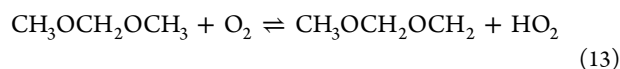
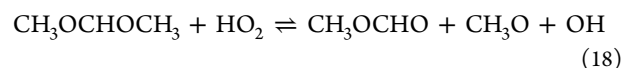
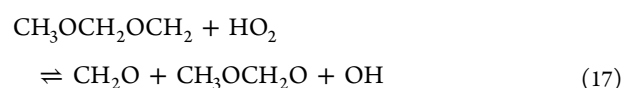
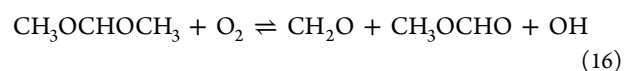
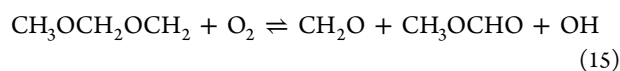


Figure 1. Influence of pressure on the DMM, CO₂, CO, CH₂O, CH₃OCHO and CH₄ concentration profiles as a function of temperature for a given air excess ratio ($\lambda = 0.7$). Sets 1–3 in Table 1.

the values used by Dias et al.¹⁴ are not the corresponding ones to the source specified, as also was indicated in the case of reaction 6), and the parameters for reaction 14 were estimated by Daly et al.¹³ as previously done in the case of reactions involving HO₂ radicals.



Although the reactions of CH₃OCH₂OCH₂ and CH₃OCHOCH₃ radicals with O₂ (reactions 15 and 16) and HO₂ (reactions 17 and 18) were omitted in previous DMM mechanisms,^{14,15,34} they can play an important role in the oxidation of DMM, particularly under high pressure and high oxygen concentration conditions and, therefore, these reactions have been included in our final mechanism.



For reactions 15 and 16, the rate constants have been estimated, establishing an analogy with the reaction of methoxy-methyl radical (CH₃OCH₂·, generated in the dimethyl ether thermal decomposition) and oxygen molecular, as previously done by Daly et al.¹³ In that case, they chose the kinetic parameters given by Dagaut et al.,²⁴ namely, $1.70 \times 10^{10} \exp(337/T) \text{ cm}^3 \text{ mol}^{-1} \text{ s}^{-1}$, which were estimated based on C₂H₅ + O₂ kinetics. However, here, we have chosen a value of the CH₃OCH₂ + O₂ rate constant of $2.50 \times 10^{11} \exp(850/T) \text{ cm}^3 \text{ mol}^{-1} \text{ s}^{-1}$, obtained by Alzueta et al.²⁰ from averaging three room-temperature determinations,^{35–37} and adopting the temperature dependence reported in Hoyermann and

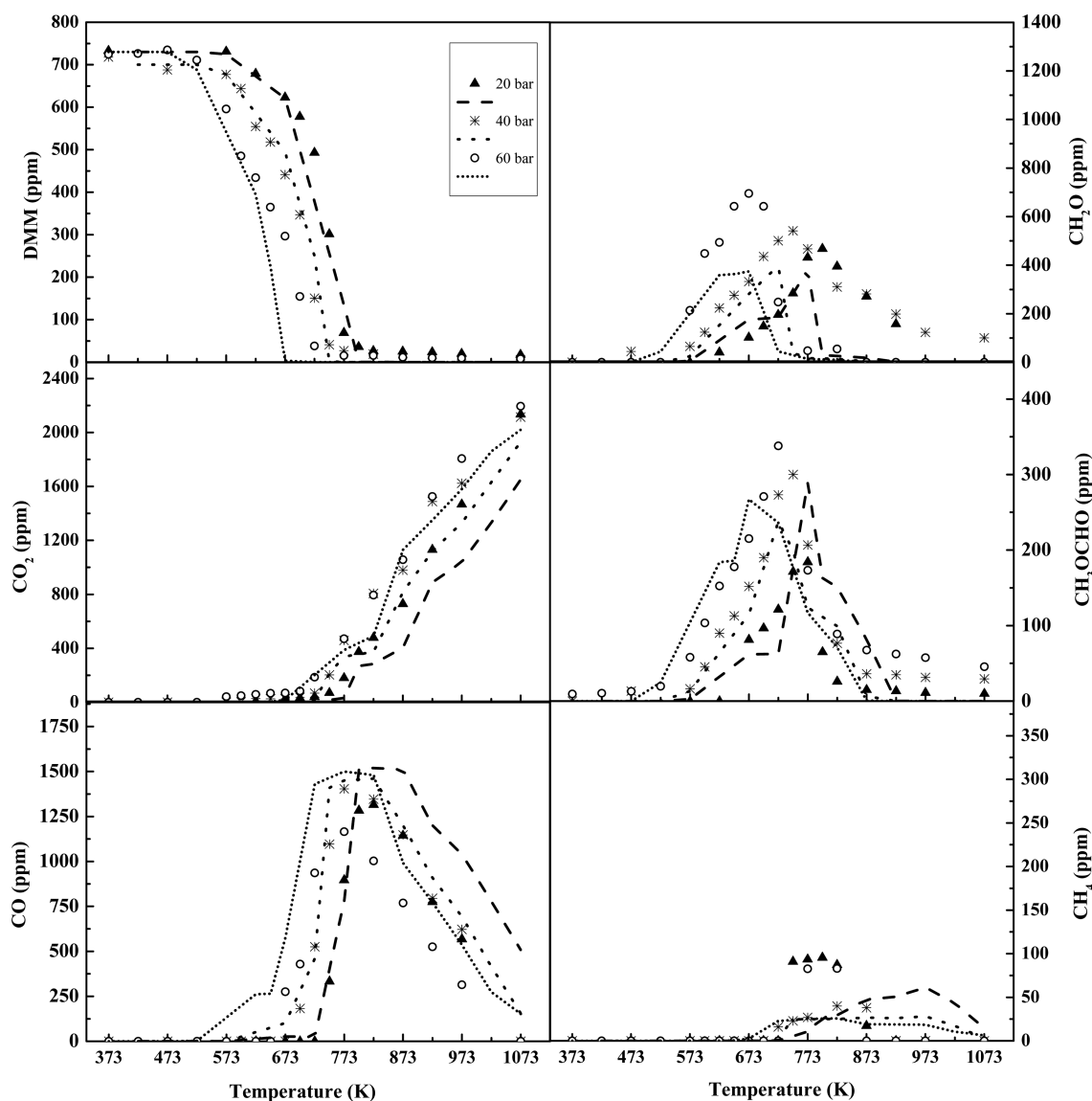


Figure 2. Influence of pressure on the DMM, CO_2 , CO, CH_2O , CH_3OCHO and CH_4 concentration profiles as a function of temperature for a given air excess ratio ($\lambda = 1$). Sets 4–6 in Table 1.

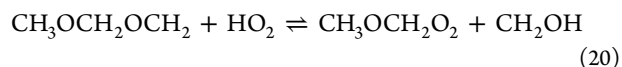
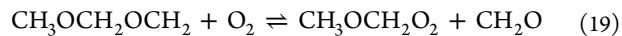
Nacke,³⁷ which is significantly faster than that proposed in the mechanism of Dagaut et al.²⁴

In the same way, the analogy used before in the case of reactions with molecular oxygen ($\text{CH}_3\text{OCH}_2 + \text{O}_2$) has been applied to obtain the rate constants of reactions 17 and 18, i.e., $\text{CH}_3\text{OCH}_2 + \text{HO}_2$. Not much information has been found related to these reactions, and the value proposed by Daly et al.,¹³ based on estimations made by Dagaut et al.²⁴ has been chosen. This value is, for reaction 17, $3.00 \times 10^{11} \text{ cm}^3 \text{ mol}^{-1} \text{ s}^{-1}$ and, for reaction 18, they increased this value to $1.00 \times 10^{12} \text{ cm}^3 \text{ mol}^{-1} \text{ s}^{-1}$.

Curran et al.³⁴ stated that the pathway involving peroxy intermediates may be important at low temperatures (below approximately 900 K) and pressures higher than 10 bar, because the bimolecular addition of methoxy-methyl radical to O_2 has a lower activation energy barrier than the β -scission to yield CH_2O and CH_3 , the two main pathways that methoxy-methyl radicals can undergo. At atmospheric pressure (e.g., Alzueta et al.²⁰), the formation of methoxy methyl-peroxy

intermediate is not predicted to be significant, except for a minor contribution for very lean stoichiometries.

Under the conditions studied in this work, high pressures (20, 40 and 60 bar) and fuel lean conditions ($\lambda = 20$), the reactions forming peroxy species (reactions 19 and 20) may have an important impact on the oxidation chemistry of DMM and, therefore, these reactions have been included in our final mechanism.



For reaction 19, the kinetic parameters have been estimated by analogy with the reaction of methoxy-methyl radical with molecular oxygen. The $6.40 \times 10^{12} \exp(-45.80/T) \text{ cm}^3 \text{ mol}^{-1} \text{ s}^{-1}$ value for $\text{CH}_3\text{OCH}_2 + \text{O}_2$ was considered in an earlier mechanism by our group.²⁰ For reaction 20, no values of kinetic parameters were found, and we have considered initially a reaction rate of $1.0 \times 10^{12} \text{ cm}^3 \text{ mol}^{-1} \text{ s}^{-1}$. The results of

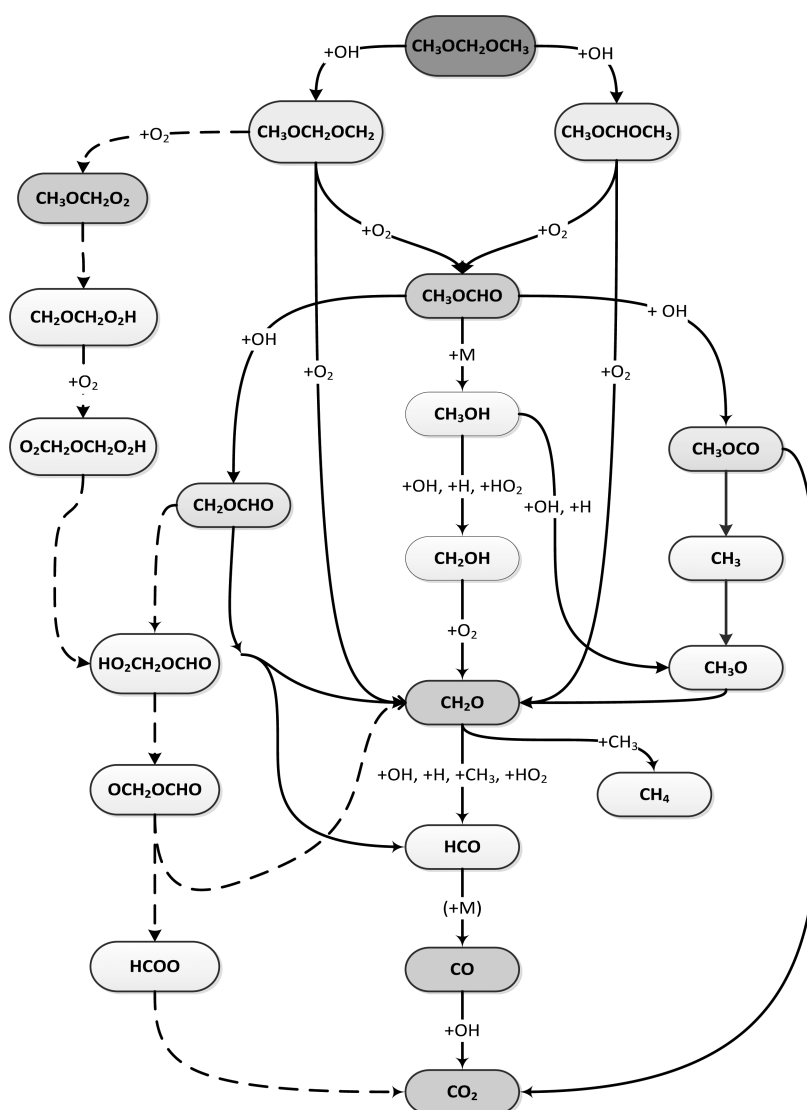


Figure 3. Reaction path diagram for DMM oxidation according to the current kinetic model in the 373–1073 K temperature range. Solid lines represent the main reaction pathways for all the conditions considered in the present work. Dashed lines refer to reaction paths that become more relevant under oxidizing conditions ($\lambda = 20$) and increasing pressure.

sensitivity analysis, shown later, indicate no significant impact of this estimation.

Model calculations have been performed using both SENKIN³⁸ from the CHEMKIN II software package³⁹ and CHEMKIN-PRO,⁴⁰ considering pressure constant in the reaction zone and the corresponding temperature profile. An example of temperature profiles inside the reactor can be found in ref 16. The full mechanism listing and thermochemistry used can be found as Supporting Information.

RESULTS AND DISCUSSION

In this work, a study of the oxidation of DMM at different pressures (20, 40 and 60 bar), and in the 373–1073 K temperature range, has been carried out. In addition to temperature and pressure, the influence of stoichiometry ($\lambda = 0.7, 1$ and 20) on the oxidation process has also been analyzed. As mentioned, the experimental results have been interpreted in terms of the detailed kinetic mechanism previously described.

Figures 1 and 2 show the influence of the temperature and pressure for specific air excess ratios, $\lambda = 0.7$ and $\lambda = 1$, respectively, on the concentration of DMM and the formation of the main products of its oxidation at high pressures: CH_2O , CO_2 , CO , CH_3OCHO and CH_4 . No other products have been detected in an appreciable amount. At atmospheric pressure, other products such as C_2H_4 , C_2H_6 and C_2H_2 , were detected through micro GC analysis in amounts lower than 100 ppm, and especially for reducing ($\lambda = 0.7$), very reducing ($\lambda = 0.4$) and pyrolysis ($\lambda = 0$) conditions.¹⁵ Methanol is highly formed at atmospheric pressure,¹⁵ while at higher pressures (20–60 bar) formaldehyde is predominant, although the distinction between methanol and formaldehyde with micro-GC techniques sometimes is quite tricky.

Both Figures 1 and 2 compare experimental (symbols) and model calculation (lines) results. Working at 20, 40 or 60 bar does not have a big effect neither on the oxidation of DMM nor on the formation of the main products. The suggested model predicts the general trend of the different concentration profiles, although there are some discrepancies between experimental and simulation results. These discrepancies are

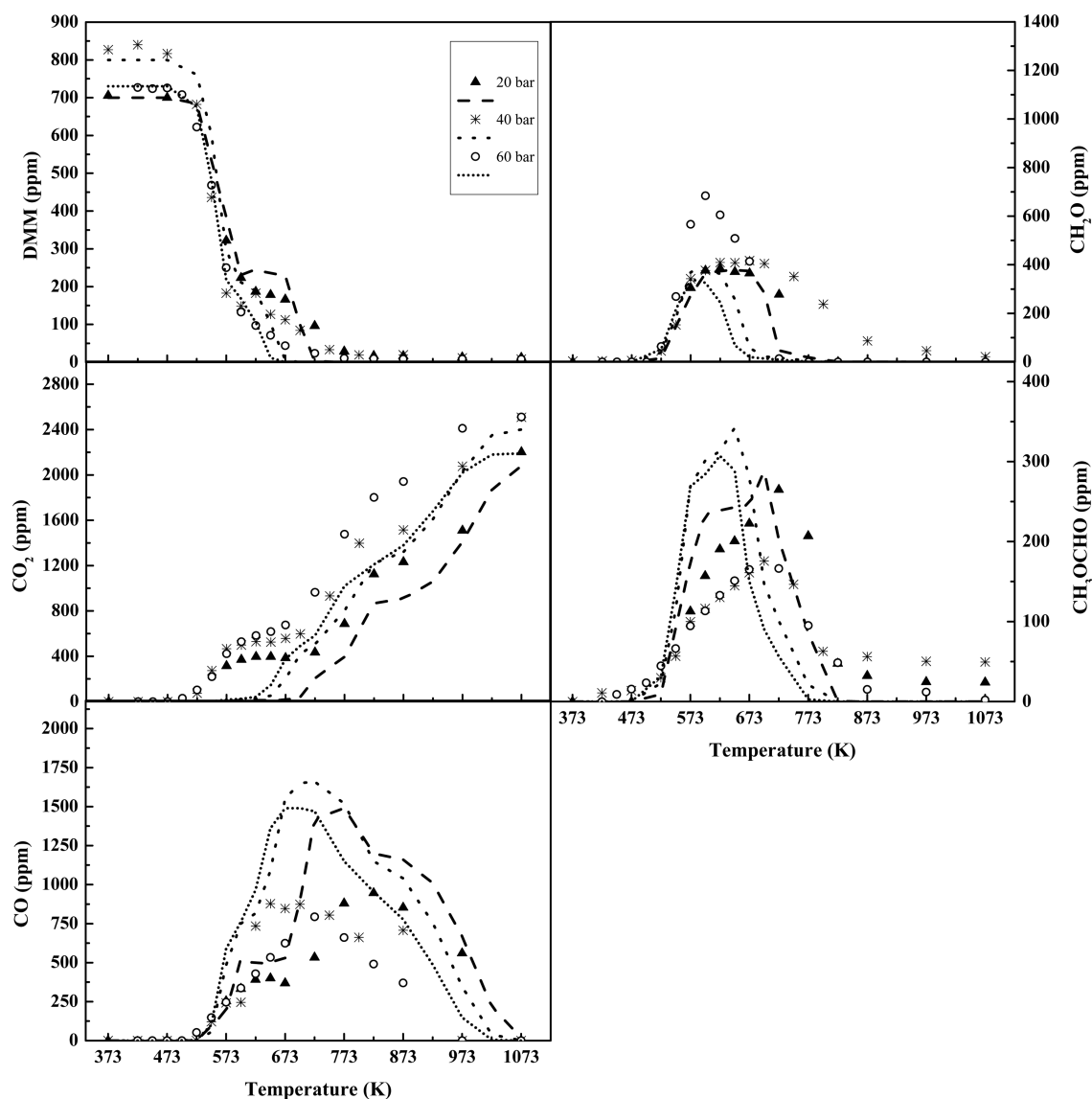


Figure 4. Influence of pressure on the DMM, CO_2 , CO, CH_2O and CH_3OCHO concentration profiles as a function of temperature for a given air excess ratio ($\lambda = 20$). Sets 7–9 in Table 1.

especially remarkable for $\lambda = 0.7$, where the CO_2 concentration values at high temperatures are underestimated, whereas the CO values are overestimated. It is difficult to isolate the origin of those discrepancies, and may be attributed to the uncertainty in the conversion of intermediates. This fact is not observed for the other values of λ considered. The oxygen concentration in the reactant mixture slightly influences the conversion of DMM, similar to what has been observed in the oxidation behavior of other oxygenated compounds such as DME²⁰ or MF.¹⁶

Figure 3 shows a reaction path diagram for DMM oxidation through a reaction rate analysis with the mechanism used in the present work. For the conditions analyzed in the present work, the main consumption of DMM is through H abstraction reactions by the hydroxyl radical (OH) to form $\text{CH}_3\text{OCH}_2\text{OCH}_2$ and $\text{CH}_3\text{OCHOCH}_3$ radicals (reactions 9 and 10), which is in agreement with other previous works.¹³ Both reactions have a relative importance of 38%. This value increases up to near 50% under oxidizing conditions.

Both radicals react with molecular oxygen to form methyl formate (CH_3OCHO) and formaldehyde as main products (reactions 15 and 16).

Formaldehyde continues the $\text{CH}_2\text{O} \rightarrow \text{HCO} \rightarrow \text{CO} \rightarrow \text{CO}_2$ reaction sequence with CO_2 as final product. As shown in Figure 3, MF seems to be an important intermediate in the total oxidation of DMM. In previous MF oxidation works, at atmospheric pressure²³ and higher pressures,¹⁶ the MF oxidation was seen to be initiated by its decomposition reaction to methanol (reaction 21). In this work, as an intermediate, MF is directly consumed by hydrogen abstraction reactions in order to produce CH_2OCHO and CH_3OCO radicals (reactions 22 and 23), with a relative importance, for example at 20 bar and oxidizing conditions ($\lambda = 20$), of 62% for reaction 22 and 20% for reaction 23.

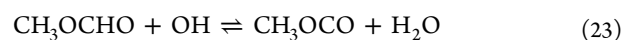
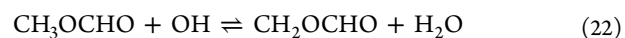
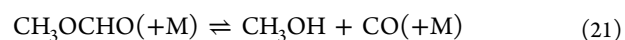


Table 3. Linear Sensitivity Coefficients for CO for Sets 1–9 in Table 1^a

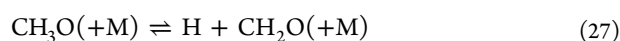
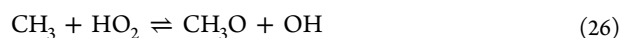
reaction	set 1 (623 K)	set 2 (623 K)	set 3 (573 K)	set 4 (673 K)	set 5 (623 K)	set 6 (523 K)	set 7 (548 K)	set 8 (548 K)	set 9 (548 K)
9 CH ₃ OCH ₂ OCH ₃ +OH=CH ₃ OCH ₂ OCH ₂ +H ₂ O	1.019	0.958	0.989	1.303	0.974	1.160	1.397	1.350	1.303
10 CH ₃ OCH ₂ OCH ₃ +OH=CH ₃ OCHOCH ₃ +H ₂ O	-0.219	-0.230	-0.352	-0.479	-0.251	-0.392	-0.487	-0.485	-0.479
11 CH ₃ OCH ₂ OCH ₃ +HO ₂ =CH ₃ OCH ₂ OCH ₂ +H ₂ O ₂	0.112	0.126	0.025	0.025	0.097	0.046	0.022	0.025	0.025
12 CH ₃ OCH ₂ OCH ₃ +HO ₂ =CH ₃ OCHOCH ₃ +H ₂ O ₂	0.126	0.124	0.022	0.033	0.087	0.086	0.035	0.036	0.033
14 CH ₃ OCH ₂ OCH ₃ +O ₂ =CH ₃ OCHOCH ₃ +HO ₂			0.001	0.001		0.017	0.007	0.003	0.001
16 CH ₃ OCH ₂ OCH ₂ +O ₂ =CH ₂ O+CH ₃ OCHO+OH	-0.184	-0.177	-0.216	-0.302	-0.182	-0.280	-0.322	-0.312	-0.302
19 CH ₃ OCH ₂ OCH ₂ +O ₂ (+M)=CH ₃ OCH ₂ O ₂ +CH ₂ O(+M)	0.179	0.174	0.214	0.301	0.179	0.279	0.317	0.309	0.301
CH ₃ OCH ₂ +O ₂ =CH ₂ O+CH ₂ O+OH	-0.021	-0.017	-0.008	-0.001	-0.017	-0.002	-0.001	-0.001	-0.001
CH ₂ OCH ₂ O ₂ H=CH ₂ O+CH ₂ O+OH	-1.479	-1.223	-0.705	-0.024	-1.164	-0.167	-0.075	-0.037	-0.024
CH ₃ OCH ₂ O ₂ =CH ₂ OCH ₂ O ₂ H	0.001	0.001	0.001	0.006	0.001	0.016	0.017	0.009	0.006
O ₂ CH ₂ OCH ₂ O ₂ H=CH ₂ OCH ₂ O ₂ H+O ₂	1.503	1.242	0.725	0.028	1.183	0.296	0.107	0.045	0.028
HO ₂ CH ₂ OCHO=OCH ₂ OCHO+OH	-0.028	-0.008	0.559	1.468	-0.006	1.659	1.795	1.614	1.468
CH ₃ OCHO+OH=CH ₂ OCHO+H ₂ O	0.071	0.059	0.023	-0.031	0.061	-0.054	-0.057	-0.044	-0.031
CH ₃ OCHO+OH=CH ₃ OCO+H ₂ O	0.002	0.004	-0.011	-0.021	0.004	-0.017	-0.023	-0.022	-0.021
CH ₂ OCHO+HO ₂ =HO ₂ CH ₂ OCHO	0.011	0.017	0.007	-0.010	0.017	-0.002	-0.007	-0.009	-0.010
H+O ₂ +N ₂ =HO ₂ +N ₂	-0.014	-0.010	-0.001	0.000	-0.005	0.000	0.000	0.000	0.000
OH+HO ₂ =H ₂ O+O ₂	-0.006	-0.005	-0.001	-0.002	-0.005	-0.002	-0.006	-0.003	-0.002
HO ₂ +HO ₂ =H ₂ O ₂ +O ₂	-0.160	-0.234	-0.056	-0.039	-0.192	-0.063	-0.026	-0.036	-0.039
H ₂ O ₂ +M=OH+OH+M	0.091	0.310	0.008	0.001	0.291	0.000	0.000	0.001	0.001
H ₂ O ₂ +OH=H ₂ O+HO ₂	-0.012	-0.030	-0.027	-0.025	-0.037	-0.002	-0.008	-0.017	-0.025
CH ₂ O+OH=HCO+H ₂ O	-0.851	-0.749	-0.608	-0.732	-0.735	-0.692	-0.811	-0.771	-0.732
CH ₂ O+HO ₂ =HCO+H ₂ O ₂	0.094	0.231	0.063	0.037	0.209	0.013	0.013	0.027	0.037
HCO+M=H+CO+M	0.014	0.009	0.003	0.000	0.004	0.001	0.000	0.000	0.000
HCO+O ₂ =HO ₂ +CO	-0.016	-0.012	0.095	0.001	-0.007	0.255	0.006	0.003	0.001

^aThe sensitivity coefficients are given as $A_i \delta Y_j / Y_j \delta A_i$, where A_i is the pre-exponential constant for reaction i and Y_j is the mass fraction of j th species. Therefore, the sensitivity coefficients listed can be interpreted as the relative change in predicted concentration for the species j caused by increasing the rate constant for reaction i by a factor of 2.

Both radicals decompose thermally, CH₂OCHO to give formaldehyde and formyl radical and CH₃OCO to form methyl radical and CO₂, through reactions 24 and 25, respectively:



As reported in an earlier work by our group for methyl formate oxidation,¹⁶ under high-pressure conditions, high concentration of methyl and hydroperoxy radicals accumulate and thus, the interaction of those radicals can generate methoxy radicals through reaction 26, which further decomposes to formaldehyde (reaction 27).



Therefore, formaldehyde is detected instead of methanol (highly formed in both MF oxidation²³ and DMM oxidation¹⁵ at atmospheric pressure) when working under high pressure.

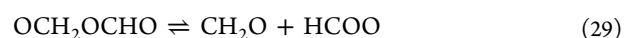
The formaldehyde obtained by this way continues the above-mentioned CH₂O → HCO → CO → CO₂ reaction sequence. A fraction of this formaldehyde reacts with methyl radicals generating methane (reaction 28), which is detected as a final product.



Figure 4 shows the influence of pressure on the DMM, CO₂, CO, CH₂O and MF concentration profiles as a function of temperature and for very oxidizing conditions, $\lambda = 20$. As previously seen, working under high pressure conditions no appreciable influence of pressure on the conversion regime of DMM and products formation is found. Thus, similar results

have been obtained for 20, 40 and 60 bar, and the slight differences that can be observed include a higher amount of methyl formate for 20 bar, whereas for the other two values of pressure, more CO₂ is produced. For the pressures of 40 and 60 bar, in the 598–673 K temperature range, a constant concentration zone in the DMM profile and in the main products, CO₂, CO, CH₃OCHO and CH₂O, can be observed. This zone appears to be associated with the oxygenated CH₃OCH₂O₂ species. In the mechanism taken as starting point and used in the previous atmosphere work on DMM conversion,¹⁵ the formation reactions of this species were not included, and thus the predictions of the mechanism were significantly worse. Therefore, the formation reactions of this species from the interaction of CH₃OCH₂OCH₂ and O₂/HO₂ (active species under oxidizing and high pressure conditions), reactions 19 and 20, were added to the mechanism.

With these two reactions, the current mechanism has been able to represent the plateau observed in DMM, CO₂ and CO concentration, in the 598–673 K temperature range. The kinetic parameters of these reactions have been estimated due to the lack of literature determinations above-mentioned, as has been described in the Modeling section. Reaction pathway analysis allows us to identify how the species are formed and proceed through the following reaction sequence: CH₃OCH₂O₂ → CH₂OCH₂O₂H → O₂CH₂OCH₂O₂H → HO₂CH₂OCHO → OCH₂OCHO. The last one decomposes to give CH₂O and HCOO through reaction 29:



Formaldehyde continues the CH₂O → HCO → CO → CO₂ well-known reaction sequence, whereas the hydrocarboxyl radical decomposes generating CO₂ as a final product:



A first-order sensitivity analysis for CO has been performed for all the sets in Table 1. The results obtained, shown in Table 3, indicate that the conversion of DMM is highly sensitive to the DMM reactions with OH radicals (reactions 9 and 10), which have been previously discussed. Reactions involving MF (CH_3OCHO) and its radicals also present a high sensitivity, as an important intermediate in the DMM oxidation under the conditions studied in the present work.

Figure 5 shows the experimental results obtained for stoichiometric conditions by our research group for the

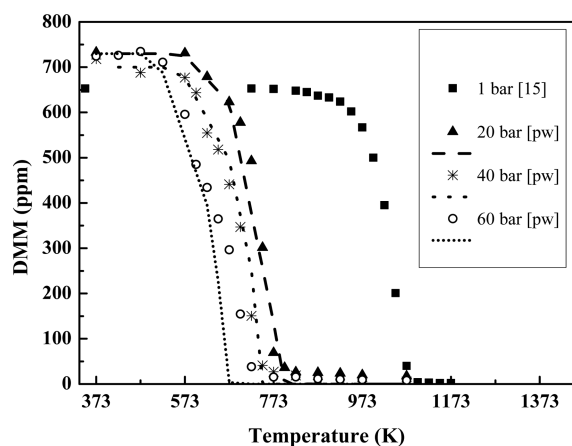


Figure 5. Results for stoichiometric conditions, at 1 bar (experimental) from Marrodán et al.¹⁵ and at high pressure (experimental and modeling) from the present work [pw], sets 4–6 in Table 1.

DMM oxidation at atmospheric pressure¹⁵ and the high-pressure results, experimental and modeling, discussed in the present work. Although it can be observed a huge shift to lower temperatures when moving from atmospheric pressure to higher ones, the results can not be directly compared because both gas residence times are significantly different. The gas residence time for the high pressure installation (t_r (s) = $261 \cdot P$ (bar)/ T (K)) is longer than at atmospheric pressure (t_r (s) = $195/T$ (K)) by a factor of 27–80 and, therefore, it is not possible to distinguish between the effect of pressure or residence time. To overcome this problem, model calculations have been carried out, modifying either the residence time or the pressure input value.

To do this, the kinetic mechanism used to simulate the high pressure experiments of this work has also been used to simulate the results obtained in the DMM oxidation at atmospheric pressure.¹⁵

Figure 6 shows, as an example, a comparison (only for DMM, CO and CO_2 concentrations) between the modeling results obtained with the initial mechanism¹⁵ (dashed lines) or with the mechanism modified in the present work (solid lines) and the experimental results (symbols) attained at atmospheric pressure in the 573–1373 K temperature range, for an initial concentration of 700 ppm of DMM and stoichiometric conditions.¹⁵ N_2 was used to achieve a total flow rate of 1000 mL (STP)/min, resulting in a gas residence time dependent on the reaction temperature of t_r (s) = $195/T$ (K).¹⁵ As can be seen in Figure 6, the modified mechanism generates almost the same results of the mechanism of reference¹⁵ and thus is able to

predict the main trends of the DMM consumption profile and CO and CO_2 formation.

With the validated kinetic mechanism of the present work, that describes well both low and high pressure experimental results, we have made different simulations to try to distinguish between the effect of residence time or pressure.

Figure 7 includes calculations for $\lambda = 1$ and 20 bar, with a residence time of t_r (s) = $5220/T$ (K) (solid lines) and for the same conditions ($\lambda = 1$ and 20 bar) but for a lower residence time of t_r (s) = $261/T$ (K) (short dashed lines), which would be the same as the residence time corresponding to 1 bar. As a reference, in Figure 7, also the experimental data of set 4 in Table 1 are included ($\lambda = 1, 20$ bar) and denoted by symbols. As can be seen, when only residence time is changed, increasing residence time shifts significantly the conversion of DMM toward lower temperatures.

Additionally, Figure 7 also includes calculations made with 1 bar of pressure and the residence time of the 20 bar experiments, i.e., t_r (s) = $5220/T$ (K) (long-dashed lines). Increasing pressure from 1 bar (long-dashed lines) to 20 bar (solid lines) but keeping a given residence time of t_r (s) = $5220/T$ (K) results in a similar shift of the DMM concentration profile as that reported for the change in time residence.

Thus, both the pressure and the residence time have an appreciable impact and are responsible for a significant shift in the oxidation regime of DMM.

CONCLUSIONS

The DMM conversion has been investigated in a quartz flow reactor in the 373–1073 K temperature range, for different air excess ratios ($\lambda = 0.7, 1$ and 20) and pressures (20–60 bar). The experimental results have been interpreted in terms of a detailed kinetic mechanism, compiled in a previous work about the DMM oxidation at atmospheric pressure by our research group,¹⁵ and modified in the present work to account also for the high pressure conditions studied. The modeling results obtained with the modified mechanism are similar to those attained without any modification; that is, the new mechanism is able to predict the main trends observed for the DMM oxidation at atmospheric pressure.

Experimental results and model calculations are, in general, in good agreement, and the main trends are well predicted for the theoretical model. Slight differences are noticed when working under stoichiometric or somewhat fuel-rich conditions, although the DMM conversion is a bit different for oxidizing conditions. Working at 20, 40 or 60 bar does not have a big effect on neither the oxidation of DMM nor the formation of the main products.

Independently of the conditions (stoichiometric, oxidizing or reducing), the main consumption of DMM occurs through H abstraction reactions by the hydroxyl radical (OH). Under oxidizing conditions, the conversion of DMM is fast until approximately the 598 to 673 K temperature zone, where the concentration of DMM presents a plateau and remains constant. This zone appears to be associated with the formation of the intermediate $\text{CH}_3\text{OCH}_2\text{O}_2$ oxygenated species. The formation reactions of this species from the interaction of $\text{CH}_3\text{OCH}_2\text{OCH}_2$ and O_2/HO_2 , active species under oxidizing and high pressure conditions, were not initially considered in the DMM reaction subset taken from the literature.¹⁴ Therefore, these reactions were added to the mechanism.

The analysis of the main reaction pathways involved in the DMM conversion, occurring under the conditions studied in

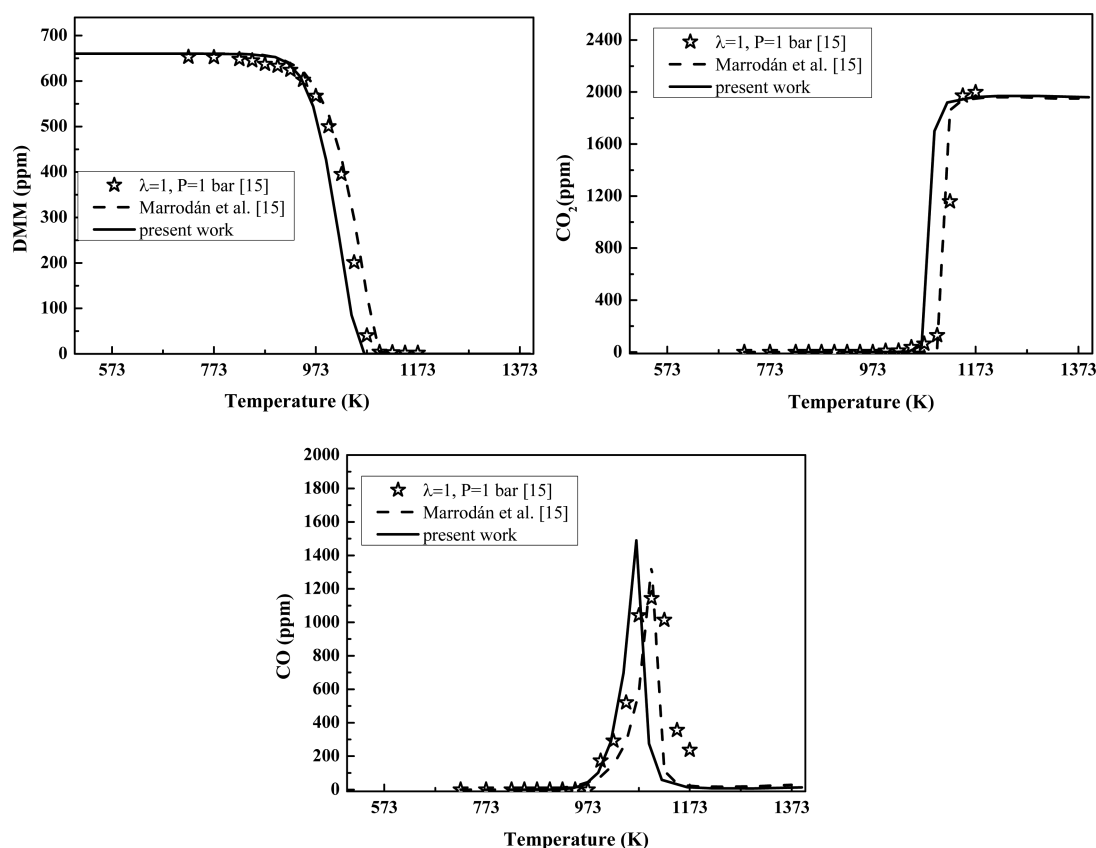


Figure 6. Comparison (for DMM, CO and CO₂ concentrations) between modeling calculations obtained with the initial mechanism¹⁵ and the mechanism used in the present work for the experimental results obtained at atmospheric pressure and $\lambda = 1$, for the conditions indicated in ref 15.

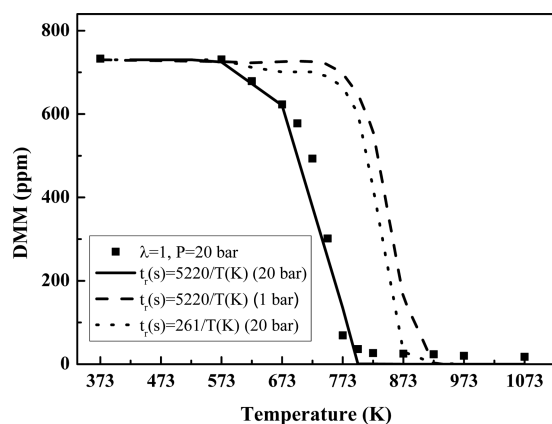


Figure 7. Evaluation through model calculations of the effect of gas residence time (comparison between solid lines, t_r (s) = 5220/ T (K), and short-dashed lines, t_r (s) = 261/ T (K)) and pressure (comparison between solid lines, t_r (s) = 5220/ T (K), and long-dashed lines, t_r (s) = 5220/ T (K)) for a selected example under the conditions indicated in set 4, Table 1.

the present work, has shown that methyl formate plays an important role in this process.

The experimental results obtained under high-pressure conditions in the present work are shifted toward lower temperatures compared to those obtained at atmospheric pressure by Marrodán et al.,¹⁵ for different residence times. Model calculations have been performed to evaluate independently the effect of pressure and gas residence time

and results indicate that both variables have remarkable influence on the DMM oxidation process.

■ ASSOCIATED CONTENT

📄 Supporting Information

The full mechanism listing including the thermodynamic data additional to THERMDAT.⁴¹ The Supporting Information is available free of charge on the ACS Publications website at DOI: 10.1021/acs.energyfuels.5b00459.

■ AUTHOR INFORMATION

Corresponding Author

*M. U. Alzueta. E-mail: uxue@unizar.es.

Notes

The authors declare no competing financial interest.

■ ACKNOWLEDGMENTS

The authors express their gratitude to the Aragón Government (GPT group) and to MINECO and FEDER (Project CTQ2012-34423) for financial support.

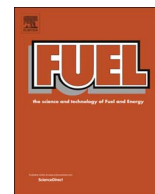
■ REFERENCES

- (1) Zhu, R.; Wang, X.; Miao, H.; Yang, X.; Huang, Z. *Fuel* **2011**, *90*, 1731–1737.
- (2) Vertin, K. D.; Ohi, J. M.; Naegeli, D. W.; Childress, K. H.; Hagen, G. P.; McCarthy, C. I.; Cheng, A. S.; Dibble, R. W. *Methylal and Methylal-Diesel Blended Fuels for Use in Compression-Ignition Engines*; SAE Technical Paper 1999-01-1508; SAE International: Warrendale, PA, 1999.
- (3) Yanfeng, G.; Shenghua, L.; Hejun, G.; Tiegang, H.; Longbao, Z. *Appl. Therm. Eng.* **2007**, *27*, 202–207.

- (4) Zhu, R.; Miao, H.; Wang, X.; Huang, Z. *Proc. Combust. Inst.* **2013**, *34*, 3013–3020.
- (5) Ren, Y.; Huang, Z.; Miao, H.; Di, Y.; Jiang, D.; Zeng, K.; Liu, B.; Wang, X. *Fuel* **2008**, *87*, 2691–2697.
- (6) Ying, W.; Longbao, Z.; Hewu, W. *Atmos. Environ.* **2006**, *40*, 2313–2320.
- (7) Arcoumanis, C.; Bae, C.; Crookes, R.; Kinoshita, E. *Fuel* **2008**, *87*, 1014–1030.
- (8) Ren, Y.; Huang, Z.; Jiang, D.; Liu, L.; Zeng, K.; Liu, B.; Wang, X. *Appl. Therm. Eng.* **2006**, *26*, 327–337.
- (9) Huang, Z. H.; Ren, Y.; Jiang, D. M.; Liu, L. X.; Zeng, K.; Liu, B.; Wang, X. B. *Energy Convers. Manage.* **2006**, *47*, 1402–1415.
- (10) Sathiyagnanam, A. P.; Saravanan, C. G. *Fuel* **2008**, *87*, 2281–2285.
- (11) Chen, G.; Yu, W.; Fu, J.; Mo, J.; Huang, Z.; Yang, J.; Wang, Z.; Jin, H.; Qi, F. *Combust. Flame* **2012**, *159*, 2324–2335.
- (12) Zhang, C.; Li, P.; Li, Y.; He, J.; Li, X. *Energy Fuels* **2014**, *28*, 4603–4610.
- (13) Daly, C. A.; Simmie, J. M.; Dagaut, P.; Cathonnet, M. *Combust. Flame* **2001**, *125*, 1106–1117.
- (14) Dias, V.; Lories, X.; Vandooren, J. *Combust. Sci. Technol.* **2010**, *182*, 350–364.
- (15) Marrodán, L.; Monge, F.; Millera, A.; Bilbao, R.; Alzueta, M. U. *Ninth Mediterranean Combustion Symposium*, Rhodes, Greece, June 7–11, 2015, accepted for presentation.
- (16) Marrodán, L.; Millera, A.; Bilbao, R.; Alzueta, M. U. *Energy Fuels* **2014**, *28*, 6107–6115.
- (17) Glarborg, P.; Alzueta, M. U.; Dam-Johansen, K.; Miller, J. A. *Combust. Flame* **1998**, *115*, 1–27.
- (18) Glarborg, P.; Alzueta, M. U.; Kjærsgaard, K.; Dam-Johansen, K. *Combust. Flame* **2003**, *132*, 629–638.
- (19) Skjøth-Rasmussen, M. S.; Glarborg, P.; Østberg, M.; Johannessen, J. T.; Livbjerg, H.; Jensen, A. D.; Christensen, T. S. *Combust. Flame* **2004**, *136*, 91–128.
- (20) Alzueta, M. U.; Muro, J.; Bilbao, R.; Glarborg, P. *Isr. J. Chem.* **1999**, *39*, 73–86.
- (21) Alzueta, M. U.; Hernández, J. M. *Energy Fuels* **2002**, *16*, 166–171.
- (22) Alzueta, M. U.; Borruey, M.; Callejas, A.; Millera, A.; Bilbao, R. *Combust. Flame* **2008**, *152*, 377–386.
- (23) Alzueta, M. U.; Aranda, V.; Monge, F.; Millera, A.; Bilbao, R. *Combust. Flame* **2013**, *160*, 853–860.
- (24) Dagaut, P.; Boettner, J. C.; Cathonnet, M. *Proc. Combust. Inst.* **1996**, *26*, 627–632.
- (25) Mallard, W. G.; Westley, F.; Herron, J. T.; Hampson, R. F. *NIST Chemical Kinetics Database*, version 6.01, 1994.
- (26) Foucaut, J. F.; Martin, R. *J. Chim. Phys.* **1978**, *75*, 132–144.
- (27) Dean, A. M. *J. Phys. Chem.* **1985**, *89*, 4600–4608.
- (28) Dagaut, P.; Daly, C.; Simmie, J. M.; Cathonnet, M. *Proc. Combust. Inst.* **1998**, *27*, 361–369.
- (29) Faubel, C.; Hoyermann, K.; Strofer, E.; Wagner, H. *Ber. Bunsenges Phys. Chem.* **1979**, *83*, 532–538.
- (30) Herron, J. T. *J. Phys. Chem. Ref. Data* **1988**, *17*, 967–1026.
- (31) Arif, M.; Dellinger, B.; Taylor, P. H. *J. Phys. Chem. A* **1997**, *101*, 2436–2441.
- (32) DeMore, W. B.; Bayes, K. D. *J. Phys. Chem. A* **1999**, *103*, 2649–2654.
- (33) Cook, R. D.; Davidson, D. F.; Hanson, R. K. *J. Phys. Chem. A* **2009**, *113*, 9974–9980.
- (34) Curran, H. J.; Pitz, W. J.; Westbrook, C. K.; Dagaut, P.; Boettner, J. C.; Cathonnet, M. *Int. J. Chem. Kinet.* **1998**, *30*, 229–241.
- (35) Sehested, J.; Sehested, K.; Platz, J.; Egsgaard, H.; Nielsen, O. J. *Int. J. Chem. Kinet.* **1997**, *29*, 627–637.
- (36) Sehested, J.; Mogelberg, T.; Wallington, T. J.; Kaiser, E. W.; Nielsen, O. J. *J. Phys. Chem.* **1996**, *100*, 17218–17225.
- (37) Hoyerman, K.; Nacke, F. *Proc. Combust. Inst.* **1996**, *26*, 505–512.
- (38) Lutz, A. E.; Kee, R. J.; Miller, J. A. *SENKIN: A FORTRAN Program for Predicting Homogeneous Gas Phase Chemical Kinetics with Sensitivity Analysis*; Sandia National Laboratories: Livermore, CA, 1988; Report SAND87-8248.
- (39) Kee, R. J.; Rupley, F. M.; Miller, J. A. *CHEMKIN-II: A FORTRAN Chemical Kinetics Package for the Analysis of Gas-Phase Chemical Kinetics*; Sandia National Laboratories: Albuquerque, NM, 1991; Report SAND87-8215.
- (40) CHEMKIN-PRO, Release 15131; Reaction Design: San Diego, 2013.
- (41) Burcat, A.; Ruscic, B. *Third Millennium Ideal Gas and Condensed Phase Thermochemical Database for Combustion with Updates from Active Thermochemical Tables*; Report TAE960; Technion Israel Institute of Technology: Haifa, Israel, 2005.

Article III:

Marrodán, L.; Arnal, Á.J.; Millera, Á.; Bilbao, R.; Alzueta, M.U. (2018). High-pressure ethanol oxidation and its interaction with NO. *Fuel* 223, 394-400.



Full Length Article

High-pressure ethanol oxidation and its interaction with NO

Lorena Marrodán, Álvaro J. Arnal, Ángela Millera, Rafael Bilbao, María U. Alzueta*

Aragón Institute of Engineering Research (I3A), Department of Chemical and Environmental Engineering, University of Zaragoza, C/Mariano Esquillor, s/n, 50018 Zaragoza, Spain



ARTICLE INFO

Keywords:

Ethanol
Oxidation
High-pressure
Nitrogen oxides
Modeling

ABSTRACT

Ethanol has become a promising biofuel, widely used as a renewable fuel and gasoline additive. Describing the oxidation kinetics of ethanol with high accuracy is required for the development of future efficient combustion devices with lower pollutant emissions. The oxidation process of ethanol, from reducing to oxidizing conditions, and its pressure dependence (20, 40 and 60 bar) has been analyzed in the 500–1100 K temperature range, in a tubular flow reactor under well controlled conditions. The effect of the presence of NO has been also investigated. The experimental results have been interpreted in terms of a detailed chemical kinetic mechanism with the GADM mechanism (Glarborg P, Alzueta MU, Dam-Johansen K and Miller JA, 1998) as a base mechanism but updated, validated, extended by our research group with reactions added from the ethanol oxidation mechanism of Alzueta and Hernández (Alzueta MU and Hernández JM, 2002), and revised according to the present high-pressure conditions and the presence of NO. The final mechanism is able to reproduce the experimental trends observed on the reactants consumption and main products formation during the ethanol oxidation under the conditions studied in this work. The results show that the oxygen availability in the reactant mixture has an almost imperceptible effect on the temperature for the onset of ethanol consumption at a constant pressure, but this consumption is faster for the highest value of air excess ratio (λ) analyzed. Moreover, as the pressure becomes higher, the oxidation of ethanol starts at lower temperatures. The presence of NO promotes ethanol oxidation, due to the increased relevance of the interactions of CH_3 radicals and NO_2 (from the conversion of NO to NO_2 at high pressures and in presence of O_2) and the increased concentration of OH radicals from the interaction of NO_2 and water.

1. Introduction

Minimizing particulate matter and nitrogen oxides (NO_x) emissions from combustion, especially from transport, is a pressing need to improve the air quality, preserve the environment and comply with the increasingly restrictive laws. A prospective solution is fuel reformulation since its effects on emissions are immediate and can be implemented, without significant changes, in the design of the equipment. This reformulation implies the total or partial replacement of the conventional fuel by alternative ones, that may have been obtained in a more environmentally friendly way, for example, alcohols such as ethanol or butanol from biomass or wastes by biorefinery processes [1].

Ethanol ($\text{C}_2\text{H}_5\text{OH}$) is one of the most studied alcohols and its use, directly or as a gasoline additive, is spread worldwide. However, the cetane number, flash point and calorific value of ethanol are lower than those corresponding to diesel fuel, so it cannot be used directly in diesel engines. Therefore, ethanol must be blended with diesel fuel or biodiesel [2] and, working under the appropriate conditions, the emissions

of CO, particulate matter and NO_x could be reduced [3].

The ethanol oxidation has been investigated in several works using laminar flames, shock tubes, flow reactors and rapid compression machines, as it has been summarized in the study of Mittal et al. [4]. More recently, Barraza-Botet et al. [5] carried out ignition and speciation studies in ethanol combustion in a rapid compression facility. For modeling predictions, they [5] used the detailed mechanism of Burke et al. [6,7] developed for C_1 - C_3 hydrocarbons and oxygenated species oxidation, obtaining a good agreement with the experimental results.

However, despite its relevance for its applicability to internal combustion engines, the ethanol oxidation in flow reactors under high-pressure conditions has not been previously studied. Therefore, reliable experimental data for validation of the kinetic models in this high-pressure regime become of high importance.

In this context, the aim of the present work is to extend the experimental database on ethanol oxidation with the study of its conversion under high-pressure conditions, in a flow reactor, for different air excess ratios, both in the absence and presence of nitric oxide (NO).

* Corresponding author.

E-mail address: uxue@unizar.es (M.U. Alzueta).

NO may be formed in the combustion chamber of a diesel engine, mainly through the thermal NO mechanism and, once it has been formed, NO may interact with ethanol or its derivatives. The experimental results are analyzed in terms of a detailed chemical kinetic mechanism to identify the main reaction routes occurring and to better understand the possible ethanol-NO interactions.

2. Experimental methodology

The ethanol oxidation experiments, both in the absence and presence of NO, have been carried out in a high-pressure flow reactor designed to approximate gas plug flow. The experimental set up is described in detail in Marrodán et al. [8] and only a brief description is provided here. A controlled evaporator mixer (CEM) has been used to feed an aqueous solution of ethanol (10% by weight) into the reaction system. The oxygen required to carry out each oxidation experiment depends on the air excess ratio analyzed (λ , defined as the inlet oxygen concentration divided by stoichiometric oxygen), and it has been supplied from gas cylinder through a Bronkhorst Hi-Tech mass flow controller. In the case of the experiments in the presence of NO, 500 ppm of NO have been added to the feed gas flow. Table 1 lists the conditions of the different experiments.

The gas reactants are premixed before entering the reaction system, which consists of a tubular quartz reactor (inner diameter of 6 mm and 1500 mm in length) enclosed in a stainless-steel tube that acts as a pressure shell. The longitudinal temperature profile in the reactor was experimentally determined. An isothermal zone (± 10 K) of 56 cm was obtained in the reactor, which was considered as reaction zone. Nitrogen to balance up to obtain a total flow rate of 1 L (STP)/min has been used, resulting in a gas residence time dependent of the pressure and the temperature according to: t_r (s) = 261 P(bar)/T(K).

The products were analyzed using an on-line 3000A Agilent micro-chromatograph equipped with TCD detectors and an URAS26 ABB continuous IR NO analyzer. The uncertainty of the measurements is estimated as $\pm 5\%$, but not less than 10 ppm.

3. Modeling

Simulations of the experimental results obtained in the ethanol high-pressure oxidation, in the absence and presence of NO, have been made using a gas-phase chemical kinetic model and the software Chemkin-Pro [9]. The detailed mechanism used in this work has been built up by our research group from the GADM mechanism [10], progressively updated (e.g. [11,12]) and modified to consider the different experimental conditions, such as the high-pressure and/or the different compounds

Table 1
Matrix of experimental conditions.

Set	Ethanol (ppm)	O ₂ (ppm)	NO (ppm)	λ	P (bar)
1	5000	10,500	0	0.7	20
2	5000	10,500	0	0.7	40
3	5000	10,500	0	0.7	60
4	5000	15,000	0	1	20
5	5000	15,000	0	1	40
6	5000	15,000	0	1	60
7	5000	60,000	0	4	20
8	5000	60,000	0	4	40
9	5000	60,000	0	4	60
10	5000	10,500	500	0.7	20
11	5000	10,500	500	0.7	40
12	5000	10,500	500	0.7	60
13	5000	15,000	500	1	20
14	5000	15,000	500	1	40
15	5000	15,000	500	1	60
16	5000	60,000	500	4	20
17	5000	60,000	500	4	40
18	5000	60,000	500	4	60

involved [13–17]. In the case of ethanol, the reaction subset proposed by Alzueta and Hernández [18] in an atmospheric ethanol oxidation study has been included in the mechanism compiled in this work. Formic acid (HCOOH) has been identified as an intermediate in oxidation of dimethyl ether [19], which is an isomer of ethanol, so the reaction subset for formic acid oxidation proposed by Marshall and Glarborg [20] has also been included in the mechanism. The thermodynamic data for the species involved are taken from the same sources as the original mechanisms. The complete mechanism (137 species and 798 reactions) is provided as [Supplementary Material](#) in CHEMKIN format.

4. Results and discussion

A study of ethanol oxidation at high pressure (20, 40 and 60 bar), in the 500–1100 K temperature range, has been carried out, for different air excess ratios ($\lambda = 0.7, 1$ and 4), both in the absence and in the presence of NO.

4.1. Oxidation of ethanol in the absence of NO

Fig. 1 shows an example of the results for ethanol consumption and CO and CO₂ formation as a function of temperature for the conditions of set 4 in Table 1, i.e., 20 bar, stoichiometric conditions ($\lambda = 1$) and in the absence of NO. From now on, experimental results are denoted by symbols, and modeling calculations by lines. In general, there is a good agreement between the experimental results and model predictions. Under these conditions, the ethanol conversion starts at approximately 725 K, the same temperature as for the onset of CO formation whose concentration peaks at 775 K. At the highest temperatures, ethanol and CO are completely oxidized to CO₂.

Fig. 2 shows the concentration of ethanol and of the main products quantified (CO, CO₂, CH₃CHO, C₂H₄, CH₄, CH₃OH, H₂), for different air excess ratios (from $\lambda = 0.7$ to $\lambda = 4$), at a constant pressure of 20 bar, and in the absence of NO. The oxygen availability in the reactant mixture does not modify significantly the temperature for the onset of ethanol conversion at a given pressure. In an ethanol oxidation study at atmospheric pressure, Alzueta and Hernández [18] observed that the ethanol oxidation occurs at lower temperatures for very oxidizing conditions ($\lambda = 35$), and small differences between $\lambda = 0.7$ and $\lambda = 1$ were found.

The biggest discrepancies can be found in the experimental and modeling results for CH₄, for reducing and stoichiometric conditions, and CH₃OH, minor products compared to CO and CO₂. The same tendencies can be observed for the other pressures studied in this work, although these results are not shown.

In order to further evaluate the influence of air excess ratio on ethanol oxidation, given the little influence found for $\lambda = 1$ and $\lambda = 4$,

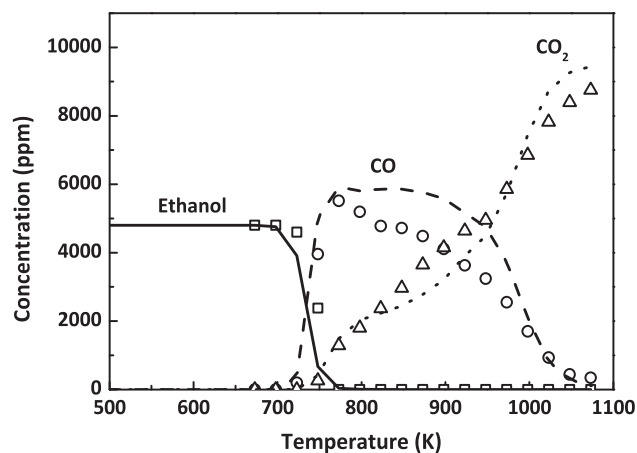


Fig. 1. Concentration of ethanol, CO and CO₂ as a function of temperature, for the conditions named as set 4 in Table 1 ($\lambda = 1, 20$ bar).

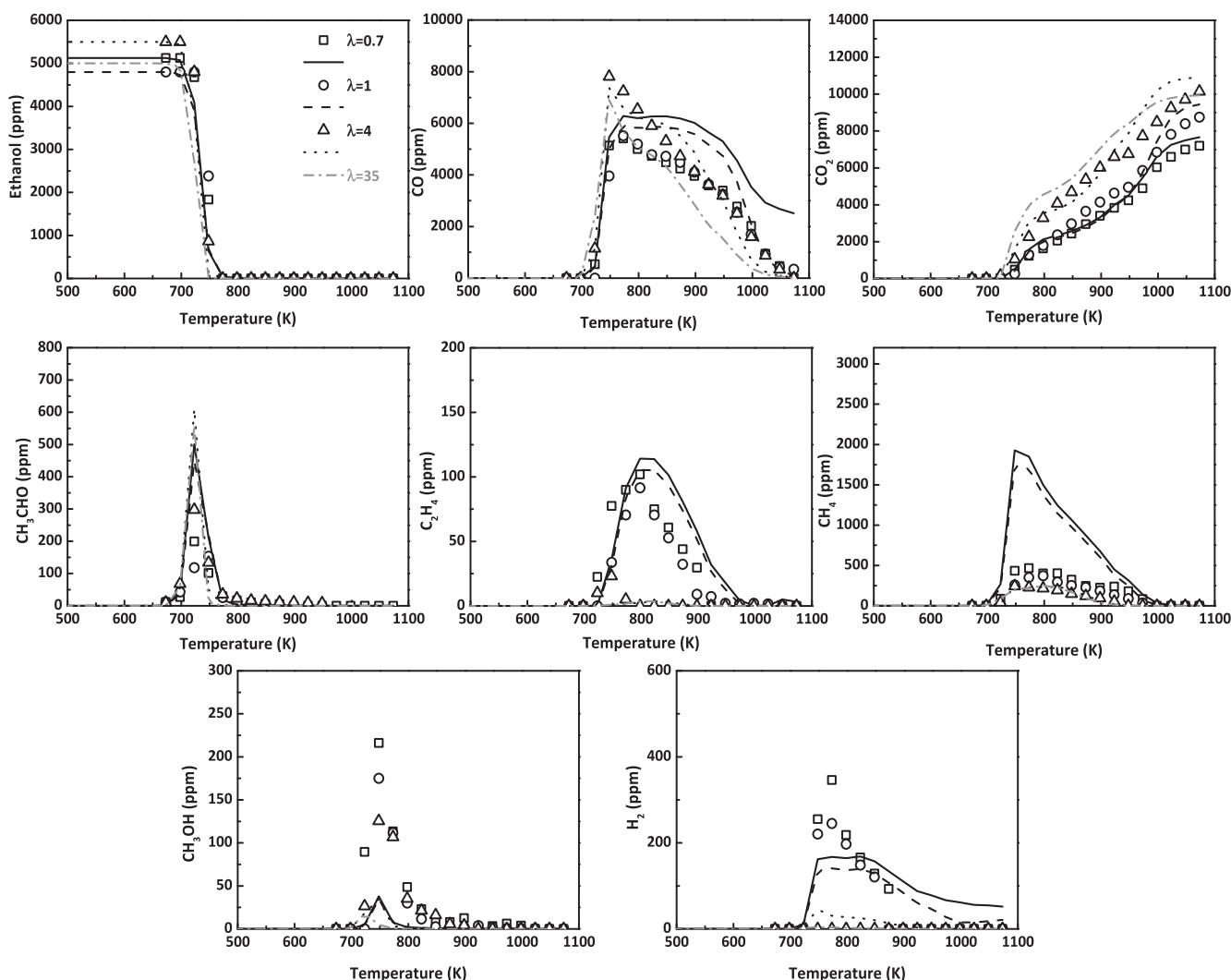


Fig. 2. Influence of the air excess ratio on the concentration profiles of ethanol and main products (CO, CO₂, CH₃CHO, C₂H₄, CH₄, CH₃OH, H₂) during ethanol oxidation, as a function of temperature, for the conditions named as sets 1, 4 and 7 in Table 1 (20 bar).

model calculations for $\lambda = 35$, very fuel-lean conditions, have been carried out. The theoretical results obtained for $\lambda = 35$ (Fig. 2) are almost the same than those for $\lambda = 4$, for ethanol, acetaldehyde (CH₃CHO) and CO and CO₂ concentrations, but lower amounts of CH₄, C₂H₄ and CH₃OH are predicted. So, it can also be deduced that for the high-pressure conditions studied in this work, there is almost no influence of the oxygen availability on the temperature for the onset of ethanol oxidation.

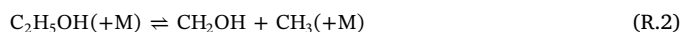
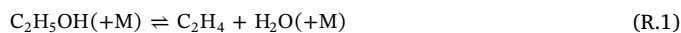
Fig. 3 shows the influence of the pressure change (20, 40 and 60 bar) on the ethanol consumption and CO formation, which has been selected as one of the main products of ethanol oxidation. Independently of the stoichiometry analyzed, the consumption of ethanol starts at lower temperatures as the pressure is increased, approximately 100 K when moving from 20 to 60 bar. This behavior is also observed in the formation of CO, which peaks at lower temperatures for the highest pressure analyzed. The oxidation of CO to CO₂ is favored by an increase in pressure, as well as by an increase in the lambda value.

Considering the experimental procedure utilized in this work, a change in the pressure maintaining the total gas flow rate, also implies a change in the gas residence time (t_r (s) = 261 P(bar)/T(K)). Therefore, with the present mechanism, that describes well the experimental results, we have made different simulations to try to distinguish between the effect of gas residence time or pressure. This evaluation can be found as Supplementary Material, Fig. S.1. The

results indicate that both the pressure and the residence time have an appreciable effect on the ethanol conversion, which is shifted to lower temperatures when any of the above variables is increased. Accordingly, the results presented in Fig. 3 correspond to the joint effect of pressure and residence time.

In general, modeling predictions are in good agreement with the experimental observations. Consequently, in this work, reaction rate analysis has been performed to identify the main ethanol consumption routes and products formation and the obtained results have been represented in a reaction pathway diagram in Fig. 4 (left).

The ethanol consumption is initiated by its thermal dehydration to ethylene (reaction R.1), as this latter has been detected by gas chromatography, and also by its thermal decomposition through bond cleavage to CH₂OH and CH₃ radicals (reaction R.2). For example, for 20 bar and $\lambda = 0.7$, at 725 K, 86% of the ethanol is being consumed through reaction R.2, and for $\lambda = 4$, 95% of the ethanol consumption is produced through reaction R.1. This fact could explain the almost negligible effect of the oxygen availability on the temperature for the onset of ethanol consumption.



In earlier studies involving ethanol oxidation in flow reactors [18,21], and in flames and jet stirred reactors [22], the main reaction

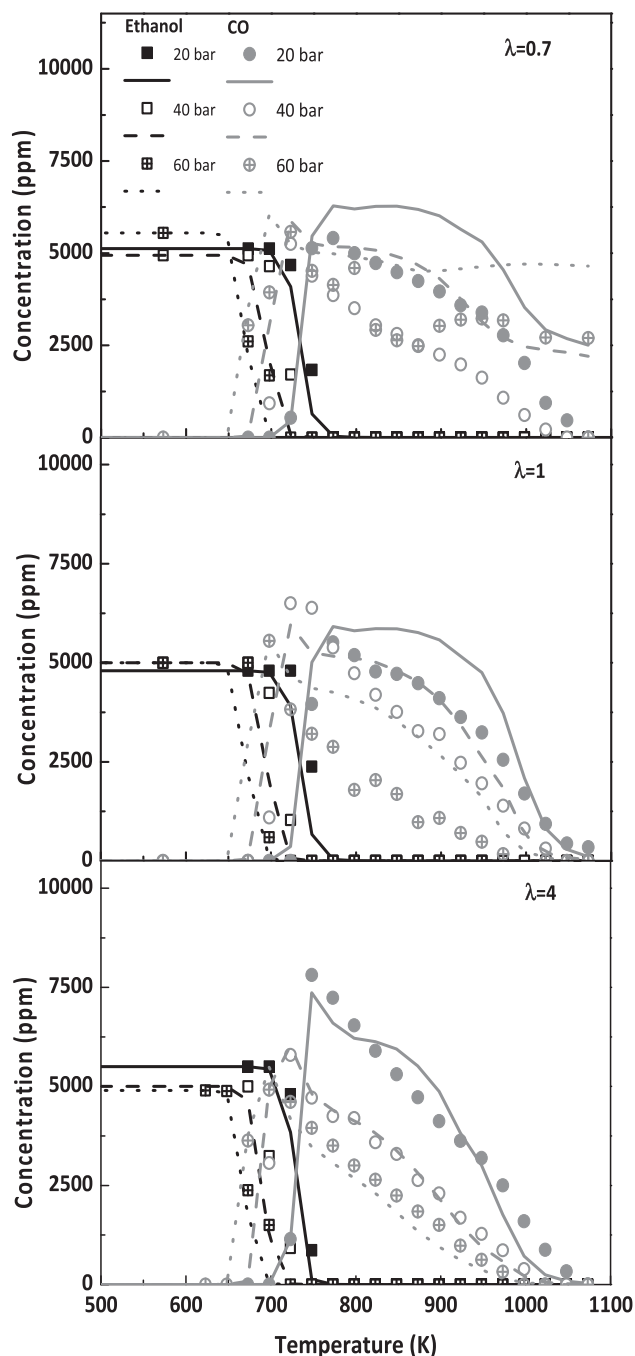
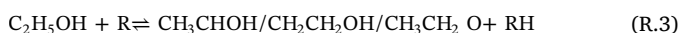


Fig. 3. Influence of the pressure change on the concentration profiles of ethanol and CO, as a function of temperature, for the conditions named as sets 1–9 in Table 1.

pathways for ethanol consumption were identified. The proposed reaction routes are based on a hydrogen abstraction that may occur on three different sites, leading to the formation of three different C_2H_5O radical isomers (reaction R.3, where R can be O, H, OH, CH_3 or HO_2 radicals).



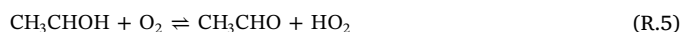
Under the conditions of the present work, these reactions also take place, especially that one involving HO_2 radicals, as it was previously observed in the oxidation of other oxygenated compounds, such as dimethoxymethane [23], under high-pressure conditions. The hydroxymethyl radical (CH_2OH), formed in reaction R.2 from ethanol, reacts with molecular oxygen to produce formaldehyde and more HO_2 radicals (reaction R.4), which interact with ethanol (reaction R.3)

producing the CH_3CHOH radical, the dominant radical under the present conditions.



An example of the evolution along the reactor of the main consumption reactions for ethanol can be observed in Fig. 4 (right), for 20 bar, $\lambda = 1$ and 725 K. At the beginning of the reactor, the ethanol consumption is mainly through its thermal dehydration (reaction R.1), but hydrogen abstraction reaction by HO_2 (reaction R.3) becomes more relevant with the distance.

The CH_3CHOH radical reacts with molecular oxygen (reaction R.5) producing acetaldehyde, which has been quantified by gas chromatography. Acetaldehyde interacts with the radical pool producing the acetyl radical (CH_3CO), which thermally decomposes to CO and CH_3 radicals.



The reaction pathways involving the other two C_2H_5O radicals are of minor relevance compared to those already described, and very similar to those described in previous ethanol oxidation works (e.g. [22]).

As it has been mentioned in the introduction, the mechanism of Burke et al. [6,7] has been used in previous ethanol studies, e.g. [5]. Therefore, it has been considered interesting to compare the experimental results obtained in this work with those predicted with the present model and the Burke et al. model. This comparison can be found as Supplementary Material, Figs. S2–S10.

It can be observed that, in general, the model proposed in this work fits better the experimental results corresponding to the ethanol conversion onset temperature and the concentrations of ethanol, CO, CO_2 , H_2 and C_2H_4 , while the Burke et al. model fits better the concentrations corresponding to CH_4 and CH_3OH .

4.2. Oxidation of ethanol in the presence of NO

In the present work, the influence of the presence of NO in the reactant mixture on ethanol oxidation has also been analyzed. When burning any fuel in an air atmosphere at high temperatures, NO may be formed through the thermal NO formation mechanism by nitrogen fixation from the combustion air [24]. NO may be reduced by its interaction with ethanol and/or its derivatives, or may promote the ethanol oxidation in a mutually sensitized oxidation [25]. Therefore, the interaction between ethanol and NO has been considered in the present work from both experimental and modeling points of view.

As it can be drawn from the discussion of the main reaction pathways for ethanol conversion in the absence of NO, a high concentration of CH_3 radicals is also expected in the presence of NO. Furthermore, under the present experimental conditions, it has been observed that, due to the high-pressure conditions and the presence of O_2 , NO added to the reactant mixture is converted to NO_2 before entering the reactor. From the interaction between CH_3 radicals and NO_2 (reaction R.6), the mechanism initially compiled in this work predicted an accumulation of nitromethane (CH_3NO_2), whose formation was not detected experimentally. Another possible interaction between CH_3 radicals and NO_2 leading to CH_3ONO may occur (reaction R.7).



In a high-pressure flow reactor study, Rasmussen and Glarborg [16] analyzed the effects of NO_x on CH_4 oxidation, through ab initio calculations. Their calculations indicated that the formation of CH_3ONO is energetically unfavorable, but, if formed, it would dissociate to NO and methoxy radical (CH_3O).

Therefore, because of the high CH_3 and NO_2 concentrations expected and no CH_3NO_2 detection, the CH_3ONO reaction to CH_3 and NO_2

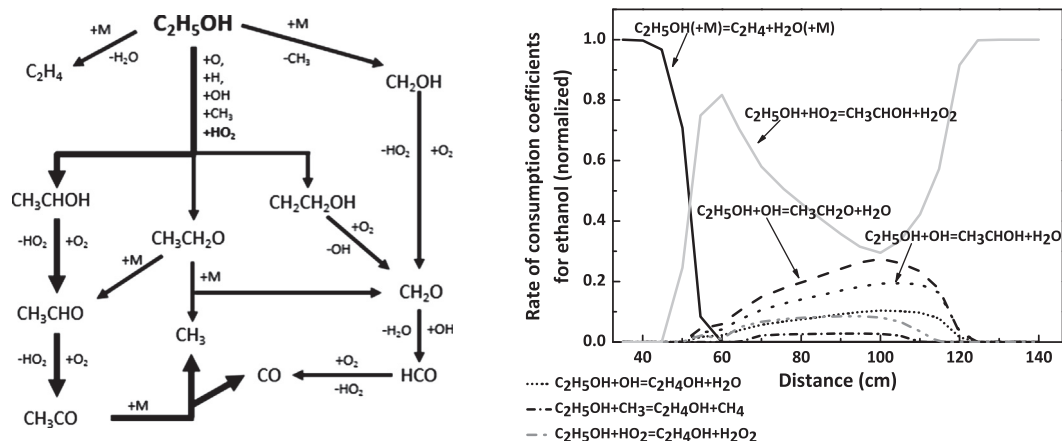


Fig. 4. Left: reaction path diagram for ethanol consumption and product formation. Right: normalized rate-of-consumption coefficients for ethanol along the reactor (for the conditions of set 4 in Table 1: 20 bar, $\lambda = 1$ and 725 K).

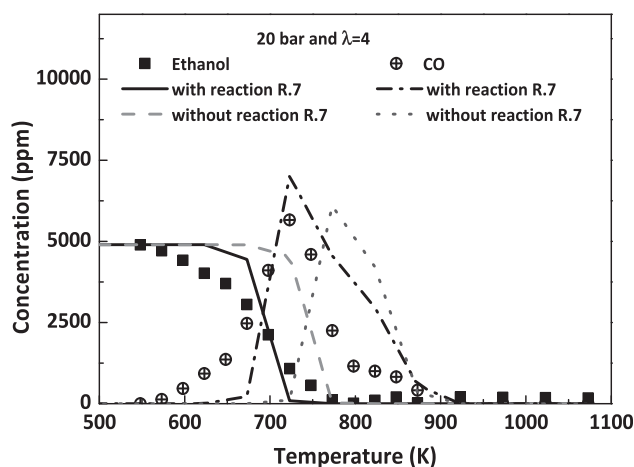


Fig. 5. Improvement in modeling predictions for ethanol and CO concentration, with and without reaction R.7 in our mechanism, for the conditions named as set 16 in Table 1.

(reaction R.7) has been included in our mechanism. There is not much information in bibliography regarding this reaction and its kinetic parameters. So, the value of $7.00 \times 10^{10} \text{ cm}^3 \text{ mol}^{-1} \text{ s}^{-1}$ proposed by Canosa et al. [26] has been adopted for reaction R.7. As it can be seen in Fig. 5, in the concentration profiles of ethanol and CO, the predictions of the model improved considerably after including reaction R.7 in the mechanism.

Fig. 6 (top) shows a comparison between the experimental results (symbols) and model predictions (lines) obtained during ethanol oxidation, in the presence of NO, for different air excess ratios and different pressures. Compared to Fig. 3, the presence of NO promotes ethanol oxidation shifting the onset of ethanol oxidation to lower temperatures, a difference of 100–125 K approximately. As also occurred in the absence of NO, the available oxygen in the reactant mixture does not modify the temperature for the onset of ethanol conversion at a constant pressure of 20 bar. The same tendency was observed for the other pressures analyzed (results not shown), but the higher the pressure the lower the ethanol conversion onset temperature. Fig. 6 (bottom) shows the experimental and theoretical NO concentration results for different air excess ratios and 20 bar, and also other pressures for $\lambda = 4$. Modeling predictions are shifted to higher temperatures, approximately 50 K, compared to experimental results. At low temperatures, as previously mentioned, the NO fed to the system is converted to NO_2 through reaction R.8, and it is not thus experimentally detected until approximately 750 K. Unlike what was observed for ethanol, both λ and pressure values influence the NO concentration, in the way that increasing the amount of oxygen in the

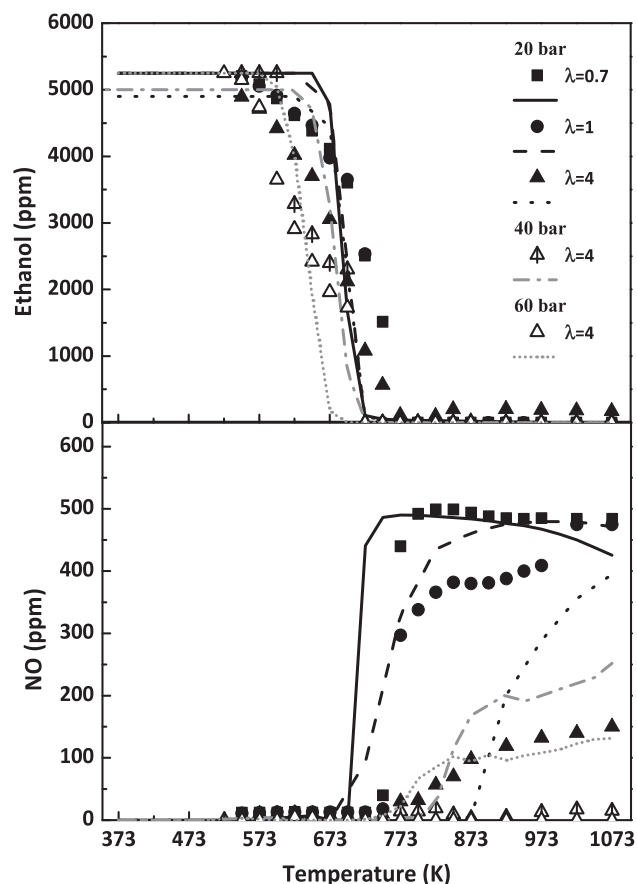


Fig. 6. Influence of the air excess ratio and pressure on the concentration profiles of ethanol (top) and NO (bottom) for the conditions named as sets 10, 13 and 16–18 in Table 1.

reactant mixture or increasing the pressure, results in a lower amount of NO experimental or predicted.



Once formed, NO_2 reacts with CH_3 radicals originated from ethanol to produce CH_3ONO (reaction R.7), which decomposes rapidly into $CH_3O + NO$. As a consequence, NO is detected again, especially for 20 bar and $\lambda = 0.7$, because an increase in the value of pressure or lambda favors reaction R.8.

NO_2 can also react with H_2O to produce HONO and OH radicals (reaction R.9), which promote ethanol conversion. The HONO formed

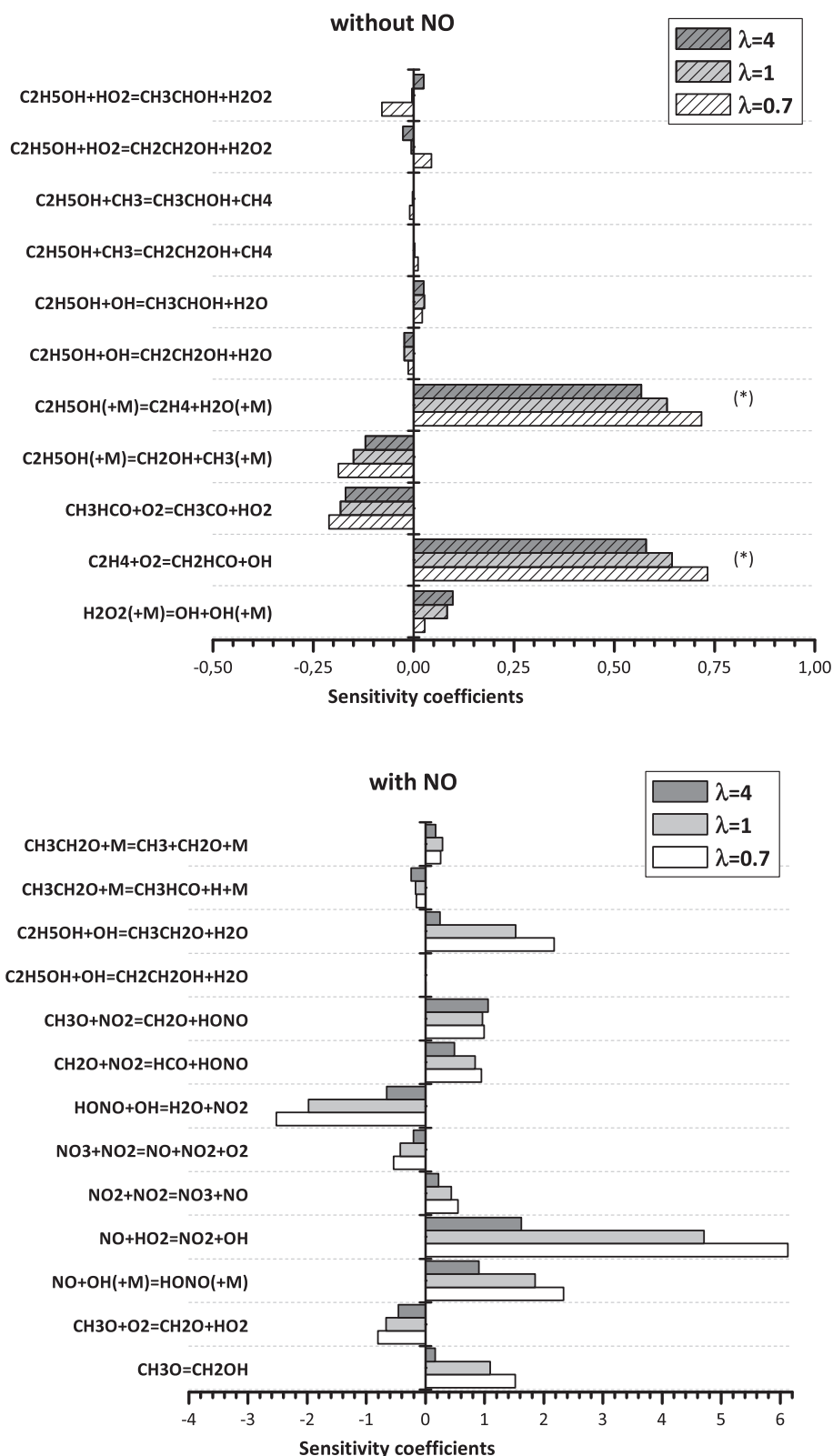


Fig. 7. Sensitivity analysis for CO for different air excess ratios and 20 bar. Top: in the absence of NO (at 698 K). Bottom: in the presence of NO (at 648 K). (*) The sensitivity coefficients have been divided by two.

decomposes to produce NO (reaction R.10).



The same reactions (R.9 and R.10), but in the reverse sense, were

the cause of a slightly inhibiting effect of ethanol conversion by NO observed in the ethanol oxidation at atmospheric pressure [18], under certain conditions.

In the presence of NO, the ethanol consumption routes are the same as those already described in the absence of NO. However, in the

presence of NO, the reaction pathways involving the $\text{CH}_3\text{CH}_2\text{O}$ radical (formed through R.3) acquire more relevance, becoming the pre-dominating reaction pathways. This radical decomposes through reactions R.11 and R.12 to produce acetaldehyde or CH_3 radicals and formaldehyde, respectively.



First-order sensitivity analyses for ethanol and CO have been performed for different air excess ratios and 20 bar, in the absence of NO and in the presence of NO.

The obtained ethanol results are in agreement with the ethanol consumption pathways previously described and can be found as [Supplementary Material, Fig. S11](#). In the absence of NO, the most sensitive reaction is the hydrogen abstraction reaction by HO_2 (reaction R.3), which is the main reaction pathway for ethanol consumption. The reaction $\text{H}_2\text{O}_2 + \text{M} = \text{OH} + \text{OH} + \text{M}$ is also very sensitive due to the generation of OH radicals which can promote the consumption of ethanol by H abstraction reactions. In the presence of NO, the formation of $\text{CH}_3\text{CH}_2\text{O}$ radical from ethanol (reaction R.3, $\text{C}_2\text{H}_5\text{OH} + \text{OH} = \text{CH}_3\text{CH}_2\text{O} + \text{H}_2\text{O}$) and its thermal decomposition (reactions R.11 and R.12) present a high sensitivity coefficient, becoming the dominant ethanol consumption under these conditions. The CH_3 radicals generated in reaction R.12 may interact with ethanol promoting its consumption. The formation of HONO from the interaction of $\text{CH}_2\text{O} + \text{NO}_2$ ($\text{CH}_2\text{O} + \text{NO}_2 = \text{HCO} + \text{HONO}$) and its subsequent decomposition (reaction R.10, $\text{HONO} + \text{M} = \text{NO} + \text{OH} + \text{M}$) producing OH radicals are sensitive in the presence of NO, because of the OH radicals generated that promote ethanol conversion.

Moreover, the first-order sensitivity analysis for CO (Fig. 7) indicates that, in the absence of NO, the most sensitive reaction is the thermal dehydration of ethanol to ethylene (reaction R.1). The subsequent reaction of ethylene with O_2 presents a high sensitivity for all the values of lambda analyzed. Hydrogen abstraction reactions from ethanol with different radicals are also sensitive. In the presence of NO, as in the case of the sensitivity results for ethanol, hydrogen abstraction reactions by OH radicals to produce $\text{CH}_3\text{CH}_2\text{O}$ radical and its subsequent decomposition are highly sensitive. The interaction of NO_2 with CH_2O to produce HONO and HCO presents the highest sensitivity coefficient for all the lambdas analyzed.

5. Conclusions

The oxidation of ethanol has been analyzed from both experimental and modeling points of view. The influence on the process of the available oxygen in the reactant mixture (different air excess ratios: $\lambda = 0.7, 1$ and 4), the change of pressure (20, 40 and 60 bar) and the presence or absence of NO has been analyzed in a tubular flow reactor, in the 500–1100 K temperature range.

In general, there is a good agreement between experimental and modeling predictions. The results show that, for the conditions studied in this work, at a constant pressure, the temperature for the onset of ethanol oxidation is roughly independent of the amount of oxygen available in the reactant mixture, but the ethanol conversion starts at lower temperatures as the pressure is increased. A reaction rate analysis indicates that the ethanol consumption is mainly initiated by thermal dehydration or decomposition.

When NO is fed to the high-pressure system, it converts to NO_2 before entering in the reactor. In view of the high expected concentration of NO_2 and CH_3 radicals (from the ethanol conversion), the reaction $\text{CH}_3\text{ONO} \rightleftharpoons \text{CH}_3 + \text{NO}_2$ has been included in our mechanism, with clear improvements of the model predictions. In the presence of NO, the ethanol conversion is promoted due to the increased

concentration of OH in the radical pool from the interaction of NO_2 and water. As observed in the absence of NO, the stoichiometry does not have a clear influence on the ethanol oxidation regime, whereas an increase in the pressure shifts the temperature for the onset of ethanol consumption to lower temperatures.

Acknowledgements

The authors express their gratitude to Aragón Government and European Social Fund (GPT group), and to MINECO and FEDER (Project CTQ2015-65226) for financial support. Ms. Marrodán acknowledges Aragón Government for the predoctoral grant awarded.

Appendix A. Supplementary data

Supplementary data associated with this article can be found, in the online version, at <http://dx.doi.org/10.1016/j.fuel.2018.03.048>.

References

- [1] Sarathy SM, Oßwald P, Hansen N, Kohse-Höinghaus K. Alcohol combustion chemistry. *Prog Energy Combust Sci* 2014;44:40–102.
- [2] Alviso D, Krauch F, Román R, Maldonado H, dos Santos RG, Rolón JC, et al. Development of a diesel-biodiesel-ethanol combined chemical scheme and analysis of reactions pathways. *Fuel* 2017;191:411–26.
- [3] An H, Yang WM, Li J. Effects of ethanol addition on biodiesel combustion: a modeling study. *Appl Energy* 2015;143:176–88.
- [4] Mittal G, Burke SM, Davies VA, Parajuli B, Metcalfe WK, Curran HJ. Autoignition of ethanol in a rapid compression machine. *Combust Flame* 2014;161:1164–71.
- [5] Barraza-Botet CL, Wagnon SW, Wooldridge MS. Combustion chemistry of ethanol: ignition and speciation studies in a rapid compression facility. *J Phys Chem A* 2016;120:7408–18.
- [6] Burke SM, Metcalfe W, Herbinet O, Batton-Leclerc F, Haas FM, Santner J, et al. An experimental and modeling study of propene oxidation. Part 1: speciation measurements in jet-stirred and flow reactors. *Combust Flame* 2014;161:2765–84.
- [7] Burke SM, Burke U, Mc Donagh R, Mathieu O, Osorio I, Keesece C, et al. An experimental and modeling study of propene oxidation. Part 2: ignition delay time and flame speed measurements. *Combust Flame* 2015;162:296–314.
- [8] Marrodán L, Millera Á, Bilbao R, Alzueta MU. High-pressure study of methyl formate oxidation and its interaction with NO. *Energy Fuels* 2014;28:6107–15.
- [9] ANSYS Chemkin-Pro 17.2, Release 15151; Reaction Design: San Diego, 2016.
- [10] Glarborg P, Alzueta MU, Dam-Johansen K, Miller JA. Kinetic modeling of hydrocarbon/nitric oxide interactions in a flow reactor. *Combust Flame* 1998;115:1–27.
- [11] Glarborg P, Alzueta MU, Kærsgaard K, Dam-Johansen K. Oxidation of formaldehyde and its interaction with nitric oxide in a flow reactor. *Combust Flame* 2003;132:629–38.
- [12] Glarborg P, Østberg M, Alzueta MU, Dam-Johansen K, Miller JA. The recombination of hydrogen atoms with nitric oxide at high temperatures. *Proc Combust Inst* 1999;27:219–27.
- [13] Rasmussen CL, Hansen J, Marshall P, Glarborg P. Experimental measurements and kinetic modeling of $\text{CO}/\text{H}_2/\text{O}_2/\text{NO}_x$ conversion at high-pressure. *Int J Chem Kin* 2008;40:454–80.
- [14] Rasmussen CL, Glarborg P. Measurements and kinetic modeling of CH_4/O_2 and $\text{CH}_4/\text{C}_2\text{H}_6/\text{O}_2$ conversion at high pressure. *Int J Chem Kin* 2008;40:778–807.
- [15] Rasmussen CL, Andersen KH, Dam-Johansen K, Glarborg P. Methanol oxidation in a flow reactor: implications for the branching ratio of $\text{CH}_3\text{OH} + \text{OH}$ reaction. *Int J Chem Kin* 2008;40:423–41.
- [16] Rasmussen CL, Glarborg P. Sensitizing effects of NO_x on CH_4 oxidation at high pressure. *Combust Flame* 2008;154:529–45.
- [17] Giménez-López J, Rasmussen CT, Hashemi H, Alzueta MU, Gao Y, Marshall P, et al. Experimental and kinetic modeling study of C_2H_2 oxidation at high pressure. *Int J Chem Kin* 2016;48:724–38.
- [18] Alzueta MU, Hernández JM. Ethanol oxidation and its interaction with nitric oxide. *Energy Fuels* 2002;16:166–71.
- [19] Fischer SL, Dryer FL, Curran HJ. The reaction kinetics of dimethyl ether. I: high-temperature pyrolysis and oxidation in flow reactors. *Int J Chem Kinet* 2000;32:713–40.
- [20] Marshall P, Glarborg P. Ab initio and kinetic modeling studies of formic acid oxidation. *Proc Combust Inst* 2015;35:153–60.
- [21] Abián M, Esarte C, Millera Á, Bilbao R, Alzueta MU. Oxidation of acetylene-ethanol mixtures and their interaction with NO. *Energy Fuels* 2008;22:3814–23.
- [22] Leplat N, Dagaut P, Togbé C, Vandooen J. Numerical and experimental study of ethanol combustion and oxidation in laminar premixed flames and jet-stirred reactor. *Combust Flame* 2011;158:705–25.
- [23] Marrodán L, Royo E, Millera Á, Bilbao R, Alzueta MU. High-pressure oxidation of dimethoxymethane. *Energy Fuels* 2015;29:3507–17.
- [24] Abián M, Alzueta MU, Glarborg P. Formation of NO from N_2/O_2 mixtures in a flow reactor: toward and accurate prediction of thermal NO. *Int J Chem Kinet* 2015;47:518–32.
- [25] Taylor PH, Cheng L, Dellinger B. The influence of nitric oxide on the oxidation of methanol and ethanol. *Combust Flame* 1998;115:561–7.
- [26] Canosa C, Penzhorn RD, Sonntag C. Product quantum yields from the photolysis of NO₂ at 366 nm in presence of ethylene. The role of NO₃. *Ber Bunsenges Phys Chem* 1979;83:217–25.

HIGH-PRESSURE ETHANOL OXIDATION AND ITS INTERACTION WITH NO

Lorena Marrodán, Álvaro J. Arnal, Ángela Millera, Rafael Bilbao, María U. Alzueta*

Aragón Institute of Engineering Research (I3A). Department of Chemical and Environmental
Engineering. University of Zaragoza. C/ Mariano Esquillor, s/n. 50018 Zaragoza. Spain

SUPPLEMENTARY MATERIAL

Table of contents

1) Evaluation through model calculations of the effect of pressure and gas residence time.

Figure S1. Evaluation through model calculations of the effect of pressure and gas residence time on the ethanol (5000 ppm) conversion, under stoichiometric conditions ($\lambda=1$). Figure S1 (left) includes calculations made at different pressures (20, 40 and 60 bar) and at a constant residence time. Figure S1 (right) includes calculations made at 20 bar and different residence times.

2) Comparison of modeling predictions using the present mechanism (solid lines) and a mechanism from literature (dashed lines) with the high-pressure plug flow reactor experimental data obtained in this work (symbols).

Figure S2. Species concentrations as a function of temperature for the high-pressure ethanol oxidation (20 bar and $\lambda=0.7$). Comparison of experimental results (symbols) with modeling predictions: present model (solid lines) and Burke et al. model (dashed lines).

Figure S3. Species concentrations as a function of temperature for the high-pressure ethanol oxidation (20 bar and $\lambda=1$). Comparison of experimental results (symbols) with modeling predictions: present model (solid lines) and Burke et al. model (dashed lines).

Figure S4. Species concentrations as a function of temperature for the high-pressure ethanol oxidation (20 bar and $\lambda=4$). Comparison of experimental results (symbols) with modeling predictions: present model (solid lines) and Burke et al. model (dashed lines).

Figure S5. Species concentrations as a function of temperature for the high-pressure ethanol oxidation (40 bar and $\lambda=0.7$). Comparison of experimental results (symbols) with modeling predictions: present model (solid lines) and Burke et al. model (dashed lines).

Figure S6. Species concentrations as a function of temperature for the high-pressure ethanol oxidation (40 bar and $\lambda=1$). Comparison of experimental results (symbols) with modeling predictions: present model (solid lines) and Burke et al. model (dashed lines).

Figure S7. Species concentrations as a function of temperature for the high-pressure ethanol oxidation (40 bar and $\lambda=4$). Comparison of experimental results (symbols) with modeling predictions: present model (solid lines) and Burke et al. model (dashed lines).

Figure S8. Species concentrations as a function of temperature for the high-pressure ethanol oxidation (60 bar and $\lambda=0.7$). Comparison of experimental results (symbols) with modeling predictions: present model (solid lines) and Burke et al. model (dashed lines).

Figure S9. Species concentrations as a function of temperature for the high-pressure ethanol oxidation (60 bar and $\lambda=1$). Comparison of experimental results (symbols) with modeling predictions: present model (solid lines) and Burke et al. model (dashed lines).

Figure S10. Species concentrations as a function of temperature for the high-pressure ethanol oxidation (60 bar and $\lambda=4$). Comparison of experimental results (symbols) with modeling predictions: present model (solid lines) and Burke et al. model (dashed lines).

3) Sensitivity analysis for ethanol.

Figure S11. Sensitivity analysis for ethanol for different air excess ratios and 20 bar. Top: in the absence of NO (at 725 K). Bottom: in the presence of NO (at 698 K)

1) Evaluation through model calculations of the effect of pressure and gas residence time.

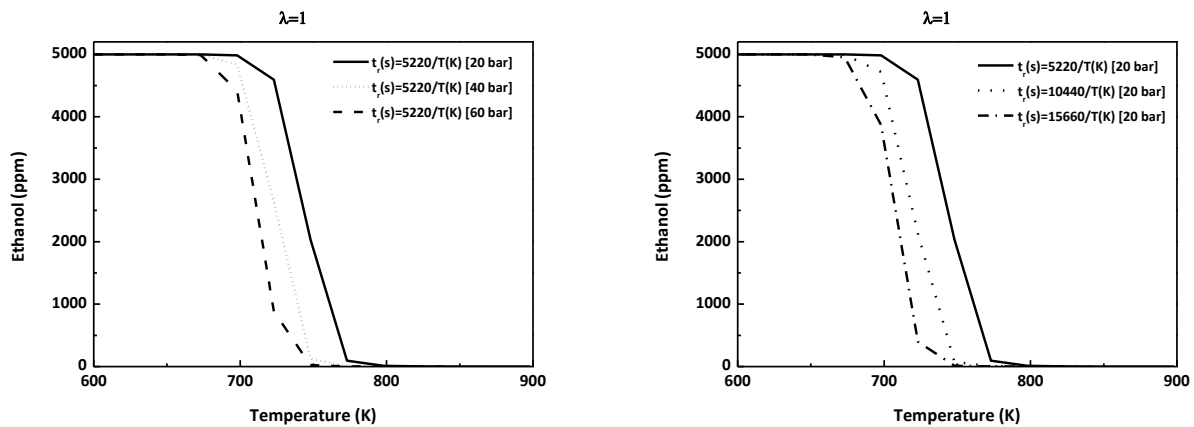


Figure S1. Evaluation through model calculations of the effect of pressure and gas residence time on the ethanol (5000 ppm) conversion, under stoichiometric conditions ($\lambda=1$). Figure S1 (left) includes calculations made at different pressures (20, 40 and 60 bar) and at a constant residence time. Figure S1 (right) includes calculations made at 20 bar and different residence times.

2) Comparison of modeling predictions using the present mechanism (solid lines) and a mechanism from literature (dashed lines) with the high-pressure plug flow reactor experimental data obtained in this work (symbols).

Literature mechanism:

- Burke SM, Metcalfe W, Herbinet O, Battin-Leclerc F, Haas FM, Santner J, Dryer FL, Curran HJ. An experimental and modeling study of propene oxidation. Part 1: speciation measurements in jet-stirred and flow reactors. *Combust. Flame* 2014;161:2765-2784.
- Burke SM, Burke U, Mc Donagh R, Mathieu O, Osorio I, Keese C, Morones A, Petersen EL, Wang W; DeVerter TA, et al. An experimental and modeling study of propene oxidation. Part 2: ignition delay time and flame speed measurements. *Combust. Flame* 2015;162:296-314.

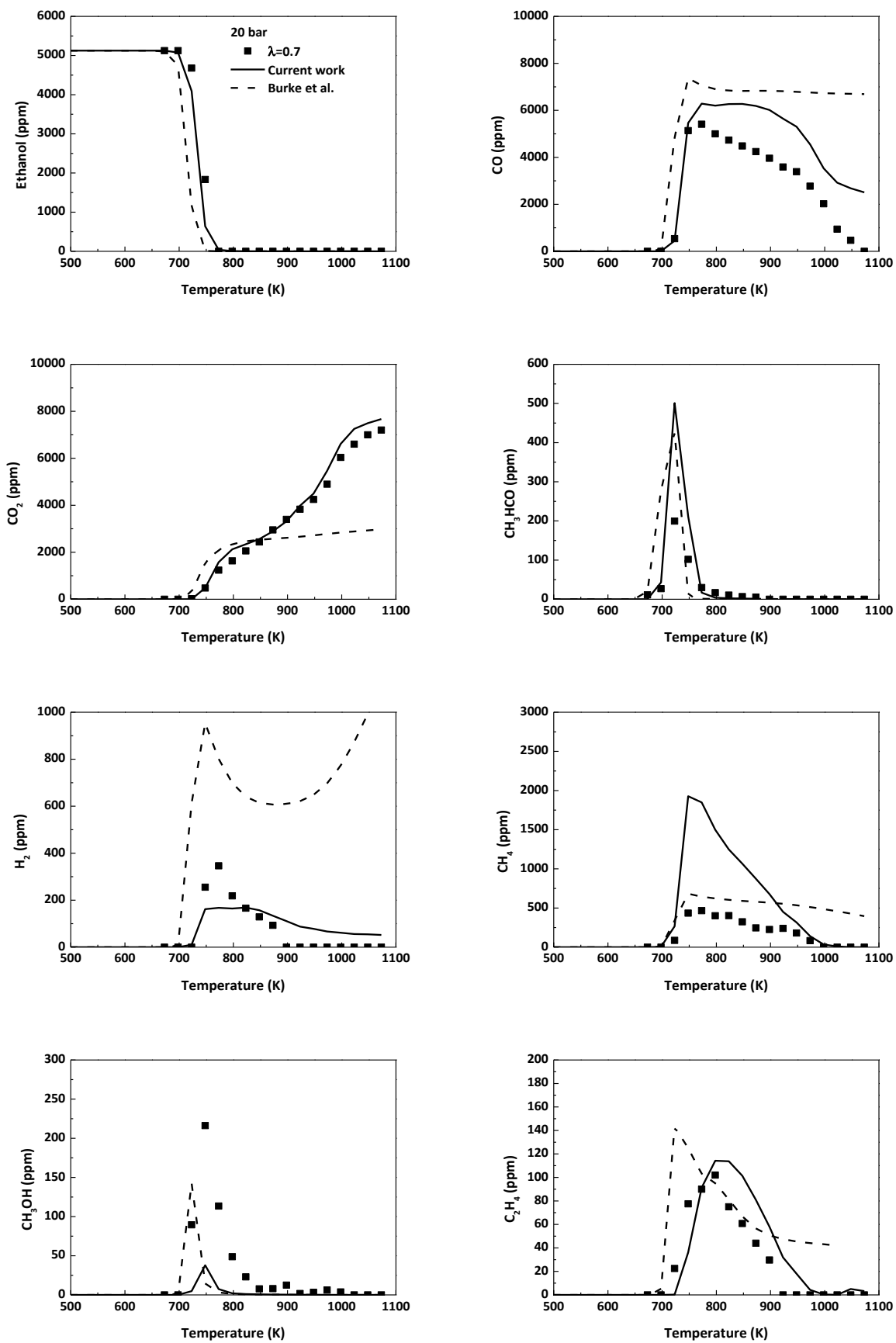


Figure S2. Species concentrations as a function of temperature for the high-pressure ethanol oxidation (20 bar and $\lambda=0.7$). Comparison of experimental results (symbols) with modeling predictions: present model (solid lines) and Burke et al. model (dashed lines).

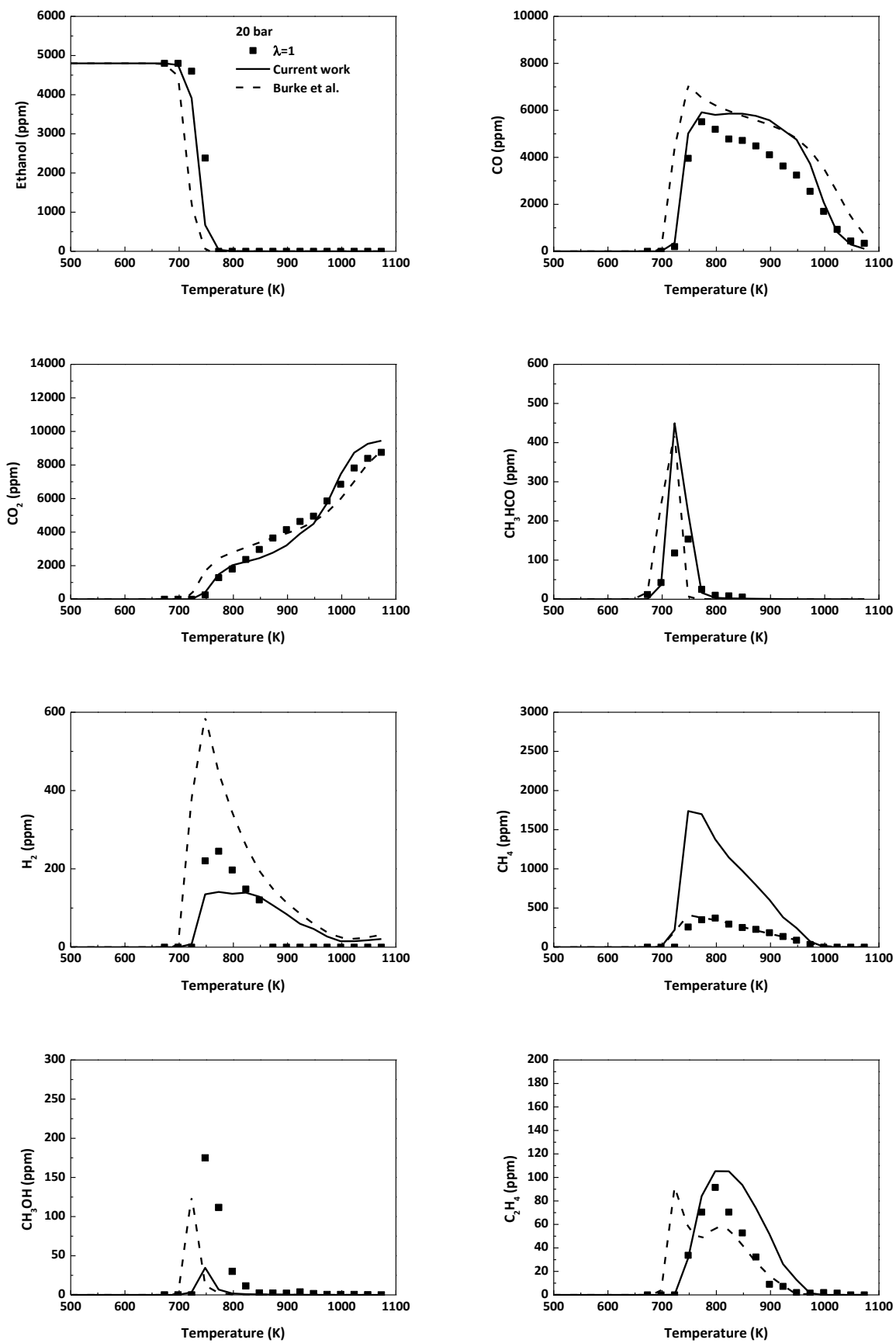


Figure S3. Species concentrations as a function of temperature for the high-pressure ethanol oxidation (20 bar and $\lambda=1$). Comparison of experimental results (symbols) with modeling predictions: present model (solid lines) and Burke et al. model (dashed lines).

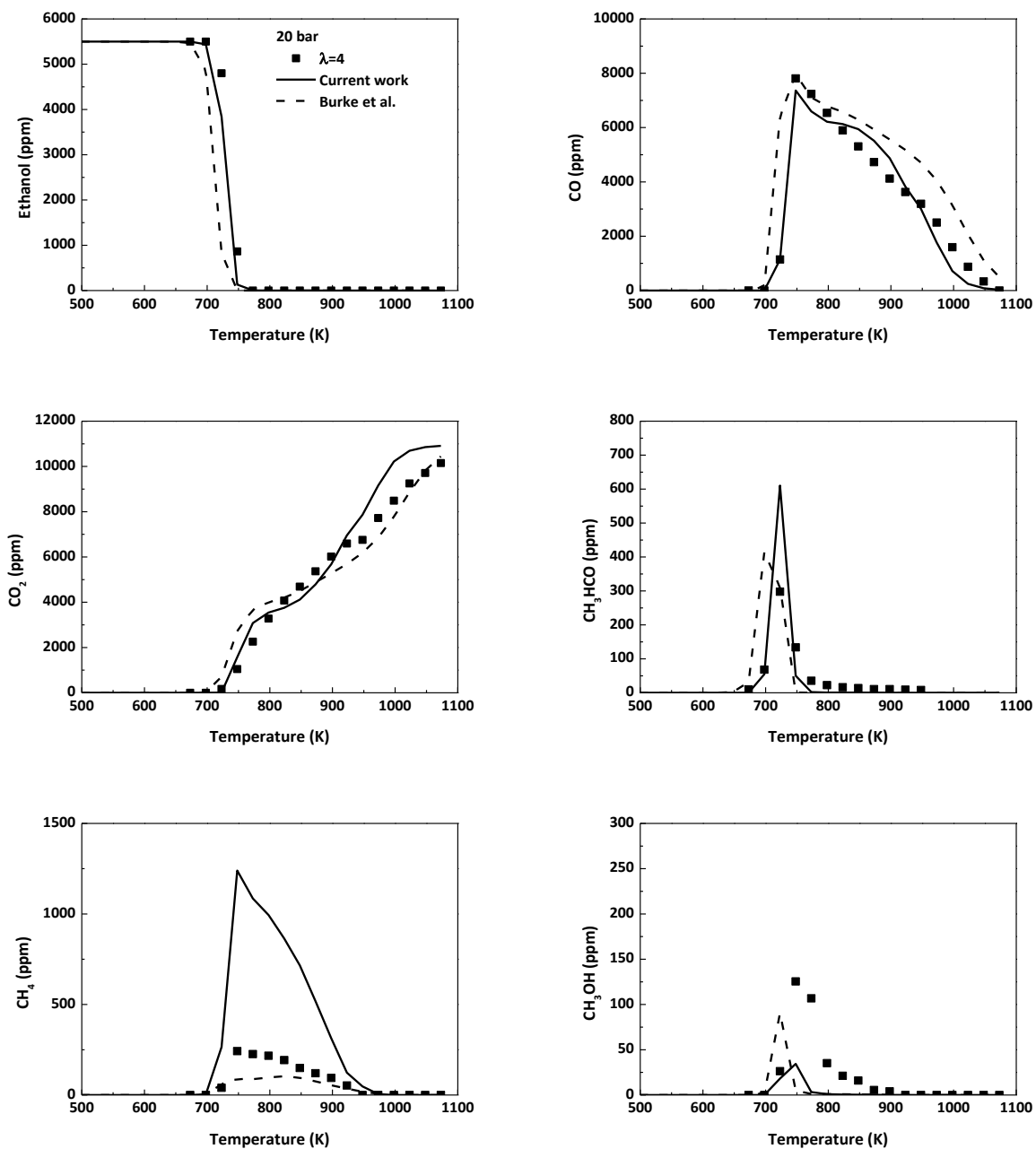


Figure S4. Species concentrations as a function of temperature for the high-pressure ethanol oxidation (20 bar and $\lambda=4$). Comparison of experimental results (symbols) with modeling predictions: present model (solid lines) and Burke et al. model (dashed lines).

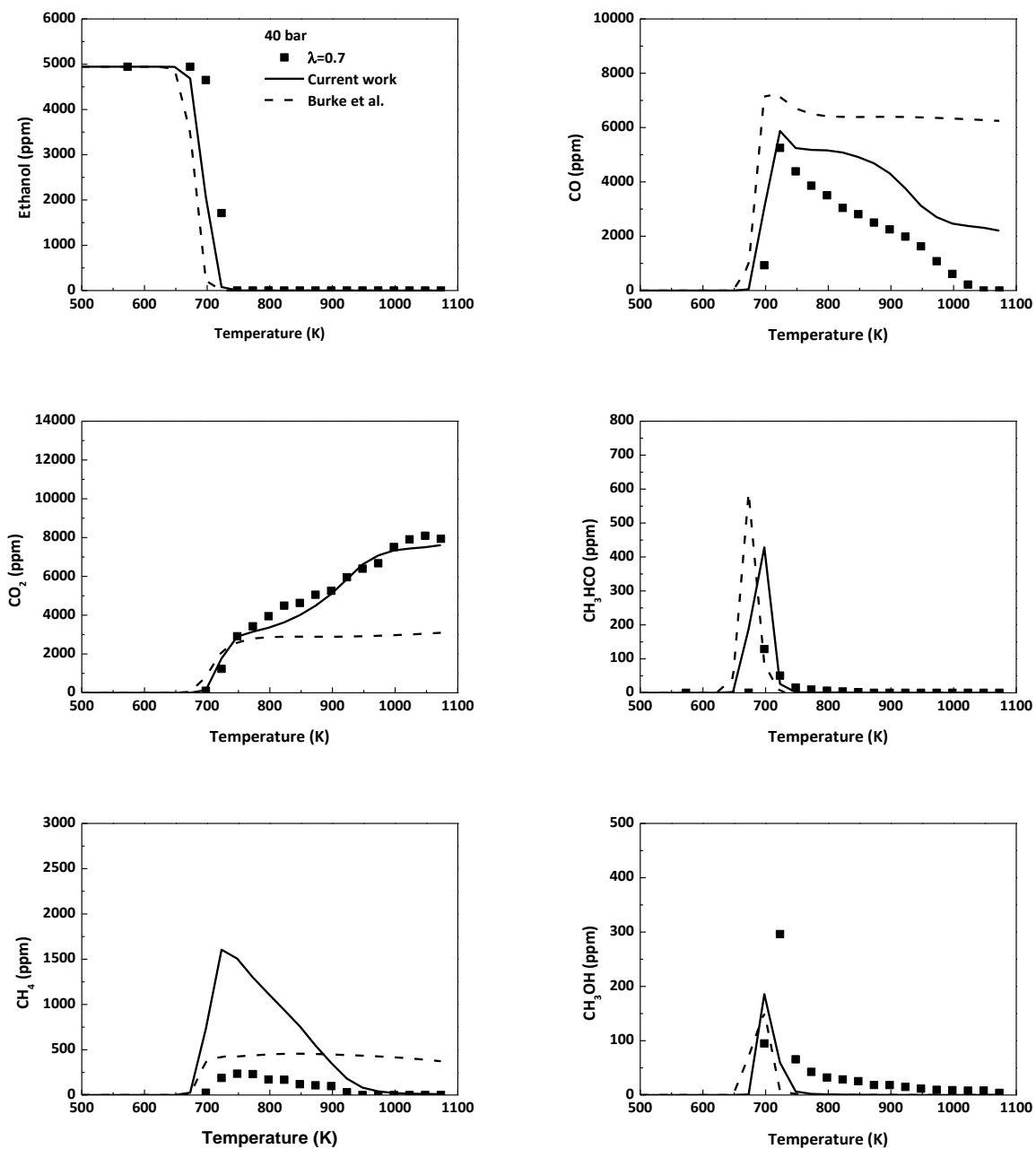


Figure S5. Species concentrations as a function of temperature for the high-pressure ethanol oxidation (40 bar and $\lambda=0.7$). Comparison of experimental results (symbols) with modeling predictions: present model (solid lines) and Burke et al. model (dashed lines).

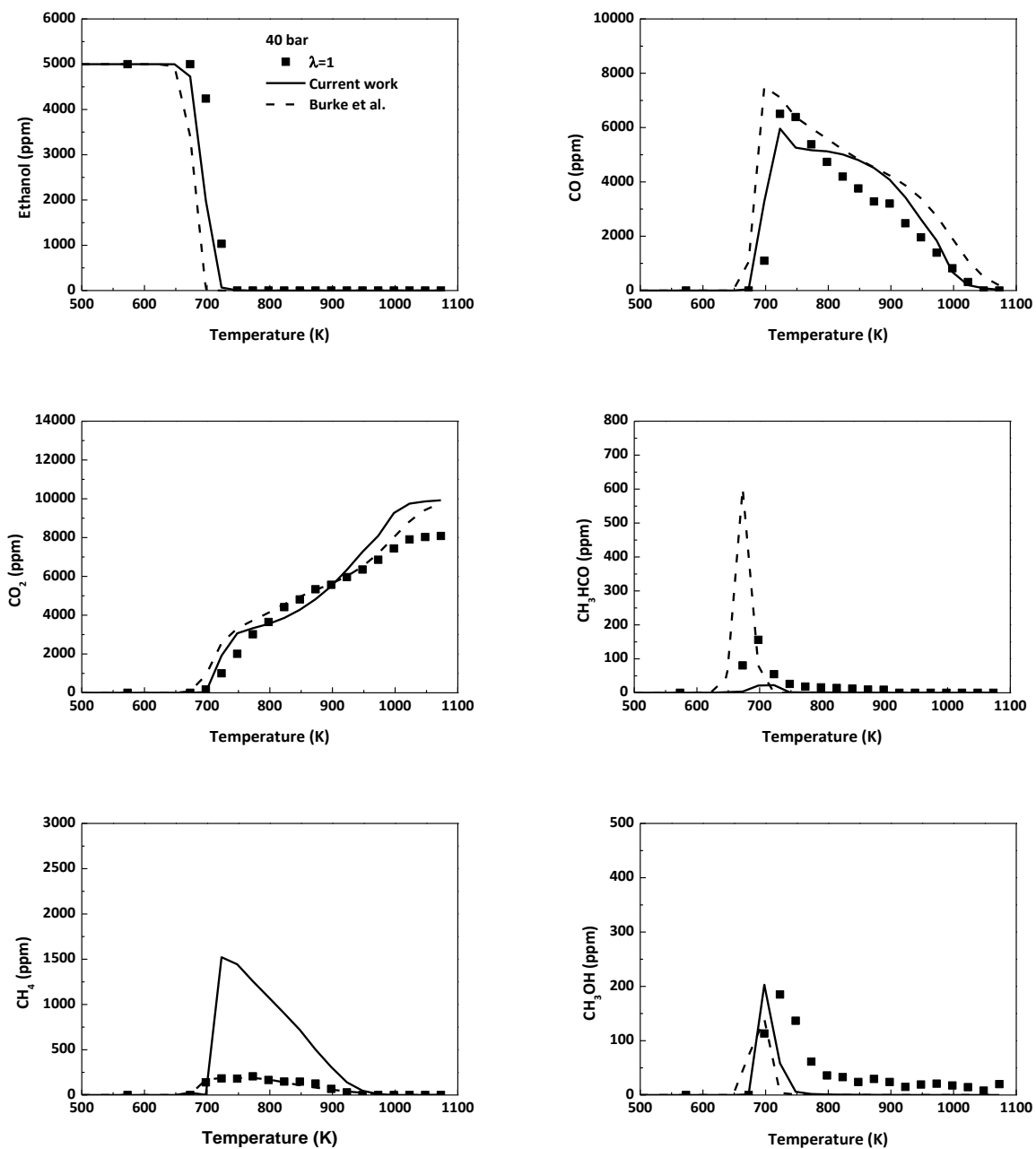


Figure S6. Species concentrations as a function of temperature for the high-pressure ethanol oxidation (40 bar and $\lambda=1$). Comparison of experimental results (symbols) with modeling predictions: present model (solid lines) and Burke et al. model (dashed lines).

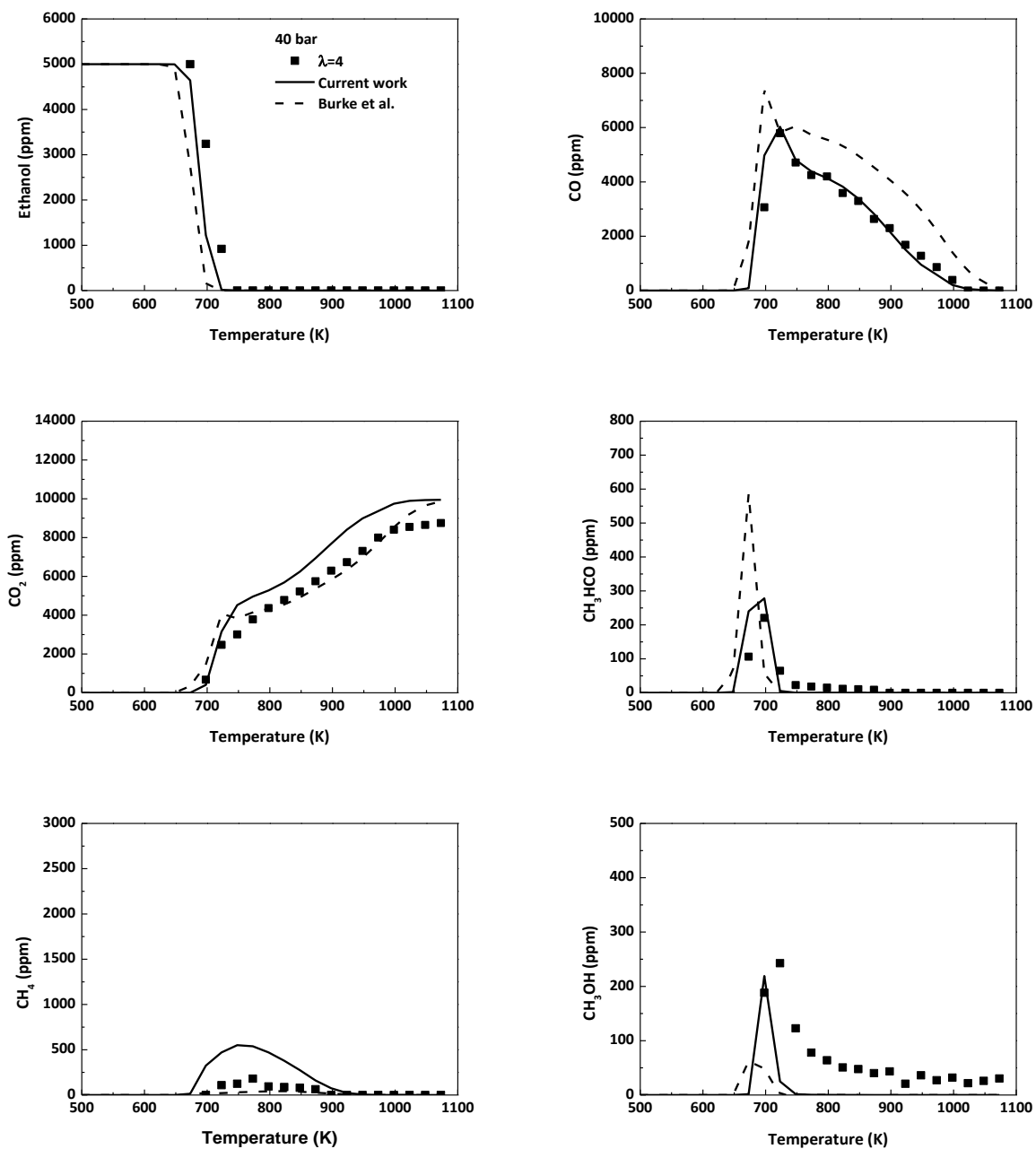


Figure S7. Species concentrations as a function of temperature for the high-pressure ethanol oxidation (40 bar and $\lambda=4$). Comparison of experimental results (symbols) with modeling predictions: present model (solid lines) and Burke et al. model (dashed lines).

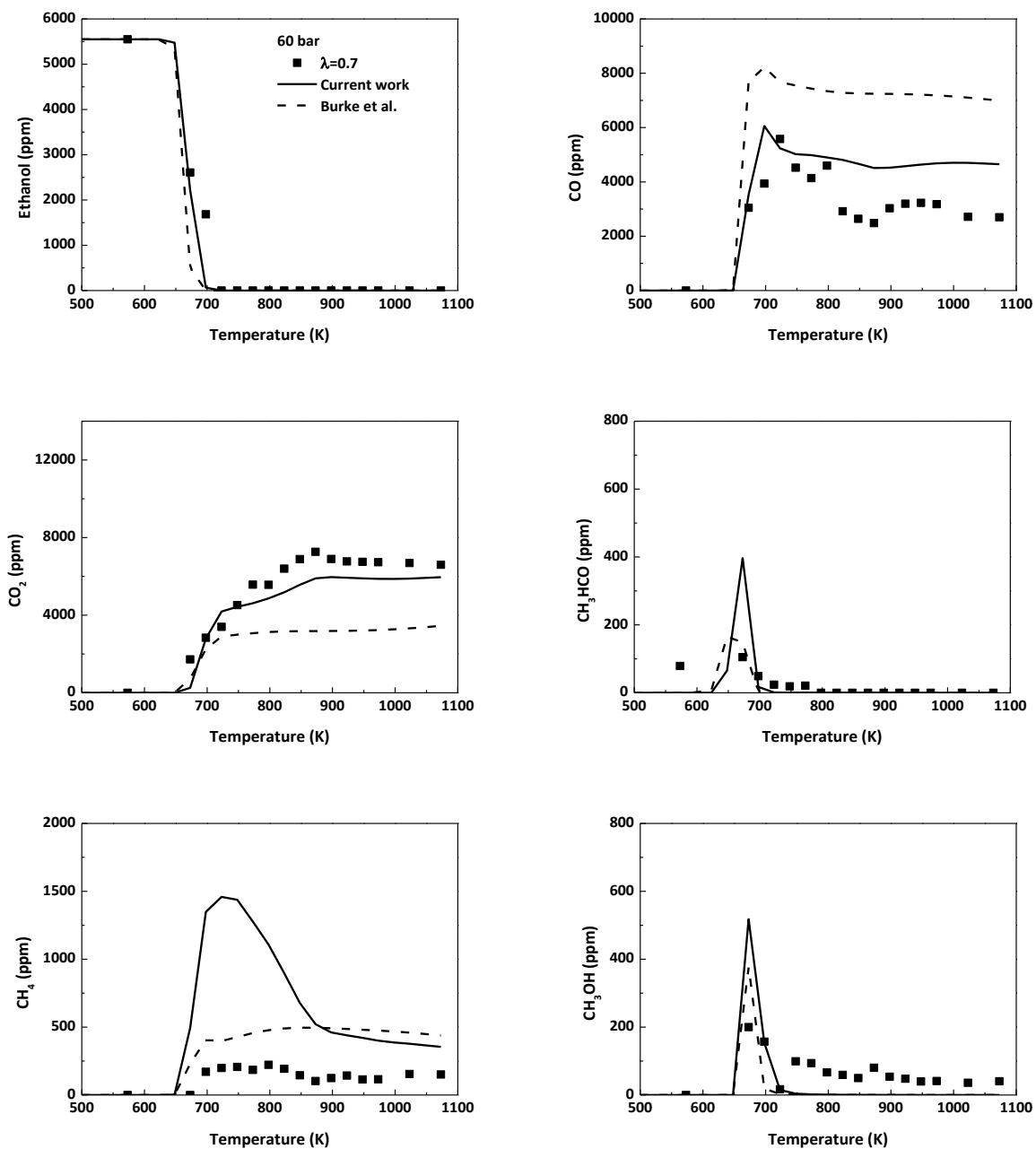


Figure S8. Species concentrations as a function of temperature for the high-pressure ethanol oxidation (60 bar and $\lambda=0.7$). Comparison of experimental results (symbols) with modeling predictions: present model (solid lines) and Burke et al. model (dashed lines).

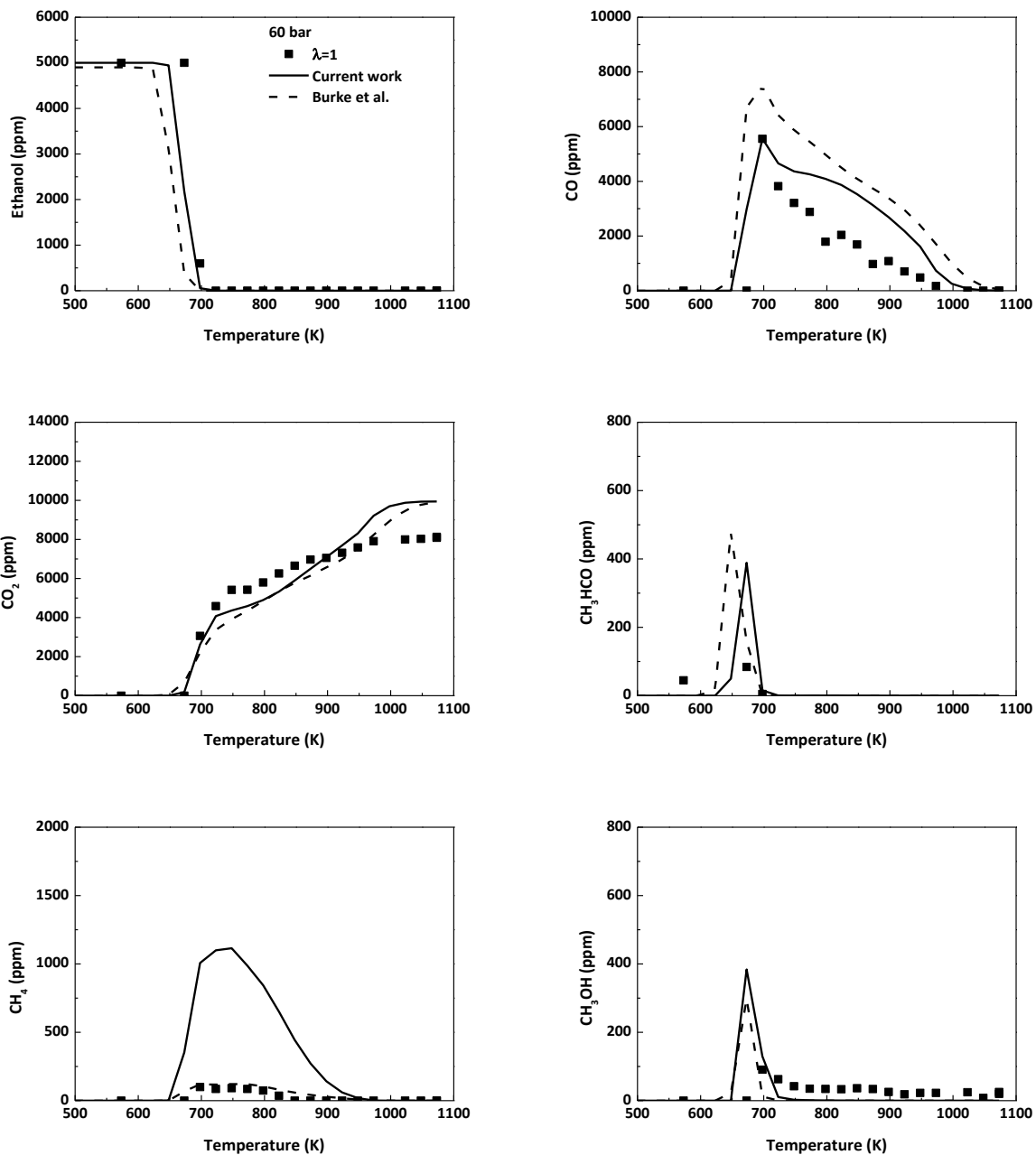


Figure S9. Species concentrations as a function of temperature for the high-pressure ethanol oxidation (60 bar and $\lambda=1$). Comparison of experimental results (symbols) with modeling predictions: present model (solid lines) and Burke et al. model (dashed lines).

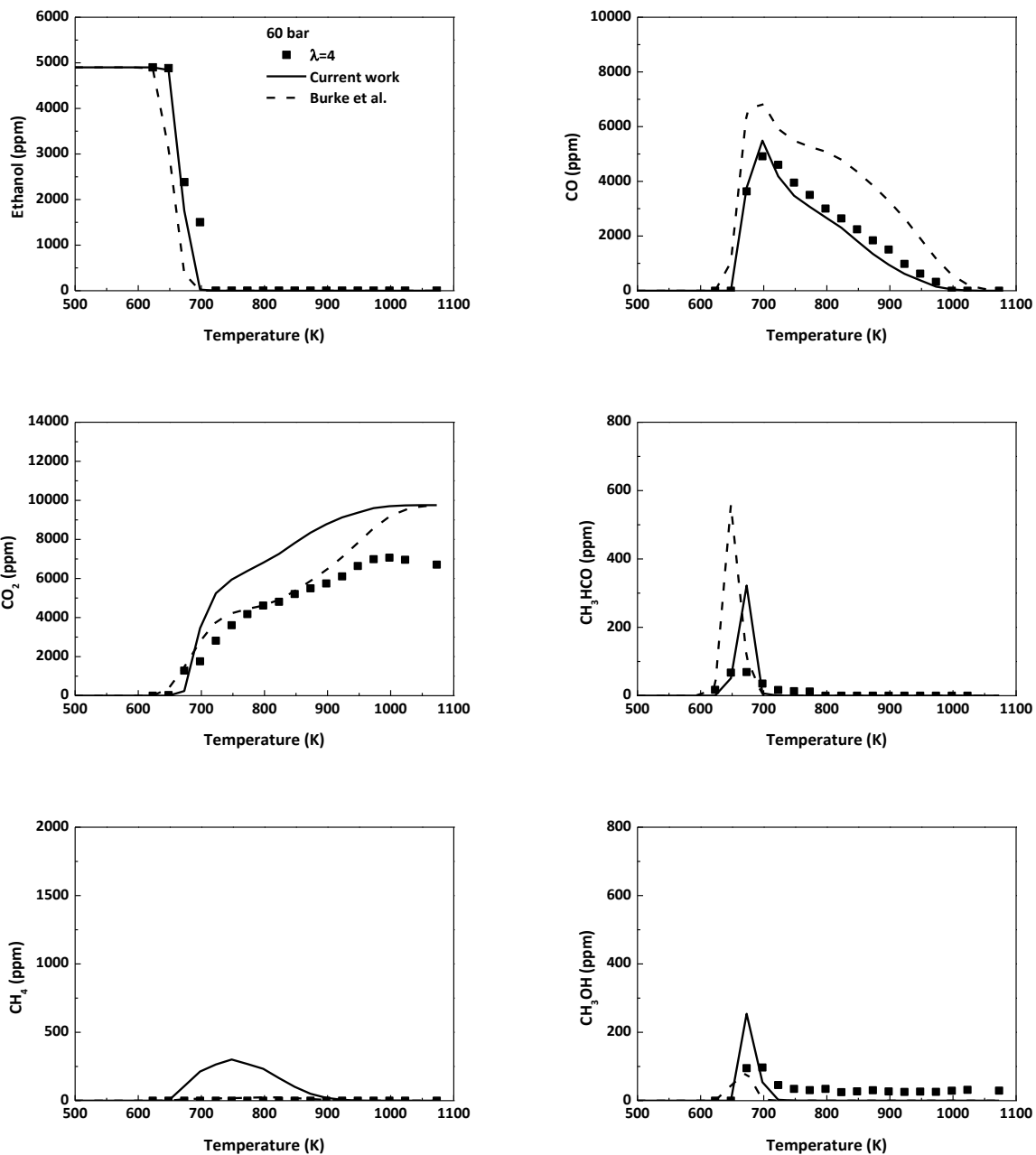


Figure S10. Species concentrations as a function of temperature for the high-pressure ethanol oxidation (60 bar and $\lambda=4$). Comparison of experimental results (symbols) with modeling predictions: present model (solid lines) and Burke et al. model (dashed lines).

3) Sensitivity analysis for ethanol.

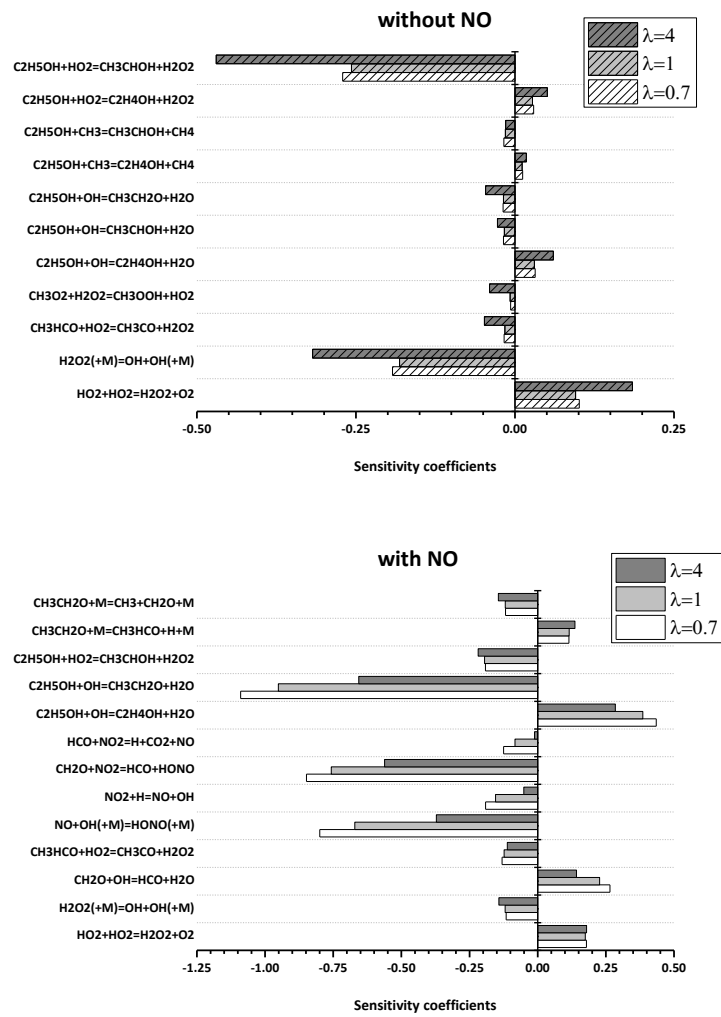


Figure S11. Sensitivity analysis for ethanol for different air excess ratios and 20 bar. Top: in the absence of NO (at 725 K). Bottom: in the presence of NO (at 698 K).

Article IV:

Marrodán, L.; Berdusán, L.; Aranda, V.; Millera, Á.; Bilbao, R.; Alzueta, M.U. (2016). Influence of dimethyl ether addition on the oxidation of acetylene in the absence and presence of NO. *Fuel* 183, 1-8.



Full Length Article

Influence of dimethyl ether addition on the oxidation of acetylene in the absence and presence of NO



Lorena Marrodán, Laura Berdusán, Verónica Aranda, Ángela Millera, Rafael Bilbao, María U. Alzueta*

Aragón Institute of Engineering Research (I3A), Department of Chemical and Environmental Engineering, University of Zaragoza, C/ Mariano Esquillor, S/N, 50018 Zaragoza, Spain

HIGHLIGHTS

- Experimental and modeling study of the C₂H₂-DME mixtures oxidation.
- For fuel-rich conditions, DME presence in the mixtures delays C₂H₂ consumption.
- For fuel-lean conditions, DME presence in the mixtures promotes C₂H₂ consumption.
- An effective NO diminution could be achieved depending on the oxygen availability.
- Competition between HCCO + NO and HCCO + O₂ determines the final NO diminution.

ARTICLE INFO

Article history:

Received 5 March 2016

Received in revised form 20 May 2016

Accepted 2 June 2016

Keywords:

Dimethyl ether
C₂H₂-DME mixtures
Oxidation
Nitrogen oxides

ABSTRACT

Dimethyl ether (DME) is a promising diesel fuel additive for reducing soot and NO_x emissions, because of its interesting properties and the possibility of a renewable production. An experimental and modeling study of the oxidation of acetylene (C₂H₂, considered as an important soot precursor) and DME mixtures has been performed under well-controlled flow reactor conditions. The influence of temperature, air excess ratio (λ) and presence of NO on the oxidation process has been analyzed. Under fuel-rich conditions, the presence of DME in these mixtures modifies the radical pool delaying the acetylene consumption. C₂H₂ and DME, and the radicals generated in their conversion, interact with NO achieving different levels of NO concentration diminution depending upon the operating conditions. Under fuel-lean conditions, the presence of DME in the mixtures increases the NO diminution, whereas for the other values of λ considered, the maximum NO decrease reached is lower than that obtained in the case of pure acetylene.

© 2016 Published by Elsevier Ltd.

1. Introduction

The use of oxygenated compounds as additives to diesel fuels is considered nowadays as a promising alternative for minimizing soot emissions and maybe also NO_x under appropriate conditions [1,2]. Classical oxygenated compounds include alcohols and ethers, and among them, ethanol (C₂H₅OH) and dimethyl ether (CH₃OCH₃, DME) are two of the most popular candidates to be used as additives. The use of ethanol has been extensively studied in the last years and it is already being used in reformulated gasolines, like E85 (85% ethanol and 15% gasoline) [3]. Similarly, DME has received considerable attention because of its high cetane number, vaporization characteristics, low toxicity, and low tendency to produce smoke and volatile organic compounds (VOCs) [4]. Additionally, DME can be produced from renewable materials [5,6].

Ethanol and DME have the same molecular formula (C₂H₆O) but different structure and functional group, and, as it has been discussed in several previous works (e.g. [7,8]), the oxygen content and the specific structure of the oxygenated compound strongly influence the capacity for pollutant emission minimization. Song et al. [9] concluded that, under the conditions of their modeling study, both DME and ethanol were effective in reducing aromatic species (important soot precursors). However, DME exhibited a greater effectiveness due to its higher enthalpy of formation, which led to a higher final flame temperature and consequently to a decrease in aromatic species production in premixed flames [10], but also because of its structure. For fuel-rich conditions, the reaction flux analysis conducted by these authors [9] determined that reactions involving DME convert only approximately 15% of its carbon to C₂-species (key species in the production of aromatic species), whereas reactions of ethanol convert approximately 35% of its carbon to C₂-species.

In previous works of our group, focused on the formation of soot (e.g. [11–13]), acetylene was selected as fuel because it is

* Corresponding author.

E-mail address: uxue@unizar.es (M.U. Alzueta).

recognized as an important soot precursor [14,15]. Furthermore, to analyze the influence of the addition of oxygenated compounds on the reduction of soot emissions, pyrolysis experiments of acetylene-ethanol mixtures were performed [16]. Results indicated that increasing the amount of ethanol in the mixture leads to a diminution on the soot production compared to the acetylene case. The influence of the oxygenated structure was also analyzed by considering the sooting tendency of two isomers, ethanol and DME [17], and the origin of both carbon and, in particular, oxygen appears to be critical for the formation of soot. DME has no C–C bonds and this fact can be the reason for DME to produce less soot than ethanol.

The performance, suitability and proper diesel engine operation of diesel-DME blends have already been reported in different works [18,19]. Therefore, taking into account these promising results, studies under well-controlled laboratory conditions may help to understand the influence of DME addition on the behavior of soot precursors in the overall oxidation process.

In this context, the present work aims to achieve a better knowledge of the C₂H₂-DME mixtures oxidation, as well as of the interaction of these mixtures with NO. A parametric study of the conversion of C₂H₂-DME mixtures has been done, analyzing the influence of temperature, air excess ratio and DME concentration in these mixtures. Experiments have been performed both in the absence and presence of NO, thus allowing to determine both the impact of the NO presence on the oxidation regime of the mixtures and the capability of these mixtures to reduce NO. The experimental results have been interpreted in terms of a detailed kinetic mechanism built up from different individual reaction subsets taken from literature.

2. Experimental

Oxidation experiments of C₂H₂-DME mixtures, both in the absence and presence of NO, have been carried out in a gas-phase installation at atmospheric pressure, which has been described in detail elsewhere (e.g. [7]) and, therefore, only a brief description is given here.

Gases are fed to the system from gas cylinders through mass flow controllers in four separate streams: a main flow containing N₂ and water vapor (fed by saturating a N₂ stream through a water bubbler), and three injector tubes for the reactants (C₂H₂, DME, O₂ and NO). N₂ is used to balance, to obtain a total flow rate of 1000 mL(STP)/min. The injection system has been configured following the investigations of Alzueta et al. [20].

The experiments have been carried out at atmospheric pressure, in the 575–1475 K temperature range and for different values of the air excess ratio (λ), ranging from fuel-rich ($\lambda = 0.2$) to fuel-lean ($\lambda = 20$) conditions. The air excess ratio is defined as the inlet oxygen concentration divided by the stoichiometric oxygen. Approximately, 500 ppm of C₂H₂ and 5000 ppm of water vapor were introduced in all the experiments, whereas for DME, two different amounts, 50 and 200 ppm, have been used. Table 1 lists the conditions of the different experiments.

Reaction takes place in a quartz plug flow reactor, following the design of Kristensen et al. [21], which has a reaction zone of 8.7 mm inside diameter and 200 mm in length. The reactor is placed in a three-zone electrically heated furnace, ensuring a uniform temperature profile throughout the reaction zone within ± 10 K. The temperature in the reaction zone is measured with a type K fine-wire thermocouple placed into a thin tube along the reactor without contact with gases. The total flow rate (1000 mL (STP)/min) is kept constant during the experiments leading to different gas residence times (t_r : 340–132 ms) depending on the temperature in the isothermal reaction zone, being $t_r (s) = 195/T(K)$.

Table 1

Matrix of experimental conditions. The experiments are conducted at constant flow rate of 1000 mL(STP)/min, in the temperature interval of 575–1475 K. The balance is closed with N₂. $t_r (s) = 195/T(K)$.

Set	λ	C ₂ H ₂ (ppm)	DME (ppm)	O ₂ (ppm)	NO (ppm)	H ₂ O (ppm)	Source ^a
1	0.2	500	50	280	0	5000	pw
2	0.2	500	200	370	0	5000	pw
3	0.2	500	200	370	500	5000	pw
4	0.2	500	0	250	500	7000	[23]
5	0.7	500	50	980	0	5000	pw
6	0.7	500	200	1295	0	5000	pw
7	0.7	500	200	1295	500	5000	pw
8	0.7	500	0	875	500	7000	[23]
9	0.7	500	0	875	0	7000	[22]
10	1	500	50	1400	0	5000	pw
11	1	500	200	1850	0	5000	pw
12	1	500	200	1850	500	5000	pw
13	1	500	0	1250	500	7000	[23]
14	20	500	50	28,000	0	5000	pw
15	20	500	200	37,000	0	5000	pw
16	20	500	200	37,000	500	5000	pw
17	20	500	0	25,000	500	5000	pw
18	20	500	0	25,000	0	7000	[22]

^a "pw" denotes present work.

At the end of the reactor, the reaction is efficiently quenched by means of external refrigeration with air. The outlet gas composition is analyzed by a micro-gas chromatograph (Agilent 3000) equipped with TCD detectors. In addition to C₂H₂, CO, CO₂, which are the majority gases, other compounds can be detected by chromatography. Among these, only H₂, CH₄, C₂H₆ and C₂H₄ were detected in appreciable amounts. The DME concentration is measured with an Ati Mattson Fourier transform infrared (FTIR) spectrometer. The NO concentration is measured using a continuous IR analyzer (URAS 26, ABB). The uncertainty of the measurements is estimated as $\pm 5\%$ but not less than 10 ppm, for both the continuous analyzers and the gas chromatograph.

An atomic carbon balance was performed in the experiments by a comparison of the carbon contained in the product gas and the carbon contained in the reactants fed to the reactor, and in all the experiments was closed within $100 \pm 10\%$.

Additional experimental data have been taken from previous works of Alzueta et al. [22] and Abián et al. [23] who, in the same experimental installation, carried out different oxidation experiments of acetylene in the absence and presence of NO, respectively.

3. Reaction mechanism

The experimental results have been analyzed in terms of a detailed gas-phase chemical kinetic model. The mechanism used as starting point for the modeling study is that previously developed by our group for the oxidation of acetylene-ethanol mixtures in the absence and presence of NO [7]. The initial mechanism included the reactions to describe interactions between C₁-C₂ hydrocarbons and NO by Glarborg et al. [24,25], reactions for acetylene conversion by Alzueta et al. [22], and reactions for ethanol oxidation by Alzueta and Hernández [26].

In the present work, the DME reaction subset proposed by Alzueta et al. [27] has been added to the initial mechanism. Moreover, a reaction subset for glyoxal (OCHCHO) oxidation [28] has also been included, because this species is recognized as an important intermediate in hydrocarbons combustion and, at low to medium temperatures, it can be formed during the C₂H₂ oxidation through the sequence: C₂H₂ $\xrightarrow{+OH}$ C₂H₂OH $\xrightarrow{+O_2}$ OCHCHO + OH. In the starting mechanism [7], only one global reaction involving glyoxal decomposition was taken into account.

The full reaction mechanism includes 100 species and 613 reactions. Thermodynamic data for the involved species have been taken from the same sources as the origin mechanisms. The most important reactions are discussed below, and the final updated mechanism is provided as Supplementary material. The Chemkin version can be obtained directly from the authors.

Calculations have been performed using the Senkin code [29], the plug flow reactor code that runs in conjunction with the Chemkin-II library [30], considering constant pressure and temperature in the reaction zone.

4. Results and discussion

A study of the oxidation of C_2H_2 -DME mixtures at atmospheric pressure in the 575–1475 K temperature range has been performed. The influence of temperature, air excess ratio (λ), amount of DME present in the mixture and the presence of NO on the conversion of these mixtures has been analyzed. The study of the influence of these variables has been done by analyzing the outlet concentration of the majority carbon species (C_2H_2 , DME, CO and CO_2) and NO. Other species (CH_4 , C_2H_6 and C_2H_4) have also been detected but in very small amounts and, therefore, their results are not shown.

4.1. C_2H_2 -DME mixtures oxidation in the absence of NO

The air excess ratio (λ) has been varied from fuel-rich ($\lambda = 0.2$) to fuel-lean conditions ($\lambda = 20$), keeping constant the concentration of C_2H_2 (500 ppm) and DME (200 ppm) and the results obtained (corresponding to sets 2, 6, 11 and 15 in Table 1) have been compared. Similar results (not shown) have been obtained for 50 ppm of DME (sets 1, 5, 10 and 14 in Table 1).

Fig. 1 shows the influence of the temperature and air excess ratio on the concentration of DME, C_2H_2 , CO and CO_2 . For CO and CO_2 , the carbon yield has been defined as the $CO_{outlet}/2[C_2H_2 + DME]_{inlet}$ and $CO_{2outlet}/2[C_2H_2 + DME]_{inlet}$ ratios. In general, the

used model provides good agreement between experimental results and modeling calculations, reproducing well the main experimental trends observed. However, certain discrepancies are observed, especially for acetylene. This can be due to the fact that the model exclusively includes gas-phase reactions; it does not consider PAH and soot formation pathways involving C_2H_2 according to HACA route [14], which may be important under given conditions, such as the very fuel-rich conditions ($\lambda = 0.2$) of this work.

As it can be observed in Fig. 1, the onset temperature for C_2H_2 and DME conversion depends on the oxygen availability. This temperature increases as the value of λ decreases, being quite similar for fuel-rich ($\lambda = 0.7$) and very fuel-rich conditions ($\lambda = 0.2$) for acetylene, and also for stoichiometric conditions for DME. The results differ from those reported by Alzueta et al. [22] in a study of pure C_2H_2 oxidation, where the onset for the C_2H_2 conversion was approximately the same, independent of the stoichiometry (values of λ up to $\lambda = 20$). Something similar can be said about DME. In the DME oxidation work by Alzueta et al. [27], the oxygen availability had a slightly influence on the onset of pure DME oxidation. Thus, the results of the present work indicate an effective interaction of the compounds and/or their derivatives in the mixtures.

At the highest temperatures considered, DME is completely consumed for all the λ values studied, even under reducing conditions, because it mainly decomposes thermally above a given temperature, as it is later discussed. Alzueta et al. [27] stated that DME oxidation does not take place or proceeds very slowly at temperatures lower than 1000 K, and this is the behavior observed for the different air excess ratios analyzed, except for $\lambda = 20$, where DME conversion starts at lower temperatures, approximately 100 K less. On the other hand, acetylene is not always completely consumed. For $\lambda = 0.2$, when the oxygen availability is lower, and at the highest temperatures reached, about 250 ppm of C_2H_2 still remain unconverted, which is also predicted by the model. Once DME is completely consumed, C_2H_2 shows a steeper decay. Moreover, at the fuel leanest conditions studied ($\lambda = 20$), the full conversion of

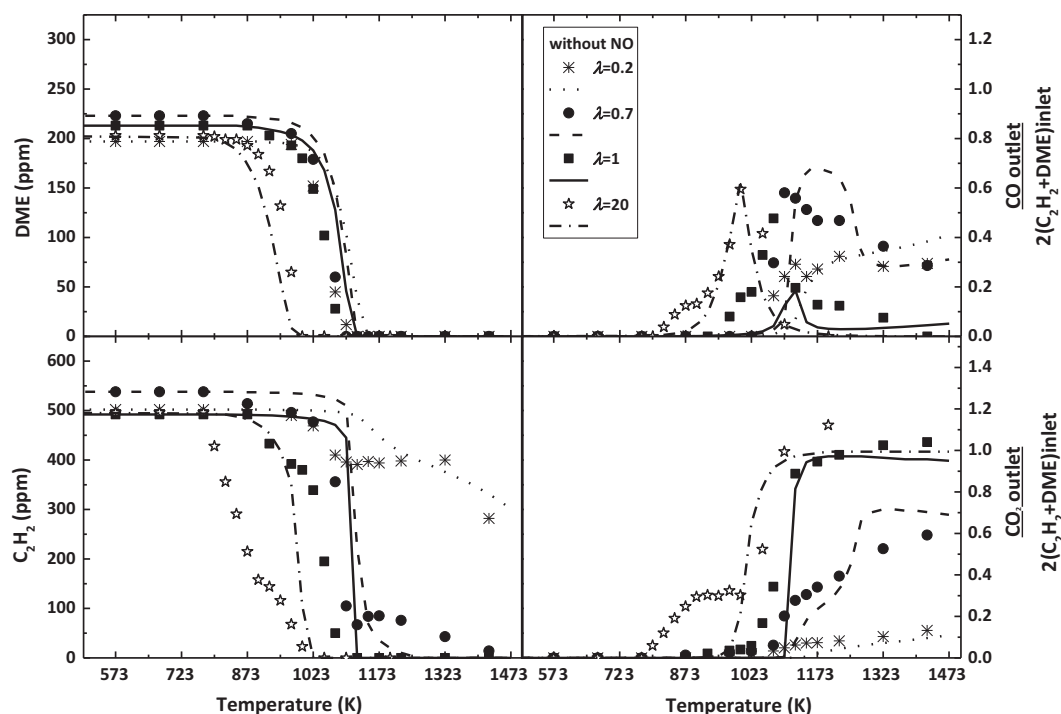


Fig. 1. Concentrations of DME and C_2H_2 , and $CO_{outlet}/2[C_2H_2 + DME]_{inlet}$ and $CO_{2outlet}/2[C_2H_2 + DME]_{inlet}$ ratios as a function of the temperature for different air excess ratios. Comparison between experimental (symbols) and modeling results (lines) (sets 2, 6, 11 and 15 in Table 1).

acetylene occurs approximately at 75 K below compared to stoichiometric conditions. Obviously, what is seen for $\lambda = 20$ is reflected in the CO and CO₂ experimental concentration profiles, which start to be formed as C₂H₂ starts to be consumed. The CO concentration reaches a maximum, and the CO₂ concentration continuously increases reaching a higher value as the conditions become fuel leaner. This is attributed to the fact that after the initiation of the acetylene conversion, mainly by its reaction with O₂ forming formyl radical (HCO) (reaction (R.1)), the main consumption of acetylene occurs through the interaction with O radicals (reaction (R.2)) generating HCCO species. Afterwards, both HCO and HCCO give CO and subsequently CO₂ (reactions (R.3)–(R.6)).



The availability of oxygen affects the temperature at which CO peaks. As the mixture becomes fuel leaner, the CO peak is shifted to lower temperatures and becomes sharper, except for $\lambda = 0.2$, for which the CO concentration increases in all the temperature range studied.

Reaction rate analyses for the oxidation of different C₂H₂-DME mixtures have been performed to identify the reactions that contribute to the C₂H₂ and DME consumption. The results indicate that the main routes for C₂H₂ consumption are similar to those reported by Alzueta et al. [22] for the individual C₂H₂ conversion and that the DME reaction pathways hardly differ from those described by Alzueta et al. [27], even though the presence of certain radicals (e.g. OH radicals) may increase the relevance of some of these routes as described below.

The initiation reactions for C₂H₂ conversion include its interaction with O₂ (reaction (R.1)) and the H, O and OH radicals. The addition of H to C₂H₂ to form vinyl radicals (reaction (R.7)) appears to be an important C₂H₂ consumption reaction, especially for $\lambda = 0.2, 0.7$ and 1.

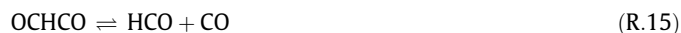
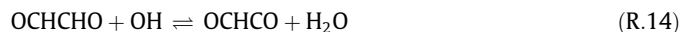
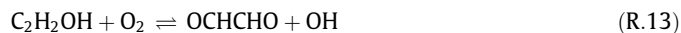
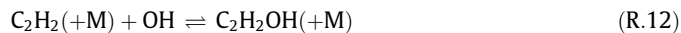


This reaction is in competition with others involving interactions of C₂H₂ with O radicals (reactions (R.2) and (R.8)) and also with OH radicals, but with a minor relevance (reactions (R.9)–(R.11)).



Under fuel-lean conditions, the C₂H₂ interaction with OH radicals to form C₂H₂OH gains relevance (reaction (R.12)). For example, at 873 K, the net rate of production of C₂H₂OH through reaction (R.12) increases from 1.00×10^{-15} mol/cm³ s, for $\lambda = 0.2$, to 1.00×10^{-11} mol/cm³ s, for $\lambda = 20$. The generated species are involved in reactions with oxygen molecular to form glyoxal (OCHCHO, reaction (R.13)), which seems to be an important intermediate in combustion of hydrocarbons as it can be formed from C₂H₂

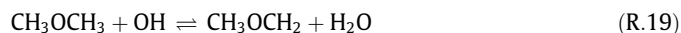
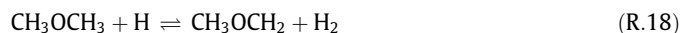
oxidation [28]. Glyoxal reacts with OH radicals to form OCHCO (reaction (R.14)), which finally decomposes to formyl radicals and CO (reaction (R.15)).



On the other hand, the conversion of DME is mainly initiated by its unimolecular decomposition:



Other important consumption reactions include hydrogen abstraction of DME by the radical pool (reactions (R.17)–(R.19)) and interaction of DME with CH₃ radicals (reaction (R.20)) to produce CH₃OCH₂ radicals, which decompose to obtain formaldehyde (reaction (R.21)), that follows the CH₂O → HCO → CO → CO₂ reaction sequence.



To evaluate the influence of the DME amount present in the mixture on the C₂H₂ and DME consumption, in Fig. 2, the results obtained for the experiments performed under fuel-rich ($\lambda = 0.7$) and fuel-lean ($\lambda = 20$) conditions for two different inlet DME amounts (50 and 200 ppm) have been compared (sets 5, 6, 9, 14, 15 and 18 in Table 1). From a previous work of our group [22], results of the C₂H₂ oxidation without DME have been taken as reference. For stoichiometric conditions, similar results (not shown) as those for $\lambda = 0.7$ have been obtained.

The temperature for the onset of the DME conversion is almost independent of the amount present in the mixture (50 or 200 ppm), although for $\lambda = 0.7$ DME is consumed completely at lower temperatures, approximately 75 K less in the experiments, for the DME lowest amount considered.

The DME presence in the mixture has a different impact whether the ambient is fuel-rich or fuel-lean. Whereas for $\lambda = 0.7$, increasing the amount of DME seems to have an inhibiting effect on acetylene consumption, for $\lambda = 20$, the presence of DME shifts the C₂H₂ concentration profiles towards lower temperatures.

Reaction rate analyses have been performed to elucidate this fact. As mentioned before, the main C₂H₂ conversion occurs through its reactions with O₂ (reaction (R.1)) and O and OH radicals (reactions (R.2), (R.8)–(R.11)), but for fuel-rich conditions, reaction (R.7), that involves H addition to form vinyl radicals, becomes a really important C₂H₂ consumption reaction. When DME is present in the mixture, some of these H radicals are then involved in DME consumption (reaction (R.18), DME + H ⇌ CH₃OCH₂ + H₂). For example, at 1023 K, when DME is not present in the mixture, H radical consumption by reaction (R.7) (C₂H₂ + H(+M) ⇌ C₂H₃(+M)) is approximately 34%; when 50 ppm of DME are present in the mixture, this value decreases to 29% (a 33% of H radical consumption is by reaction (R.18)); and, when the amount of DME is increased to 200 ppm, only a 13% of H radicals is consumed by reaction (R.7) (and a 68% by reaction (R.18)). As a result, less H radicals participate in C₂H₂ consumption, and its conversion is shifted

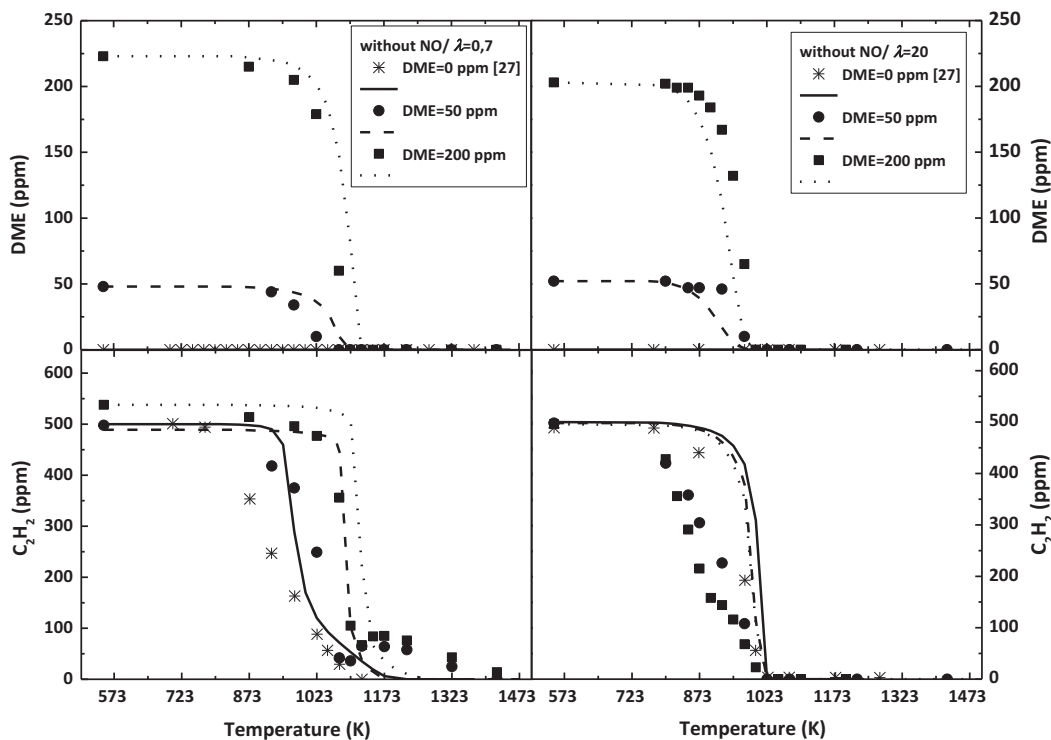


Fig. 2. Concentrations of DME and C_2H_2 as a function of the temperature depending on the DME inlet concentration for $\lambda = 0.7$ (left) and $\lambda = 20$ (right). Comparison between experimental (symbols) and modeling results (lines) (sets 5, 6, 9, 14, 15 and 18 in Table 1).

to higher temperatures when DME is present in the mixture (the higher the DME amount, the higher C_2H_2 conversion temperatures).

On the other hand, when the oxygen availability is increased ($\lambda = 20$, right in Fig. 2), the conversion of both DME and acetylene occurs at lower temperatures than for fuel-rich conditions, and the presence of DME in the reactant mixture promotes C_2H_2 conversion (there is not a big difference in adding 50 or 200 ppm of DME to the reactant mixture), although it can only be observed experimentally. One probable explanation could be that the presence of DME in the mixture entails a greater amount of oxygen that can react with both C_2H_2 and DME. The formation of OH radicals is enlarged because of the increase in the available oxygen and DME is mainly consumed by its reaction with OH (reaction (R.19)). Acetylene reacts with O_2 too (reaction (R.1)), but also with O and OH radicals (reactions (R.2) and (R.8)–(R.11)), which formation is increased because of the fuel-leaner conditions. As a result, both DME and C_2H_2 conversions are shifted to lower temperatures than for fuel-rich conditions. However, at present, the model fails to reproduce the C_2H_2 profile, probably due to uncertainties in the mechanism describing C_2H_2 conversion.

4.2. C_2H_2 -DME mixtures oxidation in the presence of NO

Although some authors indicate that NO_x emissions when DME is used as fuel are higher or of a similar level than with diesel fuel in a compression ignition engine at the same operating conditions (e.g. [31]), others indicate that when operating under optimized conditions (such as changing the injection system), NO_x emissions from DME are lower than from diesel [32]. Those studies correspond to experiments in real engines, and may be significantly different or involve many different parameters affecting the global results. Thus, studies carried out under well-controlled conditions may be helpful to understand how the DME-NO interaction proceeds. Therefore, oxidation experiments of C_2H_2 -DME mixtures in

the presence of NO, for different air excess ratios, have also been carried out (Table 1).

NO may interact with C_2H_2 , DME and their derivatives, achieving some degree of diminution depending on the conditions. Under fuel-rich conditions, NO could be decreased by reburn reactions by reacting with hydrocarbon radicals produced during the oxidation of DME and C_2H_2 [20,33–35]. Under fuel-lean conditions, NO may favor the oxidation of the C_2H_2 -DME mixture in a mutually sensitized oxidation process, similar to what has been observed for other compounds such as methane [36], ethanol and methanol [37].

To elucidate the impact of the DME presence in the C_2H_2 -DME mixtures for NO diminution, the present experimental results have been compared (Fig. 3) with those of Abián et al. [23] for the interaction between C_2H_2 and NO for different air excess ratios

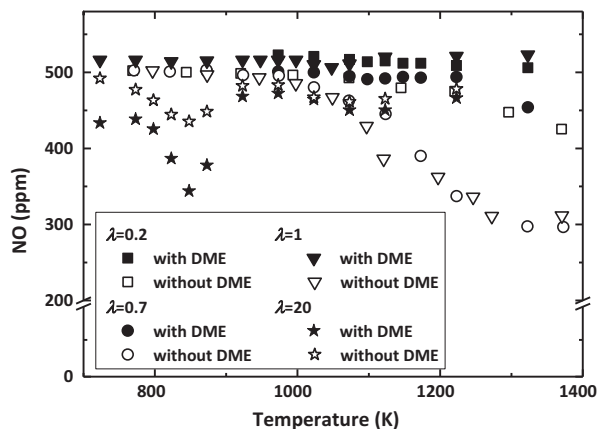


Fig. 3. Experimental results for NO concentration as a function of the temperature for different air excess ratios in the presence (solid symbols) and absence (empty symbols) [23] of DME (sets 3, 4, 7, 8, 12, 13, 16 and 17 in Table 1).

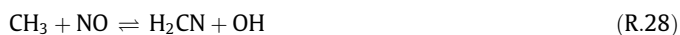
(corresponding to sets 4, 8 and 13 in Table 1). To complete that work, an experiment under similar conditions, but for $\lambda = 20$, has been performed in the present work (set 17 in Table 1).

When no DME is present in the mixture, at temperatures higher than 1300 K and for $\lambda = 0.7$ and 1, the NO amount decreases from 500 ppm to about 300 ppm, which means a 40% diminution in NO. This represents the highest NO decrease percentage achieved under the conditions of this work, because for $\lambda = 0.2$ only a 15% and for $\lambda = 20$ a 13% (at lower temperatures) decrease in NO were respectively obtained. When DME is present in the mixture, it has its main effect under fuel-lean conditions, when the NO decrease percentage rises from 13% up to 30%.

Consistent with modeling predictions, and in concordance with literature [22,23], acetylene is an important source of HCCO radicals ($C_2H_2 + O \rightleftharpoons HCCO + H$, reaction (R.2)). These radicals can be involved in the NO concentration diminution. For fuel-rich conditions, HCCO radicals interact with NO (reactions (R.22) and (R.23)) explaining the NO experimental decrease of 40% for $\lambda = 0.7$ and 1, and 15% for $\lambda = 0.2$, at 1300 K, in the absence of DME. However, by increasing the oxygen concentration ($\lambda = 20$), the HCCO + NO reactions are less important and the HCCO + O₂ reactions (reactions (R.24) and (R.25)) predominate. Due to this fact, for $\lambda = 20$, when no DME is added, the NO diminution occurs only by conversion to NO₂ (reaction (R.26)), resulting in a lower NO lessening achieved. Thus, the competition between these two HCCO radicals consumption steps (with NO or O₂) determines the final level of NO lessening achieved.



Under fuel-lean conditions, the DME addition causes an increase in the NO diminution (experimentally from a 13% up to 30%) due to its interaction with CH₃ radicals (which are generated by DME decomposition, reaction (R.16)) by reactions (R.27) and (R.28).



To deeply analyze the influence of the NO presence on the oxidation of the C₂H₂-DME mixtures, the DME and C₂H₂ experimental results and calculations (Fig. 4) can be compared with those earlier represented in Fig. 1 (under similar experimental conditions but in the absence of NO). Calculations predict reasonably well the trends obtained, with the exception of NO conversion under fuel-rich conditions, which is overestimated.

The presence of NO has its major effect under fuel-lean conditions, causing both C₂H₂ and DME concentration profiles to shift to lower temperatures; a shift of more than 200 K in the temperature for the onset of DME oxidation, similar to that observed by Alzueta et al. [27] in the study of pure DME oxidation in the presence of NO.

Reaction rate analyses performed indicate that the main routes for C₂H₂ and DME conversion, already described in the absence of NO, are mostly the same than those obtained in the presence of NO for the conditions studied in this work. In the initial steps of C₂H₂ conversion (approximately 850–875 K), the reaction of C₂H₂ with OH (reaction (R.12)), important under oxidizing conditions, becomes even more relevant in presence of NO. It represents the

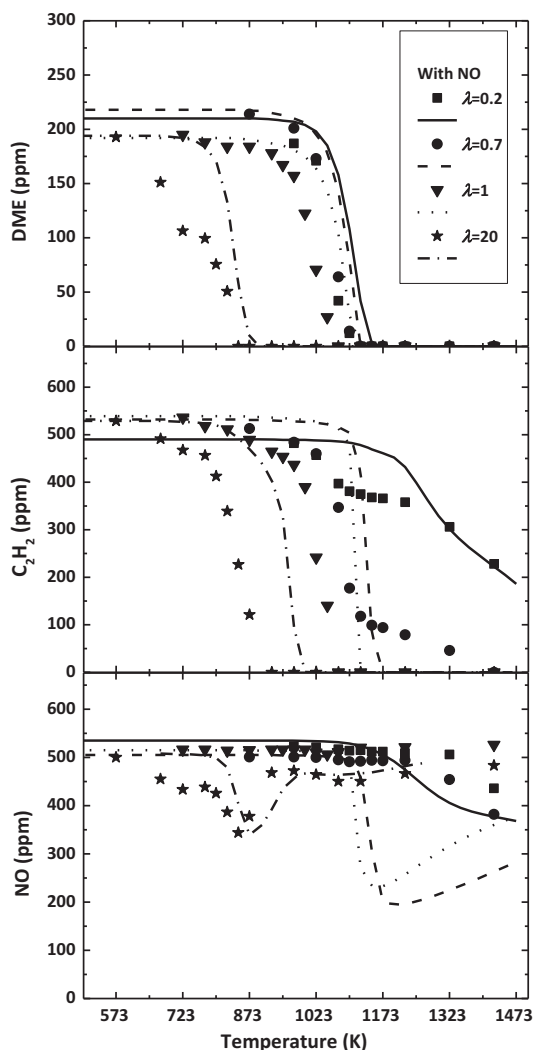


Fig. 4. Concentrations of DME, C₂H₂ and NO as a function of temperature for different air excess ratios. Comparison between experimental (symbols) and modeling results (lines) (sets 3, 7, 12 and 16 in Table 1).

first step in the formation of glyoxal (reaction (R.13)), an important intermediate under these conditions. The presence of NO also enhances reactions of acetylene consumption and HCCO and CH₂ radicals generation (reactions (R.2) and (R.8), respectively). As a result, the C₂H₂ oxidation in the presence of NO becomes faster under oxidizing conditions.

For $\lambda = 20$ and in the presence of NO, the main reaction routes for DME change slightly. The main consumption of DME is by interaction with OH radicals through reaction (R.19) (i.e. $CH_3OCH_3 + OH \rightleftharpoons CH_3OCH_2 + H_2O$). The DME radicals (CH_3OCH_2) generated react with O₂ forming peroxy species, which continue reacting until formaldehyde is obtained (reactions (R.29)–(R.31)). Alzueta et al. [27] stated that, at temperatures lower than 900 K, the DME oxidation route through methoxymethyl-peroxy ($CH_3OCH_2-O_2$) may be important, similarly to that observed in the oxidation of dimethoxymethane ($CH_3OCH_2OCH_3$) under oxidizing conditions and increasing pressure [38].

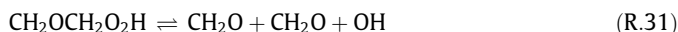
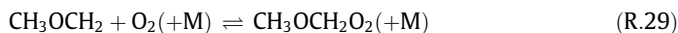


Table 2
Linear sensitivity coefficients for CO for the selected sets^a.

Reaction	Set 2 1073 K	Set 3 1073 K	Set 6 1023 K	Set 7 1023 K	Set 10 973 K	Set 11 998 K	Set 12 998 K	Set 15 848 K	Set 16 798 K
$C_2H_2 + O_2 \rightleftharpoons HCO + HCO$	0.433	0.402	0.929	0.930	1.128	1.001	1.023	1.056	1.714
$C_2H_2 + O \rightleftharpoons HCCO + H$	0.018	-0.004	0.025	0.003	0.060	0.029	0.008	0.025	0.053
$C_2H_2 + H(+M) \rightleftharpoons C_2H_3(+M)$	0.011	0.009	0.039	0.039	0.114	0.047	0.057	0.013	0.037
$C_2H_2OH + O_2 \rightleftharpoons OCHCHO + OH$	-	-	-	-	-	-	-	0.005	0.056
$OCHCHO + OH \rightleftharpoons OCHCO + H_2O$	-	-	-	-	-	-	-	0.002	0.066
$C_2H_3 + O_2 \rightleftharpoons CH_2O + HCO$	0.072	0.081	0.038	0.055	0.055	0.024	0.042	-0.001	-0.008
$CH_3 + CH_3(+M) \rightleftharpoons C_2H_6(+M)$	-0.185	-0.212	-0.063	-0.074	-0.084	-0.049	-0.063	-0.104	-0.256
$CH_3 + HO_2 \rightleftharpoons CH_3O + OH$	0.007	-	0.021	-	0.183	0.037	-	0.286	0.001
$CH_4 + OH \rightleftharpoons CH_3 + H_2O$	0.057	0.055	0.015	0.015	0.019	0.011	0.013	0.000	0.001
$CH_2O + OH \rightleftharpoons HCO + H_2O$	0.053	0.063	0.033	0.041	0.126	0.035	0.054	0.051	0.541
$CH_2O + H \rightleftharpoons HCO + H_2$	0.137	0.154	0.032	0.038	0.020	0.021	0.030	0.001	0.003
$CH_2O + CH_3 \rightleftharpoons HCO + CH_4$	0.387	0.405	0.107	0.112	0.046	0.067	0.076	0.005	0.009
$HCO + M \rightleftharpoons H + CO + M$	-0.006	-0.012	-0.007	-0.035	0.068	0.001	-0.043	0.037	0.017
$HCO + O_2 \rightleftharpoons CO + HO_2$	0.006	0.009	0.007	0.017	-0.067	-0.001	0.021	-0.038	0.035
$HCCO + O_2 \rightleftharpoons CO + CO + OH$	0.007	0.004	0.007	0.012	-0.003	0.007	0.016	0.007	0.010
$CH_3OCH_3 \rightleftharpoons CH_3O + CH_3$	0.839	0.861	0.167	0.170	0.024	0.073	0.071	-	-
$CH_3OCH_3 + H \rightleftharpoons CH_3OCH_2 + H_2$	-0.348	-0.313	-0.304	-0.304	-0.479	-0.295	-0.353	-0.008	-0.008
$CH_3OCH_3 + O \rightleftharpoons CH_3OC + H_2 + OH$	-0.012	-0.003	-0.021	-0.011	-0.016	-0.026	-0.014	-0.017	0.023
$CH_3OCH_3 + OH \rightleftharpoons CH_3OCH_2 + H_2O$	-0.057	-0.067	-0.041	-0.051	-0.159	-0.043	-0.069	-0.033	0.831
$CH_3OCH_3 + CH_3 \rightleftharpoons CH_3OCH_2 + CH_4$	0.063	0.065	0.024	0.024	0.007	0.016	0.016	0.002	0.000
$CH_3OCH_2 \rightleftharpoons CH_3 + CH_2O$	-	-	-	-	-0.001	-	0.000	-0.026	0.140
$CH_3OCH_3 + O_2(+M) \rightleftharpoons CH_3OCH_2O_2(+M)$	-	-	-	-	-	-	-	0.006	-0.035
$CH_3OCH_2 + O_2 \rightleftharpoons CH_2O + CH_2O + OH$	-	-	-	-	-	-	-	0.007	-0.041
$CH_2OCH_2O_2H \rightleftharpoons CH_2O + CH_2O + OH$	-	-	-	-	-	-	-	0.001	-0.027
$O + OH \rightleftharpoons O_2 + H$	0.110	0.061	0.118	0.077	0.269	0.122	0.093	0.158	0.277
$H + O_2 + N_2 \rightleftharpoons HO_2 + N_2$	0.007	0.010	0.004	0.011	-0.062	0.000	0.014	-0.173	-0.204
$CH_3 + NO \rightleftharpoons HCN + H_2O$	-	-0.011	-	-0.004	-	-	-0.003	-	-0.008
$CH_3 + NO \rightleftharpoons H_2CN + OH$	-	0.072	-	0.033	-	-	0.031	-	0.020
$C_2H_3 + NO \rightleftharpoons C_2H_2 + HNO$	-	0.005	-	0.011	-	-	0.014	-	0.080
$HCO + NO \rightleftharpoons HNO + CO$	-	0.004	-	0.019	-	-	0.024	-	-0.022
$HCCO + NO \rightleftharpoons HCN + CO_2$	-	-0.010	-	-0.017	-	-	-0.021	-	-0.012
$CH_3 + NO_2 \rightleftharpoons CH_3O + NO$	-	0.004	-	0.015	-	-	0.035	-	0.049
$NO_2 + H \rightleftharpoons NO + OH$	-	-0.002	-	-0.007	-	-	-0.015	-	-0.069

^a The sensitivity coefficients are given as $A_i \delta Y_j / Y_j \delta A_i$, where A_i is the pre-exponential constant for reaction i and Y_j is the mass fraction of the j th species. Therefore, the sensitivity coefficients listed can be interpreted as the relative change in predicted concentration for the species j caused by increasing the rate constant for reaction i by a factor of 2.

The interactions between DME and NO, that could produce a NO diminution, were also analyzed by Alzueta et al. [27]. These authors indicated that, under fuel-rich and stoichiometric conditions and temperatures above 1100 K, some NO is reduced and converted into HCN and N_2 by reburn-type reactions with the radicals generated from DME decomposition. However, under fuel-lean conditions and in the 800–1000 K temperature range, a considerable fraction of NO is oxidized to NO_2 (a 20% experimentally and a 40% based on modeling predictions), while no net NO_x reduction is observed.

In the case of C_2H_2 -DME mixtures, NO decreases of approximately 30% have been achieved (Fig. 4) only under oxidizing conditions and temperatures near 850 K, where the production of glyoxal (reaction (R.13)) seems to be important. The glyoxal produced decomposes to formyl radicals (reactions (R.14) and (R.15)), and subsequently produces HO_2 (reaction (R.32)).



Moreover, under these conditions of high oxygen availability ($\lambda = 20$, and NO presence), DME is initially converted into CH_3OCH_2 radicals through reaction (R.33), increasing the formation of HO_2 radicals.



Reaction rate analyses indicate that NO is converted into NO_2 by reaction with HO_2 radicals (reaction (R.26)), but NO_2 is recycled back to NO by reaction with hydrogen atoms (reaction (R.34)) and CH_3 radicals (reaction (R.35)), so no net reduction of NO_x is achieved.



A first-order sensitivity analysis to the kinetic parameters included in the mechanism used for modeling calculations has been performed for selected experiments, both in the absence and presence of NO. The impact on the CO concentration has been evaluated. Table 2 shows the results obtained. The temperatures chosen for the analysis correspond to the initiation conditions of the conversion of the mixtures, i.e., when CO has reached a value of approximately 10 ppm.

The results obtained indicate that C_2H_2 conversion in the presence of DME is sensitive to almost the same reactions as in the absence of this additive [22]. It is worth to note that only under fuel-lean conditions the reactions involving glyoxal (OCHCHO) present a high sensitivity, and also the DME oxidation route through methoxymethyl-peroxy ($CH_3OCH_2O_2$). Results are also sensitive to reactions involved in NO reduction, in particular to those that imply the competition between $HCCO + NO$ and $HCCO + O_2$, and also $CH_3 + NO_2$.

5. Conclusions

A study of the conversion of C_2H_2 -DME mixtures at atmospheric pressure, analyzing the influence of temperature, air excess ratio (λ) and presence of NO has been performed under flow reactor conditions. The results obtained have been interpreted in terms of a detailed kinetic mechanism. An extensive discussion including a comparison of the results with the literature data of individual C_2H_2 [22] and DME [27] oxidation, in the absence and presence of NO [23], has been made.

Unlike what observed in their individual behaviors, the onset temperature for the C_2H_2 and DME conversion in the oxidation of their mixtures depends on the oxygen availability, being lower for the highest value of the air excess ratio considered ($\lambda = 20$). The reaction pathways for C_2H_2 conversion in the presence of DME are basically the same as those in its absence. In this way, the DME addition only modifies the radical pool, and it could act as an inhibitor or promoter in acetylene consumption depending on the oxygen availability and the amount of DME present in the mixture. For fuel-rich conditions, increasing the amount of DME in the mixture seems to have an inhibitory effect on C_2H_2 consumption. When DME is present in the mixture, less H radicals participate in acetylene consumption through the H addition to form vinyl radicals, and as a consequence, acetylene conversion is shifted to higher temperatures. However, for fuel-lean conditions, the trend is the opposite, and the DME presence promotes C_2H_2 conversion, probably due to the increasing of O and OH radical formation which is favored because of the fuel-leaner conditions. Therefore, both DME and C_2H_2 conversions are shifted to lower temperatures.

Acetylene, DME and their intermediates may interact with NO, reaching different NO diminution levels depending on the conditions. The higher NO decrease levels were achieved in absence of DME for temperatures above 1100 K and fuel-rich ($\lambda = 0.7$) and stoichiometric conditions ($\lambda = 1$). This is due to the competition between reactions of HCCO with NO and with O_2 . By increasing the oxygen availability, the HCCO + O_2 reactions predominate reaching a lower NO decrease level. However, under fuel-lean conditions ($\lambda = 20$), the presence of DME increases the NO diminution from 13 to 30% mainly due to CH_3 radicals generated from its conversion, which can react with NO or NO_2 .

In general, modeling predictions are in good agreement with the experimental data trends obtained for the conditions studied. The model is able to reproduce the main experimental trends for C_2H_2 , DME, CO, CO_2 , and NO concentrations. However, it only includes gas-phase reactions and improvements are still needed, especially in reactions related to acetylene conversion, where higher discrepancies have been observed.

Acknowledgements

The authors express their gratitude to Aragón Government and European Social Fund (GPT group), and to MINECO and FEDER (Project CTQ2015-65226) for financial support. Ms. Marrodán acknowledges Aragón Government for the predoctoral grant awarded.

Appendix A. Supplementary material

Supplementary data associated with this article can be found, in the online version, at <http://dx.doi.org/10.1016/j.fuel.2016.06.011>.

References

- [1] Yanfeng G, Shenghua L, Hejun G, Tiegang H, Longbao Z. A new diesel oxygenate additive and its effects on engine combustion and emissions. *Appl Therm Eng* 2007;27:202–7.
- [2] Tran LS, Sirjean B, Glaude P, Fournet R, Battin-Leclerc F. Progress in detailed kinetic modeling of the combustion of oxygenated components of biofuels. *Energy* 2012;43:4–18.
- [3] Tutak W, Lukács K, Szwaja S, Bereczky Á. Alcohol-diesel fuel combustion in the compression ignition engine. *Fuel* 2015;154:196–206.
- [4] Crookes RJ, Bob-Manuel KD. RME or DME: a preferred alternative fuel option for future diesel engine operation. *Energy Convers Manage* 2007;48:2971–7.
- [5] Verbeek R, Van der Weide J. Global assessment of dimethyl-ether: comparison with other fuels. *SAE Tech. Pap.* 1997; 971607.
- [6] Arcoumanis C, Bae C, Crookes R, Kinoshita E. Synergistic effect of mixing dimethyl ether with methane, ethane, propane, and ethylene fuels on polycyclic aromatic hydrocarbon and soot formation. *Fuel* 2008;87:1014–30.
- [7] Abián M, Esarte C, Millera A, Bilbao R, Alzueta MU. Oxidation of acetylene-ethanol mixtures and their interaction with NO. *Energy Fuels* 2008;22:3814–23.
- [8] Härtl M, Seidenspinner P, Jacob E, Wachtmeister G. Oxygenate screening on a heavy-duty diesel engine and emission characteristics of highly oxygenated oxymethylene ether fuel OME₁. *Fuel* 2015;153:328–35.
- [9] Song KH, Nag P, Litzinger TA, Haworth DC. Effects of oxygenated additives on aromatics species in fuel-rich, premixed ethane combustion: a modeling study. *Combust Flame* 2003;135:341–9.
- [10] Glassman I, Yetter RA. *Combustion*. 4th ed. Burlington: Academic Press; 2008.
- [11] Ruiz MP, Guzmán de Villoria R, Millera A, Alzueta MU, Bilbao R. Influence of different operation conditions on soot formation from C_2H_2 pyrolysis. *Ind Eng Chem Res* 2007;46:7550–60.
- [12] Mendiara T, Domene MP, Millera A, Bilbao R, Alzueta MU. An experimental study of the soot formed in the pyrolysis of acetylene. *J Anal Appl Pyrolysis* 2005;74:486–93.
- [13] Saggese C, Sánchez NE, Frassoldati A, Cuoci A, Faravelli T, Alzueta MU, et al. Kinetic modeling study of polycyclic aromatic hydrocarbons and soot formation in acetylene pyrolysis. *Energy Fuels* 2014;28:1489–501.
- [14] Frenklach M. Reaction mechanism of soot formation in flames. *Phys Chem Chem Phys* 2002;4:2028–37.
- [15] Omidvarborna H, Kumar A, Kim DS. Recent studies on soot modeling for diesel combustion. *Renew Sust Energy Rev* 2015;48:635–47.
- [16] Esarte C, Callejas A, Millera A, Bilbao R, Alzueta MU. Influence of the concentration of ethanol and the interaction of compounds in the pyrolysis of acetylene and ethanol mixtures. *Fuel* 2011;90:844–9.
- [17] Esarte C, Millera A, Bilbao R, Alzueta MU. Effect of ethanol, dimethylether, and oxygen, when mixed with acetylene, on the formation of soot and gas products. *Ind Eng Chem Res* 2010;49:6772–9.
- [18] Bo Z, Weibiao F, Jingsong G. Study of fuel consumption when introducing DME or ethanol into diesel engine. *Fuel* 2006;85:778–82.
- [19] Ying W, Longbao Z, Hewu W. Diesel emission improvements by the use of oxygenated DME/diesel blend fuels. *Atmos Environ* 2006;40:2313–20.
- [20] Alzueta MU, Glarborg P, Dam-Johansen K. Low temperature interactions between hydrocarbons and nitric oxide: an experimental study. *Combust Flame* 1997;109:25–36.
- [21] Kristensen PG, Glarborg P, Dam-Johansen K. Nitrogen chemistry during burnout in fuel-staged combustion. *Combust Flame* 1996;107:211–22.
- [22] Alzueta MU, Borruey M, Callejas A, Millera A, Bilbao R. An experimental and modeling study of the oxidation of acetylene in a flow reactor. *Combust Flame* 2008;152:377–86.
- [23] Abián M, Silva SL, Millera A, Bilbao R, Alzueta MU. Effect of operating conditions on NO reduction by acetylene-ethanol mixtures. *Fuel Process Technol* 2010;91:1204–11.
- [24] Glarborg P, Alzueta MU, Dam-Johansen K, Miller JA. Kinetic modeling of hydrocarbon/nitric oxide interactions in a flow reactor. *Combust Flame* 1998;115:1–27.
- [25] Glarborg P, Alzueta MU, Kjærsgaard K, Dam-Johansen K. Oxidation of formaldehyde and its interaction with nitric oxide in a flow reactor. *Combust Flame* 2003;132:629–38.
- [26] Alzueta MU, Hernández JM. Ethanol oxidation and its interaction with nitric oxide. *Energy Fuels* 2002;16:166–71.
- [27] Alzueta MU, Muro J, Bilbao R, Glarborg P. Oxidation of dimethyl ether and its interaction with nitrogen oxides. *Isr J Chem* 1999;39:73–86.
- [28] Faßheber N, Friedrichs G, Marshall P, Glarborg P. Glyoxal oxidation mechanism: implications for the reactions HCO+ O_2 and OCHCHO+ HO_2 . *J Phys Chem A* 2015;119:7305–15.
- [29] Lutz AE, Kee RJ, Miller JA. Senkin: A fortran program for predicting homogeneous gas phase chemical kinetics with sensitivity analysis. Sandia Natl Lab Rep. SAND87-8248; 1988.
- [30] Kee RJ, Rupley FM, Miller JA. Chemkin-II: A fortran chemical kinetics package for the analysis of gas-phase chemical kinetics. Sandia Lab Rep. SAND87-8215; 1991.
- [31] Cipolat D. Analysis of energy release and NO_x emissions of a CI engine fueled by diesel and DME. *Appl Therm Eng* 2007;27:2095–103.
- [32] Park SH, Yoon SH. Injection strategy for simultaneous reduction of NO_x and soot emissions using two-stage injection in DME fueled engine. *Appl Energy* 2015;143:262–70.
- [33] Bilbao R, Millera A, Alzueta MU. Influence of the temperature and oxygen concentration on NO_x reduction in the natural gas reburning process. *Ind Eng Chem Res* 1994;33:2846–52.
- [34] Miller JA, Klippenstein SJ, Glarborg P. A kinetic issue in reburning: the fate of HCNO. *Combust Flame* 2003;135:357–62.
- [35] Faravelli T, Frassoldati A, Ranzi E. Kinetic modeling of the interactions between NO and hydrocarbons in the oxidation of hydrocarbons at low temperatures. *Combust Flame* 2003;132:188–207.
- [36] Dagaut P, Nicolle A. Experimental study and detailed kinetic modeling of the effect of exhaust gas on fuel combustion: mutual sensitization of the oxidation of nitric oxide and methane over extended temperature and pressure ranges. *Combust Flame* 2005;140:161–71.
- [37] Taylor PH, Cheng L, Dellinger B. The influence of nitric oxide on the oxidation of methanol and ethanol. *Combust Flame* 1998;115:561–7.
- [38] Marrodán L, Royo E, Millera A, Bilbao R, Alzueta MU. High pressure oxidation of dimethoxymethane. *Energy Fuels* 2015;29:3507–17.

Article V:

Marrodán, L.; Arnal, Á.J.; Millera, Á.; Bilbao, R.; Alzueta, M.U. (2018). The inhibiting effect of NO addition on dimethyl ether high-pressure oxidation. *Combustion and Flame* 197, 1-10.



The inhibiting effect of NO addition on dimethyl ether high-pressure oxidation



Lorena Marrodán, Álvaro J. Arnal, Ángela Millera, Rafael Bilbao, María U. Alzueta*

Aragón Institute of Engineering Research (I3A), Department of Chemical and Environmental Engineering, University of Zaragoza, C/Mariano Esquillor, s/n. 50018, Zaragoza, Spain

ARTICLE INFO

Article history:

Received 9 March 2018

Revised 3 July 2018

Accepted 4 July 2018

Keywords:

Dimethyl ether

Oxidation

High-pressure

Nitrogen oxides

Modeling

ABSTRACT

The high-pressure dimethyl ether (DME, CH_3OCH_3) oxidation has been investigated in a plug flow reactor in the 450–1050 K temperature range. Different pressures (20, 40 and 60 bar), air excess ratios ($\lambda = 0.7, 1$ and 35), and the absence/presence of NO have been tested, for the first time under these conditions. An early reactivity of DME and a negative temperature coefficient (NTC) zone have been observed under the studied conditions, although under very oxidizing conditions ($\lambda = 35$), NTC zone is almost imperceptible because DME is completely consumed at lower temperatures. A chemical kinetic mechanism has been used to describe the DME high-pressure oxidation, with a good agreement with the experimental trends observed. In general, modeling calculations with the present mechanism have been successfully compared with experimental data from literature. The presence of NO has an inhibiting effect on DME high-pressure consumption at low-temperatures because of: (i) the competition between $\text{CH}_3\text{OCH}_2 + \text{O}_2 \rightleftharpoons \text{CH}_3\text{OCH}_2\text{O}_2$ and $\text{CH}_3\text{OCH}_2 + \text{NO}_2 \rightleftharpoons \text{CH}_3\text{OCH}_2\text{O} + \text{NO}$ reactions, and (ii) the participation of NO in $\text{CH}_3\text{OCH}_2\text{O}_2 + \text{NO} \rightleftharpoons \text{CH}_3\text{OCH}_2\text{O} + \text{NO}_2$ reaction, preventing $\text{CH}_3\text{OCH}_2\text{O}_2$ radicals continue reacting through a complex mechanism, which includes a second O_2 addition and several isomerizations and decompositions, during which highly reactive OH radicals are generated. Consequently, NO and NO_2 are interchanged in a cycle but never consumed.

© 2018 The Combustion Institute. Published by Elsevier Inc. All rights reserved.

1. Introduction

Current problems derived from the intense use of fossil fuels make the search for more environmentally friendly fuels and new combustion techniques urgent. The second-generation biofuels, derived from biomass wastes, are considered to be clean and CO_2 neutral. Dimethyl ether (DME, CH_3OCH_3), due to its high cetane number (>55), almost immediate vaporization as sprayed into the cylinder, rich oxygen content (around 35 % by mass), no C–C bonds, and lower autoignition temperature compared to diesel fuel, is considered as a good alternative [1]. It can be a substitute for Liquefied Petroleum Gas (LPG), diesel fuel and Liquefied Natural Gas (LNG) [2,3]. Therefore, DME conversion has been subject of numerous studies carried out in different types of reactors and conditions. For example, Rodriguez et al. [4], in their study of low-temperature oxidation of DME, performed a great review of some of the most recent experimental studies, 34 different works performed in jet-stirred reactors, flow tubes, shock tubes, rapid compression machines, burners and spherical bombs.

Diesel engines involve conditions where interactions between fuel components and nitrogen oxides are possible. For example, the recycling of some of the exhaust gas back into the engine system, commonly known as exhaust gas recirculation (EGR), is a strategy of limiting the production of pollutants by diluting the reactants with exhaust gas, allowing operation under fuel-lean conditions and lower temperatures. New combustion techniques, such as low temperature combustion (LTC), homogeneous charge compression ignition (HCCI) and premixed charge compression ignition (PCCI), also include EGR systems to achieve low emissions of NO_x and soot [5,6]. Thereby, it is interesting to analyze the role of the NO formed during the fuel combustion and once it has been recycled, because it may have a significant impact on autoignition.

Numerous previous studies have analyzed the interaction between NO and different fuels such as hydrocarbons [7–13] or alcohols [14,15] showing that, depending on the combustion conditions, the impact of NO can be completely different. At high temperatures and fuel-rich conditions, NO may be reduced to N_2 and HCN by reacting with hydrocarbon radicals in reburn-type reactions (e.g., [16]); whereas at low to intermediate temperatures, the presence of NO may promote the oxidation of the fuel (e.g., [12]), but also the oxidation of NO to NO_2 may be promoted by the fuel

* Corresponding author.

E-mail address: uxue@unizar.es (M.U. Alzueta).

in a mutually sensitized oxidation process, as reported by Dagaut and Nicolle during the oxidation of methane in the presence of NO [10]. However, the presence of NO can also have inhibiting effects on fuel conversion. Moréac et al. [8], in a n-heptane jet-stirred oxidation work at 10 atm, reported that the effects of the NO presence vary with temperature; that is, at low temperatures NO may have an inhibiting effect, whereas at temperatures higher than 675 K, NO may accelerate the reactivity. The addition of NO may inhibit the reaction to the point of extinction in the negative temperature coefficient (NTC) region, that is of primary importance for the autoignition, due to the $\text{NO} + \text{OH} = \text{HONO}$ reaction; but at higher temperatures, the HO_2 concentration is increased and it allows the regeneration of reactive OH radicals through $\text{NO} + \text{HO}_2 = \text{NO}_2 + \text{OH}$. Moreover, Anderlohr et al. [13] suggested a mechanism to explain this inhibiting effect of NO in the NTC zone of n-heptane oxidation. The competition between $\text{RO}_2 + \text{NO} = \text{RO} + \text{NO}_2$ and the second O_2 addition could be the main cause for the inhibiting effect at temperatures higher than 650 K. Below this temperature, the $\text{NO} + \text{OH} = \text{HONO}$ reaction seems to be the inhibiting one.

Despite the large number of studies concerning the interaction of fuel components with NO or the DME oxidation, to our knowledge, only a previous work of our group focuses on the direct interaction of DME and NO in an atmospheric plug flow reactor [17]. Other study [18], also from our group and under atmospheric conditions, analyzes the effect of the addition of NO to mixtures of DME and acetylene, as a soot precursor. Besides, since engine efficiency is increased by working under high-pressure conditions, reliable experimental data for validation of the kinetic models at these conditions become very relevant.

In this scenario, the present work aims to analyze the influence of the presence of NO on the high-pressure oxidation of DME, which, to our knowledge, has not been considered earlier. For this analysis, it is also interesting to first characterize the DME oxidation under high-pressure conditions. Therefore, an experimental and kinetic study of DME high-pressure (20, 40 and 60 bar) oxidation has been carried out in the 450–1050 K temperature range. In addition to stoichiometric conditions, oxidation data have been collected under strongly oxidizing and slightly reducing conditions, both in the absence and presence of NO (500 ppm).

2. Experimental section

The experimental setup used to perform the high-pressure DME oxidation experiments, in the absence and presence of NO, has been previously described in detail [19], so only a description of the main features is provided here. Reactants, DME (approximately 700 ppm), NO (approximately 500 ppm) and O_2 , and N_2 as carrier gas, were supplied from gas cylinders through mass flow controllers with an uncertainty in the flow rate measurements of approximately 0.5%. The oxygen required to carry out each oxidation experiment is determined by the air excess ratio (λ , defined as the inlet oxygen divided by stoichiometric oxygen). Table 1 contains the conditions for the different experiments.

The reactant gases were premixed before entering the reactor, which consists of a tubular quartz tube (inner diameter of 6 mm and 1500 mm in length) designed to approximate plug flow [20]. The reactor is enclosed in a stainless-steel pressure shell and it, in turn, in an electrically heated oven. The temperature is monitored by K-thermocouples placed between the quartz reactor and the steel shell. The longitudinal temperature profiles were experimentally determined in N_2 atmosphere, obtaining an isothermal (± 10 K) reaction zone of 56 cm. An example of the temperature profiles inside the reactor for a flow rate of 1 L(STP)/min, and 20, 40 and 60 bar can be found in the Supplementary Material (Figs. S1–S3). Moreover, an excel spreadsheet with all the temperature-distance profiles is provided as Supplementary Mate-

Table 1

Matrix of experimental conditions. Experiments were conducted in the 450–1050 K temperature range. The balance is closed with N_2 .

Set	DME [ppm]	NO [ppm]	P [bar]	λ	t_r [s]	Flow rate [L(STP)/min]
1	700	-	20	0.7	5220/T	1
2	698	-	20	1	5220/T	1
3	700	-	20	35	5220/T	1
4	692	-	40	0.7	10440/T	1
5	695	-	40	1	10440/T	1
6	700	-	40	35	10440/T	1
7	704	-	60	0.7	15660/T	1
8	702	-	60	1	15660/T	1
9	700	-	60	35	15660/T	1
10	732	-	40	0.7	5220/T	2
11	698	-	40	1	5220/T	2
12	700	-	40	35	5220/T	2
13	710	518	20	0.7	5220/T	1
14	700	498	20	1	5220/T	1
15	700	490	20	35	5220/T	1
16	702	502	40	0.7	10440/T	1
17	695	485	40	1	10440/T	1
18	723	497	40	35	10440/T	1
19	710	479	60	0.7	15660/T	1
20	703	515	60	1	15660/T	1
21	700	487	60	35	15660/T	1

rial. Two different gas flow rates were tested (1 and 2 L(STP)/min) resulting in different temperature-dependent gas residence times (t_r) according to the working pressure. In the case of the higher gas flow rate studied in this work, 2 L(STP)/min, the temperature profiles were also checked, and they were very similar to those determined for 1 L(STP)/min. In all the cases, nitrogen was used to balance.

The gases leaving the reactor were on-line analyzed by a micro-gas chromatograph (Agilent 3000A) equipped with Thermal Conductivity Detectors (TCD), an ATI Mattson Fourier Transform Infrared (FTIR), and a continuous IR NO analyzer (URAS26 ABB). The uncertainty of the measurements is estimated as $\pm 5\%$, except for the FTIR spectrometer, which is estimated $\pm 10\%$.

3. Chemical kinetic model

The first detailed gas-phase chemical kinetic mechanism, used for chemistry description and analysis of the present experimental results, was taken from a study of the atmospheric oxidation of acetylene-dimethyl ether mixtures, in the absence and presence of NO, developed by our research group [18], to which modifications have been made in this work as described below. The basis of this first mechanism consists of reactions to describe C_1 – C_2 and NO interactions and it was initially proposed by Glarborg et al. [16] and progressively updated (e.g., [21]). This mechanism [18] also includes reactions to describe acetylene [22], ethanol [14], glyoxal [23] and DME [17] conversion. When the mechanism of reference [18] was used to simulate the present high-pressure experimental results, the mechanism was not able to describe properly the characteristic NTC behavior of DME occurring at low temperature and high pressure. Therefore, improvements of the mechanism from reference [18], which was validated at atmospheric pressure, are required.

This mechanism has been updated and modified to consider the high-pressure experimental conditions of this work [20,24–27]. The subset for DME has also been revised according to DME kinetic mechanisms from literature, Zhao's et al. [28] and Burke's et al. mechanisms [29], validated against a wide range of experimental data. Burke et al. [29] assessed the pressure dependencies of the reactions involved in the low-temperature oxidation pathways for DME. Under the experimental conditions studied in that work, the prediction of the ignition delay times was found to be

Table 2Reactions for DME modified or added compared to Alzueta et al.'s work [17]; units: cm³, mol, s and cal.

Reaction		A	n	E _a	Source
CH ₃ OCH ₃ (+M) = CH ₃ + CH ₃ O(+M)	(high-pressure)	4.37 × 10 ²¹	-1.57	83842	[28]
	(low-pressure)	1.13 × 10 ⁶²	-12.19	94882	
CH ₃ OCH ₃ + OH = CH ₃ OCH ₂ + H ₂ O		6.71 × 10 ⁶	2.00	-629.88	[28]
CH ₃ OCH ₃ + HO ₂ = CH ₃ OCH ₂ + H ₂ O ₂		2.00 × 10 ¹³	0.00	16500	[28]
CH ₃ OCH ₃ + CH ₃ = CH ₃ OCH ₂ + CH ₄		2.68 × 10 ¹	3.78	9631.3	[28]
CH ₃ OCH ₃ + CH ₃ O ₂ = CH ₃ OCH ₂ + CH ₃ O ₂ H		1.27 × 10 ⁻³	4.64	10556	[29]
CH ₃ OCH ₃ + CH ₃ OCH ₂ O ₂ = CH ₃ OCH ₂ + CH ₃ OCH ₂ O ₂ H		5.00 × 10 ¹²	0.00	17690	[29]
CH ₃ OCH ₃ + OCHO = CH ₃ OCH ₂ + HOCHO		1.00 × 10 ¹³	0.00	17690	[29]
CH ₃ OCH ₂ = CH ₃ + CH ₂ O		8.03 × 10 ¹²	0.44	26490	[29]
CH ₃ OCH ₂ + O ₂ = CH ₃ OCH ₂ O ₂	(0.001 atm)	7.49 × 10 ²³	-4.52	25236	
	(0.01 atm)	6.92 × 10 ²⁸	-5.73	27494	
	(1 atm)	4.23 × 10 ²⁹	-5.61	28898	
	(10 atm)	6.61 × 10 ²⁷	-4.71	29735	
	(100 atm)	2.66 × 10 ²⁹	-4.94	31785	
	(0.001 atm)	1.12 × 10 ¹⁸	-3.37	-4294	[29]
	(0.01 atm)	1.33 × 10 ²¹	-3.95	-2615	
	(1 atm)	1.13 × 10 ²⁸	-5.24	4088	
	(2 atm)	3.91 × 10 ²⁷	-5.00	4512	
	(10 atm)	2.75 × 10 ²⁴	-3.87	4290	
CH ₃ OCH ₂ + O ₂ = CH ₂ OCH ₂ O ₂ H	(20 atm)	2.97 × 10 ²²	-3.23	3781	
	(50 atm)	5.19 × 10 ¹⁹	-2.35	2908	
	(100 atm)	5.43 × 10 ¹⁷	-1.73	2210	
	(0.001 atm)	5.08 × 10 ²⁰	-4.39	469	[29]
	(0.01 atm)	5.47 × 10 ²³	-4.96	2183	
	(1 atm)	2.81 × 10 ²⁸	-5.63	7848	
	(2 atm)	5.19 × 10 ²⁷	-5.33	8144	
	(10 atm)	9.67 × 10 ²⁴	-4.40	8417	
	(20 atm)	4.08 × 10 ²³	-3.90	8494	
	(50 atm)	5.08 × 10 ²¹	-3.30	8585	
CH ₃ OCH ₂ + O ₂ = CH ₂ O + CH ₂ O + OH	(100 atm)	1.62 × 10 ²⁰	-2.80	8619	
	(0.001 atm)	8.01 × 10 ²¹	-3.20	3067	[29]
	(0.01 atm)	1.73 × 10 ²³	-3.50	4050	
	(1 atm)	2.04 × 10 ³¹	-5.80	11594	
	(2 atm)	5.99 × 10 ³¹	-5.90	12710	
	(10 atm)	9.39 × 10 ³⁰	-5.60	14517	
	(20 atm)	1.09 × 10 ³⁰	-5.30	15051	
	(50 atm)	3.58 × 10 ²⁸	-4.90	15664	
	(100 atm)	2.41 × 10 ²⁷	-4.50	16107	
			9.72 × 10 ¹⁵	-1.10	20640
CH ₃ OCH ₂ O = CH ₃ O + CH ₂ O		1.60 × 10 ²³	-4.50	0	[28]
CH ₃ OCH ₂ O ₂ + CH ₃ OCH ₂ O ₂ = O ₂ + CH ₃ OCH ₂ O + CH ₃ OCH ₂ O		6.84 × 10 ²²	-4.50	0	[28]
CH ₃ OCH ₂ O ₂ + CH ₃ OCH ₂ O ₂ = O ₂ + CH ₃ OCHO + CH ₃ OCH ₂ OH		1.94 × 10 ²⁹	-6.99	22446	[29]
CH ₃ OCH ₂ O ₂ = CH ₂ OCH ₂ O ₂ H	(0.001 atm)	4.07 × 10 ²⁷	-6.16	21619	
	(0.01 atm)	2.52 × 10 ²⁵	-4.76	22691	
	(1 atm)	5.97 × 10 ²⁴	-4.48	22868	
	(2 atm)	4.44 × 10 ²¹	-3.38	22386	
	(10 atm)	4.52 × 10 ¹⁹	-2.74	21803	
	(20 atm)	5.72 × 10 ¹⁶	-1.82	20829	
	(50 atm)	3.70 × 10 ¹⁴	-1.13	20034	
CH ₃ OCH ₂ O ₂ = CH ₂ O + CH ₂ O + OH	(100 atm)	2.06 × 10 ³⁶	-8.30	33415	[29]
	(0.01 atm)	2.07 × 10 ³⁹	-8.90	35842	
	(1 atm)	1.12 × 10 ⁴⁰	-8.40	39835	
	(2 atm)	9.72 × 10 ³⁸	-8.00	39923	
	(10 atm)	6.28 × 10 ³⁵	-7.00	39900	
	(20 atm)	1.60 × 10 ³⁴	-6.50	39850	
	(50 atm)	8.32 × 10 ³¹	-5.80	39719	
	(100 atm)	1.22 × 10 ³⁰	-5.20	39549	
	(0.001 atm)	1.66 × 10 ²³	-4.53	22243	[29]
	(0.01 atm)	5.30 × 10 ²⁵	-4.93	24158	
CH ₂ OCH ₂ O ₂ H = OH + CH ₂ O + CH ₂ O	(1 atm)	7.81 × 10 ²²	-3.50	23156	
	(2 atm)	4.98 × 10 ²²	-3.35	23062	
	(10 atm)	8.46 × 10 ²²	-3.22	23559	
	(20 atm)	9.09 × 10 ²²	-3.14	23899	
	(50 atm)	4.59 × 10 ²²	-2.94	24262	
	(100 atm)	1.40 × 10 ²²	-2.72	24407	
	(0.001 atm)	9.42 × 10 ¹²	-1.68	-4998	[29]
	(0.01 atm)	8.16 × 10 ¹⁶	-2.50	-2753	
	(1 atm)	1.06 × 10 ²²	-3.30	3389	
	(2 atm)	3.48 × 10 ²⁰	-2.79	3131	
CH ₂ OCH ₂ O ₂ H + O ₂ = > O ₂ CH ₂ OCH ₂ O ₂ H	(10 atm)	2.86 × 10 ¹⁶	-1.48	1873	
	(20 atm)	8.55 × 10 ¹⁴	-1.01	1312	
	(50 atm)	2.68 × 10 ¹³	-0.54	727	
	(100 atm)	4.87 × 10 ¹²	-0.32	428	

(continued on next page)

Table 2 (continued)

Reaction		A	n	E _a	Source		
CH ₂ OCH ₂ O ₂ H + O ₂ => HO ₂ CH ₂ OCHO + OH	(0.001 atm)	5.90 × 10 ²⁰	-2.88	3234	[29]		
	(0.01 atm)	2.06 × 10 ²³	-3.59	5116			
	(1 atm)	4.45 × 10 ²⁹	-5.29	12791			
	(2 atm)	2.44 × 10 ²⁸	-4.92	12891			
	(10 atm)	9.42 × 10 ²³	-3.68	12049			
	(20 atm)	1.04 × 10 ²²	-3.16	11505			
	(50 atm)	6.95 × 10 ¹⁹	-2.60	10861			
	(100 atm)	3.96 × 10 ¹⁸	-2.31	10500			
	O ₂ CH ₂ OCH ₂ O ₂ H = HO ₂ CH ₂ OCHO + OH	(0.001 atm)	9.05 × 10 ²³	-4.88		18805	[29]
		(0.01 atm)	6.84 × 10 ²⁶	-5.32		22533	
(1 atm)		5.07 × 10 ¹⁶	-1.81	21175			
(2 atm)		2.66 × 10 ¹⁴	-1.11	20310			
(10 atm)		1.69 × 10 ¹⁰	0.18	18604			
(20 atm)		1.11 × 10 ⁻⁹	0.54	18100			
(50 atm)		1.07 × 10 ⁻⁸	0.84	17661			
(100 atm)		3.86 × 10 ⁻⁷	0.98	17467			
HO ₂ CH ₂ OCHO => OCH ₂ OCHO + OH			3.00 × 10 ¹⁶	0.00	43000	[28]	
CH ₂ O + OCHO = OCH ₂ OCHO			1.25 × 10 ¹¹	0.00	11900	[29]	
HOCH ₂ OCO = HOCH ₂ O + CO		2.18 × 10 ¹⁶	-2.69	17200	[28]		
HOCH ₂ OCO = CH ₂ OH + CO ₂		5.31 × 10 ¹⁵	-2.61	20810	[28]		
HOCH ₂ O = HCOOH + H		1.00 × 10 ¹⁴	0.00	14900	[28]		
CH ₂ O + OH = HOCH ₂ O		4.50 × 10 ¹⁵	-1.11	0	[28]		

particularly sensitive to the decomposition of the CH₃OCH₂ radical (CH₃OCH₂ = CH₃ + CH₂O). Therefore, only the pressure dependency of this reaction was updated through a more sophisticated treatment by Burke et al. [29]. However, under the present conditions, results are sensitive to the isomerization of alkyl-peroxy radicals to form hydroperoxy alkyl radicals (CH₃OCH₂O₂ = CH₂OCH₂O₂H). The impact of such reaction is later discussed.

The reactions for DME, that have been modified or added compared to Alzueta et al. reaction subset [17], are specified in Table 2.

As previously mentioned, the variety of experimental and modeling studies on DME conversion is very large. The performance of some of the most recent mechanisms [4,28,30,31] has been compared against the present high-pressure experimental data. The comparisons can be found in Figs. S4–S6 in Supplementary Material. In general, those mechanisms are able to reproduce the experimental trends. An interesting issue when comparing the different mechanisms is the different reaction pathways considered. An aspect of interest is related to the presence and reactions of formic acid (HCOOH). Our experimental results evidence the formation of HCOOH from DME and, actually, HCOOH has a significant role under our conditions. The mechanism proposed by Rodriguez et al. [4] does not include HCOOH as intermediate, and although other mechanisms (for example, Zhao et al.'s mechanism [28]) suggested some reactions involving formic acid, in the present work, we have included the more recent subset for the oxidation of formic acid based on ab initio calculations proposed by Marshall and Glarborg [32].

The present mechanism also includes reaction subsets for methyl formate [19], dimethoxymethane [33] and ethanol [34], validated in previous works under similar experimental conditions, even though they are not especially relevant to this study.

In the case of reactions involving NO and NO₂, no major modifications have been made with respect to previous works from our group under similar conditions (e.g., [34]). The basis mechanism from Glarborg et al. [16] contains reactions to describe the interactions between C₁–C₂ and NO. These reactions have been updated according to more recent works involving NO_x, which were developed and validated for high-pressure conditions [20,26]. Reactions for coupling both DME and NO_x subsets, such as CH₃OCH₂ + NO₂ = CH₃OCH₂O + NO or CH₃OCH₂O₂ + NO = CH₃OCH₂O + NO₂, were already considered in

the initial DME reaction subset [17]. Only one modification was made in our previous study [34], we included reaction (R₁) to reproduce the highly expected interaction between CH₃ radicals and NO₂ under high-pressure conditions.



Thermochemistry involved in modeling DME conversion has been extensively studied, and significant discrepancies can be found in enthalpy and entropy of formation as well as heat capacities for the different species involved in the conversion of DME. We have done a review of the different thermodynamic values of the literature and Table S1 in the Supplementary Material lists the different thermodynamic properties for those selected species of relevance for DME conversion: CH₃OCH₂, CH₃OCH₂O₂ and CH₂OCH₂O₂H. In Table S1, thermodynamic data calculated from the mechanism information given by different authors [4,28–31], together with the theoretical determination by Yamada et al. [35], are shown. As it can be observed, there is a large discrepancy between the values used for the different authors, especially for CH₃OCH₂. Moreover, the values can differ depending on the temperature range used for calculations, low or high temperature range.

The thermodynamic data that we have used for the species involved in DME reaction subset have been taken from Burke et al. [29] to be consistent with the source of the kinetic parameters.

The final mechanism, which involves 138 species and contains 792 reactions, and the thermodynamic data files, both in CHEMKIN format, are provided as Supplementary Material. Numerical calculations were conducted with the plug-flow reactor module of CHEMKIN-PRO software package [36] and taking into account the temperature profiles experimentally determined.

An example of the relevance of the different modifications done to the mechanism [18] is shown in Fig. S7 in Supplementary Material. As it can be observed, the match between experimental results and modeling calculations improves considerably with the modifications in Table 2.

Moreover, modeling calculations obtained with the present mechanism have been compared against several sets of data from literature covering a wide range of experimental devices and conditions (Figs. S8–S17 in Supplementary Material). In general, the present mechanism reproduces well the different experimental data from literature.

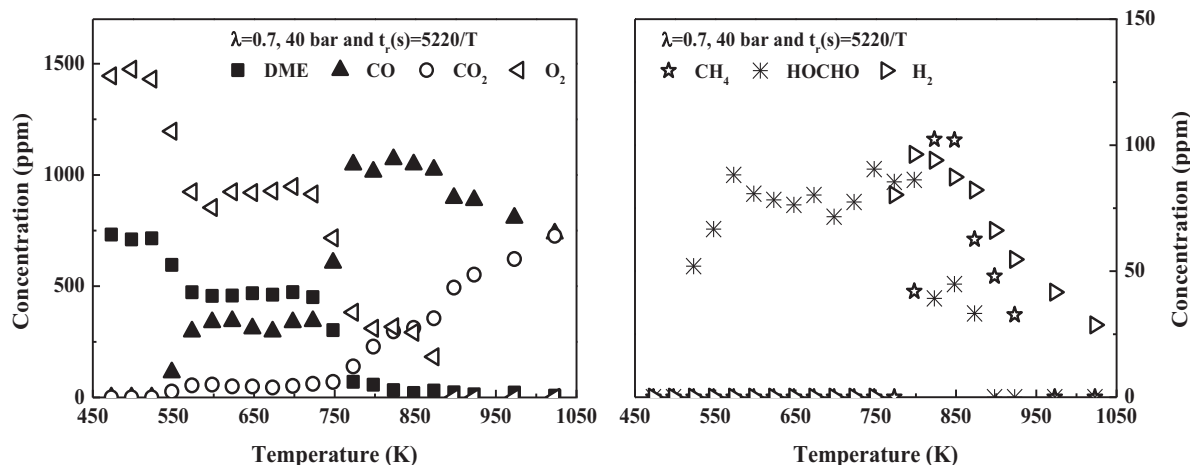


Fig. 1. Evolution for DME, O₂, CO, CO₂, CH₄, HCOOH and H₂ concentrations with temperature during the high-pressure (20 bar) oxidation of DME, for the conditions denoted as set 10 in Table 1 ($\lambda = 0.7$, 2 L(STP)/min, in the absence of NO).

4. Results and discussion

The main purpose of this work is to analyze the effect of the addition of NO on the high-pressure oxidation of DME. Therefore, before analyzing its effect, the high-pressure oxidation of DME should be well characterized.

4.1. High-pressure DME oxidation in the absence of NO

The influence of the pressure (20, 40 and 60 bar), the oxygen availability (determined by different air excess ratios, λ), and the presence of NO has been evaluated in the 450–1050 K high-pressure DME oxidation.

Figure 1 shows, for a selected experiment (set 10 in Table 1), the evolution with temperature of the reactants (DME and O₂) and main products (CO, CO₂, CH₄, HCOOH, H₂) concentration experimentally obtained. In the 550–750 K temperature range, there is a “plateau” in DME where it remains constant. It corresponds to the negative temperature coefficient (NTC) zone, where DME reactivity is constant or decreases with temperature, and it is also reflected in the concentration profile of the other compounds. It is more pronounced in the oxygen concentration profile, in which two inflection points characterizing the NTC zone can be identified. From now on, we will focus mainly on DME concentration profile to analyze the influence of the different variables.

Considering the experimental procedure followed in the current setup, a change in the working pressure while maintaining the total gas flow rate, also implies a change in the gas residence time. That is, for 1 L(STP)/min of total flow rate, the gas residence time is $t_r(s) = 261 P(\text{bar})/T(K)$, which implies that residence time depends on both pressure and temperature. Therefore, we have performed different experiments to try to distinguish between the effect of gas residence time or pressure. To analyze the influence of the pressure, the gas residence time was kept “constant”, only as a function of temperature, $t_r(s) = 5220/T(K)$, and the pressure was increased from 20 to 40 bar. On the other hand, to analyze the influence of the gas residence time, the pressure was kept constant (40 bar) and the residence time was changed from $t_r(s) = 5220/T(K)$ to $t_r(s) = 10,440/T(K)$. Figure 2 shows the experimental results (symbols) and modeling calculations (lines) obtained in this way for the three different values of lambda analyzed.

As shown in Fig. 2, in general, there is a good agreement between experimental results and modeling calculations for DME conversion. In the 550–700 K temperature range, the NTC behavior

is observed for all the conditions analyzed, although is less pronounced under very oxidizing ($\lambda = 35$) conditions because the high oxygen availability causes the DME to be completely consumed at lower temperatures. This will be discussed later when analyzing the influence of pressure and lambda on DME oxidation. For the same residence time, increasing the pressure from 20 to 40 bar, does not seem to have a big effect on DME conversion for any of the lambda values analyzed. For the same pressure and $\lambda = 0.7$ and $\lambda = 1$, the oxidation of DME is favored by increasing the gas residence time, whereas for $\lambda = 35$ no big changes are noticed. In conclusion, under the operating conditions used in this work, the effect on DME high-pressure oxidation of the residence time is clear and more noticeable than the effect of pressure. In a previous high-pressure oxidation of ethanol under similar conditions to those of this work [34], an analysis of the influence of pressure and residence time was also carried out, but only from a modeling point of view, elucidating that both pressure and residence time had an appreciable impact shifting ethanol conversion to lower temperatures when any of these variables was increased.

4.2. High-pressure DME oxidation in the presence of NO

The influence of NO presence (500 ppm) on the high-pressure (20, 40 and 60 bar) DME oxidation has been analyzed in the 450–1050 K temperature range, from reducing ($\lambda = 0.7$) to very oxidizing conditions ($\lambda = 35$). As it has been explained, the results presented from now on, correspond to the joint effect of pressure and residence time, with a more relevance of the latter. Furthermore, under the present experimental conditions, it has been observed that NO added to the reactant mixture can be converted to NO₂ before entering the reactor, because of the high-pressure conditions and the presence of O₂, through reaction (R₂).



Figure 3 shows the evolution with temperature of theoretical and experimental NO outlet concentrations for the different pressures and values of lambda analyzed. Model reproduces quite well the experimental trends observed although some improvements could be done, in particular at high pressure and high temperature, where the model deviates from experimental results. At present, we are not able to explain the reasons for such discrepancy. Under these conditions, the formation of stable peroxide nitrogenous species may occur, but not easy to be detected experimentally. At temperatures below 650 K, for $\lambda = 0.7$ and 1, the experimental NO concentration remains in a low value and, at higher temperatures,

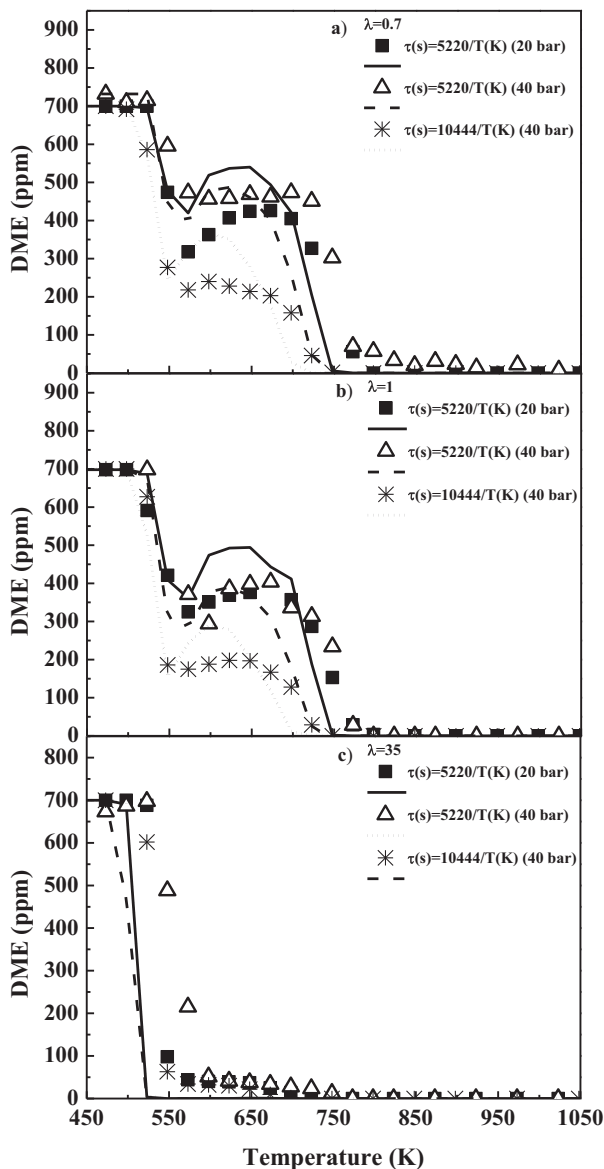


Fig. 2. Evaluation of the effect of pressure and gas residence time on the high-pressure (20 or 40 bar) oxidation of DME, for the conditions denoted as (a) sets 1, 10 and 4 in Table 1 for $\lambda=0.7$; (b) sets 2, 11 and 5 in Table 1 for $\lambda=1$; and (c) sets 3, 12 and 6 in Table 1 for $\lambda=35$.

it starts to increase to reach almost the inlet concentration value in the case of 20 bar and a slightly lower concentration for 40 and 60 bar. Only for $\lambda=35$, the experimental NO concentration remains almost constant in very low concentration, less than 50 ppm, in the highest case.

In the same way, Fig. 4 shows the evolution with temperature of the DME concentration profile for different pressures and values of lambda, in the presence and absence of NO.

In the absence of NO (denoted by open symbols), for the same value of lambda, as the pressure is increased, that is, to descend in a column in Fig. 4, the consumption of DME occurs at lower temperatures and the NTC zone, instead of a curve, presents the shape of a plateau. For a constant value of pressure, an increase of the oxygen availability in the reactant mixture, that is, to move to the right in the same row of Fig. 4, makes the NTC zone less pronounced. For oxidizing conditions ($\lambda=35$), it is less noticed because it occurs when the conversion of DME is near the 100%.

The inhibiting effect of NO addition is evident. The NTC zone disappears and the onset of DME conversion is shifted to higher temperatures for all the conditions analyzed in this work. However, due to the OH radicals generated during the NO_2 conversion to NO ($\text{NO}_2 + \text{H} \rightleftharpoons \text{NO} + \text{OH}$), NO can also promote DME conversion at higher temperatures above NTC zone, as can be observed, for example, at 20 bar, reducing conditions ($\lambda=0.7$) and temperatures around 775 K, and stoichiometric conditions ($\lambda=1$) and temperatures around 700 K. Once the DME conversion is initiated, its consumption occurs very fast, with a sharp decay in the DME concentration profile.

The inhibiting or promoting impact of NO on hydrocarbon oxidation has been previously discussed during the oxidation of alkanes that present the NTC zone, such as n-heptane in jet-stirred reactors [8,13], or n-pentane in an atmospheric quartz flow reactor [9]. The previous work of Alzueta et al. [17] on the interaction of DME with NO, in an atmospheric flow reactor, pointed out the promoting effect of NO addition on DME conversion under oxidizing conditions. However, unlike the present work, in the atmospheric pressure study, the NTC zone was not observed and DME consumption occurred at much higher temperatures, above 1000 K in the absence of NO. Nevertheless, it is worth to mention that because of the different pressures analyzed in each study (atmospheric or high pressure) there is a huge difference in the residence time between the Alzueta et al.'s [17] and the present works, $\tau_r(s) = 190/T(K)$ and $\tau_r(s) = 261 P(\text{bar})/T(K)$, respectively.

Regarding modeling calculations, under very oxidizing conditions ($\lambda=35$), the experimental trend observed for DME concentration in the presence of NO (Fig. 4) is not accurately reproduced by the model. In this case, simulations are almost the same with

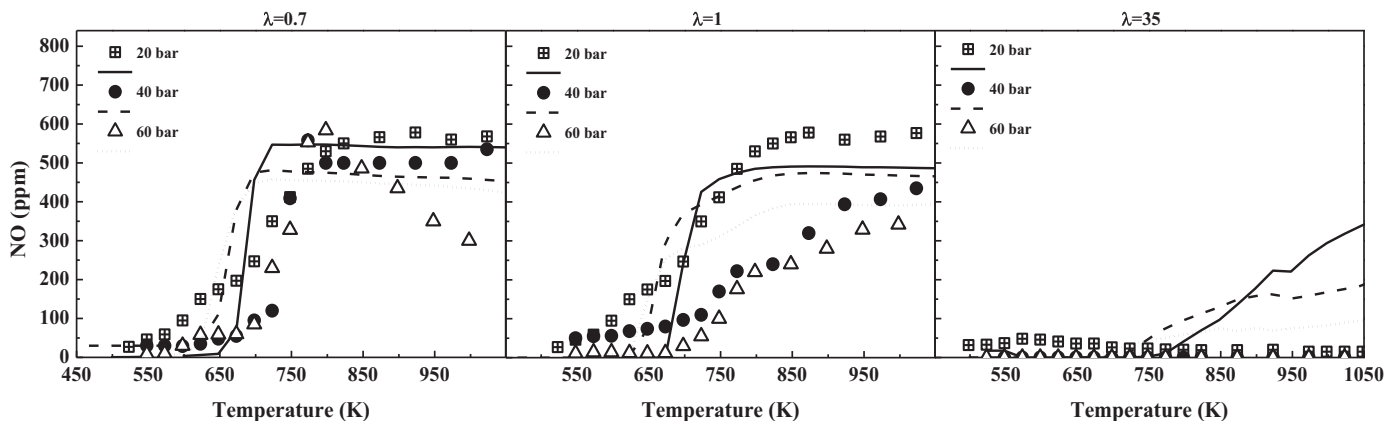


Fig. 3. Evolution for NO concentration with temperature during the high-pressure (20, 40 and 60 bar) oxidation of DME, for the conditions denoted as sets 13–21 in Table 1.

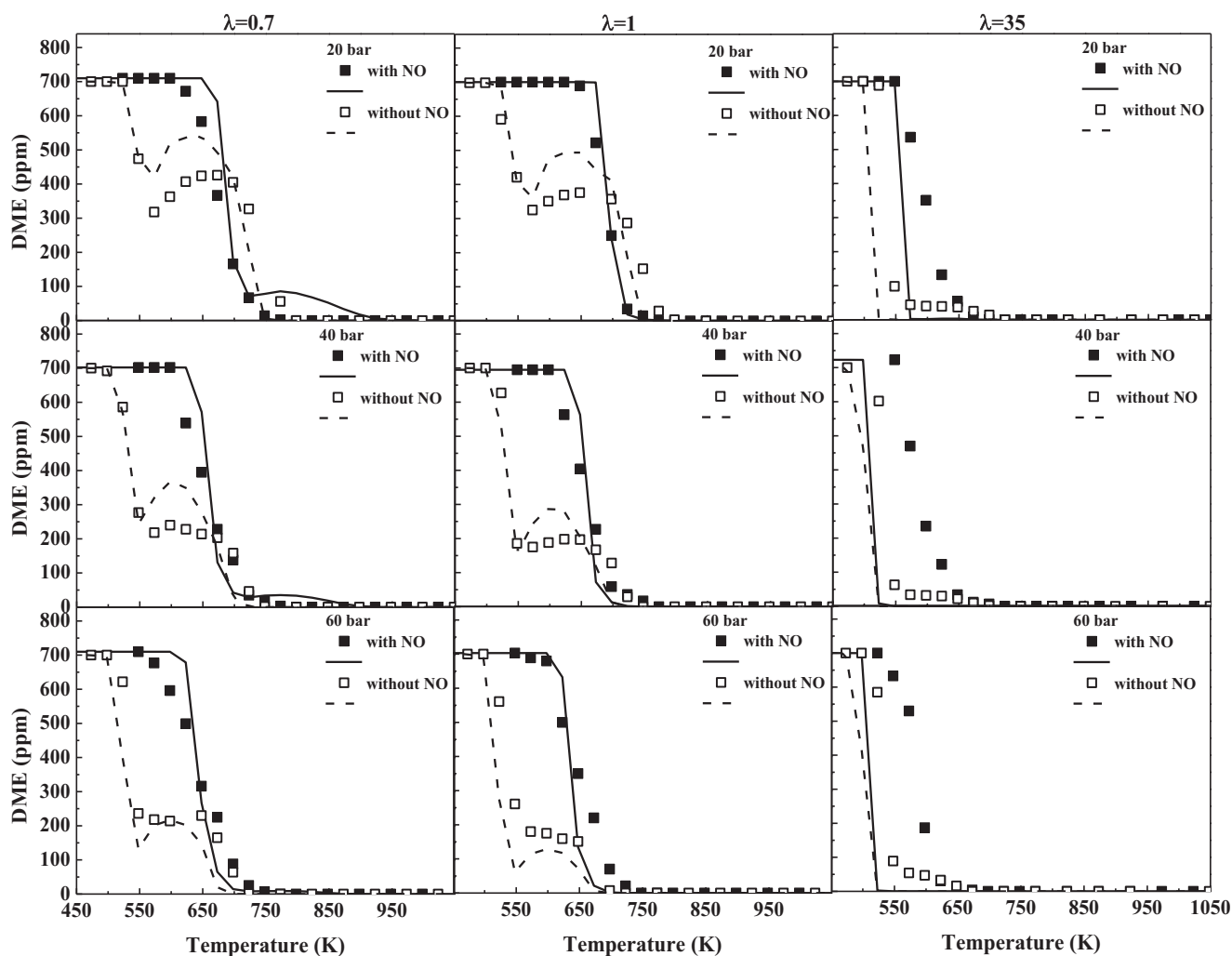


Fig. 4. Evaluation of the effect of NO presence (500 ppm) on the high-pressure (20, 40 and 60 bar) oxidation of DME, for the conditions denoted as sets 1–9 and 13–21 in Table 1. Open symbols correspond to results in the absence of NO and full symbols, in the presence of NO.

and without NO, but experimental results obtained in the presence of NO are shifted to higher temperatures, approximately 25 K. As will be seen later in the sensitivity analysis, calculations indicate that the concentration profiles are sensitive to the isomerization of alkyl peroxy radicals ($\text{CH}_3\text{OCH}_2\text{O}_2 = \text{CH}_2\text{OCH}_2\text{O}_2\text{H}$). In order to evaluate the sensitivity of this reaction, Fig. S18 in Supplementary Material shows the comparison between experimental and calculations using both the mechanism used along the present work and the same mechanism substituting the Burke et al. [29] determination by a non-pressure dependent value by Zhao et al. [28]. As seen, the fitting of experimental data and calculated results vary with the use of the non-dependent rate constant, and it improves for $\lambda = 35$. Therefore, we believe that a deeper study for this important reaction for the flow reactor experiments would be of interest. Despite of this, in general, there is a good agreement between experimental results and modeling calculations, both in the absence and presence of NO.

4.3. Reaction rate and first-order sensitivity analyses

Once the effectiveness of the present model has been proved, and in order to identify the main reaction routes for DME consumption, and especially, the routes responsible for NO inhibiting effect, reaction rate analyses have been performed. The DME oxidation chemistry at low-temperatures is more complex than at

higher temperatures as pointed out previously by Rodriguez et al. [4] in a JSR experimental work, and Tomlin et al. [37] and Eskola et al. [38] in theoretical works. Therefore, Fig. 5 shows a diagram with the main DME consumption routes in the absence of NO, for 600 K, a temperature included in the NTC zone.

The main consumption of DME is through hydrogen abstraction reactions by radicals to form the CH_3OCH_2 radical (R_3). This radical leads to the formation of methoxy methyl peroxy radical ($\text{CH}_3\text{OCH}_2\text{O}_2$) after the addition of a molecule of oxygen (R_4). The $\text{CH}_3\text{OCH}_2\text{O}_2$ radical leads to the formation of the hydroperoxyl-methylformate ($\text{HO}_2\text{CH}_2\text{OCHO}$) through a complex mechanism which involves an isomerization (R_5), a second O_2 addition (R_6) and a new isomerization followed by a decomposition (R_7).



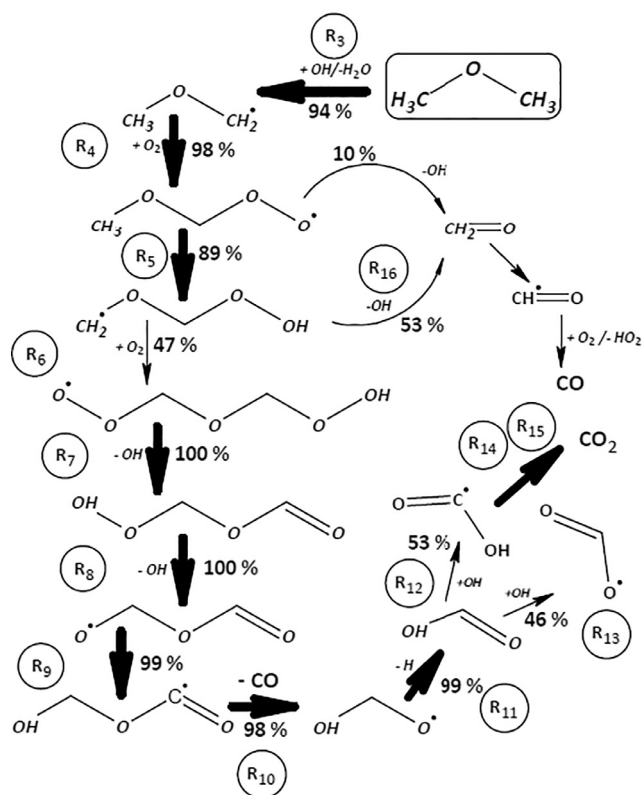
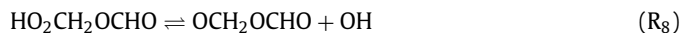


Fig. 5. Main reaction pathways for DME oxidation at 600 K. Conditions denoted as set 2 in Table 1 (20 bar, $\lambda=1$, in the absence of NO). The selected position in the reactor corresponds to 57.4 cm, the point at which the temperature profile reaches the plateau.

After subsequent isomerization and decomposition reactions formic acid is formed (sequence of reactions R_8 – R_{11})



and it continues reacting until CO_2 is produced (sequence of reactions R_{12} – R_{15}).



During this complex reaction mechanism, hydroxyl radicals are released, which are responsible for the high reactivity of DME at low temperatures. As temperature increases, β -scission of the $\text{CH}_2\text{OCH}_2\text{O}_2\text{H}$ radical forming 2 molecules of formaldehyde and only one reactive hydroxyl radical (R_{16}) becomes more relevant and, therefore, the DME reactivity decreases (NTC zone appears). For example, at 20 bar, in the absence of NO and $\lambda=1$, reaction (R_{16}) at 525 K represents a 6% of the $\text{CH}_2\text{OCH}_2\text{O}_2\text{H}$ radical total

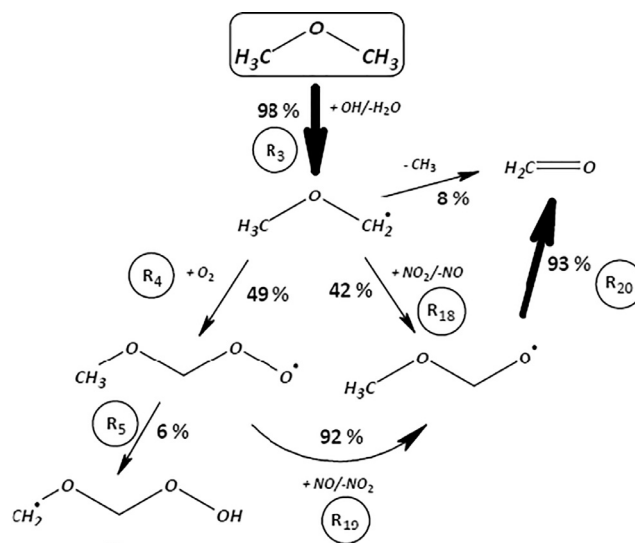
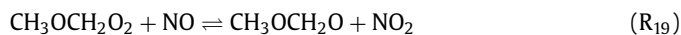
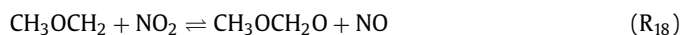


Fig. 6. Main reaction pathways for DME oxidation at 700 K. Conditions denoted as set 14 in Table 1 (20 bar, $\lambda=1$, in the presence of NO). The selected position in the reactor corresponds to 57.4 cm, the point at which the temperature profile reaches the plateau.

consumption, whereas at 600 K it represents a 53% and at 700 K, a 94%. Another β -scission reaction with increasing relevance with increasing temperature is the decomposition of CH_3OCH_2 radical forming formaldehyde and CH_3 radicals (R_{17}). Decomposition of CH_3OCH_2 radical (R_{17}) is almost negligible at 600 K, it represents a 20% of radical consumption at 700 K and a 53% at 750 K, under the same conditions above specified.



Figure 6 shows the main reaction pathways for DME consumption at 700 K, in the presence of NO (500 ppm). As in the absence of NO, the main consumption for DME is through H abstraction reactions forming the CH_3OCH_2 radical (R_3). This radical can lead to the formation of $\text{CH}_3\text{OCH}_2\text{O}_2$ radical by the addition of an oxygen molecule (R_4) and continues the reaction mechanism described above in the absence of NO, although this pathway has a lower relevance. However, a new reaction route involving NO and NO_2 competes with this first addition of O_2 . CH_3OCH_2 radical can react with NO_2 leading to the formation of NO and a new radical, $\text{CH}_3\text{OCH}_2\text{O}$ (R_{18}). This radical, which can also be produced by reaction of $\text{CH}_3\text{OCH}_2\text{O}_2$ and NO (R_{19}), later decomposes to formaldehyde (R_{20}). Therefore, in addition to reaction (R_2), NO and NO_2 are interchanged through reactions (R_{18} – R_{19}), but never consumed.



In the decomposition of $\text{CH}_3\text{OCH}_2\text{O}$ (R_{20}), besides formaldehyde, methoxy radicals (CH_3O) are also formed, and then react with O_2 , NO_2 or NO to produce more formaldehyde (R_{21} – R_{23}). There is a competition between these three CH_3O consumption reactions, with reaction with O_2 (R_{21}) being the most relevant, followed by the reaction with NO_2 (R_{22}) and finally by the reaction with NO (R_{23}).



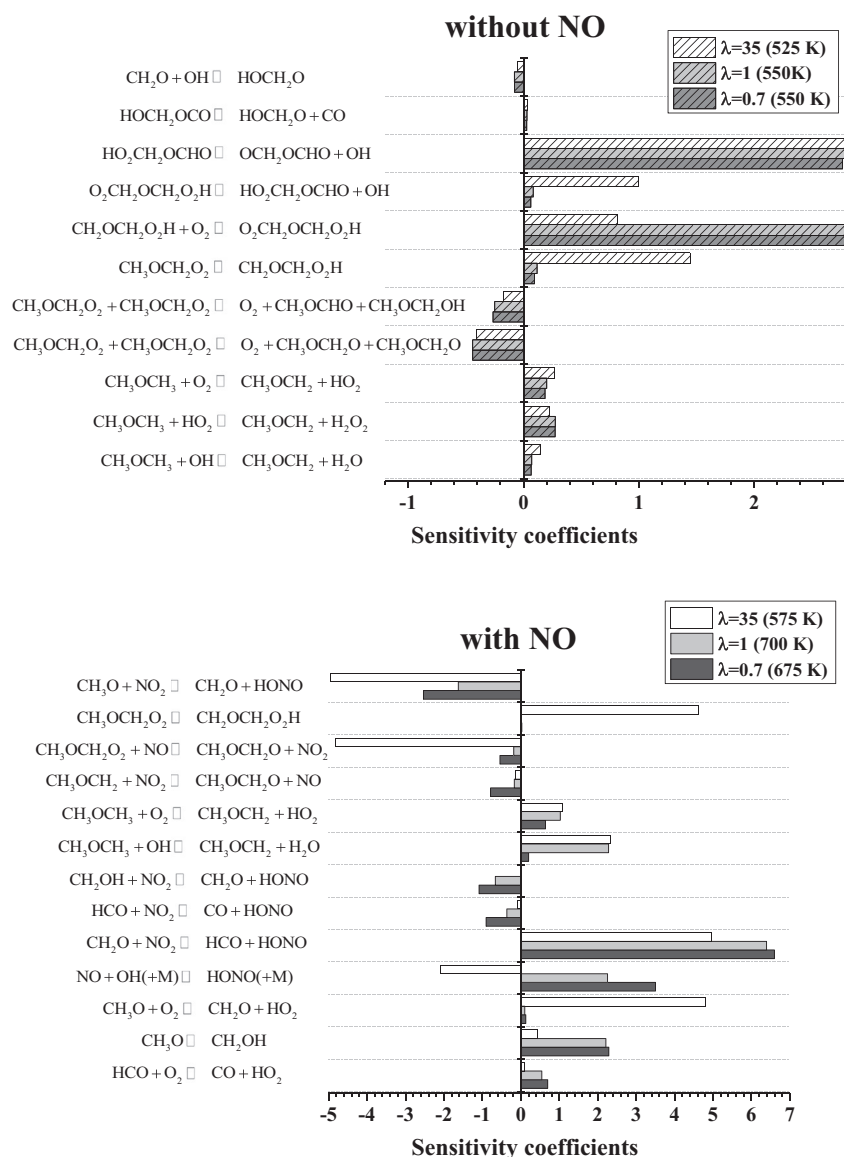


Fig. 7. Sensitivity analysis for CO for different air excess ratios and 20 bar. Top: in the absence of NO. Bottom: in the presence of NO.



The analysis of the reaction pathways has been completed with a first-order sensitivity analysis for CO for the different air excess ratios analyzed, 20 bar and in the absence and presence of NO. In each case, temperatures near the initiation of DME conversion, at which the CO concentration predicted by the model corresponds to a value around 30 ppm, have been selected. Figure 7 shows a comparison of the sensitivity coefficients obtained in the presence and in the absence of NO.

In the absence of NO, the isomerization of the methoxy methyl peroxy radical ($\text{CH}_3\text{OCH}_2\text{O}_2$) (R_5) and the decomposition of the hydroperoxyl-methylformate ($\text{HO}_2\text{CH}_2\text{OCHO}$) (R_8) present a high sensitivity due to the OH radicals generated directly, in the decomposition, or indirectly through the low-temperature mechanism described previously and represented in Fig. 5. This mechanism involves the $\text{CH}_3\text{OCH}_2\text{O}_2$ isomerization (R_5) and the O_2 addition to $\text{CH}_2\text{OCH}_2\text{O}_2\text{H}$ (R_6), also with a high sensitivity coefficient. In an

opposite way, the self-reaction of $\text{CH}_3\text{OCH}_2\text{O}_2$ radicals results in less CO formation because it reduces the amount of $\text{CH}_3\text{OCH}_2\text{O}_2$ radicals than can react through the low-temperature mechanism.

In the presence of NO, the reaction of $\text{CH}_3\text{OCH}_2\text{O}_2$ with NO (generally represented as $\text{RO}_2 + \text{NO} = \text{RO} + \text{NO}_2$, R_{19}) decreases the global system reactivity. This reaction, that is in competition with reaction (R_5), reduces the availability of hydroperoxide species (RO_2) and, therefore, the formation of hydroxyl radicals from hydroperoxide decomposition reactions during the low-temperature mechanism, because the resulting RO radical decomposes directly to formaldehyde (R_{20}). On the contrary, the isomerization of $\text{CH}_3\text{OCH}_2\text{O}_2$ has a positive sensitivity coefficient (R_5), because, as in the absence of NO, this reaction corresponds to the initial steps of the low-temperature mechanism.

5. Conclusions

The effect of NO presence on the DME high pressure oxidation has been evaluated by means of novel experimental results obtained in a plug flow reactor at 20, 40 and 60 bar, in the 450–1050 K range and for different values of the air excess ratio ($\lambda = 0.7$,

1 and 35). Additionally, a chemical kinetic mechanism has been used which provides a good agreement with the trends experimentally observed. Moreover, modeling calculations with the present mechanism have been successfully compared with experimental data from literature.

The presence of NO clearly inhibits DME oxidation in the 550–700K temperature range, where the NTC zone was previously observed in the absence of NO. Reaction rate analyses performed indicate that the main consumption of DME is through H abstraction forming the CH_3OCH_2 radical ($\text{CH}_3\text{OCH}_3 + \text{R} \Rightarrow \text{CH}_3\text{OCH}_2 + \text{RH}$). In the absence of NO, it reacts with O_2 to form $\text{CH}_3\text{OCH}_2\text{O}_2$ ($\text{CH}_3\text{OCH}_2 + \text{O}_2 \Rightarrow \text{CH}_3\text{OCH}_2\text{O}_2$) and it continues reacting through a complex mechanism while OH radicals are generated. But, in the presence of NO, the $\text{CH}_3\text{OCH}_2 + \text{O}_2$ reaction is in competition with $\text{CH}_3\text{OCH}_2 + \text{NO}_2$ channel producing NO which reacts with $\text{CH}_3\text{OCH}_2\text{O}_2$ ($\text{CH}_3\text{OCH}_2\text{O}_2 + \text{NO} \Rightarrow \text{CH}_3\text{OCH}_2\text{O} + \text{NO}_2$), inhibiting the low-temperature DME oxidation. Consequently, NO and NO_2 are interchanged in a cycle but never consumed.

Acknowledgments

The authors express their gratitude to Aragón Government and European Social Fund (GPT group), and to MINECO and FEDER (Project CTQ2015-65226) for financial support. Ms. Marrodán acknowledges Aragón Government for the predoctoral grant awarded.

Supplementary materials

Supplementary material associated with this article can be found, in the online version, at doi:10.1016/j.combustflame.2018.07.005.

References

- [1] C. Arcoumanis, C. Bae, R. Crookes, E. Kinoshita, The potential of di-methyl ether (DME) as an alternative fuel for compression-ignition engines: a review, *Fuel* 87 (2008) 1014–1030.
- [2] S.H. Park, C.S. Lee, Combustion performance and emission reduction characteristics of automotive DME engine system, *Prog. Energy Combust. Sci.* 39 (2013) 147–168.
- [3] T.A. Semelsberger, R.L. Borup, H.L.J. Greene, Dimethyl ether (DME) as an alternative fuel, *J. Power Sources* 156 (2006) 497–511.
- [4] A. Rodriguez, O. Frottier, O. Herbinet, R. Fournet, R. Bounaceur, C. Fittschen, F. Battin-Leclerc, Experimental and modeling investigation of the low-temperature oxidation of dimethyl ether, *J. Phys. Chem. A* 119 (2015) 7905–7923.
- [5] U. Asad, M. Zheng, Exhaust gas recirculation for advanced diesel combustion cycles, *Appl. Energy* 123 (2014) 242–252.
- [6] J.E. Dec, Advanced compression-ignition engines. Understanding the in-cylinder processes, *Proc. Combust. Inst.* 32 (2009) 2727–2742.
- [7] Z. Chen, P. Zhang, Y. Yang, M.J. Brear, X. He, Z. Wang, Impact on nitric oxide (NO) on n-heptane autoignition in a rapid compression machine, *Combust. Flame* 186 (2017) 94–104.
- [8] G. Moréac, P. Dagaut, J.F. Roesler, M. Cathonnet, Nitric oxide interactions with hydrocarbon oxidation in a jet-stirred reactor at 10 atm, *Combust. Flame* 145 (2006) 512–520.
- [9] P.A. Glaude, N. Marinov, Y. Koshiishi, N. Matsunaga, M. Hori, Kinetic modeling of the mutual oxidation of NO and larger alkanes at low temperature, *Energy Fuels* 19 (2005) 1839–1849.
- [10] P. Dagaut, A. Nicolle, Experimental study and detailed kinetic modeling of the effect of exhaust gas on fuel combustion: mutual sensitization of the oxidation of nitric oxide and methane over extended temperature and pressure ranges, *Combust. Flame* 140 (2005) 161–171.
- [11] P. Dagaut, J. Luche, M. Cathonnet, Reduction of NO by n-butane in a JSR: experiments and kinetic modeling, *Energy Fuels* 14 (2000) 712–719.
- [12] A.B. Bendtsen, P. Glarborg, K. Dam-Johansen, Low temperature oxidation of methane: the influence of nitrogen oxides, *Combust. Sci. Technol.* 151 (2000) 31–71.
- [13] J.M. Anderlohr, R. Bounaceur, A. Pires Da Cruz, F. Battin-Leclerc, Modeling of autoignition and NO sensitization for the oxidation of IC engine surrogate fuels, *Combust. Flame* 156 (2009) 505–521.
- [14] M.U. Alzueta, J.M. Hernández, Ethanol oxidation and its interaction with nitric oxide, *Energy Fuels* 16 (2002) 166–171.
- [15] M.U. Alzueta, R. Bilbao, M. Finestra, Methanol oxidation and its interaction with nitric oxide, *Energy Fuels* 15 (2001) 724–729.
- [16] P. Glarborg, M.U. Alzueta, K. Dam-Johansen, J.A. Miller, Kinetic modeling of hydrocarbon/nitric oxide interactions in a flow reactor, *Combust. Flame* 115 (1998) 1–27.
- [17] M.U. Alzueta, J. Muro, R. Bilbao, P. Glarborg, Oxidation of dimethyl ether and its interaction with nitrogen oxides, *Isr. J. Chem.* 39 (1999) 73–86.
- [18] L. Marrodán, L. Berdusán, V. Aranda, Á. Millera, R. Bilbao, M.U. Alzueta, Influence of dimethyl ether addition on the oxidation of acetylene in the absence and presence of NO, *Fuel* 183 (2016) 1–8.
- [19] L. Marrodán, Á. Millera, R. Bilbao, M.U. Alzueta, High-pressure study of methyl formate oxidation and its interaction with NO, *Energy Fuels* 28 (2014) 6107–6115.
- [20] C.L. Rasmussen, J. Hansen, P. Marshall, P. Glarborg, Experimental measurements and kinetic modeling of $\text{CO}/\text{H}_2/\text{O}_2/\text{NO}_x$ conversion at high pressure, *Int. J. Chem. Kinet.* 40 (2008) 454–480.
- [21] P. Glarborg, M. Østberg, M.U. Alzueta, K. Dam-Johansen, J.A. Miller, The recombination of hydrogen atoms with nitric oxide at high temperatures, *Proc. Combust. Inst.* 27 (1999) 219–227.
- [22] M.U. Alzueta, M. Borruey, A. Callejas, Á. Millera, R. Bilbao, An experimental and modeling study of the oxidation of acetylene in a flow reactor, *Combust. Flame* 152 (2008) 377–386.
- [23] N. Faßheber, G. Friedrichs, P. Marshall, P. Glarborg, Glyoxal oxidation mechanism: implications for the reactions $\text{HCO} + \text{O}_2$ and $\text{OCHCHO} + \text{HO}_2$, *J. Phys. Chem. A* 119 (2015) 7305–7315.
- [24] C.L. Rasmussen, P. Glarborg, Measurements and kinetic modeling of CH_4/O_2 and $\text{CH}_4/\text{C}_2\text{H}_6/\text{O}_2$ conversion at high-pressure, *Int. J. Chem. Kinet.* 40 (2008) 778–807.
- [25] C.L. Rasmussen, K.H. Andersen, K. Dam-Johansen, P. Glarborg, Methanol oxidation in a flow reactor: implications for the branching ratio of the $\text{CH}_3\text{OH} + \text{OH}$ reaction, *Int. J. Chem. Kinet.* 40 (2008) 423–441.
- [26] C.L. Rasmussen, P. Glarborg, Sensitizing effects of NO_x on CH_4 oxidation at high pressure, *Combust. Flame* 154 (2008) 529–545.
- [27] J. Giménez-López, C.T. Rasmussen, H. Hashemi, M.U. Alzueta, Y. Gao, P. Marshall, C.F. Goldsmith, P. Glarborg, Experimental and kinetic modeling study of C_2H_2 oxidation at high pressure, *Int. J. Chem. Kinet.* 48 (2016) 724–738.
- [28] Z. Zhao, M. Chaos, A. Kazakov, F.L. Dryer, Thermal decomposition reaction and a comprehensive kinetic model of dimethyl ether, *Int. J. Chem. Kinet.* 40 (2008) 1–18.
- [29] U. Burke, K.P. Somers, P. O’Toole, C.M. Zinner, N. Marquet, G. Bourque, E.L. Petersen, W.K. Metcalfe, Z. Serinyel, H.J. Curran, An ignition delay and kinetic modeling study of methane, dimethyl ether, and their mixtures at high pressures, *Combust. Flame* 162 (2015) 315–330.
- [30] Z. Wang, X. Zhang, L. Xing, L. Zhang, F. Herrmann, K. Moshhammer, F. Qi, K. Kohse-Höinghaus, Experimental and kinetic modeling study of the low- and intermediate-temperature oxidation of dimethyl ether, *Combust. Flame* 162 (2015) 1113–1125.
- [31] E.E. Dames, A.S. Rosen, B.W. Weber, C.W. Gao, C.-J. Sung, W.H. Green, A detailed combined experimental and theoretical study on dimethyl ether/propane blended oxidation, *Combust. Flame* 168 (2016) 310–330.
- [32] P. Marshall, P. Glarborg, Ab initio and kinetic modeling studies of formic acid oxidation, *Proc. Combust. Inst.* 35 (2015) 153–160.
- [33] L. Marrodán, E. Royo, Á. Millera, R. Bilbao, M.U. Alzueta, High pressure oxidation of dimethoxymethane, *Energy Fuels* 29 (2015) 3507–3517.
- [34] L. Marrodán, Á.J. Arnal, Á. Millera, R. Bilbao, M.U. Alzueta, High-pressure ethanol oxidation and its interaction with NO, *Fuel* 223 (2018) 394–400.
- [35] T. Yamada, J.W. Bozelli, T.H. Lay, Comparisons of CBS-q and G2 calculations on thermodynamic properties, transition states, and kinetics on dimethyl-ether+ O_2 reaction system, *Int. J. Chem. Kinet.* 32 (2000) 435–452.
- [36] ANSYS Chemkin-Pro 17.2; Reaction Design: San Diego, 2016.
- [37] A.S. Tomlin, E. Agbro, V. Nevrlý, J. Dlabka, M. Vašínek, Evaluation of combustion mechanisms using global uncertainty and sensitivity analyses: a case study for low-temperature dimethyl ether oxidation, *Int. J. Chem. Kinet.* 46 (2014) 662–682.
- [38] A.J. Eskola, S.A. Carr, R.J. Shannon, B. Wang, M.A. Blitz, M.J. Pilling, P.W. Seakins, S.H. Robertson, Analysis of the kinetics and yields of OH radical production from the $\text{CH}_3\text{OCH}_2 + \text{O}_2$ reaction in the temperature range 195–650 K: an experimental and computational study, *J. Phys. Chem. A* 118 (2014) 6773–6788.

THE INHIBITING EFFECT OF NO ADDITION ON DIMETHYL ETHER HIGH-PRESSURE OXIDATION

Lorena Marrodán, Álvaro J. Arnal, Ángela Millera, Rafael Bilbao, María U. Alzueta*

Aragón Institute of Engineering Research (I3A). Department of Chemical and Environmental
Engineering. University of Zaragoza. C/ Mariano Esquillor, s/n. 50018 Zaragoza. Spain

**SUPPLEMENTARY
MATERIAL**

Table of contents^(a)

1) Temperature profiles inside the reactor.

Figure S1. Temperature profiles for different nominal temperatures as a function of distance for a flow rate of 1 L(STP)/min and 20 bar.

Figure S2. Temperature profiles for different nominal temperatures as a function of distance for a flow rate of 1 L(STP)/min and 40 bar.

Figure S3. Temperature profiles for different nominal temperatures as a function of distance for a flow rate of 1 L(STP)/min and 60 bar.

2) Comparison of high-pressure flow reactor data obtained in the present work and modeling calculations obtained using models from literature.

Figure S4. Comparison of high-pressure (20 bar) flow reactor data obtained in the present work and modeling calculations obtained using models from literature: Zhao et al. [1], Rodriguez et al. [2], Wang et al. [3] and Dames et al. [4].

Figure S5. Comparison of high-pressure (40 bar) flow reactor data obtained in the present work and modeling calculations obtained using models from literature: Zhao et al. [1], Rodriguez et al. [2], Wang et al. [3] and Dames et al. [4].

Figure S6. Comparison of high-pressure (60 bar) flow reactor data obtained in the present work and modeling calculations obtained using models from literature: Zhao et al. [1], Rodriguez et al. [2], Wang et al. [3] and Dames et al. [4].

3) Review of the different thermodynamic values proposed in recent mechanisms of the literature.

Table S1. Calculations for enthalpy of formation, entropy and heat capacity for the different values found in literature.

4) Comparison of modeling calculations obtained with the mechanism from our research group previously validated for atmospheric conditions [7] and the present mechanism.

Figure S7. Comparison of modeling calculations obtained with our mechanism previously validated for atmospheric conditions [7] and the present mechanism, for the conditions denoted as sets 1-3 in Table 1. Experimental results are denoted by symbols and modeling calculations by lines.

5) Comparison of simulations using the present mechanism with data from literature.

A) Shock tube

Figure S8. Comparison with shock tube data from Pfahl et al. [8] (P=13 and 40 bar, stoichiometric mixtures). Symbols represent literature experimental data and lines modeling calculations obtained using the present mechanism.

Figure S9. Comparison with shock tube data from Li et al. [9] (P=22 bar, $\phi=1$ and 0.5). Symbols represent literature experimental data and lines modeling calculations obtained using the present mechanism.

B) Rapid compression machine and shock tube

Figure S10. Comparison with RCM data from Burke et al. [5] (P=11.9 and 25 atm, stoichiometric mixtures). Symbols represent literature experimental data and lines modeling calculations obtained using the present mechanism.

C) Jet-stirred reactor

Figure S11. Comparison with jet-stirred data from Dagaut et al. [10] (P=10 atm, $t_r=1$ s, $\phi=1$ and 0.2, 0.2% DME, dilution in N₂). Symbols represent literature experimental data and lines modeling calculations obtained using the present mechanism.

Figure S12. Comparison with jet-stirred data from Rodriguez et al. [2] (P=106.7 kPa, $t_r=2$ s, $\phi=2$, 1 and 0.25, 2% DME, dilution in He). Symbols represent literature experimental data and lines modeling calculations obtained using the present mechanism.

D) Flow reactor

Figure S13. Comparison with flow reactor data from Alzueta et al. [11] (P=1 atm, $\lambda=1$, 500 ppm DME, dilution in N₂). Symbols represent literature experimental data and lines modeling calculations obtained using the present mechanism.

Figure S14. Comparison with flow reactor data from Alzueta et al. [11] (P=1 atm, $\lambda=1$, 500 ppm DME, 500 ppm NO, dilution in N₂). Symbols represent literature experimental data and lines modeling calculations obtained using the present mechanism.

Figure S15. Comparison with flow reactor data from Curran et al. [12] (P=12.5 atm, $t_r=1.8$, $\phi=1.13$, 3030 ppm DME, dilution in N₂). Symbols represent literature experimental data and lines modeling calculations obtained using the present mechanism.

Figure S16. Comparison with flow reactor data from Hermann et al. [13] (P=0.97 bar, $\phi=1.2$, 1 and 0.8, dilution in Ar). Symbols represent literature experimental data and lines modeling calculations obtained using the present mechanism.

Figure S17. Comparison with flow reactor data from Kurimoto et al. [14] (P=1 atm, $\phi=0.2$, 0.5 % DME, dilution in He/Ar). Symbols represent literature experimental data and lines modeling calculations obtained using the present mechanism.

6) Evaluation of the sensitivity of the $\text{CH}_3\text{OCH}_2\text{O}_2=\text{CH}_2\text{OCH}_2\text{O}_2\text{H}$ reaction in modeling calculations.

Figure S18. Comparison between experimental and modeling results with and without pressure dependency for the $\text{CH}_3\text{OCH}_2\text{O}_2=\text{CH}_2\text{OCH}_2\text{O}_2\text{H}$ reaction, for 20 bar, different values of λ and in the absence/presence of NO.

7) References

^(a) References used along the Supplementary Material file have their own numeration, which can be different from the one used in the main body of the paper. They are listed at the end of this file.

1) Temperature profiles inside the reactor.

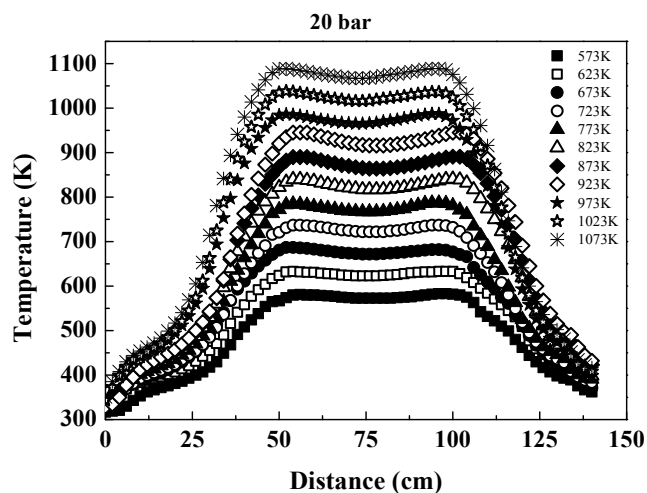


Figure S1. Temperature profiles for different nominal temperatures as a function of distance for a flow rate of 1 L(STP)/min and 20 bar.

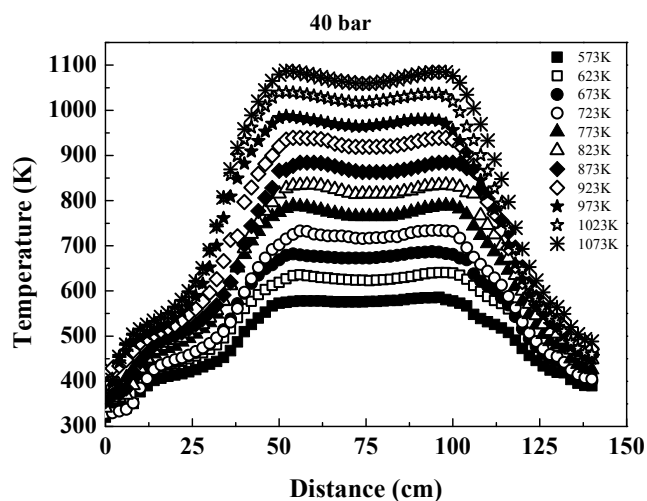


Figure S2. Temperature profiles for different nominal temperatures as a function of distance for a flow rate of 1 L(STP)/min and 40 bar.

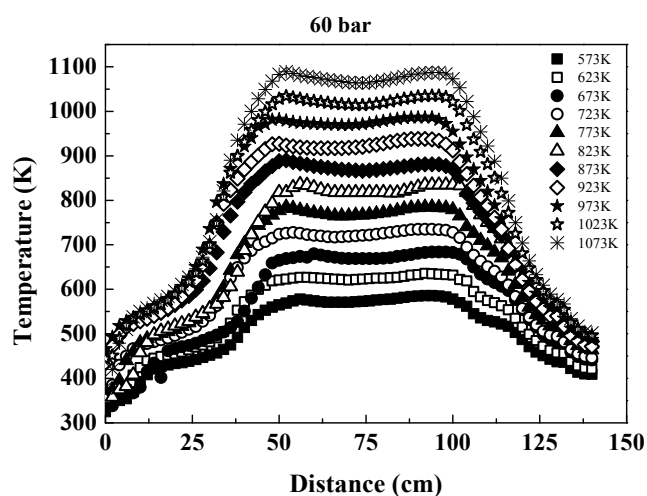


Figure S3. Temperature profiles for different nominal temperatures as a function of distance for a flow rate of 1 L(STP)/min and 60 bar.

2) Comparison of high-pressure flow reactor data obtained in the present work and modeling calculations obtained using models from literature.

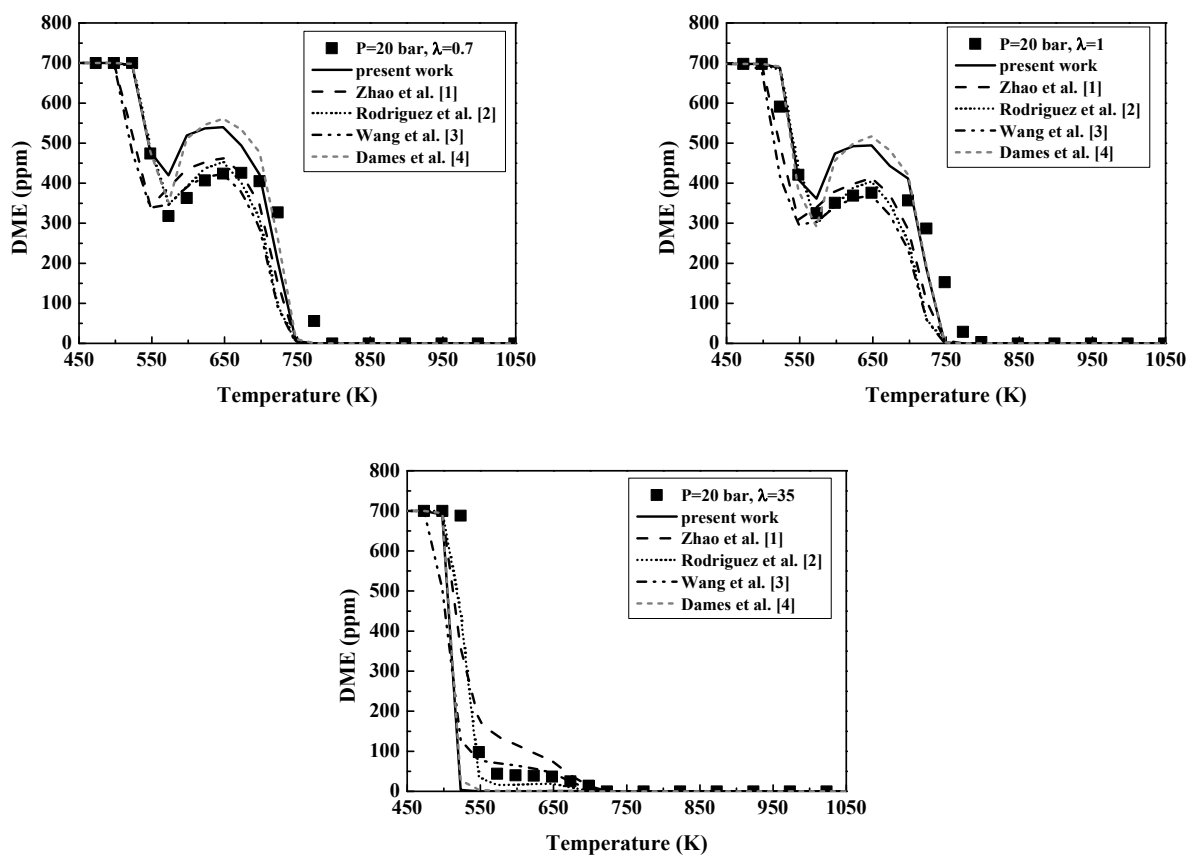


Figure S4. Comparison of high-pressure (20 bar) flow reactor data obtained in the present work and modeling calculations obtained using models from literature: Zhao et al. [1], Rodriguez et al. [2], Wang et al. [3] and Dames et al. [4].

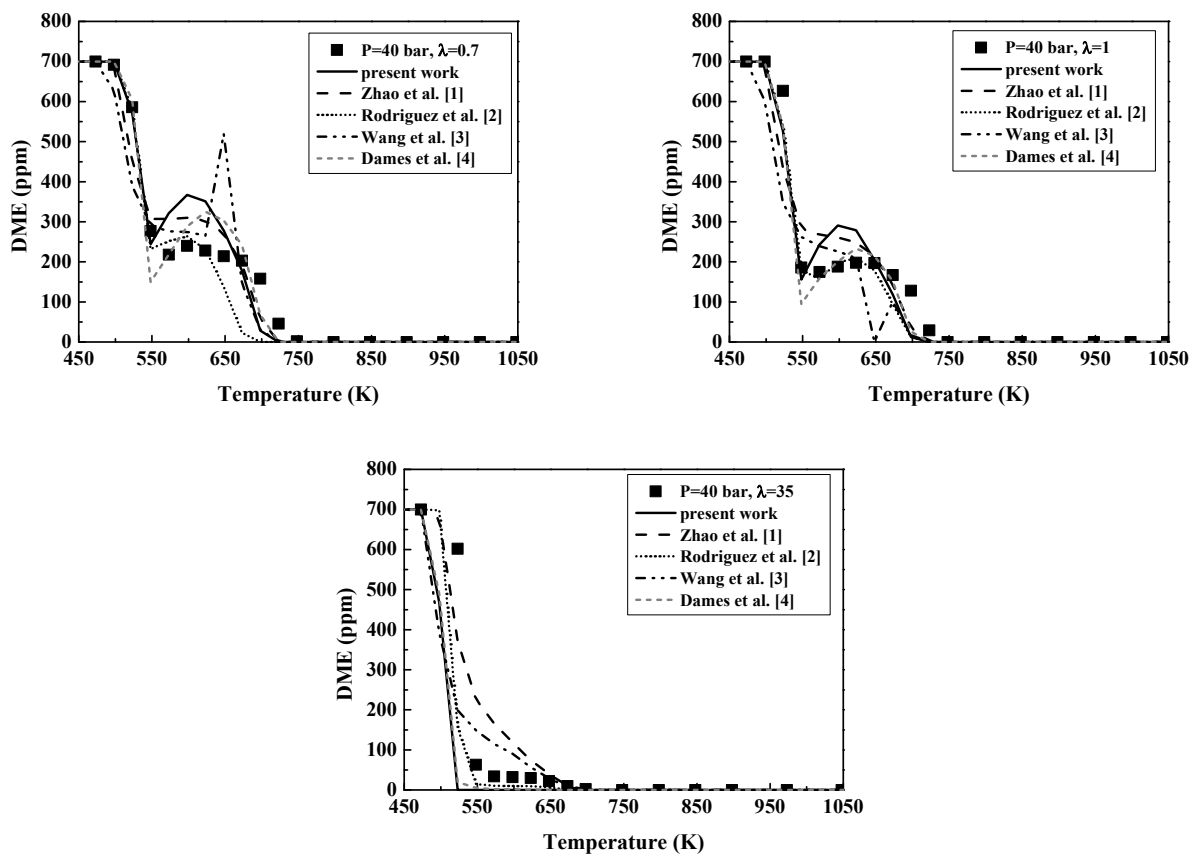


Figure S5. Comparison of high-pressure (40 bar) flow reactor data obtained in the present work and modeling calculations obtained using models from literature: Zhao et al. [1], Rodriguez et al. [2], Wang et al. [3] and Dames et al. [4].

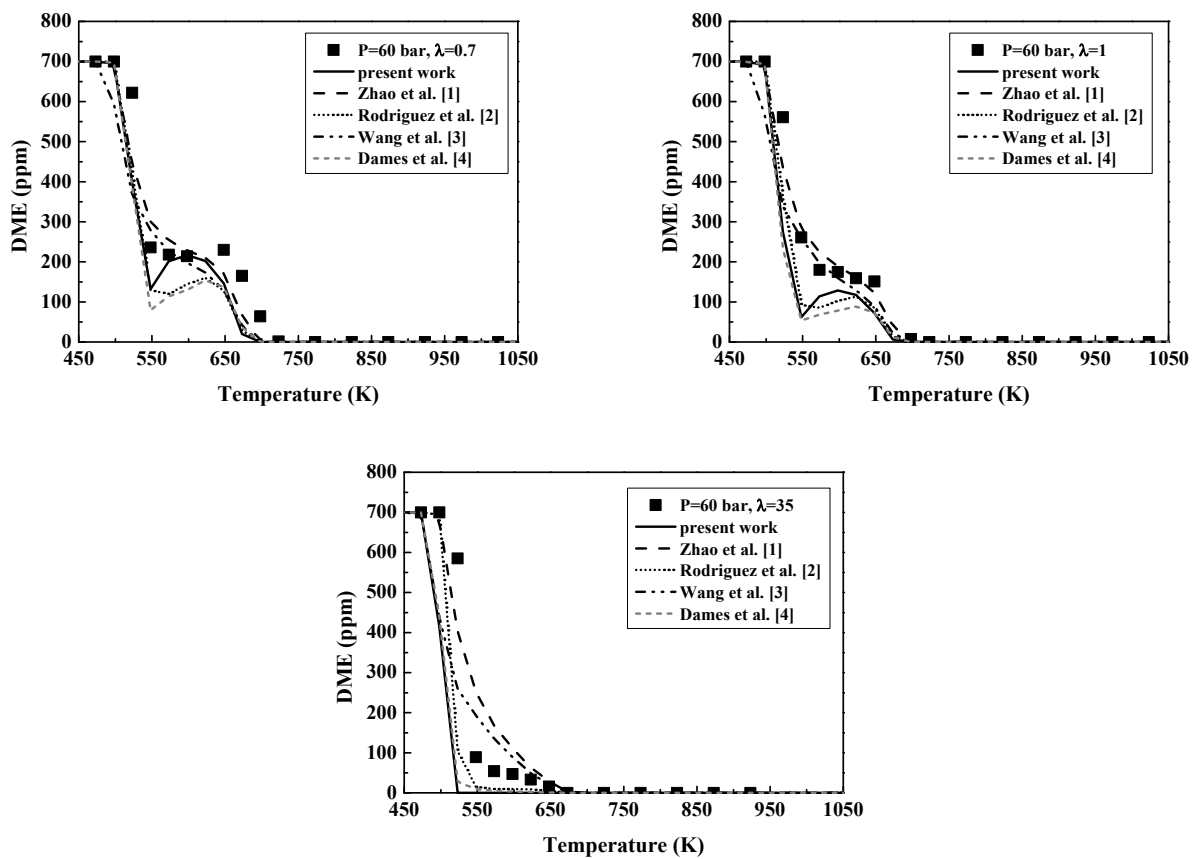


Figure S6. Comparison of high-pressure (60 bar) flow reactor data obtained in the present work and modeling calculations obtained using models from literature: Zhao et al. [1], Rodriguez et al. [2], Wang et al. [3] and Dames et al. [4].

3) Review of the different thermodynamic values proposed in recent mechanisms of the literature.

Table S1. Calculations for enthalpy of formation, entropy and heat capacity for the different values found in literature.

		Enthalpy of formation at 298 K (kcal/mol) (300-1000K)	Entropy of formation at 298 K (cal/mol) (300-1000K)	Heat capacity at 300 K (cal/mol K) (300-1000K)
CH₃OCH₂	Burke et al. [5]	-1.70	64.10	19.75
	Dames et al. [4]	0.63	44.87	16.04
	Rodriguez et al. [2]	-0.55	65.55	18.77
	Wang et al. [3]	-1.05	63.19	22.15
	Zhao et al. [1]	-1.05	63.19	22.15
	Yamada et al. [6] ^(a)	0.1	67.67	14.79
CH₃OCH₂O₂	Burke et al. [5]	-38.50	78.04	30.13
	Dames et al. [4]	-35.25	82.99	20.90
	Rodriguez et al. [2]	-36.07	77.83	28.33
	Wang et al. [3]	-37.30	77.04	31.07
	Zhao et al. [1]	-37.30	77.04	31.07
	Yamada et al. [6] ^(a)	-33.9	83.10	21.34
CH₂OCH₂O₂H	Burke et al. [5]	-27.61	81.07	81.07
	Dames et al. [4]	-25.52	85.98	85.98
	Rodriguez et al. [2]	-27.24	81.86	81.86
	Wang et al. [3]	-26.87	79.83	79.83
	Zhao et al. [1]	-26.87	79.83	79.83
	Yamada et al. [6] ^(a)	-1.8	87.73	22.40

^(a) The values have been taken directly from the paper.

4) Comparison of modeling calculations obtained with the mechanism from our research group previously validated for atmospheric conditions [7] and the present mechanism.

As an example of the relevance of modifications done to the mechanism, Figure S7 shows a comparison of modeling predictions obtained with the first mechanism from our research group [7] without any modifications, which was validated for atmospheric pressure conditions, and the present mechanism after the changes detailed in the manuscript, for the experimental conditions denoted as sets 1-3 in Table 1. As it can be observed, the match between experimental results and modeling calculations improves considerably with the described modifications.

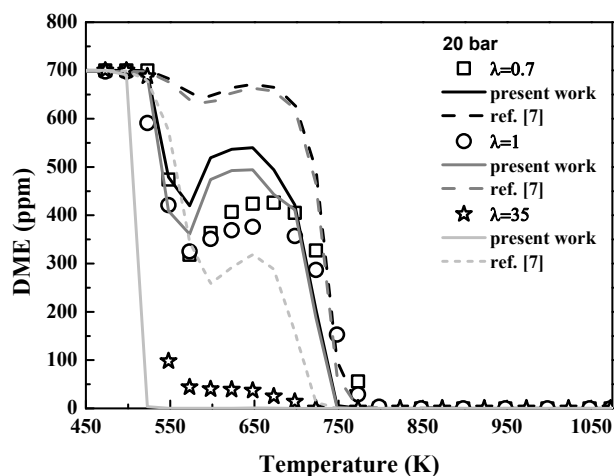


Figure S7. Comparison of modeling calculations obtained with our mechanism previously validated for atmospheric conditions [7] and the present mechanism, for the conditions denoted as sets 1-3 in Table 1. Experimental results are denoted by symbols and modeling calculations by lines.

5) Comparison of simulations using the present mechanism with data from literature.

A) Shock tube

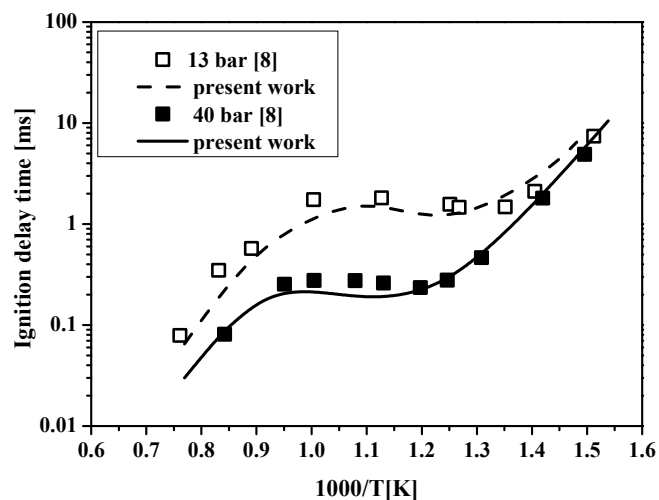


Figure S8. Comparison with shock tube data from Pfahl et al. [8] ($P=13$ and 40 bar, stoichiometric mixtures). Symbols represent literature experimental data and lines modeling calculations obtained using the present mechanism.

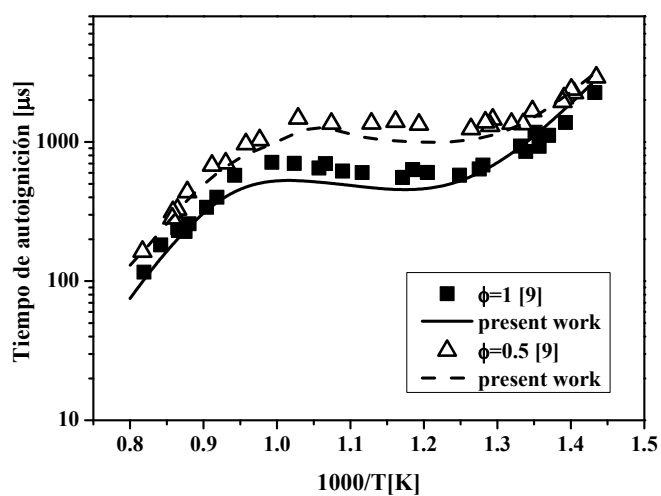


Figure S9. Comparison with shock tube data from Li et al. [9] ($P=22$ bar, $\phi=1$ and 0.5). Symbols represent literature experimental data and lines modeling calculations obtained using the present mechanism.

B) Rapid compression machine and shock tube

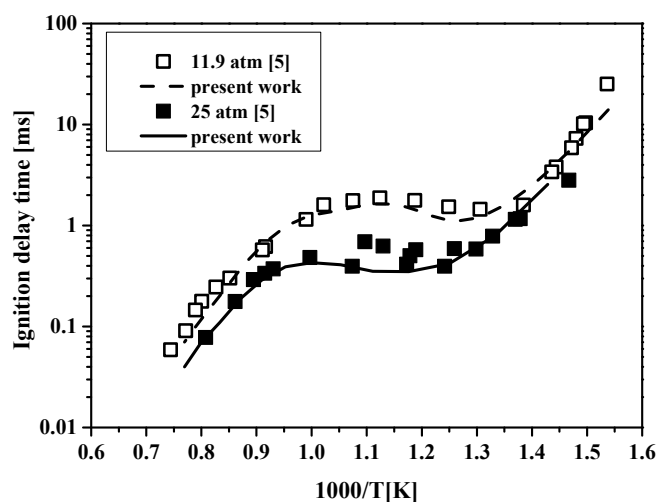


Figure S10. Comparison with rapid compression machine and shock tube data from Burke et al. [5] ($P=11.9$ and 25 atm, stoichiometric mixtures). Symbols represent literature experimental data and lines modeling calculations obtained using the present mechanism.

C) Jet-stirred reactor

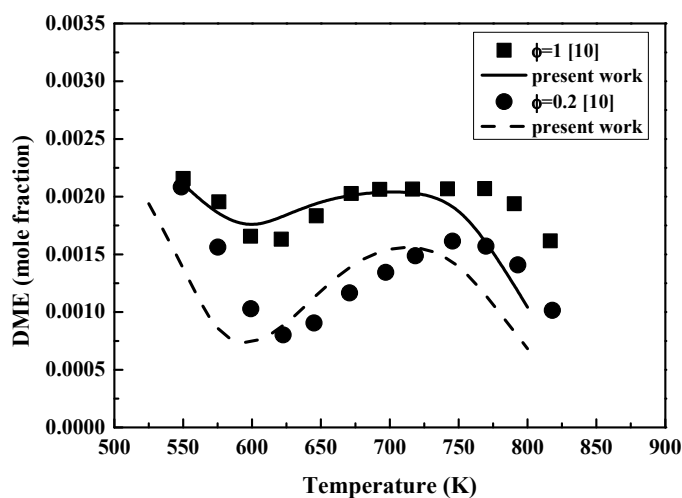


Figure S11. Comparison with jet-stirred data from Dagaut et al. [10] ($P=10$ atm, $t_r=1$ s, $\phi=1$ and 0.2, 0.2% DME, dilution in N_2). Symbols represent literature experimental data and lines modeling calculations obtained using the present mechanism.

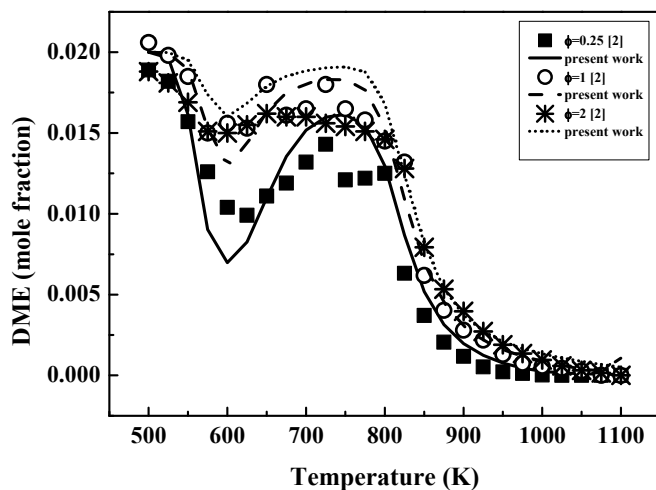


Figure S12. Comparison with jet-stirred data from Rodriguez et al. [2] ($P=106.7$ kPa, $t_r=2$ s, $\phi=2, 1$ and 0.25 , 2% DME, dilution in He). Symbols represent literature experimental data and lines modeling calculations obtained using the present mechanism.

D) Flow reactor

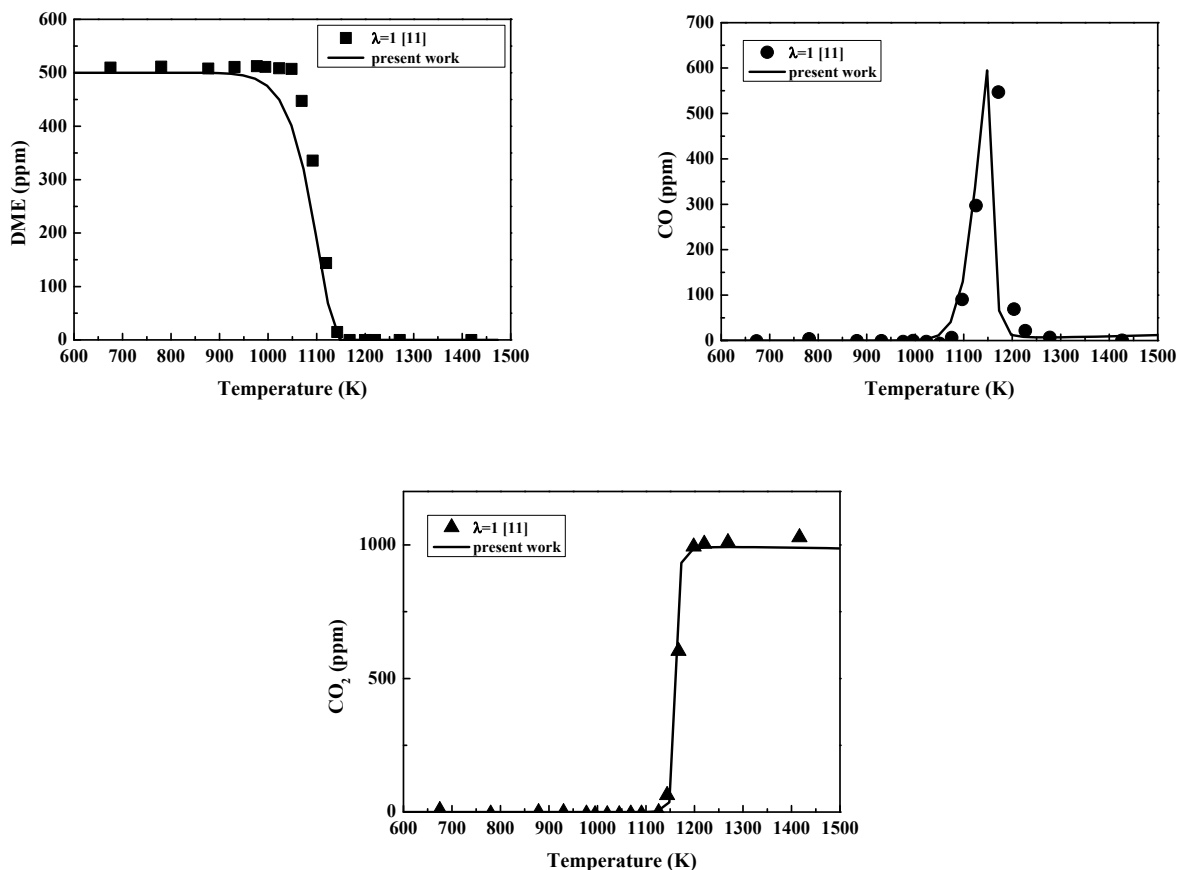


Figure S13. Comparison with flow reactor data from Alzueta et al. [11] ($P=1$ atm, $\lambda=1$, 500 ppm DME, dilution in N_2). Symbols represent literature experimental data and lines modeling calculations obtained using the present mechanism.

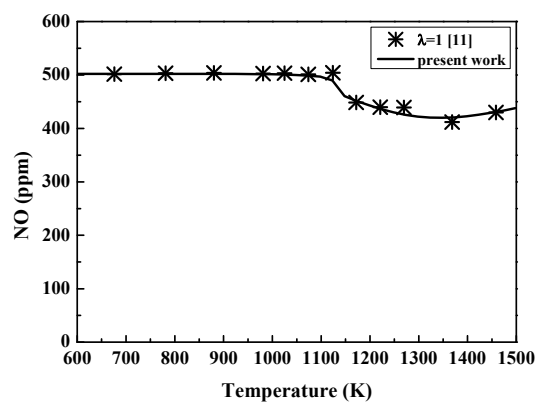
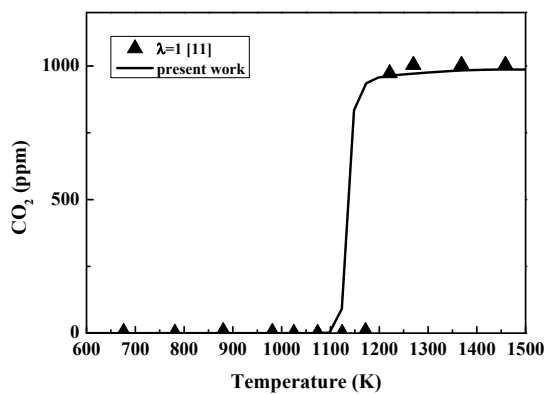
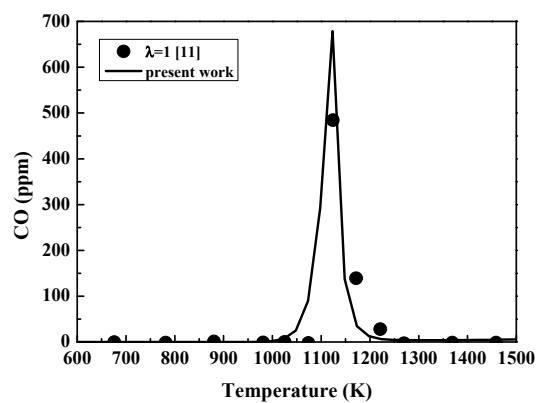
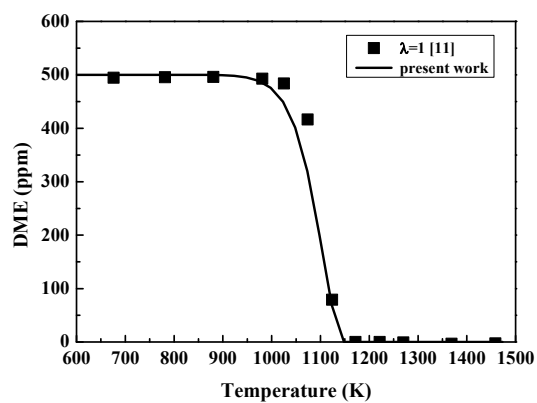


Figure S14. Comparison with flow reactor data from Alzueta et al. [11] ($P=1$ atm, $\lambda=1$, 500 ppm DME, 500 ppm NO, dilution in N_2). Symbols represent literature experimental data and lines modeling calculations obtained using the present mechanism.

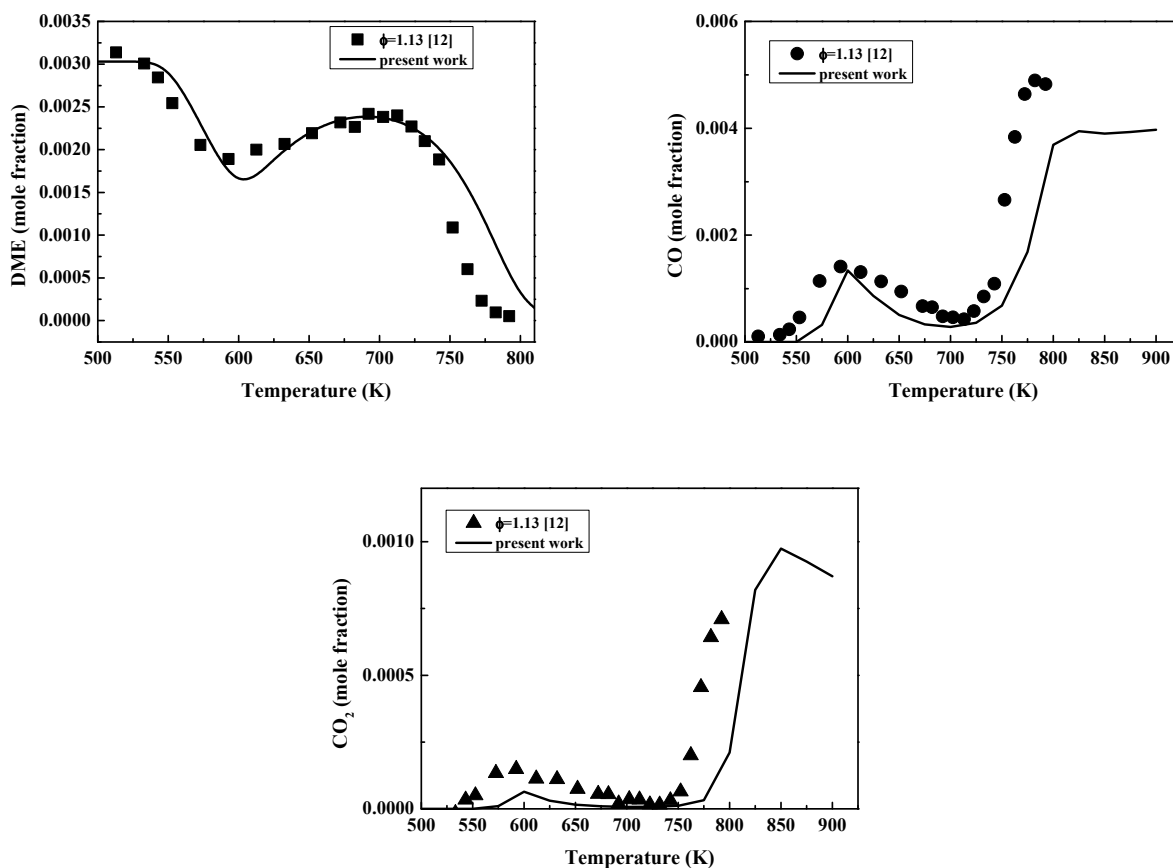


Figure S15. Comparison with flow reactor data from Curran et al. [12] ($P=12.5$ atm, $\tau_r=1.8$, $\phi=1.13$, 3030 ppm DME, dilution in N_2). Symbols represent literature experimental data and lines modeling calculations obtained using the present mechanism.

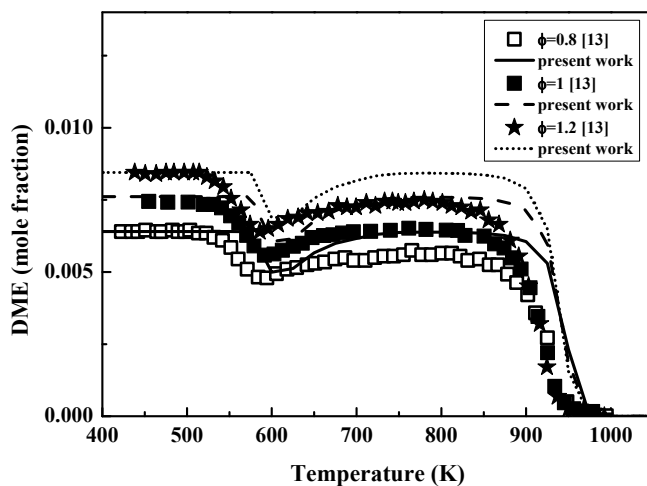


Figure S16. Comparison with flow reactor data from Hermann et al. [13] ($P=0.97$ bar, $\phi=1.2$, 1 and 0.8, dilution in Ar). Symbols represent literature experimental data and lines modeling calculations obtained using the present mechanism.

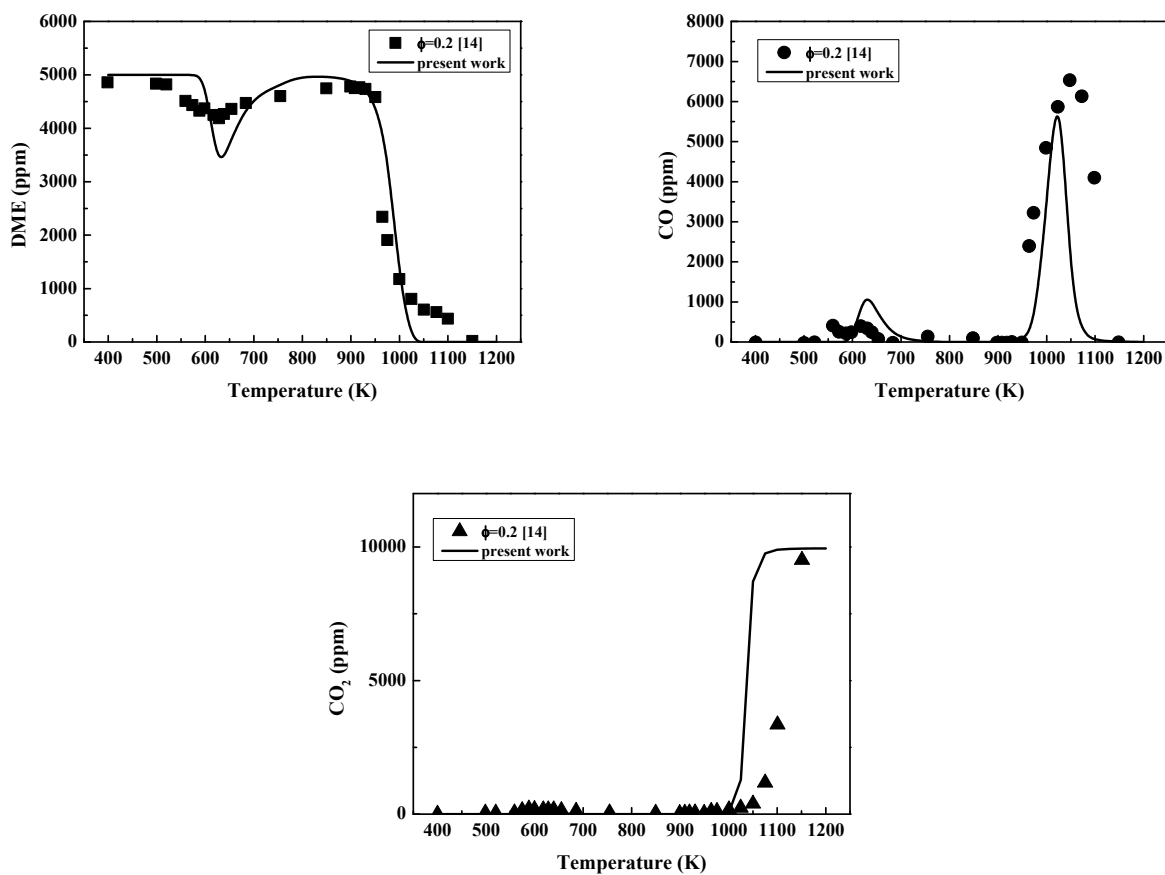


Figure S17. Comparison with flow reactor data from Kurimoto et al. [14] ($P=1$ atm, $\phi=0.2$, 0.5 % DME, dilution in He/Ar). Symbols represent literature experimental data and lines modeling calculations obtained using the present mechanism.

6) Evaluation of the sensitivity of the $\text{CH}_3\text{OCH}_2\text{O}_2=\text{CH}_2\text{OCH}_2\text{O}_2\text{H}$ reaction in modeling calculations.

In order to evaluate the sensitivity of the $\text{CH}_3\text{OCH}_2\text{O}_2=\text{CH}_2\text{OCH}_2\text{O}_2\text{H}$ reaction, Figure S18 shows the comparison between experimental results and modeling calculations using both the mechanism used along the present work and the same mechanism substituting the Burke et al. [29] determination by a non-pressure dependent value by Zhao et al. [28].

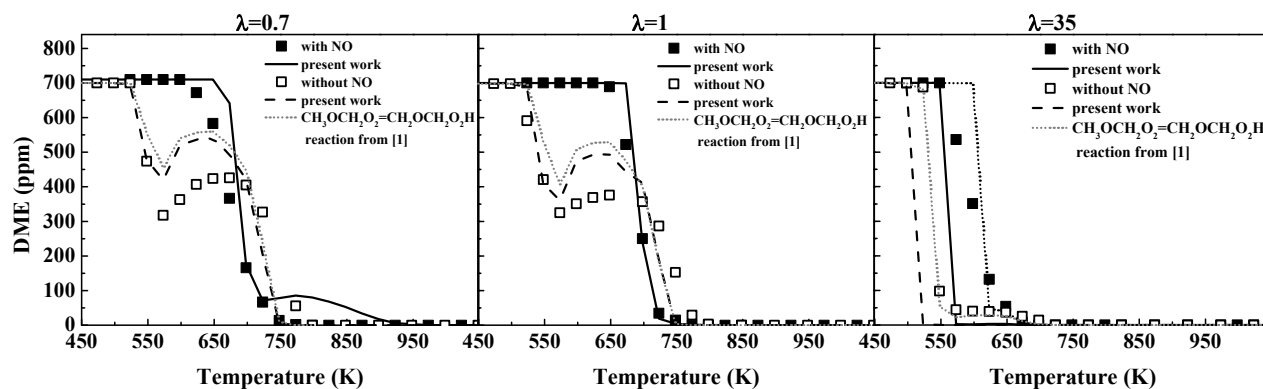


Figure S18. Comparison between experimental and modeling results with and without pressure dependency for the $\text{CH}_3\text{OCH}_2\text{O}_2=\text{CH}_2\text{OCH}_2\text{O}_2\text{H}$ reaction, for 20 bar, different values of lambda and in the absence/presence of NO.

7) References

- [1] Z. Zhao, M. Chaos, A. Kazakov, F.L. Dryer, Thermal decomposition reaction and a comprehensive kinetic model of dimethyl ether, *Int. J. Chem. Kinet.* 40 (2008) 1-18.
- [2] A. Rodriguez, O. Frottier, O. Herbinet, R. Fournet, R. Bounaceur, C. Fittschen, F. Battin-Leclerc, Experimental and modeling investigation of the low-temperature oxidation of dimethyl ether, *J. Phys. Chem. A* 119 (2015) 7905-7923.
- [3] Z. Wang, X. Zhang, L. Xing, L. Zhang, F. Herrmann, K. Moshhammer, F. Qi, K. Kohse-Höinghaus, Experimental and kinetic modeling study of the low- and intermediate-temperature oxidation of dimethyl ether, *Combust. Flame* 162 (2015) 1113-1125.
- [4] E.E. Dames, A.S. Rosen, B.W. Weber, C.W. Gao, C-J. Sung, W.H. Green, A detailed combined experimental and theoretical study on dimethyl ether/propane blended oxidation, *Combust. Flame* 168 (2016) 310-330.
- [5] U. Burke, K.P. Somers, P. O'Toole, C.M. Zinner, N. Marquet, G. Bourque, E.L. Petersen, W.K. Metcalfe, Z. Serinyel, H.J. Curran, An ignition delay and kinetic modeling study of methane, dimethyl ether, and their mixtures at high pressures, *Combust. Flame* 162 (2015) 315-330.
- [6] T. Yamada, J.W. Bozelli, T.H. Lay, Comparisons of CBS-q and G2 calculations on Thermodynamic properties, transition states, and kinetics on dimethyl-ether+O₂ reaction system, *Int. J. Chem. Kinet.* 32 (2000) 435-452.
- [7] L. Marrodán, L. Berdusán, V. Aranda, Á. Millera, R. Bilbao, M.U. Alzueta, Influence of dimethyl ether addition on the oxidation of acetylene in the absence and presence of NO, *Fuel* 183 (2016) 1-8.
- [8] U. Pfahl, K. Fieweger, G. Adomeit, Self-ignition of diesel-relevant hydrocarbon-air mixtures under engine conditions, *Proc. Combust. Inst.* 26 (1996) 781-789.
- [9] Z. Li, W. Wang, Z. Huang, M.A. Oehlschlaeger, Dimethyl ether autoignition at engine-relevant conditions, *Energy Fuels* 27 (2013) 2811-2817.
- [10] P. Dagaut, C. Daly, J.M. Simmie, M. Cathonnet, The oxidation and ignition of dimethylether from low to high temperature (500-1600 K): experiments and kinetic modeling, *Proc. Combust. Inst.* 27 (1998) 361-369.
- [11] M.U. Alzueta, J. Muro, R. Bilbao, P. Glarborg, Oxidation of dimethyl ether and its interaction with nitrogen oxides, *Isr. J. Chem.* 39 (1999) 73-86.

- [12] H.J. Curran, S.L. Fischer, F.L. Dryer, The reaction kinetics of dimethyl ether. II: Low-temperature oxidation in flow reactors, *Int. J. Chem. Kinet.* 32 (2000) 741-759.
- [13] F. Herrmann, B. Jochim, P. Oßwald, L. Cai, H. Pitsch, K. Kohse-Höinghaus, Experimental and numerical low-temperature oxidation study of ethanol and dimethyl ether, *Combust. Flame* 161 (2014) 384-397.
- [14] N. Kurimoto, B. Brumfield, X. Yang, T. Wada, P. Diévar, G. Wysocki, Y. Ju, Quantitative measurements of HO₂/H₂O₂ and intermediate species in low and intermediate temperature oxidation of dimethyl ether, *Proc. Combust. Inst.* 35 (2015) 457-464.

Article VI:

Song, Y.; **Marrodán, L.**; Vin, N.; Herbinet, O.; Assaf, E.; Fittschen, C.; Stagni, A.; Faravelli, T.; Alzueta, M.U.; Battin-Leclerc, F. (2018). The sensitizing effects of NO₂ and NO on methane low temperature oxidation in a jet stirred reactor. *Proceedings of the Combustion Institute*, DOI: 10.1016/j.proci.2018.06.115.



ELSEVIER

Available online at www.sciencedirect.com

ScienceDirect

Proceedings of the Combustion Institute 000 (2018) 1–9

www.elsevier.com/locate/prociProceedings
of the
Combustion
Institute

The sensitizing effects of NO₂ and NO on methane low temperature oxidation in a jet stirred reactor

Y. Song^a, L. Marrodán^b, N. Vin^a, O. Herbinet^{a,*}, E. Assaf^c,
C. Fittschen^c, A. Stagni^d, T. Faravelli^d, M.U. Alzueta^b, F. Battin-Leclerc^a

^a Laboratoire Réactions et Génie des Procédés, CNRS-Université de Lorraine, 1 rue Grandville, 54000 Nancy, France

^b Aragón Institute of Engineering Research (I3A), Department of Chemical and Environmental Engineering, University of Zaragoza, Mariano Esquillor s/n, 50018 Zaragoza, Spain

^c Université Lille, CNRS, UMR 8522- PC2A-PhysicoChimie des Processus de Combustion et de l'Atmosphère, F59000 Lille, France

^d Department of Chemistry, Materials and Chemical Engineering "G. Natta", Politecnico di Milano, Piazza Leonardo da Vinci 32, 20133 Milano, Italy

Received 29 November 2017; accepted 18 June 2018

Available online xxx

Abstract

The oxidation of neat methane (CH₄) and CH₄ doped with NO₂ or NO in argon has been investigated in a jet-stirred reactor at 107 kPa, temperatures between 650 and 1200 K, with a fixed residence time of 1.5 s, and for different equivalence ratios (Φ), ranging from fuel-lean to fuel-rich conditions. Four different diagnostics have been used: gas chromatography (GC), chemiluminescence NO_x analyzer, continuous wave cavity ring-down spectroscopy (cw-CRDS) and Fourier transform infrared spectroscopy (FTIR). In the case of the oxidation of neat methane, the onset temperature for CH₄ oxidation was above 1025 K, while it is shifted to 825 K with the addition of NO₂ or NO, independently of equivalence ratio, indicating that the addition of NO₂ or NO highly promotes CH₄ oxidation. The consumption rate of CH₄ exhibits a similar trend with the presence of both NO₂ and NO. The amount of produced HCN has been quantified and a search for HONO and CH₃NO₂ species has been attempted. A detailed kinetic mechanism, derived from POLIMI kinetic framework, has been used to interpret the experimental data with a good agreement between experimental data and model predictions. Reaction rate and sensitivity analysis have been conducted to illustrate the kinetic regimes. The fact that the addition of NO or NO₂ seems to have similar effects on promoting CH₄ oxidation can be explained by the fact that both species are involved in a reaction cycle interchanging them and whose result is $2\text{CH}_3 + \text{O}_2 = 2\text{CH}_2\text{O} + 2\text{H}$. Additionally, the direct participation of NO₂ in the $\text{NO}_2 + \text{CH}_2\text{O} = \text{HONO} + \text{HCO}$ reaction has a notable accelerating effect on methane oxidation.

© 2018 Published by Elsevier Inc. on behalf of The Combustion Institute.

Keywords: Jet-stirred reactor; NO_x methane combustion; Low-temperature oxidation

* Corresponding author.

E-mail address: olivier.herbinet@univ-lorraine.fr (O.

Herbinet).

<https://doi.org/10.1016/j.proci.2018.06.115>

1540-7489 © 2018 Published by Elsevier Inc. on behalf of The Combustion Institute.

1. Introduction

The limited fossil fuel resource and its harmful effects on the climate have increased the interest for environmentally friendly fuels. Biomass seems to be a promising fuel source due to its sustainability, secure supply and low threat to the environment. Produced from the biomass anaerobic digestion, the so-called “biogas”, consists mainly of methane (CH_4) and carbon dioxide (CO_2) with trace amounts of nitrogen and sulfur compounds. Biogas plays an important role as potential renewable gas-phase fuel. The main nitrogen compound present in biogas is ammonia, which could easily convert to NO in the presence of oxygen even at low temperatures. The mutual effects of CH_4/NO_x or CH_4/NH_3 have attracted considerable attention in the past decade.

A large number of experimental reports concerning the hydrocarbon- NO_x interactions in ideal reactors are available [1–12]. Most studies related to reburning technology were performed in tubular flow reactors (FR) for CH_4 high-temperature oxidation. Over a relatively low-temperature range (800–1150 K), Dagaut and Nicolle [6] demonstrated the effects of NO on methane oxidation at pressures of 1–10 atm in a jet stirred reactor. A simplified reaction path was proposed, in which the reaction $\text{NO} + \text{HO}_2 = \text{OH} + \text{NO}_2$ followed by $\text{OH} + \text{CH}_4 = \text{CH}_3 + \text{H}_2\text{O}$ were highlighted. In addition, the investigation of mutual effects of NO_2 on CH_4 oxidation is also of significant value. Bendtsen et al. [4] and Chan et al. [9] examined the impact of NO and NO_2 as promoters to CH_4 oxidation under fuel-lean conditions in a FR. The different key reactions at the onset for NO ($\text{CH}_3\text{O}_2 + \text{NO} = \text{CH}_3\text{O} + \text{NO}_2$) or NO_2 ($\text{NO}_2 + \text{CH}_4 = \text{CH}_3 + \text{HONO}$) sensitization were identified. However, some minor reaction paths such as $\text{NO}_2 + \text{CH}_2\text{O} = \text{HONO} + \text{HCO}$, which could play a role in mutual effects on CH_4 oxidation, have been ignored so far. Moreover, to the authors' knowledge, the sensitizing effects of NO_2 on methane low-temperature oxidation in a jet-stirred reactor have not been investigated yet.

Despite the abundant kinetic studies for the CH_4 - NO_x interactions, the knowledge of some notable intermediate nitrogen species (such as HONO) is not comprehensively understood. Chai and Goldsmith [13] calculated the rate coefficients for $\text{H}_2 + \text{NO}_2$ and $\text{CH}_4 + \text{NO}_2$ with the formation of HONO. The fate of these species is of importance to the hydrocarbon- NO_x interactions during the biogas oxidation. However, until now, HONO has never been detected during fuel oxidation.

Therefore, the aim of this work is to investigate the hydrocarbon- NO_x (NO and NO_2) interactions in biogas oxidation at atmospheric pressure and temperatures ranging from 650 to 1200 K. A search for intermediate species HONO, CH_3NO_2 and

HCN has been made with the aid of continuous wave Cavity Ring-Down Spectroscopy (cw-CRDS) and Fourier Transform Infrared (FTIR), respectively. A detailed kinetic mechanism, recently updated according to the latest available *ab initio* calculations, is used to interpret the experimental data.

2. Experimental setup

The experimental setup was a laboratory-scale spherical fused silica JSR (volume of 85 cm^3 ; detailed description provided elsewhere [14]). A more detailed description of the experimental setup is available in Supplementary material (SM1). The reactant gases were premixed in a preheating zone before entering the reactor center through four nozzles which create high turbulence resulting in homogeneity in composition and temperature of the gas phase. The residence time inside the preheater was only 1% with respect to the one in the reactor which was fixed at 1.5 s (± 0.1 s) within all the experiments performed. Both the reactor and the preheater were heated using Thermocoax resistances. The reactor temperature was measured by a type-K thermocouple (± 5 K) located at the center of the reactor. The pressure in the reactor was controlled by a needle valve (± 0.2 kPa) positioned downstream of the reactor and kept at 107 kPa. Argon, oxygen, NO, NO_2 and methane were provided by Messer (purities of 99.99%, respectively). The flow rates of the reactants were controlled by mass flow controllers ($\pm 0.05\%$). The gases leaving the reactor were analyzed on-line using two gas chromatographs (GCs), a NO_x analyzer (Thermo Scientific Model 42i), a FTIR (Thermo Scientific Antaris) spectrometer and a cw-CRDS spectroscopy cell.

- The first GC equipped with a thermal conductivity detector was used to quantify O_2 . The second GC equipped with flame-ionization detector preceded by a methanizer and a PlotQ capillary column was used to quantify CH_4 , CO, CO_2 , C_2H_4 , C_2H_6 and C_2H_2 .
- The chemiluminescence NO_x analyzer was adopted to measure NO and NO_2 . The quantitative range is 0–5000 ppm for NO and 0–500 ppm for NO_2 with 0.1 ppm sensitivity, respectively. Two pumps are used for outlet and bypass channels, respectively.
- The FTIR spectrometer was used to detect the CH_3NO_2 (if any) and HCN (calibrated using a HCN diluted (1000 ppm in N_2) cylinder) species.
- cw-CRDS infrared spectroscopy was used to detect H_2O , CH_2O and HONO (if any) species, the description of this instrument is also provided in [15].

The uncertainty for the different diagnostic instruments is estimated to be $\pm 5\%$ except for the

FTIR and CRDS measurements which is ± 10 –15%. All the experimental data presented hereafter are detailed in a spreadsheet in SM2.

3. Kinetic model

The kinetic mechanism used for chemistry description and analysis of experimental results was obtained by relying on the POLIMI kinetic framework, describing the pyrolysis and oxidation of hydrocarbon fuels [16]. Its core C_0 – C_3 mechanism was recently revised by coupling the H_2/O_2 and C_1/C_2 subsets from Metcalfe et al. [17], C_3 from Burke et al. [18], and heavier fuels from Ranzi et al. [19]. For the low temperature conditions of interest in this work, particular attention was devoted to updating the (equilibrated) reaction rates of peroxy radical formation from methyl radical [20], as well as the related thermodynamic properties. They were adopted, when available, from the database of Burcat and Ruscic [21].

Following the modularity principle behind the POLIMI mechanism, a NO_x sub-mechanism was integrated into the main framework: a complete characterization of its basic structure is provided in [22, 23]. It describes the major paths leading to NO_x formation. Apart from the three well-studied reactions responsible of thermal NO_x mechanism [24], the mechanism underwent a major update for the prompt path, especially in relation to the NCN-route: the kinetic laws of the reactions involving NCN were updated after the *ab initio* calculations by Harding et al. [25] and Faßheber et al. [26]. Moreover, the chemistry of HNC and HNCN was also updated according to the modifications proposed by Lamoureux et al. [27]. On the other side, the high-temperature reburning mechanism of methane implements the rates proposed by Dean and Bozzelli [28] for the reactions of methyl with NO. The methoxy activation by NO ($CH_3O_2 + NO = CH_3O + NO_2$) was obtained from Atkinson et al. [29], and validated in the 200–430 K temperature range, while its direct formation via NO_2 ($CH_3 + NO_2 = CH_3O + NO$) was updated following Glarborg and Bendtsen [30], which is temperature independent over the range 295–1400 K. Rate coefficients of HONO and HNO_2 formation from methane and NO_2 were implemented following Chai and Goldsmith [13]. The complete mechanism (153 species and 2361 reactions) is provided as supplemental material of this paper in CHEMKIN format, along with thermodynamic and transport properties (SM3). The present mechanism is able to reproduce experimental data from literature [6, 7, 9] as shown in SM1.

4. Results

Experiments for the oxidation of CH_4 doped with NO and NO_2 with argon as bath gas were

Table 1

Experimental conditions (Inlet composition volume basis; balanced Ar).

Exp.	X_{CH_4}	X_{NO} ppm	X_{NO_2} ppm	X_{O_2}	Φ
1	0.01	–	–	0.04	0.5
2	0.01	–	–	0.02	1
3	0.01	–	–	0.01	2
4	0.01	500	–	0.04	0.5
5	0.01	500	–	0.02	1
6	0.01	500	–	0.01	2
7	0.01	100	–	0.02	1
8	0.01	–	400	0.04	0.5
9	0.01	–	400	0.02	1
10	0.01	–	400	0.01	2
11	0.01	–	100	0.02	1
12	0.01	1000	–	0.02	1

performed under fuel-lean ($\Phi = 0.5$) to fuel-rich ($\Phi = 2$) conditions over the 650–1200 K temperature range. Equivalence ratios were calculated neglecting the amounts of added NO_x compounds which were around 4–10% that of CH_4 . The experimental conditions investigated in this study are presented in Table 1. Numerical calculations were conducted with CHEMKIN-PRO software package [31]. Transient solver was applied in the simulation tasks with sufficient time allowed to reach the steady state solution.

4.1. Profiles of carbon compound species and water

Figure 1 shows the evolution of major products with temperature for the oxidation of CH_4 (left), methane doped with NO_2 (middle) and NO (right) for the three studied equivalence ratios ($\Phi = 0.5, 1$ and 2). With respect to the pure CH_4 oxidation, the initial oxidation temperatures are 1025 K, 1075 K and 1175 K for $\Phi = 0.5, 1$ and 2, respectively. Dynamic behaviors (oscillations) occur under oxidizing and stoichiometric conditions when the temperature is above 1050 K and 1100 K, respectively. This is, too, an interesting topic of research in such systems, but beyond the goals of this specific study.

In the presence of NO_2 (400 ppm) under fuel-lean conditions, the reaction is initiated at 825 K. The rise of consumption of CH_4 is extremely fast with the increase of temperature. At 950 K, 98% of the inlet methane concentration was oxidized. Under stoichiometric conditions, the onset temperature for CH_4 oxidation is around 825 K as well. However, CH_4 consumption is slower than that under fuel-lean conditions: there is still 24% CH_4 left in the reactor outlet at 1000 K. Similarly as under the above two conditions, the consumption of methane also starts at 825 K under fuel-rich conditions, whereas the consumption of methane is even slower compared to that under stoichiometric conditions. Differing from what is observed under stoichiometric and oxidizing conditions, the mole fraction of methane reaches a minimum at 950 K

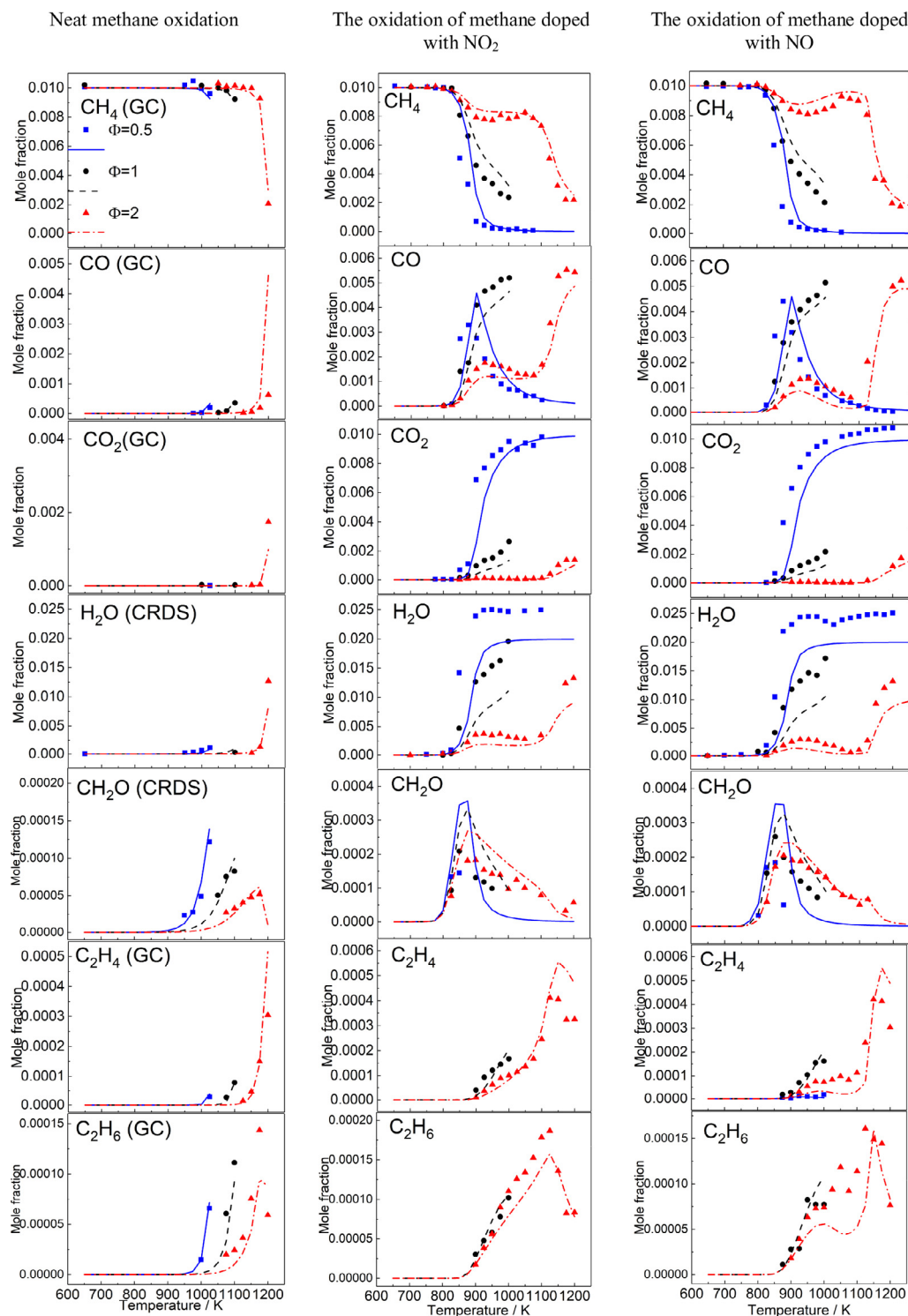


Fig. 1. Species profile comparison between experimental data and model predictions. The left column is for the oxidation of neat methane; the middle column is for the oxidation of methane doped with NO_2 (400 ppm); the right column is for the oxidation of methane doped with NO (500 ppm). Here and in further figures in this paper, symbols represent experiments and lines denote simulations. Experiments and simulations are not presented for conditions where oscillations were observed.

under reducing conditions, and the mole fraction of methane increases at higher temperatures until 1050 K. After that, methane is consumed again. Compared to the oxidation of neat methane (left column), the enhancing effect for the addition of NO_2 into the oxidizing environment system is quite obvious especially for reducing conditions.

In the presence of NO (500 ppm), the evolution of methane profiles is quite similar to what is obtained in the presence of NO_2 . This indicates that the promoting effects of NO and NO_2 on methane oxidation is almost the same although the amount of the addition of NO and NO_2 is a little different.

Note that oscillations even occur under stoichiometric ($T > 1000$ K) and oxidizing conditions ($T > 1100$ K, with NO_2 addition) in the presence of NO and NO_2 . The present model could reproduce the above mentioned dynamic behavior as shown in SM1.

The peak mole fraction of CH_2O profile occurs at a temperature of 850 K, which is independent of equivalence ratios in the presence of both NO and NO_2 . Likewise, the mole fraction of CO reaches its utmost value at 850 K under fuel-lean conditions, which indicates that the methane oxidation is very fast at this specific temperature. Under fuel-rich conditions, the temperature for the peak CO mole fraction shifts to 900 K. C_2 species (C_2H_4 , C_2H_6) mainly appear under stoichiometric and reducing conditions at higher temperature ($T > 900$ K). Under oxidizing conditions, the mole fraction of C_2 species are below the detection limit and this behavior is well captured by the model as is shown in SM1. The global carbon balance has been checked and the deviation is below 5% (SM2).

The agreement between the experimental data and simulated results is generally good within all the investigated conditions except for that the model underestimates the experimental profile of H_2O under stoichiometric and fuel-lean conditions, which was also observed by Bugler et al. [32]. It might be ascribed to the uncertainty in cw-CRDS measurements derived from its significant concentrations. Also, the performance of different literature models against present experimental data is displayed in SM1. It is found that the current POLIMI model is better capturing the experimental data than the other models.

In order to evaluate the effect of the amount of added NO_2 and NO on the methane oxidation, three more sets of experiments with addition of 100 ppm NO_2 or NO and addition of 1000 ppm NO (sets 7, 11 and 12 in Table 1), respectively, were conducted. Figure 2 shows both the experimental and model results. It was found that the onset temperature for methane oxidation is independent of the added amount of NO_2 and NO. Moreover, with the lower added amount of NO_2 or NO, the methane conversion is slower. When 1000 ppm of NO is present, methane conversion shows a

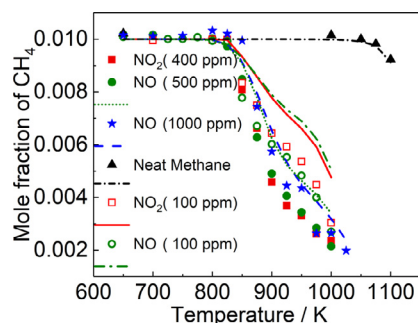


Fig. 2. Mole fractions of methane with various additions of NO_2 (400 and 100 ppm) and NO (1000, 500 and 100 ppm) under stoichiometric condition.

trend similar to that with 500 ppm NO addition. Furthermore, the consumption rate for methane also exhibits the similar trend in the presence of both NO_2 (100 ppm) and NO (100 ppm) which differs from what was previously observed by Chan et al. [9] in a FR.

4.2. Profiles of nitrogen containing species

4.2.1. NO_2 and NO

Figure 3 shows the evolution of NO_2 and NO profiles as a function of temperature for methane oxidation in the presence of NO_2 (left) and NO (right), respectively. In the presence of 400 ppm NO_2 , the consumption of NO_2 is approximately similar for all investigated equivalence ratios. The increase of the NO mole fraction is quite sharp over the range 800–900 K, and is independent of equivalence ratio. After that, it attains a “plateau” level of 280 ppm in stoichiometric and oxidizing conditions and 300 ppm in reducing conditions, with the increase of temperature. Only under rich conditions the NO concentration drops from 300 to 100 ppm when the temperature increases from 1100 K to 1200 K. The model accurately predicts the onset for both the consumption of NO_2 and production of NO. It overestimates the amount of NO when the temperature is above 800 K.

In the presence of NO (500 ppm), the mole fraction of NO_2 peaks at 850 K, which corresponds to the maximum consumption of NO with all equivalence ratios. The amount of NO_2 drops gradually as the temperature is above 850 K, meanwhile, the mole fraction of NO increases to a stable value until the temperature is beyond 900 K. Under reducing conditions, the mole fraction of NO decreases dramatically over the temperature range 1100–1200 K. Although the model underestimates the formation of NO_2 , the initiation temperature for NO– NO_2 conversion is well captured.

4.2.2. HCN

HCN has been quantified by FTIR at the highest temperatures (1175–1200 K) studied in this

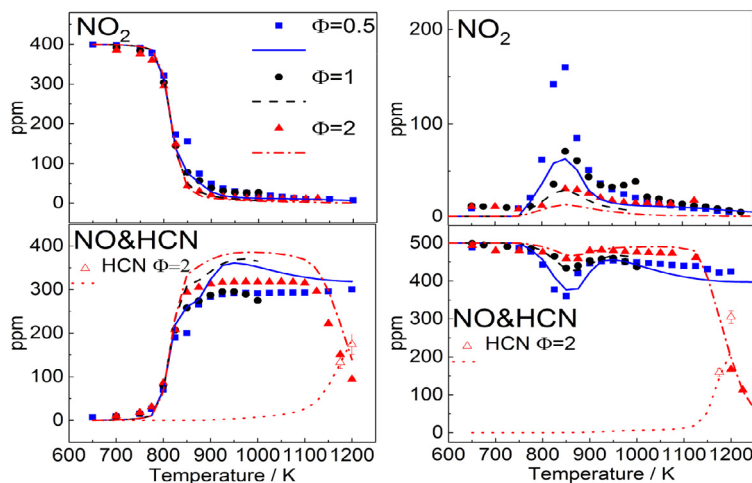
The oxidation of methane doped with NO₂ The oxidation of methane doped with NO

Fig. 3. The comparison of NO₂, NO and HCN profiles between experimental data and model predictions. Left: the oxidation of methane doped with NO₂ (400 ppm). Right: the oxidation of methane doped with NO (500 ppm).

work for both NO₂ and NO additions as shown in Fig. 3. The measured HCN spectrum is displayed in SM1. At a same temperature, the amount of HCN is higher in the presence of NO than with NO₂ addition. Moreover, the quantification of HCN could somewhat help to close the nitrogen balance at the highest temperatures. The model predicts the formation of HCN quite well in the presence of NO₂, although it underestimates the amount of HCN in the presence of NO at 1200 K.

The mass balance of nitrogen deteriorates with the increase of temperature when temperature is above 850 K in the presence of NO₂ condition. The reason could be ascribed to the detection failure for some nitrogenated species with the currently available diagnostic instruments. Also, the overprediction of NO in the presence of NO₂ indicates that the NO₂ conversion channel needs to be further investigated.

4.2.3. A search for HONO and CH₃NO₂ species

The absorption spectrum of HONO has been previously measured by Jain et al. [33]. This previous work indicates that HONO, if any, should be detected in the present study. In our study, the cw-CRDS product analyses were conducted in the near infrared at wavenumbers in the 6638.0–6643.5 cm⁻¹ range. The absorption line at 6643.17 cm⁻¹ was chosen as the most suitable for the quantification of HONO with an absorption cross-section of $4.2 \pm 1.7 \times 10^{-21}$ cm² [33] due to the fact that there are no interferences at this specific absorption line. There were obvious signals at this absorption line in the spectrum around a temperature of 850 K. However, for some less intense absorption lines, such as 6642.45 cm⁻¹, no signals could be observed in our

spectra. Therefore, the maximum produced HONO mole fraction is then below the estimated detection limit of 3 ppm. No obvious FTIR absorption lines for CH₃NO₂ could be observed. The maximum produced CH₃NO₂ mole fraction is then below the estimated detection limit of 5 ppm. The measured spectra of HONO and CH₃NO₂ of this study can be found in SM1. Modeling calculations (see SM1) predict low mole fraction (1–2 ppm) of HONO, which is consistent with what is observed in these experimental data. Note that the discrepancy between experimental and modeling calculations found in the 800–1000 K range for NO₂ (right upper in Fig. 3), can be explained by the too high predicted formation of CH₃NO₂. However, no experimental detection of this species by FTIR was achieved although it could be done.

4.3. Discussion

Reaction rate and sensitivity analyses have been performed to identify the main reaction routes and the utmost sensitive reactions for CH₄ consumption in the presence of NO_x, respectively, as shown in Fig. 4. The characteristic temperature of 850 K is selected because the consumption of methane is quite significant and the formation of carbon species peaks at this specific temperature.

In the case of neat CH₄, the reaction path analysis is conducted at 1100 K, its consumption proceeds through methyl radicals (CH₃) which can continue reacting following 4 different routes: (a) a self-reaction forming ethane; reactions with O₂, (b) forming directly CH₂O + OH radicals, (c) giving CH₃O radicals which also lead to formaldehyde via reaction (1) CH₃O(+M) = CH₂O + H(+M)

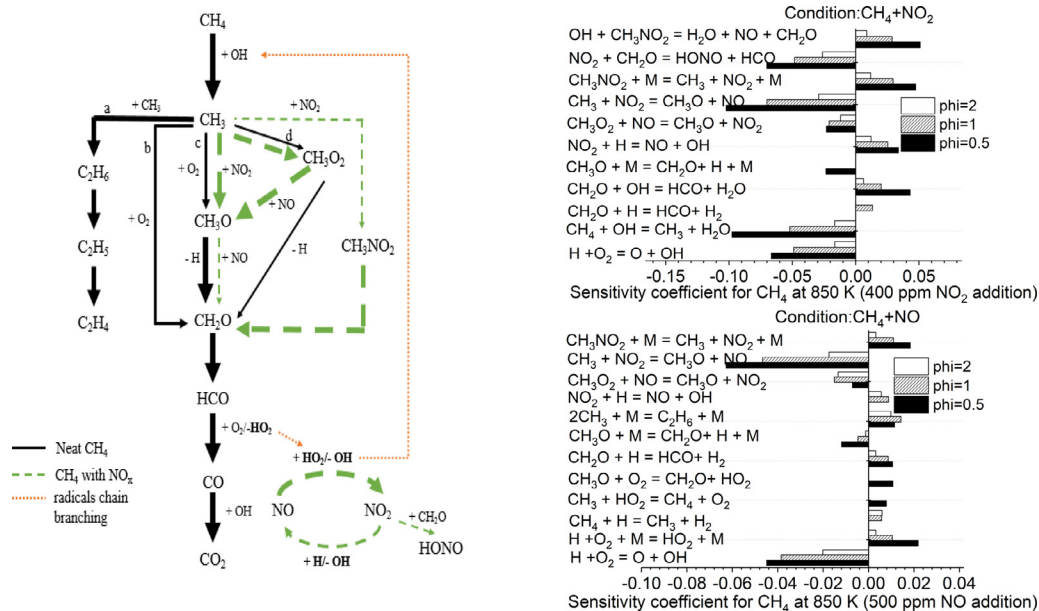


Fig. 4. Left: Reaction path diagram for CH₄ oxidation in presence of NO_x ($\Phi = 1$, $T = 850$ K). Solid lines represent the main reaction routes occurring during the oxidation of neat CH₄ (1100 K); dashed lines highlight the main changes due to the presence of NO_x. The size of the arrow is proportional to the flow rate of the given reactions. Right: CH₄ sensitivity coefficient at 850 K in the presence of NO₂ (upper: 400 ppm) and NO (bottom: 500 ppm).

or (d) producing CH₃O₂ radical via reaction (2) $\text{CH}_3 + \text{O}_2(+\text{M}) = \text{CH}_3\text{O}_2(+\text{M})$, which is also a minor source of formaldehyde.

At 850 K, in the presence of NO_x, methoxy radical formation through reaction (3) $\text{CH}_3 + \text{NO}_2 = \text{CH}_3\text{O} + \text{NO}$ is the most sensitive as shown in sensitivity analysis except for the addition of NO under reducing condition, when reaction (3) is slightly less sensitive than chain branching reaction $\text{H} + \text{O}_2 = \text{O} + \text{OH}$. In this case, CH₃O radicals are also formed in large extent by the reaction of NO with CH₃O₂ radicals: reaction (4) $\text{CH}_3\text{O}_2 + \text{NO} = \text{CH}_3\text{O} + \text{NO}_2$. The whole reaction cycle (1)–(4) results in an overall balance: $2\text{CH}_3 + \text{O}_2 = 2\text{CH}_2\text{O} + 2\text{H}$ and produces a strong acceleration of methane oxidation, since 2 H atoms are obtained from 2 CH₃ radicals and one O₂ molecule. The reaction route involving C₂ species becomes more relevant as the temperature is increased being almost negligible at 850 K.

The above mentioned reaction loop (1)–(4) acts as a “catalytic” cycle and it can explain the fact that the addition of NO or NO₂ seems to have similar effects on promoting methane oxidation. Note that NO/NO₂ interchanging occurs via the reaction of NO and HO₂ radicals giving NO₂ and OH radicals and the reaction of NO₂ with H radicals reforming NO and OH radicals. The OH radicals produced during the NO–NO₂ interchanging cycle interact with CH₄ promoting its conversion,

whereas the H and HO₂ radicals produced during the conversion of CH₄ (i.e. mainly through $\text{CH}_3\text{O} + \text{M} = \text{CH}_2\text{O} + \text{M}$) + H and $\text{HCO} + \text{O}_2 = \text{CO} + \text{HO}_2$) promote the NO–NO₂ conversion as described earlier. The role of the radicals in the mutual sensitization of the oxidation of CH₄ and NO_x has been highlighted in Fig. 4.

Moreover, in the presence of NO or NO₂, CH₃ radical is consumed by an alternative route, leading to the formation of nitromethane, CH₃NO₂. This acts as an inhibitor of the whole system for two different reasons: (i) it traps both CH₃ and NO₂, slowing down their successive reactions and the formation of the very reactive methoxy radical (CH₃O), and (ii) it also acts as an OH scavenger via $\text{OH} + \text{CH}_3\text{NO}_2 = \text{H}_2\text{O} + \text{NO} + \text{CH}_2\text{O}$.

The main formation route for HONO is from NO₂ by reactions $\text{NO}_2 + \text{CH}_2\text{O} = \text{HONO} + \text{HCO}$ and $\text{NO}_2 + \text{HNO} = \text{HONO} + \text{NO}$. It only represents 4% in the total NO₂ consumption at 850 K and $\Phi = 0.5$, hence the expected HONO mole fraction is small, which agrees with the experimental data. However, these reactions play an essential role for the consumption of methane because the unstable HONO can readily convert to OH radical. In turn this favors the abstraction reaction $\text{CH}_4 + \text{OH} = \text{CH}_3 + \text{H}_2\text{O}$, which is the second most sensitive reaction for methane depletion in the conditions with NO₂ addition. Note that the sensitivity analysis in

Fig. 4 shows a strong promoting effect of the reaction $\text{NO}_2 + \text{CH}_2\text{O} = \text{HONO} + \text{HCO}$.

At high temperatures, when HCN has been experimentally detected, NO reacts with HCCO and CH_3 radicals to form HCNO and H_2CN , respectively, and later HCN is obtained; thus, NO is reduced by means of well-known reburn type reactions [3].

5. Conclusions

In this work, the oxidation of neat methane and methane doped with NO_2 or NO at 107 kPa and temperatures of 650–1200 K with a fixed residence time of 1.5 s has been investigated in a jet-stirred reactor under oxidizing to reducing conditions from both experimental and modeling points of view. In general, there is a good agreement between experimental results and modeling calculations. New experimental data and new species detection, along with the confirmation of a detailed kinetic model under these new conditions, have provided insights into understanding the mutual effect of CH_4 – NO_x interaction. The addition of NO_2 or NO produces comparable results on methane oxidation, anticipating the onset temperature for CH_4 consumption to lower temperatures (825 K) regardless of the equivalence ratio. Kinetic analysis showed that the parallel behavior of NO and NO_2 is connected to their interchanging via $\text{NO}_2 + \text{H}/\text{CH}_3 = \text{NO} + \text{OH}/\text{CH}_2\text{O}$ and $\text{NO} + \text{HO}_2/\text{CH}_3\text{O}_2 = \text{NO}_2 + \text{OH}/\text{CH}_3\text{O}$ reactions. This allows relating both actions to a common, oxidation-sensitizing mechanism, activated by methoxy radical formation, whilst counteracted by the parallel formation of nitromethane. The mole fraction of HCN has been quantified with FTIR, and the agreement between the experimental data and model prediction is generally good. Modeling calculations predict the formation of CH_3NO_2 , which was not detected experimentally although it could be, partially explaining the discrepancy between experimental and modeling results in the NO_2 profile at 800–1000 K. The contribution of HONO in the activation of the system was pointed out, too. The amount of HONO was under the detection limit, consistently with the modeling predictions.

Acknowledgments

This work has received funding from the European Union H2020 (H2020-SPIRE-04-2016) under Grant agreement no. 723706 and from the COST Action CM1404 “Chemistry of smart energy carriers and technologies”. Ms. Marrodán acknowledges Aragón Government for the predoctoral grant awarded.

Supplementary materials

Supplementary material associated with this article can be found, in the online version, at doi:10.1016/j.proci.2018.06.115.

References

- [1] J.H. Bromly, F.J. Barnes, S. Muris, X. You, B.S. Haynes, *Combust. Sci. Technol.* 115 (1996) 259–296.
- [2] M.U. Alzueta, P. Glarborg, K. Dam-Johansen, *Combust. Flame* 109 (1997) 25–36.
- [3] P. Glarborg, M.U. Alzueta, K. Dam-Johansen, J.A. Miller, *Combust. Flame* 115 (1998) 1–27.
- [4] A.B. Bendtsen, P. Glarborg, K.I.M. Dam-Johansen, *Combust. Sci. Technol.* 151 (2000) 31–71.
- [5] P. Dagaut, J. Luche, M. Cathonnet, *Proc. Combust. Inst.* 28 (2000) 2459–2465.
- [6] P. Dagaut, A. Nicolle, *Combust. Flame* 140 (2005) 161–171.
- [7] C.L. Rasmussen, A.E. Rasmussen, P. Glarborg, *Combust. Flame* 154 (2008) 529–545.
- [8] T. Mendiara, P. Glarborg, *Energy Fuels* 23 (2009) 3565–3572.
- [9] Y.L. Chan, F.J. Barnes, J.H. Bromly, A.A. Konnov, D.K. Zhang, *Proc. Combust. Inst.* 33 (2011) 441–447.
- [10] J. Giménez-López, V. Aranda, A. Millera, R. Bilbao, M.U. Alzueta, *Fuel Process. Technol.* 92 (2011) 582–589.
- [11] Y. Chan, J. Bromly, A. Konnov, D. Zhang, *Combust. Sci. Technol.* 184 (2012) 114–132.
- [12] J. Zhang, V. Burkle-Vitzthum, P.-M. Marquaire, *Combust. Sci. Technol.* 187 (2015) 1139–1156.
- [13] J. Chai, C.F. Goldsmith, *Proc. Combust. Inst.* 36 (2017) 617–626.
- [14] O. Herbinet, F. Battin-Leclerc, *Int. J. Chem. Kinet.* 46 (2014) 619–639.
- [15] C. Bahrini, O. Herbinet, P.-A. Glaude, C. Schaeffer, C. Fittschen, F. Battin-Leclerc, *Chem. Phys. Lett.* 534 (2012) 1–7.
- [16] E. Ranzi, A. Frassoldati, R. Grana, et al., *Prog. Energy Combust. Sci.* 38 (2012) 468–501.
- [17] W.K. Metcalfe, S.M. Burke, S.S. Ahmed, H.J. Curran, *Int. J. Chem. Kinet.* 45 (2013) 638–675.
- [18] S.M. Burke, U. Burke, R. Mc Donagh, et al., *Combust. Flame* 162 (2015) 296–314.
- [19] E. Ranzi, A. Frassoldati, A. Stagni, M. Pelucchi, A. Cuoci, T. Faravelli, *Int. J. Chem. Kinet.* 46 (2014) 512–542.
- [20] R.X. Fernandes, K. Luther, J. Troe, *J. Phys. Chem. A* 110 (2006) 4442–4449.
- [21] A. Burcat, B. Ruscic, *Third Millennium Ideal Gas and Condensed Phase Thermochemical Database for Combustion With Updates from Active Thermochemical Tables*, Argonne National Laboratory Argonne, IL, 2005.
- [22] T. Faravelli, A. Frassoldati, E. Ranzi, *Combust. Flame* 132 (2003) 188–207.
- [23] A. Frassoldati, T. Faravelli, E. Ranzi, *Combust. Flame* 135 (2003) 97–112.
- [24] J.A. Miller, C.T. Bowman, *Prog. Energy Combust. Sci.* 15 (1989) 287–338.
- [25] L.B. Harding, S.J. Klippenstein, J.A. Miller, *J. Phys. Chem. A* 112 (2008) 522–532.

- [26] N. Faßheber, J. Dammeier, G. Friedrichs, *Phys. Chem. Chem. Phys.* 16 (2014) 11647–11657.
- [27] N. Lamoureux, H. El Merhubi, L. Pillier, S. de Persis, P. Desgroux, *Combust. Flame* 163 (2016) 557–575.
- [28] A.M. Dean, J.W. Bozzelli, in: *Gas-phase Combustion Chemistry*, Springer, 2000, pp. 125–341.
- [29] R. Atkinson, D. Baulch, R. Cox, et al., *Atmos. Chem. Phys.* 6 (2006) 3625–4055.
- [30] P. Glarborg, A.B. Bendtsen, J.A. Miller, *Int. J. Chem. Kinet.* 31 (1999) 591–602.
- [31] CHEMKIN-PRO 15151, Reaction Design, San Diego, (2013).
- [32] J. Bugler, A. Rodriguez, O. Herbinet, et al., *Proc. Combust. Inst.* 36 (2017) 441–448.
- [33] C. Jain, P. Morajkar, C. Schoemaeker, B. Viskolcz, C. Fittschen, *J. Phys. Chem. A* 115 (2011) 10720–10728.

The sensitizing effects of NO₂ and NO on methane low temperature oxidation in a jet stirred reactor

Y. Song^a, L. Marrodán^b, N. Vin^a, O. Herbinet^{a,*}, E. Assaf^c, C. Fittschen^c, A. Stagni^d, T. Faravelli^d,
M.U. Alzueta^b, F. Battin-Leclerc^a

^aLaboratoire Réactions et Génie des Procédés, CNRS-Université de Lorraine, 1 rue Grandville, 54000 Nancy, France. *olivier.herbinet@univ-lorraine.fr

^bAragón Institute of Engineering Research (I3A), Department of Chemical and Environmental Engineering, University of Zaragoza, Mariano Esquillor s/n, 50018 Zaragoza, Spain.

^cUniversité Lille, CNRS, UMR 8522- PC2A-PhysicoChimie des Processus de Combustion et de l'Atmosphère, F59000 Lille, France.

^dDepartment of Chemistry, Materials and Chemical Engineering "G. Natta", Politecnico di Milano, P.zza Leonardo da Vinci 32, 20133 Milano, Italy.

**SUPPLEMENTAL
INFORMATION**

Table of content

1) Additional description of the experimental setup

- A) Jet-stirred reactor
- B) Gas chromatography
- C) NO_x Analysis
- D) FTIR apparatus
- E) cw-CRDS apparatus

Fig.S1. Schematic view of the JSR and CRDS coupling.

2) Comparison of simulations using the present mechanism (POLIMI mechanism) with literature data.

Fig.S2. Comparison of modeling predictions using POLIMI mechanism (solid lines) and experimental (symbols) and modeling predictions (dashed lines) reported by Dagaut and Nicolle [1] for the oxidation of methane and NO in a JSR (1 atm, $\Phi=0.1$, 2500 ppm of CH₄, 50000 ppm of O₂, dilution in N₂, $\tau=120$ ms).

Fig.S3. Comparison of modeling predictions using POLIMI mechanism (solid lines) and experimental (symbols) and modeling predictions (dashed lines) reported by Dagaut and Nicolle [1] for the oxidation of methane and NO in a JSR (10 atm, $\Phi=0.5$, 2500 ppm of CH₄, 10000 ppm of O₂, dilution in N₂, $\tau=1000$ ms).

Fig.S4. Comparison of modeling predictions using POLIMI mechanism (lines) and experimental (symbols) reported by Chan et al. [2] for the oxidation of methane and different amounts of NO in a flow reactor (1 atm, 2.5% methane-in-air mixture, 0-100 ppm NO added, residence time of 2 s).

Fig.S5. Comparison of modeling predictions using POLIMI mechanism (lines) and experimental (symbols) reported by Chan et al. [2] for the oxidation of methane and different amounts of NO₂ in a flow reactor (1 atm, 2.5% methane-in-air mixture, 0-100 ppm NO₂ added, residence time of 2 s).

Fig.S6. Comparison of modeling predictions using POLIMI mechanism (lines) and experimental (symbols) reported by Rasmussen et al. [3] for the oxidation of methane and NO in a high-pressure flow reactor (20 bar, 4.58% methane, 925 ppm O₂, 200 ppm NO, 14 ppm NO₂, $\Phi=99$, $\tau=2440/T$).

3) The evolution profiles of methane as a function of time at both steady and oscillation states

Fig.S7. The simulation work of the evolution profiles of methane as a function of time for the neat methane oxidation at 1100 K under stoichiometric condition. (**Steady state**)

Fig.S8. The simulation work of the evolution profiles of methane as a function of time for the neat methane oxidation at 1200 K under stoichiometric condition. (**Oscillations**)

Fig.S9. The simulation work of the evolution profiles of methane as a function of time for the oxidation of methane doped with NO at 900 K under stoichiometric condition. (**Steady state**)

Fig.S10. The simulation work of the evolution profiles of methane as a function of time for the oxidation of methane doped with NO at 1000 K under stoichiometric condition. (**Oscillations**)

Fig.S11. The simulation work of the evolution profiles of methane as a function of time for the oxidation of methane doped with NO₂ at 900 K under stoichiometric condition. (**Steady state**)

Fig.S12. The simulation work of the evolution profiles of methane as a function of time for the oxidation of methane doped with NO₂ at 1100 K under stoichiometric condition. (**Oscillations**)

4) Evolution with temperature of mole fractions of the different species according to model calculations with POLIMI mechanism.

A) For the addition of 400 ppm of NO₂ and $\Phi=2$.

Fig.S13. Evolution with temperature of mole fractions for the carbon compound species, H₂O and H₂ predicted by the POLIMI mechanism for the addition of 400 ppm of NO₂ and $\Phi=2$.

Fig.S14. Evolution with temperature of mole fractions for the nitrogen containing species predicted by the POLIMI mechanism for the addition of 400 ppm of NO₂ and $\Phi=2$

B) For the addition of 400 ppm of NO₂ and $\Phi=0.5$.

Fig.S15. Evolution with temperature of mole fractions for the carbon compound species, H₂O and H₂ predicted by the POLIMI mechanism for the addition of 400 ppm of NO₂ and $\Phi=0.5$.

Fig.S16. Evolution with temperature of mole fractions for the nitrogen containing species predicted by the POLIMI mechanism for the addition of 400 ppm of NO₂ and $\Phi=0.5$.

C) For the addition of 500 ppm of NO and $\Phi=2$.

Fig.S17. Evolution with temperature of mole fractions for the carbon compound species, H₂O and H₂ predicted by the POLIMI mechanism for the addition of 500 ppm of NO and $\Phi=2$.

Fig.S18. Evolution with temperature of mole fractions for the nitrogen containing species predicted by the POLIMI mechanism for the addition of 500 ppm of NO and $\Phi=2$.

D) For the addition of 500 ppm of NO and $\Phi=0.5$.

Fig.S19. Evolution with temperature of mole fractions for the carbon compound species, H₂O and H₂ predicted by the POLIMI mechanism for the addition of 500 ppm of NO and $\Phi=0.5$.

Fig.S20. Evolution with temperature of mole fractions for the nitrogen containing species predicted by the POLIMI mechanism for the addition of 500 ppm of NO and $\Phi=0.5$.

5) The performance of literature models against the experimental data

Fig.S21. The performance of different models against the experiment data (mole fraction of methane) with neat methane oxidation under stoichiometric conditions.

Fig.S22. The performance of different models against the experiment data (mole fraction of methane) with the oxidation of methane doped with NO₂ under stoichiometric conditions.

Fig.S23. The performance of different models against the experiment data (mole fraction of methane) with the oxidation of methane doped with NO under stoichiometric conditions.

Fig.S24. The performance of different models against the experiment data (mole fraction of NO_x) with the oxidation of methane doped with NO₂ under stoichiometric conditions.

Fig.S25. The performance of different models against the experiment data (mole fraction of NO_x) with the oxidation of methane doped with NO under stoichiometric conditions.

6) Comparison of FTIR spectra for HCN with the spectra obtained during the oxidation of methane doped with NO.

Fig.S26. Comparison of the FTIR spectra for HCN [7] with the spectra obtained during the oxidation of methane doped with NO (500 ppm NO, 1200 K and $\Phi=2$).

7) Comparison of FTIR spectra for CH_3NO_2 with the spectra obtained during the oxidation of methane doped with NO_2 .

Fig.S27. Comparison of the FTIR spectra obtained for CH_3NO_2 with the spectra obtained during the oxidation of methane doped with NO_2 (400 ppm NO_2 , 900 K and $\Phi=0.5$).

8) Comparison of cw-CRDS spectra for HONO with the spectra obtained during the oxidation of methane doped with NO_2 .

Fig.S28. Comparison of the HONO cw-CRDS spectra with the spectra obtained during the oxidation of CH_4 doped with 400 ppm NO_2 , at 850 K and $\Phi=0.5$. Red line: absorption spectrum measured in this work (left axis), black line: HONO spectrum from Jain et al. [4], green line: CH_2O absorption spectrum from Ruth et al. [5], multiplied by 12, blue bars: CH_4 line strengths from Liu et al. [6], multiplied by 10^4 .

9) Comparisons between the original POLIMI model and POLIMI model with $\text{CH}_3+\text{NO}_2=\text{CH}_2\text{O}+\text{NO}$ modified against the experimental data under different conditions

Fig.S29. Comparisons between the original POLIMI model and POLIMI model with $\text{CH}_3+\text{NO}_2=\text{CH}_2\text{O}+\text{NO}$ modified against the experimental results from the oxidation of methane doped with NO_2 under stoichiometric conditions

Fig.S30. Comparisons between the original POLIMI model and POLIMI model with $\text{CH}_3+\text{NO}_2=\text{CH}_2\text{O}+\text{NO}$ modified against the experimental results from the oxidation of methane doped with NO under stoichiometric conditions

1) Additional description of the experimental setup

A) Jet-stirred reactor (JSR)

The jet-stirred reactor (JSR) used in this study is spherical with a volume of about 85 cm³. It is preceded by an annular preheater in which the reacting mixture is progressively heated up to the reaction temperature. Then the reacting mixture enters the reactor through four injectors with nozzles which creates high turbulence and homogenous mixing. The annular preheater and the reactor are made of fused silica. The heating is provided through Thermocoax resistances rolled around the preheater and the reactor. The reaction temperature is measured with a type K thermocouple located in a glass finger (the intraannular part of the preheater) at the center of the spherical reactor. Mass flow controllers (Bronkhorst) are used to control the volumetric flow rates of the reactants (CH₄, O₂, NO and NO₂) and the inert gas (Ar). The role of the inert gas is to dilute the reacting mixture in order to slow down the exothermicity of the reactions and to get a better control of the temperature. The pressure inside the reactor (800 Torr=106.7 kPa) is controlled using a manual valve located downstream of the reactor. The gas stream is analyzed online downstream of the reactor with the different diagnostic techniques as followed:

B) Gas chromatography

Two gas chromatographs were used for the online quantification of oxygen and carbon containing species. The first one, a Perichrom PR1250, was used to quantify oxygen. Injection were performed using a six-way gas sampling valve. The column used for the separation was a molecular sieve packed column and the detection was carried out with a thermal conductivity detector. The carrier gas was helium to have a good sensibility for oxygen. The second one, a Perichrom PR2500, was used for the quantification of CO, CO₂ and C₁-C₂ hydrocarbons. Injection were performed using a six-way gas sampling valve. A split of 1:5 was applied in the split injector. The column used for species separation was a PlotQ capillary one. The detection was performed using a flame ionization detector. The gas flow from the column was passed over a heated nickel catalyst for hydrogenation to convert CO and CO₂ to methane before detection. The calibration was performed with calibration bottles provided by Air-Liquide, France. The detection limit is about 10 ppm for the FID, 100 ppm for the TCD and the relative uncertainty is mole fractions is $\pm 5\%$.

C) NO_x Analysis

A chemiluminescence NO_x analyzer (Model 42i from ThermoFisher Scientific) was used to measure NO and NO₂ mole fractions. The quantitative range is 0-5000 ppm for NO and 0-500 ppm for NO₂ with 0.1 ppm sensitivity, respectively. Two pumps are used for outlet and bypass channels, respectively, enabling the simultaneous measurement of the concentrations of NO and NO₂. Briefly, the detection is based on the reaction of NO with O₃ leading to NO₂ + O₂ + *hν*. The light emitted, which is proportional to the concentration of NO, is detected using a photomultiplier tube (PMT). The measurement of NO₂ is indirectly obtained by measuring the total NO_x concentrations and subtracting the concentration of NO. The total NO_x concentrations are determined by converting NO₂ to NO over a heated catalyst prior the reaction chamber where the reaction with ozone takes place. The calibration was made with two calibration bottles provided by Air-Liquide, France, with 5000 ppm NO and 500 ppm NO₂ in argon, respectively. Note that the diluent gas is of importance as it has an effect on the flow rate through the analyzer and that it should be the same as the carrier gas used in experiments. The detection limit is about 1 ppm and the relative uncertainty is NO mole fractions is $\pm 5\%$, ± 10 for NO₂.

D) FTIR analyses

A Fourier Transform InfraRed spectrometer (FTIR) from Thermo Scientific Antaris equipped with a Mercure Cadmium Tellure photoelectric detector was used to analyze HCN and nitromethane. FTIR calibrations were obtained by injecting standards. Nitromethane was provided by Sigma (purity greater than 98.5%) and diluted mixtures were obtained by mixing nitromethane and helium using a Coriolis, a mass flow controller and an evaporation system provided by Bronkhorst, France. HCN was calibrated using a calibration gas bottle provided by Air-Liquide, France (1000 ppm of HCN in nitrogen). Different concentrations were used for calibration by

mixing the diluted HCN with an auxiliary nitrogen flow. The two flows were controlled by mass flow controllers provided by Bronkhorst, France. All FTIR analyses were performed at 373.15 K and 150 Torr. 32 scans were recorded for each analysis. A resolution of 0.5 cm^{-1} was used. The detection limit is about 10 ppm and the relative uncertainty in mole fractions is $\pm 10\%$,

E) cw-CRDS apparatus

The cw-CRDS cell is composed of a quartz tube with an outer diameter of 8 mm and a length of 80 cm. The total volume of the cell including the sampling probe is estimated to be 40 cm^3 . The cell is maintained at ambient temperature through convection and the pressure in the CRDS cavity is kept at approximately 10 Torr. The low pressure is obtained using a rotary vane pump (Alcatel 1015SD with a nominal flow rate of $15\text{ m}^3\cdot\text{h}^{-1}$). CRDS analyses were carried out in the near infrared at wavelengths from $6638 - 6643\text{ cm}^{-1}$. The near-infrared beam was provided by a fibred distributed feed-back (DFB) diode laser (Fitel-Furukawa FOL15DCWB-A81-W1509) emitting up to 40 mW, the wavelength can be varied in the range $6640\pm 13\text{ cm}^{-1}$ through changing the current applied to the diode laser. The diode laser emission is directly fibred and passes through a fibred optical isolator and a fibred acousto-optical modulator (AOM, AA Opto-Electronic). The AOM allows the laser beam to be deviated within 350 ns with respect to a trigger signal for a total duration of 1.5 ms. The zero order beam is connected to a fibred optical wave meter (228 Bristol Instruments) for monitoring the wavelength of the laser emission with an accuracy of 0.01 cm^{-1} . The main first order laser beam is coupled into the CRDS optical cavity through a short focal length lens ($f = 10\text{ mm}$) for mode matching so as to excite the fundamental TEM₀₀ mode. Two folding micrometric mirrors allow easy alignment of the beam, as shown in Figure 1. After many round trips, the optical signal transmitted through the cavity is converted into current by an avalanche photodiode (Perkin Elmer C30662E). A home designed amplifier-threshold circuit converts the current signal to an exploitable voltage signal and triggers the AOM to deviate the laser beam (turn off of the first order) as soon as the cavity comes into resonance and the photodiode signal exceeds a user-defined threshold. The photodiode signal is connected to a fast 16 bit analogue acquisition card (PCI-6259, National Instruments) in a PC, which is triggered also by the amplifier-threshold circuit. The acquisition card has an acquisition frequency of 1.25 MHz and thus the ring-down signal is sampled every 800 ns and the data are transferred to PC in real time. The ring-down time is obtained by fitting the exponential decay over a time range of seven lifetimes by a Levenberg-Marquardt exponential fit in LabView. The concentration of a species being formed or consumed during the hydrocarbon oxidation process in a jet-stirred reactor (JSR), can be obtained by measuring the ring-down time of the empty cavity τ_0 , i.e., the ring down time before heating the reactor, and the ring down time τ , after turning on the heater:

$$\alpha = [X] \times \sigma = \frac{R}{c} \left(\frac{1}{\tau} - \frac{1}{\tau_0} \right)$$

where σ is the absorption cross section, R is the ratio between the cavity length L , i.e. the distance between the two cavity mirrors to the length LA over which the absorber is present, c is the speed of light. Knowing the absorption cross section, one can extract the concentration $[A]$ of the target molecule. The relative uncertainty is around $\pm 10\text{-}15\%$,

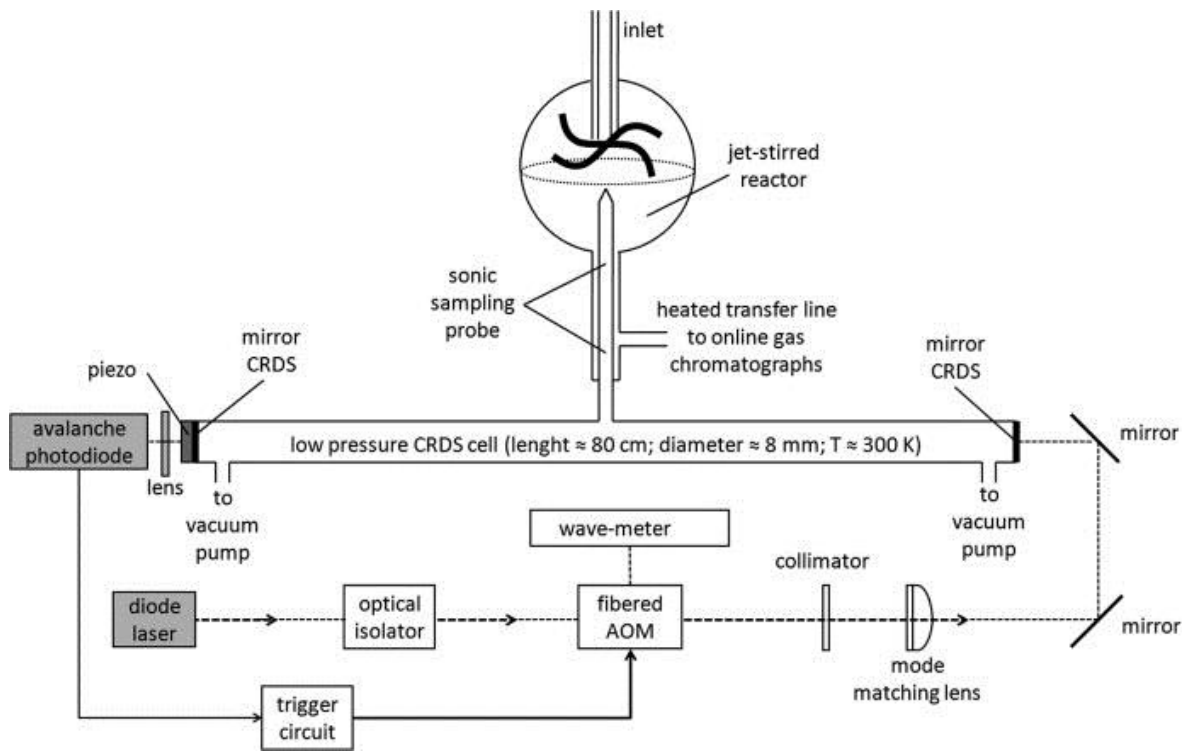


Fig.S1. Schematic view of the JSR and CRDS coupling.

2) Comparison of simulations using the present mechanism (POLIMI mechanism) with literature data.

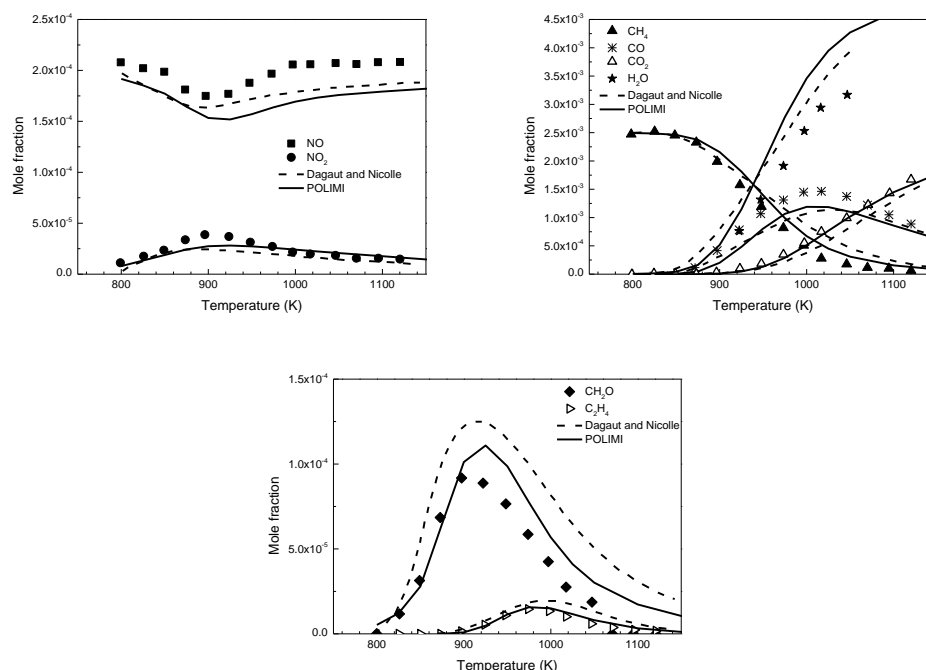


Fig.S2. Comparison of modeling predictions using POLIMI mechanism (solid lines) and experimental (symbols) and modeling predictions (dashed lines) reported by Dagaut and Nicolle [1] for the oxidation of methane and NO in a JSR (1 atm, $\Phi=0.1$, 2500 ppm of CH_4 , 50000 ppm of O_2 , dilution in N_2 , $\tau=120$ ms).

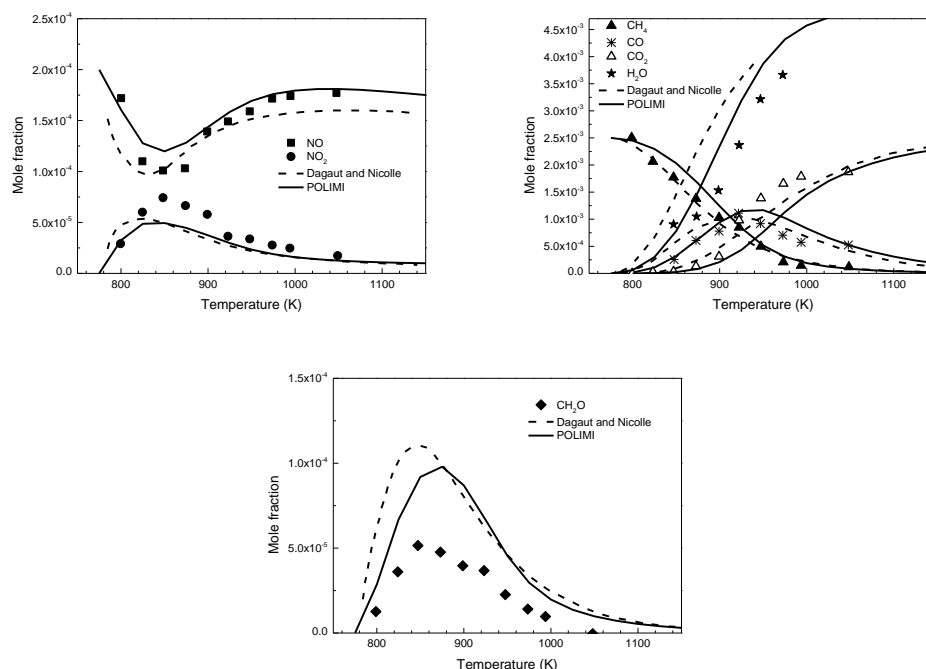


Fig.S3. Comparison of modeling predictions using POLIMI mechanism (solid lines) and experimental (symbols) and modeling predictions (dashed lines) reported by Dagaut and Nicolle [1] for the oxidation of methane and NO in a JSR (10 atm, $\Phi=0.5$, 2500 ppm of CH_4 , 10000 ppm of O_2 , dilution in N_2 , $\tau=1000$ ms).

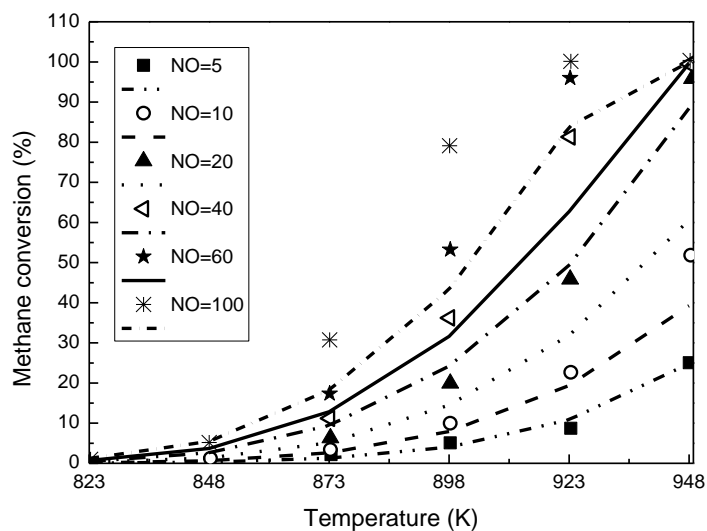


Fig.S4. Comparison of modeling predictions using POLIMI mechanism (lines) and experimental (symbols) reported by Chan et al. [2] for the oxidation of methane and different amounts of NO in a flow reactor (1 atm, 2.5% methane-in-air mixture, 0-100 ppm NO added, residence time of 2 s).

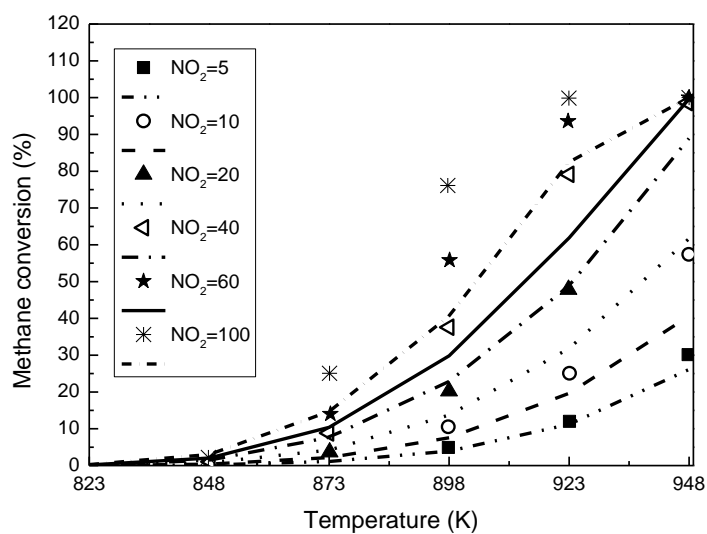


Fig.S5. Comparison of modeling predictions using POLIMI mechanism (lines) and experimental (symbols) reported by Chan et al. [2] for the oxidation of methane and different amounts of NO₂ in a flow reactor (1 atm, 2.5% methane-in-air mixture, 0-100 ppm NO₂ added, residence time of 2 s).

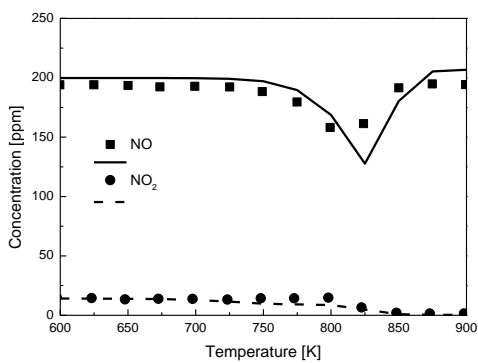
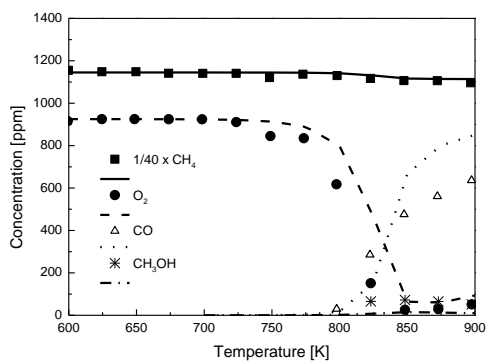


Fig.S6. Comparison of modeling predictions using POLIMI mechanism (lines) and experimental (symbols) reported by Rasmussen et al. [3] for the oxidation of methane and NO in a high-pressure flow reactor (20 bar, 4.58% methane, 925 ppm O₂, 200 ppm NO, 14 ppm NO₂, $\Phi=99$, $\tau=2440/T$).

3) The evolution profiles of methane as a function of time at both steady and oscillation states

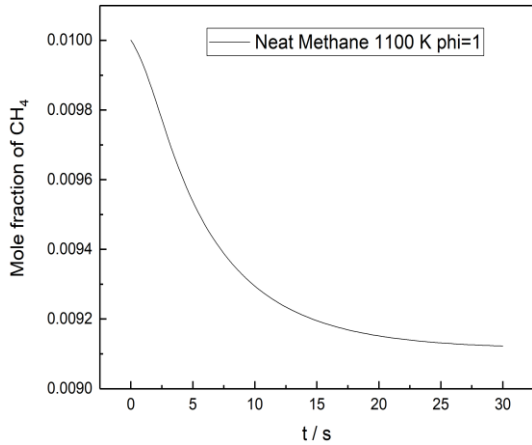


Fig.S7. The simulation work of the evolution profiles of methane as a function of time for the neat methane oxidation at 1100 K under stoichiometric condition. **(Steady state)**

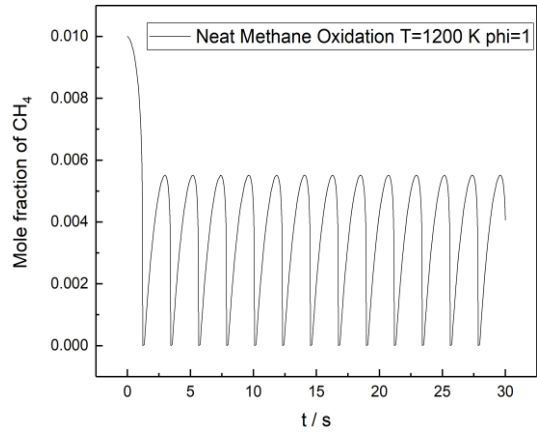


Fig.S8. The simulation work of the evolution profiles of methane as a function of time for the neat methane oxidation at 1200 K under stoichiometric condition. **(Oscillations)**

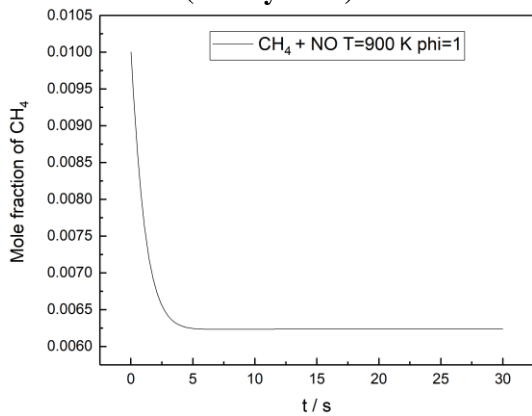


Fig.S9. The simulation work of the evolution profiles of methane as a function of time for the oxidation of methane doped with NO at 900 K under stoichiometric condition. **(Steady state)**

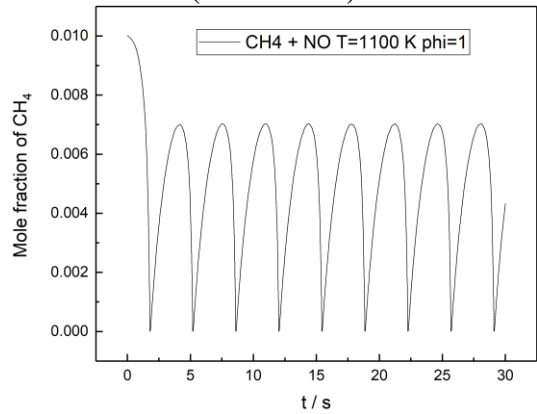


Fig.S10. The simulation work of the evolution profiles of methane as a function of time for the oxidation of methane doped with NO at 1000 K under stoichiometric condition. **(Oscillations)**

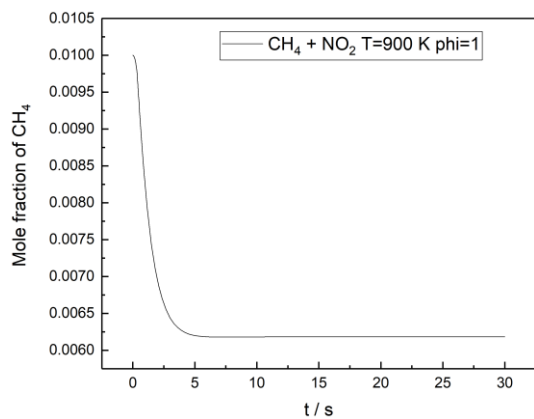


Fig.S11. The simulation work of the evolution profiles of methane as a function of time for the oxidation of methane doped with NO₂ at 900 K under stoichiometric condition. **(Steady state)**

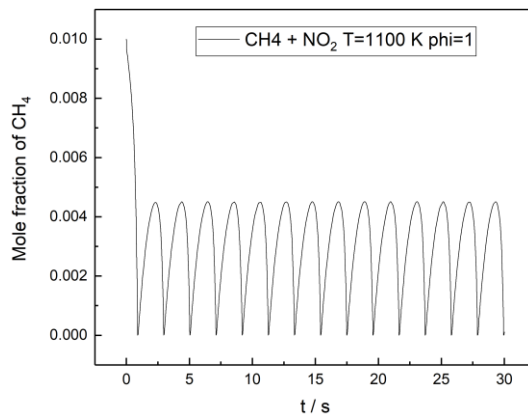


Fig.S12. The simulation work of the evolution profiles of methane as a function of time for the oxidation of methane doped with NO₂ at 1100 K under stoichiometric condition. **(Oscillations)**

4) Evolution with temperature of mole fractions of the different species according to model calculations with POLIMI mechanism.

A) For the addition of 400 ppm of NO_2 and $\Phi=2$.

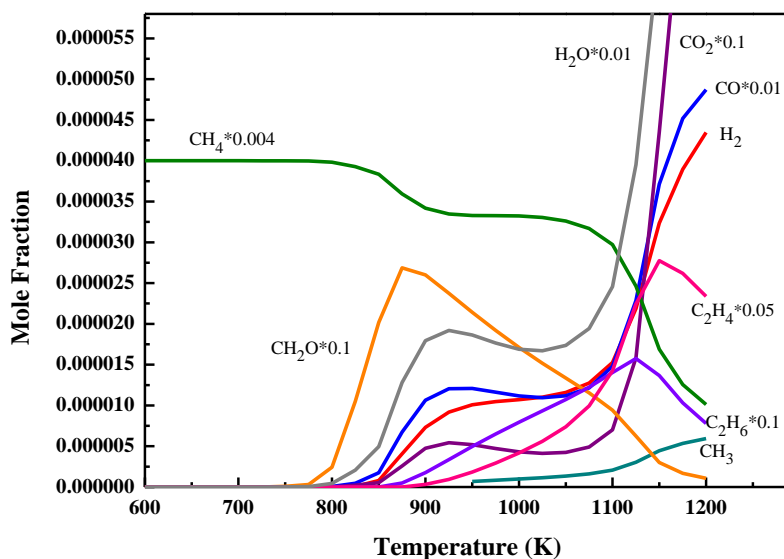


Fig.S13. Evolution with temperature of mole fractions for the carbon compound species, H_2O and H_2 predicted by the POLIMI mechanism for the addition of 400 ppm of NO_2 and $\Phi=2$.

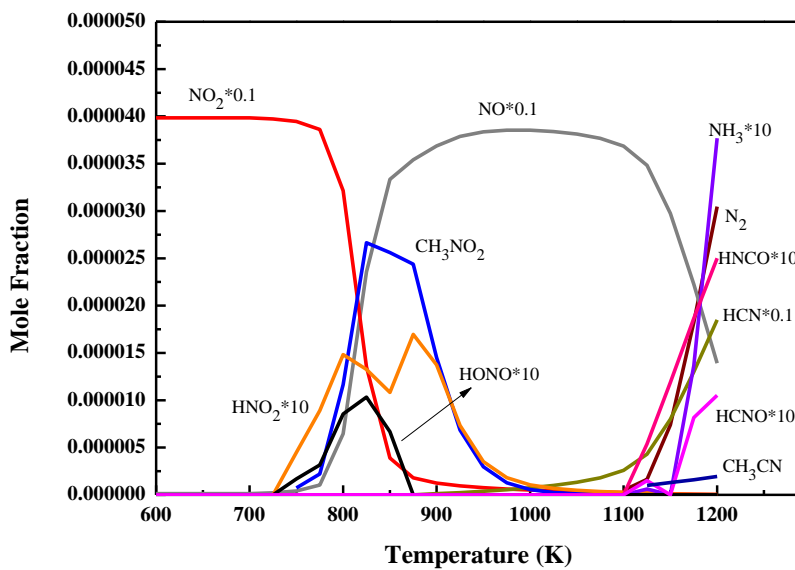


Fig.S14. Evolution with temperature of mole fractions for the nitrogen containing species predicted by the POLIMI mechanism for the addition of 400 ppm of NO_2 and $\Phi=2$.

B) For the addition of 400 ppm of NO₂ and $\Phi=0.5$

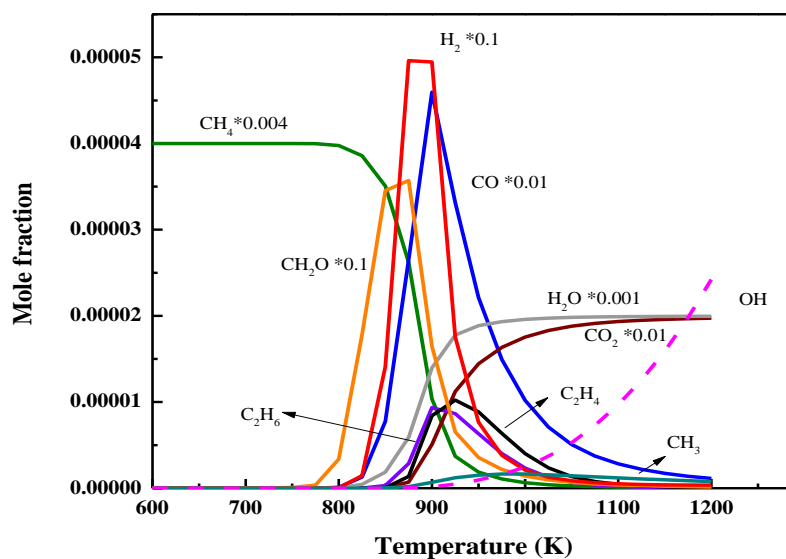


Fig.S15. Evolution with temperature of mole fractions for the carbon compound species, H₂O and H₂ predicted by the POLIMI mechanism for the addition of 400 ppm of NO₂ and $\Phi=0.5$.

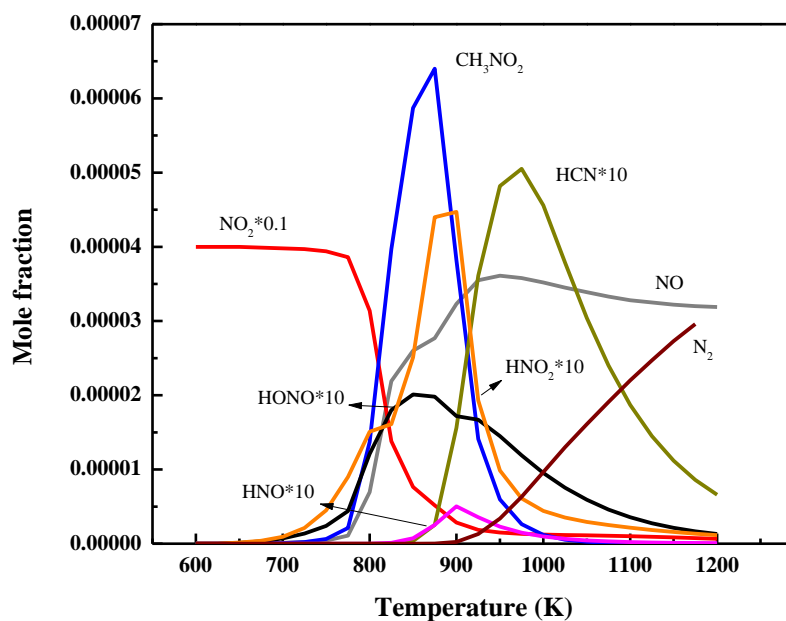


Fig.S16. Evolution with temperature of mole fractions for the nitrogen containing species predicted by the POLIMI mechanism for the addition of 400 ppm of NO₂ and $\Phi=0.5$.

C) For the addition of 500 ppm of NO and $\Phi=2$.

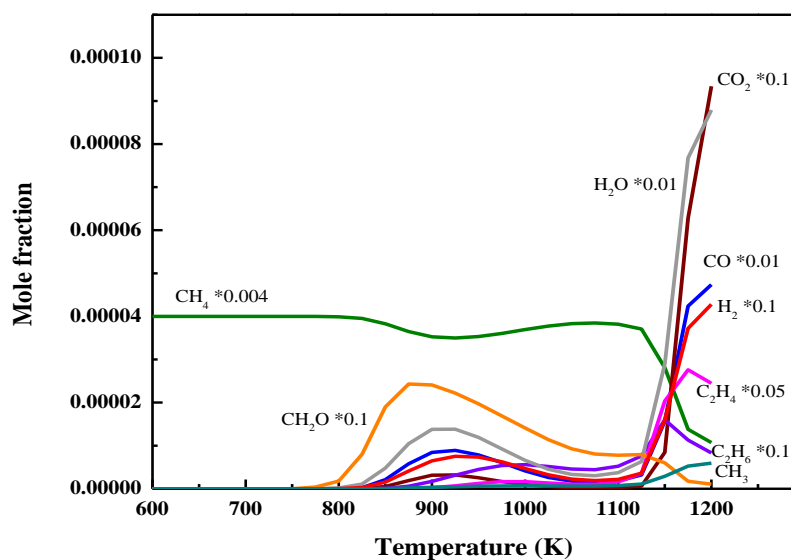


Fig.S17. Evolution with temperature of mole fractions for the carbon compound species, H₂O and H₂ predicted by the POLIMI mechanism for the addition of 500 ppm of NO and $\Phi=2$.

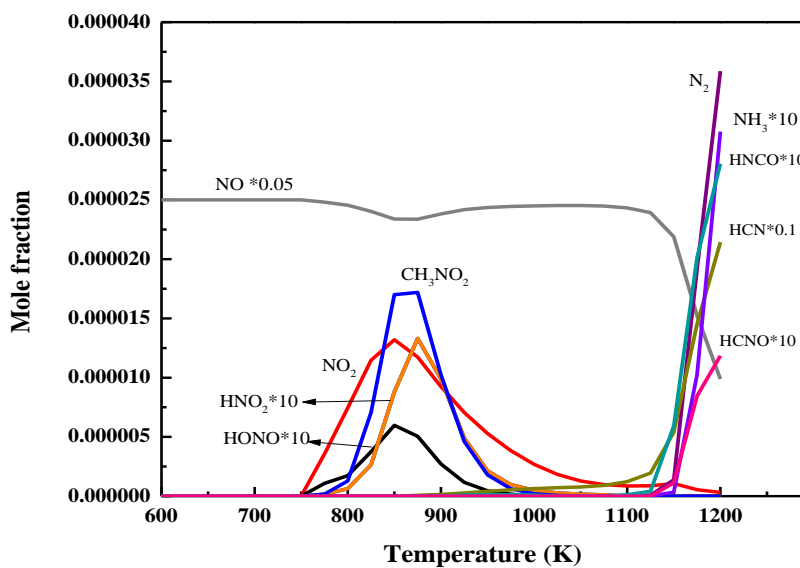


Fig.S18. Evolution with temperature of mole fractions for the nitrogen containing species predicted by the POLIMI mechanism for the addition of 500 ppm of NO and $\Phi=2$.

D) For the addition of 500 ppm of NO and $\Phi=0.5$.

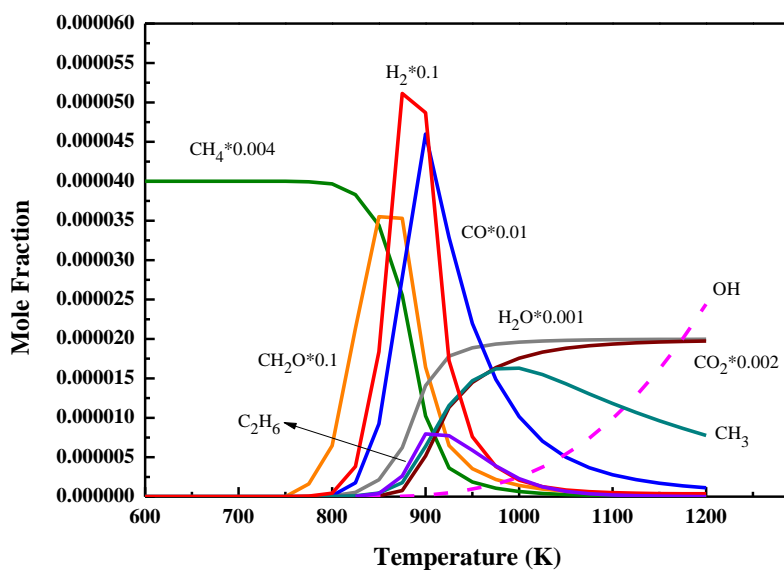


Fig.S19. Evolution with temperature of mole fractions for the carbon compound species, H₂O, H₂ and OH radicals predicted by the POLIMI mechanism for the addition of 500 ppm of NO and $\Phi=0.5$.

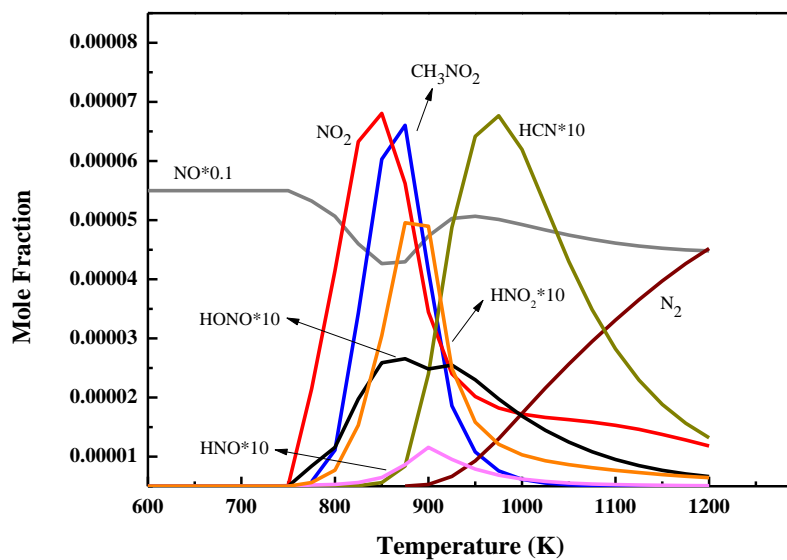


Fig.S20. Evolution with temperature of mole fractions for the nitrogen containing species predicted by the POLIMI mechanism for the addition of 500 ppm of NO and $\Phi=0.5$.

5) The performance of literature models against the experimental data

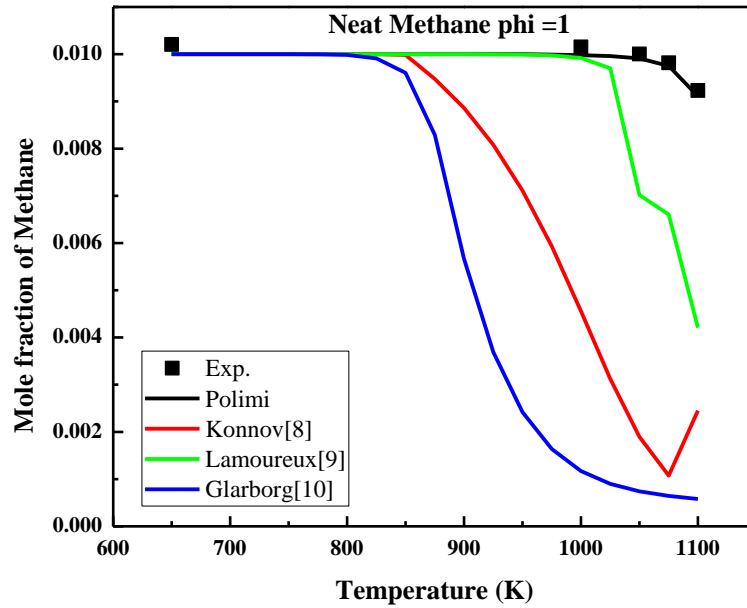


Fig.S21. The performance of different models against the experiment data (mole fraction of methane) with neat methane oxidation under stoichiometric conditions.

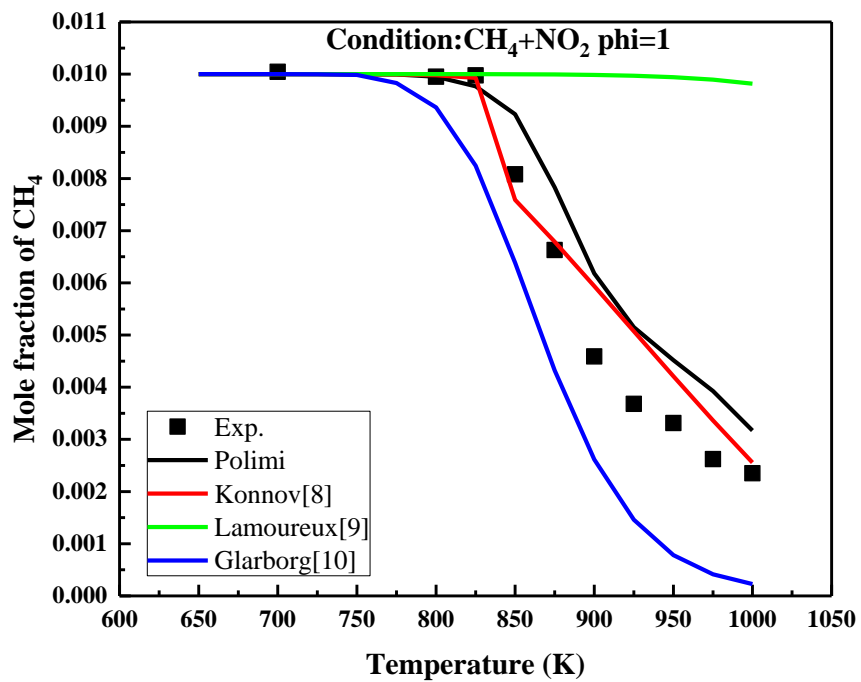


Fig.S22. The performance of different models against the experiment data (mole fraction of methane) with the oxidation of methane doped with NO_2 under stoichiometric conditions.

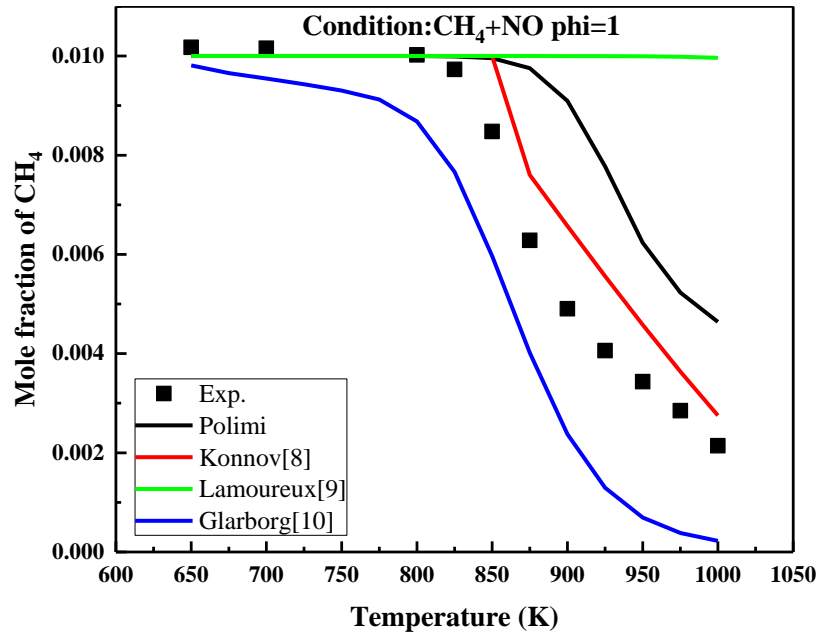


Fig.S23. The performance of different models against the experiment data (mole fraction of methane) with the oxidation of methane doped with NO under stoichiometric conditions.

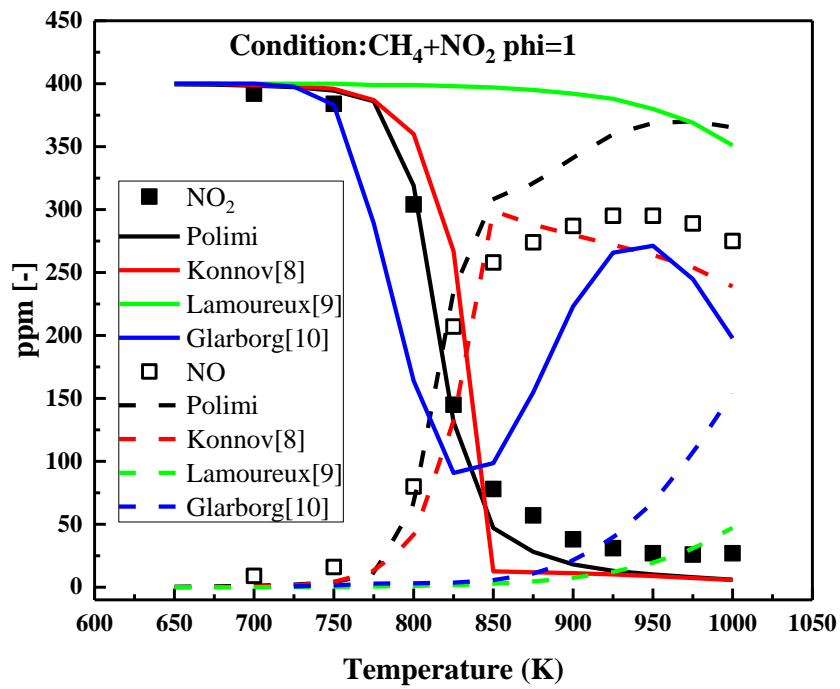


Fig.S24. The performance of different models against the experiment data (mole fraction of NO_x) with the oxidation of methane doped with NO_2 under stoichiometric conditions.

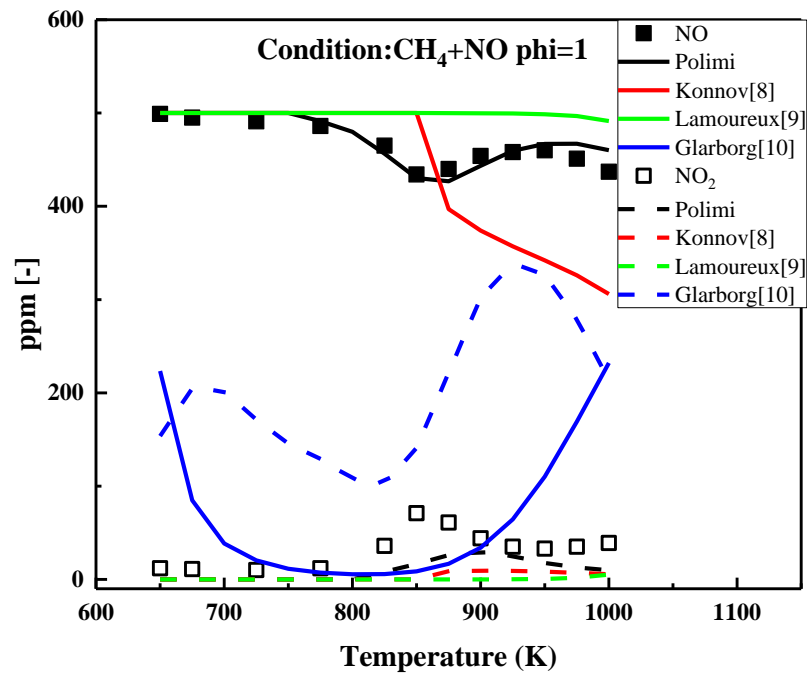


Fig.S25. The performance of different models against the experiment data (mole fraction of NO_x) with the oxidation of methane doped with NO under stoichiometric conditions.

6) Comparison of FTIR spectra for HCN with the spectra obtained during the oxidation of methane doped with NO.

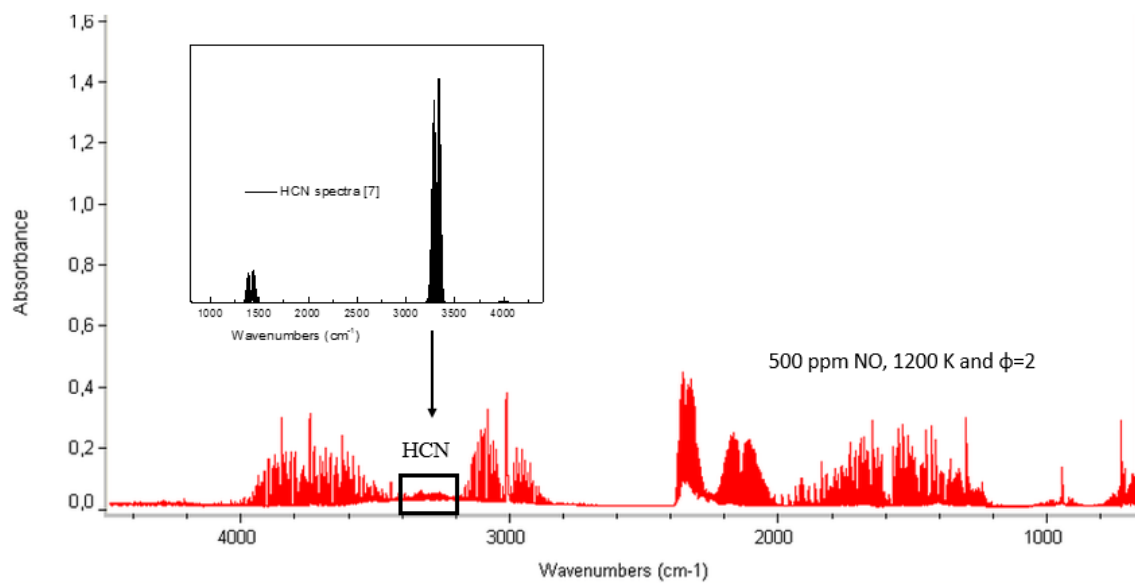


Fig.S26. Comparison of the FTIR spectra for HCN [7] with the spectra obtained during the oxidation of methane doped with NO (500 ppm NO, 1200 K and $\Phi=2$).

7) Comparison of FTIR spectra for CH_3NO_2 with the spectra obtained during the oxidation of methane doped with NO_2 .

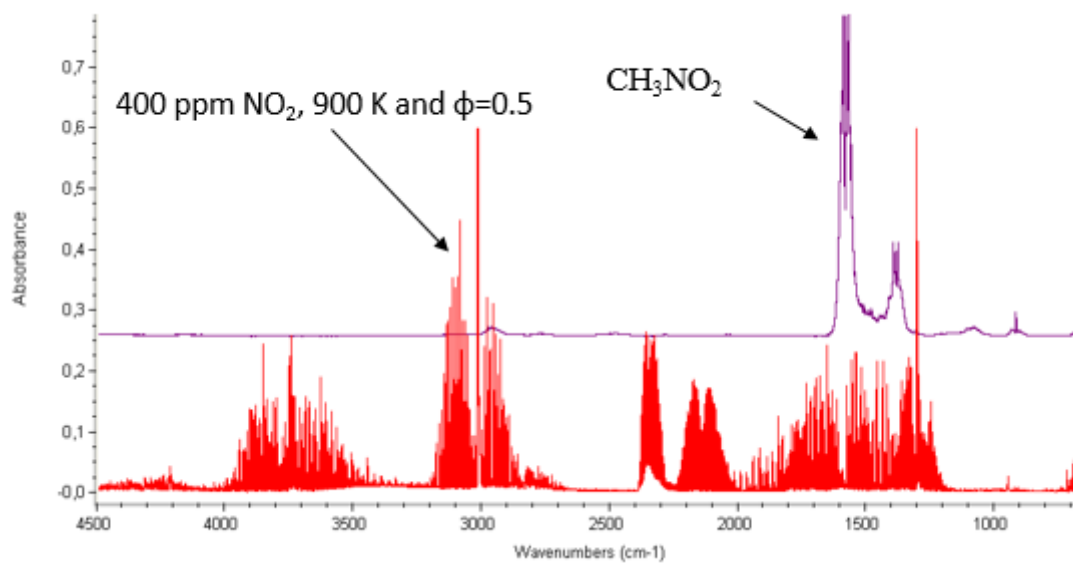


Fig.S27. Comparison of the FTIR spectra obtained for CH_3NO_2 with the spectra obtained during the oxidation of methane doped with NO_2 (400 ppm NO_2 , 900 K and $\Phi=0.5$).

8) Comparison of cw-CRDS spectra for HONO with the spectra obtained during the oxidation of methane doped with NO₂

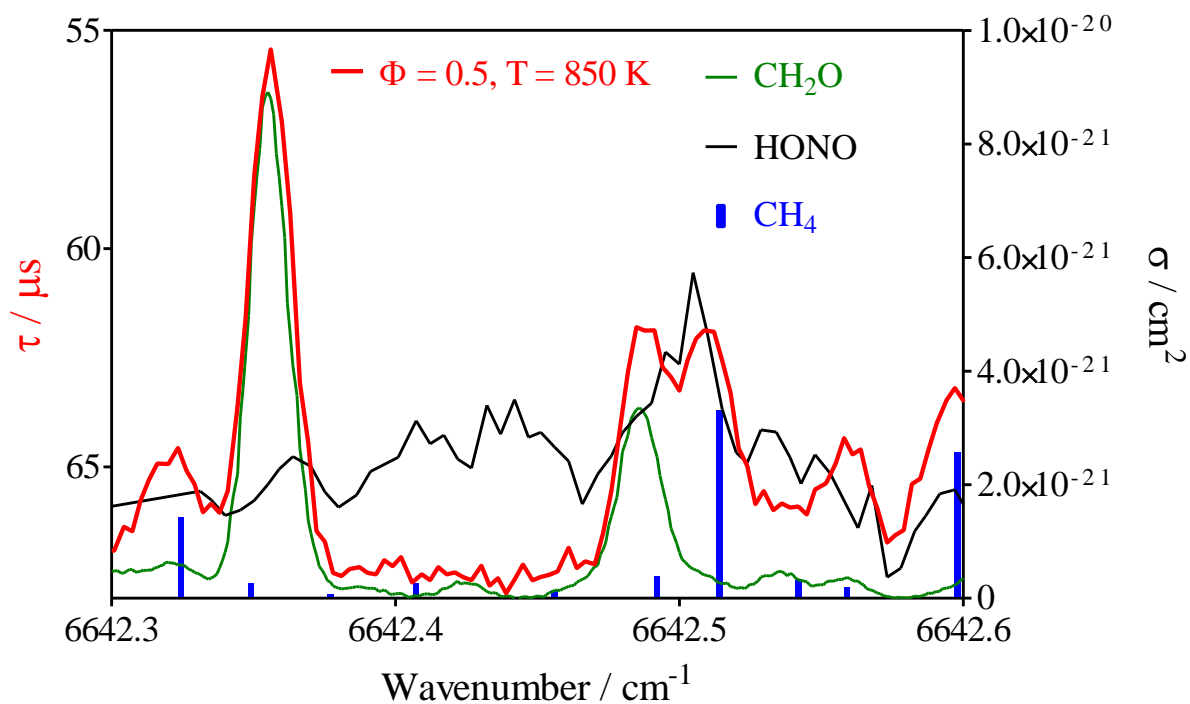


Fig.S28. Comparison of the HONO cw-CRDS spectra with the spectra obtained during the oxidation of CH₄ doped with 400 ppm NO₂, at 850 K and $\Phi=0.5$. Red line: absorption spectrum measured in this work (left axis), black line: HONO spectrum from Jain et al. [4], green line: CH₂O absorption spectrum from Ruth et al. [5], multiplied by 12, blue bars: CH₄ line strengths from Liu et al. [6], multiplied by 10^4 .

9) Comparisons between the original POLIMI model and POLIMI model with $\text{CH}_3+\text{NO}_2=\text{CH}_2\text{O}+\text{NO}$ modified against the experimental data under different conditions

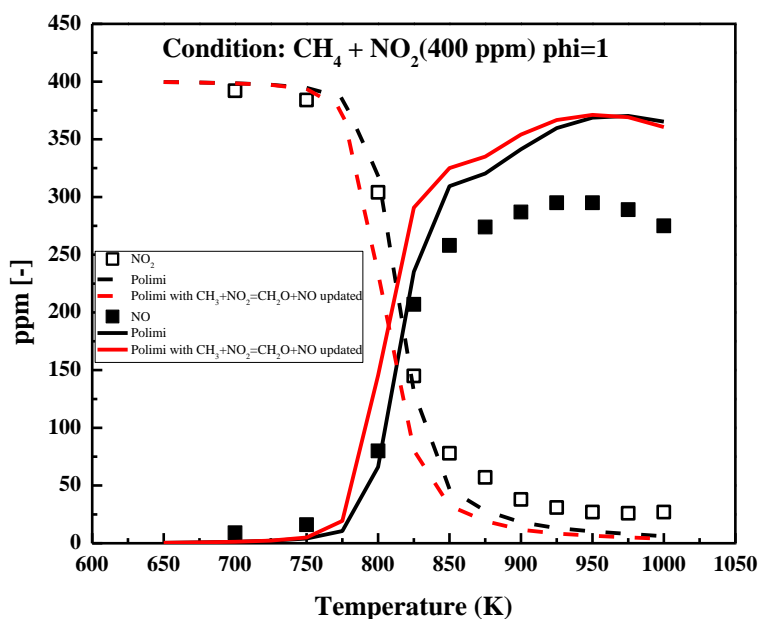


Fig.S29. Comparisons between the original POLIMI model and POLIMI model with $\text{CH}_3+\text{NO}_2=\text{CH}_2\text{O}+\text{NO}$ modified against the experimental results from the oxidation of methane doped with NO_2 under stoichiometric conditions.

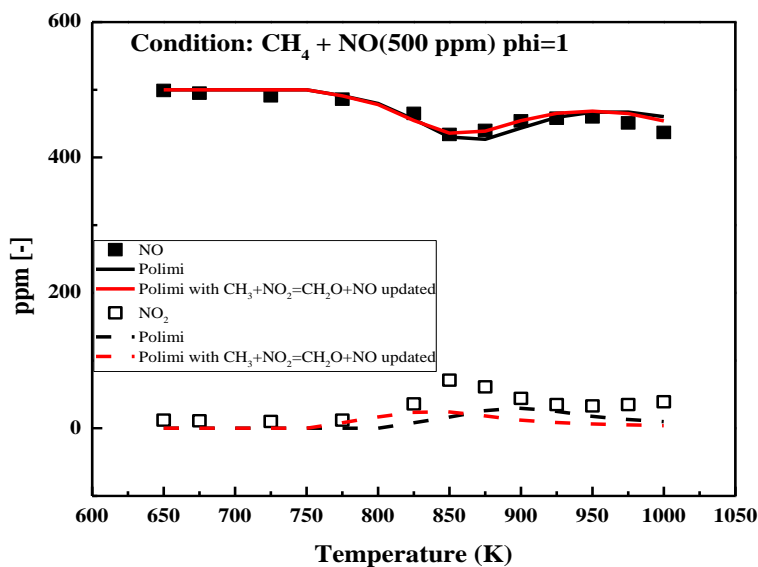


Fig.S30. Comparisons between the original POLIMI model and POLIMI model with $\text{CH}_3+\text{NO}_2=\text{CH}_2\text{O}+\text{NO}$ modified against the experimental results from the oxidation of methane doped with NO under stoichiometric conditions.

References

- [1] P. Dagaut, A. Nicolle, *Combust. Flame* 140 (2005) 161-171.
- [2] Y.L. Chan, F.J. Barnes, J.H. Bromly, A.A. Konnov, D.K. Zhang, *Proc. Combust. Inst.* 33 (2011) 441-447.
- [3] C.L. Rasmussen, A.E. Rasmussen, P. Glarborg, *Combust. Flame* 154 (2008) 529-545.
- [4] C. Jain, P. Morajkar, C. Schoemaeker, B. Viskolcz, C. Fittschen, *J. Phys. Chem. A* 115 (2011) 10720-10728.
- [5] A.W. Liu, S. Kassi, A. Campargue, *Chem. Phys. Lett.* 447 (2007) 16-20.
- [6] A.A. Ruth, U. Heitmann, E. Heinecke, C. Fittschen, *Z. Phys. Chem.* 229 (2015) 1609.
- [7] The HITRAN Database, Website: <http://hitran.org/>
- [8] A.A. Konnov, *Combustion and Flame*, 156 (2009) 2093-2105.
- [9] N. Lamoureux, H. El Merhubi, L. Pillier, S. de Persis, P. Desgroux, *Combustion and Flame*, 163 (2016) 557-575.
- [10] T. Mendiara, P. Glarborg, *Combustion and Flame*, 156 (2009) 1937-1949.

Article VII:

Marrodán, L.; Fuster, M.; Millera, Á.; Bilbao, R.; Alzueta, M.U. (2018). Ethanol as a fuel additive: high-pressure oxidation of its mixtures with acetylene. *Energy and Fuels* 32, 10078-10087.

Ethanol as a Fuel Additive: High-Pressure Oxidation of Its Mixtures with Acetylene

Lorena Marrodán,¹ Miguel Fuster, Ángela Millera, Rafael Bilbao, and María U. Alzueta*¹

Aragón Institute of Engineering Research (I3A), Department of Chemical and Environmental Engineering, University of Zaragoza, 50018 Zaragoza, Spain

Supporting Information

ABSTRACT: An experimental and modeling study of the oxidation of acetylene–ethanol mixtures under high-pressure conditions (10–40 bar) has been carried out in the 575–1075 K temperature range in a plug-flow reactor. The influence on the oxidation process of the oxygen inlet concentration (determined by the air excess ratio, λ) and the amount of ethanol (0–200 ppm) present in the reactant mixture has also been evaluated. In general, the predictions obtained with the proposed model are in satisfactory agreement with the experimental data. For a given pressure, the onset temperature for acetylene conversion is almost the same independent of the oxygen or ethanol concentration in the reactant mixture but is shifted to lower temperatures when the pressure is increased. Under the conditions of this study, the ethanol presence does not modify the main reaction routes for acetylene conversion, with its main effect being the modification of the radical pool composition.

INTRODUCTION

Fuel reformulation seems to be a promising strategy for minimizing important pollutants emitted to the atmosphere during combustion processes, especially from transportation, such as nitrogen oxides (NO_x) and soot, the principal component of particulate matter. Government regulations are becoming stricter; there is an increasing global warming concern; and fossil fuel resources are finite. Therefore, bio-derived oxygenated fuels and fuel additives have been given more attention in the last few years and awaken the research community interest, as shown by Kohse-Höinghaus et al.¹ when reviewing biofuel combustion chemistry.

Among all possible biofuels, ethanol is one of the most common biofuels and has been widely studied and used, either directly or as a gasoline additive. However, its application in diesel engines is restricted because its cetane number, flash point, and calorific values are lower compared to diesel fuel. For this reason, ethanol must be blended with diesel or biodiesel to overcome all of these difficulties. In this way, with regard to the exhaust pollutant emissions, although there is certain controversy about if it is possible to reduce simultaneously CO, soot, or nitrogen oxides emissions, authors, such as An et al.,² indicate that, working under given conditions, for example, at comparatively lower temperatures, soot and nitrogen oxides emissions could be reduced using ethanol. This controversy makes a systematic study at laboratory scale necessary under well-controlled operating conditions to acquire better knowledge of the possible effects of the ethanol addition to fuel.

In recent years, the role of ethanol as an additive to diesel or gasoline has been studied in engines (e.g., refs 3 and 4) and when added to different hydrocarbons (such as acetylene, ethylene, *n*-heptane, propene, iso-octane, or benzene, among others) in laboratory flames [for example, refs 5–9], jet-stirred reactors (JSRs),^{10,11} and plug-flow reactors,¹² to investigate its influence on combustion performance and pollutant emissions.

Dagaut and Togbé¹⁰ carried out an experimental and modeling study of the oxidation of different mixtures of iso-octane with ethanol and 1-butanol in a JSR at an equivalence ratio of 1 and a pressure of 10 atm with good agreement between experimental and modeling calculations. Reaction rate analyses showed that the reaction paths were very similar when increasing the alcohol fraction in the mixture. In a similar way, Rezgui and Guemini¹¹ carried out a computational study based on the experimental results previously obtained by Ristori et al.¹³ and Aboussi¹⁴ on the effects of ethanol addition on the formation of some pollutants during benzene JSR oxidation, and their results indicated that the mole fractions of acetylene (C_2H_2), cyclopentadienyl radical (C_5H_5), and propargyl radical (C_3H_3) decreased when increasing the ethanol percentage in the mixture. In an atmospheric plug-flow reactor, Abián et al.¹² analyzed the effect of the temperature (775–1375 K), air excess ratio (from fuel-rich to fuel-lean conditions), and ethanol concentration (0–200 ppm) on the oxidation of acetylene–ethanol mixtures. They stated that the main reaction pathways observed for acetylene conversion in the presence of ethanol were basically the same as those in its absence, and the influence of ethanol addition comes from its capacity to modify the composition of the radical pool. Moreover, Esarte et al.¹⁵ analyzed soot formation from the pyrolysis of acetylene, ethanol, and their mixtures, and the results showed that adding small concentrations of ethanol (600 times lower than the acetylene concentration) leads to a diminution on the production of soot from acetylene pyrolysis.

However, despite its relevance for its applicability to internal combustion engines and the current tendency in designing combustion systems working at high pressure to increase

Special Issue: SMARTCAT's COST Action

Received: March 19, 2018

Revised: July 6, 2018

Published: July 9, 2018

efficiency, to our knowledge, no experimental or modeling studies have been carried out evaluating the impact of ethanol addition to hydrocarbons at pressures higher than 10 atm.

In this context, the aim of the present work is to study the high-pressure oxidation of acetylene–ethanol mixtures, which will extend the experimental database on the behavior of ethanol as an additive. Therefore, the oxidation of acetylene–ethanol mixtures in a quartz flow reactor under high-pressure conditions has been studied from both experimental and modeling points of view. Acetylene (C_2H_2) has been set as the main fuel because it is recognized as one of the main soot precursors and is an important intermediate in combustion of hydrocarbons and a recent chemical kinetic mechanism for modeling its conversion under high-pressure conditions is available.¹⁶ The experimental results obtained have been used to validate a chemical kinetic mechanism able to describe the oxidation of both compounds and their mixtures under the conditions studied. This will extend the applicability of the model to other operating conditions, and it can be used as a predicting tool.

EXPERIMENTAL SECTION

The experiments have been carried out in a laboratory-scale high-pressure flow reactor designed to approximate plug flow,¹⁷ which has been described elsewhere,¹⁸ and therefore, only the most relevant details are mentioned here. The oxidation of C_2H_2 (approximately 500 ppm) and ethanol (C_2H_5OH , 0–200 ppm) mixtures has been analyzed in the 575–1075 K temperature range. To evaluate the influence of the pressure on the oxidation process, different manometric pressures have been tested, 10–40 bar. The oxygen inlet concentration has been varied from reducing to oxidizing conditions by modifying the value of λ (0.7, 1, and 20), defined as inlet oxygen divided by stoichiometric oxygen, and considering both fuel components, acetylene and ethanol. Nitrogen is used to balance up to obtain a total gas flow rate of 1 L [1 L (STP)/min (STP)]/min. Reactants are highly diluted, minimizing the reaction thermal effects. Reactant gases, supplied from gas cylinders, are premixed before entering the reactor. Table 1 lists the conditions for the different experiments.

The oxidation reactions take place in a tubular quartz tube (inner diameter of 6 mm and length of 1500 mm) enclosed in a steel pressure shell and placed in an electrically heated oven. Type K

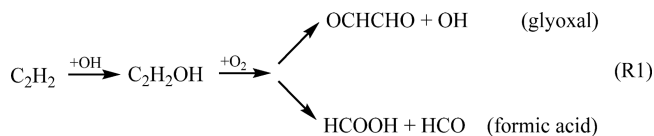
thermocouples, positioned in the void between the quartz reactor and the steel shell, were used to measure the longitudinal temperature profiles, obtaining an isothermal reaction zone (± 10 K) of 56 cm. The temperature profiles, for 10 and 40 bar, can be found as Figures S1 and S2 of the Supporting Information, respectively. The gas residence time in the isothermal zone can be represented by t_r (s) = $261 \times P$ (bar)/ T (K), which implies that the residence time depends upon both the pressure and temperature. Downstream of the reactor, the pressure of the system is reduced to the atmospheric level before product analysis, which is performed using a micro gas chromatograph (Agilent 3000A) equipped with a Thermal Conductivity Detector (TCD) and an ATI Mattson Fourier transform infrared spectrometer. The uncertainty of measurements is estimated as $\pm 5\%$, except for the FTIR spectrometer, which is estimated as $\pm 10\%$. The atomic carbon balance was checked, and the deviations were below 10% in most of the cases.

CHEMICAL KINETIC MODEL

The experimental results have been analyzed in terms of a detailed gas-phase chemical kinetic mechanism for chemistry description and analysis of the oxidation under high-pressure conditions of C_2H_2 – C_2H_5OH mixtures.

The mechanism and thermodynamic data proposed by our group to describe the ethanol high-pressure oxidation¹⁹ have been taken in the present work without any modifications. This mechanism includes the reaction subset for ethanol conversion suggested by Alzueta and Hernández.²⁰ Calculations coincide, in general, well with the main experimental trends observed. Other mechanisms in the literature are available. As an example, we have tested a very recent mechanism by Hashemi et al.,²¹ proposed to describe the pyrolysis and oxidation of ethanol under high-pressure conditions. The results indicate that modeling predictions are also in good agreement with the experimental trends observed in the present work (Figures S3–S5 of the Supporting Information).

The present mechanism takes as a basis the GADM mechanism,²² progressively updated (e.g., refs 23 and 24) and modified to consider the high-pressure conditions and the different compounds involved.^{17,25–27} The reaction subset proposed by Giménez-López et al.¹⁶ for oxidation of acetylene at intermediate temperatures and a high pressure was also included. These authors indicated that, through the sequence represented in reaction R1, significant amounts of glyoxal and formic acid may be formed from acetylene. Therefore, the reaction subsets for these compounds (refs 28 and 29, respectively) were also added to the present mechanism.



Although no special implication of compounds, such as methyl formate, dimethoxymethane, or dimethyl ether, is expected, the present mechanism also includes reaction subsets for these compounds, which have been validated under high-pressure conditions (refs 18, 30, and 31, respectively). We found that some reactions involving HCOOH proposed by Zhao et al.³² slightly improve the present model calculations. Most of these reactions (Table S1 of the Supporting Information) are H-abstraction and decomposition reactions, which occur in only one step (e.g., $HCOOH + OH = H_2O + CO_2 + H$), whereas in the formic acid subset by Marshall and Glarborg,²⁹ this is produced in two steps: a H abstraction (e.g., $HCOOH + OH = HOCO + H_2O$), followed by the decomposition of the

Table 1. Matrix of Experimental Conditions^a

set	C_2H_2 (ppm)	C_2H_5OH (ppm)	P (bar)	λ
1	569		10	1
2	467	49	10	0.7
3	537	42		1
4	424	46		20
5	544	52	20	1
6	490	51	40	0.7
7	566	48		1
8	565	50		20
9	574	96	10	1
10	559	140	10	1
11	552	170	10	0.7
12	531	242		1
13	420	210		20
14	554	210	40	0.7
15	575	204		1
16	551	211		20

^aExperiments are conducted in the 575–1075 K temperature range. The balance is closed with N_2 .

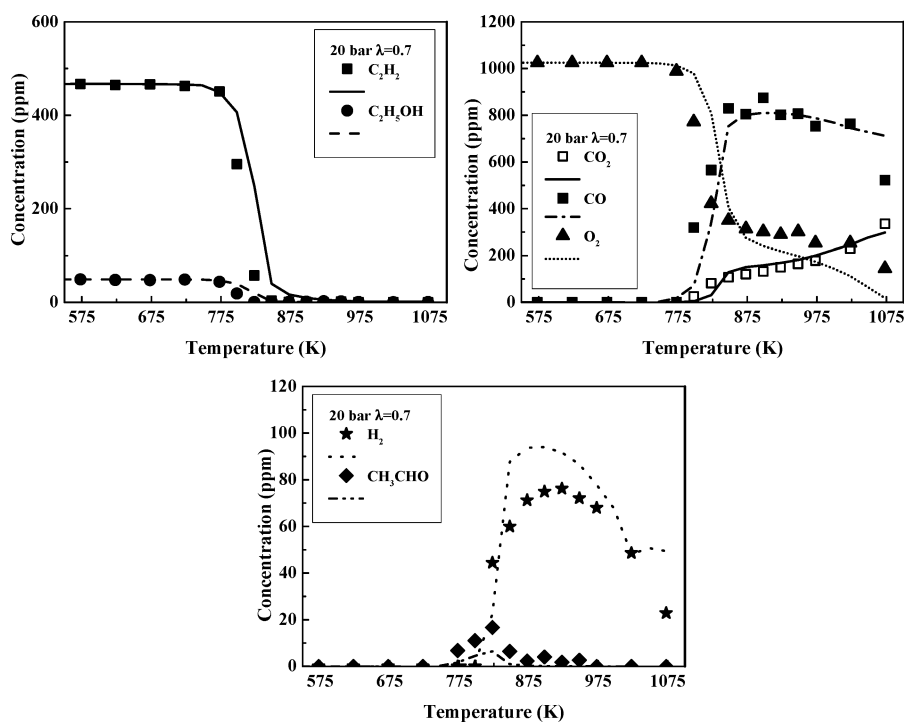


Figure 1. Evolution of C_2H_2 , C_2H_5OH , O_2 , CO , CO_2 , H_2 , and CH_3CHO concentrations with the temperature during the high-pressure (10 bar) oxidation of C_2H_2 – C_2H_5OH mixtures for the conditions denoted as set 2 in Table 1.

hydrocarboxyl radical produced [e.g., $HOCO (+M) = CO + OH (+M)$]. Examples of the discrepancies obtained in modeling calculations with or without these reactions, for conditions denoted as sets 1–4 in Table 1, are given in Figures S6–S9 of the Supporting Information. The influence of these reactions, although low, indicates an uncertainty in the behavior of $HCOOH$, and therefore, effort should be made in better understanding its oxidation.

The mechanism obtained by this way involves 137 species and contains 798 reactions, and as mentioned above, it is the same successfully used in a high-pressure ethanol oxidation study.¹⁹ The complete mechanism and thermodynamic data are provided as Supporting Information.

Numerical calculations were conducted with the plug-flow reactor module of the CHEMKIN-PRO software package³³ and considering the corresponding temperature profiles determined experimentally.

RESULTS AND DISCUSSION

The oxidation of C_2H_2 – C_2H_5OH mixtures has been studied in the 575–1075 K temperature range. In addition to the temperature, the influence of the pressure (10 and 40 bar), air excess ratio (λ), and concentration of ethanol in the mixture (0–200 ppm) has been analyzed from both experimental and modeling points of view. Figure 1 shows an example of the results for the consumption with the temperature of the reactants C_2H_2 , C_2H_5OH , and oxygen and for the formation of different products quantified (CO , CO_2 , H_2 , and CH_3CHO) for the conditions denoted as set 2 in Table 1. From now on, experimental results are denoted by symbols, whereas model calculations are denoted by lines. In general, there is good agreement between experimental and modeling results. Moreover, all of the experimental results obtained in the present work can be found in an Excel spreadsheet as Supporting Information.

Figures 2 and 3 show the evolution with the temperature of C_2H_2 , C_2H_5OH , CO , and CO_2 concentrations for stoichiometric conditions ($\lambda = 1$), 10 bar, and different inlet ethanol concentrations. Apparently, under the present high-pressure conditions, neither the presence nor the amount of ethanol significantly modifies the onset temperature for acetylene oxidation or the acetylene conversion profile, in contrast to what was observed by Abián et al.¹² in their atmospheric pressure oxidation work of C_2H_2 – C_2H_5OH mixtures [t_r (s) = $195/T$ (K), 500 ppm of C_2H_2 , and 0–200 ppm of C_2H_5OH]. In that study, as the amount of ethanol was increased, the acetylene conversion occurred at higher temperatures. Under the present high-pressure conditions (10 bar), the oxidation of C_2H_2 starts at 775–800 K approximately, independent of the amount of ethanol present in the reactant mixture. In the case of ethanol, it also starts to be consumed at the same temperature as C_2H_2 , that is, 775–800 K approximately, and independent of the amount added to the mixture, whereas under atmospheric conditions,¹² ethanol was more reactive, being completely consumed at lower temperatures than acetylene, and once ethanol was consumed, the C_2H_2 concentration sharply decayed.

On the other hand, for the lower amounts of ethanol, 0 and 50 ppm, the modeling predictions for CO and CO_2 seem to be in good agreement with the experimental data. However, for higher amounts of ethanol, the CO concentration is under-predicted by the model, whereas the concentration of CO_2 is overestimated. This indicates that, although the experimental trends of both compounds are well-predicted by the model, further work could be performed to improve modeling predictions in the oxidation pathways of C_2H_2 and C_2H_5OH to CO and CO_2 . At present, we are not able to clearly identify what is the reason for the poor fitting of the calculations versus experimental individual data of CO and CO_2 . However, the sum of both CO and CO_2 is well-described by calculations

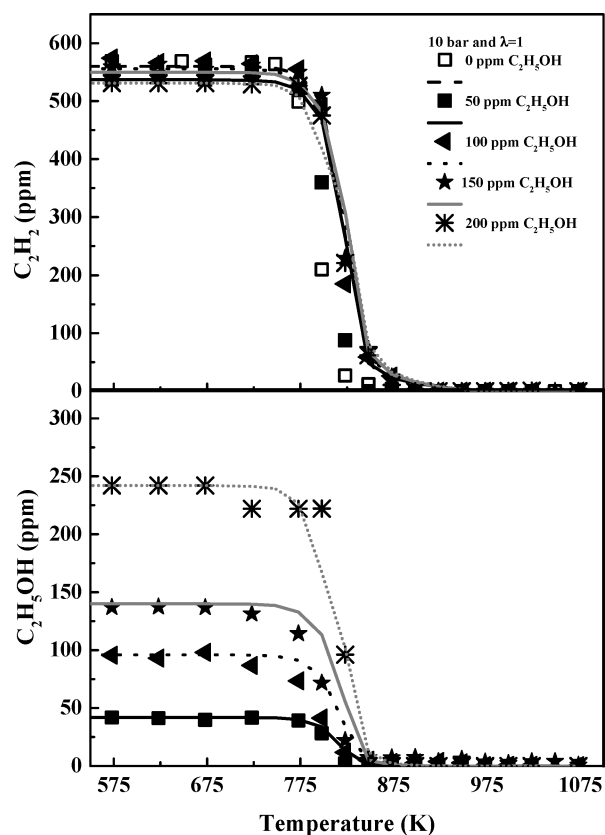


Figure 2. Influence of the amount of ethanol added to the mixture on the concentration profiles of C_2H_2 and C_2H_5OH during the C_2H_2 – C_2H_5OH mixture oxidation as a function of the temperature for stoichiometric conditions ($\lambda = 1$) and 10 bar. Experimental results are denoted by symbols, and modeling calculations are denoted by lines. The inlet conditions correspond to sets 1, 3, 9, 10, and 12 in Table 1.

(bottom part of Figure 3). Because the reaction rate of the conversion of CO to CO_2 is known with certain confidence, the differences may be attributed to inaccuracies in predicting the H/O radical pool composition, which may arise from a number of reactions involved in the mechanism feeding the radical pool.

To evaluate the influence of the oxygen availability in the reactant mixture on the oxidation of the mixtures, different air excess ratios (λ) have been used for two different ethanol concentrations in the mixture, 50 or 200 ppm, while keeping the value of the pressure at 10 bar and the C_2H_2 concentration constant (500 ppm, approximately). The experimental results obtained for acetylene and ethanol consumption and CO formation, as one of the major oxidation products, are compared to modeling calculations and represented in Figure 4. The inlet oxygen concentration does not significantly modify acetylene for either the lowest concentration of ethanol in the mixture (50 ppm, left part of Figure 4) or for the highest concentration of ethanol in the mixture (200 ppm, right part of Figure 4). The temperature for the onset of C_2H_2 oxidation and, therefore, the onset of CO formation is almost independent of the value of λ analyzed. In the case of ethanol, as previously reported in a high-pressure (20, 40, and 60 bar) ethanol oxidation study,¹⁹ for a given pressure, the inlet oxygen concentration does not clearly modify the C_2H_5OH oxidation and ethanol is completely consumed for all of the stoichiometries analyzed. One possible explanation to the

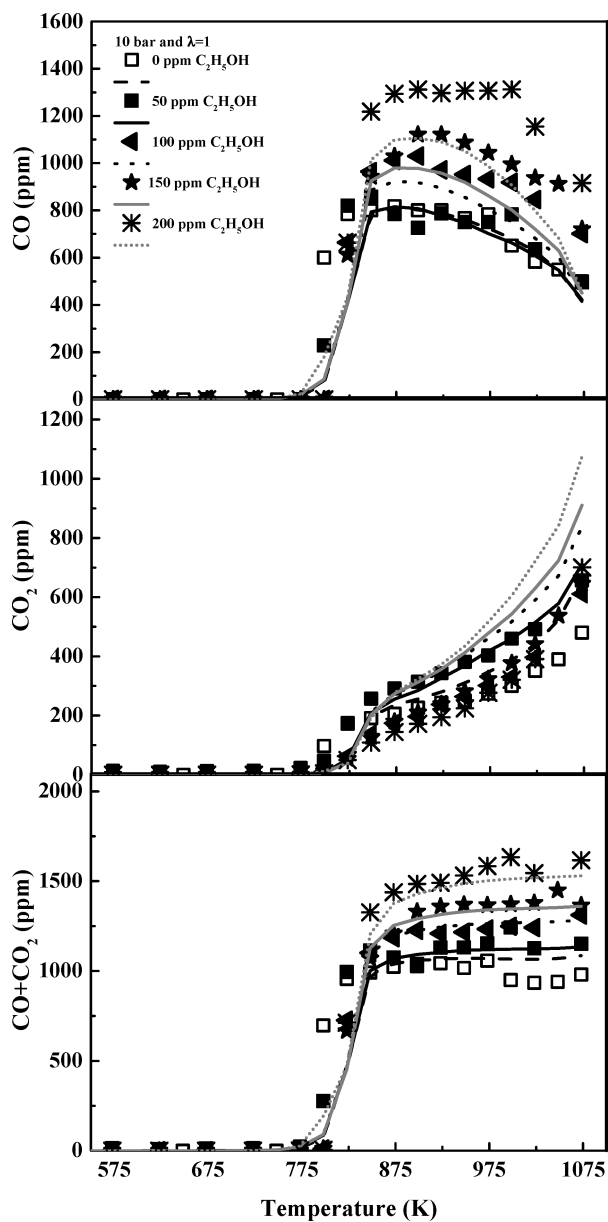
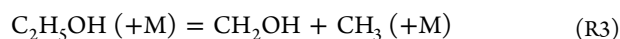
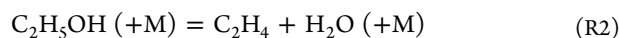


Figure 3. Influence of the amount of ethanol added to the mixture on the concentration profiles of CO, CO_2 , and the sum of both during the C_2H_2 – C_2H_5OH mixture oxidation as a function of the temperature for stoichiometric conditions ($\lambda = 1$) and 10 bar. Experimental results are denoted by symbols, and modeling calculations are denoted by lines. The inlet conditions correspond to sets 1, 3, 9, 10, and 12 in Table 1.

almost negligible effect of the oxygen availability on the onset temperature for ethanol consumption could be that ethanol oxidation is initiated by its thermal dehydration to ethylene (reaction R2) and its thermal decomposition through bond cleavage to CH_2OH and CH_3 radicals (reaction R3).¹⁹



Another study of the oxidation of C_2H_2 – C_2H_5OH mixtures but under atmospheric pressure conditions¹² also indicates that the onset temperature of acetylene and ethanol conversion is almost the same (around 900 K) for all of the values of λ

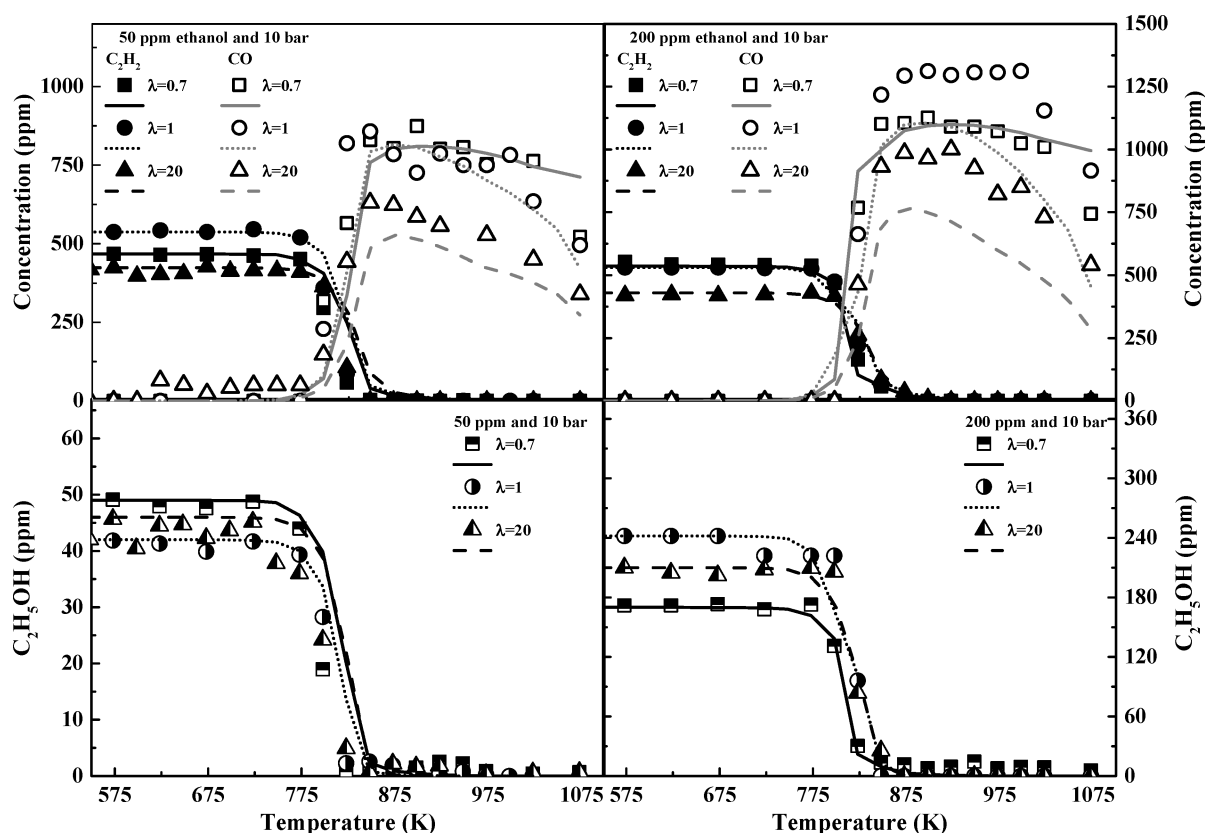


Figure 4. Influence of the air excess ratio (λ) on the concentration profiles of C_2H_2 and CO (upper part) and C_2H_5OH (lower part) during the C_2H_2 – C_2H_5OH mixture oxidation as a function of the temperature for 10 bar and two different amounts of ethanol added to the blend, (left part) 50 ppm and (right part) 200 ppm. Experimental results are denoted by symbols, and modeling calculations are denoted by lines. The inlet conditions correspond to sets 2–4 and 11–13 in Table 1.

analyzed but the temperature range for full consumption of acetylene and ethanol was different depending upon the value of λ analyzed, unlike what is observed at a high pressure. Thus, at atmospheric pressure and the leanest conditions studied ($\lambda = 20$), the full conversion of acetylene was produced at approximately 100 K below compared to $\lambda = 0.7$ and stoichiometric conditions ($\lambda = 1$), while for $\lambda = 0.2$, C_2H_2 was not completely consumed, even for the highest temperature analyzed in that study, 1375 K.

The influence of a change in the working pressure (from 10 to 40 bar) on the oxidation of C_2H_2 – C_2H_5OH mixtures has also been evaluated (Figure 5). As listed in Table 1, for ethanol concentrations in the mixture of 50 and 200 ppm, the three different values of λ have been tested for both pressures, although not all of them have been represented in Figure 5. As previously mentioned, the impact of the inlet oxygen on the C_2H_2 – C_2H_5OH mixture oxidation is almost negligible.

As seen in Figure 5, an increase in the working pressure appears to shift the onset of C_2H_2 oxidation to lower temperatures, approximately 50–75 K. Therefore, the conversion of C_2H_2 at 40 bar starts at 725 K, which is approximately the same temperature as that obtained under similar experimental conditions by Giménez-López et al.¹⁶ in their high-pressure (60 bar) oxidation study of C_2H_2 [total flow rate of 3 L (STP)/min and residence times of 10–15 s in the isothermal reaction zone]. Therefore, a change in the pressure from 10 to 40 bar has significant effects on the conversion of C_2H_2 and C_2H_5OH , but the effects are less pronounced when the pressure is further increased.

Because the model provides good performance when simulating the oxidation of C_2H_2 – C_2H_5OH mixtures, model calculations at different pressures were run to compare modeling predictions for C_2H_2 consumption for different pressures, stoichiometric conditions, and approximately 50 ppm of ethanol. The results obtained from this theoretical evaluation are shown in Figure 6. As seen, the most significant changes occur in the 1–10 pressure range. As described in the Experimental Section, the residence time of the gas in the isothermal zone can be represented by t_r (s) = $261 \times P$ (bar) / T (K). Therefore, when the pressure is increased from 1 to 10 bar, the residence time is also increased by a factor of 10, in addition to the increase in the species concentration by increasing the system pressure. As a consequence, the onset temperature changes steeply. In the same way, a change from 10 to 20 bar implies an increase in the residence time of 2, and a change from 60 to 100 bar implies an increase of 1.7 times, with the effect in the onset temperature less pronounced in the last case. Additionally, an experiment at 20 bar, which is within the pressure range object of this study, has been performed under similar conditions (set 5 in Table 1). As seen, the present mechanism is able to reproduce again the trend experimentally observed, strengthening the reliability of the present mechanism.

In general, model predictions reproduce the experimental observations. Therefore, with the present mechanism, a reaction rate analysis has been performed, which has allowed for the identification of the main routes for C_2H_2 and C_2H_5OH consumption and product formation during the oxidation of

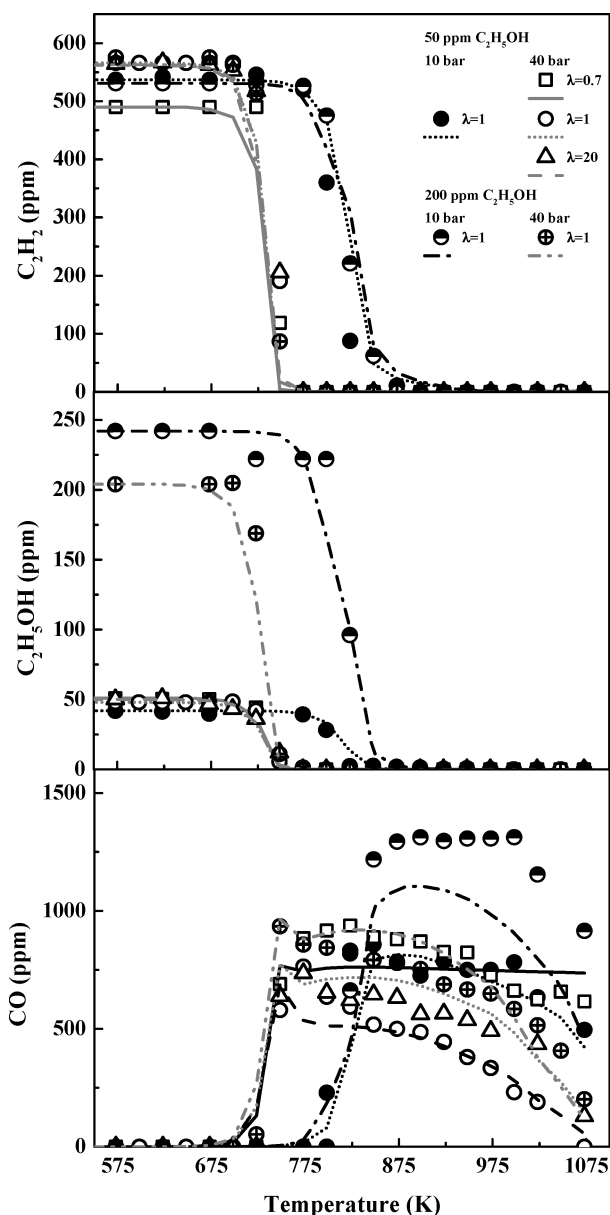


Figure 5. Influence of the pressure on the concentration profiles of C_2H_2 , C_2H_5OH , and CO during the C_2H_2 – C_2H_5OH mixture oxidation as a function of the temperature and for different values of the air excess ratio. Experimental results are denoted by symbols, and modeling calculations are denoted by lines. The inlet conditions correspond to sets 3, 6–8, 12, and 15 in Table 1.

C_2H_2 – C_2H_5OH mixtures. A diagram with the main reaction pathways is represented in Figure 7. The width of the arrows and the values included in the figure correspond to the percentage of consumption of the corresponding compound for the conditions and reactor distance indicated in its caption. In the case of acetylene, its conversion is initiated through the sequence described in reaction R4 and reactions with O_2 , such as reaction R5, to form HCO, which may react with oxygen, producing HO_2 radicals and more CO (reaction R6). Upon initiation, C_2H_2 undergoes addition reactions generating intermediate adducts; that is, C_2H_2 reacts with OH radicals to produce the CHCHOH adduct (reaction R7), which is the main acetylene consumption route independent of the value of

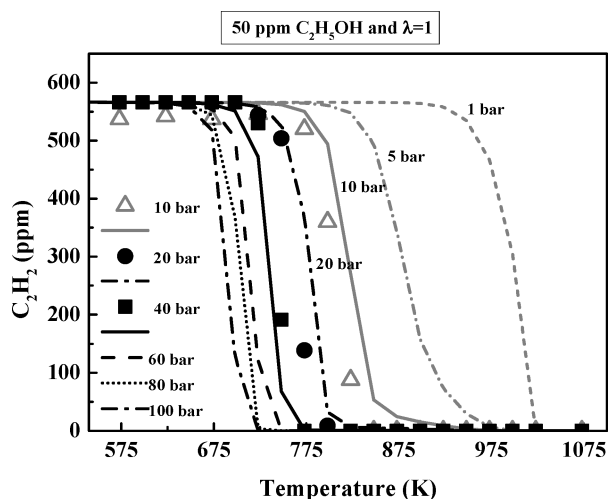
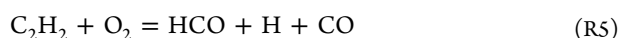
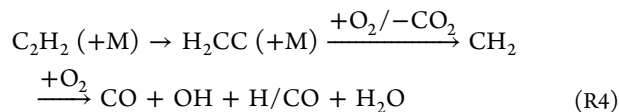
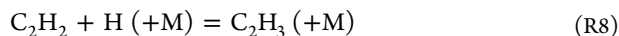


Figure 6. Evaluation through model calculations of the pressure effect on the temperature evolution of the C_2H_2 concentration predicted by the model for a mixture of C_2H_2 and C_2H_5OH and stoichiometric conditions ($\lambda = 1$).

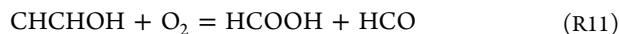
the air excess ratio analyzed but becomes more relevant as the oxygen availability increases.



The C_2H_2 combination with H radicals to form vinyl radicals (C_2H_3), reaction R8, is important under stoichiometric ($\lambda = 1$) and, especially, fuel-rich conditions ($\lambda = 0.7$). Reactions of C_2H_2 with O radicals (reactions R9 and R10) are of less importance compared to the previous reaction. For example, under the same conditions described in the caption of Figure 7, i.e., 800 K, and the experimental conditions denoted as set 3 in Table 1 (10 bar and $\lambda = 1$ and 42 ppm of ethanol in the blend), reaction R8 represents 20% of the total C_2H_2 consumption, whereas reactions R9 and R10 represent only 6% of the total C_2H_2 consumption.



Although the CHCHOH adduct could decompose thermally or react with O/H radicals, under the conditions of this work, it mainly reacts with O_2 to form formic acid, HCOOH (reaction R11). Giménez-López et al.¹⁶ indicated that glyoxal (OCHCHO) could also be formed in considerable concentration from the reaction of the CHCHOH adduct with O_2 , but under the present conditions, this route is almost negligible.



The slight discrepancies in model calculations related to HCOOH reactions from Zhao et al.,³² mentioned in the

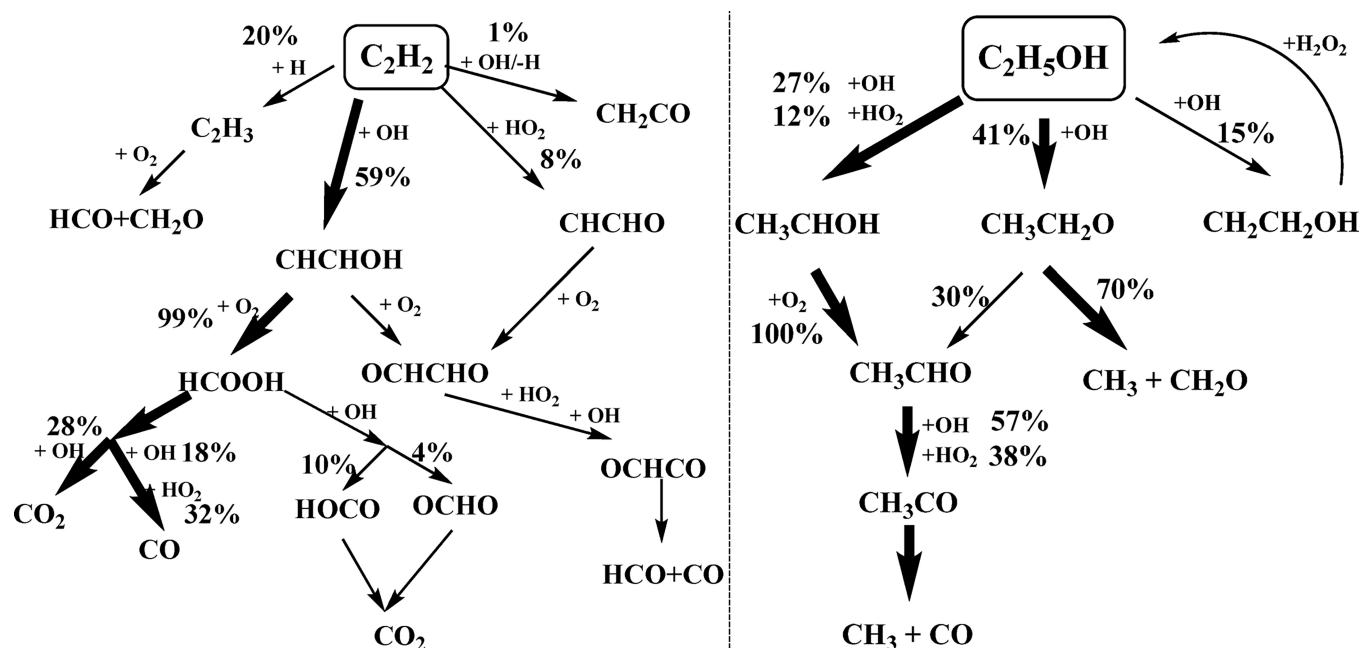
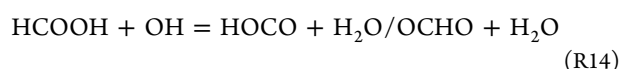
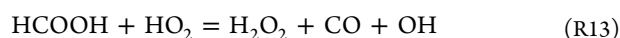
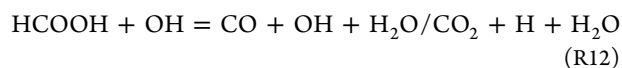
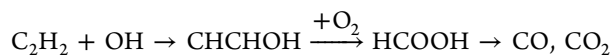


Figure 7. Main reaction pathways for (left part) C₂H₂ and (right part) C₂H₅OH consumption and product formation. The percentages in the diagram correspond to 800 K and the experimental conditions denoted as set 3 in Table 1. The selected position in the reactor is 105 cm, which corresponds to the point at which the concentration of C₂H₂ is about 470 ppm and the C₂H₅OH concentration is about 34 ppm.

Chemical Kinetic Model section, do not modify the mentioned reaction routes. It only changes the way in which formic acid is converted, that is, directly to CO and CO₂ (reactions R12 and R13) or through HOCO and OCHO (reaction R14), which later decompose to produce CO and CO₂.



In conclusion, acetylene is mainly consumed following the sequence:



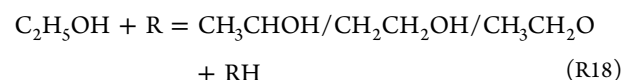
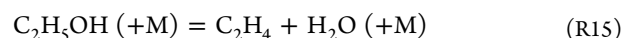
independent of the value of λ . However, in a previous study of the oxidation of C₂H₂–C₂H₅OH mixtures at atmospheric pressure,¹² although the possible reaction routes were almost the same, the predominant reactions were those involving interactions of C₂H₂ and H and O radicals.

The reaction routes for C₂H₂ described above are almost the same than those described in a high-pressure acetylene oxidation work,¹⁶ only with differences under reducing conditions. In that work, C₂H₂ was mostly consumed by recombination with H to form vinyl radicals. However, under the present conditions, C₂H₂ is mainly consumed by the reaction with OH radicals under all of the stoichiometries analyzed. Therefore, apparently, under the present conditions, the addition of ethanol to the reactant mixture does not modify the acetylene oxidation regime. It only modifies the composition of the radical pool, increasing the relevance of C₂H₂ reactions with OH radicals. Therefore, the effectiveness of ethanol in reducing soot formation from acetylene, that has been proven in different works (e.g., ref 15), is probably

produced by oxygen present in ethanol, which contributes to an increase of the O/OH radical pool, therefore favoring C₂H₂ oxidation toward CO and CO₂ and, hence, removing carbon from the reaction paths, which leads to soot formation.

On the other hand, ethanol conversion is initiated by its thermal dehydration to ethylene and water (reaction R15). The water generated may react with O₂ (reaction R16) or H radicals (reaction R17) generated from the oxidation of C₂H₂ (for example, in reaction R5), and therefore, HO₂ and OH radicals are formed.

After initiation, C₂H₅OH is mainly consumed by H abstraction reactions, leading to the formation of three different ethanol radicals (CH₃CHOH, CH₂CH₂OH, or CH₃CH₂O), depending upon the site where the H abstraction occurs¹⁹ (represented in reaction R18, where R can be O, H, OH, CH₃, or HO₂ radicals).



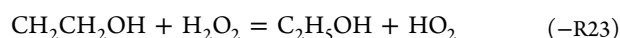
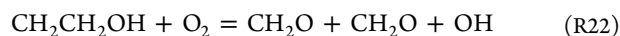
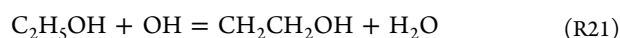
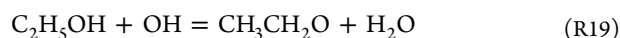
The abstraction of hydrogen from ethanol by HO₂ radicals is very important in the initial steps of ethanol consumption, but as OH radicals are generated, this becomes the more relevant oxidation route. As represented in Figure 7, 41% of the ethanol conversion occurs through H abstraction by OH radicals to form CH₃CH₂O (reaction R19) and 27% also occurs through H abstraction by OH radicals to form the other ethanol radical, CH₃CHOH (reaction R20). The third option of the H-abstraction reaction from ethanol by OH radicals is to produce the CH₂CH₂OH radical (reaction R21), but it is less relevant compared to the other routes (15%). Previous ethanol

Table 2. Normalized Sensitivity Coefficients for CO for Sets 2–4, 6–8, and 11–13 in Table 1^a

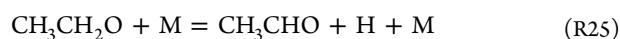
reaction	set 2	set 3	set 4	set 6	set 7	set 8	set 11	set 12	set 13
	775 K	775 K	775 K	700 K	700 K	700 K	775 K	775 K	775 K
$\text{HO}_2 + \text{HO}_2 = \text{H}_2\text{O}_2 + \text{O}_2$	-0.81	-0.83	-0.78	-1.01	-1.02	-1.02	-0.84	-0.85	-0.81
$\text{H}_2\text{O}_2 (+\text{M}) = \text{OH} + \text{OH} (+\text{M})$	0.70	0.72	0.73	0.78	0.78	0.81	0.80	0.85	0.85
$\text{CH}_2 + \text{O}_2 = \text{CO} + \text{H}_2\text{O}$	-0.14	-0.13	-0.14	-0.07	-0.07	-0.07	-0.11	-0.10	-0.11
$\text{CH}_2 + \text{O}_2 = \text{CO}_2 + \text{H} + \text{H}$	0.05	0.05	0.05	0.03	0.03	0.03	0.04	0.04	0.05
$\text{CH}_2 + \text{O}_2 = \text{CH}_2\text{O} + \text{O}$	0.04	0.04	0.05	0.02	0.02	0.03	0.03	0.03	0.04
$\text{C}_2\text{H}_2 (+\text{M}) = \text{H}_2\text{CC} (+\text{M})$	0.01	0.01	0.08	0.00	0.00	0.02	0.01	0.01	0.09
$\text{C}_2\text{H}_2 + \text{O} = \text{HCCO} + \text{H}$	0.26	0.26	0.21	0.19	0.19	0.18	0.21	0.18	0.14
$\text{C}_2\text{H}_2 + \text{O} = \text{CH}_2 + \text{CO}$	-0.26	-0.25	-0.21	-0.19	-0.19	-0.18	-0.19	-0.15	-0.12
$\text{C}_2\text{H}_2 + \text{OH} = \text{CHCHOH}$	0.21	0.18	0.22	0.15	0.13	0.11	0.36	0.39	0.43
$\text{C}_2\text{H}_2 + \text{HO}_2 = \text{CH}_2\text{CHOO}$	-0.02	-0.02	-0.01	-0.06	-0.05	-0.05	-0.02	-0.01	-0.01
$\text{C}_2\text{H}_2 + \text{HO}_2 = \text{CHCHO} + \text{OH}$	2.16	2.14	1.87	1.89	1.92	1.87	1.81	1.64	1.42
$\text{H}_2\text{CC} + \text{O}_2 = \text{CH}_2 + \text{CO}_2$	0.08	0.07	0.04	0.02	0.01	0.02	0.07	0.07	0.03
$\text{C}_2\text{H}_5\text{OH} + \text{OH} = \text{CH}_2\text{CH}_2\text{OH} + \text{H}_2\text{O}$	-0.11	-0.09	-0.10	-0.07	-0.06	-0.06	-0.22	-0.26	-0.26
$\text{C}_2\text{H}_5\text{OH} + \text{HO}_2 = \text{CH}_3\text{CHOH} + \text{H}_2\text{O}_2$	0.22	0.17	0.23	0.26	0.23	0.25	0.53	0.68	0.69

^aThe normalized sensitivity coefficients are given as $A_i \delta Y_j / Y_j \delta A_i$, where A_i is the pre-exponential constant for reaction i and Y_j is the mass fraction of the j th species. Therefore, the sensitivity coefficients listed can be interpreted as the relative change in the predicted concentration for the species j caused by increasing the rate constant for reaction i by a factor of 2.

oxidation works, under high and atmospheric pressure conditions,^{19,20} indicate that the $\text{CH}_2\text{CH}_2\text{OH}$ radical may react with O_2 to form formaldehyde (reaction R22). Under the present conditions, this radical reacts with H_2O_2 (reaction –R23) to give back ethanol as a result of the high concentration of H_2O_2 under high-pressure conditions ($\text{HO}_2 + \text{HO}_2 = \text{H}_2\text{O}_2 + \text{O}_2$). Oxygen is preferably consumed in other routes than in reaction R22.



The ethanol radicals, CH_3CHOH and $\text{CH}_3\text{CH}_2\text{O}$, react with O_2 or just decompose thermally (reactions R24 and R25, respectively) to form acetaldehyde (CH_3CHO), or in the case of $\text{CH}_3\text{CH}_2\text{O}$, it can also decompose and produce CH_3 radicals and formaldehyde (reaction R26).

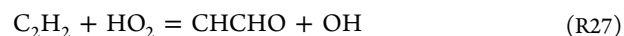


The reaction routes for ethanol, described above and represented in Figure 7, are the most relevant reactions under the conditions of this work and are almost the same than those previously described in earlier studies concerning the oxidation of ethanol or its mixtures.^{12,19}

Therefore, it seems that, during the joint oxidation of ethanol and acetylene, there is no direct interaction between both compounds; each of them follows their corresponding reaction routes, and their oxidation is only modified by an increase in the O/OH radical pool generated during the conversion of the other reactant.

Moreover, a first-order sensitivity analysis for CO has been performed for the conditions denoted as sets 2–4, 6–8, and 11–13 in Table 1 in the very beginning of the C_2H_2 – $\text{C}_2\text{H}_5\text{OH}$

mixture conversion, which means when the concentration of CO is around 10 ppm. The results obtained, as shown in Table 2, indicate the most sensitive reactions for the different values of λ (0.7, 1, and 20), pressures (10 and 40 bar), and concentrations of ethanol (50 or 200 ppm) in the blend. In general, the normalized sensitivity coefficients obtained for all of the conditions analyzed are very similar, indicating that there is not a huge difference between the coefficients if λ , pressure, and/or amount of ethanol are changed. In the case of acetylene, its reaction with HO_2 radicals (reaction R27) is very sensitive as a result of the OH radicals generated, which interact with acetylene and ethanol (reactions R7 and R18, respectively).



To our knowledge, there is no direct determination for the rate constant of reaction R27. The temperature- and pressure-dependent rate coefficients, together with the whole reaction subset for C_2H_2 , as mentioned in the Chemical Kinetic Model section, have been adopted from the recent work on high-pressure acetylene oxidation by Giménez-López et al.¹⁶ The authors stated that the $\text{C}_2\text{H}_2 + \text{HO}_2$ reaction involves nine different pressure- and temperature-dependent product channels, with the formation of CHCHO being the dominant under the studied conditions. In that paper, it is also indicated that the rate constant for these reactions had not been previously determined experimentally, and only a room-temperature upper limit of $3 \times 10^9 \text{ cm}^3 \text{ mol}^{-1} \text{ s}^{-1}$ was available in the literature.³⁴ Therefore, considering the similarities between the $\text{C}_2\text{H}_3\text{O}_2$ potential energy surface (PES) relative to $\text{C}_2\text{H}_2 + \text{HO}_2$ and $\text{C}_2\text{H}_3 + \text{O}_2$ systems, Giménez-López et al.¹⁶ adopted the temperature- and pressure-dependent rate coefficients for these reactions from the $\text{C}_2\text{H}_3 + \text{O}_2$ kinetic analysis by Goldsmith et al.³⁵ A better determination of this reaction rate would be desirable.

On the other hand, in the case of ethanol, two H abstraction reactions to form $\text{CH}_2\text{CH}_2\text{OH}$ and CH_3CHOH radicals appear among the most sensitive reactions (Table 2). The coefficients obtained for the first reaction are negative, and OH radicals are removed from the main oxidation pathways, whereas the H abstraction from ethanol by HO_2 radicals is

promoting, the ethanol radical generated in this case is more reactive, and H_2O_2 also produced decomposes, generating very reactive OH radicals.

As mentioned before, although some uncertainties in modeling calculations related to HCOOH reactions were found, none of these reactions appeared among the most sensitive reactions; therefore, they do not have a significant influence on the results.

CONCLUSION

The influence of the temperature (575–1075 K), pressure (10 or 40 bar), inlet oxygen concentration ($\lambda = 0.7, 1, \text{ or } 20$), and concentration of ethanol in the reactant mixture (50–200 ppm) has been evaluated in the high-pressure oxidation of acetylene–ethanol mixtures. The detailed chemical kinetic mechanism previously compiled by our group in a high-pressure ethanol oxidation work¹⁹ has been used in this work for calculations. In general, the mechanism is able to reproduce the wide range of conditions experimentally tested. Neither the oxygen concentration nor the amount of ethanol added to the reaction mixture have a significant influence on the onset temperature for the conversion of C_2H_2 . Only an increase in the pressure (when moving from 10 to 40 bar) shifts the onset for acetylene conversion to lower temperatures. The reaction routes for acetylene consumption remain practically unaltered by the addition of ethanol in comparison to those obtained in the high-pressure oxidation study of acetylene,¹⁶ with the C_2H_2 interaction with OH radicals being the main consumption route for λ values analyzed. Apparently, there is no interaction between acetylene and ethanol; their respective oxidation is only modified by an increase in the O/OH radical pool produced during the conversion of the other reactant.

ASSOCIATED CONTENT

Supporting Information

The Supporting Information is available free of charge on the ACS Publications website at DOI: 10.1021/acs.energyfuels.8b00920.

Temperature profiles inside the reactor, comparison of modeling predictions using the present mechanism and the mechanism by Hashemi et al.²¹ for the conditions denoted as sets 2–4 in Table 1, list of HCOOH reactions from Zhao et al.,³² and comparison of modeling calculations obtained with the present mechanism, with or without HCOOH reactions from Zhao et al.,³² for the conditions denoted as sets 1–4 in Table 1 (PDF)

Complete mechanism (TXT)

Thermodynamic data (TXT)

All of the experimental results obtained in the present work (XLSX)

AUTHOR INFORMATION

Corresponding Author

*E-mail: uxue@unizar.es.

ORCID

Lorena Marrodán: 0000-0002-7767-3057

María U. Alzueta: 0000-0003-4679-5761

Notes

The authors declare no competing financial interest.

ACKNOWLEDGMENTS

The authors express their gratitude to the Aragón Government and European Social Fund [Thermochemical Processes Group (GPT)] and the Ministry of Economy and Competitiveness (MINECO) and European Regional Development Fund (FEDER) (Project CTQ2015-65226) for financial support. Lorena Marrodán acknowledges the Aragón Government for the predoctoral grant awarded.

REFERENCES

- (1) Kohse-Höinghaus, K.; Oßwald, P.; Cool, T. A.; Kasper, T.; Hansen, N.; Qi, F.; Westbrook, C. K.; Westmoreland, P. R. Biofuel combustion chemistry: From ethanol to biodiesel. *Angew. Chem., Int. Ed.* **2010**, *49*, 3572–3597.
- (2) An, H.; Yang, W. M.; Li, J. Effects of ethanol addition on biodiesel combustion: A modeling study. *Appl. Energy* **2015**, *143*, 176–188.
- (3) Alptekin, E. Evaluation of ethanol and isopropanol as additives with diesel fuel in a CRDI diesel engine. *Fuel* **2017**, *205*, 161–172.
- (4) Sakai, S.; Rothamer, D. Effect of ethanol blending on particulate formation from premixed combustion in spark-ignition engines. *Fuel* **2017**, *196*, 154–168.
- (5) Bierkandt, T.; Kasper, T.; Akyildiz, E.; Lucassen, A.; Oßwald, P.; Köhler, M.; Hemberger, P. Flame structure of a low-pressure laminar premixed and lightly sooting acetylene flame and the effect of ethanol addition. *Proc. Combust. Inst.* **2015**, *35*, 803–811.
- (6) Bennett, B. A. V.; McEnally, C. S.; Pfeifferle, L. D.; Smooke, M. D.; Colket, M. B. Computational and experimental study of the effects of adding dimethyl ether and ethanol to nonpremixed ethylene/air flames. *Combust. Flame* **2009**, *156*, 1289–1302.
- (7) Inal, F.; Senkan, S. M. Effects of oxygenate concentration on species mole fractions in premixed n-heptane flames. *Fuel* **2005**, *84*, 495–503.
- (8) Kohse-Höinghaus, K.; Oßwald, P.; Struckmeier, U.; Kasper, T.; Hansen, N.; Taatjes, C. A.; Wang, J.; Cool, T. A.; Gon, S.; Westmoreland, P. R. The influence of ethanol addition on premixed fuel-rich propene–oxygen–argon flames. *Proc. Combust. Inst.* **2007**, *31*, 1119–1127.
- (9) Liu, D. Detailed influences of ethanol as fuel additive on combustion chemistry of premixed fuel-rich ethylene flames. *Sci. China: Technol. Sci.* **2015**, *58*, 1696–1704.
- (10) Dagaut, P.; Togbé, C. Oxidation kinetics of mixtures of iso-octane with ethanol or butanol in a jet-stirred reactor: Experimental and modeling study. *Combust. Sci. Technol.* **2012**, *184*, 1025–1038.
- (11) Rezgui, Y.; Guemini, M. Effect of ethanol on soot precursors emissions during benzene oxidation in a jet-stirred reactor. *Environ. Sci. Pollut. Res.* **2014**, *21*, 6671–6686.
- (12) Abián, M.; Esarte, C.; Millera, Á.; Bilbao, R.; Alzueta, M. U. Oxidation of acetylene-ethanol mixtures and their interaction with NO. *Energy Fuels* **2008**, *22*, 3814–3823.
- (13) Ristori, A.; Dagaut, P.; El Bakali, A.; Pengloan, G.; Cathonnet, M. Benzene oxidation: Experimental results in a JSR and comprehensive kinetic modeling in JSR, shock-tube and flame. *Combust. Sci. Technol.* **2001**, *167*, 223–256.
- (14) Aboussi, B. Etude expérimentale et modélisation de l'oxydation de l'éthanol. Ph.D. Thesis, University of Orléans, Orléans, France, 1991.
- (15) Esarte, C.; Callejas, A.; Millera, Á.; Bilbao, R.; Alzueta, M. U. Influence of the concentration of ethanol and the interaction of compounds in the pyrolysis of acetylene and ethanol mixtures. *Fuel* **2011**, *90*, 844–849.
- (16) Giménez-López, J.; Rasmussen, C. T.; Hashemi, H.; Alzueta, M. U.; Gao, Y.; Marshall, P.; Goldsmith, F.; Glarborg, P. Experimental and kinetic modeling study of C_2H_2 oxidation at high pressure. *Int. J. Chem. Kinet.* **2016**, *48*, 724–738.
- (17) Rasmussen, C. L.; Hansen, J.; Marshall, P.; Glarborg, P. Experimental measurements and kinetic modeling of $\text{CO}/\text{H}_2/\text{O}_2/$

NO_x conversion at high pressure. *Int. J. Chem. Kinet.* **2008**, *40*, 454–480.

(18) Marrodán, L.; Millera, Á.; Bilbao, R.; Alzueta, M. U. High-pressure study of methyl formate oxidation and its interaction with NO. *Energy Fuels* **2014**, *28*, 6107–6115.

(19) Marrodán, L.; Arnal, Á.J.; Millera, Á.; Bilbao, R.; Alzueta, M. U. High-pressure ethanol oxidation and its interaction with NO. *Fuel* **2018**, *223*, 394–400.

(20) Alzueta, M. U.; Hernández, J. M. Ethanol oxidation and its interaction with nitric oxide. *Energy Fuels* **2002**, *16*, 166–171.

(21) Hashemi, H.; Christensen, J. M.; Glarborg, P. High-pressure pyrolysis and oxidation of ethanol. *Fuel* **2018**, *218*, 247–257.

(22) Glarborg, P.; Alzueta, M. U.; Dam-Johansen, K.; Miller, J. A. Kinetic modeling of hydrocarbon/nitric oxide interactions in a flow reactor. *Combust. Flame* **1998**, *115*, 1–27.

(23) Glarborg, P.; Alzueta, M. U.; Kærsgaard, K.; Dam-Johansen, K. Oxidation of formaldehyde and its interaction with nitric oxide in a flow reactor. *Combust. Flame* **2003**, *132*, 629–638.

(24) Glarborg, P.; Østberg, M.; Alzueta, M. U.; Dam-Johansen, K.; Miller, J. A. The recombination of hydrogen atoms with nitric oxide at high temperatures. *Symp. Combust., [Proc.]* **1998**, *27*, 219–226.

(25) Rasmussen, C. L.; Jakobsen, J. G.; Glarborg, P. Measurements and kinetic modeling of CH₄/O₂ and CH₄/C₂H₆/O₂ conversion at high-pressure. *Int. J. Chem. Kinet.* **2008**, *40*, 778–807.

(26) Rasmussen, C. L.; Wassard, K. H.; Dam-Johansen, K.; Glarborg, P. Methanol oxidation in a flow reactor: Implications for the branching ratio of CH₃OH + OH reaction. *Int. J. Chem. Kinet.* **2008**, *40*, 423–441.

(27) Rasmussen, C. L.; Rasmussen, A. E.; Glarborg, P. Sensitizing effects of NO_x on CH₄ oxidation at high pressure. *Combust. Flame* **2008**, *154*, 529–545.

(28) Fafsheber, N.; Friedrichs, G.; Marshall, P.; Glarborg, P. Glyoxal oxidation mechanism: Implications for the reactions HCO + O₂ and OCHCHO + HO₂. *J. Phys. Chem. A* **2015**, *119*, 7305–7315.

(29) Marshall, P.; Glarborg, P. Ab initio and kinetic modeling studies of formic acid oxidation. *Proc. Combust. Inst.* **2015**, *35*, 153–160.

(30) Marrodán, L.; Royo, E.; Millera, Á.; Bilbao, R.; Alzueta, M. U. High pressure oxidation of dimethoxymethane. *Energy Fuels* **2015**, *29*, 3507–3517.

(31) Marrodán, L.; Arnal, Á. J.; Millera, Á.; Bilbao, R.; Alzueta, M. U. The inhibiting effect of NO addition on dimethyl ether high-pressure oxidation. *Combust. Flame*, In Press. DOI: [10.1016/j.combust-flame.2018.07.005](https://doi.org/10.1016/j.combust-flame.2018.07.005).

(32) Zhao, Z.; Chaos, M.; Kazakov, A.; Dryer, F. L. Thermal decomposition reaction and a comprehensive kinetic model of dimethyl ether. *Int. J. Chem. Kinet.* **2008**, *40*, 1–18.

(33) Reaction Design. ANSYS Chemkin-Pro 17.2; Reaction Design: San Diego, CA, 2016.

(34) Bohn, B.; Zetzsch, C. J. Formation of HO₂ from OH and C₂H₂ in the presence of O₂. *J. Chem. Soc., Faraday Trans.* **1998**, *94*, 1203–1210.

(35) Goldsmith, C. F.; Harding, L. B.; Georgievskii, Y.; Miller, J. A.; Klippenstein, S. J. Temperature and pressure-dependent rate coefficients for the reaction of vinyl radical with molecular oxygen. *J. Phys. Chem. A* **2015**, *119*, 7766–7779.

ETHANOL AS FUEL ADDITIVE: HIGH-PRESSURE OXIDATION OF ITS MIXTURES WITH ACETYLENE

Lorena Marrodán, Miguel Fuster, Ángela Millera, Rafael Bilbao, María U. Alzueta*

Aragón Institute of Engineering Research (I3A). Department of Chemical and Environmental

Engineering. University of Zaragoza. C/ Mariano Esquillor, s/n. 50018 Zaragoza. Spain

**SUPPORTING
INFORMATION**

Table of contents

1) Temperature profiles inside the reactor.

Figure S1. Temperature profiles for different nominal temperatures as a function of distance for a flow rate of 1 L (STP)/min and 10 bar.

Figure S2. Temperature profiles for different nominal temperatures as a function of distance for a flow rate of 1 L (STP)/min and 40 bar.

2) Comparison of modeling predictions using the present mechanism and Hashemi et al. [21] mechanism for the conditions denoted as sets 2-4 in Table 1 of the manuscript.

Figure S3. Comparison of modeling calculations obtained with the present mechanism and the mechanism from Hashemi et al. [21] for the conditions denoted as set 2 in Table 1 of the manuscript.

Figure S4. Comparison of modeling calculations obtained with the present mechanism and the mechanism from Hashemi et al. [21] for the conditions denoted as set 3 in Table 1 of the manuscript.

Figure S5. Comparison of modeling calculations obtained with the present mechanism and the mechanism from Hashemi et al. [21] for the conditions denoted as set 4 in Table 1 of the manuscript.

3) List of HCOOH reactions from Zhao et al. [32].

Table S1. Reactions for HCOOH from Zhao et al. [32]; cm³, mol, s and cal units.

4) Comparison of modeling calculations obtained with the present mechanism, with or without HCOOH reactions from Zhao et al. [32], for the conditions denoted as sets 1-4 in Table 1 of the manuscript.

Figure S6. Comparison of modeling calculations obtained with the present mechanism with or without HCOOH reactions from Zhao et al. [32] for the conditions denoted as set 1 in Table 1 of the manuscript.

Figure S7. Comparison of modeling calculations obtained with the present mechanism with or without HCOOH reactions from Zhao et al. [32] for the conditions denoted as set 2 in Table 1 of the manuscript.

Figure S8. Comparison of modeling calculations obtained with the present mechanism with or without HCOOH reactions from Zhao et al. [32] for the conditions denoted as set 3 in Table 1 of the manuscript.

Figure S9. Comparison of modeling calculations obtained with the present mechanism with or without HCOOH reactions from Zhao et al. [32] for the conditions denoted as set 4 in Table 1 of the manuscript.

1) Temperature profiles inside the reactor.

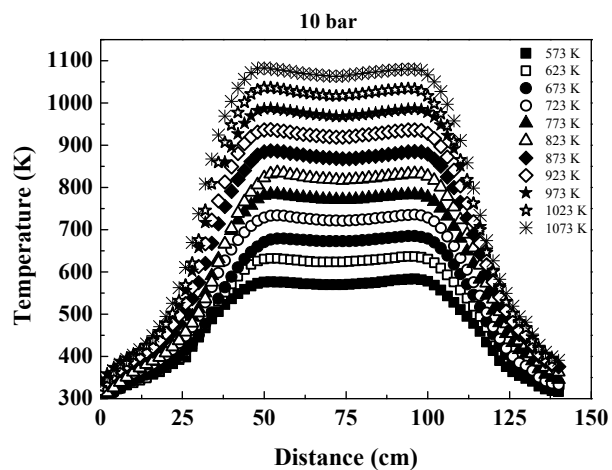


Figure S1. Temperature profiles for different nominal temperatures as a function of distance for a flow rate of 1 L (STP)/min and 10 bar.

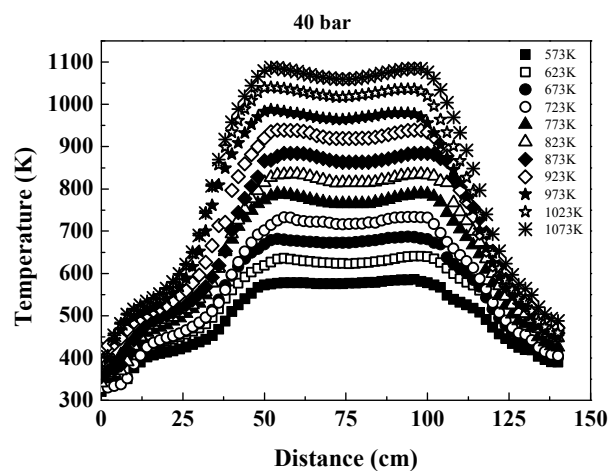


Figure S2. Temperature profiles for different nominal temperatures as a function of distance for a flow rate of 1 L (STP)/min and 40 bar.

2) Comparison of predictions using the present mechanism and Hashemi et al. [21] mechanism for the conditions denoted as sets 2-4 in Table 1 of the manuscript.

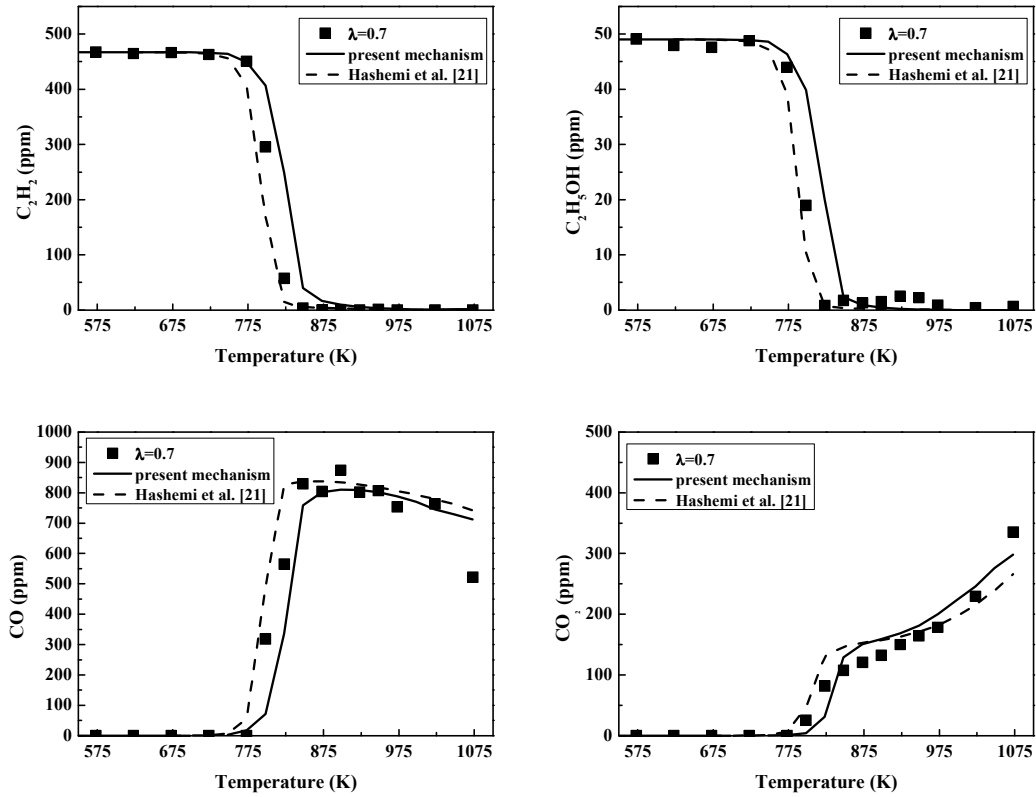


Figure S3. Comparison of modeling calculations obtained with the present mechanism and the mechanism from Hashemi et al. [21] for the conditions denoted as set 2 in Table 1 of the manuscript.

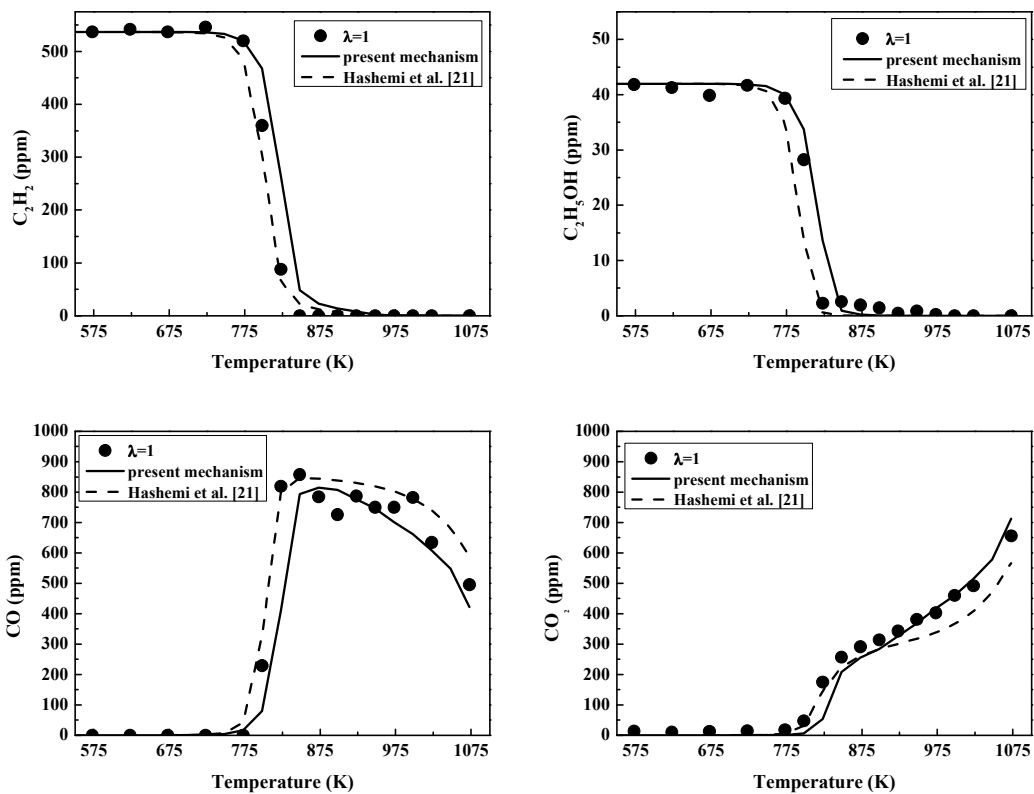


Figure S4. Comparison of modeling calculations obtained with the present mechanism and the mechanism from Hashemi et al. [21] for the conditions denoted as set 3 in Table 1 of the manuscript.

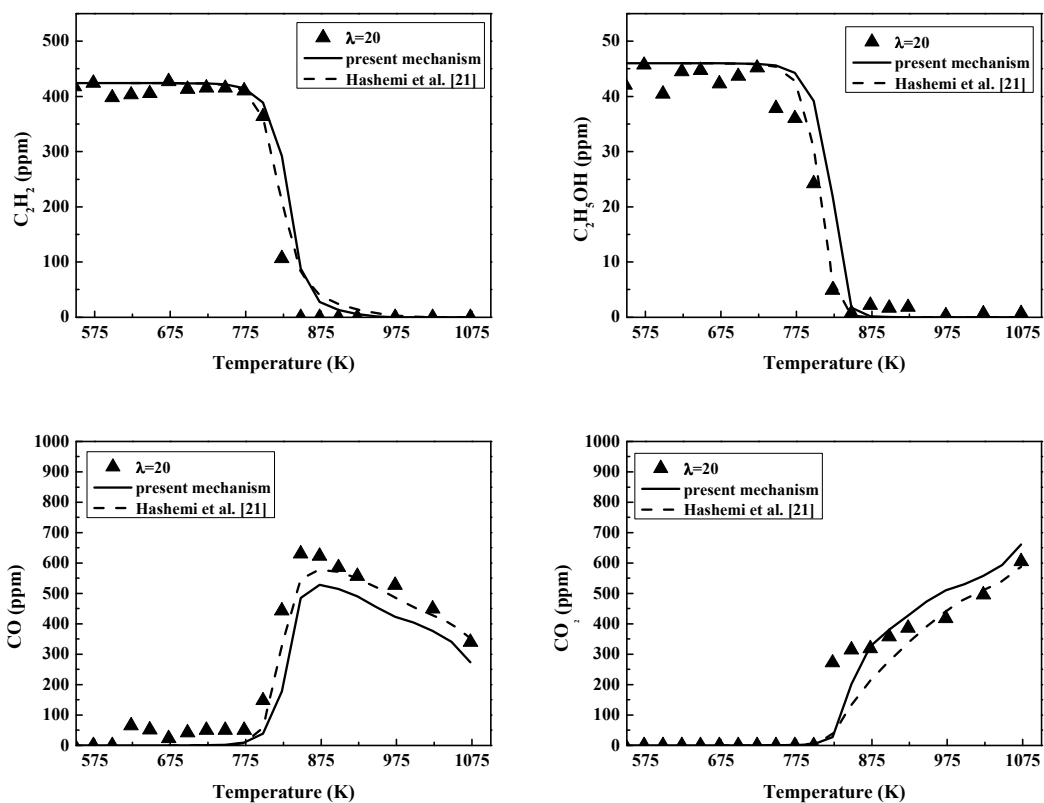


Figure S5. Comparison of modeling calculations obtained with the present mechanism and the mechanism from Hashemi et al. [21] for the conditions denoted as set 4 in Table 1 of the manuscript.

3) List of HCOOH reactions from Zhao et al. [32].

Table S1. Reactions for HCOOH from Zhao et al. [32]; cm³, mol, s and cal units.

Reaction	A	n	E _a	source
HCOOH+OH=H ₂ O+CO ₂ +H	2.62 x 10 ⁶	2.06	916	[32]
HCOOH+OH=H ₂ O+CO+OH	1.85 x 10 ⁷	1.51	-962	[32]
HCOOH+H=H ₂ +CO ₂ +H	4.24 x 10 ⁶	2.10	4868	[32]
HCOOH+H=H ₂ +CO+H	6.03 x 10 ¹³	-0.35	2988	[32]
HCOOH+CH ₃ =CH ₄ +CO+OH	3.90 x 10 ⁻⁷	5.80	2200	[32]
HCOOH+HO ₂ =H ₂ O ₂ +CO+OH	1.00 x 10 ¹²	0.00	11920	[32]

4) Comparison of modeling calculations obtained with the present mechanism, with or without HCOOH reactions from Zhao et al. [32], for the conditions denoted as sets 1-4 in Table 1 of the manuscript.

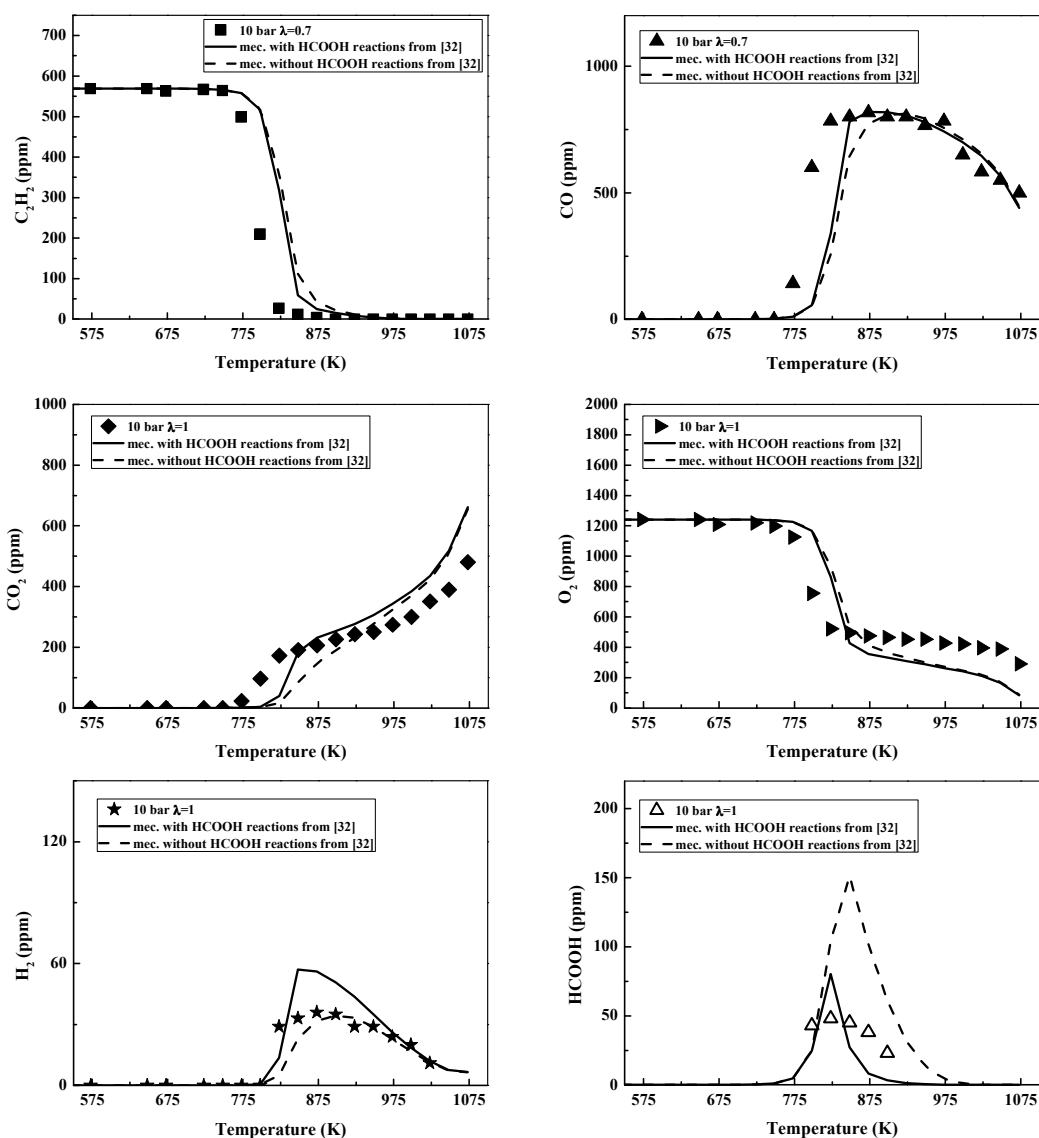


Figure S6. Comparison of modeling calculations obtained with the present mechanism with or without HCOOH reactions from Zhao et al. [32] for the conditions denoted as set 1 in Table 1 of the manuscript.

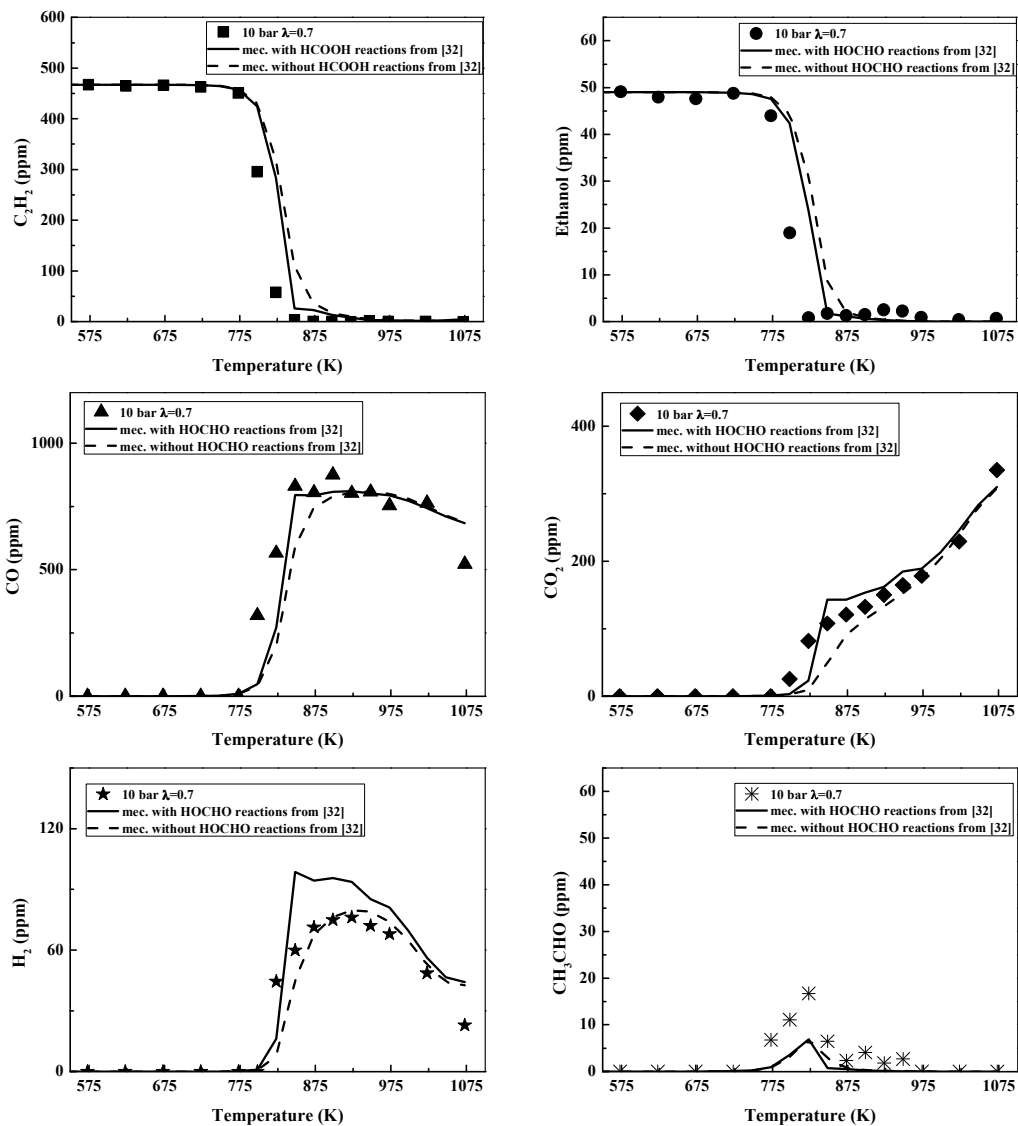


Figure S7. Comparison of modeling calculations obtained with the present mechanism with or without HCOOH reactions from Zhao et al. [32] for the conditions denoted as set 2 in Table 1 of the manuscript.

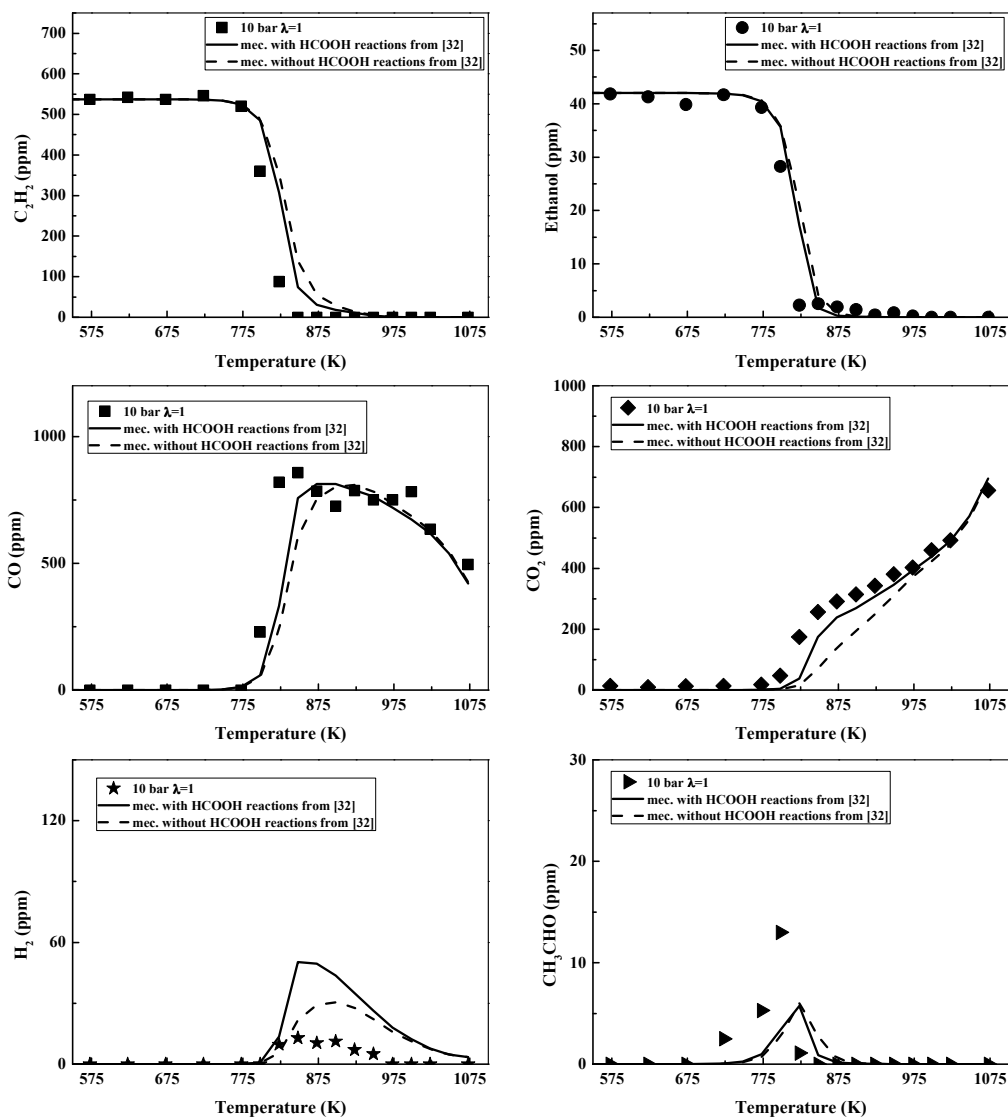


Figure S8. Comparison of modeling calculations obtained with the present mechanism with or without HCOOH reactions from Zhao et al. [32] for the conditions denoted as set 3 in Table 1 of the manuscript.

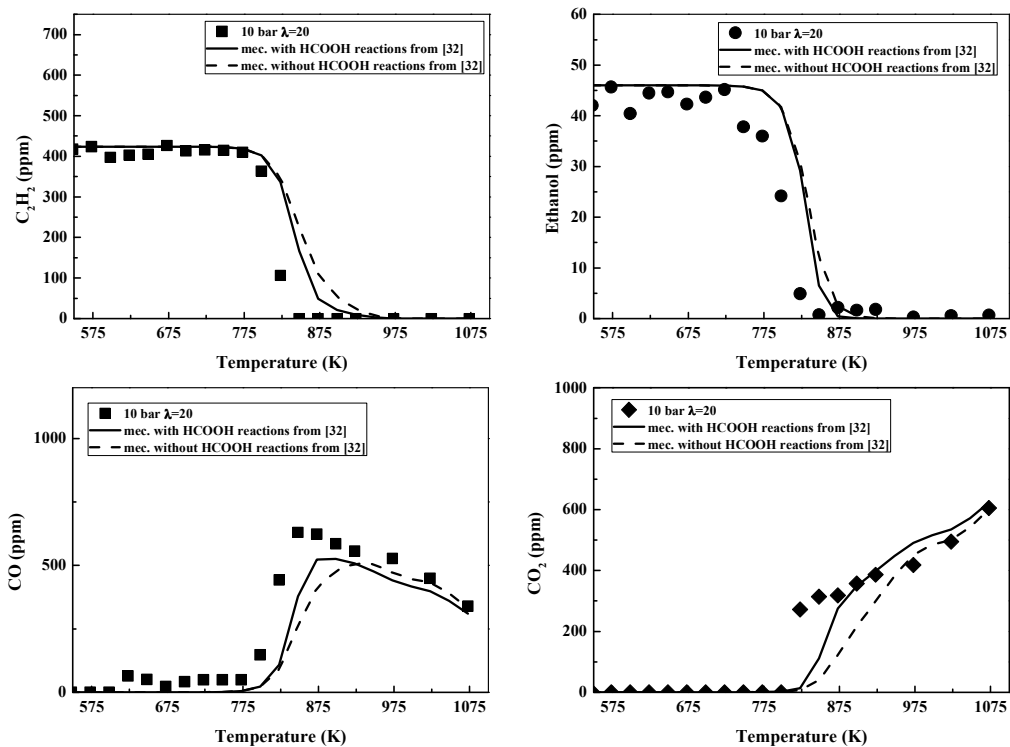


Figure S9. Comparison of modeling calculations obtained with the present mechanism with or without HCOOH reactions from Zhao et al. [32] for the conditions denoted as set 4 in Table 1 of the manuscript.

References

- [21] Hashemi, H.; Christensen, J.M.; Glarborg, P. High-pressure pyrolysis and oxidation of ethanol. *Fuel* 2018, 218, 247-257.
- [32] Zhao, Z.; Chaos, M.; Kazakov, A.; Dryer, F.L. Thermal decomposition reaction and a comprehensive kinetic model of dimethyl ether. *Int. J. Chem. Kin.* 2008, 40, 1-18.

Final mechanism

“This annex contains the final mechanism compiled in the present work”.


```

!
!
!*****
!***
!***  OXIDATION OF ORGANIC COMPOUNDS PRESENT IN FUELS UNDER CONDITIONS OF INTEREST  *****
!***                                FOR COMBUSTION PROCESSES                                *****
!***
!***                                PhD: L. Marrodan; Supervisors: M.U. Alzueta and A. Millera *****
!*****
!
ELEMENTS
  O H C N AR HE
END
!
SPECIES
!***inert***
AR N2 HE
!
!***H2***
H O OH H2 O2 H02 H2O H2O2
!
!***CO/CO2***
CO CO2
!
!***CH2O***
CH2O HCO
!
!***CH4***
CH3 CH4 CH2 CH2(S) CH C
CH3O CH2OH
!
!***C2***
C2 C2H2 C2H C2H3 C2H4 C2H5 C2H6
CH2CO HCCO C2O
CH2HCO C2H2OH CH3HCO CH3CO HCCOH
C2H5CHO C2H5CO
CHCHO H2CC CH2CHO0 CH2CHO
!
!***C3***
C3H2 C3H4 H2CCCH
!
!***C4***
C4H2
!
!***H/N/O***
NO NO2 NO3 N2O HNO HON HONO HNO2 H2NO HNOH HONO2
NH3 NH2 NH N
N2H4 N2H3 N2H2 H2NN NNH
CH3ONO CH3ONO2
!
!***cyanides***
HCN HNC CN HNCO HOCN HCNO NCO H2CN HCNH CH3CN CH2CN NCCN NCN
C2N2
!
!***DME***
CH3OCH3 CH3OCH2 CH3O2
CH3OCH2O2H O2CH2OCH2O2H H02CH2OCHO
CH3OCH2O CH3OCH2O2 CH2OCH2O2H CH3OCH2OH CH3OOH
CH3NO CH3NO2 H2CNO2
!
!***Ethano]***
C2H5OH C2H4OH CH3CHOH CH3CH2O
!
!***Methano]***
CH3OH
!
!***Methyl formate***
CH3OCHO CH2OCHO CH3OCO
HC00H CH3CO2CH3 CH3OC002H OCH2O2H OCH2OCO
CH3CH2OCHO OCH2OCHO O0CH2OCHO CH2OOH
CH3OC0O CH3OC00O H00CH2OCO CH2OC00OH
OCH0C00OH O0CH2OC00OH H00CH2OC00O CH00CO
H00CH2O
!
!***DMM***

```

```

CH3OCH2OCH3 CH3OCH2OCH2 CH3OCHOCH3
CH3O2H
CH3OCH2O2
!
!***Glyoxal***
OCHCHO HOCH(OO)CHO HOCH(OOH)CHO OCHCO HOCHO
!
!Acid formic
HOCH2OCO HOCH2O HOCHO OCHO HOCHOH HOCO
!
!
!
END
!
THERMO
300.00 1000.00 5000.00
CH2(S) 83194H 2C 1 0 OG 300.000 4000.000 1400.00 1
0.40752106E+01 0.15779120E-02-0.10806129E-06-0.84592437E-10 0.14033284E-13 2
0.50007492E+05-0.15480316E+01 0.35932946E+01 0.13151238E-02 0.30756846E-06 3
0.42637904E-09-0.34178712E-12 0.50451547E+05 0.17780241E+01 4
CH2 83194H 2C 1 0 OG 300.000 4000.000 1400.00 1
0.39737520E+01 0.16097502E-02-0.10785119E-06-0.86399922E-10 0.14301196E-13 2
0.45608973E+05 0.75549729E-01 0.36872995E+01 0.15066403E-02 0.69679857E-07 3
0.23537297E-09-0.19397147E-12 0.45863672E+05 0.20267601E+01 4
C2H 83194H 1C 2 0 OG 300.000 4000.000 1400.00 1
0.52086663E+01 0.12875765E-02-0.10398387E-06-0.67526325E-10 0.11751871E-13 2
0.64697773E+05-0.53721781E+01 0.39396334E+01 0.32114412E-02-0.39412765E-06 3
-0.74782530E-09 0.27493521E-12 0.65224684E+05 0.17814000E+01 4
C2H3 83194H 3C 2 0 OG 300.000 4000.000 1400.00 1
0.71861677E+01 0.34552682E-02-0.29435373E-06-0.20681942E-09 0.36797774E-13 2
0.32229627E+05-0.15977573E+02 0.24955740E+01 0.10269993E-01-0.10226917E-05 3
-0.27594382E-08 0.96919825E-12 0.34232813E+05 0.10614626E+02 4
C2H5 83194H 5C 2 0 OG 300.000 4000.000 1400.00 1
0.87349157E+01 0.54537677E-02-0.37647177E-06-0.31297920E-09 0.52844000E-13 2
0.10265269E+05-0.23104086E+02 0.24398923E+01 0.13747212E-01-0.85500653E-06 3
-0.31469924E-08 0.93754355E-12 0.13158588E+05 0.13099146E+02 4
H2CCCH 032599C 3H 3 G 0300.00 4000.00 1000.00 1
0.08831047E+02 0.04357194E-01-0.04109066E-05-0.02368723E-08 0.04376520E-12 2
0.39983875E+05-0.22559194E+02 0.04754199E+02 0.11080277E-01 0.02793323E-05 3
-0.05479212E-07 0.01949629E-10 0.41398515E+05 -1.94548824E-01 4
C2H2OH HCCO TRAN 121196H 3C 20 1 OG 300.000 3000.000 1000.00 1
0.57206843E+01 0.10704185E-01-0.50358494E-05 0.11324499E-08-0.10086621E-12 2
0.12849424E+05-0.47081776E+01 0.81498282E-01 0.31640644E-01-0.34085361E-04 3
0.18978838E-07-0.41950165E-11 0.14060783E+05 0.22908977E+02 4
CH3O2 C 1H 30 2 G 300.00 4000.00 1000.00 1
.480390863E+01 .995844638E-02-.385301026E-05 .684740497E-09-.458402955E-13 2
-.747135460E+03 .145281400E+01 .362497097E+01 .359397933E-02 .226538097E-04 3
-.295391947E-07 .111977570E-10 .793040410E+02 .996382194E+01 4
CH3OOH BUR95 H 4C 10 2 OOG 200.000 6000.000 1000.000 1
0.61600316E+01 0.10239957E-01-0.36101507E-05 0.57550301E-09-0.34178147E-13 2
-0.17654526E+05-0.61911544E+01 0.49652507E+01 0.92343510E-03 0.34455956E-04 3
-0.44469600E-07 0.17456120E-10-0.16726970E+05 0.29880275E+01-0.14980760E+05 4
OCHCHO 120596H 2C 20 2 OG 300.000 3000.000 1000.00 1
0.49087462E+01 0.13182673E-01-0.71416730E-05 0.18461316E-08-0.18525858E-12 2
-0.27116386E+05 0.59148768E+00 0.25068862E+01 0.18899139E-01-0.10302623E-04 3
0.62607508E-09 0.88114253E-12-0.26427374E+05 0.13187043E+02 4
CH3CN 111596H 3C 2N 1 OG 300.000 3000.000 1000.00 1
0.23924046E+01 0.15618873E-01-0.79120497E-05 0.19372333E-08-0.18611956E-12 2
0.84999377E+04 0.11145236E+02 0.25197531E+01 0.13567523E-01-0.25764077E-05 3
-0.30893967E-08 0.14288692E-11 0.85533762E+04 0.10920868E+02 4
CH2CN 111596H 2C 2N 1 OG 300.000 3000.000 1000.00 1
0.46058146E+01 0.94485160E-02-0.47116329E-05 0.11389957E-08-0.10828942E-12 2
0.29171486E+05 0.10084415E+01 0.25296724E+01 0.18114138E-01-0.18960575E-04 3
0.11944583E-07-0.32544142E-11 0.29592293E+05 0.10993441E+02 4
HNO pg9601H 1N 10 1 G 0300.00 5000.00 1000.00 1
0.03615144E+02 0.03212486E-01-0.01260337E-04 0.02267298E-08-0.01536236E-12 2
0.11769108E+05 0.04810264E+02 0.02784403E+02 0.06609646E-01-0.09300223E-04 3
0.09437980E-07-0.03753146E-10 0.12025976E+05 0.09035629E+02 4
C2H5OH BUR 8/88C 2H 60 1 G 200.000 6000.000 1000.00 1
0.65624365E+01 0.15204222E-01-0.53896795E-05 0.86225011E-09-0.51289787E-13 2
-0.31525621E+05-0.94730202E+01 0.48586957E+01-0.37401726E-02 0.69555378E-04 3
-0.88654796E-07 0.35168835E-10-0.29996132E+05 0.48018545E+01-0.28257829E+05 4
CH3CHOH 103190C 2H 50 1 G 0300.00 4000.00 1500.00 1

```


0.01161148E+03	0.05173117E-01	-0.04856685E-05	-0.02202895E-08	0.03913721E-12	2						
-0.01248811E+06	-0.03688213E+03	0.01415940E+02	0.02870648E+00	-0.02373820E-03	3						
0.01148886E-06	-0.02391420E-10	-0.08638718E+05	0.01844256E+03		4						
C2H4OH	MARI99C	2H	50	1	OG	200.000	4000.000	1000.00	1		
0.74564000E+00	0.02930200E-00	-2.18510000E-05	8.85746000E-09	-1.38170000E-12	2						
-0.54736000E+04	0.22235000E+02	0.74564000E+00	0.02930200E-00	-2.18510000E-05	3						
8.85746000E-09	-1.38170000E-12	-0.54736000E+04	0.22235000E+02		4						
OCHCO		C	20	2H	1	G	350.000	2900.000	1000.00	1	
0.49499388E+01	0.10163032E-01	-0.55772010E-05	0.14572026E-08	-0.14743475E-12	2						
-0.96593808E+04	0.25798798E+01	0.33940561E+01	0.14362856E-01	-0.88413766E-05	3						
0.16096129E-08	0.32038938E-12	-0.92479810E+04	0.10592041E+02		4						
HOCH(OO)CHO	dummy	C	2H	30	4	OG	300.000	5000.000	1394.000	1	
0.15404761E+01	0.31924787E-01	-0.29631306E-04	0.13499252E-07	-0.23583024E-11	2						
0.17876151E+05	0.17757938E+02	0.15404761E+01	0.31924787E-01	-0.29631306E-04	3						
0.13499252E-07	-0.23583024E-11	0.17876151E+05	0.17757938E+02		4						
HOCH(OOH)CHO	dummy	C	2H	40	4	OG	300.000	5000.000	1394.000	1	
0.15404761E+01	0.31924787E-01	-0.29631306E-04	0.13499252E-07	-0.23583024E-11	2						
0.17876151E+05	0.17757938E+02	0.15404761E+01	0.31924787E-01	-0.29631306E-04	3						
0.13499252E-07	-0.23583024E-11	0.17876151E+05	0.17757938E+02		4						
HOCHO FORMIC ACID	L	8/88H	2C	10	2	OG	200.000	6000.000	1000.	1	
0.46138316E+01	0.64496364E-02	-0.22908251E-05	0.36716047E-09	-0.21873675E-13	2						
-0.47514850E+05	0.84788383E+00	0.38983616E+01	-0.35587795E-02	0.35520538E-04	3						
-0.43849959E-07	0.17107769E-10	-0.46770609E+05	0.73495397E+01	-0.45531246E+05	4						
HON	HF	MELIUS93H	1N	10	1	OG	300.00	5000.00	1671.000	1	
3.78577430E+00	2.86062728E-03	-1.02423922E-06	1.64463139E-10	-9.77943616E-15	2						
2.93319701E+04	3.12193293E+00	3.33656431E+00	2.67682939E-03	5.61801303E-07	3						
-1.11362279E-09	2.84076438E-13	2.95979751E+04	5.96343188E+00		4						
H2NN DBOZ00M93/JBPM3	96 N	2H	2	0	OG	300.000	5000.000	1695.000	1		
3.13531032E+00	5.68632569E-03	-1.93983467E-06	3.01290501E-10	-1.74978144E-14	2						
3.33678346E+04	7.04815840E+00	2.88544262E+00	4.69495999E-03	7.01983230E-07	3						
-1.53359038E-09	3.79345858E-13	3.36030690E+04	8.95096779E+00		4						
NCCN		C	2N	20	00	OG	300.00	5000.00	1000.00	1	
0.65480000E+01	0.39847100E-02	-0.16342200E-05	0.30386000E-09	-0.21110000E-13	2						
0.34907200E+05	-0.97360000E+01	0.42654600E+01	0.11922570E-01	-0.13420140E-04	3						
0.91923000E-08	-0.27789400E-11	0.35478900E+05	0.17130000E+01		4						
OCHO		1104	C	1H	1N	00	2G	298.150	3000.000	1000.00	1
4.41052368E+00	7.50888367E-03	-4.25889679E-06	1.12761124E-09	-1.14144138E-13	2						
-1.70297531E+04	3.43148293E+00	3.62860375E+00	8.12496033E-03	-1.41560718E-06	3						
-3.27951824E-09	1.61553900E-12	-1.67477889E+04	7.83169538E+00		4						
CH3O2H	7/13/98	thermC	1H	40	2	OG	300.000	5000.000	1390.000	1	
8.43117091E+01	8.06817909E-03	-2.77094921E-06	4.31332243E-10	-2.50692146E-14	2						
-1.96678771E+04	-1.91170629E+01	3.23442817E+00	1.90129767E-02	-1.13386287E-05	3						
3.40306653E-09	-4.11830222E-13	-1.77197926E+04	9.25623949E+00		4						
HOCH2OCO	8/31/99	THERMC	2H	30	3	OG	300.000	5000.000	1603.000	1	
4.13737391E+01	8.17663898E-03	-2.92034021E-06	4.66695616E-10	-2.76276823E-14	2						
-4.65575743E+04	-2.86035265E+01	6.08180801E+00	1.28768359E-02	2.04419418E-06	3						
-6.10154921E-09	1.79820559E-12	-4.39526183E+04	2.54054449E+00		4						
HOCH2O	8/ 4/99	THERMC	1H	30	2	OG	300.000	5000.000	1452.000	1	
6.43121515E+00	7.43673043E-03	-2.50422354E-06	3.84879712E-10	-2.21778689E-14	2						
-2.47500385E+04	-7.29290847E+00	4.11183145E+00	7.53850697E-03	3.77337370E-06	3						
-5.38746005E-09	1.45615887E-12	-2.34414546E+04	6.81381989E+00		4						
CH3OCH2OH	2/ 9/96	THERMC	2H	60	2	OG	300.000	5000.000	2014.000	1	
8.70981570E+01	1.53602372E-02	-5.41003788E-06	8.60573446E-10	-5.08819752E-14	2						
-4.76607115E+04	-1.80226702E+01	3.15851876E+00	2.44325751E-02	-8.66984784E-06	3						
-5.93319328E-11	4.36400003E-13	-4.54488899E+04	1.30511235E+01		4						
HOCHOH		1311	C	1H	3N	00	2G	298.150	3000.000	1000.00	1
4.86295370E+00	1.23471277E-02	-5.95787471E-06	1.34757724E-09	-1.18911894E-13	2						
-2.71063590E+04	1.47289499E+00	1.70704907E+00	2.28906928E-02	-1.86531423E-05	3						
7.73103555E-09	-1.19476312E-12	-2.63711754E+04	1.72183239E+01		4						
HOCO	equilib	ATCT/AC	1.0	2.H	1.	O.G	200.000	6000.000	1000.	1	
5.39206152E+00	4.11221455E-03	-1.48194900E-06	2.39875460E-10	-1.43903104E-14	2						
-2.36480760E+04	-2.23529091E+00	2.92207919E+00	7.62453859E-03	3.29884437E-06	3						
-1.07135205E-08	5.11587057E-12	-2.33512327E+04	1.12925886E+01	-2.21265065E+04	4						
CHCHO		C	2H	2N	00	1G	298.150	3000.000	1000.00	1	
1.48500000E+00	2.31400000E-02	-2.37600000E-05	1.23300000E-08	-2.55200000E-12	2						
2.97960000E+04	1.72100000E+01	1.48500000E+00	2.31400000E-02	-2.37600000E-05	3						
1.23300000E-08	-2.55200000E-12	2.97960000E+04	1.72100000E+01		4						
H2CC vinylidene	T	7/11C	2.H	2.	0.	O.G	200.000	6000.000	1000.	1	
4.27807305E+00	4.75622626E-03	-1.63007378E-06	2.54622680E-10	-1.48860086E-14	2						
4.80140478E+04	6.39978600E-01	3.28154941E+00	6.97642650E-03	-2.38527914E-06	3						
-1.21077631E-09	9.82041734E-13	4.83191706E+04	5.92035686E+00	4.95846418E+04	4						
CH2CHOO		OC	2H	30	2	G	300.00	2000.00	1000.00	1	
0.14160300E+01	0.29933721E-01	-0.26385173E-04	0.11770709E-07	-0.20511571E-11	2						
0.11361727E+05	0.18969526E+02	0.14146113E+01	0.29754629E-01	-0.25839387E-04	3						
0.11222085E-07	-0.18678097E-11	0.11371249E+05	0.19022561E+02		4						

```

CH2CHO Vinyl- T04/O6C 2.H 3.0 1. 0.G 200.000 6000.000 1000. 1
5.91636535E+00 8.84650426E-03-3.14954895E-06 5.05413189E-10-3.01304621E-14 2
-1.04779892E+03-6.10649981E+00 2.66873956E+00 9.62329538E-03 1.60617438E-05 3
-2.87681820E-08 1.25030066E-11 2.19438429E+02 1.25694476E+01 1.53380440E+03 4
HE Ranzi OHE 2C OH 00 OG 0300.00 5000.00 1000.00 1
3.1250000E+00 -1.4062505E-03 9.3750049E-07 -1.5625008E-10 0.0000000E+00 2
-940.68700E+00 -2.4124130E+00 2.5000000E+00 0.0000000E+00 0.0000000E+00 3
0.0000000E+00 0.0000000E+00 -745.37510E+00 0.9153489E+00 4
CH3OCH3 2/11/14 thermC 2H 60 1 OG 300.000 5000.000 1999.000 1
6.03232751E+00 1.56155270E-02-5.50761030E-06 8.75666140E-10-5.17180562E-14 2
-2.52690354E+04-8.25885183E+00 2.05597390E+00 2.07019456E-02-5.00382376E-06 3
-1.62279885E-09 6.84330155E-13-2.35494445E+04 1.45029944E+01 4
CH3OCH2 2/11/14 thermC 2H 50 1 OG 300.000 5000.000 1395.000 1
6.62621974E+00 1.22219496E-02-4.12416696E-06 6.34127512E-10-3.65317390E-14 2
-3.33965890E+03-8.95305753E+00 1.58874948E+00 2.24414123E-02-1.19434933E-05 3
3.37160213E-09-4.15077249E-13-1.37208255E+03 1.87548958E+01 4
CH3OCH2OH 2/12/14 thermC 2H 60 3 OG 300.000 5000.000 1404.000 1
1.28159161E+01 1.34818095E-02-4.50397729E-06 6.88229286E-10-3.94883680E-14 2
-4.06745921E+04-3.78047802E+01 1.05786981E+00 4.36787095E-02-3.46383899E-05 3
1.44808830E-08-2.46100643E-12-3.68851076E+04 2.43391936E+01 4
CH3OCH2O2 2/12/14 thermC 2H 50 3 OG 300.000 5000.000 1441.000 1
1.19179361E+01 1.19412867E-02-3.93526185E-06 5.95756132E-10-3.39597705E-14 2
-2.34231833E+04-3.20096863E+01 3.39930541E+00 3.09460407E-02-1.92548181E-05 3
5.76033887E-09-6.16081571E-13-2.04433218E+04 1.39429608E+01 4
CH2OCH2OH 2/12/14 thermC 2H 50 5 OG 300.000 5000.000 1418.000 1
1.23892901E+01 1.11758961E-02-3.59249095E-06 5.34196366E-10-3.00536541E-14 2
-1.80551598E+04-3.29576862E+01 1.62245477E-01 4.76101093E-02-4.52046954E-05 3
2.18379311E-08-4.11295947E-12-1.46498100E+04 2.98253164E+01 4
O2CH2OCH2OH 2/12/14 ermC 2H 50 5 OG 300.000 5000.000 1433.000 1
1.77378326E+01 1.13589899E-02-3.67382539E-06 5.49255712E-10-3.10405899E-14 2
-3.82903058E+04-5.66609932E+01 2.39977678E+00 5.39881943E-02-4.87969524E-05 3
2.19792134E-08-3.86106979E-12-3.37824638E+04 2.30683371E+01 4
HO2CH2OCHO 2/12/14 thermC 2H 40 4 OG 300.000 5000.000 1386.000 1
1.57136128E+01 9.64430166E-03-3.44136025E-06 5.49722196E-10-3.25360322E-14 2
-6.29409094E+04-5.29505242E+01 1.21909586E+00 4.28858235E-02-3.17634222E-05 3
1.11542676E-08-1.49753153E-12-5.79287926E+04 2.49759193E+01 4
CH3OCH2O 5/15/14 thermC 2H 50 2 OG 300.000 5000.000 1523.000 1
9.81288609E+00 1.21313106E-02-4.30285768E-06 6.84443177E-10-4.03862658E-14 2
-2.50760742E+04-2.51866352E+01 5.63414373E+00 8.92830283E-03 1.37225633E-05 3
-1.40497059E-08 3.54625624E-12-2.22825214E+04 1.93588846E+00 4
HOCH2OCO 5/29/14 thermC 2H 30 3 OG 300.000 5000.000 1443.000 1
1.11498410E+01 9.34736520E-03-3.35541548E-06 5.38037115E-10-3.19260183E-14 2
-4.75012119E+04-2.95983867E+01 5.95255071E+00 8.42196282E-03 1.36741678E-05 3
-1.46786275E-08 3.84143533E-12-4.44470269E+04 2.85657217E+00 4
OCH2OCHO 5/29/14 thermC 2H 30 3 OG 300.000 5000.000 1523.000 1
1.24013200E+01 7.83738243E-03-2.82992688E-06 4.55558739E-10-2.71061389E-14 2
-4.68453470E+04-3.78084549E+01 1.89539692E+00 2.74118545E-02-1.36476090E-05 3
1.26325603E-09 5.17970476E-13-4.27879440E+04 2.02333278E+01 4
HOOC2O C 1H 30 3 G 0300.00 5000.00 1000.00 1
0.49785396E+00 0.18224888E-01-0.62859067E-05 0.10141499E-08-0.63038970E-13 2
-0.12036847E+05 0.30297577E+02-0.16220864E+01 0.39559957E-01-0.40179089E-04 3
0.17700215E-07-0.20797537E-11-0.13054886E+05 0.35495285E+02 4
CH3NO2 T01/O0C 1H 3N 10 2G 200.000 6000.000 1000. 1
6.73034758E+00 1.09601272E-02-4.05357875E-06 6.67102246E-10-4.04686823E-14 2
-1.29143475E+04-1.01800883E+01 3.54053638E+00 1.86559899E-03 4.44946580E-05 3
-5.87057133E-08 2.30684496E-11-1.11385976E+04 1.06884657E+01-9.71208165E+03 4
!END
!
!
REACTIONS
!
!*****
! H2/O2
!*****
!
H+O2=O+OH 3.6E15 -0.410 16600 !
H+H+M=H2+M 7.0E17 -1.000 0 !
N2/O/ H2O/O/ H2/O/ !
H+H+N2=H2+N2 5.4E18 -1.300 0 !
H+H+H2=H2+H2 1.0E17 -0.600 0 !
H+H+H2O=H2+H2O 1.0E19 -1.000 0 !

```

H+O+M=OH+M	6.2E16	-0.600	0 !
H2O/5/			!
H+O2(+M)=HO2(+M)	1.5E12	0.600	0 !
LOW / 3.5E16 -0.41 -1116 /			!
TROE / 0.5 1.0E-30 1.0E30 /			!
N2/0/ AR/0/ H2O/11/ H2/2/ O2/0.78/			!
H+O2(+AR)=HO2(+AR)	1.5E12	0.600	0 !
LOW / 9.04E19 -1.500 490 /			!
TROE / 0.5 1.0E-30 1.0E30 /			!
H+O2(+N2)=HO2(+N2)	1.5E12	0.600	0 !
LOW / 6.37E20 -1.720 520 /			!
TROE / 0.8 1.0E-30 1.0E30 /			!
O+O+M=O2+M	1.9E13	0.000	-1788 !
N2/1.5/ O2/1.5/ H2O/10/			!
O+H2=OH+H	3.8E12	0.000	7948 !
DUPLICATE			!
O+H2=OH+H	8.8E14	0.000	19175 !
DUPLICATE			!
OH+OH=O+H2O	4.3E03	2.700	-1822 !
OH+H+M=H2O+M	4.5E22	-2.000	0 !
AR/0.38/ H2/0.73/ H2O/12/ !HE/0.38/			!
OH+H2=H+H2O	2.1E08	1.520	3449 !
H2+O2=HO2+H	7.4E05	2.433	53502 !
HO2+H=OH+OH	8.4E13	0.000	400 !
HO2+H=H2O+O	1.4E12	0.000	0 !
HO2+O=OH+O2	1.6E13	0.000	-445 !
HO2+OH=H2O+O2	3.6E21	-2.100	9000 !
DUPLICATE			!
HO2+OH=H2O+O2	2.0E15	-0.600	0 !
DUPLICATE			!
HO2+OH=H2O+O2	-2.2E96	-24.000	49000 !
DUPLICATE			!
HO2+HO2=H2O2+O2	1.9E11	0.000	-1408 !
DUPLICATE			!
HO2+HO2=H2O2+O2	1.0E14	0.000	11034 !
DUPLICATE			!
H2O2(+M)=OH+OH(+M)	4.0E11	0.000	37137 !
LOW /2.291E16 0.0 43638/			!
TROE /0.5 1E-30 1E30 1E30/			!
H2O/12/ H2/2.5/ AR/0.64/			!
H2O2+H=H2O+OH	1.0E13	0.000	3580 !
H2O2+H=HO2+H2	1.7E12	0.000	3760 !
H2O2+O=HO2+OH	9.6E06	2.000	3970 !
H2O2+OH=H2O+HO2	1.9E12	0.000	427 !
DUPLICATE			!
H2O2+OH=H2O+HO2	1.6E18	0.000	29410 !
DUPLICATE			!
!			!
! *****			!
! CO/CO2 subset			!
! *****			!
!			!
CO+O(+M)=CO2(+M)	1.8E10	0.000	2384 !
LOW /1.35E24 -2.79 4191/			!
TROE /1.0 1E-30 1E30 1E30/			!
H2/2.5/ H2O/12/ CO/1.9/ CO2/3.8/			!
CO+O2=CO2+O	4.7E12	0.000	60500 !
CO+HO2=CO2+OH	1.6E05	2.180	17943 !
CO+OH=CO2+H	8.7E05	1.730	-685 !
PLOG/ 0.01315	2.1E05	1.900	-1064/
PLOG/ 0.1315	2.5E05	1.880	-1043/
PLOG/ 1.315	8.7E05	1.730	-685/
PLOG/ 13.158	6.8E06	1.480	48/
PLOG/ 131.58	2.3E07	1.350	974/
CO+OH=HOCO	2.0E20	-3.500	1309 !
PLOG/ 0.013158	1.7E15	-2.680	859
PLOG/ 0.13158	5.9E18	-3.350	887/
PLOG/ 1.3158	2.6E20	-3.500	1309/
PLOG/ 13.158	7.1E20	-3.320	1763/
PLOG/ 131.58	1.1E20	-2.780	2056/
HOCO+OH=CO2+H2O	4.6E12	0.000	-89 !

```

    DUPLICATE
HOCO+OH=CO2+H2O          9.5E06   2.000   -89 !
    DUPLICATE
HOCO+O2=CO2+HO2          9.9E11   0.000    0 !
HOCO(+M)=CO+OH(+M)       5.9E12   0.53   33980 !
LOW/2.20E23  -1.83   35260/
HOCO(+M)=CO2+H(+M)       1.7E12   0.31   32920 !
LOW/2.9E26  -3.02   35070/
!
! *****
! CH2O
! *****
!
CH2O(+M)=HCO+H(+M)       8.0E15   0.000  87726 !
LOW /                     1.3E36  -5.500  93932/
CH2O(+M)=CO+H2(+M)       3.7E13   0.000  71969 !
LOW /                     4.4E38  -6.100  93932/
CH2O+H=HCO+H2    1      1      1
PLOG/0.04              7.4E23  -2.732  16379/
PLOG/0.04              2.1E10   1.057   3720/
PLOG/1                 1.4E23  -2.355  17519/
PLOG/1                 1.6E15  -0.444   5682/
PLOG/10                7.3E23  -2.665  17634/
PLOG/10                4.2E09   1.294   3591/
CH2O+H=H+CO+H2        5.1E07   2.182  11524
PLOG/0.04              7.2E08   1.903  11733/
PLOG/1                 5.1E07   2.182  11524/
PLOG/10                1.1E09   1.812  13163/
CH2O+O=HCO+OH         5.6E31  -5.189  19968
DUPLICATE
CH2O+O=HCO+OH          1.4E15  -0.530   4011
DUPLICATE
CH2O+O=H+CO+OH         2.5E21  -1.903  22674
CH2O+O2=HCO+HO2        2.4E05   2.500  36461
DUPLICATE
CH2O+O2=HCO+HO2       -1.4E15   0.027  56388
DUPLICATE
CH2O+O2=H+CO+HO2       1.4E15   0.027  56388
CH2O+OH=HCO+H2O        1.9E09   1.256   -302
PLOG/0.04              3.6E09   1.167  -206/
PLOG/1                 1.9E09   1.256  -302/
PLOG/10                1.1E09   1.330  -392/
CH2O+OH=H+CO+H2O       7.2E10   0.892   9310
PLOG/0.04              7.0E10   0.911  8646/
PLOG/1                 7.2E10   0.892   9310/
PLOG/10                8.4E10   0.879  9843/
CH2O+HO2=HCO+H2O2      4.1E04   2.500  10206
DUPLICATE
CH2O+HO2=HCO+H2O2     -2.5E14   0.027  30133
DUPLICATE
CH2O+HO2=H+CO+H2O2     2.5E14   0.027  30120
CH2O+CH3=HCO+CH4       3.2E01   3.360   4310
DUPLICATE
CH2O+CH3=HCO+CH4      -1.9E11   0.887  24237
DUPLICATE
CH2O+CH3=H+CO+CH4       1.9E11   0.887  24224
HCO(+M)=H+CO(+M)       4.9E16  -0.930  19724
LOW/                     7.4E21  -2.360  19383/
TROE/ 0.103 139 10900 4550/
N2/1.5/ O2/1.5/ CO/1.5/ H2/2.0/ CH4/5.0/ CO2/3./ H2O/15./
HCO+H=CO+H2            1.1E14   0.000    0 !
HCO+O=CO+OH            3.0E13   0.000    0 !
HCO+O=CO2+H            3.0E13   0.000    0 !
HCO+OH=CO+H2O          1.1E14   0.000    0 !
HCO+O2=CO+HO2          6.9E06   1.900  -1369 !
HCO+HO2=CO2+OH+H       3.0E13   0.000    0 !
HCO+HCO=CO+CH2O        2.7E13   0.000    0 !
!
! *****
! CH4/CH3/CH2/CH/C
! *****
!
CH3+H(+M)=CH4(+M)       2.1E14   0.000    0 !

```

```

LOW /6.467E23 -1.8 0/
TROE /0.6376 1E-30 3230 1E30/
CH4/1.9/ C2H6/4.8/
CH4+H=CH3+H2 4.1E03 3.156 8755 !
CH4+O=CH3+OH 4.4E05 2.500 6577 !
CH4+OH=CH3+H2O 1.0E06 2.182 2506 !
CH4+HO2=CH3+H2O2 4.7E04 2.500 21000 !
CH3+H=CH2+H2 9.0E13 0.0 15100 !
CH3+O=CH2O+H 8.0E13 0.0 0 !
CH3+OH=CH2+H2O 7.5E06 2.0 5000 !
CH3+HO2=CH4+O2 2.5E08 1.25 -1630 !
CH3+HO2=CH3O+OH 2.0E13 0.00 1075 !
CH3+O2=CH3O+O 2.87E13 0.0 30481 !
CH3+O2<=>CH2O+OH 2.64E00 3.28 8105 !
CH3+CH3(+M)=C2H6(+M) 2.1E16 -0.97 620 !
LOW /1.26E50 -9.67 6220/
TROE/ 0.5325 151 1038 4970 /
N2/1.43/ H2O/8.59/
CH3+HCO=CH4+CO 1.2E14 0.0 0 !
CH2+H=CH+H2 1.00E18 -1.56 0 !
CH2+O=CO+H+H 5.00E13 0.00 0 !
CH2+O=CO+H2 3.00E13 0.00 0 !
CH2+OH=CH+H2O 1.13E7 2.00 3000 !
CH2+OH=CH2O+H 2.50E13 0.00 0 !
CH2+O2=CO+H2O 2.20E22 -3.3 2867 !
CH2+O2=CO2+H+H 3.3E21 -3.3 2867 !
CH2+O2=CH2O+O 3.29E21 -3.3 2867 !
CH2+O2=CO2+H2 2.63E21 -3.3 2867 !
CH2+O2=CO+OH+H 1.64E21 -3.3 2867 !
CH2+CO2=CO+CH2O 1.10E11 0.00 1000 !
CH2+CH4=CH3+CH3 4.3E12 0.0 10030 !
CH2+CH3=C2H4+H 4.20E13 0.00 0 !
CH2+CH2=C2H2+H+H 4.00E13 0.00 0 !
CH2+C2H2=H2CCCH+H 1.20E13 0.00 6600 !
CH2+HCCO=C2H3+CO 3.00E13 0.00 0 !
CH2(S)+M=CH2+M 1.00E13 0.00 0 !
H/20/ H2O/3/ N2/0.0/ AR/0.0/
CH2(S)+AR=CH2+AR 1.45E13 0.0 884 !
CH2(S)+N2=CH2+N2 1.26E13 0.0 430 !
CH2(S)+H=CH+H2 3.0E13 0.0 0 !
CH2(S)+H=CH2+H 2.00E14 0.00 0 !
CH2(S)+H2=CH3+H 7.2E13 0.0 0 !
CH2(S)+H2O=CH3+OH 3.0E15 -0.6 0 !
CH2(S)+H2O=CH2+H2O 3.0E13 0.0 0 !
CH2(S)+O=CO+H+H 3.0E13 0.0 0 !
CH2(S)+OH=CH2O+H 3.0E13 0.0 0 !
CH2(S)+O2=CO+OH+H 7.0E13 0.0 0 !
CH2(S)+CO2=CH2O+CO 3.0E12 0.0 0 !
CH2(S)+CH4=CH3+CH3 4.3E13 0.0 0 !
CH2(S)+CH3=C2H4+H 2.0E13 0.0 0 !
CH2(S)+C2H6=CH3+C2H5 1.2E14 0.0 0 !
CH2(S)+CH2CO=C2H4+CO 1.6E14 0.0 0 !
CH+H=C+H2 1.5E14 0.0 0 !
CH+O=CO+H 5.7E13 0.0 0 !
CH+OH=HCO+H 3.0E13 0.0 0 !
CH+OH=C+H2O 4.0E7 2.0 3000 !
CH+O2=HCO+O 3.30E13 0.0 0 !
CH+H2O=CH2O+H 5.72E12 0.0 -755 !
CH+CO2=HCO+CO 3.4E12 0.0 686 !
CH+CH2O=CH2CO+H 9.5E13 0.0 -517 !
CH+C2H2=C3H2+H 1.0E14 0.0 0 !
CH+CH4=C2H4+H 6.00E13 0.0 0 !
CH+CH3=C2H3+H 3.00E13 0.0 0 !
CH+CH2=C2H2+H 4.00E13 0.0 0 !
CH+HCCO=C2H2+CO 5.0E13 0.0 0 !
C+OH=CO+H 5.0E13 0.0 0 !
C+O2=CO+O 2.0E13 0.0 0 !
C+CH3=C2H2+H 5.0E13 0.0 0 !
C+CH2=C2H+H 5.0E13 0.0 0 !
!
! *****
! CH3OH/CH2OH/CH3O
! *****
CH3OH(+M)=CH3+OH(+M) 2.1E18 -0.6148 92540 !
LOW /2.60E49 -8.80 101500/
!

```

```

TROE /0.7656 1910 59.51 9374/
CH3OH+H<=>CH2OH+H2      3.07E05  2.55    5440 !
CH3OH+H=CH3O+H2         4.1E04   2.658   9221 !
CH3OH+O=CH2OH+OH        2.1E13   0.000   5305 !
CH3OH+O=CH3O+OH         3.7E12   0.000   5305 !
CH3OH+OH=CH2OH+H2O      1.5E08   1.4434   113 !
CH3OH+OH=CH3O+H2O       2.7E07   1.4434   113 !
CH3OH+HO2=CH2OH+H2O2    3.5E-4   4.850   10346 !
CH3OH+HO2=CH3O+H2O2     1.5E-3   4.610   15928 !
CH3OH+O2=CH2OH+HO2      3.6E05   2.270   42760 !
CH2OH=CH2O+H            5.7E34  -6.640  46430 !
CH2OH+H=CH2O+H2         1.4E13   0.000    0 !
CH2OH+H=CH3+OH          6.0E12   0.000    0 !
CH2OH+H(+M)=CH3OH(+M)   4.3E15  -0.790    0 !
  LOW /3.844E37 -6.21 1333/
  TROE /0.25 210 1434 1E30/
CH2OH+O=CH2O+OH         6.6E13   0.000   -693 !
CH2OH+OH=CH2O+H2O       2.4E13   0.000    0 !
CH2OH+HO2=CH2O+H2O2     1.2E13   0.000    0 !
CH2OH+O2=CH2O+HO2      7.2E13   0.000   3736 !
  DUPLICATE
CH2OH+O2=CH2O+HO2      2.9E16  -1.500    0 !
  DUPLICATE
CH2OH+HCO=CH3OH+CO      1.0E13   0.000    0 !
CH2OH+HCO=CH2O+CH2O     1.5E13   0.000    0 !
CH2OH+CH2O=CH3OH+HCO    5.5E03   2.810   5862 !
CH2OH+CH2OH=CH3OH+CH2O  4.8E12   0.000    0 !
CH2OH+CH3O=CH3OH+CH2O  2.4E12   0.000    0 !
CH2OH+CH4=CH3OH+CH3     2.2E01   3.100  16227 !
CH3O=CH2O+H             4.2E107 -29.490  63410 !
CH3O=CH2OH              5.4E111 -30.460  62690 !
CH3O+H=CH2O+H2          5.3E13   0.000   745 !
CH3O+H=CH3+OH           4.6E12   0.000   745 !
CH3O+H(+M)=CH3OH(+M)    2.4E12   0.515   50 !
  LOW /4.66E41 -7.44 14080/
  TROE /0.7 100 90000 10000/
  N2/1/ H2/2/ H2O/6/ CH4/2/ CO/1.5/ CO2/2/ C2H6/3/
CH3O+O=CH2O+OH          3.8E12   0.000    0 !
CH3O+OH=CH2O+H2O        1.8E13   0.000    0 !
CH3O+HO2=CH3OH+O2       1.4E11   0.000    0 !
CH3O+O2=CH2O+H2O        4.8E-1   3.567  -1055 !
CH3O+CO=CH3+CO2         9.5E25  -4.930   9080 !
CH3O+CH3=CH2O+CH4       2.4E13   0.000    0 !
CH3O+CH4=CH3OH+CH3      1.3E14   0.000  15073 !
CH3O+CH2O=CH3OH+HCO     1.0E11   0.000   2981 !
CH3O+CH3O=CH3OH+CH2O    6.0E13   0.000    0 !
!
! *****
! C2 subset
! *****
!
C2H6+H=C2H5+H2          5.4E02   3.50    5210 !
C2H6+O=C2H5+OH          3.0E07   2.00    5115 !
C2H6+OH=C2H5+H2O        7.2E6    2.0     864 !
C2H6+HO2=C2H5+H2O2      1.3E13   0.00   20460 !
C2H6+O2=C2H5+HO2        5.0E13   0.0    55000 !
C2H6+CH3=C2H5+CH4       5.5E-1   4.00    8300 !
C2H4+H(+M)=C2H5(+M)     1.08E12  0.45   1822 !
  LOW/1.112E34 -5.0 4448.0/
  TROE/0.5 95.0 95.0 200./
  H2/2/ CO/2/ CO2/3/ H2O/5/
C2H5+H(+M)=C2H6(+M)     5.2E17  -0.99   1580 !
  LOW / 2.0E41 -7.08 6685/
  TROE/ 0.8422 125 2219 6882 /
  H2/2/ CO/2/ CO2/3/ H2O/5/
C2H5+H=CH3+CH3          4.9E12   0.35    0 !
C2H5+O=CH3+CH2O         4.2E13   0.00    0 !
C2H5+O=CH3HCO+H         5.3E13   0.00    0 !
C2H5+O=C2H4+OH          3.0E13   0.00    0 !
C2H5+OH=C2H4+H2O        2.4E13   0.00    0 !
C2H5+O2=C2H4+HO2        1.0E10   0.00  -2190 !
C2H5+CH2O=C2H6+HCO      5.5E03   2.81   5860 !
C2H5+HCO=C2H6+CO        1.2E14   0.00    0 !
C2H5+CH3=C2H4+CH4       1.1E12   0.00    0 !
C2H5+C2H5=C2H6+C2H4     1.5E12   0.00    0 !

```

C2H3+H(+M)=C2H4(+M)	6.1E12	0.27	280 !
LOW /0.98E30 -3.86 3320./			
TROE /0.7820 207.50 2663.00 6095.00/			
N2/1.4/ H2O/7.14/			
C2H4+M=C2H2+H2+M	3.50E16	0.00	71500 !
N2/1.5/ H2O/10/			
C2H4+H=C2H3+H2	5.42E14	0.00	14902 !
C2H4+O=CH2HCO+H	4.7E06	1.88	180 !
C2H4+O2=CH2HCO+OH	2.0E08	1.500	39000 !
C2H4+O2=C2H3+HO2	4.2E13	0.0	57630 !
C2H4+O=CH3+HCO	8.1E6	1.88	180 !
C2H4+O=CH2CO+H2	6.8E5	1.88	180 !
C2H4+OH=C2H3+H2O	2.0E13	0.00	5940 !
C2H4+HO2=CH3HCO+OH	2.2E12	0.00	17200 !
C2H4+CH3=C2H3+CH4	5.0E11	0.0	15000 !
C2H3+H=C2H2+H2	4.00E13	0.00	0 !
C2H3+O=CH2CO+H	3.00E13	0.00	0 !
C2H3+OH=C2H2+H2O	2.0E13	0.00	0 !
C2H3+O2=CH2O+HCO	4.58E16	-1.39	1015 !
C2H3+O2=CH2HCO+O	3.03E11	-0.29	10.73 !
C2H3+O2=C2H2+HO2	1.3E6	1.61	-383 !
C2H3+CH2O=C2H4+HCO	5.4E3	2.81	5860 !
C2H3+HCO=C2H4+CO	9.0E13	0.0	0 !
C2H3+CH3=C2H2+CH4	2.1E13	0.0	0 !
C2H3+C2H3=C2H4+C2H2	6.3E13	0.0	0 !
C2H3+CH2=C3H4+H	3.0E13	0.0	0 !
C2H3+C2H=C2H2+C2H2	3.0E13	0.0	0 !
C2H3+CH=CH2+C2H2	5.0E13	0.0	0 !
C2H3+C2H3=H2CCCH+CH3	1.8E13	0.0	0 !
!			
!*****			
! C2H2			
!*****			
!			
C2H2+M=C2H+H+M	9.1E30	-3.700	127138 !
H2/2/ CO/2/ CO2/3/ H2O/5/			
C2H2(+M)=H2CC(+M)	1.80E4	3.510	43300
LOW /2.5E15 -0.640 49700/			
TROE/0.5 1E-30 1E+30/			
C2H2+H(+M)=C2H3(+M)	1.7E10	1.266	2709
LOW /6.3E31 -4.664 3780/			
TROE/0.7878 -10212 1E-30/			
C2H+H2=C2H2+H	4.1E5	2.390	864
C2H2+O=HCCO+H	1.4E7	2.000	1900
C2H2+O=CH2+CO	6.1E6	2.000	1900
C2H2+O=C2H+OH	3.2E15	-0.6	15000
C2H2+OH=C2H2OH	3.5E31	-6.200	6635 !
PLOG / .01	2.9E64	-18.570	10009. /
PLOG / .01	2.6E33	-7.360	6392. /
PLOG / .025	4.7E59	-16.870	9087. /
PLOG / .025	4.4E32	-7.020	5933. /
PLOG / 0.1	1.2E28	-5.560	3724. /
PLOG / 0.1	6.4E42	-9.960	11737. /
PLOG / 1.0	1.9E44	-11.380	6299. /
PLOG / 1.0	3.5E31	-6.200	6635. /
PLOG / 10.0	1.5E24	-4.060	3261. /
PLOG / 10.0	4.5E31	-5.920	8761. /
PLOG / 100.	6.2E20	-2.800	2831. /
PLOG / 100.	1.6E29	-4.910	9734. /
C2H2+OH=CH3+CO	1.3E09	0.730	2579 !
PLOG / .01	4.8E05	1.680	-330. /
PLOG / .025	4.4E06	1.400	227. /
PLOG / 0.1	7.7E07	1.050	1115. /
PLOG / 1.0	1.3E09	0.730	2579. /
PLOG / 10.0	4.3E08	0.920	3736. /
PLOG / 100.	8.3E05	1.770	4697. /
C2H2+OH=HCCOH+H	2.4E06	2.000	12713 !
PLOG / .01	2.8E05	2.280	12419. /
PLOG / .025	7.5E05	2.160	12547. /
PLOG / .1	1.8E06	2.040	12669. /
PLOG / 1.0	2.4E06	2.000	12713. /
PLOG / 10.	3.2E06	1.970	12810. /
PLOG / 100.	7.4E06	1.890	13603. /
C2H2+OH=CH2CO+H	7.5E06	1.550	2106 !
PLOG / .01	1.7E03	2.560	-844. /

PLOG / .025	1.5E04	2.280	-292. /
PLOG / 0.1	3.0E05	1.920	598. /
PLOG / 1.0	7.5E06	1.550	2106. /
PLOG / 10.0	5.1E06	1.650	3400. /
PLOG / 100.	1.5E04	2.450	4477. /
C2H2+OH=C2H+H2O	2.6E6	2.140	8586
C2H2+HO2=CH2CHO	7.11E20	-3.15	15650
PLOG/1.000E-02	5.0E06	-1.020	9152/
PLOG/1.000E-02	1.9E26	-8.34	9249/
PLOG/1.000E-01	6.0E17	-3.82	10790/
PLOG/1.000E-01	5.3E129	-41.74	35930/
PLOG/3.160E-01	2.5E48	-12.82	25220/
PLOG/3.160E-01	2.0E18	-3.67	10480/
PLOG/1.000E+00	4.1E50	-13.07	27220/
PLOG/1.000E+00	4.9E21	-4.37	12220/
PLOG/3.160E+00	9.1E46	-11.57	26880/
PLOG/3.160E+00	1.9E22	-4.28	13080/
PLOG/1.000E+01	4.6E43	-10.24	26930/
PLOG/1.000E+01	2.1E21	-3.78	13380/
PLOG/3.160E+01	5.6E38	-8.49	26210/
PLOG/3.160E+01	1.4E20	-3.30	13410/
PLOG/1.000E+02	2.5E35	-7.26	26390/
PLOG/1.000E+02	1.4E19	-2.91	13420/
C2H2+HO2=CHCHO+OH	3.24E09	1.05	16950
PLOG/1.000E-02	5.5E09	0.91	18500/
PLOG/1.000E-02	2.4E07	1.54	14690/
PLOG/1.000E-01	5.9E09	0.90	18550/
PLOG/1.000E-01	2.5E07	1.54	14700/
PLOG/3.160E-01	6.8E09	0.88	18640/
PLOG/3.160E-01	2.6E07	1.54	14730/
PLOG/1.000E+00	1.6E10	0.77	19040/
PLOG/1.000E+00	2.5E07	1.56	14790/
PLOG/3.160E+00	3.5E09	0.99	18810/
PLOG/3.160E+00	1.5E08	1.32	15090/
PLOG/1.000E+01	5.4E10	0.61	20740/
PLOG/1.000E+01	1.6E08	1.36	15420/
PLOG/3.160E+01	3.7E08	1.23	15960/
PLOG/3.160E+01	1.7E07	1.59	15910/
PLOG/1.000E+02	1.5E11	0.48	17730/
PLOG/1.000E+02	7.2E06	1.73	16020/
CHCHO+H=CH2CO+H	1.0E14	0.000	0 !
CHCHO+O2=CO2+H+HCO	2.1E09	0.9929	-269 !
CHCHO+O2=OCHCHO+O	1.3E06	2.4202	1604 !
C2H2+HO2=CH2CHO+O	1.41E05	1.86	15460
PLOG/1.000E-02	5.5	1.19	12880/
PLOG/1.000E-02	2.9E-4	4.16	7736/
PLOG/1.000E-01	1.1E08	0.77	13600/
PLOG/1.000E-01	6.1E03	3.81	8394/
PLOG/3.160E-01	1.2E07	1.09	13050/
PLOG/3.160E-01	5.4E-4	4.09	8044/
PLOG/1.000E+00	3.0E07	0.98	13310/
PLOG/1.000E+00	2.5E-4	4.19	8203/
PLOG/3.160E+00	2.0E74	-16.33	109200/
PLOG/3.160E+00	6.6E04	1.85	12360/
PLOG/1.000E+01	7.5E14	-1.17	18350/
PLOG/1.000E+01	2.9E-1	3.38	10590/
PLOG/3.160E+01	8.6E18	-2.27	22230/
PLOG/3.160E+01	2.0E00	3.17	11740/
PLOG/1.000E+02	5.8E18	-2.09	24350/
PLOG/1.000E+02	1.1E-1	3.52	11980/
C2H2+HO2=CH2O+HCO	8.66E7	0.87	14170
PLOG/1.000E-02	3.9E13	-1.17	13750/
PLOG/1.000E-02	8.4E00	2.56	7382/
PLOG/1.000E-01	4.3E00	2.64	7253/
PLOG/1.000E-01	1.6E13	-1.05	13520/
PLOG/3.160E-01	2.6E-6	4.34	4525/
PLOG/3.160E-01	6.9E09	-0.00	11720/
PLOG/1.000E+00	3.3E102	-24.18	138600/
PLOG/1.000E+00	8.1E07	0.60	10850/

PLOG/3.160E+00	5.2E15	-1.75	15180/
PLOG/3.160E+00	3.5E00	2.69	8025/
PLOG/1.000E+01	7.3E35	-7.77	26970/
PLOG/1.000E+01	9.8E06	0.91	11710/
PLOG/3.160E+01	1.8E28	-5.30	25130/
PLOG/3.160E+01	1.8E04	1.70	11250/
PLOG/1.000E+02	2.5E16	-1.70	20030/
PLOG/1.000E+02	4.3E-6	4.31	6829/
C2H2+HO2=CH2O+H+CO	8.66E07	0.87	14170
PLOG/1.000E-02	9.1E13	-1.17	13750/
PLOG/1.000E-02	2.0E01	2.56	7382/
PLOG/1.000E-01	9.9E00	2.64	7253/
PLOG/1.000E-01	3.6E13	-1.05	13520/
PLOG/3.160E-01	6.1E-6	4.34	4525/
PLOG/3.160E-01	1.6E10	-0.00	11720/
PLOG/1.000E+00	7.8E102	-24.18	138600/
PLOG/1.000E+00	1.9E08	0.60	10850/
PLOG/3.160E+00	1.2E16	-1.75	15180/
PLOG/3.160E+00	8.3E00	2.69	8025/
PLOG/1.000E+01	1.7E36	-7.77	26970/
PLOG/1.000E+01	2.3E07	0.91	11710/
PLOG/3.160E+01	4.1E28	-5.30	25130/
PLOG/3.160E+01	4.2E04	1.70	11250/
PLOG/1.000E+02	5.8E16	-1.70	20030/
PLOG/1.000E+02	1.0E-5	4.31	6829/
C2H2+HO2=OCHCHO+H	3.94E04	1.68	13980
PLOG/1.000E-02	8.5E07	0.48	11720/
PLOG/1.000E-02	2.4E-6	4.43	5578/
PLOG/1.000E-01	7.4E07	0.50	11690/
PLOG/1.000E-01	2.0E-6	4.45	5564/
PLOG/3.160E-01	7.9E07	0.49	11700/
PLOG/3.160E-01	1.8E-6	4.46	5654/
PLOG/1.000E+00	2.2E09	0.06	12470/
PLOG/1.000E+00	2.2E-5	4.17	6416/
PLOG/3.160E+00	7.0E49	-10.18	77110/
PLOG/3.160E+00	7.7E05	1.18	11340/
PLOG/1.000E+01	4.1E16	-2.03	17630/
PLOG/1.000E+01	2.0E-2	3.38	8696/
PLOG/3.160E+01	9.4E16	-2.03	19590/
PLOG/3.160E+01	6.1E-3	3.53	9217/
PLOG/1.000E+02	5.9E21	-3.32	25030/
PLOG/1.000E+02	6.8E-2	3.27	10760/
C2H2+HO2=CH2CO+OH	5.16E-04	3.99	18890
PLOG/1.000E-02	6.3E-7	4.75	15530/
PLOG/1.000E-02	1.3E-14	6.58	10270/
PLOG/1.000E-01	6.7E-7	4.74	15550/
PLOG/1.000E-01	1.3E-14	6.59	10330/
PLOG/3.160E-01	4.2E-7	4.81	15410/
PLOG/3.160E-01	4.0E-14	6.36	10270/
PLOG/1.000E+00	5.3E-7	4.78	15460/
PLOG/1.000E+00	3.3E-15	6.70	10090/
PLOG/3.160E+00	1.0E-6	4.69	15640/
PLOG/3.160E+00	8.7E-21	8.30	8107/
PLOG/1.000E+01	4.7E-5	4.22	16780/
PLOG/1.000E+01	8.4E-22	8.76	8804/
PLOG/3.160E+01	9.0E-1	2.97	19730/
PLOG/3.160E+01	6.9E-14	6.67	13130/
PLOG/1.000E+02	3.6E03	1.97	23010/
PLOG/1.000E+02	6.6E-12	6.15	14730/
C2H2+HO2=CO+CH3O	3.06E05	1.07	14220
PLOG/1.000E-02	3.5E11	0.00	49510/
PLOG/1.000E-02	2.9E04	1.23	9903/

PLOG/1.000E-01	2.8E08	0.01	11920/
PLOG/1.000E-01	9.7E-7	4.15	5173/
PLOG/3.160E-01	8.1E07	0.18	11650/
PLOG/3.160E-01	1.8E-8	4.62	4517/
PLOG/1.000E+00	8.9E69	-15.85	102500/
PLOG/1.000E+00	5.4E05	0.86	10700/
PLOG/3.160E+00	5.7E12	-1.25	14570/
PLOG/3.160E+00	5.4E-4	3.42	7218/
PLOG/1.000E+01	3.3E23	-4.45	21210/
PLOG/1.000E+01	2.9E02	1.84	10460/
PLOG/3.160E+01	2.4E22	-3.96	22650/
PLOG/3.160E+01	8.1E00	2.30	10560/
PLOG/1.000E+02	1.2E18	-2.57	22360/
PLOG/1.000E+02	6.9E-4	3.42	9329/
C2H2+HO2=CO2+CH3	4.13E5	0.96	14140
PLOG/1.000E-02	1.2E-7	4.31	4614/
PLOG/1.000E-02	2.0E08	0.00	11790/
PLOG/1.000E-01	1.1E-7	4.32	4622/
PLOG/1.000E-01	2.0E08	0.00	11780/
PLOG/3.160E-01	1.8E142	-35.04	188700/
PLOG/3.160E-01	1.6E05	0.95	10200/
PLOG/1.000E+00	4.0E84	-19.80	119800/
PLOG/1.000E+00	1.4E06	0.68	10810/
PLOG/3.160E+00	5.0E13	-1.60	14980/
PLOG/3.160E+00	9.3E-3	3.00	7659/
PLOG/1.000E+01	8.6E28	-6.15	24030/
PLOG/1.000E+01	1.9E04	1.26	11230/
PLOG/3.160E+01	1.3E27	-5.42	25380/
PLOG/3.160E+01	2.9E02	1.79	11240/
PLOG/1.000E+02	1.7E15	-1.80	20370/
PLOG/1.000E+02	3.9E-7	4.21	7314/
C2H2+O2=HCO+HCO	6.1E12	0.000	53250
DUPLICATE			
C2H2+O2=HCO+HCO	1.7E07	1.670	70960 !
DUPLICATE			
C2H2+O2=HCO+HCO	-7.3E22	-2.473	73164
DUPLICATE			
C2H2+O2=HCO+HCO	-2.2E32	-4.946	93078
DUPLICATE			
C2H2+O2=HCO+H+CO	7.3E22	-2.473	73164
C2H2+O2=H+CO+H+CO	2.2E32	-4.946	93078
C2H2+CH2(S)=C2H2+CH2	4.0E13	0.000	0 !
H2CC+H=C2H2+H	1.0E14	0.000	0 !
H2CC+OH=CH2CO+H	2.0E13	0.000	0 !
H2CC+O2=CH2+CO2	1.0E13	0.000	0 !
C2H2OH+O2=OCHCHO+OH	1.0E12	0.0	5000 !
C2H2OH+O2=HOCHO+HCO	4.2E12	0.0	0 !
C2H+O=CH+CO	5.0E13	0.0	0 !
C2H+OH=HCCO+H	2.0E13	0.0	0 !
C2H+OH=C2+H2O	4.0E7	2.0	8000 !
!C2H+O2=CO+HCO	2.5E13	0.0	0 !
C2H+O2=CO+CO+H	2.52E13	0.0	0 !
C2H+CH4=C2H2+CH3	7.2E13	0.0	980 !
C2H+C2H2=C4H2+H	2.47E12	0.5	-391 !
C2+OH=C2O+H	5.0E13	0.0	0 !
C2+O2=CO+CO	5.0E13	0.0	0 !
!			
!*****			
! CH3HCO/CH2HCO/CH3CO/CH2CO/HCCOH/HCCO/C2O			
!*****			
!			
CH3HCO=CH3+HCO	7.1E15	0.0	81280 !
CH3HCO+H=CH3CO+H2	4.1E9	1.16	2400 !
CH3HCO+O=CH3CO+OH	5.8E12	0.0	1800 !
CH3HCO+OH=CH3CO+H2O	2.3E10	0.73	-1110 !
CH3HCO+HO2=CH3CO+H2O2	3.0E12	0.0	12000 !
CH3HCO+O2=CH3CO+HO2	3.0E13	0.0	39000 !
CH3HCO+CH3=CH3CO+CH4	2.0E-6	5.60	2460 !
CH2HCO=CH3+CO	1.0E13	0.0	42000 !

CH2HCO+H=CH3+HCO	1.0E14	0.0	0 !
CH2HCO+H=CH3CO+H	3.0E13	0.0	0 !
CH2HCO+O=CH2O+HCO	5.0E13	0.0	0 !
CH2HCO+OH=CH2CO+H2O	2.0E13	0.0	0 !
CH2HCO+OH=CH2OH+HCO	1.0E13	0.0	0 !
CH2HCO+O2=CH2O+CO+OH	1.1E14	-0.610	11422 !
CH2HCO+CH3=C2H5CHO	5.0E13	0.0	0 !
CH2HCO+CH2=C2H4+HCO	5.0E13	0.0	0 !
CH2HCO+CH=C2H3+HCO	1.0E14	0.0	0 !
C2H2OH=HCCOH+H	1.5E32	-6.168	52239 !
C2H2OH+H=CH2HCO+H	5.0E13	0.0	0 !
C2H2OH+O=OCHCHO+H	5.0E13	0.0	0 !
CH3CO(+M)=CH3+CO(+M)	2.8E13	0.0	17100 !
LOW/2.1E15 0.0 14000./			
TROE/ 0.5 1.0E-30 1.0E30 /			
H2/2/ CO/2/ CO2/3/ H2O/5/			
CH3CO+H=CH3+HCO	2.1E13	0.00	0 !
CH3CO+H=CH2CO+H2	1.2E13	0.00	0 !
CH3CO+O=CH3+CO2	1.5E14	0.00	0 !
CH3CO+O=CH2CO+OH	4.0E13	0.00	0 !
CH3CO+OH=CH2CO+H2O	1.2E13	0.00	0 !
CH2+CO(+M)=CH2CO(+M)	8.1E11	0.5	4510 !
LOW/ 1.88E33 -5.11 7095./			
TROE/ 0.5907 275 1226 5185/			
H2/2/ CO/2/ CO2/3/ H2O/8.58/ N2/1.43/			
CH2CO+H=CH3+CO	5.93E6	2.0	1300 !
CH2CO+H=HCCO+H2	3.0E7	2.0	10000 !
CH2CO+O=CH2+CO2	1.8E12	0.0	1350 !
CH2CO+O=HCCO+OH	2.0E7	2.0	10000 !
CH2CO+OH=CH2OH+CO	7.2E12	0.0	0 !
CH2CO+OH=CH3+CO2	3.0E12	0.0	0 !
CH2CO+OH=HCCO+H2O	1.0E7	2.0	3000 !
HCCOH+H=HCCO+H2	3.0E7	2.0	1000 !
HCCOH+OH=HCCO+H2O	1.0E7	2.0	1000 !
HCCOH+O=HCCO+OH	2.0E7	3.0	1900 !
CH+CO(+M)=HCCO(+M)	5.0E13	0.0	0 !
LOW/ 1.88E28 -3.74 1936 /			
TROE/ 0.5757 237 1652 5069 /			
N2/1.43/ H2O/8.58/ CO/2/ CO2/3/ H2/2/			
HCCO+H=CH2(S)+CO	1.00E14	0.0	0 !
HCCO+O=CO+CO+H	1.00E14	0.0	0 !
HCCO+OH=C2O+H2O	6.0E13	0.0	0 !
HCCO+O2=CO+CO2+H	1.4E7	1.7	1000 !
HCCO+O2=CO+CO+OH	2.88E7	1.7	1000 !
HCCO+HCCO=C2H2+CO+CO	1.00E13	0.0	0 !
HCCO+C2H2=H2CCCH+CO	1.0E11	0.0	3000 !
C2O+H=CH+CO	1.0E13	0.0	0 !
C2O+O=CO+CO	5.0E13	0.0	0 !
C2O+OH=CO+CO+H	2.0E13	0.0	0 !
C2O+O2=CO+CO+O	2.0E13	0.0	0 !
C2H5+HCO=C2H5CHO	1.8E13	0.0	0 !
C2H5CHO+H=C2H5CO+H2	8.0E13	0.0	0 !
C2H5CHO+O=C2H5CO+OH	7.8E12	0.0	1730 !
C2H5CHO+OH=C2H5CO+H2O	1.2E13	0.0	0 !
C2H5+CO=C2H5CO	1.5E11	0.0	4800 !
!			
! *****			
! H/N/O subset			
! *****			
!			
NO+H(+M)=HNO(+M)	1.52E15	-0.410	0 !
LOW /2.357E+14 0.206 -1550/			!
TROE /0.82 1E-30 1E+30 1E+30/			!
N2/1.6/			!
NO+H+N2=HNO+N2	7.0E19	-1.50	0 !
NO+O(+M)=NO2(+M)	1.3E15	-0.750	0 !
LOW /4.72E+24 -2.87 1550/			!
TROE /0.850 1E-30 1E+30 1E+30/			!
AR/0/			!
NO+OH(+M)=HONO(+M)	1.1E14	-0.300	0 !
LOW /3.392E+23 -2.5 0/			!
TROE /0.75 1E-30 1E+30 1E+30/			!
NO+HO2=NO2+OH	2.1E12	0.00	-479 !

NO2+H=NO+OH	8.4E13	0.0	0 !
NO2+O=NO+O2	3.9E12	0.0	-238 !
NO2+O(+M)=NO3(+M)	1.3E13	0.0	0 !
LOW/1.0E28 -4.08 2470./			
N2/1.5/ O2/1.5/ H2O/18.6/			
NO+NO+O2=NO2+NO2	1.2E9	0.0	-1053 !
NO2+NO2=NO3+NO	9.6E09	0.73	20900 !
NO3+H=NO2+OH	6.0E13	0.0	0 !
NO3+O=NO2+O2	1.0E13	0.0	0 !
NO3+OH=NO2+HO2	1.4E13	0.0	0 !
NO3+HO2=NO2+O2+OH	1.5E12	0.0	0 !
NO3+NO2=NO+NO2+O2	5.0E10	0.0	2940 !
HNO+H=H2+NO	4.5E11	0.72	655 !
HNO+O=NO+OH	1.0E13	0.0	0 !
HNO+OH=NO+H2O	3.6E13	0.0	0 !
HNO+O2=HO2+NO	1.0E13	0.0	25000 !
HNO+NO2=HONO+NO	6.0E11	0.0	2000 !
HNO+HNO=N2O+H2O	9.0E08	0.0	3100 !
HNO+NH2=NH3+NO	3.63E6	1.63	-1252 !
H2NO+M=HNO+H+M	2.5E15	0.0	50000 !
H2O/5/ N2/2/			
H2NO+H=HNO+H2	3.0E7	2.0	2000 !
H2NO+H=NH2+OH	5.0E13	0.0	0 !
H2NO+O=NH2+O2	2.0E14	0.0	0 !
H2NO+O=HNO+OH	3.0E7	2.0	2000 !
H2NO+OH=HNO+H2O	2.0E7	2.0	1000 !
H2NO+NO=HNO+HNO	2.0E04	2.0	13000 !
H2NO+NO2=HONO+HNO	6.0E11	0.0	2000 !
HONO+H=H2+NO2	1.2E13	0.0	7352 !
HONO+O=OH+NO2	1.2E13	0.0	5961 !
HONO+OH=H2O+NO2	4.0E12	0.0	0 !
NH3+M=NH2+H+M	2.2E16	0.0	93470 !
NH3+H=NH2+H2	6.4E05	2.39	10171 !
NH3+O=NH2+OH	9.4E06	1.94	6460 !
NH3+OH=NH2+H2O	2.0E06	2.04	566 !
NH3+HO2=NH2+H2O2	3.0E11	0.0	22000 !
NH2+H=NH+H2	4.0E13	0.00	3650 !
NH2+O=HNO+H	6.6E14	-0.50	0 !
NH2+O=NH+OH	6.8E12	0.0	0 !
NH2+OH=NH+H2O	4.0E06	2.0	1000 !
NH2+HO2=H2NO+OH	5.0E13	0.0	0 !
NH2+HO2=NH3+O2	1.0E13	0.0	0 !
NH2+NO=NNH+OH	8.9E12	-0.35	0 !
NH2+NO=N2+H2O	1.3E16	-1.25	0 !
DUP			
NH2+NO=N2+H2O	-8.9E12	-0.35	0 !
DUP			
NH2+NO2=N2O+H2O	3.2E18	-2.2	0 !
NH2+NO2=H2NO+NO	3.5E12	0.0	0 !
NH2+H2NO=NH3+HNO	3.0E12	0.0	1000 !
NH2+HONO=NO2+NH3	7.1E1	3.02	-4941 !
NH2+NH2=N2H2+H2	8.5E11	0.0	0 !
NH2+NH=N2H2+H	5.0E13	0.0	0 !
NH2+N=N2+H+H	7.2E13	0.0	0 !
NH+H=N+H2	3.0E13	0.0	0 !
NH+O=NO+H	9.2E13	0.0	0 !
NH+OH=HNO+H	2.0E13	0.0	0 !
NH+OH=N+H2O	5.0E11	0.50	2000 !
NH+O2=HNO+O	4.6E05	2.0	6500 !
NH+O2=NO+OH	1.3E06	1.5	100 !
NH+NO=N2O+H	2.9E14	-0.4	0 !
DUP			
NH+NO=N2O+H	-2.2E13	-0.23	0 !
DUP			
NH+NO=N2+OH	2.2E13	-0.23	0 !
NH+NO2=N2O+OH	1.0E13	0.0	0 !
NH+NH=N2+H+H	2.5E13	0.0	0 !
NH+N=N2+H	3.0E13	0.0	0 !
N+OH=NO+H	3.8E13	0.0	0 !
N+O2=NO+O	6.4E09	1.0	6280 !
N+NO=N2+O	3.3E12	0.30	0 !
N2H2+M=NNH+H+M	5.0E16	0.0	50000 !
H2O/15/ O2/2/ N2/2/ H2/2/			
N2H2+H=NNH+H2	5.0E13	0.0	1000 !
N2H2+O=NH2+NO	1.0E13	0.0	0 !

N2H2+O=NNH+OH	2.0E13	0.0	1000 !
N2H2+OH=NNH+H2O	1.0E13	0.0	1000 !
N2H2+NO=N2O+NH2	3.0E12	0.0	0 !
N2H2+NH2=NH3+NNH	1.0E13	0.0	1000 !
N2H2+NH=NNH+NH2	1.0E13	0.0	1000 !
NNH=N2+H	1.0E7	0.0	0 !
NNH+H=N2+H2	1.0E14	0.0	0 !
NNH+O=N2O+H	1.0E14	0.0	0 !
NNH+O=N2+OH	8.0E13	0.0	0 !
NNH+O=NH+NO	5.0E13	0.0	0 !
NNH+OH=N2+H2O	5.0E13	0.0	0 !
NNH+O2=N2+HO2	2.0E14	0.0	0 !
NNH+O2=N2+O2+H	5.0E13	0.0	0 !
NNH+NO=N2+HNO	5.0E13	0.0	0 !
NNH+NH2=N2+NH3	5.0E13	0.0	0 !
NNH+NH=N2+NH2	5.0E13	0.0	0 !
N2O+M=N2+O+M	4.0E14	0.0	56100 !
N2/1.7/ O2/1.4/ H2O/12/ CO/1.5/ CO2/3/			
N2O+H=N2+OH	3.3E10	0.0	4729 !
DUP			
N2O+H=N2+OH	4.4E14	0.0	19254 !
DUP			
N2O+O=NO+NO	6.6E13	0.0	26630 !
N2O+O=N2+O2	1.0E14	0.0	28000 !
N2O+OH=N2+HO2	1.3E-2	4.72	36561 !
N2O+OH=HNO+NO	1.2E-4	4.33	25081 !
N2O+NO=NO2+N2	5.3E05	2.23	46281 !
HONO2+OH=NO3+H2O	1.0E10	0.0	-1240 !
H2NO+O2=HNO+HO2	3.0E12	0.0	25000 !
HONO+HONO=>NO+NO2+H2O	3.5E-1	3.64	12100 !
H2NO+HO2=HNO+H2O2	2.9E04	2.69	1600 !
HNOH+H=NH2+OH	4.0E13	0.0	0 !
HNOH+H=HNO+H2	4.8E8	1.5	378 !
HNOH+O=HNO+OH	7.0E13	0.0	0 !
DUP			
HNOH+O=HNO+OH	3.3E08	1.5	-358 !
DUP			
HNOH+OH=HNO+H2O	2.4E6	2.0	-1192 !
HNOH+NH2=NH3+HNO	1.8E6	1.94	-1152 !
HNOH+HO2=HNO+H2O2	2.9E4	2.69	-1600 !
HNOH+M=HNO+H+M	2.0E24	-2.84	58934 !
H2O/10/			
HNOH+O2=HNO+HO2	3.0E12	0.0	25000 !
HNOH+NO2=HONO+HNO	6.0E11	0.0	2000 !
!			
! *****			
! cyanide subset			
! *****			
!			
CN+H2=HCN+H	3.0E05	2.45	2237 !
HCN+O=NCO+H	1.4E04	2.64	4980 !
HCN+O=NH+CO	3.5E03	2.64	4980 !
HCN+O=CN+OH	2.7E09	1.58	29200 !
HCN+OH=CN+H2O	3.9E06	1.83	10300 !
HCN+OH=HOCN+H	5.9E04	2.40	12500 !
HCN+OH=HNCO+H	2.0E-3	4.00	1000 !
HCN+OH=NH2+CO	7.8E-4	4.00	4000 !
HCN+CN=C2N2+H	1.5E07	1.71	1530 !
CN+O=CO+N	7.7E13	0.0	0 !
CN+OH=NCO+H	4.0E13	0.0	0 !
CN+O2=NCO+O	7.5E12	0.0	-389 !
CN+CO2=NCO+CO	3.7E06	2.16	26884 !
CN+NO2=NCO+NO	5.3E15	-0.752	344 !
CN+NO2=CO+N2O	4.9E14	-0.752	344 !
CN+NO2=N2+CO2	3.7E14	-0.752	344 !
CN+HNO=HCN+NO	1.8E13	0.00	0 !
CN+HONO=HCN+NO2	1.2E13	0.00	0 !
CN+N2O=NCN+NO	3.9E03	2.6	3696 !
CN+HNCO=HCN+NCO	1.5E13	0.0	0 !
CN+NCO=NCN+CO	1.8E13	0.0	0 !
HNCO+M=NH+CO+M	1.1E16	0.0	86000 !
HNCO+H=NH2+CO	2.2E07	1.7	3800 !
HNCO+O=NCO+OH	2.2E6	2.11	11425 !
HNCO+O=NH+CO2	9.8E7	1.41	8524 !
HNCO+O=HNO+CO	1.5E08	1.57	44012 !

HNCO+HO2=NCO+H2O2	3.0E11	0.0	22000 !
HNCO+O2=HNO+CO2	1.0E12	0.0	35000 !
HNCO+NH2=NH3+NCO	5.0E12	0.0	6200 !
HNCO+NH=NH2+NCO	3.0E13	0.0	23700 !
HOCN+H=NCO+H2	2.0E07	2.0	2000 !
HOCN+O=NCO+OH	1.5E04	2.64	4000 !
HOCN+OH=NCO+H2O	6.4E05	2.0	2563 !
HCNO+H=HCN+OH	1.0E14	0.0	12000 !
HCNO+O=HCO+NO	2.0E14	0.0	0 !
HCNO+OH=CH2O+NO	4.0E13	0.0	0 !
NCO+M=N+CO+M	3.1E16	-0.50	48000 !
NCO+H=NH+CO	5.0E13	0.0	0 !
NCO+O=NO+CO	4.7E13	0.0	0 !
NCO+OH=NO+HCO	5.0E12	0.0	15000 !
NCO+O2=NO+CO2	2.0E12	0.0	20000 !
NCO+H2=HNCO+H	7.6E02	3.0	4000 !
NCO+HCO=HNCO+CO	3.6E13	0.0	0 !
NCO+NO=N2O+CO	6.2E17	-1.73	763 !
NCO+NO=N2+CO2	7.8E17	-1.73	763 !
NCO+NO2=CO+NO+NO	2.5E11	0.0	-707 !
NCO+NO2=CO2+N2O	3.0E12	0.0	-707 !
NCO+HNO=HNCO+NO	1.8E13	0.0	0 !
NCO+HONO=HNCO+NO2	3.6E12	0.0	0 !
NCO+N=N2+CO	2.0E13	0.0	0 !
NCO+NCO=N2+CO+CO	1.8E13	0.0	0 !
C2N2+O=NCO+CN	4.6E12	0.0	8880 !
C2N2+OH=HOCN+CN	1.9E11	0.0	2900 !
NCN+H=HCN+N	1.0E14	0.0	0 !
NCN+O=CN+NO	1.0E14	0.0	0 !
NCN+OH=HCN+NO	5.0E13	0.0	0 !
NCN+O2=NO+NCO	1.0E13	0.0	0 !
CH3CN+H=HCN+CH3	4.0E7	2.0	2000 !
CH3CN+H=CH2CN+H2	3.0E7	2.0	1000 !
CH3CN+O=NCO+CH3	1.5E4	2.64	4980 !
CH3CN+OH=CH2CN+H2O	2.0E7	2.0	2000 !
CH2CN+O=CH2O+CN	1.0E14	0.0	0 !
CH2OH+CN=CH2CN+OH	5.0E13	0.0	0 !
H2CN+M=HCN+H+M	3.0E14	0.0	22000 !
!			
!*****			
! subset for CxHyOz+nitrogen species reactions			
!*****			
!			
CO+NO2=CO2+NO	9.0E13	0.0	33779 !
CO+N2O=N2+CO2	3.2E11	0.0	20237 !
CO2+N=NO+CO	1.9E11	0.0	3400 !
CH2O+NO2=HCO+HONO	8.0E02	2.77	13730 !
CH2O+NCO=HNCO+HCO	6.0E12	0.0	0 !
HCO+NO=HNO+CO	7.2E12	0.0	0 !
HCO+HNO=CH2O+NO	6.0E11	0.0	2000 !
HCO+NO2=CO+HONO	1.2E23	-3.29	2355 !
HCO+NO2=H+CO2+NO	8.4E15	-0.75	1930 !
CH4+CN=CH3+HCN	6.2E04	2.64	-437 !
NCO+CH4=CH3+HNCO	9.8E12	0.00	8120 !
CH3+NO=HCN+H2O	1.5E-1	3.523	3950 !
CH3+NO=H2CN+OH	1.5E-1	3.523	3950 !
CH3+NO2=CH3O+NO	4.0E13	-0.20	0 !
CH3+N=H2CN+H	7.1E13	0.0	0 !
CH3+CN=CH2CN+H	1.0E14	0.0	0 !
CH3+HOCN=CH3CN+OH	5.0E12	0.0	2000 !
CH2+NO=HCN+OH	2.2E12	0.0	-378 !
CH2+NO=HCNO+H	1.3E12	0.0	-378 !
CH2+NO2=CH2O+NO	5.9E13	0.0	0 !
CH2+N=HCN+H	5.0E13	0.0	0 !
CH2+N2=HCN+NH	1.0E13	0.0	74000 !
H2CN+N=N2+CH2	2.0E13	0.0	0 !
CH2(S)+NO=HCN+OH	2.0E13	0.0	0 !
CH2(S)+NO=CH2+NO	1.0E14	0.0	0 !
CH2(S)+HCN=CH3+CN	5.0E13	0.0	0 !
CH+NO=HCN+O	4.8E13	0.0	0 !
CH+NO=HCO+N	3.4E13	0.0	0 !
CH+NO=NCO+H	1.9E13	0.0	0 !
CH+NO2=HCO+NO	1.0E14	0.0	0 !
CH+N=CN+H	1.3E13	0.0	0 !
CH+N2=HCN+N	3.7E07	1.42	20723 !

```

CH+N2O=HCN+NO          1.9E13  0.0   -511 !
C+NO=CN+O              2.0E13  0.0     0 !
C+NO=CO+N              2.8E13  0.0     0 !
C+N2=CN+N              6.3E13  0.0  46019 !
C+N2O=CN+NO            5.1E12  0.0     0 !
C2H6+CN=C2H5+HCN      1.2E05  2.77  -1788 !
C2H6+NCO=C2H5+HNCO    1.5E-9  6.89  -2910 !
C2H4+CN=C2H3+HCN      5.9E14  -0.24  0 !
C2H3+N=HCN+CH2        2.0E13  0.0     0 !
C2H3+NO=C2H2+HNO      1.0E12  0.0   1000 !
C2H2+NCO=HCCO+HCN     1.4E12  0.0   1815 !
C2H+NO=HCN+CO         2.1E13  0.0     0 !
CH2CO+CN=HCCO+HCN     2.0E13  0.0     0 !
HCCO+NO=HCNO+CO       7.2E12  0.0     0 !
HCCO+NO=HCN+CO2       1.6E13  0.0     0 !
HCCO+NO2=HCNO+CO2     1.6E13  0.0     0 !
HCCO+N=HCN+CO         5.0E13  0.0     0 !
C2H+NO=CN+HCO         6.03E13 0.0   570 !
CH3OH+NO2=CH2OH+HONO  3.7E11  0.0  21400 !
CH2OH+NO=CH2O+HNO     1.3E12  0.0     0 !
CH2OH+NO2=CH2O+HONO   5.0E12  0.0     0 !
CH2OH+HNO=CH3OH+NO    3.0E12  0.0     0 !
!
! *****
! CH3OCH3 reactions
! *****
CH3OCH3(+M)=CH3+CH3O(+M) 4.38E21 -1.565 83842 !
  LOW / 1.1253E+62 -1.2019E+01 9.4882E+04/
  TROE / 0.0 5.1603E+02 1.0 3.6670E+03/
CH3OCH3+OH=CH3OCH2+H2O 6.71E06 2.00 -629.88 !
CH3OCH3+H=CH3OCH2+H2 1.2E01 4.00 2050 !
CH3OCH3+O=CH3OCH2+OH 5.0E13 0.00 4600 !
CH3OCH3+HO2=CH3OCH2+H2O2 2.0E13 0.00 1650 !
CH3OCH3+CH3O2=CH3OCH2+CH3O2H 1.27e-3 4.640 10556 !
CH3OCH3+O2=CH3OCH2+HO2 4.1E13 0.00 44910 !
CH3OCH3+CH3=CH3OCH2+CH4 2.68E01 3.7779 9631 !
CH3OCH3+CH3O=CH3OCH2+CH3OH 6.0E11 0.00 4075 !
CH3OCH3+CH3OCH2O2=CH3OCH2+CH3OCH2O2H 5.0e12 0.000 17690 !
CH3OCH3+OCHO=CH3OCH2+HOCHO 1.0e13 0.000 17690 !
CH3OCH2=CH3+CH2O 8.03e+12 0.440284 26490.7 !
plog/ 1.00e-02 7.494e+23 -4.5152 25236.1/
plog/ 1.00e-01 6.921e+28 -5.7271 27494.9/
plog/ 1.00e+00 4.229e+29 -5.6103 28898.3/
plog/ 1.00e+01 6.608e+27 -4.7073 29735.2/
plog/ 1.00e+02 2.659e+29 -4.9358 31785.5/
CH3OCH2+O2=CH3OCH2O2 1.0 1.0 1.0
plog/ 1.000e-003 1.120e+018 -3.37 -4294./
plog/ 1.000e-002 1.330e+021 -3.95 -2615./
plog/ 1.000e+000 1.130e+028 -5.24 4088./
plog/ 2.000e+000 3.910e+027 -5.00 4512./
plog/ 1.000e+001 2.750e+024 -3.87 4290./
plog/ 2.000e+001 2.970e+022 -3.23 3781./
plog/ 5.000e+001 5.190e+019 -2.35 2908./
plog/ 1.000e+002 5.430e+017 -1.73 2210./
CH3OCH2+CH3O=CH3OCH3+CH2O 2.4E13 0.00 0
CH3OCH2+CH2O=CH3OCH3+HCO 5.5E03 2.80 5860
CH3OCH2+CH3HCO=CH3OCH3+CH3CO 1.3E12 0.00 8500
CH3OCH2+HO2=CH3OCH2O+OH 9.6E12 0.00 0
CH3OCH2+NO2=CH3OCH2O+NO 1.0E13 0.00 0
CH3OCH2+O2=CH2OCH2O2H 1.0 1.0 1.0
plog/ 1.000e+001 9.670e+024 -4.36 8417./
plog/ 2.000e+001 4.080e+023 -3.90 8494./
plog/ 5.000e+001 5.080e+021 -3.28 8585./
plog/ 1.000e+002 1.620e+020 -2.81 8619./
CH3OCH2+O2=CH2O+CH2O+OH 1.0 1.0 1.0
plog/ 1.000e-003 8.010e+021 -3.18 3067./
plog/ 1.000e-002 1.730e+023 -3.55 4050./
plog/ 1.000e+000 2.040e+031 -5.76 11594./
plog/ 2.000e+000 5.990e+031 -5.87 12710./
plog/ 1.000e+001 9.390e+030 -5.59 14517./
plog/ 2.000e+001 1.090e+030 -5.30 15051./
plog/ 5.000e+001 3.580e+028 -4.88 15664./
plog/ 1.000e+002 2.410e+027 -4.55 16107./
CH3OCH2O+OH=CH3OCH2O2H 2.0E13 0.000 0
CH3OCH2O = CH3O+CH2O 9.72E15 -1.10 20640 !

```

```

CH3OCH2O2+CH2O=CH3OCH2O2H+HCO          2.0E12   0.00   11665
CH3OCH2O2+NO=CH3OCH2O+NO2                2.5E12   0.00    -258
CH3OCH2O2+CH3HCO=CH3OCH2O2H+CH3CO       2.8E12   0.00   13600
CH3OCH2O2+CH3OCH2O2=O2+CH3OCH2O+CH3OCH2O 1.597E+23 -4.50  0.000E+00 !
CH3OCH2O2+CH3OCH2O2=O2+CH3OCHO+CH3OCH2OH 6.844E+22 -4.50  0.000E+00 !
CH3OCH2O2 = CH2OCH2O2H 1.0 1.0 1.0!
plog/ 1.000e-003 1.940e+029 -6.99 22446./
plog/ 1.000e-002 4.070e+027 -6.16 21619./
plog/ 1.000e+000 2.520e+025 -4.76 22691./
plog/ 2.000e+000 5.970e+024 -4.48 22868./
plog/ 1.000e+001 4.440e+021 -3.38 22386./
plog/ 2.000e+001 4.520e+019 -2.74 21803./
plog/ 5.000e+001 5.720e+016 -1.82 20829./
plog/ 1.000e+002 3.700e+014 -1.13 20034./
CH3OCH2O2=CH2O+CH2O+OH 1.0 1.0 1.0
plog/ 1.000e-003 2.060e+036 -8.32 33415./
plog/ 1.000e-002 2.070e+039 -8.86 35842./
plog/ 1.000e+000 1.120e+040 -8.42 39835./
plog/ 2.000e+000 9.720e+038 -8.04 39923./
plog/ 1.000e+001 6.280e+035 -6.97 39900./
plog/ 2.000e+001 1.600e+034 -6.46 39850./
plog/ 5.000e+001 8.320e+031 -5.75 39719./
plog/ 1.000e+002 1.220e+030 -5.20 39549./
CH2OCH2O2H = OH+CH2O+CH2O 1.0 1.0 1.0!
plog/ 1.000e-003 1.660e+023 -4.53 22243./
plog/ 1.000e-002 5.300e+025 -4.93 24158./
plog/ 1.000e+000 7.810e+022 -3.50 23156./
plog/ 2.000e+000 4.980e+022 -3.35 23062./
plog/ 1.000e+001 8.460e+022 -3.22 23559./
plog/ 2.000e+001 9.090e+022 -3.14 23899./
plog/ 5.000e+001 4.590e+022 -2.94 24262./
plog/ 1.000e+002 1.400e+022 -2.72 24407./
CH2OCH2O2H+O2 => O2CH2OCH2O2H 1.0 1.0 1.0!
plog/ 1.000e-003 9.420e+012 -1.68 -4998./
plog/ 1.000e-002 8.160e+016 -2.50 -2753./
plog/ 1.000e+000 1.060e+022 -3.30 3389./
plog/ 2.000e+000 3.480e+020 -2.79 3131./
plog/ 1.000e+001 2.860e+016 -1.48 1873./
plog/ 2.000e+001 8.550e+014 -1.01 1312./
plog/ 5.000e+001 2.680e+013 -0.54 727./
plog/ 1.000e+002 4.870e+012 -0.32 428./
CH2OCH2O2H+O2<=>HO2CH2OCHO+OH 1.0 1.0 1.0 !
plog/ 1.000e-003 5.900e+020 -2.88 3234./
plog/ 1.000e-002 2.060e+023 -3.59 5116./
plog/ 1.000e+000 4.450e+029 -5.29 12791./
plog/ 2.000e+000 2.440e+028 -4.92 12891./
plog/ 1.000e+001 9.420e+023 -3.68 12049./
plog/ 2.000e+001 1.040e+022 -3.16 11505./
plog/ 5.000e+001 6.950e+019 -2.60 10861./
plog/ 1.000e+002 3.960e+018 -2.31 10500./
O2CH2OCH2O2H = HO2CH2OCHO+OH 1.0 1.0 1.0
plog/ 1.000e-003 9.050e+023 -4.88 18805./
plog/ 1.000e-002 6.840e+026 -5.32 22533./
plog/ 1.000e+000 5.070e+016 -1.81 21175./
plog/ 2.000e+000 2.660e+014 -1.11 20310./
plog/ 1.000e+001 1.690e+010 0.18 18604./
plog/ 2.000e+001 1.110e+009 0.54 18100./
plog/ 5.000e+001 1.070e+008 0.84 17661./
plog/ 1.000e+002 3.860e+007 0.98 17467./
HO2CH2OCHO => OCH2OCHO+OH          3E16      0.0   4.300E+04 !
CH2O+OCHO=OCH2OCHO          1.25e11   0.000   11900 !
OCH2OCHO = HOCH2OCO          1.0E11      0.00   1.400E+04
HOCH2OCO = HOCH2O+CO        2.177E16  -2.69   1.720E+04 !
HOCH2OCO = CH2OH+CO2        5.311E15  -2.61   2.081E+04 !
HOCH2O = HOCHO+H            1.000E14   0.00   1.490E+04
CH2O+OH = HOCH2O            4.50E15   -1.11   0.000E+00 !
CH3+O2(+M)=CH3O2(+M)        7.8E8      1.2      0
  LOW/5.8E25 -3.3 0/
  TROE/0.664 0.1E6 0.1E2/
CH4+NO2=CH3+HONO            1.2E13      0.0     30000
CH3O+NO=CH2O+HNO            1.3E14     -0.70      0
CH3O+NO(+M)=CH3ONO(+M)      5.99E14   -0.600      0 !
  LOW /8.14E+25 -2.8 0/
  TROE /1.0 1E-30 900 1E+30/
CH3O+NO2=CH2O+HONO          6.0E12      0.0     2285

```


CH3O+NO2 (+M)=CH3ONO2 (+M) LOW/1.4E30 -4.5 0/	1.2E13	0.0	0
CH3O2+H=CH3O+OH	9.64E13	0.0	0
CH3O2+O=CH3O+O2	2.59E13	0.0	0
CH3O2+OH=CH3O+HO2	6.00E13	0.0	0
CH3O2+HO2=CH3OOH+O2	2.50E11	0.0	0
CH3O2+H2O2=CH3OOH+HO2	2.40E12	0.0	9940
CH3O2+CH2O=CH3OOH+HCO	2.00E12	0.0	11665
CH3O2+CH4=CH3OOH+CH3	1.8E11	0.0	18500
CH3O2+CH3=CH3O+CH3O	2.4E13	0.0	0
CH3O2+CH3O=CH2O+CH3OOH	3.0E11	0.0	0
CH3O2+CH2OH=CH2O+CH3OOH	1.2E13	0.0	0
CH3O2+CH3OH=CH3O+CH2OH+OH	1.8E12	0.0	13700
CH3O2+CH3O2=CH3O+CH3O+O2	1.0E11	0.0	300
CH3O2+CH3O2=CH3OH+CH2O+O2	4.0E9	0.0	-2210
CH3O2+NO=CH3O+NO2	0.169E13	0.0	-570
CH3OOH=CH3O+OH	6.3E14	0.0	42300
CH3OOH+H=CH3O2+H2	8.8E10	0.0	1860
CH3OOH+H=CH3O+H2O	8.2E10	0.0	1860
CH3OOH+O=CH3O2+OH	1.0E12	0.0	3000
CH3OOH+OH=CH3O2+H2O	1.8E12	0.0	-378
NO+CH3 (+M)=CH3NO (+M) LOW /2.5E+16 0.0 -2841/ TROE /5.0 1E-30 120 1E+30/	9.00E12	0.0	192 !
CH3ONO=CH3+NO2	7E10	0.0	0 !
CH3NO2 (+M)=CH3+NO2 (+M) LOW/1.3E17 0.00 42000/ TROE/0.183 0.1E-29 0.1E31/	1.8E16	0.0	58500
CH3NO2+H=HONO+CH3	3.3E12	0.0	3730
CH3NO2+H=CH3NO+OH	1.4E12	0.0	3730
CH3NO2+H=H2CNO2+H2	5.4E02	3.50	5200
CH3NO2+O=H2CNO2+OH	1.5E13	0.00	5350
CH3NO2+OH=H2CNO2+H2O	5.05E05	2.00	1000 !
CH3NO2+OH=CH3OH+NO2	2.0E10	0.00	-1000
CH3NO2+HO2=H2CNO2+H2O2	3.0E12	0.00	23000
CH3NO2+O2=H2CNO2+HO2	2.0E13	0.00	57000
CH3NO2+CH3=H2CNO2+CH4	5.5E-1	4.00	8300
CH3NO2+CH3O=H2CNO2+CH3OH	3.0E11	0.00	7000
CH3NO2+NO2=H2CNO2+HONO	3.0E11	0.00	32000
H2CNO2=CH2O+NO	1.0E13	0.00	36000
! *****			
! C2H5OH			
! *****			
! C2H5OH (+M)=CH2OH+CH3 (+M) LOW /2.9E85 -18.9 109914/ TROE/ 0.5 200 890 4600 / H2O/5.0/ H2/2/ CO/2/ CO2/3/	5.9E23	-1.68	91163!
C2H5OH (+M)=C2H5+OH (+M) LOW /3.2E85 -18.8 114930/ TROE/ 0.5 300 900 5000 / H2O/5.0/ H2/2/ CO/2/ CO2/3/	1.2E23	-1.54	96005!
C2H5OH (+M)=C2H4+H2O (+M) LOW /2.6E83 -18.8 86452/ TROE/ 0.7 350 800 3800 / H2O/5.0/	2.8E13	0.09	66136!
C2H5OH (+M)=CH3HCO+H2 (+M) LOW /4.5E87 -19.4 115586/ TROE/ 0.9 900 1100 3500 / H2O/5.0/	7.2E11	0.09	91007!
C2H5OH+OH=C2H4OH+H2O	1.7E11	0.27	600!
C2H5OH+OH=CH3CHOH+H2O	4.6E11	0.15	0!
C2H5OH+OH=CH3CH2O+H2O	7.5E11	0.30	1634!
C2H5OH+H=C2H4OH+H2	1.2E07	1.80	5098!
C2H5OH+H=CH3CHOH+H2	2.6E07	1.65	2827!
C2H5OH+H=CH3CH2O+H2	1.5E07	1.60	3038!
C2H5OH+O=C2H4OH+OH	9.4E07	1.70	5459!
C2H5OH+O=CH3CHOH+OH	1.9E07	1.85	1824!
C2H5OH+O=CH3CH2O+OH	1.6E07	2.00	4448!
C2H5OH+CH3=C2H4OH+CH4	2.2E02	3.18	9622!
C2H5OH+CH3=CH3CHOH+CH4	7.3E02	2.99	7948!
C2H5OH+CH3=CH3CH2O+CH4	1.4E02	2.99	7649!
C2H5OH+HO2=C2H4OH+H2O2	1.2E04	2.55	15750!
C2H5OH+HO2=CH3CHOH+H2O2	8.2E03	2.55	10750!

C2H5OH+HO2=CH3CH2O+H2O2	2.5E12	0.00	24000!
CH3CH2O+M=CH3HCO+H+M	1.2E35	-5.89	25274!
CH3CH2O+M=CH3+CH2O+M	1.3E38	-6.96	23800!
CH3CH2O+CO=C2H5+CO2	4.7E02	3.16	5380!
CH3CH2O+O2=CH3HCO+HO2	4.0E10	0.00	1100!
CH3CH2O+H=CH3+CH2OH	3.0E13	0.00	0!
CH3CH2O+H=C2H4+H2O	3.0E13	0.00	0!
CH3CH2O+OH=CH3HCO+H2O	1.0E13	0.00	0!
CH3CHOH+O2=CH3HCO+HO2	4.8E14	0.00	5017!
DUP			
CH3CHOH+O2=CH3HCO+HO2	8.4E15	-1.20	0!
DUP			
CH3CHOH+O=CH3HCO+OH	1.0E14	0.00	0!
CH3CHOH+H=CH3+CH2OH	3.0E13	0.00	0!
CH3CHOH+H=C2H4+H2O	3.0E13	0.00	0!
CH3CHOH+HO2=CH3HCO+OH+OH	4.0E13	0.00	0!
CH3CHOH+OH=CH3HCO+H2O	5.0E12	0.00	0!
CH3CHOH+M=CH3HCO+H+M	1.0E14	0.00	25000!
C2H4OH+O2=CH2O+CH2O+OH	6.0E10	0.00	4500!
!			
!*****			
! CH3OCHO			
!*****			
!			
CH3OCHO(+M)=CH3OH+CO(+M)	2.00e13	0.000	60000
LOW /2.40e59 -11.8 71400/			
TROE /0.239 5.551e2 8.34e9 8.21e9/			
H2/3.0/ H2O/6/ O2/1.1/ CO/2.7/ CO2/5.4/			
CH3OCHO(+M)=CH4+CO2(+M)	1.50e12	0.000	59700
LOW /5.63e61 -12.79 71100/			
TROE / 0.179 3.575e2 9.918e9 3.28e9/			
H2/3.0/ H2O/6/ O2/1.1/ CO/2.7/ CO2/5.4/			
CH3OCHO(+M)=CH2O+CH2O(+M)	1.00e12	0.000	60500
LOW /1.55e57 -11.57 71700/			
TROE /0.781 6.49e2 6.18e2 6.71e9/			
H2/3.0/ H2O/6/ O2/1.1/ CO/2.7/ CO2/5.4/			
CH3OCHO(+M)=CH3+OCHO(+M)	2.17e24	-2.4	92600
LOW /5.71e47 -8.43 98490/			
TROE /6.89E-15 4.73e3 9.33e9 1.78e9/			
H2/3.0/ H2O/6/ O2/1.1/ CO/2.7/ CO2/5.4/			
CH3OCHO(+M)=CH3O+HCO(+M)	4.18e16	0.000	97400
LOW /5.27e63 -1.23e1 109180/			
TROE /0.894 7.49e9 6.47e2 6.69e8/			
H2/3.0/ H2O/6/ O2/1.1/ CO/2.7/ CO2/5.4/			
!			
CH3OCHO+H=CH2OCHO+H2	6.65E5	2.500	6496
CH3OCHO+H=CH3OCO+H2	2.58E5	2.500	5736
CH3OCHO+OH=CH2OCHO+H2O	8.86E12	0.100	3340
CH3OCHO+OH=CH3OCO+H2O	1.22E16	-1.0	4946
CH3OCHO+O=CH2OCHO+OH	8.84E5	2.4	4593
CH3OCHO+O=CH3OCO+OH	2.45E5	2.5	4047
CH3OCHO+O2=CH2OCHO+HO2	1.53E13	0.1	51749
CH3OCHO+O2=CH3OCO+HO2	3.85E12	0.1	50759
CH3OCHO+HO2=CH2OCHO+H2O2	5.66E4	2.4	16594
CH3OCHO+HO2=CH3OCO+H2O2	1.57E5	2.2	16544
CH3OCHO+CH3=CH2OCHO+CH4	2.91E-1	3.7	6823
CH3OCHO+CH3=CH3OCO+CH4	9.21E-2	3.7	6052
CH3OCHO+CH3O2=CH2OCHO+CH3OOH	5.66E4	2.4	16594
CH3OCHO+CH3O=CH2OCHO+CH3OH	4.59E9	0.5	4823
CH3OCHO+HCO=CH2OCHO+CH2O	1.02E5	2.5	18430
CH3OCHO+OCHO=CH2OCHO+HOCHO	5.66E4	2.4	16594
CH3OCHO+C2H5=CH2OCHO+C2H6	1.00E11	0.0	10400

CH3OCHO+C2H3=CH2OCHO+C2H4	1.00E11	0.0	10400
CH3OCHO+CH3O2=CH3OCO+CH3OOH	1.57E5	2.2	16544
CH3OCHO+CH3O=CH3OCO+CH3OH	5.27E9	0.8	2912
CH3OCHO+OCHO=CH3OCO+HOCHO	1.57E5	2.2	16544
CH3OCHO+HCO=CH3OCO+CH2O	5.40E6	1.9	17010
CH3OCHO+C2H5=CH3OCO+C2H6	1.00E11	0.0	10400
CH3OCHO+C2H3=CH3OCO+C2H4	1.00E11	0.0	10400
CH3+CO2=CH3OCO	4.76E7	1.5	34700
CH3O+CO=CH3OCO	1.55E6	2.02	5730
CH2OCHO=CH3OCO	2.62E11	0.0	38178 !
CH2O+HCO=CH2OCHO	3.89E11	0.0	22000
H+CH2OCHO=CH3OCHO	1.00E14	0.0	0
H+CH3OCO=CH3OCHO	1.00E14	0.0	0
CH3OCO+CH3OCHO=CH3OCHO+CH2OCHO	3.00E11	0.0	10400
CH2OCHO+HO2=HO2CH2OCHO	7.00E12	0.0	-1000
CH3OCO+HO2=CH3OCO2H	7.00E12	0.0	-1000
CH3OCO+OH=CH3OCO2H	1.55E6	2.41	-4132
CO2+CH3O=CH3OCO	1.00E11	0.00	9200
CH3OCO+O2=CH3OCO2O	4.52E12	0.00	0
CH2OCHO+O2=O2CH2OCHO	4.52E12	0.00	0
O2CH2OCHO=HO2CH2OCO	2.47E11	0.00	28900
HO2CH2OCO=>CO2+CH2O+OH	1.50E13	0.00	20500
HO2CH2OCO=>CO+HO2CH2O	2.00E13	0.00	17150
HO2CH2O=CH2O+HO2	1.28E12	0.00	13500
CH3OCO+OH=CH2OCO+OH	7.41E11	0.00	28900
CH2OOH+CO2=HO2CH2OCO	2.92E6	1.6	36591
OCH2O2H+CO=HO2CH2OCO	1.08E7	1.6	5588
OH+CH2O=CH2OOH	2.3E10	0.0	12900
OCH2O2H=CH2O+HO2	1.27E18	-1.8	10460
CH2OCO+OH=CH2O+CO2+OH	3.8E18	-1.5	37360
CH2OCO+OH=CH2O+CO+HO2	3.8E18	-1.5	37360
CH2OCO+OH=>OCH2OCO+OH	7.5E10	0.0	15250
HO2CH2OCO=>OCH2OCO+OH	7.5E10	0.0	15250
CH2OCO+OH+O2=O2CH2OCO	4.52E12	0.0	0
HO2CH2OCO+O2=HO2CH2OCO2O	4.52E12	0.0	0
O2CH2OCO+OH=>OCH2OCO+OH	2.89E10	0.0	21863
HO2CH2OCO=>OCH2OCO+OH	2.48E11	0.0	20900
OCH2OCO+OH=>CO2+OCHO+OH	1.05E16	0.0	41600
OCH2OCO+H=>CHO+CO+H2	4.8E8	1.5	2005
OCH2OCO+OH=>CHO+CO+H2O	2.40E6	2.0	-1192
OCH2OCO+HO2=>CHO+CO+H2O2	4.00E12	0.0	12976
OCHO+CO=CHOOCO	1.08E7	1.6	5588
HCO+CO2=CHOOCO	2.92E6	1.6	36591
!			
! *****			
! DMM			
! *****			
CH3OCH2OCH3+H=CH3OCH2OCH2+H2	9.70E13	0.00	6210
CH3OCH2OCH3+H=CH3OCHOCH3+H2	3.70E12	0.00	3240
CH3OCH2OCH3+O=CH3OCH2OCH2+OH	5.00E13	0.00	4570
CH3OCH2OCH3+O=CH3OCHOCH3+OH	6.00E13	0.00	3970
CH3OCH2OCH3+M=CH3+CH3OCH2O+M	2.62E16	0.00	82200
CH3OCH2OCH3+M=CH3O+CH3OCH2+M	2.51E15	0.00	76800
CH3OCH2OCH3+O2=CH3OCH2OCH2+HO2	4.10E13	0.00	44900
CH3OCH2OCH3+O2=CH3OCHOCH3+HO2	3.33E12	0.00	43500
CH3OCH2OCH3+CH3=CH3OCH2OCH2+CH4	2.26E-5	5.35	5810
CH3OCH2OCH3+CH3=CH3OCHOCH3+CH4	5.00E12	0.00	9750
CH3OCH2OCH3=CH3OCH2OCH2+H	4.35E16	0.00	100000
CH3OCH2OCH3=CH3OCHOCH3+H	6.31E15	0.00	94700
CH3OCH2OCH2=CH2O+CH3OCH2	1.00E13	0.00	32500
CH3OCHOCH3=CH3OCHO+CH3	1.00E13	0.00	32500
CH3OCH2O+M=CH3OCHO+H+M	7.00E15	0.00	22800
CH3OCH2O+O2=CH3OCHO+HO2	6.03E10	0.00	1650
CH3OCH2O+OH=CH3OCHO+H2O	1.00E13	0.00	0
CH3OCH2O+O=CH3OCHO+OH	1.00E13	0.00	0
CH3OCH2O+H=CH3OCHO+H2	2.00E13	0.00	0
CH3OH+H=CH3+H2O	5.01E12	0.00	5300
CH3+CH2OH=CH2O+CH4	2.41E12	0.00	0
CH3O+HCO=CH2O+CH2O	6.03E12	0.00	0
CH3OCH2OCH3=CH3OH+CH3+HCO	1E13	0.00	6E+04
CH3OCH2OCH3+CH3O2=CH3OCH2OCH2+CH3O2H	1.68E13	0.00	1.769E+04
CH3OCH2OCH3+CH3O2=CH3OCHOCH3+CH3O2H	5.6E12	0.0	1.44E4
CH3OCH2OCH3+CH3O=CH3OCH2OCH2+CH3OH	6.02E11	0.00	4.074E+03
CH3OCH2OCH3+CH3O=CH3OCHOCH3+CH3OH	2.01E11	0.00	2.873E+03
CH3OCH2OCH3+CH3OCH2O2=CH3OCH2OCH2+CH3OCH2O2H	5E12	0.0	17960

```

CH3OCH2OCH3+CH3OCH2O2=CH3OCHOCH3+CH3OCH2O2H 5E12 0.0 17960
CH3OCH2OCH3+OH=CH3OCH2OCH2+H2O 6.32E6 2.00 -652
CH3OCH2OCH3+OH=CH3OCHOCH3+H2O 6.32E6 2.00 -652
CH3OCH2OCH3+HO2=CH3OCH2OCH2+H2O2 1E13 0.00 17686
CH3OCH2OCH3+HO2=CH3OCHOCH3+H2O2 2E12 0.00 15296
CH3OCH2OCH2+O2=CH2O+CH3OCHO+OH 2.5E11 0.00 -1700
CH3OCH2OCH2+HO2=CH2O+CH3OCH2O+OH 3E11 0.0 0
CH3OCHOCH3+O2=CH2O+CH3OCHO+OH 2.5E11 0.0 -1700
CH3OCHOCH3+HO2=CH3OCHO+CH3O+OH 1E12 0.0 0
CH3OCH2OCH2+O2(+M)=CH3OCH2O2+CH2O(+M) 6.40E12 0.0 91
LOW /1.3E26 -3.0 0/
CH3OCH2OCH2+HO2=CH3OCH2O2+CH2OH 1E12 0.00 0
!
! *****
! OCHCHO
! *****
!
OCHCHO=CH2O+CO 8.04E55 -12.6 76713 !
DUPLICATE !
PLOG/ 0.009869 4.17E53 -12.5 70845/
PLOG/ 0.04935 5.12E54 -12.6 73012/
PLOG/ 0.09869 1.03E55 -12.6 73877/
PLOG/ 0.4935 4.50E55 -12.6 75869/
PLOG/ 0.9869 8.04E55 -12.6 76713/
PLOG/ 4.935 1.05E55 -12.2 77643/
PLOG/ 9.869 5.48E56 -12.6 79964/
OCHCHO=CO+CO+H2 6.12E57 -13.1 80147 !
PLOG/ 0.009869 6.02E51 -12.1 71854/
PLOG/ 0.04935 1.43E54 -12.5 74751/
PLOG/ 0.09869 1.78E55 -12.7 76137/
PLOG/ 0.4935 1.31E57 -13.0 78972/
PLOG/ 0.9869 6.12E57 -13.1 80147/
PLOG/ 4.935 5.79E57 -12.9 81871/
PLOG/ 9.869 3.42E59 -13.3 84294/
OCHCHO=CH2O+CO 2.62E57 -13.2 79754 !
DUPLICATE !
PLOG/ 0.009869 8.36E52 -12.6 72393/
PLOG/ 0.04935 8.25E54 -12.9 75113/
PLOG/ 0.09869 4.37E55 -13.0 76257/
PLOG/ 0.4935 1.32E57 -13.2 78851/
PLOG/ 0.9869 2.62E57 -13.2 79754/
PLOG/ 4.935 1.00E57 -12.9 81161/
PLOG/ 9.869 5.69E59 -13.3 83539/
OCHCHO=HCO+HCO 1.89E57 -12.8 84321 !
PLOG/ 0.009869 1.03E42 -9.7 73534/
PLOG/ 0.04935 6.02E48 -11.1 77462/
PLOG/ 0.09869 1.65E51 -11.6 79111/
PLOG/ 0.4935 5.33E55 -12.5 82774/
PLOG/ 0.9869 1.89E57 -12.8 84321/
PLOG/ 4.935 2.22E59 -13.1 87258/
PLOG/ 9.869 2.99E60 -13.3 88993/
OCHCHO+H=OCHCO+H2 5.4E13 0.000 4302 !
OCHCHO+O=OCHCO+OH 4.2E11 0.570 2760 !
OCHCHO+OH=OCHCO+H2O 4.0E06 2.000 -1630 !
OCHCHO+HO2=>HOCH(OO)CHO 1.3E31 -7.532 1440 !
HOCH(OO)CHO => OCHCHO+HO2 1.9E29 -5.781 15790 !
HOCH(OO)CHO => HOCHO+CO+OH 1.6E10 0.051 15190 !
OCHCHO+HO2=OCHCO+H2O2 8.2E04 2.500 10206 !
OCHCHO+O2=OCHCO+HO2 4.8E05 2.500 36461 !
OCHCHO+HO2=HOCHO+CO+OH 3.3E-4 3.995 300 !
OCHCO=HCO+CO 4.1E14 0.000 8765 !
PLOG/ 0.01 3.8E12 0.000 8610/
PLOG/ 0.1 3.8E13 0.000 8665/
PLOG/ 1.0 4.1E14 0.000 8765/
OCHCO+O2=CO+CO2+OH 3.3E14 0.000 2075 !
PLOG/ 0.01 1.6E14 0.000 1540/
PLOG/ 0.1 1.1E14 0.000 1300/
PLOG/ 1.0 3.3E14 0.000 2075/
!
! *****
! HOCHO
! *****
!
HOCHO(+M)=CO+H2O(+M) 7.5E14 0.000 68710 !
LOW /4.1E15 0 52980/

```

HOCHO(+M)=CO2+H2(+M)	4.5E13	0.000	68240 !
LOW /1.7E15 0 51110/			!
HOCHO+H=HOCO+H2	2.3E02	3.272	4858 !
HOCHO+H=OCHO+H2	4.2E05	2.255	14091 !
HOCHO+H=HOCHOH	2.5E05	2.357	9783 !
HOCHO+O=HOCO+OH	5.1E01	3.422	4216 !
HOCHO+O=OCHO+OH	1.7E05	2.103	9880 !
HOCHO+OH=HOCO+H2O	7.8E-6	5.570	-2365 !
HOCHO+OH=OCHO+H2O	4.9E-5	4.910	-5067 !
HOCHO+HO2=HOCO+H2O2	4.7E-1	3.975	16787 !
HOCHO+HO2=OCHO+H2O2	3.9E01	3.080	25206 !
HOCO+HO2=HOCHO+O2	4.0E11	0.000	0 !
HOCHO+O2=OCHO+HO2	3.0E13	0.000	63000 !
HOCO+H=CO2+H2	3.1E17	-1.3475	555 !
HOCO+H=CO+H2O	6.0E15	-0.525	2125 !
HOCO+O=CO2+OH	9.0E12	0.000	0 !
HOCO+OH=CO2+H2O	4.6E12	0.000	-89 !
DUPLICATE			!
HOCO+OH=CO2+H2O	9.5E06	2.000	-89 !
DUPLICATE			!
HOCO+HO2=CO2+H2O2	4.0E13	0.000	0 !
OCHO=CO2+H	1.0E10	0.000	0 !
OCHO+O2=CO2+HO2	5.0E13	0.000	0 !
HOCH2O=HCO+H2O	2.0E11	0.449	41259 !
HOCH2O+O2=HOCHO+HO2	7.2E13	0.000	3736 !
DUPLICATE			!
HOCH2O+O2=HOCHO+HO2	2.9E16	-1.500	0 !
DUPLICATE			!
!			!
END			!

